

NISTIR 8271 DRAFT SUPPLEMENT

Face Recognition Vendor Test (FRVT) Part 2: Identification

Patrick Grother
Mei Ngan
Kayee Hanaoka
*Information Access Division
Information Technology Laboratory*

This document is a draft supplement of [NIST Interagency Report 8271](#)

2023/04/04



NISTIR 8271 DRAFT SUPPLEMENT

Face Recognition Vendor Test (FRVT) Part 2: Identification

Patrick Grother
Mei Ngan
Kayee Hanaoka
*Information Access Division
Information Technology Laboratory*

This document is a draft supplement of [NIST Interagency Report 8271](#)

November 2022



U.S. Department of Commerce
Gina M. Raimondo, Secretary

National Institute of Standards and Technology
Laurie E. Locascio, NIST Director and Undersecretary of Commerce for Standards and Technology

RELEASE NOTES

2023-03-29: The 1:N track of the FRVT remains open.

- ▷ This document is the twenty third draft update to [NIST Interagency Report 8271](#). It contains results for one first-time participant: Recognito.
- ▷ The document also includes results for algorithms for one returning developer: AllGoVision Technologies.

2023-03-14: The 1:N track of the FRVT remains open.

- ▷ This document is the twenty second draft update to [NIST Interagency Report 8271](#). It contains results for no first-time participants.
- ▷ The document also includes results for algorithms from nine returning developers: Cloudwalk - Moon-time Smart Technology, Line Corporation, Intema-LGL Group Neurotechnology, NEC, Paravision, Samsung S1, Veridas Digital Authentication Solutions, and Thales Group

2023-02-06: The 1:N track of the FRVT remains open.

- ▷ This document is the twenty first draft update to [NIST Interagency Report 8271](#). It contains results for no first-time participants.
- ▷ The document also includes results for algorithms from seven returning developers: Dermalog, DiluSense Technology, Hangzhuo Allu Network Information Technology, Idemia, Innovatrics, Rank One Computing, and Sensetime Group.

2022-12-15: The 1:N track of the FRVT remains open.

- ▷ This document is the twentieth draft update to [NIST Interagency Report 8271](#). It contains results for one first-time participant: First Credit Bureau Kazakhstan.
- ▷ The document also includes results for algorithms from five returning developers: Gorilla Technology, Pangiam, Qnap Security, SQLsoft, Vixvizon (formerly known as Imagus).

2022-11-09: The 1:N track of the FRVT remains open.

- ▷ This document is the nineteenth draft update to [NIST Interagency Report 8271](#). It contains results for four first-time participant: Mukh, Turing Technology VIP, Verijelas and Verihubs Inteligensia
- ▷ The document also includes results for algorithms from two returning developers: Maxvision and Samsung S1.

2022-09-23: The 1:N track of the FRVT remains open.

- ▷ This document is the eighteenth draft update to [NIST Interagency Report 8271](#). It contains results for two first-time participants: Intema-LGL Group and T4iSB.
- ▷ The document also includes results for algorithms from two returning developers: Cloudwalk - Moon-time Smart Technology, Dermalog, Griaule, Hangzhuo Allu Network Information Technology, Intelivision, Line Corporation, NEC, Sensetime Group, Realnetworks Inc and Vietnam Posts and Telecommunications Group.

2022-07-28: The 1:N track of the FRVT remains open.

- ▷ This document is the seventeenth draft update to [NIST Interagency Report 8271](#). It contains results for one first-time participant: Maxvision.
- ▷ The document also includes results for algorithms from two returning developers: Rank One Computing, and Viettel Group.

- ▷ We have replaced the probe set used in the visa-border benchmark. It was previously comprised of 80 000 images; it now has size 1 212 892 - see amended entries in Table 1. False negative identification rates have increased.
- ▷ We have added images to the probe set used in the visa-kiosk benchmark. It was previously comprised of 21 016 mates and the same number of non-mates; it now has 31 579 mates and 45 460 non-mates - see amended and entries in Table 1. False negative identification rates are improved (reduced) slightly.

2022-06-08: The 1:N track of the FRVT remains open.

- ▷ This document is the seventeenth draft update to [NIST Interagency Report 8271](#). It includes results for algorithms submitted by three first-time participants: Digidata, DiluSense Technology, and Vietnam Posts and Telecommunications Group.
- ▷ The document also includes results for algorithms from five returning developers: Canon Inc, Imagus Technology, Neurotechnology, Thales, and Samsung S1.

2022-04-28: The 1:N track of the FRVT remains open.

- ▷ This document is the sixteenth draft update to [NIST Interagency Report 8271](#). It includes results for algorithms submitted by one first-time participants: Hangzhuo Allu Network Information Technology.
- ▷ The document also includes results for algorithms from three returning developers: HyperVerge Inc, Qnap Security, and Realnetworks Inc.
- ▷ The [1:N results page](#) has been updated.

2022-03-30: The 1:N track of the FRVT remains open.

- ▷ This document is the sixteenth draft update to [NIST Interagency Report 8271](#). It includes results for algorithms submitted by two first-time participants: Intellivision, and Pangiam.
- ▷ The document also includes results for algorithms from three returning developers: Fujitsu Research and Development Center, Idemia, and Gorilla Technology.
- ▷ The [1:N results page](#) has been updated.

2022-02-23: The 1:N track of the FRVT remains open.

- ▷ This document is the fifteenth draft update to [NIST Interagency Report 8271](#). It includes results for algorithms submitted by four first-time participants: Cloudwalk - Moontime Smart Technology, Decatur Industries Inc, NotionTag Technologies Private Limited, and Reveal Media Ltd.
- ▷ The document also includes results for algorithms from three returning developers: Cognitec Systems GmbH, Sensetime Group, and Viettel Group
- ▷ The [1:N results page](#) has been updated.

2022-01-20: The 1:N track of the FRVT remains open.

- ▷ This document is the fourteenth draft update to [NIST Interagency Report 8271](#). It includes results for algorithms recently submitted by two first-time participants: Daon and SQIsoft.
- ▷ The document also includes results for algorithms from five returning developers: Cyberlink Corp, NEC, Neurotechnology, Paravision, and Rank One Computing.
- ▷ The [1:N results page](#) has been updated.

2021-12-16: The 1:N track of the FRVT remains open.

- ▷ This document is the thirteenth draft update to [NIST Interagency Report 8271](#). It includes results for algorithms from six returning developers: Dahua Technology, Imagus Technology, Line Corporation, N-Tech Lab, Qnap Security, and Realnetworks Inc.

- ▷ The [1:N results page](#) has been updated.

2021-11-22: The 1:N track of the FRVT remains open.

- ▷ This document is the twelfth draft update to [NIST Interagency Report 8271](#). It includes results for algorithms recently submitted by three first-time participants Clearview AI, Griaule, and Mantra Softech India.
- ▷ This document and the [1:N results page](#) also include results for algorithms from six returning developers: Acer Incorporated, Canon, Dermalog, Samsung S1, VisionLabs, and Veridas Digital Authentication.

2021-10-28: The 1:N track of the FRVT remains open.

- ▷ This document is the eleventh draft update to [NIST Interagency Report 8271](#). It includes results for algorithms recently submitted by three first-time participants (20Face, Fujitsu Research and Development Center, and Vision-Box), and five returning participants (Alchera, Gorilla Technology, Tevian, Thales-Cogent, and Visidon). Visidon
- ▷ Both the main [1:N results page](#) and the small-gallery [paperless travel page](#) have been updated.

2021-09-21: The 1:N track of the FRVT remains open. Three news items:

- ▷ This document is the tenth draft update to [NIST Interagency Report 8271](#). It includes results for algorithms recently submitted by six first-time developers: Cubox, Fincore, HyperVerge, Qnap Security, Staqu Technologies, and Tripleize (Aize, 3-ize).
- ▷ It includes results also for four returning developers: Cognitec Systems, Incode Technologies, Innovatrics, Neurotechnology, and Rank One Computing.

2021-08-02: The 1:N track of the FRVT remains open. Three news items:

- ▷ This document is the ninth draft update to [NIST Interagency Report 8271](#). It includes results for algorithms recently submitted by eight participants: Cyberlink Corp, NEC Corp, N-Tech Lab, Realnetworks Inc., Sensetime Group, Veridas Digital, Viettel Group, and Vigilant Solutions.
- ▷ Algorithms submitted since July 24 will be included in the next update scheduled for September 9, 2021.
- ▷ A new report, NIST Interagency Report 8381 - FRVT Part 7: Identification for Paperless Travel and Immigration, has been released [[PDF](#), [webpage](#)]. It documents the use of FRVT 1:N algorithms in positive access control and immigration status update travel applications where the enrolled population size is as low as 420 people for aircraft boarding, and 42 000 for an airport security line. These population sizes are much smaller than those used in the main [1:N evaluation](#). Going forward, we will update the report and webpage with results for new algorithms.

2021-07-07: The 1:N track of the FRVT remains open. One update:

- ▷ This document is the eighth draft update to [NIST Interagency Report 8271](#). It include results for an algorithm from one participant: Kakao Enterprises.

2021-06-22: The 1:N track of the FRVT remains open. Three updates:

- ▷ This is the seventh draft of the update to [NIST Interagency Report 8271](#). It includes results for algorithms from three new participants: Line Corporation, Rendip, and Samsung S1 Corp.
- ▷ We have also added results for algorithms from five returning developers: Imagus Technology, Kneron, Tevian, Visidon, and Xforward AI Technology.

- ▷ The algorithm-specific report cards (examples: [1](#), [2](#), and [3](#)) now include figures showing how low threshold values can be used to reduce candidate list lengths for human review, while (usually) elevating miss rates (FNIR) only modestly. The reports also feature some minor additions and clarifications.

2021-03-26: The 1:N track of the FRVT remains open. Three updates:

- ▷ This is the sixth draft of the update to [NIST Interagency Report 8271](#). It includes results for algorithms from three returning developers: Neurotechnology, Guangzhou Pixel Solutions, and Tech5 SA.
- ▷ We have added results on the webpage and in the report for a new ageing dataset in which border crossing photos are searched against a gallery of border crossing photos collected between 10 and 15 years prior to the mated search photos. See section [2](#) for a description of the images. Table [1](#) has a new entry describing the experiment.
- ▷ We will mostly discontinue running the mugshot ageing test, reserving it for algorithms that show high accuracy on the new border-crossing set.

2021-03-26: Regarding the fifth draft of the update to [NIST Interagency Report 8271](#):

- ▷ In addition have added results for first algorithms from two new participants: Viettel Group and Veridas Digital Authentication Solutions.
- ▷ We have added results for algorithms from two returning developers: Idemia and Cognitec Systems.
- ▷ In addition to the report, the [results page](#) and its hyperlinked [report cards](#) have been updated.

2021-02-08: Regarding the fourth draft of the update to [NIST Interagency Report 8271](#):

- ▷ We have added results for eight algorithms submitted by eight developers: Cyberlink, Dermalog, Imagus, Paravision, Sensetime, Trueface, Vigilant Solutions, and X-Forward AI. With the exception of Trueface, all of these developers have participated previously.
- ▷ We anticipate updating this report again in the first week of March 2021.
- ▷ The main [results page](#) has been revised with tabs for the investigative and lights-out identification tables, and a new tab dedicated to speed and resource consumption.
- ▷ The report cards (example [here](#)) hyperlinked from the [results page](#) have been revised to improve content and format.

2020-12-14: Regarding third draft of the update to [NIST Interagency Report 8271](#):

- ▷ We have added results for fifteen algorithms submitted by thirteen developers. The four first-time participants are: Acer, Akurat Satu Indonesia, Canon, and Xforward AI Technology. The ten returning developers are: AllGoVision, Cyberlink Corp, Dahua Technology, Deepglint, Guangzhou Pixel Solutions, IIT Vision, Innovatrics, Rank One Computing, Scanovate, Sensetime Group, Synesis, and VisionLabs.
- ▷ We have added two new datasets to the evaluation: First a set of “visa-border” photos, representing search of an airport immigration lane photo against a database of closely ISO standard portraits; second a “visa-kiosk” set representing search of a photo collected in a registered traveller kiosk against the same ISO portrait gallery. The images are described in section [2.1](#).
- ▷ As in previous reports, we include results for searching mugshots against a mugshot gallery containing a single image of each of 12 million people. However we have suspending running searches against a gallery in which multiple lifetime photos per person are present, because this is computationally expensive. We retain a N = 3 million search test dedicated to ageing in which mugshots taken up to 18 years after the first photograph are searched - see Table [8](#).
- ▷ Tables containing computational resource information, Table [2](#) . . . , now include duration of the finalization step, in which search algorithms can, at their option, build fast-search data structures.

- ▷ We have linked revised per-algorithm PDF report cards from the main [results page](#).
- ▷ We have regenerated all figures and tables to drop algorithms submitted before June 2018. Results for prior algorithms appear in [archived editions](#) of this report.
- ▷ Going forward, we anticipate producing more frequent updates to this report. Developers may submit one algorithm to this evaluation every four calendar months.

2020-03-24: Regarding the second draft of the update to [NIST Interagency Report 8271](#):

- ▷ Adds results for three algorithms from three developers, Dermalog, Innovatrics, and Synesis.
- ▷ Adds Table 8 on ageing showing the increase in false negative rates with time elapsed between two photos. Some of the results were contained in graphs in prior editions of this report, but the table adds results for some newly submitted algorithms.
- ▷ Adjusts frontal mugshot results (for recent and lifetime consolidated galleries) to include the effect of removing some images that should not have been included in image test sets. These images were mostly profile views, images of tattoos containing faces, images of faces on tee shirts, and images of photographs on walls behind the intended subject. This affects many tables and reduces false negative identification rates for all algorithms. The reduction is larger for “recent” enrollments than for “lifetime consolidated” ones with the consequence that accuracy on recent images is now superior.

2020-02-26: Regarding the first draft of the update to [NIST Interagency Report 8271](#):

- ▷ Adds results for 38 algorithms from 31 different developers, eleven of whom are entirely new to the 1:N track of FRVT. These are Allgovision, Cyberlink, Deepsea Tencent, Farbar F8, Imperial College London, Intsys MSU, Kedacom, Kneron, Pixelall, and Scanovate.

DISCLAIMER

Specific hardware and software products identified in this report were used in order to perform the evaluations described in this document. In no case does identification of any commercial product, trade name, or vendor, imply recommendation or endorsement by the National Institute of Standards and Technology, nor does it imply that the products and equipment identified are necessarily the best available for the purpose.

INSTITUTIONAL REVIEW BOARD

The National Institute of Standards and Technology's Research Protections Office reviewed the protocol for this project and determined it is not human subjects research as defined in Department of Commerce Regulations, 15 CFR 27, also known as the Common Rule for the Protection of Human Subjects (45 CFR 46, Subpart A).

ACKNOWLEDGMENTS

The authors are grateful for the support and collaboration of the the Department of Homeland Security's Science & Technology Directorate (S&T), Office of Biometric Identity Management (OBIM), and Customs and Border Protection (CBP).

Additionally, the authors are grateful to staff in the NIST Biometrics Research Laboratory for infrastructure supporting rapid evaluation of algorithms.

Executive Summary

This document is a draft revision of the September 2019 report [NIST Interagency Report 8271](#). That report gave extensive documentation of face recognition applied to mugshots. This report extends that by adding more two more challenging datasets containing images with serious departures from canonical frontal image standards. The report also adds results for algorithms submitted to NIST since in 2019 and 2020. The algorithms, which implement one-to-many identification of faces appearing in two-dimensional images, are prototypes from the research and development laboratories of mostly commercial suppliers, and are submitted to NIST as compiled black-box libraries implementing a NIST-specified C++ test interface. The report therefore does not describe how algorithms operate. The report lists accuracy results alongside developer names and will therefore be useful for comparison of face recognition algorithms and assessment of absolute capability. The report is accompanied by a [webpage](#) with sortable results.

The evaluation uses six datasets: frontal mugshots, profile view mugshots, desktop webcam photos, visa-like immigration application photos, immigration lane photos, and registered traveler kiosk photos. These datasets are sequestered at NIST, meaning that developers do not have access to them for training or testing. This aspect is important because face recognition algorithms are very often deployed without the developer having access to the customers image data. A possible exception to this would be in a cloud-based application where the operational image data is uploaded to a cloud operated by a face recognition developer.

The major result in NIST IR 8271 was that massive gains in accuracy have been achieved in the years 2013 to 2018 and these far exceed improvements made in the prior period, 2010 to 2013. While the industry gains were broad - at least 30 developers' algorithms outperformed the most accurate algorithm from late 2013, there remains a wide range of capability. While this report shows accuracy gains only over the period 2018-2020, the most accurate algorithm reported here is substantially more accurate than anything reported in NIST IR 8271. This is evidence that face recognition development continues apace, and that FRVT reports are but a snapshot of contemporary capability.

From discussion with developers, the accuracy gains stem from the adoption of deep convolutional neural networks. As such, face recognition has undergone an industrial revolution, with algorithms increasingly tolerant of poorly illuminated and other low quality images, and poorly posed subjects. One related result is that a few algorithms correctly match side-view photographs to galleries of frontal photos, with search accuracy approaching that of the best c. 2010 algorithms operating on purely frontal images. The capability to recognize under a 90-degree change in viewpoint - pose invariance - has been a long-sought milestone in face recognition research.

With good quality portrait photos, the most accurate algorithms will find matching entries, when present, in galleries containing 12 million individuals, with rank one miss rates of approaching 0.1%. The remaining errors are in large part attributable to long-run ageing, facial injury and poor image quality. Given this impressive achievement - close to perfect recognition - an advocate might claim that cooperative face recognition is a solved problem, a statement that can be refuted with the following context and caveats:

- ▷ **Mugshots vs. less constrained captures:** The low error rates reported here are attained using mostly excellent cooperative live-capture mugshot images collected with an attendant present. Recognition in other circumstances, particularly those without a dedicated photographic environment and human or automated quality control checks, will lead to declines in accuracy. This is documented here for side-view images, poorer quality webcam images, and, particularly, for newly introduced ATM-style kiosk photos that were not originally intended for automated face recognition. In this case, recognition error rates are much higher, often in excess of 20% even with the more accurate algorithms which variously remain intolerant of face cropping (at image edge) and of large downward head pitch.
- ▷ **Algorithm accuracy spectrum:** Recognition accuracy is very strongly dependent on the algorithm and, more

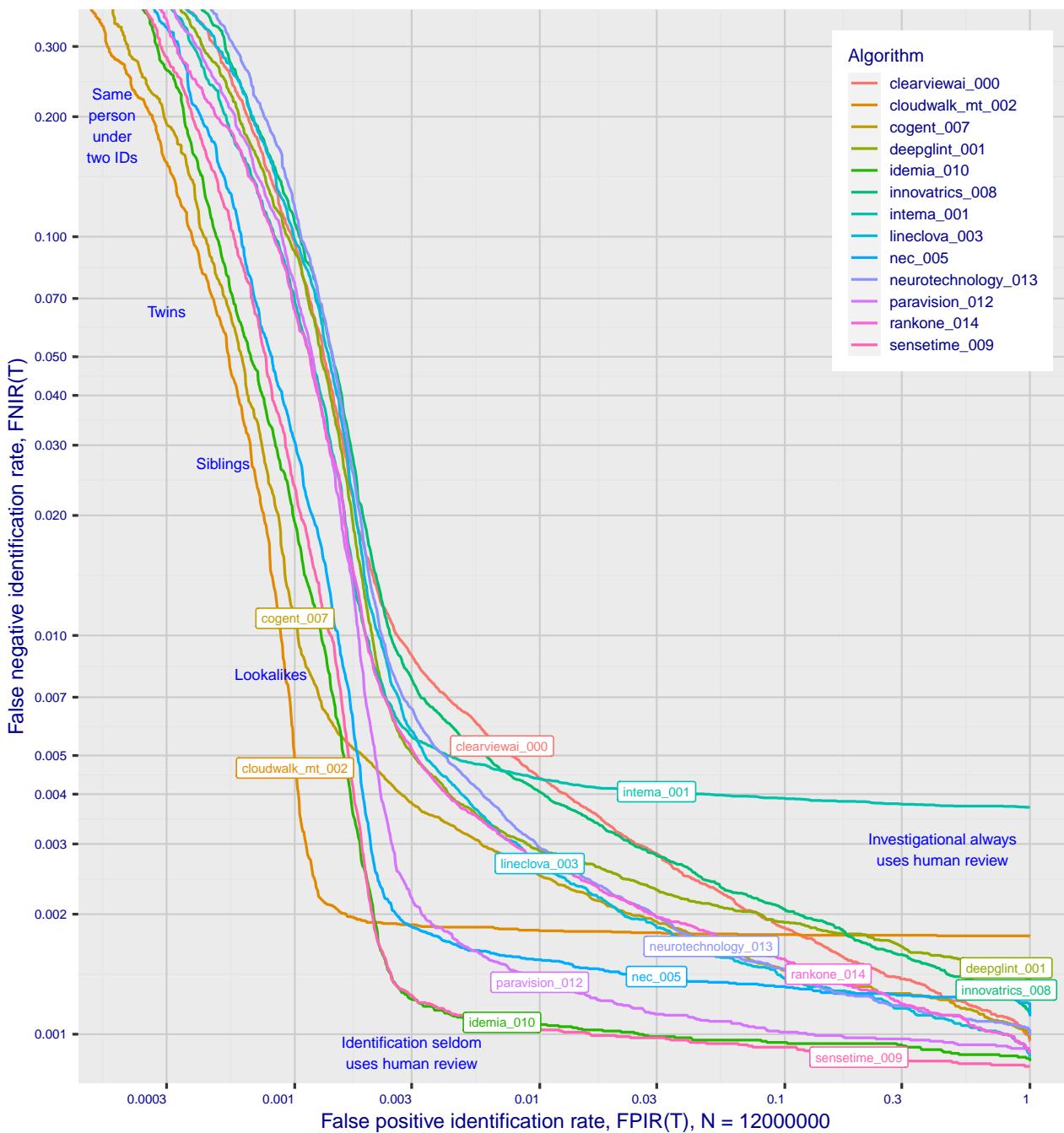


Figure 1: Identification miss rates across the false positive range. N = 12 million individuals are enrolled with one recent image.

generally, on the developer of the algorithm. False negative error rates in a particular scenario range from a few tenths of one percent to beyond fifty percent. This is tabulated exhaustively later: For example Table 13 shows accuracy across datasets. Figure 1 here compares algorithms on mugshot searches in a consolidated gallery of 12 million subjects and 12 million photos. Many algorithms do not achieve the low error rates noted above, and while many of those may still be useful and valuable to end-users, only the most accurate excel on poor quality images and those collected long after the initial enrollment sample.

▷ **Versioning:** While results for up to ten algorithms from each developer are reported here, the intra-provider

accuracy variations are usually smaller than the inter-provider variations. That said different versions give an order of magnitude fewer misses. Some developers demonstrate speed-accuracy tradeoffs¹. See Figs. 18, 19.

- ▷ **Low similarity scores:** In thousands of mugshot cases the correct gallery image is returned at rank 1 but its similarity score is nevertheless low, below some operationally required score threshold. This is not so important when face recognition is used for “lead generation” in investigational applications because human reviewers are specifically required to review potentially long candidate lists and the threshold is effectively 0. In applications where search volumes are higher and labor is not available to review the results from searches, a higher threshold must be applied. This reduces the length of candidate lists and false positive identification rates at the expense of increased false negative miss rates. The tradeoff between the two error rates is reported extensively later.
- ▷ **Population size:** As the number of enrolled subjects grows, some mates are displaced from rank one, decreasing accuracy. As tabulated later for N up to 12 million, false negative rates generally rise slowly with population size. This enables use of face recognition in very large populations. However in most positive and negative identification applications², a score threshold is set to limit the rate at which non-mate searches produce false positives. This has the consequence that some mated searches will report the mate below threshold, i.e. a miss, even if it is at rank 1. The utility of this is that many non-mated searches will return no candidate identities at all. As the error-tradeoff characteristic shows, investigational miss rates on the right side are very low but then rise steadily (in the center region) as threshold is increased to support “lights-out” applications, and ultimately rise quickly (left side) as discussed below. Thus, if we demand that just one in one thousand non-mate searches produce any false positives, the most accurate algorithms there (Sensetime-004 and NEC-3) would fail on between 3 and 5% of mated searches. Even though the graph shows results for the most accurate algorithms, all but two would fail to find the mate in more than 8% of mated searches. While the two most accurate algorithms produce a relatively flat error tradeoff until the threshold is raised to limit false positives to about 1 in 400 non-mated searches³.

Thereafter, as the threshold is raised to further reduce false positives, miss rates rise rapidly. This means that low false positive identification rates are inaccessible with these algorithms, a result that does not apply for ten-finger identification algorithms. The rapid rise occurs because the lower mate scores are mixed with very high non-mate scores, the low scores from poor image quality and ageing, the high non-mates from the presence of lookalikes persons (doppelgangers), twins (discussed next) and, ultimately, the presence of a few unconsolidated subjects i.e. persons present under multiple IDs.

- ▷ **False negatives from ageing:** A large source of error in long-run applications where subjects are not re-enrolled on a set schedule is ageing. Changes in facial appearance increase with the time elapsed between photographs. These will depress similarity scores and eventually cause false negatives. All faces age and while this usually proceeds in a graceful and progressive manner, drug use can accelerate this [28]. Elective surgery may be effective in delaying it although this has not been formally quantified with face recognition. As ageing is essentially unavoidable, it can only be mitigated by scheduled re-capture, as in passport re-issuance. To quantify ageing effects, we used the more accurate algorithms to enroll the earliest image of 3.1 million adults and then search

¹For example, NEC-0 prepares templates much faster than NEC-2 but gives twenty times more misses. Dermalog-5 executes a template search much more quickly than Dermalog-6 but is also much less accurate.

²In a positive identification application such as a registered traveler system, a user is making an implicit claim to be enrolled in the system - most users will be. In a negative application, such as with deportees, the implicit claim is that the subject is not enrolled - most will not be.

³The gallery size here is 12 million people, one image per person. Given 331 201 non-mated searches, an exhaustive implementation of one-too-many search would execute almost 4 trillion comparisons. At a false positive identification rate of 0.0025 the number of false positives is, to first order, 828 corresponding to single-comparison false match rate of $828 / 4 \text{ trillion} = 2.1 \times 10^{-10}$ i.e. about 1 in 5 billion. Strictly this FMR computation is meaningful only for algorithms that implement 1:N search using N 1:1 comparisons, which is not always the case.

with 10.3 million newer photos taken up to 18 years after the initial enrollment photo. Figure 2 puts ageing into context by contrasting it with the increase in false negatives that occurs when the number of individuals in an enrollment database becomes larger and the chance of a false positive increases such that higher thresholds may become necessary⁴.

The Figure shows, from top to bottom, increases in false negative identification rates (FNIR) with the algorithm being tested. This applies to increases due to N on the left side, and increases due to ageing on the right side. The relative spacing of the dots shows that for all algorithms the dependency of FNIR on N (up to 12 million) is considerably less than on ΔT (up to 18 years). The figure additionally shows the most accurate nine algorithms for each year in which they were submitted, limiting to only one per developer.

In the inset table, accuracy is seen to degrade progressively with time, as mate scores decline and non-mates displace mates from rank 1 position. More accurate algorithms tend to be less sensitive to ageing. The more accurate algorithms give fewer errors after 18 years of ageing than middle tier algorithms give after four. Note also we do not quantify an ageing rate - more formal methods [2] borrowed from the longitudinal analysis literature have been published for doing so (given suitable repeated measures data).

See Figures 60, 91 and 106.

⁴Some algorithms implement strategies to automatically adjust scores to account for increased population size. This relieves the system owner of having to increase thresholds as N increases.

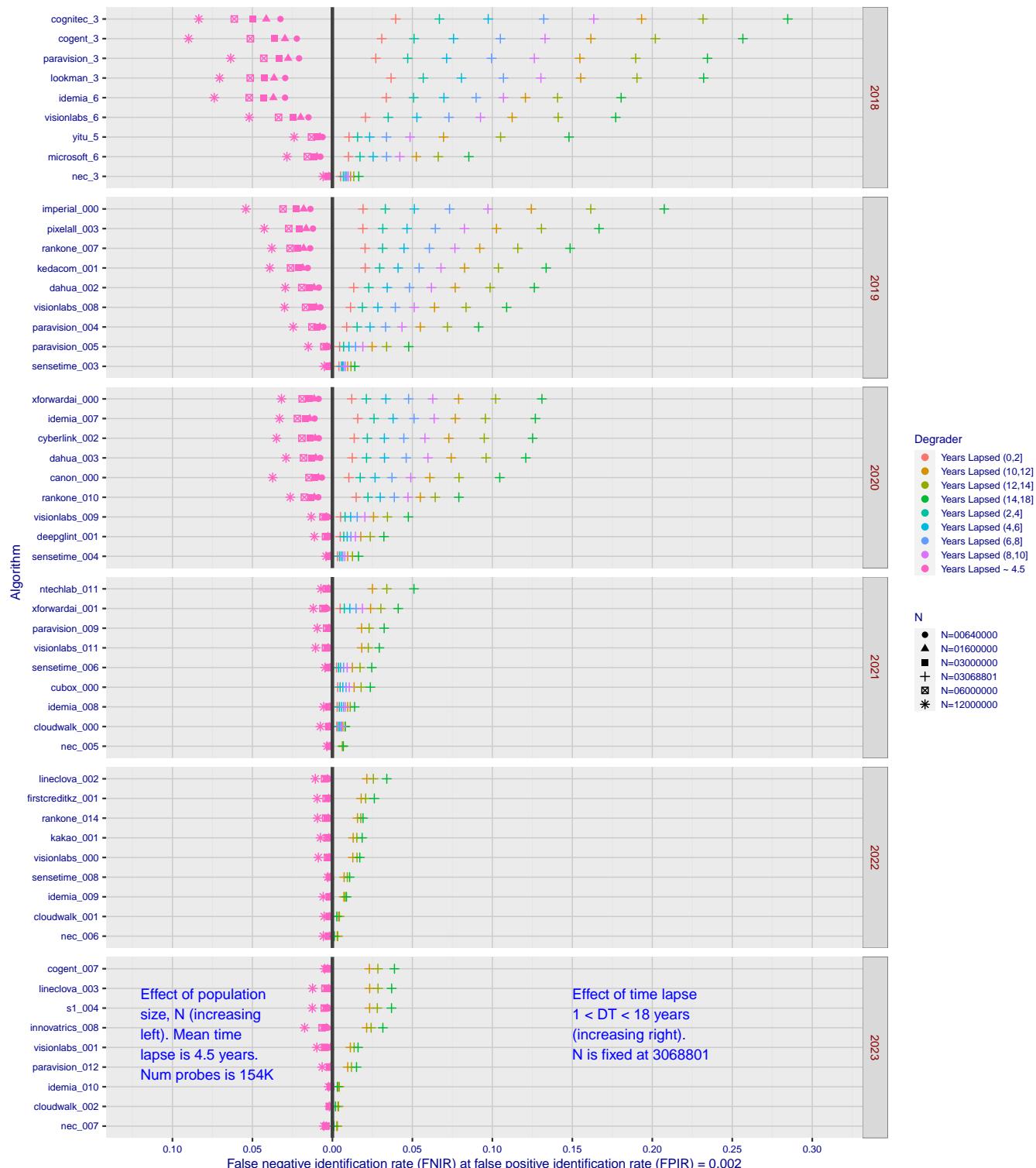


Figure 2: Identification miss rates as a function of enrolled population size, N , and time-lapse, ΔT .

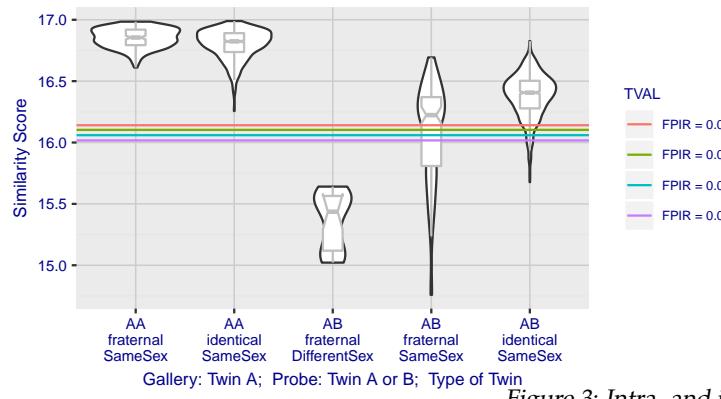


Figure 3: Intra- and inter-twin scores

▷ **False positives from twins:** By enrolling 640 000 mugshots, adding photos of one twin, and then searching photos of those subjects and their twin the inset figure shows, for one typical algorithm, the similarity is generally greater when searching twins against themselves (A) than when searching twins against their sibling (B) but very often still above even stringent thresholds i.e. those corresponding to one in one thousand searches producing a false positive. Thus twins will very often produce a high-scoring non-match on a candidate list and a false alarm in an online identification system. The plot of Fig. 3 shows that fraternal twins are sometimes correctly rejected at those thresholds - including most different sex twins (at center). Figure ?? shows substantially similar behavior for all algorithms tested. In an investigative search, a twin would typically appear at rank 1, or rank 2 if their sibling happened to also be the gallery. Twins (and triplets etc.) constituted 3.3% of all live births [17] in recent years⁵, and because that number is higher today than when the individuals in current adult databases were born, the false positives that arise from twins are now, and will increasingly be, an operational problem. Relative to the United States, twins are born with considerable regional variation. For example they are much less common in East Asia, and much more common in Sub-Saharan Africa [21].

The presence of twins in the mugshot database is inevitable given its size, around 12.3 million people. As this is not an insignificant sample of the domestic United States population, people with other familial ties will be present also. The data was collected over an extended period and because location information is not available, we are unable to estimate the proportion of the domestic population that is present in the dataset. However, if we assume twins are neither more or less disposed to arrest than the general population, we can estimate that hundreds of thousands of individuals in the dataset are twins. This will affect false positive rates because we randomly set aside 331 201 individuals for nonmate searches, and some proportion of those will be twins with siblings in the gallery.

▷ **Database integrity:** An operational error rate should be added to all false negative rates in this report reflecting the proportion of images in a real database that are un-matchable. Such anomalies arise from images that: do not contain a face; include multiple persons; cannot be decoded; are rotated by 90° or 180°; depict a face on clothing; and others introduced by a long tail of various clerical errors. While the mugshot trials in this report have been constructed to minimize such effects, they are a real problem in actual operations.

This report is being updated continuously as new algorithms are submitted to FRVT, and run on new datasets. Participation in the [one-to-many identification track](#) is independent of participation in the [one-to-one verification track](#) of FRVT.

⁵See the CDC's National Vital Statistics Report for 2017: https://www.cdc.gov/nchs/data/nvsr/nvsr67/nvsr67_08-508.pdf

Scope and Context

Audience: This report is intended for developers, integrators, end users, policy makers and others who have some familiarity with biometrics applications. The methods and metrics documented here will be of interest to organizations engaged in tests of face recognition algorithms. Some of these have been incorporated in the ISO/IEC 19795 Part 1 Biometric Testing and Reporting Framework standard, now nearing publication.

Prior benchmarks: Automated face recognition accuracy has improved massively in the two decades since initial commercialization of the various technologies. NIST has tracked that improvement through its conduct of regular independent, free, open, and public evaluations. These have fostered improvements in the state of the art. This report serves as an update to the [NIST Interagency Report 8271](#) on performance of face identification algorithms, published in September 2019.

Demographics: In December 2019, NIST published a first report on demographic dependencies in face recognition, [NIST Interagency Report 8280](#) that documented age, sex and race differentials in one-to-one and one-to-many false positive and false negative rates.

Scope: NIST IR 8271 documented recognition results for four databases containing in excess of 30.2 million still photographs of 14.4 million individuals. That constituted the largest public and independent evaluation of face recognition ever conducted. It includes results for accuracy, speed, investigative vs. identification applications, scalability to large populations, use of multiple images per person, images of cooperative and non-cooperative subjects.

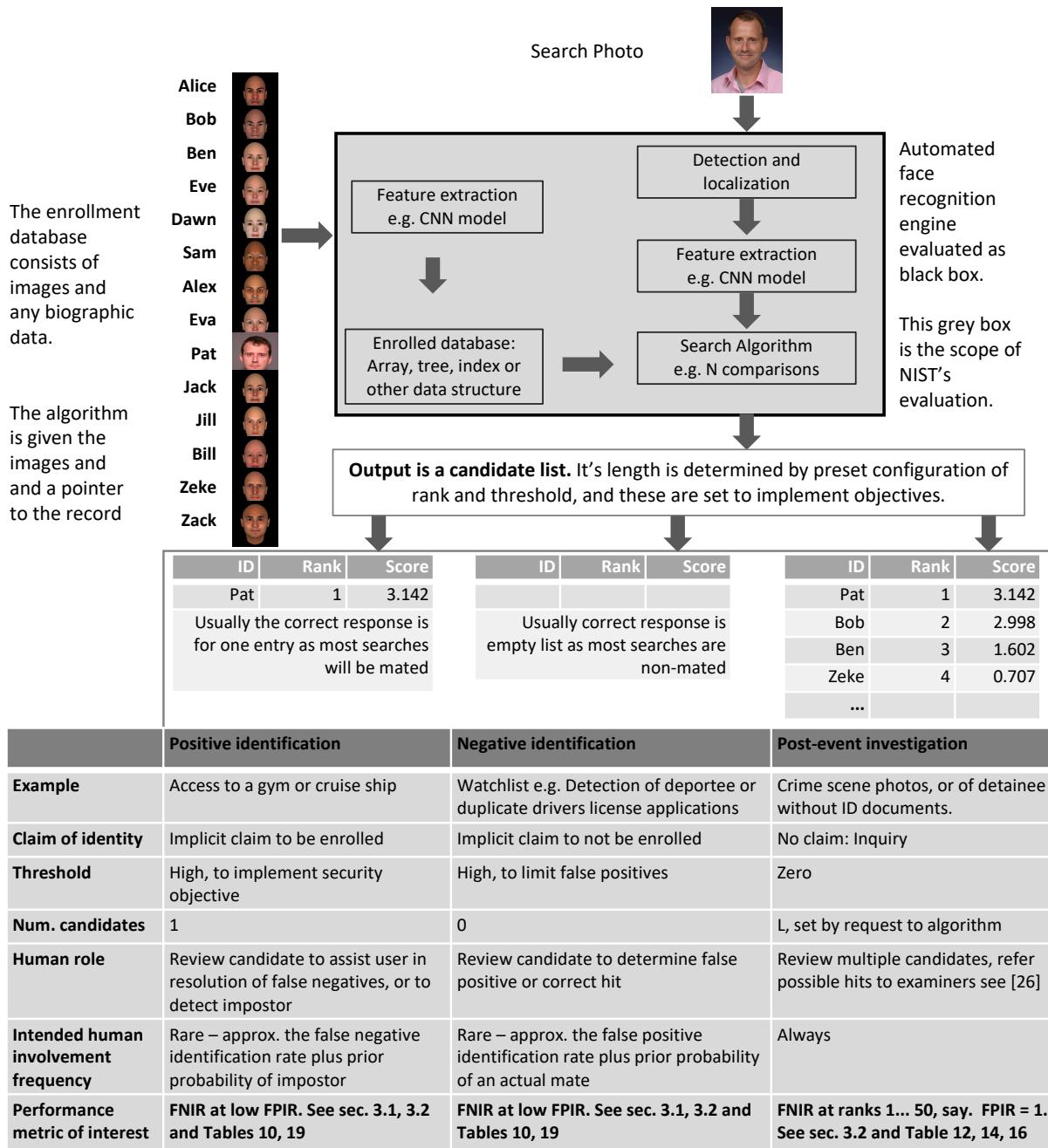
The report also includes results for ageing, recognition of twins, and recognition of profile-view images against frontal galleries. It otherwise does not address causes of recognition failure, neither image-specific problems nor subject-specific factors including demographics. Separate reports on demographic dependencies in face recognition will be published in the future. Additionally out of scope are: performance of live [human-in-the-loop transactional systems](#) like automated border control gates; human recognition accuracy as used in forensic applications; and recognition of persons in video sequences (which NIST evaluated separately [9]). Some of those applications share core matching technologies that *are* tested in this report.

Images: Five kinds of images are employed; these are either compared with images of the same kind, or against others from different capture environments as follows. The primary dataset is a set of law enforcement mugshot images (Fig. 5) which are enrolled and then searched with three kinds of images: other mugshots (i.e. within-domain); profile-view photographs (90 degree cross-view); and lower quality webcam images (Fig. 6) collected in similar detention operations (cross-domain). Additionally we compare high quality visa-like photos collected in immigration offices, with: medium quality border crossing images collected in primary immigration lanes; poor quality images collected in ATM-like registered traveller kiosks.

Participation and industry coverage: The report includes performance figures for prototype algorithms from the research laboratories of commercial developers and a few universities. This represents a substantial majority of the face recognition industry, but only a tiny minority of the academic community. Participation was open worldwide. While there is no charge for participation, developers incur some software engineering expense in implementing their algorithms behind the NIST application programming interface (API). The test is a black-box test where the function of the algorithm, and the intellectual property associated with it, is hidden inside pre-compiled libraries.

Recent technology development: Most face recognition research with deep convolutional neural networks (CNNs) has been aimed at achieving invariance to pose, illumination and expression variations that characterize photojournalism and social media images. The initial research [18, 22] employed large numbers of images of relatively few ($\sim 10^4$) individuals to learn invariance. Inevitably much larger populations ($\sim 10^7$) were employed for training [11, 20] but the benchmark, Labeled Faces in the Wild with (essentially) an equal error rate metric [12], represents an easy task,

one-to-one verification at very high false match rates. While a larger scale identification benchmark duly followed, Megaface [15], its primary metric, rank one hit rate, contrasts with the high threshold discrimination task required in most large-population applications of face recognition, namely credential de-duplication, and background checks. There, identification in galleries containing up to 10^8 individuals must be performed using a) very few images per individual and b) stringent thresholds to afford very low false positive identification rates. This track of FRVT was launched to measure the capability of the new technologies, including in these two cases. FRVT has included open-set identification tests since 2002, reporting both false negative and positive identification rates [7].



Performance metrics for applications: This report documents the performance of one-to-many face recognition algorithms. The word "performance" here refers to recognition accuracy and computational resource usage, as measured

by executing those algorithms on massive sequestered datasets.

This report includes extensive tabulation of recognition error rates germane to the main use-cases for face search technology. The Figure below, inspired by the Figure 1 in [23] differentiates different applications of the technolgy. The last row directs readers to the main tables relevant to those applications, respectively threshold-based and rank-based metrics that are special cases of the metrics given in section 3. The terms negative identification and positive identification are taken from the ISO/IEC 2382-37:2017 standardized biometrics vocabulary.

The algorithms are specifically configured for these applications by setting thresholds and candidate list lengths. Both rank-based metrics and threshold-based metrics include tradeoffs. In investigation, overall accuracy will be reduced if labor is only available to review a few candidates from the automated system. Note that when a fixed number of candidates are returned, the false positive identification rate of the automated face recognition engine will be 100%, because a probe image of anyone not enrolled will still return candidates. In identification applications where false positives must be limited to satisfy reviewer labor availability or a security objective, higher false negative rates are implied. This report includes extensive quantification of this threshold-based tradeoff.

See Sec. 3

Template diversity: The FRVT is designed to evaluate black-box technologies with the consequence that the templates that hold features extracted from face images are entirely proprietary opaque binary data that embed considerable intellectual property of the developer. Despite migration to CNN-based technologies there is no consensus on the optimal feature vector dimension. This is evidenced by template sizes ranging from below 100 bytes to more than four kilobytes. This diversity of approaches, suggests there is no prospect of a standard template something that would require a common feature set to be extracted from faces. Interoperability in automated face recognition remains solidly based on images and documentary standards for those, in particular the ICAO portrait [27] specification deriving from the ISO/IEC 19794-5 Token frontal [24] standard, which are similar to certain ANSI/NIST Type 10 [26] formats.

Training: The algorithms submitted to NIST have been developed using image datasets that developers do not disclose. The development will often include application of machine learning techniques and will additionally involve iterative training and testing cycles. NIST itself does not perform any training and does not refine or alter the algorithm in any way. Thus the model, data files, and libraries that define an algorithm are fixed for the duration of the tests. This reflects typical operational reality where recognition software, once installed, is fixed and constant until upgraded. This situation persists because on-site training of algorithms on customer data is atypical essentially because training is not a turnkey process.

Automated search and human review: Virtually all applications using automated face search require human review of the outputs at some frequency: Always for investigational applications; rarely in positive identification applications, after rejection (false or otherwise); and rarely in negative identification applications, after an alarm (false or otherwise). The human role is usually to compare a reference image with the query image or the live-subject if present, to render either a definitive decision on “exclusion” (different subjects), or “identification” (same subject), or a declaration that one or both images have “no value” and that no decision can be made. Note that automated face recognition algorithms are not built to do exclusion - low scores from a face comparison arise from different faces *and* poor quality images of the same face.

Human reviewers make recognition errors [5, 19, 25] and are sensitive to image acquisition and quality. Accurate human review is supported by high resolution - as specified in the Type 50, 51 acquisition profiles of the ANSI/NIST Type 10 record [26], and by multiple non-frontal views as specified in the same standard. These often afford views of the ear. Organizations involved in image collection should consider supporting human adjudication by collecting high-resolution frontal and non-frontal views, preparing low resolution versions for automated face recognition [24], and retaining both for any subsequent resolution of candidate matches. Along these lines, the ISO/IEC Joint Technical

Committee 1 subcommittee 37 on biometrics has just initiated projects on image quality assessment and face-aware capture.

Release Notes

FRVT Activities: Since February 2017, NIST has been evaluating one-to-one verification algorithms on an ongoing basis. NIST then restarted FRVT's one-to-many track in February 2018, inviting participants to send up to prototype algorithms. Both tracks allows developers to submit updated algorithms to NIST at any time but no more frequently than four calendar months. This more closely aligns development and evaluation schedules. Results are posted to the web within a few weeks of submission. Details and full report are linked from the [Ongoing FRVT site](#).

FRVT Reports: The results of the FRVT appear in the series NIST Interagency Reports tabulated below. The reports were developed separately and released on different schedules. In prior years NIST has mostly reported FRVT results as a single report; this had the disadvantage that results from completed sub-studies were not published until all other studies were complete.

Date	Link	Title	No.
2014-03-20	PDF	FRVT Performance of Automated Age Estimation Algorithms	7995
2015-04-20	PDF	Face Recognition Vendor Test (FRVT) Performance of Automated Gender Classification Algorithms	8052
2014-05-21	PDF	FRVT Performance of face identification algorithms	8009
2017-03-07	PDF	Face In Video Evaluation (FIVE) Face Recognition of Non-Cooperative Subjects	8173
2017-11-23	PDF	The 2017 IARPA Face Recognition Prize Challenge (FRPC)	8197
2018-11-27	PDF	Face Recognition Vendor Test - Part 2: Identification	8271
2019-09-11	PDF	Face Recognition Vendor Test - Part 2: Identification	8271
2019-12-11	PDF	Face Recognition Vendor Test - Part 3: Demographic Effects	8280
2020-01-03	WWW	Face Recognition Vendor Test (FRVT) - Part 1 Verification	Draft

Details appear on pages linked from <https://www.nist.gov/programs-projects/face-projects>.

Appendices: This report is accompanied by appendices which present exhaustive results on a per-algorithm basis. These are machine-generated and are included because the authors believe that visualization of such data is broadly informative and vital to understanding the context of the report.

Typesetting: Virtually all of the tabulated content in this report was produced automatically. This involved the use of scripting tools to generate directly type-settable L^AT_EX content. This improves timeliness, flexibility, maintainability, and reduces transcription errors.

Graphics: Many of the Figures in this report were produced using the **ggplot2** package running under **R**, the capabilities of which extend beyond those evident in this document.

Contents

Release Notes	1
Disclaimer	6
Institutional Review Board	6
Acknowledgments	6
Executive Summary	7
Scope and Context	13
Release Notes	17
1 Introduction	19
2 Evaluation datasets	20
3 Performance metrics	26
4 Results	42
Appendices	87
A Accuracy on large-population FRVT 2018 mugshots	87
B Effect of time-lapse: Accuracy after face ageing	132
C Effect of enrolling multiple images	210
D Accuracy with poor quality webcam images	217
E Accuracy for profile-view to frontal recognition	227
F Search duration	231
G Gallery Insertion Timing	265

1 Introduction

One-to-many identification represents the largest market for face recognition technology. Algorithms are used across the world in a diverse range of biometric applications: detection of duplicates in databases, detection of fraudulent applications for credentials such as passports and driving licenses, token-less access control, surveillance, social media tagging, lookalike discovery, criminal investigation, and forensic clustering.

This report contains a breadth of performance measurements relevant to many applications. Performance here refers to accuracy and resource consumption. In most applications, the core accuracy of a facial recognition algorithm is the most important performance variable. Resource consumption will be important also as it drives the amount of hardware, power, and cooling necessary to accommodate high volume workflows. Algorithms consume processing time, they require computer memory, and their static template data requires storage space. This report documents these variables.

1.1 Open-set searches

FRVT tested open-set identification algorithms. Real-world applications are almost always “open-set”, meaning that some searches have an enrolled mate, but some do not. For example, some subjects have truly not been issued a visa or drivers license before; some law enforcement searches are from first-time arrestees⁶. In an “open-set” application, algorithms make no prior assumption about whether or not to return a high-scoring result, and for a mated search, the ideal behaviour is that the search produces the correct mate at high score and first rank. For a non-mate search, the ideal behavior is that the search produces zero high-scoring candidates.

Many academic benchmarks execute only closed-set searches. The proportion of mates found in the rank one position is the default accuracy metric. This hit rate metric ignores the score with which a mate is found; weak hits count as much as strong hits. This ignores the real-world imperative that in many applications it is necessary to elevate a threshold to reduce the number of false positives.

⁶Operationally closed-set applications are rare because it is usually not the case that all searches have an enrolled mate. One counter-example, however, is a cruise ship in which all passengers are enrolled and all searches should produce exactly one identity. Another example is forensic identification of dental records from an aircraft crash.

2 Evaluation datasets

This report documents accuracy for four kinds of images - mugshots, webcam, profiles and wild - as described in the following sections.

2.1 Immigration-related images

This report includes benchmark tests sharing a common enrollment of high quality frontal portrait images collected while subject make applications for various immigration benefits. We then search that with two kinds of images, webcam images collected during in-bound immigration and also images collected from registered travelers using a ATM-style kiosk. These are described below and depicted in Figure 4.



Figure 4: Example photos.

- ▷ **Application reference photos:** The images are collected in an attended interview setting using dedicated capture equipment and lighting. The images, at size 300x300 pixels, are smaller than normally indicated by ISO. The images are all high-quality frontal portraits collected in immigration offices and with a white background. As such, potential quality related drivers of high false match rates (such as blur) can be expected to be absent. The images are encoded as ISO/IEC 10918-1 i.e. JPEG. Older images had a compression ration of about 16:1, while newer images, since 2010, are more lightly compressed at 4:1. When these images are provided as input into the algorithm, they are labeled with the type "iso". This report enrols 1 600 000 application images, one per person.
- ▷ **Border crossing photos:** Most images are have width 320 and height 240 pixels. They are JPEG compressed at 16:1 i.e. filesize just below 15KB. The images present challenges for face recognition in that subjects often exhibit non-zero yaw and pitch (associated with the rotational degrees of freedom of the camera mount), low contrast (due to varying and intense background lights), and poor spatial resolution (due to inexpensive cameras). There are often subjects standing in the background, usually at very low resolution (see Figure 4b). In such cases, algorithms should detect all faces and determine which is the largest and most centered. When these images are provided as input into the algorithm, they are labeled with the type "wild".
- ▷ **Kiosk photos:** These photos were collected from subjects whose attention was focused on interaction with an immigration kiosk. They images were not intended for use with automated face recognition. The camera is situated above a display which the user touches, and is triggered either without directing the subject to look at it, or without waiting for the subject to comply. The images are therefore characterized by pitch-down pose, sometimes exceeding 45 degrees, as in Figure 4c. Yaw-angle variation is mild, with most images close to frontal. The images

have width 320 pixels and height 240 pixels and therefore tall individuals are sometimes cropped. This is often just above the eyes and can occur at the nose or mouth. Conversely, short individuals are sometimes cropped such that only the top part of the face is visible. In a quite small number of cases, there other subjects standing just behind the primary subject such that algorithms should detect all faces and determine which is the largest and most centered. Background ceiling lighting is often visible and this sometimes leads to under-exposure of the face. When these images are provided as input into the algorithm, they are labeled with the type "wild".

2.2 Law enforcement images

The main mugshot dataset used is referred to as the FRVT 2018 set. This set was collected over the period 2002 to 2017 in routine United States law enforcement operations. This set yields three subsets

- ▷ **Mugshots:** Mugshots comprise about 86% of the database. They have reasonable compliance with the ANSI/NIST ITL1-2011 Type 10 standard's subject acquisition profiles levels 10-20 for frontal images [26]. The most common departure from the standard's requirements is the presence of mild pose variations around frontal - the images of Figure 5 are typical. The images vary in size, with many being 480x600 pixels with JPEG compression applied to produce filesizes of between 18 and 36KB with many images outside this range, implying that about 0.5 bits are being encoded per pixel. When these images are provided as input into the algorithm, they are labeled with the type "mugshot".

Example images appear in Fig. 5

[NIST Interagency Report 8238](#) includes a comparison of this set of mugshots with the smaller and easier sets of mugshots used in tests run in 2010 and 2014.

- ▷ **Profile images:** Profile-view images have been collected in law enforcement for more than 100 years, as human capability is improved with orthogonal information. The profile images used in this report were collected during the same session as the frontal mugshot photograph, in the same standardized photographic setup. These would not therefore be used with automated face recognition. A small subset, 200 000 images, were set aside for testing. When these images are provided as input into the algorithm, they are labeled with the type "wild".

Example images appear in Fig. 7

- ▷ **Webcam images:** The remaining 14% of the images were collected using an inexpensive webcam attached to a flexible operator-directed mount. These images are all of size 240x240 pixels, that are in considerable violation of most quality-related clauses of all face recognition standards. As evident in the figure, the most common defects are non-frontal pose (associated with the rotational degrees of freedom of the camera mount), low contrast (due to varying and intense background lights), and poor spatial resolution (due to inexpensive camera optics) - see examples in Fig 6. The images are overly JPEG compressed, to between 4 and 7KB, implying that only 0.5 to 1 bits are being encoded per color pixel. When these images are provided as input into the algorithm, they are labeled with the type "wild".

Example images appear in Fig. 6

These are drawn from NIST Special Database 32 which may be downloaded [here](#).

These images were partitioned in galleries and probesets for the various experiment listed in Table 1.

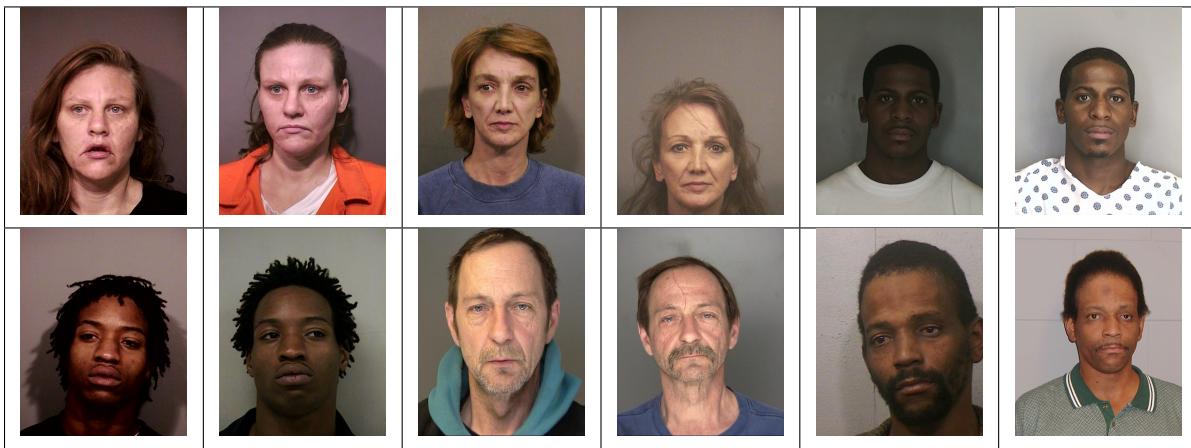


Figure 5: Six mated mugshot pairs representative of the FRVT-2014 (LEO) and FRVT-2018 datasets. The images are collected live, i.e. not scanned from paper. Image source: NIST Special Database 32 the Multiple Encounter Deceased Subjects dataset.



Figure 6: Twelve webcam images representative of probes against the FRVT-2018 mugshot gallery. The first eight images are four mated pairs. Such images present challenges to recognition including pose, non-uniform illumination, low contrast, compression, cropping, and low spatial sampling rate. Image source: NIST Special Database 32 the Multiple Encounter Deceased Subjects dataset.

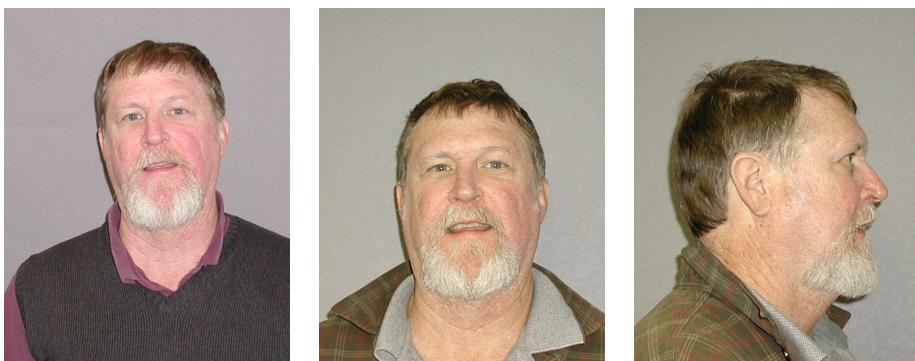


Figure 7: **[Profile views]** The three images are a frontal enrollment, subsequent frontal probe, and same-session ninety degree profile view. While collection of both frontal and profile views has been typical in law enforcement for more than a century, the recognition of profile to frontal views has essentially been impossible. However, reasonably high accuracy results is now possible - see section E.

Image				
Encounter	1	...	$K_i - 1$	K_i
Capture Time	T_1	...	$T_{K_i - 1}$	T_{K_i}
Role RECENT	Not used	Not used	Enrolled	Search
Role LIFETIME	Enrolled	Enrolled	Enrolled	Search

Figure 8: Depiction of the “recent” and “lifetime” enrollment types. Image source: NIST Special Database 32

2.3 Enrollment strategies

Many operational applications include collection and enrollment of biometric data from subjects on more than one occasion. This might be done on a regular basis, as might occur in credential (re-)issuance, or irregularly, as might happen in a criminal recidivist situation [4]. The number of images per person will depend on the application area. In civil identity credentialing (e.g. passports, driver’s licenses), the images will be acquired approximately uniformly over time (e.g. ten years for a passport). While the distribution of dates for such images of a person might be assumed uniform, a number of factors might undermine this assumption⁷. In criminal applications, the number of images would depend on the number of arrests. The distribution of dates for arrest records for a person (i.e. the recidivism distribution) has been modeled using the exponential distribution but is recognized to be more complicated⁸.

In any case, the 2010 NIST evaluation of face recognition showed that considerable accuracy benefits accrue with retention and use of *all* historical images [6].

To this end, the FRVT API document provides $K \geq 1$ images of an individual to the enrollment software. The software is tasked with producing a single proprietary undocumented “black-box” template⁹ from the K images. This affords the algorithm an ability to generate a *model* of the individual, rather than to simply extract features from each image on a sequential basis.

As depicted in Figure 8, the i -th individual in the FRVT 2018 dataset has K_i images. These are labelled as x_k for $k = 1 \dots K_i$ in chronological order of capture date. To measure the utility of having multiple enrollment images, this report evaluates three kinds of enrollment:

- ▷ **Recent:** Only the second most recent image, $x_{K_i - 1}$ is enrolled. This strategy of enrollment mimics the operational policy of retaining the imagery from the most recent encounter. This might be done operationally to ameliorate the effects of face ageing. Obviously retaining only the most recent image should only be done if the identity of the person is trusted to be correct. For example, in an access control situation retention of the most recent successful *authentication* image would be hazardous if it could be a false positive.
- ▷ **Lifetime-consolidated:** All but the most recent image are enrolled, $x_1 \dots x_{K_i - 1}$. This subject-centric strategy might be adopted if quality variations exist where an older image might be more suitable for matching, despite the ageing effect.

⁷For example, a person might skip applying for a passport for one cycle, letting it expire. In addition, a person might submit identical images (from the same photography session) to consecutive passport applications at five year intervals.

⁸A number of distributions have been considered to model recidivism, see for example [3].

⁹There are no formal face template standards. Template standards only exist for fingerprint minutiae - see ISO/IEC 19794-2:2011.

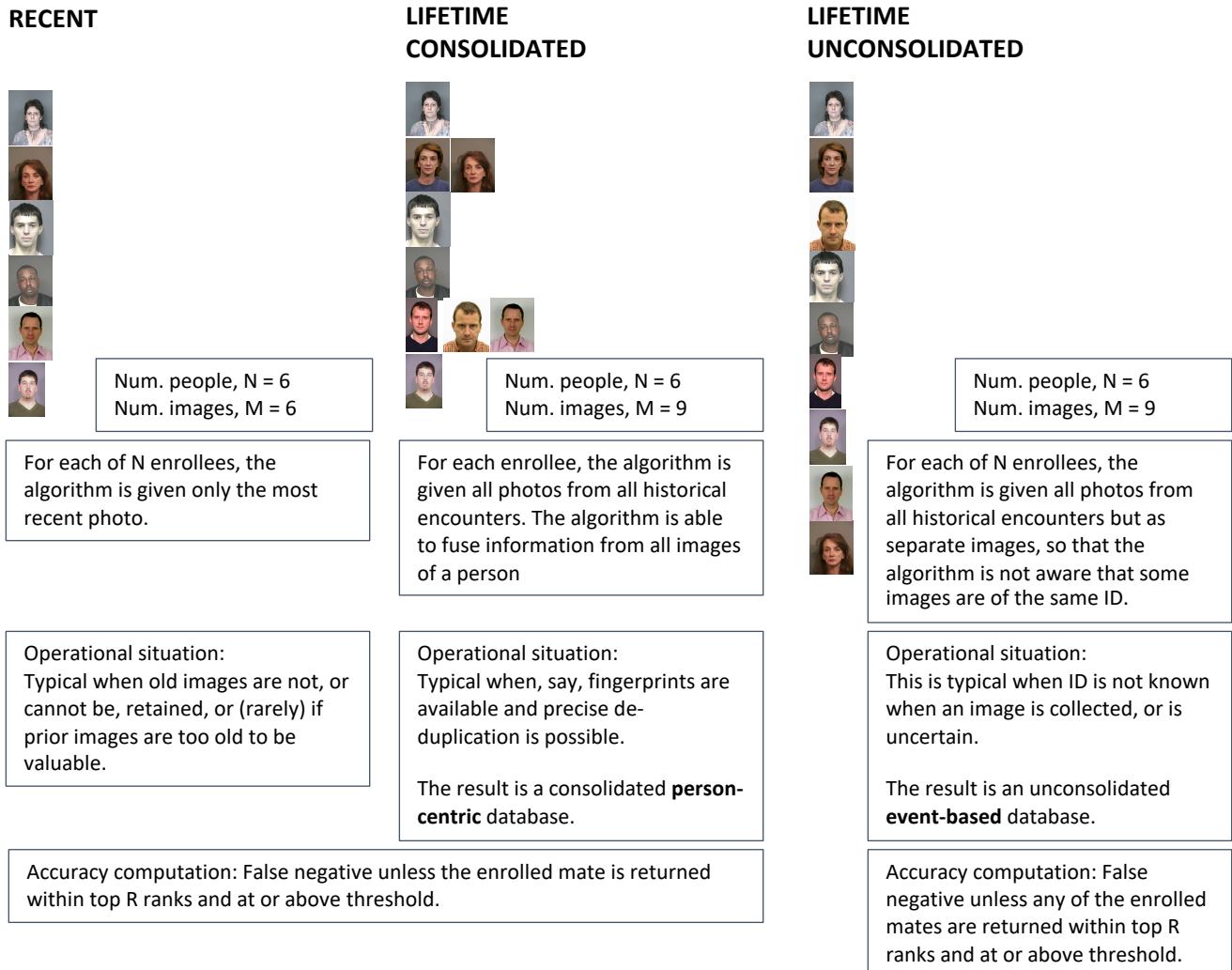


Figure 9: Enrollment strategies. The figure shows the three kinds of enrollment databases examined in this report. Image source: NIST Special Database 32

	ENROLLMENT				SEARCH			
	TYPE SEE SECTION 2.3	POPULATION FILTER	N-SUBJECTS	N-IMAGES	MATE N-SUBJECTS	NON-MATE N-IMAGES	N-SUBJECTS	N-IMAGES
Mugshot trials from enrollment of single images								
1	RECENT	NATURAL	640 000	640 000	154 549	154 549	331 254	331 254
2	RECENT	NATURAL	1 600 000	1 600 000				
3	RECENT	NATURAL	3 000 000	3 000 000				
4	RECENT	NATURAL	6 000 000	6 000 000				
5	RECENT	NATURAL	12 000 000	12 000 000				
Cross-domain								
13	MUGSHOTS AS ON ROW 2				82 106 WEBCAM	82 106 WEBCAM	331 254 WEBCAM	331 254 WEBCAM
Cross-view								
14	MUGSHOTS AS ON ROW 2				100 000 PROFILE	100 000 PROFILE	100 000 PROFILE	100 000 PROFILE
Mugshot ageing								
17	OLDEST	NATURAL	3 068 801	3 068 801	2 853 221	10 951 064	0	0
Border crossing ageing								
18	OLDEST	NATURAL	1 600 000	1 600 000	903 655	1 922 393	1 393 076	1 680 000
Visa-border								
19	PRIOR	NATURAL	1 600 000 VISA	1 600 000 VISA	577 444 BORDER	1 212 892 BORDER	79 769 BORDER	80 000 BORDER
20	VISA AS ON ROW 18				14 004 BORDER	31 579 BORDER	42 474 BORDER	45 460 BORDER

Table 1: Enrollment and search sets. Each row summarizes one identification trial. Unless stated otherwise, all entries refer to mugshot images. The term “natural” means that subjects were selected without heed to demographics, i.e. in the distribution native to this dataset. The probe images were collected in a different calendar year to the enrollment image. Missing values in rows 2-12 are the same as in row 1.

▷ **Lifetime-unconsolidated:** Again all but the most recent image are enrolled $x_1 \dots x_{K_i-1}$ but now separately, with different identifiers, such that the algorithm is not aware that the images are from the same face. This kind of event- or encounter-centric enrollment is very common when operational constraints preclude reliable consolidation of the historical encounters into a single identity. This aspect also prevents the recognition algorithm from a) building a holistic model of identity (as is common in speaker recognition systems) and b) implementing fusion, for example template-level fusion of feature vectors, or post-search score-level fusion. The result is that searches will typically yield more than one image of a person in the top ranks. This has consequences for appropriate metrics, as detailed in section 3.2.1

NIST first evaluated this kind of enrollment in mid 2018, and the results tables include some comparison of accuracy available from all three enrollment styles.

In all cases, the most recent image, x_{K_i} , is reserved as the search image. For the 1.6 million subject enrollment partition of the FRVT 2018 data, $1 \leq K_i \leq 33$ with $K_i = 1$ in 80.1% of the individuals, $K_i = 2$ in 13.4%, $K_i = 3$ in 3.7%, $K_i = 4$ in 1.4%, $K_i = 5$ in 0.6%, $K_i = 6$ in 0.3%, and $K_i > 6$ is 0.2% for everyone else. This distribution is substantially dependent on United States recidivism rates.

We did not evaluate the case of retaining only the highest quality image, since automated quality assessment is out of scope for this report. We do not anticipate that such strategies will prove beneficial when the quality assessment apparatus is imperfect and unvalidated.

3 Performance metrics

This section gives specific definitions for accuracy and timing metrics. Tests of open-set biometric algorithms must quantify frequency of two error conditions:

- ▷ **False positives:** Type I errors occur when search data from a person who has never been seen before is incorrectly associated with one or more enrollees' data.
- ▷ **Misses:** Type II errors arise when a search of an enrolled person's biometric does not return the correct identity.

Many practitioners prefer to talk about "hit rates" instead of "miss rates" - the first is simply one minus the other as detailed below. Sections 3.1 and 3.2 define metrics for the Type I and Type II performance variables.

Additionally, because recognition algorithms sometimes fail to produce a template from an image, or fail to execute a one-to-many search, the occurrence of such events must be recorded. Further because algorithms might elect to not produce a template from, for example, a poor quality image, these failure rates must be combined with the recognition error rates to support algorithm comparison. This is addressed in section 3.5.

Finally, section 3.7 discusses measurement of computation duration, and section 3.8 addresses the uncertainty associated with various measurements. Template size measurement is included with the results.

3.1 Quantifying false positives

It is typical for a search to be conducted into an enrolled population of N identities, and for the algorithm to be configured to return the closest L candidate identities. These candidates are ranked by their score, in descending order, with all scores required to be greater than or equal to zero. A human analyst might examine either all L candidates, or just the top $R \leq L$ identities, or only those with score greater than threshold, T . The workload associated with such examination is discussed later, in 3.6.

False alarm performance is quantified in two related ways. These express how many searches produces false positives, and then, how many false positives are produced in a search.

False positive identification rate: The first quantity, FPIR, is the proportion of non-mate searches that produce an adverse outcome:

$$\text{FPIR}(N, T) = \frac{\text{Num. non-mate searches where one or more enrolled candidates are returned with score at or above threshold}}{\text{Num. non-mate searches attempted.}} \quad (1)$$

Under this definition, FPIR can be computed from the highest non-mate candidate produced in a search - it is not necessary to consider candidates at rank 2 and above. FPIR is the primary measure of Type I errors in this report.

Selectivity: However, note that in any given search, several non-mate may be returned above threshold. In order to quantify such events, a second quantity, selectivity (SEL), is defined as the *number* of non-mates returned on a candidate list, averaged over all searches.

$$\text{SEL}(N, T) = \frac{\text{Num. non-mate enrolled candidates returned with score at or above threshold}}{\text{Num. non-mate searches attempted.}} \quad (2)$$

where $0 \leq \text{SEL}(N, T) \leq L$. Both of these metrics are useful operationally. FPIR is useful for targeting how often an

adverse false positive outcome can occur, while SEL as a number is related to workload associated with adjudicating candidate lists. The relationship between the two quantities is complicated - it depends on whether an algorithm concentrates the false alarms in the results of a few searches or whether it disburses them across many. This was detailed in FRVT 2014, NISTIR 8009. It has not yet been detailed in FRVT 2018.

3.2 Quantifying hits and misses

If L candidates are returned in a search, a shorter candidate list can be prepared by taking the top $R \leq L$ candidates for which the score is above some threshold, $T \geq 0$. This reduction of the candidate list is done because thresholds may be applied, and only short lists might be reviewed (according to policy or labor availability, for example). It is useful then to state accuracy in terms of R and T , so we define a “miss rate” with the general name **false negative identification rate** (FNIR), as follows:

$$\text{FNIR}(N, R, T) = \frac{\text{Num. mate searches with enrolled mate found outside top } R \text{ ranks or score below threshold}}{\text{Num. mate searches attempted.}} \quad (3)$$

This formulation is simple for evaluation in that it does not distinguish between causes of misses. Thus a mate that is not reported on a candidate list is treated the same as a miss arising from face finding failure, algorithm intolerance of poor quality, or software crashes. Thus if the algorithm fails to produce a candidate list, either because the search failed, or because a search template was not made, the result is regarded as a miss, adding to FNIR.

Hit rates, and true positive identification rates: While FNIR states the “miss rate” as how often the correct candidate is either not above threshold or not at good rank, many communities prefer to talk of “hit rates”. This is simply the **true positive identification rate**(TPIR) which is the complement of FNIR giving a positive statement of how often mated searches are successful:

$$\text{TPIR}(N, R, T) = 1 - \text{FNIR}(N, R, T) \quad (4)$$

This report does not report true positive “hit” rates, preferring false negative miss rates for two reasons. First, costs rise linearly with error rates. For example, if we double FNIR in an access control system, then we double user inconvenience and delay. If we express that as decrease of TPIR from, say 98.5% to 97%, then we mentally have to invert the scale to see a doubling in costs. More subtly, readers don’t perceive differences in numbers near 100% well, becoming inured to the “high nineties” effect where numbers close to 100 are perceived indifferently.

Reliability is a corresponding term, typically being identical to TPIR, and often cited in automated (fingerprint) identification system (AFIS) evaluations.

An important special case is the **cumulative match characteristic**(CMC) which summarizes accuracy of mated-searches only. It ignores similarity scores by relaxing the threshold requirement, and just reports the fraction of mated searches returning the mate at rank R or better.

$$\text{CMC}(N, R) = 1 - \text{FNIR}(N, R, 0) \quad (5)$$

We primarily cite the complement of this quantity, $\text{FNIR}(N, R, 0)$, the fraction of mates *not* in the top R ranks.

The **rank one hit rate** is the fraction of mated searches yielding the correct candidate at best rank, i.e. $\text{CMC}(N, 1)$. While this quantity is the most common summary indicator of an algorithm’s efficacy, it is not dependent on similarity scores, so it does not distinguish between strong (high scoring) and weak hits. It also ignores that an adjudicating reviewer is often willing to look at many candidates.

3.2.1 False negative rates for unconsolidated galleries

As detailed in section 2.3 a common type of gallery, here referred to as the lifetime unconsolidate type, is populated with all images of an individual without any association between them. That is, the gallery construction algorithm is not provided with any ID labels that would support processing of a person's images jointly. This contrasts with the lifetime consolidate type where an algorithm may explicitly fuse features from multiple images of a person, or select a best image. In such cases, where the number of enrolled images is a random variable, we define two false negative rates as follows.

The first demands that the algorithm place any of the K_i mates in the top $R \geq 1$ ranks. The proportion of searches for which this does not occur forms a false negative identification rate:

$$\text{FNIR}_{\text{any}}(N, R, T) = 1 - \frac{\text{Num. mate searches where any enrolled mate is found in the top } R \text{ ranks and at-or-above threshold}}{\text{Num. mate searches attempted.}} \quad (6)$$

The second demands that the algorithm place all K_i mates in the top $R \geq K_i$ ranks. The proportion of searches for which this does not occur forms a false negative identification rate:

$$\text{FNIR}_{\text{all}}(N, R, T) = 1 - \frac{\text{Num. mate searches where all enrolled mates are found in the top } R \text{ ranks and at-or-above threshold}}{\text{Num. mate searches attempted.}} \quad (7)$$

Placing all mates in the top ranks is a more difficult task than correctly retrieving any image, so it holds that: $\text{FNIR}_{\text{all}} \geq \text{FNIR}_{\text{any}}$. This is evident in the results presented for November 2018 algorithms in Tables starting at ??.

The information retrieval community might prefer to compute and plot *precision* and *recall*; this is a valid approach, but we advance the two metrics above because they relate to our normal definition of consolidated FNIR, and they cover the two extreme use-cases of wanting any hit vs. all hits.

3.3 DET interpretation

In biometrics, a false negative occurs when an algorithm fails to match two samples of one person – a Type II error. Correspondingly, a false positive occurs when samples from two persons are improperly associated – a Type I error.

Matches are declared by a biometric system when the native comparison score from the recognition algorithm meets some threshold. Comparison scores can be either similarity scores, in which case higher values indicate that the samples are more likely to come from the same person, or dissimilarity scores, in which case higher values indicate different people. Similarity scores are traditionally computed by fingerprint and face recognition algorithms, while dissimilarities are used in iris recognition. In some cases, the dissimilarity score is a distance possessing metric properties. In any case, scores can be either mate scores, coming from a comparison of one person's samples, or nonmate scores, coming from comparison of different persons' samples.

The words "genuine" or "authentic" are synonyms for mate, and the word "impostor" is used as a synonym for non-mate. The words "mate" and "nonmate" are traditionally used in identification applications (such as law enforcement search, or background checks) while genuine and impostor are used in verification applications (such as access control).

An error tradeoff characteristic represents the tradeoff between Type II and Type I classification errors. For identification this plots false negative vs. false positive identification rates i.e. FNIR vs. FPIR parametrically with T. Such plots

are often called detection error tradeoff (DET) characteristics or receiver operating characteristic (ROC). These serve the same function – to show error tradeoff – but differ, for example, in plotting the complement of an error rate (e.g. TPIR = 1 – FNIR) and in transforming the axes, most commonly using logarithms, to show multiple decades of FPIR. More rarely, the function might be the inverse of the Gaussian cumulative distribution function.

The slides of Figures 10 through 15 discuss presentation and interpretation of DETs used in this document for reporting face identification accuracy. Further detail is provided in formal biometrics testing standards, see the various parts of ISO/IEC 19795 Biometrics Testing and Reporting. More terms, including and beyond those to do with accuracy, appear in ISO/IEC 2382-37 Information technology – Vocabulary – Part 37: Harmonized biometric vocabulary.

2023/04/04
07:31:47FNIR(N, R, T) = False neg. identification rate
FPIR(N, T) = False pos. identification rateN = Num. enrolled subjects
R = Num. candidates examined

T = Threshold

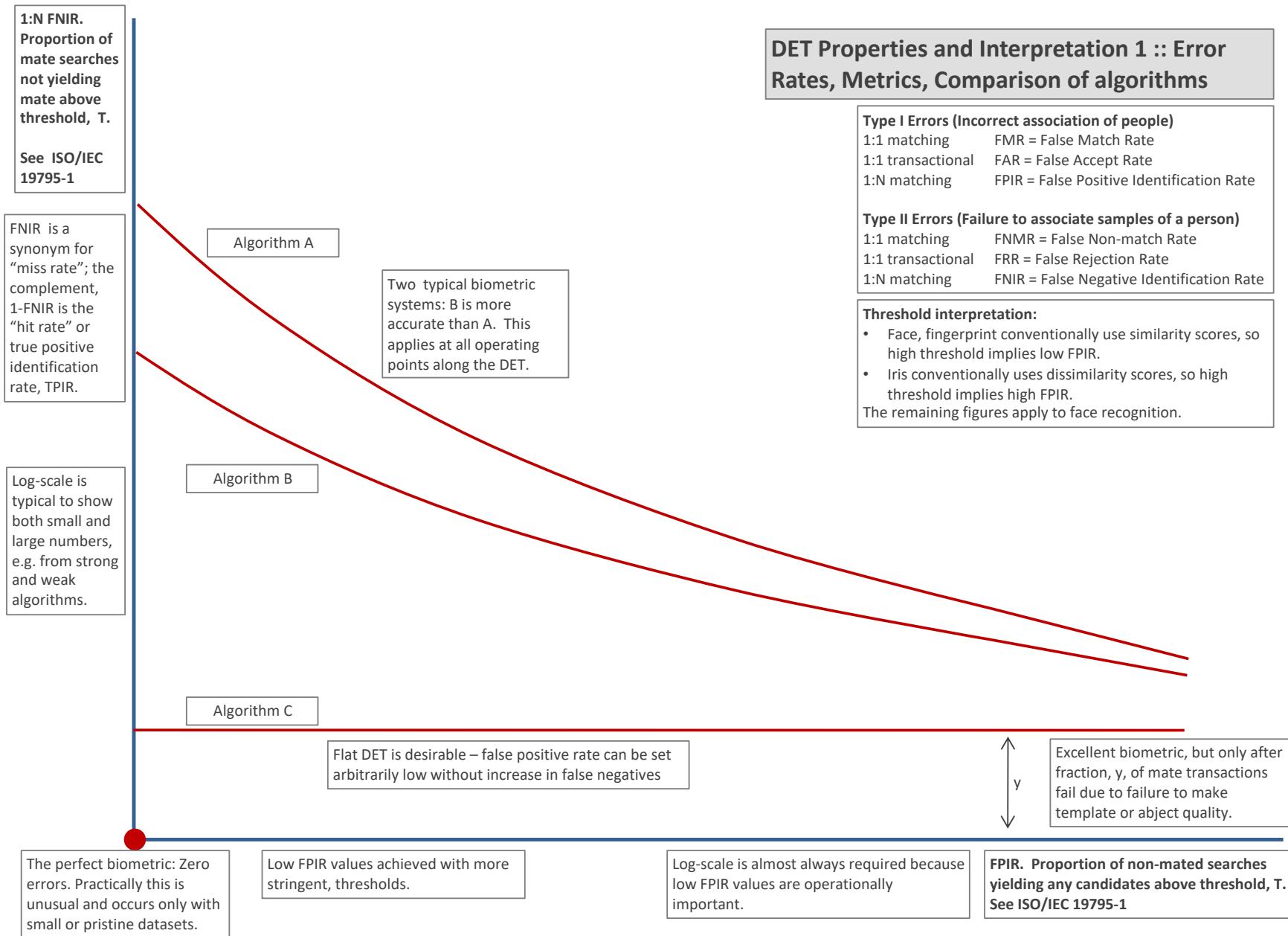
T = 0 → Investigation
T > 0 → Identification

Figure 10: DET as the primary performance reporting mechanism.

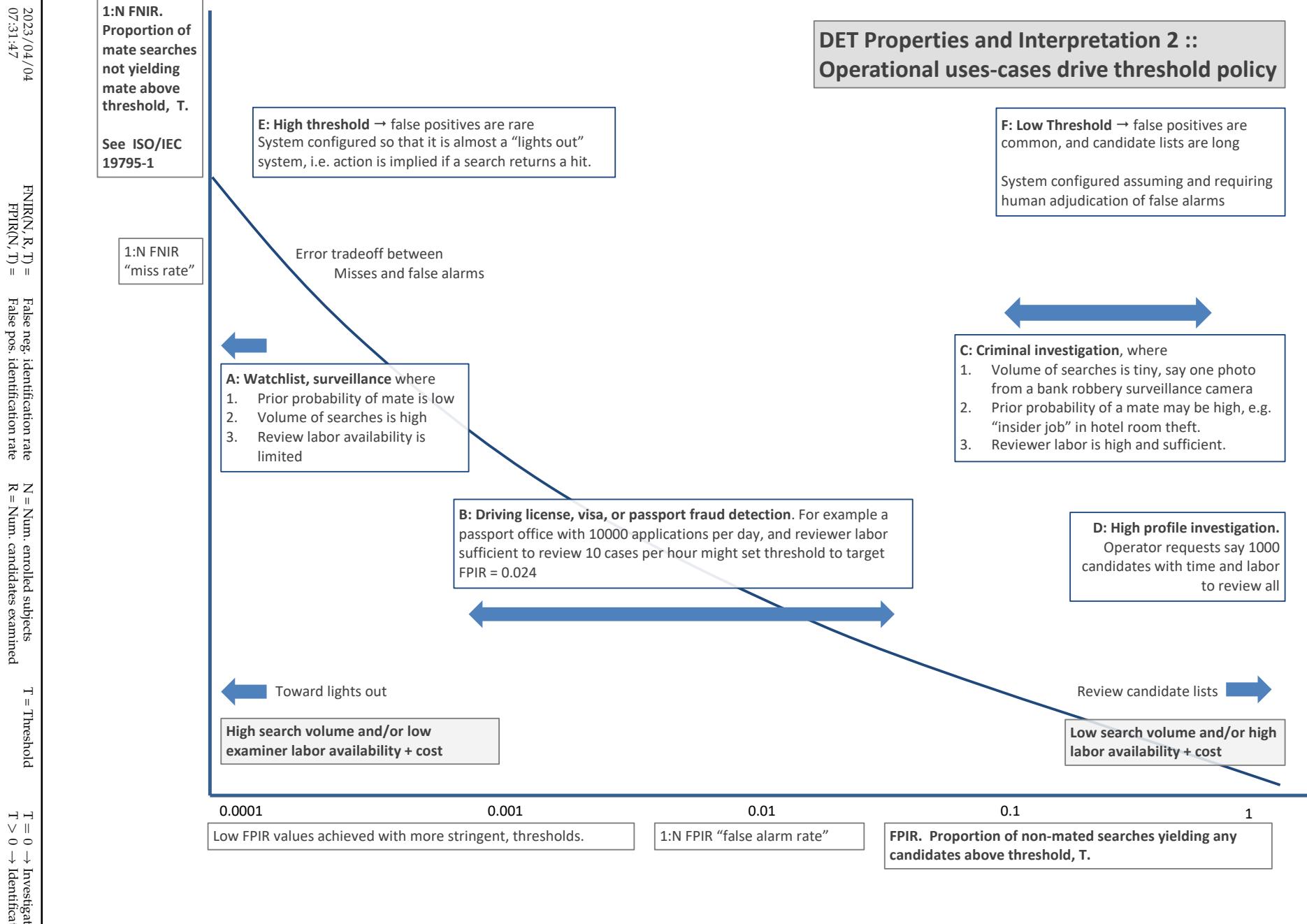


Figure 11: DET as the primary performance reporting mechanism.

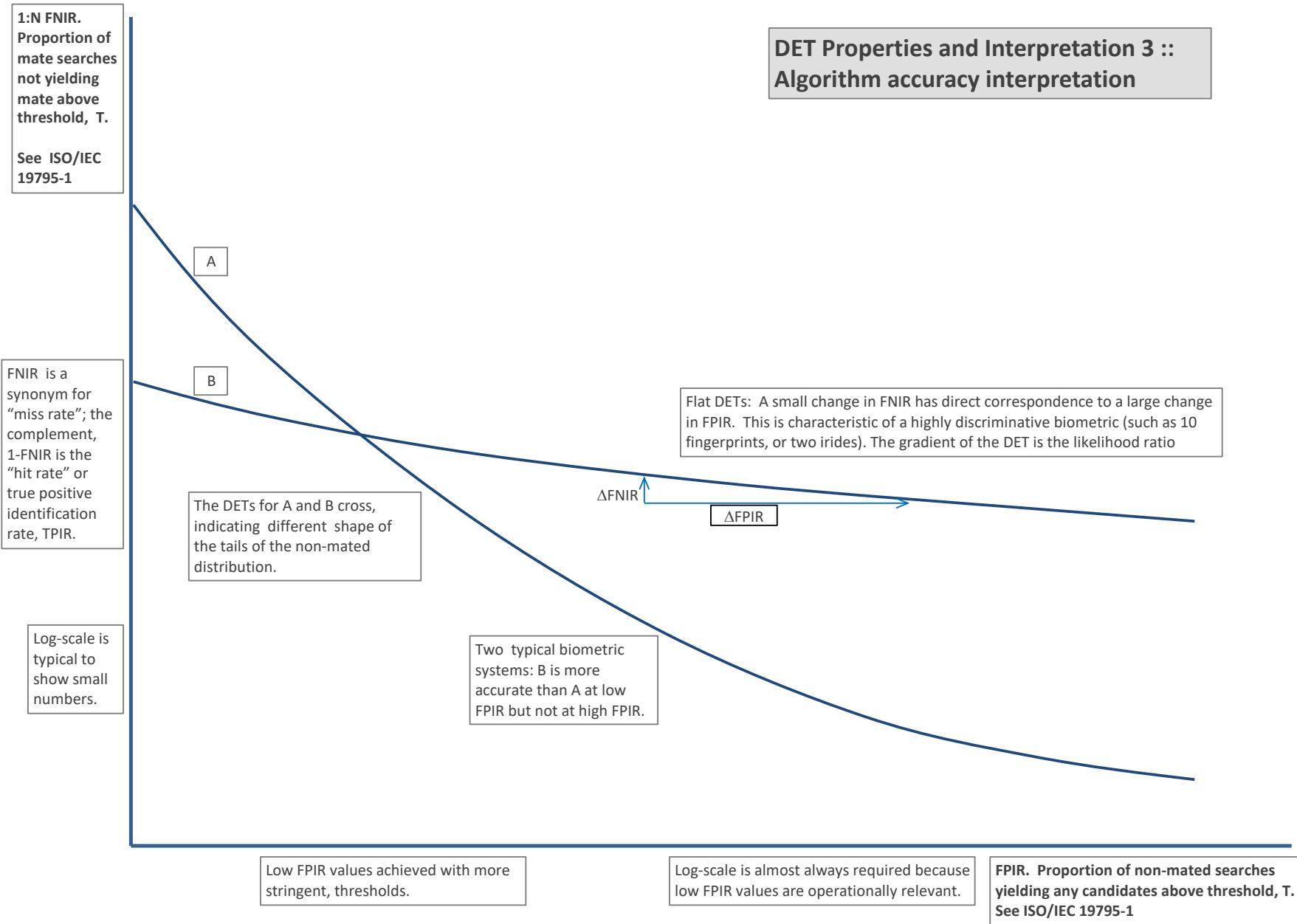
2023/04/04
07:31:47FNIR(N, R, T) = False neg. identification rate
FPIR(N, T) = False pos. identification rateN = Num. enrolled subjects
R = Num. candidates examinedT = Threshold
T = 0 → Investigation
T > 0 → Identification

Figure 12: DET as the primary performance reporting mechanism.

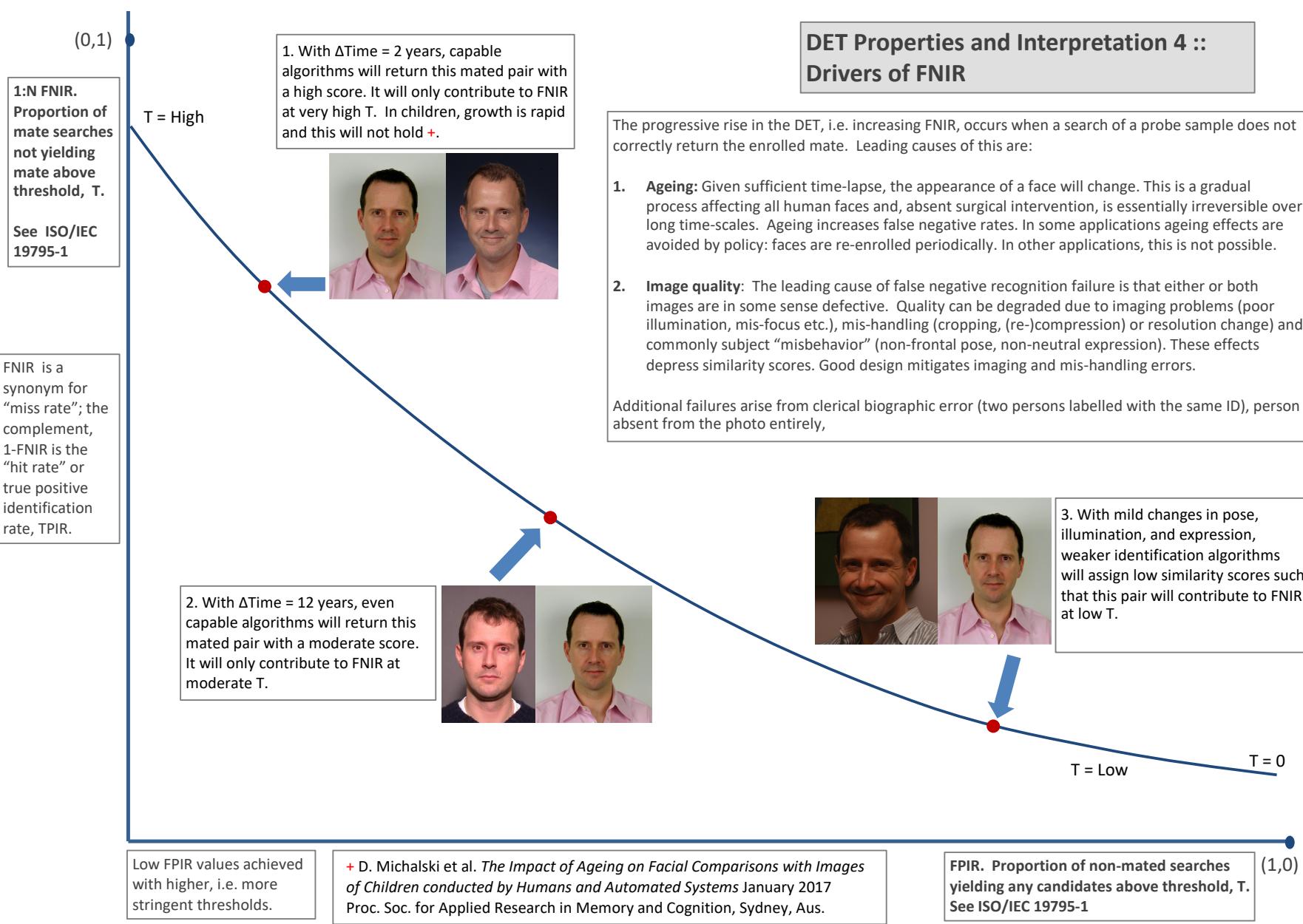


Figure 13: DET as the primary performance reporting mechanism.

2023/04/04
07:31:47

$\text{FNIR}(N, k, D) =$ False neg. identification rate
 $\text{FPIR}(N, T) =$ False pos. identification rate
 $N =$ Num. enrolled subjects
 $R =$ Num. candidates examined

T = Threshold

$T \equiv 0 \rightarrow$ Investigation
 $T > 0 \rightarrow$ Identification

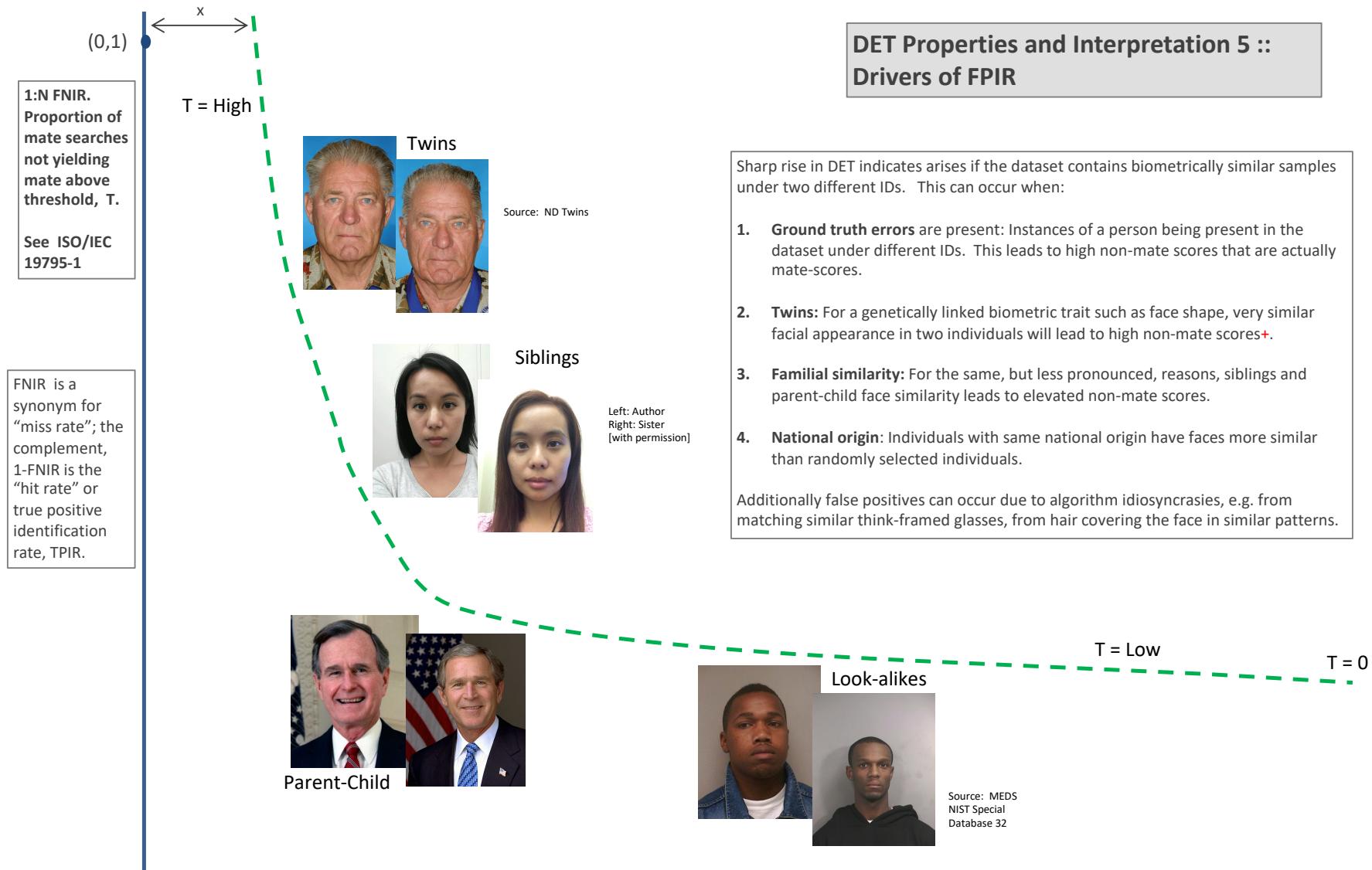


Figure 14: DET as the primary performance reporting mechanism.

2023/04/04
07:31:47

$\text{FNIR}(N, R, T) =$ False neg. identification rate
 $\text{FPIR}(N, T) =$ False pos. identification rate

N = Num. enrolled subjects
 R = Num. candidates examined

T = Threshold

$T = 0 \rightarrow$ Investigation
 $T > 0 \rightarrow$ Identification

1:N FNIR.
Proportion of mate searches not yielding mate above threshold, T .
See ISO/IEC 19795-1

Algorithm X,
Condition 1

Algorithm X,
Condition 2

If system X is used with images of different properties, say from different imaging systems, or from different populations, generally both FNIR and FPIR will change. The dotted line joins points of the same threshold. Horizontal (vertical) lines indicate change in FPIR (FNIR) only. Two cases concerning population size are shown below (A and B), for the blue curves.

FNIR is a synonym for "miss rate"; the complement, 1-FNIR is the "hit rate" or true positive identification rate, TPIR.

Log-scale is typical to show small numbers.

Algorithm Y,
Condition 1

Algorithm Y,
Condition 2

If DETs are computed for two categories (men and women) or (cameras A and B) or (indoor vs. outdoor), generally the Type I and Type II errors will differ and the line of constant threshold will be neither horizontal nor vertical.

The ideal situation in most applications is that a fixed threshold yields a fixed FPIR so that system owners see no change in false alarms across populations or conditions.

Low FPIR values achieved with higher, i.e. more stringent, thresholds.

Log-scale is often required because low FPIR values are operationally relevant.

FPIR. Proportion of non-mated searches yielding any candidates above threshold, T . See ISO/IEC 19795-1

Figure 15: DET as the primary performance reporting mechanism.

2023/04/04
07:31:47FNIR(N, R, T) = False neg. identification rate
FPIR(N, T) = False pos. identification rateN = Num. enrolled subjects
R = Num. candidates examined

T = Threshold

T = 0 → Investigation
T > 0 → Identification

1:N FNIR.
Proportion of mate searches not yielding mate above threshold, T.
See ISO/IEC 19795-1

FNIR is a synonym for "miss rate"; the complement, 1-FNIR is the "hit rate" or true positive identification rate, TPIR.

Log-scale is typical to show small numbers.

A: Typical case: In theory, and often in practice, a 1:N search is implemented by executing N 1:1 comparisons independently and then sorting by similarity score:

Mate scores: A mate comparison score is independent of the rest of enrollment data, and so independent of N. This implies the horizontal line above $\text{FNIR}(T, N) = \text{FNMR}(T, 1)$.

Non-mate scores: FPIR increases linearly with N from binomial theory: $\text{FPIR}(N, T) = 1 - (1 - \text{FMR}(T))^N \rightarrow N \text{ FMR}(T)$ for small FPIR.

Pop. N1



Pop. N2 > N1



B: Special case: An enrollment database is not just a linear data structure, it could be an index, or tree, then search is not simply N 1:1 comparisons and a sort. In that case:

Mate scores become dependent on the enrollment data, either its size or actual content, then generally $\text{FNIR}(T, N) \neq \text{FNIR}(T, 1)$.

Non-mate scores are normally no longer just the highest 1:1 comparison score. Instead, for example, scores may be normalized as the implementation attempts to make FPIR independent of N will yield the vertical line linking points of equal threshold.

Low FPIR values achieved with higher, i.e. more stringent, thresholds.

Log-scale is often required because low FPIR values are operationally important.

DET Properties and Interpretation 7 :: Effect of enrolled population size.

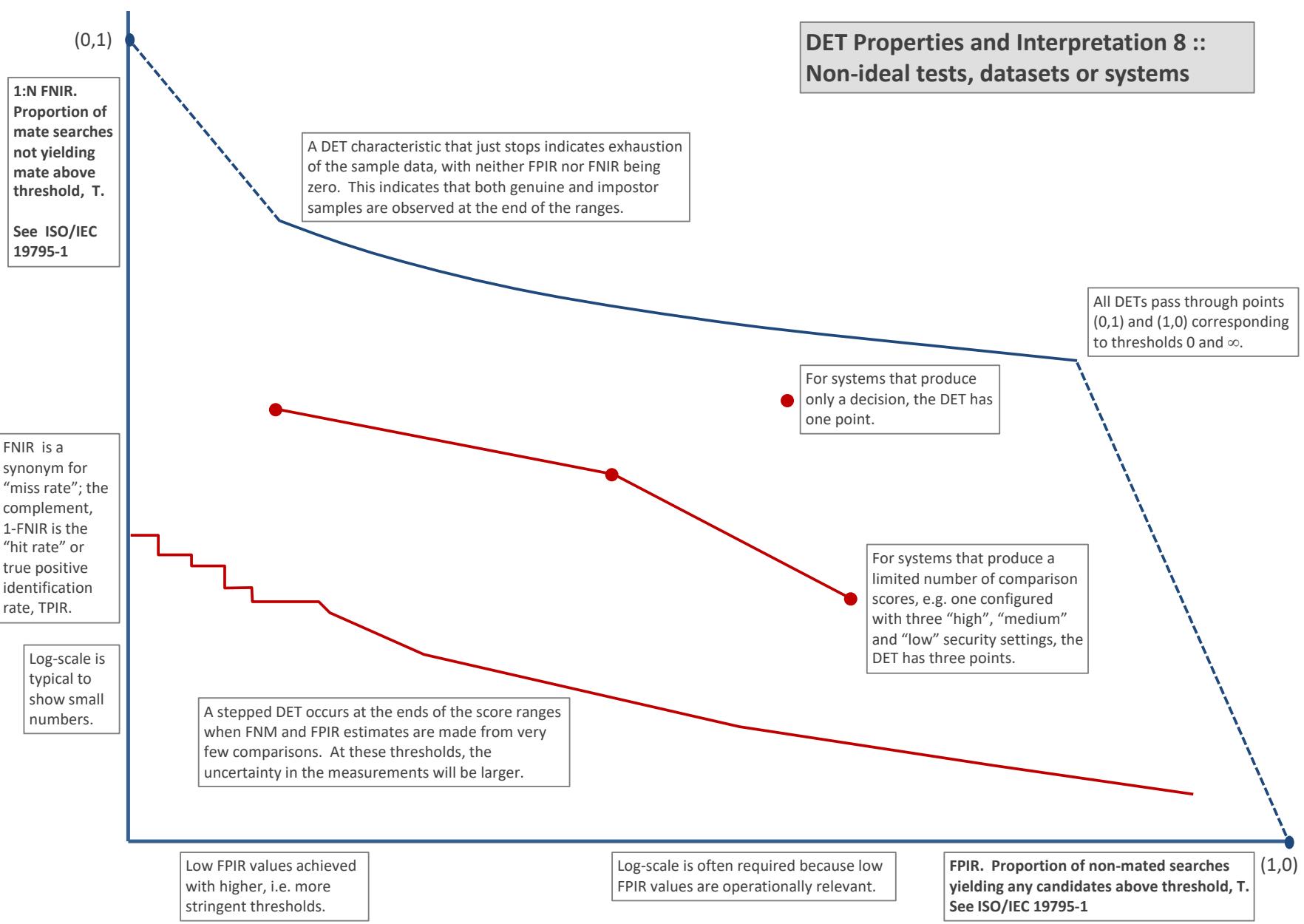


Figure 17: DET as the primary performance reporting mechanism.

3.4 Best practice testing requires execution of searches with and without mates

FRVT embeds 1:N searches of two kinds: Those for which there is an enrolled mate, and those for which there is not. The respective numbers for these types of searches appear in Table 1. However, it is common to conduct only mated searches¹⁰. The cumulative match characteristic is computed from candidate lists produced in mated searches. Even if the CMC is the only metric of interest, the actual trials executed in a test should nevertheless include searches for which no mate exists. As detailed in Table 1 the FRVT reserved disjoint populations of subjects for executing true non-mate searches.

3.5 Failure to extract features

During enrollment some algorithms fail to convert a face image to a template. The proportion of failures is the failure-to-enroll rate, denoted by FTE. Similarly, some search images are not converted to templates. The corresponding proportion is termed failure-to-extract, denoted by FTX.

We do not report FTX because we assume that the same underlying algorithm is used for template generation for enrollment and search.

Failure to extract rates are incorporated into FNIR and FPIR measurements as follows.

- ▷ **Enrollment templates:** Any failed enrollment is regarded as producing a zero length template. Algorithms are required by the API [10] to transparently process zero length templates. The effect of template generation failure on search accuracy depends on whether subsequent searches are mated, or non-mated: Mated searches will fail giving elevated FNIR; non-mated searches will not produce false positives so, to first order, FPIR will be reduced by a factor of $1 - \text{FTE}$.
- ▷ **Search templates and 1:N search:** In cases where the algorithm fails to produce a search template from input imagery, the result is taken to be a candidate list whose entries have no hypothesized identities and zero score. The effect of template generation failure on search accuracy depends on whether searches are mated, or non-mated: Mated searches will fail giving elevated FNIR; Non-mated searches will not produce false positives, so FPIR will be reduced. Thus given a measurement of false negative and positive rates made over only those where failures-to-extract did not occur, those rates - call them FNIR^\dagger and FPIR^\dagger - could be adjusted by an explicit measurement of FTX as follows

$$\text{FNIR} = \text{FTX} + (1 - \text{FTX})\text{FNIR}^\dagger \quad (8)$$

$$\text{FPIR} = (1 - \text{FTX})\text{FPIR}^\dagger \quad (9)$$

This approach is the correct treatment for positive-identification applications such as access control where cooperative users are enrolled and make attempts at recognition. This approach is not appropriate to negative identification applications, such as visa fraud detection, in which hostile individuals may attempt to evade detection by submitting poor quality samples. In those cases, template generation failures should be investigated as though a false alarm had occurred.

¹⁰For example, the [Megaface benchmark](#). This is bad practice for several reasons: First, if a developer knows, or can reasonably assume, that a mate always exists, then unrealistic gaming of the test is possible. A second reason is that it does not put FPIR on equal footing with FNIR and that matters because in most applications, not all searches have mates - not everyone has been previously enrolled in a driving license issuance or a criminal justice system - so addressing between-class separation becomes necessary.

3.6 Fixed length candidate lists, threshold independent workload

Suppose an automated face identification algorithm returns L candidates, and a human reviewer is retained to examine up to R candidates, where $R \leq L$ might be set by policy, preference or labor availability. For now, assume also that the reviewer is not provided with, or ignores, similarity scores, and thresholds are not applied. Given the algorithm typically places mates at low (good) ranks, the number of candidates a reviewer can be expected to review can be derived as follows. Note that the reviewer will:

- ▷ Always inspect the first ranked image Frac. reviewed = 1
- ▷ Then inspect those candidates where mate not confirmed at rank 1 Frac. reviewed = 1-CMC(1)
- ▷ Then inspect those candidates where mate not confirmed at rank 1 or 2 Frac. reviewed = 1-CMC(2)

etc. Thus if the reviewer will stop after a maximum of R candidates, the expected number of candidate reviews is

$$M(R) = 1 + (1 - CMC(1)) + (1 - CMC(2)) + \dots + (1 - CMC(R - 1)) \quad (10)$$

$$= R - \sum_{r=1}^{R-1} CMC(r) \quad (11)$$

A recognition algorithm that front-loads the cumulative match characteristic will offer reduced workload for the reviewer. This workload is defined only over the searches for which a mate exists. In the cases where there truly is no mate, the reviewer would review all R candidates. Thus, if the proportion of searches for which a mate does exist is β , which in the law enforcement context would be the recidivism rate [3], the full expression for workload becomes:

$$M(R) = \beta \left(R - \sum_{r=1}^{R-1} CMC(r) \right) + (1 - \beta)R \quad (12)$$

$$= R - \beta \sum_{r=1}^{R-1} CMC(r) \quad (13)$$

3.7 Timing measurement

Algorithms were submitted to NIST as implementations of the application programming interface(API) specified by NIST in the Evaluation Plan [10]. The API includes functions for initialization, template generation, finalization, search, gallery insert, and gallery delete. Two template generation functions are required, one for the preparation of an enrollment template, and one for a search template.

In NIST's test harness, all functions were wrapped by calls to the C++ std::chrono::high_resolution_clock which on the dedicated timing machine counts 1ns clock ticks. Precision is somewhat worse than that however.

3.8 Uncertainty estimation

3.8.1 Random error

This study leverages operational datasets for measurement of recognition error rates. This affords several advantages. First, large numbers of searches are conducted (see Table 1) giving precision to the measurements. Moreover, for the two mugshot datasets, these do not involve reuse of individuals so binomial statistics can be expected to apply to recognition error counts. In that case, an observed count of a particular recognition outcome (i.e. a false negative or false positive) in M trials will sustain 95% confidence that the actual error rate is no larger than some value.

As an example, the minimum number of mugshot searches conducted in this report is $M = 154\,549$, and for an observed FNIR around 0.002, the measurement supports a conclusion that the actual FNIR is no higher than 0.00228 at 99% confidence level. On the false positive side, we tabulate FNIR at FPIR values as low as 0.001. Given estimates based on 331 254 non-mate trials, the actual FPIR values will be below 0.00115 at 99% confidence. In conclusion, large scale evaluation, without reuse of subjects, supports tight uncertainty bounds on the measured error rates.

3.8.2 Systematic error

The FRVT 2018 dataset includes anomalies discovered as a result of inspecting images involved in recognition failures from the most accurate algorithms. Two kinds of failure occur: False negatives (which, for the purpose here, include failures to make templates) and false positives.

False negative errors: We reviewed 600 false negative pairs for which either or both of the leading two algorithms did not put the correct mate in the top 50 candidates. Given 154 549 searches, this number represents 0.39% of the total, resulting in $\text{FNIR} \sim 0.0039$. Of the 600 pairs:

- ▷ **A: Poor quality:** About 20% of the pairs included images of very low quality, often greyscale, low resolution, blurred, low contrast, partially cropped, interlaced, or noisy scans of paper images. Additionally, in a few cases, the face is injured or occluded by bandages or heavy cosmetics.
- ▷ **B: Ground truth identity label bugs:** About 15% of the pairs are not actually mated. We only assigned this outcome when a pair is clearly not mated.
- ▷ **C: Profile views:** About 35% included an image of a profile (side) view of the face, or, more rarely, an image that was rotated 90 degrees in-plane (roll).
- ▷ **D: Tattoos:** About 30% included an image of a tattoo that contained a face image. These arise from mis-labelling in the parent dataset metadata.
- ▷ **E: Ageing:** There is considerable time-lapse between the two captures.

All these estimates are approximate. Of these, the tattoo and mislabelled images can never be matched. These constitute an accuracy floor in the sample implying that FNIR cannot be below 0.0018¹¹. The profile-views, low-quality images, and images with considerable ageing can, in principle, be successfully matched - indeed some algorithms do so - so are not part of the accuracy floor.

¹¹This value is the sum of two partial false negative rates: $\text{FNIR}_B = 0.15 * 0.0039$ plus $\text{FNIR}_D = 0.3 * 0.0039$

For the microsoft-4 algorithm the lowest miss rate from (recent entry in Table 29) is $\text{FNIR}(640\,000, 50, 0) = 0.0018$. This is close to the value estimated from the inspection of misses. It is below the 0.0039 figure because the algorithm does match some profile and poor quality images, that the yitu-2 algorithm does not.

For many tables (e.g. Table 29), the FNIR values obtained for the FRVT-2018 mugshots could be corrected by reducing them by 0.0018. The best values would then be indistinct from zero. The results in this report *were not* adjusted to account for this systematic error.

False positive errors: As shown in Figure 1 and discussed in Figure 14 many of the DET characteristics in this report exhibit a pronounced turn upward at low false positive rates. The shape can be caused by identity labelling errors in the ground truth of a dataset, specifically persons present in the database under two IDs such that some proportion of non-mate pairs are actually mated. To look for such possibilities, we merged the highest 1000 non-mate pairs produced by three different algorithms which resulted in 1839 unique pairs. This constitutes 0.56% of all non-mate searches. We assert that it is *very* difficult for human reviewers to assign the pairs into the following three categories: twins; doppelgangers; or ground-truth errors (instances of the same person under two IDs). Given this difficulty we made no attempt to correct any possible ground truth errors except by removing 57 pairs in the following categories:

- ▷ **A: Profile views:** Thirteen pairs included one or two profile-view images. As described in Figure 150, these can cause false positives.
- ▷ **B: Same-session photographs:** For twelve pairs, the images were identical or trivially altered (e.g. cropped) versions of the same photo. These were present under a different ID likely due to some clerical or procedural mistake.
- ▷ **C: Tattoos of faces:** There were fourteen instances of tattoo photographs that contained faces causing false matches.
- ▷ **D: T-shirt faces:** There were six instances of T-shirt photographs (of Bob Marley and Che Guevara) being detected instead of the face and causing false positives.
- ▷ **E: Background faces:** There were twelve instances of one subject appearing in the background of two otherwise correct portrait photos.

Note we did not remove any images where there was a chance that the pair was actually a different person.

In any case, the results in this report have not been adjusted for this systematic error.

4 Results

This section gives extensive results for algorithms submitted to FRVT 2018. Three page “report cards” for each algorithm are contained in a [separate supplement](#). Performance metrics were described in section 3. The main results are summarized in tabular form with more exhaustive data included as DET, CMC and related graphs in appendices as follows:

- ▷ The three tables 2-4 list algorithms alongside full developer names, acceptance date, size of the provided configuration data, template size and generation time, and search duration data.
 - The **template generation duration** is most important to applications that require fast response. For example, an eGate taking more than two seconds to produce a template might be unacceptable. Note that GPUs may be of utility in expediting this operation for some algorithms, though at additional expense. Two additional factors should be considered¹²¹³.
 - The **search duration** is the time taken for a search of a search template into a gallery of N enrollment templates. This performance variable, together with the volume of searches, is influential on the amount of hardware needed to sustain an operational deployment. This is measured here with the algorithm running on a single core of a contemporary CPU. Search is most simply implemented as N computations of a distance metric followed by a sort operation to find the closest enrollments. However, considerable optimization of this process is possible, up to and including fast-search algorithms that, by various means, avoid computation of all N distances.
 - The **template size** is the size of the extracted feature vector (or vectors) and any needed header information. Large template sizes may be influential on bus or network bandwidth, storage requirements, and on search duration. While the template itself is an opaque data blob, the feature dimensionality might be estimated by assuming a four-bytes-per-float encoding. There is a wide range of encodings. For the more accurate algorithm, sizes range from 256 bytes to about 2KB bytes, indicating essentially no consensus on face modeling and template design.
 - The **template size multiplier** column shows how, given k input images, the size of the template grows. Most implementations internally extract features from each image and concatenate them, and implement some score-level fusion logic during search. Other implementations, including many of the most accurate algorithms, produce templates whose size does not grow with k . This could be achieved via selection of the best quality image - but this is not optimal in handling ageing where the oldest image could be the best quality. Another mechanism would be feature-level fusion where information is fused from all k inputs. In any case, as a black-box test, the fusion scheme is proprietary and unknown.
 - The size of the **configuration data** is the total size of all files resident in a vendor-provided directory that contains arbitrary read-only files such as parameters, recognition models (e.g caffe). Generally a large value for this quantity may prohibit the use of the algorithm on a resource-constrained device.

¹²The FRVT 2018 API prohibited threading, so some gains from parallelism may be available on multiple-cores or multiple processors, if the feature extraction code could be distributed across them.

¹³Note also that factors of two or more may be realizable by exploiting modern vector processing instructions on CPUs. It is not clear in our measurements whether all developers exploited Intel’s AVX2 instructions, for example. Our machine was so equipped, but we insisted that the same compiled library should also run on older machines lacking that instruction. The more sophisticated implementations may have detected AVX2 presence and branched accordingly. The less sophisticated may be defaulted to the reduced instruction set. Readers should see the FRVT 2018 API document for the specific chip details.

▷ Tables 29-30 report core rank-based accuracy for mugshot images. The population size is limited to $N = 1.6$ million identities because this is the largest gallery size on which all algorithms were executed. Notable observations from these tables are as follows:

- **Accuracy gains since 2018:** NIST Interagency Report 8238 documented massive gains over those reported in the FRVT 2014 report, NIST Interagency Report 8009. Further gains are documented in this report. Comparing the most accurate algorithm in November 2018, NEC-3, the value of $\text{FNIR}(N, L, T)$ reduced from 0.0031 to 0.0024 for the Sensetime-004 algorithm with $N = 12$ million recent images. The tables show broader gains: many developers have made advances since 2018 with between two and five-fold reduction in errors.

- **Wide range in accuracy:** The rank-1 miss rates vary from $\text{FNIR}(N, 1, 0) = 0.0012$ for sensetime-004 up to about 0.5 for the very fast but inaccurate microfocus-x algorithms. Among the developers who are superior to NEC in 2013, the range is from 0.002 to 0.035 for camvi-3. This large accuracy range is consistent with the buyer-beware maxim, and indicates that face recognition software is far from being commoditized.

▷ Tables 34-35 report threshold-based error rates, $\text{FNIR}(N, L, T)$, for $N = 1.6$ million for mugshot-mugshot accuracy on FRVT 2014, FRVT 2018, and also (in pink) mugshot-webcam accuracy using FRVT 2018 enrollments. Notable observations from these tables are as follows:

- **Order of magnitude accuracy gains since 2014:** As with rank-based results, the gains in accuracy are substantial, though somewhat reduced. At $\text{FPIR} = 0.01$, the best improvement over NEC in 2014 is a 27 fold reduction in FNIR using the NEC_2 algorithm. At $\text{FPIR} = 0.001$, the largest gain is a six-fold reduction in FNIR via the NEC_3 algorithm.

- **Broad gains across the industry:** About 19 companies realize accuracy better than the NEC benchmark from 2014. This is somewhat lower than the 28 developers who succeeded on the rank-1 metric. This may be due to the ubiquity of, and emphasis on, the rank-1 metric in many published algorithm development papers.

- **Webcam images:** Searches of webcam images give $\text{FNIR}(N, T)$ values around 2 to 3 times higher than mugshot searches. Notably the leading developers with mugshots are approximately the same with poorer quality webcams. But some developers e.g. Camvi, Megvii, TongYi, and Neurotechnology do improve their relative rankings on webcams, perhaps indicating their algorithms were tailored to less constrained images.

▷ Tables 21, 25, 26 and show, respectively, high-threshold, rank 1, and rank 50 FNIR values for all algorithms performing searches into five different gallery sizes, $N = 640\,000$, $N = 1\,600\,000$, $N = 3\,000\,000$, $N = 6\,000\,000$ and $12\,000\,000$. The $\text{FPIR} = 0.001$ table is included to inform high-volume duplicate detection applications. The Rank-1 table is included as a primary accuracy indicator. The Rank-50 table is included to inform agencies who routinely produce 50 candidates for human-review. The notable results are:

- **Slow growth in rank-based miss rates:** $\text{FNIR}(N, R)$ generally grows as a power law, aN^b . From the straight lines of many graphs of Figure 20 this is clearly a reasonable model for most, but not all, algorithms. The coefficient a can be interpreted as FNIR in a gallery of size 1. The more important coefficient b indicates scalability, and often, $b \ll 1$, implies very benign growth in FNIR . The coefficients of the models appear in the Tables 25 and 26.

- **Slow growth in threshold-based miss rates:** $\text{FNIR}(N, T)$ also generally grows as a power law, aN^b except at the high threshold values corresponding to low FPIR values. This is visible in the plots of Figure 36 which

show straight lines except for $FPIR = 0.001$, which increase more rapidly with N above 3 000 000. Each trace in those figures shows $FNIR(N, T)$ at fixed $FPIR$ with both N and T varying. Thus at large N , it is usually necessary to elevate T to maintain fixed $FPIR$. This causes increased $FNIR$. Why that would no-longer obey a power-law is not known. However, if we expect large galleries to contain individuals with familial relations to the non-mate search images - in the most extreme case, twins - then suppression of false positives becomes more difficult. This is discussed in the Figures starting at Fig. 10

▷ Figure ?? shows false positives from twins against their enrolled siblings, broken out by type of twin: fraternal or identical. The Figure is based on the enrollment of 104 single images on one of a pair of twins, and then the search of 2354 second images. Note that the dataset is heavily skewed towards identical twins which is not representative of the true population. There is also a skew towards same sex fraternal twin pairs compared to different sex fraternal twin pairs again not representative of the true population.

The notable results are:

- For all algorithms tested, the 1087 mated searches (Twin A vs. Twin A) produce scores almost always above typical operational thresholds, with (not shown) matches at rank 1. The images are of good quality, so this is the result expected from the rest of this report.
- For the 1066 identical twin searches (AB), almost all produce the twin at rank 1, with a few producing the mate at further down the candidate lists rank and low score.
- For the 169 fraternal searches (AB) from same sex pairs, most algorithms give a large number of very high scores, implying false positives at all thresholds. However, there are long tails containing lower scores that are correctly below threshold. In general, scores that are higher in this distribution are all rank 1 whereas the lower scores have much higher ranks.
- (Not shown) Of the 169, there are 24 fraternal searches (AB) involving different sex twins. Here most algorithms correctly report scores well below the lowest threshold, and usually not on the candidate list at all.

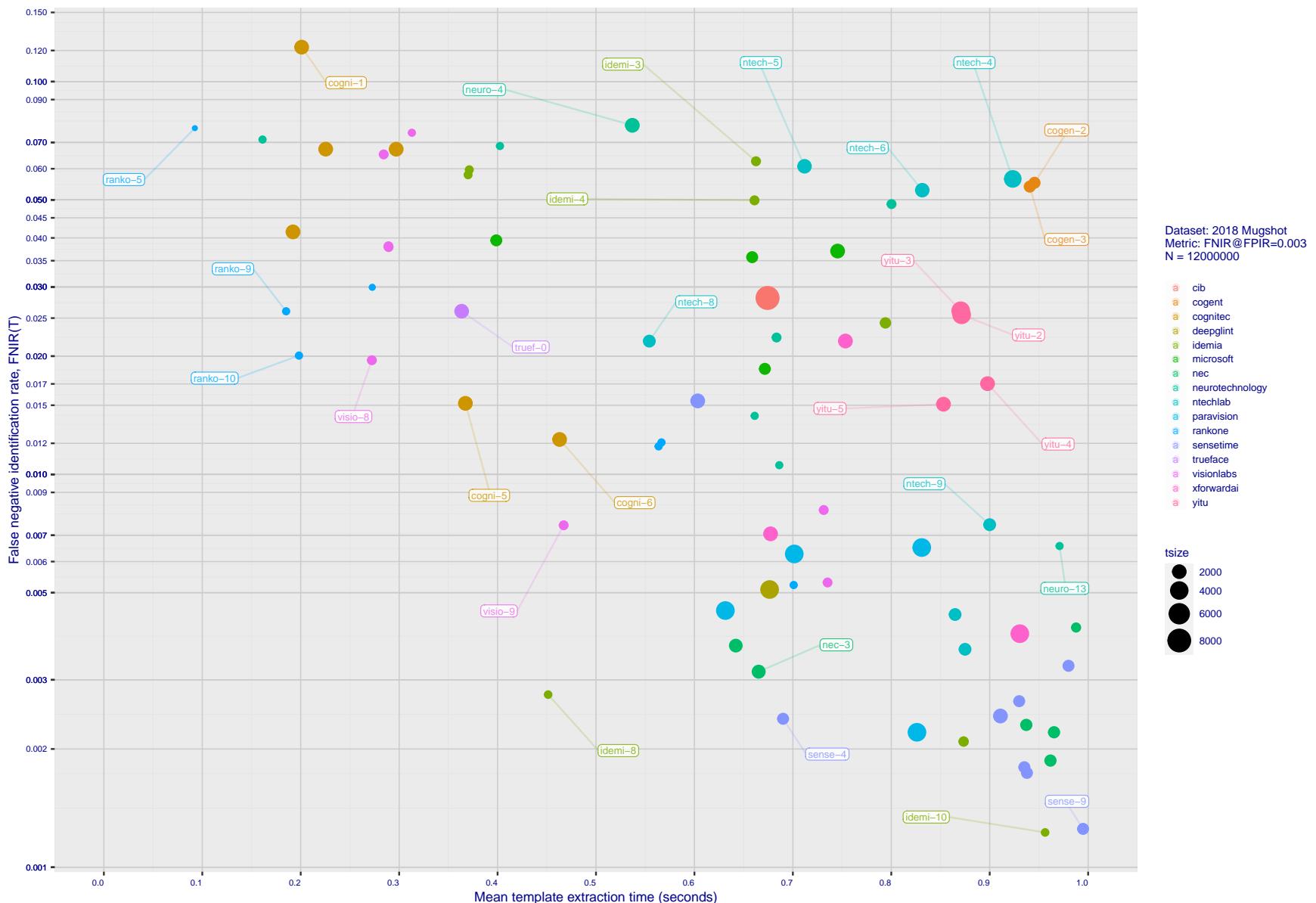
2023/04/04
07:31:47

Figure 18: [Mugshot Dataset] Speed-accuracy tradeoff. For developers of the more accurate algorithms the plot shows the tradeoff of high-threshold recognition miss-rates, $\text{FNIR}(N, N, T)$ for $\text{FPIR}(N, T) = 0.003$, and template generation time. Developers are coded by color. Template size is encoded by the size of the circle. Some labels are quite distant from the respective point, to avoid superposing text. Without any other influences, the assumption would be that taking time to localize the face, and extract features, would lead to better accuracy. The most notable result, for NEC, is that their slower algorithms are much more accurate than the version that extract features in fewer than 90 milliseconds.

2023/04/04
07:31:47FNIR(N, R, T) = False neg. identification rate
FPTR(N, T) = False pos. identification rateN = Num. enrolled subjects
R = Num. candidates examinedT = Threshold
T = 0 → Investigation

T > 0 → Identification

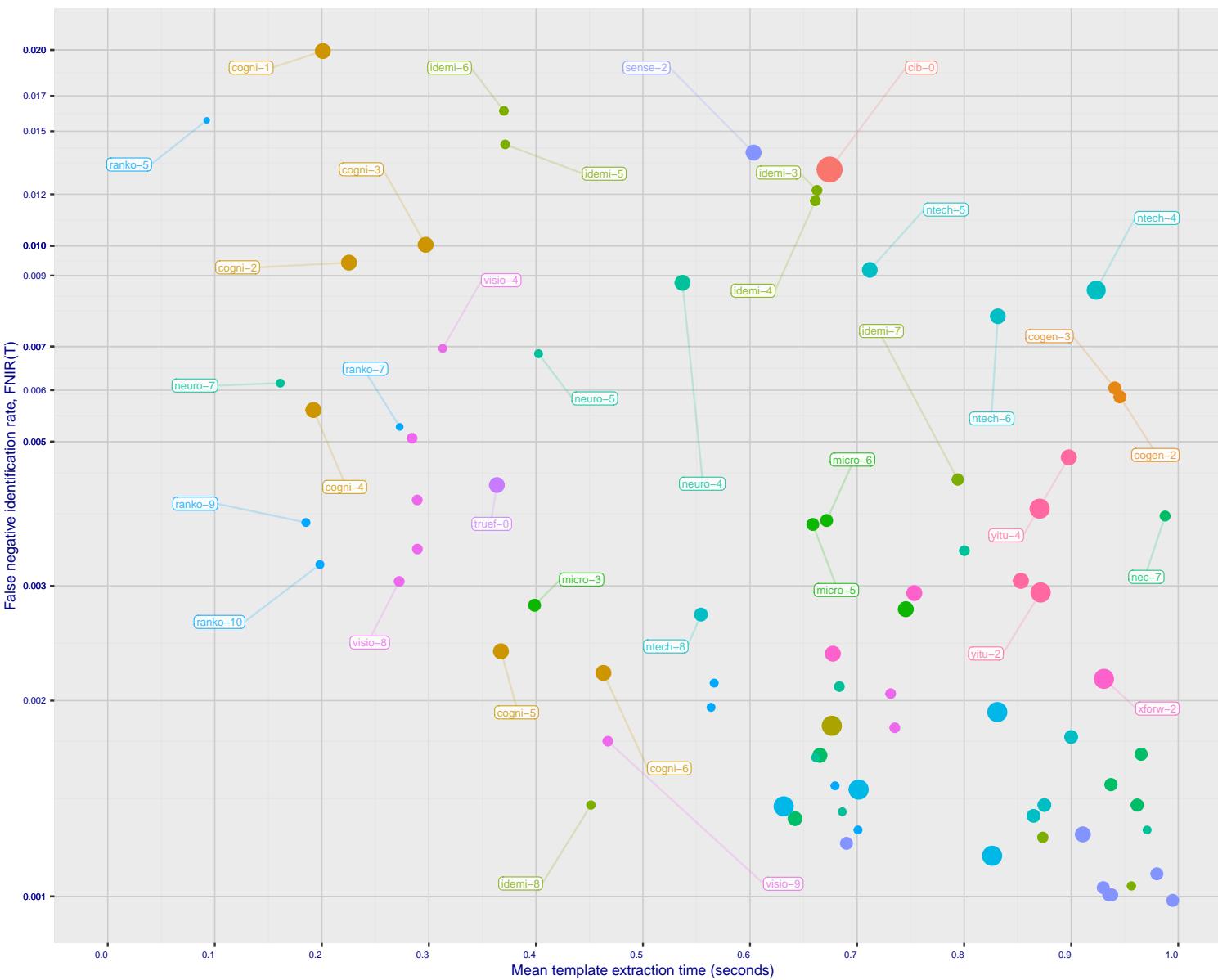


Figure 19: [Mugshot Dataset] Speed-accuracy tradeoff. For developers of the more accurate algorithms the plot shows the tradeoff of rank-one recognition miss-rates, FNIR(N, 1, 0), and template generation time. Developers are coded by color. Template size is encoded by the size of the circle. Some labels are quite distant from the respective point, to avoid superposing text. Without any other influences, the assumption would be that taking time to localize the face, and extract features, would lead to better accuracy. This occurs for NEC with their slower algorithm being much accurate than the version that extract features in fewer than 90 milliseconds.

Notes	
1	Configuration size does not capture static data present in libraries. Libraries are included but the size also includes any ancillary libraries for image processing (e.g. openCV) or numerical computation (e.g. blas).
2	Finalization is the processing of converting $N = 1600000$ templates into a searchable data structure an operation which can be a simple copy, or the building of an index or tree, for example. The duration of the operation may be data dependent, and may not be linear in the number of input templates.
3	This multiplier expresses the increase in template size when k images are passed to the template generation function.
4	All durations are measured on Intel®Xeon®CPU E5-2630 v4 @ 2.20GHz processors. Estimates are made by wrapping the API function call in calls to <code>std::chrono::high_resolution_clock</code> which on the machine in (3) counts 1ns clock ticks. Precision is somewhat worse than that however.
5	Search durations are measured as in the prior note. The power-law model in the final column mostly fits the empirical results in Figure 151. However in certain cases the model is not correct and should not be used numerically.

Table 2: Summary of algorithms and properties included in this report. The blue superscripts give ranking for the quantity in that column. Missing search durations, denoted by “-”, are absent because those runs were not executed, usually because we did not run on the larger galleries. Caution: The power-law model is sometimes an incorrect model. It is included here only to show broad sublinear behavior, which is flagged in green. The models should not be used for prediction.

DEVELOPER	FULL NAME	DEVELOPER LOCATION	SHORT NAME	SEQ. NUM.	VALIDATION DATE	CONFIG ¹ DATA (MB)	LIB ¹ DATA (MB)	TEMPLATE GENERATION			FINALIZE ² TIME (S)	SEARCH DURATION ³ MILLISEC						POWER LAW (μ s)
								SIZE (B)	MULT ³	TIME (MS) ⁴		L=1	L=50	L=50	L=50	N=3M	N=6M	
								N=1.6M	N=1.6M	N=1.6M		N=1.6M	N=1.6M	N=1.6M	N=1.6M	N=1.6M	N=1.6M	
53	Dermalog	DE	dermalog	007	2020-02-12	0	424	5 ¹²⁸	1	61 ⁴¹⁰	1	(29) ⁹⁸	(26) ⁹⁶	(29) ²¹⁸	(27) ⁴²⁹	(27) ¹⁰¹³	(27) ¹⁰¹³	178 ^{0.01N^{1.1}}
54	Dermalog	DE	dermalog	008	2021-01-25	0	531	4 ⁵¹²	-	46 ³⁷⁰	25 ⁴	(81) ³³⁵	(57) ²⁴⁶	(46) ⁴⁶²	(46) ⁹²⁴	(44) ¹⁸⁴⁹	(44) ¹⁸⁴⁹	50 ^{0.15N^{1.0}}
55	Dermalog	DE	dermalog	009	2021-11-09	0	318	4 ⁵¹²	-	40 ³⁴⁷	18 ³	(62) ²⁵³	(58) ²⁴⁶	(45) ⁴⁶¹	(45) ⁹²³	(43) ¹⁸⁴⁶	(43) ¹⁸⁴⁶	45 ^{0.16N^{1.0}}
56	Dermalog	DE	dermalog	010	2022-07-25	0	514	36 ⁵¹²	-	117 ⁶³³	21 ³	(56) ²⁴¹	(56) ²⁴²	(44) ⁴⁵⁴	(44) ⁹¹⁰	(42) ¹⁸²³	(42) ¹⁸²³	48 ^{0.15N^{1.0}}
57	Dermalog	DE	dermalog	011	2022-12-12	0	272	3 ¹²⁸	-	39 ³⁴²	2 ¹	(22) ⁸⁷	(21) ⁸⁸	(18) ¹⁶⁵	(18) ³³¹	(18) ⁶⁶⁴	(18) ⁶⁶⁴	65 ^{0.05N^{1.0}}
58	Digidata	IN	digidata	000	2022-06-03	248	33	121 ²⁰⁴⁸	-	98 ⁵⁶⁰	25 ²⁴⁴⁴	(2) ⁰	(23) ⁹⁵	-	-	-	-	-
59	DiluSense Technology	CN	dilusense	000	2022-05-26	311	56	174 ²⁰⁴⁸	-	24 ²⁴⁷	26 ²⁶	(204) ¹⁹⁰⁴	(204) ¹⁸⁹⁸	(176) ³⁵⁹⁷	(171) ⁷²⁵⁶	(174) ¹⁴⁶⁸⁹	(104) ^{0.88N^{1.0}}	
60	DiluSense Technology	CN	dilusense	001	2022-12-24	599	5	245 ⁴⁰⁹⁶	-	226 ⁸⁸³	38 ²³¹	(227) ³⁰²⁶	(230) ³⁰⁴²	(194) ⁴⁷³⁸	(191) ⁹⁴⁷³	(192) ¹⁹⁰²⁶	(24) ^{5.36N^{0.9}}	
61	FarBar Inc	TW	f8	001	2019-10-03	266	19	125 ²⁰⁴⁸	k	192 ⁸¹⁰	14 ¹⁴	-	-	-	-	-	-	-
62	Fincore Ltd	UK	fincore	000	2021-08-18	250	224	108 ²⁰⁴⁸	-	81 ⁴⁷⁵	70 ⁹	(122) ⁵⁶²	(119) ⁵⁶⁰	-	-	-	-	-
63	First Credit Bureau Kazakhstan	KZ	firstcreditkz	001	2022-11-22	548	24	24 ²⁸⁸	-	188 ⁷⁹⁹	6 ²	(20) ⁴⁶	(18) ⁴⁶	(16) ⁸⁷	(16) ¹⁷⁹	(16) ³⁵⁴	(72) ^{0.03N^{1.0}}	
64	Fujitsu Research and Development Center	CN	fujitsulab	000	2021-10-12	497	337	69 ¹⁰³²	-	254 ⁹⁴⁵	35 ⁵	(195) ¹⁶⁶⁸	(193) ¹⁶⁵⁷	(167) ³¹⁴⁰	(164) ⁶³²⁰	(163) ¹²⁷²³	(102) ^{0.78N^{1.0}}	
65	Fujitsu Research and Development Center	CN	fujitsulab	001	2022-03-15	675	386	68 ¹⁰³²	-	225 ⁸⁸²	71 ⁹	(202) ¹⁸⁵⁴	(203) ¹⁸¹⁷	(172) ³⁴⁵¹	(170) ⁶⁹⁸⁶	(171) ¹⁴¹⁶⁶	(122) ^{0.72N^{1.0}}	
66	Gorilla Technology	TW	gorilla	2	2018-10-29	91	1252	85 ¹¹³²	k	38 ³³⁸	204 ²⁴	(39) ¹⁴⁵	(40) ¹⁴⁶	(33) ²⁹³	(32) ⁶¹²	(30) ¹⁵⁰⁹	(176) ^{0.02N^{1.1}}	
67	Gorilla Technology	TW	gorilla	3	2018-10-26	94	1252	234 ²¹⁵⁶	k	97 ⁵⁵⁹	265 ¹²⁰²⁰	-	(110) ²⁰⁴⁷	-	-	-	-	-
68	Gorilla Technology	TW	gorilla	004	2020-01-06	182	1244	235 ²¹⁹²	k	53 ³⁸⁸	23 ⁴¹	(74) ²⁸⁶	(72) ²⁸⁵	(99) ¹¹⁹¹	(101) ²⁴¹⁶	(95) ⁵⁰³⁶	(221) ^{0.00N^{1.3}}	
69	Gorilla Technology	TW	gorilla	005	2021-02-22	306	1420	271 ⁶²⁸⁸	-	85 ⁴⁸³	249 ⁷⁸	(143) ⁸⁰²	(143) ⁷⁹⁹	(118) ¹⁵¹⁴	(135) ⁴⁴⁵⁴	(129) ⁸⁸²⁰	(20) ^{0.05N^{1.2}}	
70	Gorilla Technology	TW	gorilla	006	2021-09-30	377	691	274 ⁸³³⁶	-	175 ⁷⁶⁷	25 ⁹⁹	(191) ¹⁶²⁶	(190) ¹⁶¹²	(146) ²⁴²²	(134) ⁴⁴²²	(134) ⁹³⁶³	(101) ^{0.59N^{1.0}}	
71	Gorilla Technology	TW	gorilla	007	2022-02-16	392	322	272 ⁶²⁹⁰	-	93 ⁵²⁶	252 ⁸⁹	(141) ⁷⁶⁵	(137) ⁷⁴⁵	(112) ¹⁴⁰⁸	(112) ²⁸²³	(105) ⁵⁷⁶⁴	(80) ^{0.42N^{1.0}}	
72	Gorilla Technology	TW	gorilla	008	2022-10-31	321	290	265 ⁴²⁴²	-	250 ⁹³⁸	24 ⁵⁴	(111) ⁵¹³	(107) ⁵⁰⁰	(84) ⁹⁴⁹	(99) ²⁴⁰²	(108) ⁶⁰⁰⁶	(204) ^{0.03N^{1.2}}	
73	Griaule	US	griaule	000	2021-11-01	0	584	201 ²⁰⁵²	-	63 ⁴¹⁷	52 ⁸	(250) ⁵⁸²⁷	(254) ⁶¹⁵⁰	(215) ¹¹⁴⁷³	(212) ²²⁹⁵²	(209) ⁴⁶⁰⁷⁰	(42) ^{3.89N^{1.0}}	
74	Griaule	US	griaule	001	2022-07-26	0	615	210 ²⁰⁵²	-	274 ¹¹⁰²	10 ¹²	(251) ⁵⁸⁶⁶	(255) ⁶¹⁸¹	(217) ¹¹⁶²⁹	(213) ²³¹⁷⁵	(210) ⁴⁶⁵⁰⁴	(60) ^{3.74N^{1.0}}	
75	Guangzhou Pixel Solutions Co Ltd	CN	pixelall	002	2019-07-01	0	165	239 ²⁵⁶⁰	k	14 ¹⁹⁰	16 ¹⁵	(179) ¹²⁹⁶	(181) ¹³³⁴	(153) ²⁵²⁶	(148) ⁵¹³⁶	(152) ¹¹⁰⁴⁵	(128) ^{0.52N^{1.0}}	
76	Guangzhou Pixel Solutions Co Ltd	CN	pixelall	003	2019-11-05	0	690	238 ²⁵⁶⁰	k	150 ⁷⁰³	201 ²²	(176) ¹²⁷³	(177) ¹³⁰⁷	(150) ²⁴⁷⁴	(149) ⁵¹⁹⁸	(153) ¹¹⁴¹	(141) ^{0.46N^{1.0}}	
77	Guangzhou Pixel Solutions Co Ltd	CN	pixelall	004	2020-07-02	0	538	237 ²⁵⁶⁰	k	69 ⁴⁴⁹	18 ¹⁷	(179) ¹²⁵⁹	(130) ¹³⁰⁰	(149) ²⁴⁶⁵	(155) ⁵⁴⁹²	(154) ¹¹⁴⁴³	(155) ^{0.34N^{1.1}}	
78	Guangzhou Pixel Solutions Co Ltd	CN	pixelall	005	2021-03-23	0	717	236 ²⁵⁶⁰	-	205 ⁸⁴⁰	101 ¹¹	(188) ¹⁶⁰⁶	(188) ¹⁵²⁸	(155) ²⁶⁰⁹	(145) ⁴⁹²⁶	(157) ¹¹⁷⁷⁰	(92) ^{0.73N^{1.0}}	
79	Hangzhou Allu Network Information Technology	CN	hzailu	000	2022-03-18	855	97	60 ¹⁰²⁴	-	124 ⁶⁴⁹	10 ¹¹	(222) ²⁶⁰⁹	(226) ²⁵⁵¹	(196) ⁴⁸¹³	(194) ⁹⁷⁰²	(193) ¹⁹³³⁸	(70) ^{1.50N^{1.0}}	
80	Hangzhou Allu Network Information Technology	CN	hzailu	001	2022-08-18	273	162	169 ²⁰⁴⁸	-	180 ⁷⁷⁷	108 ¹²	(237) ⁴⁵³⁷	(243) ⁴⁶³⁷	(208) ⁸⁶⁶⁶	(206) ⁸⁶⁶⁶	(205) ³⁹⁸⁰⁵	(130) ^{1.79N^{1.0}}	
81	Hangzhou Allu Network Information Technology	CN	hzailu	002	2023-01-12	302	293	176 ²⁰⁴⁸	-	209 ⁷⁷⁷	11 ¹²	(238) ⁴⁵⁷⁹	(244) ⁴⁶⁵²	(202) ⁸⁷⁰⁵	(206) ⁷¹⁹²	(206) ³⁹⁸⁶⁴	(127) ^{1.82N^{1.0}}	
82	Hikvision Research Institute	CN	hikvision	5	2018-10-29	593	9	92 ¹⁴⁰⁸	1	108 ⁶⁰⁷	168 ¹⁶	(154) ⁸⁸³	(154) ⁸⁹⁵	(131) ¹⁹⁰⁸	(125) ³⁷⁹²	(136) ⁹³⁸⁷	(187) ^{0.10N^{1.1}}	
83	Hikvision Research Institute	CN	hikvision	6	2018-10-29	593	9	91 ¹⁴⁰⁸	1	106 ⁵⁹⁸	17 ¹⁶	(152) ⁸⁷¹	(153) ⁸⁷⁷	-	-	-	-	-
84	HyperVerge Inc	IN	hyperverge	001	2021-08-11	1791	212	62 ¹⁰²⁴	-	208 ⁸⁴⁵	31 ⁵	(130) ⁷⁰⁵	(130) ⁶⁸¹	(106) ¹³⁴⁶	(108) ²⁶⁸¹	(103) ⁵⁶⁸⁰	(112) ^{0.32N^{1.0}}	
85	HyperVerge Inc	IN	hyperverge	002	2022-04-13	1140	1118	61 ¹⁰²⁴	-	246 ⁹³⁴	75 ⁹	(130) ⁶⁶¹	(129) ⁶⁵⁹	(103) ¹²⁹²	(93) ²¹⁸⁸	(49) ²¹⁸¹	(19) ^{11.29N^{0.8}}	
86	Idemia	FR	idemia	5	2018-10-29	417	48	28 ³⁵²	1	48 ³⁷¹	32 ⁵	(35) ¹³⁷	(37) ¹³⁸	(41) ⁴³⁷	(37) ⁷²⁴	(38) ¹⁶³⁰	(213) ^{0.01N^{1.2}}	
87	Idemia	FR	idemia	6	2018-10-29	417	48	30 ³⁵²	1	47 ³⁷⁰	29 ⁴	(36) ¹³⁷	(36) ¹³⁸	(42) ⁴⁴²	(42) ⁸²⁷	(39) ¹⁶⁴⁶	(215) ^{0.01N^{1.2}}	
88	Idemia	FR	idemia	007	2020-01-17	738	113	98 ⁸⁶⁰	1	186 ⁷⁹⁴	145 ¹⁴	(40) ¹⁵¹	(41) ¹⁵²	(67) ⁶⁸³	(71) ¹⁴⁸¹	(68) ³⁰²²	(226) ^{0.00N^{1.4}}	
89	Idemia	FR	idemia	008	2021-03-15	378	65	28 ³⁰⁰	-	71 ⁴⁵¹	19 ³	(34) ¹³²	(35) ¹³¹	(30) ²⁴⁷	(29) ⁵⁰¹	(28) ¹⁰¹³	(83) ^{0.07N^{1.0}}	
90	Idemia	FR	idemia	009	2022-03-01	735	68	36 ⁶³⁶	-	220 ⁸⁷³	44 ⁷	(32) ²¹¹	(31) ²⁰⁵	(40) ³⁸⁹	(41) ⁷⁸⁷	(37) ¹⁶¹⁵	(107) ^{0.10N^{1.0}}	
91	Idemia	FR	idemia	010	2023-01-11	942	71	27 ³⁰⁰	-	259 ⁹⁵⁶	11 ²	(50) ¹⁹⁴	(48) ¹⁹⁵	(37) ³⁶⁹	(38) ⁷³²	(34) ¹⁴⁸⁸	(71) ^{0.11N^{1.0}}	
92	Imagus Technology Pty Ltd	AU	imagus	005	2021-01-15	222	311	127 ²⁰⁴⁸	-	183 ⁷⁸⁶	143 ¹⁴	(55) ²³⁶	(77) ³¹³	(64) ⁶⁵¹	(66) ¹³⁶¹	(54) ²⁴⁶¹	(185) ^{0.03N^{1.1}}	
93	Imagus Technology Pty Ltd	AU	imagus	006	2021-05-27	248	369	110 ²⁰⁴⁸	-	236 ⁹⁰⁴	89 ⁵	(79) ³¹⁷	(54) ²³⁴	(50) ⁴⁹⁹	(63) ¹²⁷³	(58) ²⁷²⁷	(210) ^{0.01N^{1.2}}	
94	Imagus Technology Pty Ltd	AU	imagus	007	2021-11-16	248	366	132 ²⁰⁴⁸	-	109 ⁶⁰⁹	65 ⁹	(54) ²³⁴	(53) ²³⁸	(43) ⁴⁴²	(43) ⁸⁸¹	(41) ¹⁷⁶⁵	(35) ^{0.16N^{1.0}}	
95	Imagus Technology Pty Ltd	AU	imagus	008	2022-05-26	204	335	180 ²⁰⁴⁸	-	68 ⁴⁴⁵	181 ¹⁷	(120) ⁵⁶⁶	(122) ⁵⁶⁵	-	-	-	-	
96	Imperial College London	GB	imperial	000	2019-08-28	461	15	179 ²⁰⁴⁸	1	102 ⁵⁷⁷	117 ¹³	(85) ³⁶⁰	(91) ³⁷⁹	(122) ¹⁶²⁶	(129) ⁴⁰⁵⁷	(130) ¹⁰²⁹¹	(229) ^{0.00N^{1.5}}	
97	Incode Technologies Inc	US	incode	2	2018-10-29	71	31	133 ²⁰⁴⁸	1	30 ²⁸⁹	167 ¹⁵	(95) ⁴¹¹	(94) ⁴⁰⁴	-	-	-	-	
98	Incode Technologies Inc	US	incode	3	2018-10-29	133	31	167 ²⁰⁴⁸	1	148 ⁶⁹⁷	157 ¹⁵	(94) ⁴⁰⁸	(97) ⁴¹²	(75) ⁸⁴⁷	(75) ¹⁶⁰⁸	(88) ⁴⁴⁸⁶	(180) ^{0.05N^{1.1}}	
99	Incode Technologies Inc	US	incode	004	2019-06-24	254	5											

	DEVELOPER FULL NAME	DEVELOPER LOCATION	SHORT NAME	SEQ. NUM.	VALIDATION DATE	CONFIG ¹ DATA (MB)	LIB ¹ DATA (MB)	TEMPLATE GENERATION SIZE (B) MULT ³ TIME (MS) ⁴	FINALIZE ² TIME (S)	SEARCH DURATION ⁵ MILLISEC						
										N=1.6M	N=1.6M	L=1	N=1.6M	L=50	N=12M	POWER LAW (μ s)
105	Intellivision	IN	intellivision	001	2022-03-08	62	130	222 2056 -	60 406	192 20	(89) 388	(89) 377	-	-	-	-
106	Intellivision	IN	intellivision	002	2022-07-28	114	128	225 2056 -	34 331	123 13	(266) 20542	(271) 20448	-	-	-	-
107	Intema-LGL Group	LU	intema	000	2022-08-24	1042	20	36 512 -	166 737	269 13809	(15) 27	(13) 31	(10) 36	(12) 44	(10) 54	11 791.50 N ^{0.3}
108	Intema-LGL Group	LU	intema	001	2023-02-22	723	20	31 512 -	251 938	260 4808	(14) 26	(9) 26	(14) 49	(13) 57	(11) 66	13 220.53 N ^{0.4}
109	IrexAI	US	irex	000	2021-02-09	724	46	240 3080 -	207 844	191 19	(127) 616	(124) 600	(94) 1120	(103) 2477	(106) 5863	160 0.13 N ^{1.1}
110	Kakao Enterprise	KR	kakao	000	2021-06-23	404	124	202 2052 -	204 835	54 8	(53) 213	(52) 215	(51) 510	(49) 971	(46) 1955	164 0.05 N ^{1.1}
111	Kakao Enterprise	KR	kakao	001	2022-06-08	615	102	170 2048 -	263 961	185 18	(103) 469	(103) 471	(86) 952	(87) 1887	(80) 3870	157 0.11 N ^{1.1}
112	Kedacom International Pte	SG	kedacom	001	2019-09-16	239	36	292 1 -	90 507	8 2	(140) 764	(140) 760	(132) 1940	(116) 2983	(117) 6623	135 0.31 N ^{1.0}
113	Kneron	US	kneron	000	2020-03-03	366	13	177 2048 k	92 523	122 13	(221) 2535	(224) 2506	(195) 4752	(193) 9696	(195) 20926	136 0.95 N ^{1.0}
114	Kneron	US	kneron	001	2021-06-10	270	69	123 2048 -	80 472	72 9	(223) 2690	(227) 2642	-	-	-	-
115	Line Corporation	JP	line	000	2021-06-02	138	397	114 2048 -	83 481	59 8	(249) 5433	(249) 5418	(212) 10144	-	-	39 3.65 N ^{1.0}
116	Line Corporation	JP	line	001	2021-11-21	471	396	163 2048 -	240 907	60 8	(203) 1872	(207) 1934	(176) 3647	(179) 7675	-	143 0.64 N ^{1.0}
117	Line Corporation	JP	lineclova	002	2022-07-29	560	72	155 2048 -	197 824	127 13	(63) 262	(64) 257	(49) 488	(51) 977	(47) 1963	73 0.15 N ^{1.0}
118	Line Corporation	JP	lineclova	003	2023-01-19	574	397	168 2048 -	189 799	45 7	(42) 158	(33) 103	(48) 487	(50) 972	(60) 2731	216 0.01 N ^{1.2}
119	Lomonosov Moscow State University	RU	intsysmsu	000	2019-08-19	375	168	137 2048 1	111 614	129 13	(98) 430	(100) 431	(78) 860	(79) 1730	(98) 5353	195 0.03 N ^{1.1}
120	Lookman Electroplast Industries	IN	lookman	3	2018-10-28	203	24	25 292 1	37 336	17 3	(138) 739	(136) 745	(110) 1394	(111) 2817	(124) 8286	173 0.13 N ^{1.1}
121	Lookman Electroplast Industries	IN	lookman	4	2018-10-28	184	24	51 548 1	33 320	28 4	(158) 981	(159) 998	-	-	-	-
122	Lookman Electroplast Industries	IN	lookman	005	2019-09-16	239	36	52 548 1	88 506	24 4	(160) 1005	(161) 1008	(154) 2597	(153) 5446	(130) 8939	171 0.19 N ^{1.1}
123	Mantra Softech India	IN	mantra	000	2021-10-28	460	61	200 2052 -	62 412	89 10	(156) 916	(156) 910	(126) 1714	(124) 3411	(120) 6841	46 0.57 N ^{1.0}
124	Maxvision	CN	maxvision	000	2022-06-17	167	60	182 2048 -	11 183	275 -	(243) 5044	(247) 5188	(211) 9663	(210) 19358	(204) 39552	103 2.41 N ^{1.0}
125	Maxvision	CN	maxvision	001	2022-10-28	228	63	117 2048 -	73 457	126 13	(170) 1173	(170) 1177	(140) 2233	(139) 4589	(139) 9371	86 0.65 N ^{1.0}
126	Megvii/Face++	CN	megvii	1	2018-10-28	1703	41	255 4096 1	116 631	223 32	(117) 552	(120) 561	(102) 1222	(98) 2321	(107) 5968	179 0.08 N ^{1.1}
127	Megvii/Face++	CN	megvii	2	2018-10-28	1735	42	254 4096 1	119 635	221 31	(118) 553	(117) 558	-	-	-	-
128	MicroFocus	GB	microfocus	5	2018-10-29	94	26	17 256 k	26 262	12 2	(47) 182	(46) 186	(36) 354	(36) 708	(32) 1425	75 0.11 N ^{1.0}
129	MicroFocus	GB	microfocus	6	2018-10-29	94	26	11 256 k	25 262	14 2	(48) 183	(45) 186	-	-	-	-
130	Microsoft	US	microsoft	5	2018-10-29	381	155	63 1024 1	127 658	104 11	(187) 1606	(194) 1673	(166) 3076	(163) 6302	(168) 13160	99 0.79 N ^{1.0}
131	Microsoft	US	microsoft	6	2018-10-29	478	155	59 1024 1	132 671	161 15	(192) 1642	(192) 1618	(180) 3710	(166) 6401	(165) 12892	120 0.68 N ^{1.0}
132	Mukh Technologies	US	mukh	002	2022-09-16	693	442	165 2048 -	275 1278	259 4261	(4) 5	(20) 83	(17) 106	(17) 313	(17) 628	31 0.07 N ^{1.0}
133	N-Tech Lab	RU	rtech	5	2018-10-30	1685	113	103 1940 k	156 711	243 55	(59) 243	(60) 246	(53) 538	(54) 1100	(62) 2867	191 0.02 N ^{1.1}
134	N-Tech Lab	RU	rtech	6	2018-10-30	1686	117	104 1940 k	203 831	246 63	(58) 243	(59) 246	(55) 546	(55) 1104	(63) 2873	193 0.02 N ^{1.1}
135	N-Tech Lab	RU	rtechlab	007	2019-06-25	2450	51	242 3348 k	187 795	248 73	(91) 393	(98) 427	(72) 780	(82) 1768	(77) 3499	133 0.16 N ^{1.0}
136	N-Tech Lab	RU	rtechlab	008	2020-01-06	1111	51	90 1300 k	96 554	230 36	(46) 179	(43) 184	(35) 341	(34) 683	(31) 1395	62 0.11 N ^{1.0}
137	N-Tech Lab	RU	rtechlab	009	2021-03-01	1208	42	244 899	229 35	(45) 178	(44) 184	(34) 336	(34) 676	(40) 1704	154 0.05 N ^{1.1}	
138	N-Tech Lab	RU	rtechlab	010	2021-06-24	351	213	88 1280 -	221 874	36 6	(99) 440	(101) 435	(74) 821	(76) 1645	(72) 3337	93 0.22 N ^{1.0}
139	N-Tech Lab	RU	rtechlab	011	2021-12-07	679	208	87 1280 -	215 864	39 6	(106) 488	(105) 483	(82) 912	(86) 1869	(92) 5003	175 0.07 N ^{1.1}
140	NEC	JP	nec	2	2018-10-30	705	35	99 1616 k	123 642	188 18	(92) 405	(95) 409	(92) 1072	(80) 1755	(87) 4255	182 0.06 N ^{1.1}
141	NEC	JP	nec	3	2018-10-30	774	110	100 1712 k	130 665	196 21	(5) 7	(3) 7	(5) 14	(9) 40	(12) 82	202 0.00 N ^{1.2}
142	NEC	JP	nec	004	2021-07-19	971	63	83 1104 -	264 965	40 7	(82) 349	(83) 351	(65) 662	(64) 1330	(56) 2685	78 0.20 N ^{1.0}
143	NEC	JP	nec	005	2021-12-13	922	88	84 1104 -	262 961	41 7	(104) 473	(115) 551	(90) 1017	(91) 2091	(85) 4242	90 0.28 N ^{1.0}
144	NEC	JP	nec	006	2022-08-10	701	54	82 1104 -	248 937	69 9	(83) 358	(84) 354	(66) 666	(65) 1331	(57) 2707	64 0.21 N ^{1.0}
145	NEC	JP	nec	007	2023-03-03	632	56	58 560 -	272 987	37 6	(51) 200	(49) 200	(38) 375	(39) 752	(36) 1527	56 0.12 N ^{1.0}
146	Neurotechnology	LT	neurotech	5	2018-10-30	266	53	18 256 k	55 402	132 14	(147) 835	(149) 839	(125) 1690	(122) 3219	(131) 8955	161 0.19 N ^{1.1}
147	Neurotechnology	LT	neurotech	6	2018-10-30	564	53	14 256 k	161 726	10 2	(148) 839	(150) 842	-	-	-	-
148	Neurotechnology	LT	neurotech	007	2019-10-03	57	51	18 256 k	7 161	9 2	(166) 1118	(166) 1110	(138) 2143	(133) 4397	(132) 9045	98 0.55 N ^{1.0}
149	Neurotechnology	LT	neurotechnology	008	2021-03-22	355	49	46 514 -	190 800	27 4	(169) 1167	(169) 1149	(141) 2266	(138) 4573	(140) 9586	108 0.55 N ^{1.0}
150	Neurotechnology	LT	neurotechnology	009	2021-09-01	246	82	41 513 -	139 683	15 3	(163) 1035	(163) 1049	(134) 1977	(131) 4270	(127) 8756	147 0.32 N ^{1.1}
151	Neurotechnology	LT	neurotechnology	010	2022-01-07	247	83	13 256 -	129 661	3 2	(159) 988	(157) 984	(129) 1897	(128) 3977	(123) 8048	138 0.36 N ^{1.0}
152	Neurotechnology	LT	neurotechnology	012	2022-06-07	247	84	14 256 -	141 686	16 3	(164) 1036	(165) 1063	(135) 2046	(130) 4179	(126) 8624	134 0.41 N ^{1.0}
153	Neurotechnology	LT	neurotechnology	013	2023-02-03	364	87	15 256 -	267 970	4 2	(249) 5779	(248) 5231	(214) 10886	(220) 27551	(221) 76318	219 0.05 N ^{1.3}
154	Newland Computer Co Ltd	CN	newland	2	2018-10-30	96	27	120 2048 -	212 855	163 15	(262) 8741	(267) 8854	(229) 17892	(227) 39356	-	177 1.32 N ^{1.1}
155	Nobilis	US	nobilis	1	2018-10-30	114	176	187 2048 1	18 206	159 15	(177) 1273	(174) 1272	-	-	-	-
156	Nobilis	US	nobilis	2	2018-10-30	153	176	266 6144 1	91 517	235 43	(220) 2513	(225) 2522	(197) 5649	(198) 12432	(208) 44262	218 0.04 N ^{1.3}

Notes

- Configuration size does not capture static data present in libraries. Libraries are included but the size also includes any ancillary libraries for image processing (e.g. openCV) or numerical computation (e.g. blas).
- Finalization is the processing of converting $N = 1600000$ templates into a searchable data structure an operation which can be a simple copy, or the building of an index or tree, for example. The duration of the operation may be data dependent, and may not be linear in the number of input templates.
- This multiplier expresses the increase in template size when k images are passed to the template generation function.
- All durations are measured on Intel®Xeon®@CPU E5-2630 v4 @ 2.20GHz processors. Estimates are made by wrapping the API function call in calls to std::chrono::high_resolution_clock which on the machine in (3) counts 1ns clock ticks. Precision is somewhat worse than that however.
- Search durations are measured as in the prior note. The power-law model in the final column mostly fits the empirical results in Figure 151. However in certain cases the model is not correct and should not be used numerically.

	DEVELOPER	DEVELOPER	SHORT	SEQ.	VALIDATION	CONFIG ¹	LIB ¹	TEMPLATE GENERATION			FINALIZE ²		SEARCH DURATION ³ MILLISEC														
								LOCATION	NAME	NUM.	DATE	DATA (MB)	DATA (MB)	SIZE (B)	MULT ³	TIME (MS) ⁴	TIME (S)	L=1	L=50	L=50	L=50	L=50	POWER LAW (μ s)				
N=1.6M	N=1.6M	N=1.6M	N=3M	N=6M	N=12M																						
157	NotionTag Technologies Private Limited	IN	notiontag	000	2022-01-14	265	945	233	2120	-	72	453	93	10	(261)	8619	(266)	8705	(228)	16652	(226)	38794	(223)	90607	181		
158	Pangiam	US	pangiam	000	2022-02-22	453	23	162	2048	-	120	636	182	17	(67)	276	(78)	319	(60)	601	(60)	1210	(53)	2443	76		
159	Pangiam	US	pangiam	001	2022-11-17	991	36	172	2048	-	265	966	141	14	(66)	275	(29)	323	(80)	885	(83)	1771	(78)	3592	208		
160	Paravision (EverAI)	US	everai	2	2018-10-30	224	304	138	2048	1	43	366	218	30	(69)	278	(71)	283	-	-	-	-	-	-	-		
161	Paravision (EverAI)	US	everai	3	2018-10-30	438	304	149	2048	1	158	717	211	28	(70)	281	(57)	572	(56)	1146	(50)	2278	123	0.12N ^{1.0}			
162	Paravision (EverAI)	US	everai-paravision	004	2019-06-19	527	128	241	4096	1	133	672	288	45	(119)	559	(118)	559	(156)	2611	(168)	6445	(172)	14519	227	0.00N ^{1.5}	
163	Paravision (EverAI)	US	paravision	005	2019-12-11	543	154	252	4096	1	202	830	240	48	(121)	561	(121)	564	(91)	1056	(95)	2298	(91)	4966	151	0.16N ^{1.1}	
164	Paravision (EverAI)	US	paravision	007	2021-02-01	529	235	250	4096	-	150	701	241	48	(123)	569	(116)	558	(93)	1086	(92)	2111	(86)	4254	26	1.11N ^{0.9}	
165	Paravision	US	paravision	009	2021-12-14	672	300	257	4100	-	115	631	250	82	(234)	3690	(239)	4230	(205)	8037	(204)	16532	(200)	31422	125	1.62N ^{1.0}	
166	Paravision	US	paravision	012	2023-02-07	762	182	258	4100	-	206	826	251	85	(236)	4475	(241)	4466	(207)	8552	(208)	17349	(201)	33950	132	1.66N ^{1.0}	
167	Qnap Security	TW	qnap	000	2021-07-28	182	15	193	2048	-	74	457	77	9	(172)	1231	(200)	1763	-	-	-	-	-	-	-		
168	Qnap Security	TW	qnap	001	2021-12-09	191	13	119	2048	-	110	613	58	9	(194)	1666	(189)	1429	(173)	3472	(176)	7375	(179)	15159	199	0.11N ^{1.2}	
169	Qnap Security	TW	qnap	002	2022-04-15	338	32	181	2048	-	196	822	179	17	(157)	958	(171)	1179	(143)	2312	(142)	4789	(147)	6791	163	0.24N ^{1.1}	
170	Qnap Security	TW	qnap	003	2022-12-09	239	60	136	2048	-	52	387	138	13	(196)	1671	(183)	1396	(175)	3567	(175)	7350	(177)	15014	207	0.09N ^{1.2}	
171	Quantasoft	CZ	quantasoft	1	2018-10-30	276	452	128	2048	k	51	385	36	6	(264)	15422	(289)	14858	(226)	14717	-	(185)	18323	-	-	-	
172	Rank One Computing	US	rankone	4	2018-10-09	0	101	185	k	3	36	42	7	(30)	101	(32)	101	(26)	190	-	-	-	-	-	36	0.07N ^{1.0}	
173	Rank One Computing	US	rankone	5	2018-10-24	0	101	6	133	k	4	92	43	7	(37)	140	(38)	144	(31)	266	(30)	525	(29)	1049	33	0.11N ^{1.0}	
174	Rank One Computing	US	rankone	006	2019-06-03	0	133	7	165	k	23	245	53	8	-	-	-	-	-	-	-	-	-	-	-		
175	Rank One Computing	US	rankone	007	2019-11-12	0	137	8	165	k	28	272	47	7	(33)	116	(34)	115	(28)	215	(28)	439	(26)	877	74	0.07N ^{1.0}	
176	Rank One Computing	US	rankone	009	2020-06-26	0	105	18	260	k	15	185	100	11	(24)	95	(27)	96	(21)	181	(21)	362	(22)	727	49	0.06N ^{1.0}	
177	Rank One Computing	US	rankone	010	2020-11-05	0	135	23	261	-	16	198	94	10	(25)	95	(22)	95	(19)	178	(19)	357	(20)	714	44	0.06N ^{1.0}	
178	Rank One Computing	US	rankone	011	2021-08-27	0	175	20	261	-	100	566	61	8	(27)	95	(24)	95	(22)	183	(22)	370	(19)	714	59	0.06N ^{1.0}	
179	Rank One Computing	US	rankone	012	2021-12-27	0	257	22	261	-	99	563	48	9	(26)	95	(25)	95	(20)	179	(20)	361	(21)	718	47	0.06N ^{1.0}	
180	Rank One Computing	US	rankone	013	2022-07-21	0	223	19	261	-	138	679	173	16	(31)	101	(30)	100	(24)	188	(24)	376	(24)	784	25	0.20N ^{0.9}	
181	Rank One Computing	US	rankone	014	2022-12-21	0	237	21	261	-	149	700	51	8	(32)	101	(29)	100	(25)	188	(25)	376	(23)	775	85	0.06N ^{1.0}	
182	Realnetworks Inc	US	realnetworks	2	2018-10-30	105	104	261	4104	k	22	241	210	28	(205)	2008	(211)	2048	(183)	4194	(182)	8642	(178)	15035	91	1.08N ^{1.0}	
183	Realnetworks Inc	US	realnetworks	003	2019-06-12	93	102	101	1848	k	10	173	116	13	(168)	1145	(167)	1132	(137)	2142	(150)	5241	(151)	10495	167	0.21N ^{1.1}	
184	Realnetworks Inc	US	realnetworks	004	2019-10-17	94	102	102	1848	1	9	171	99	11	(167)	1143	(168)	1137	(139)	2149	(141)	4740	(142)	6963	146	0.36N ^{1.0}	
185	Realnetworks Inc	US	realnetworks	005	2021-06-23	168	209	221	2056	-	33	32	69	8	(193)	1654	(191)	1616	(165)	3030	(161)	6068	(160)	12134	54	1.01N ^{1.0}	
186	Realnetworks Inc	US	realnetworks	006	2021-12-02	250	56	215	2056	-	41	348	56	8	(116)	543	(113)	531	(89)	996	(90)	1994	(84)	3991	52	0.33N ^{1.0}	
187	Realnetworks Inc	US	realnetworks	007	2022-04-11	455	99	218	2056	-	118	634	180	17	(146)	815	(146)	812	(119)	1559	(115)	6361	(142)	27N ^{1.0}			
188	Realnetworks Inc	US	realnetworks	008	2022-08-29	557	99	224	2056	-	266	968	109	12	(117)	538	(112)	525	(88)	986	(89)	1967	(101)	5559	168	0.09N ^{1.1}	
189	Recognito	AE	recognito	000	2023-02-17	350	242	242	1280	-	243	924	80	9	(139)	756	(139)	748	(111)	1396	(110)	2788	(93)	5030	38	0.49N ^{1.0}	
190	Remark Holdings	CN	remarkai	000	2019-06-12	234	1092	148	2048	k	125	650	115	12	(248)	5776	(251)	5703	(216)	32133	(224)	91436	(220)	0.05N ^{1.3}			
191	Remark Holdings	CN	remarkai	0	2018-10-30	187	847	158	2048	k	104	593	150	14	(247)	5685	(252)	5723	-	-	-	-	-	-	-		
192	Remark Holdings	CN	remarkai	1	2018-10-30	187	847	147	2048	k	65	427	155	14	(246)	5680	(253)	5761	(220)	12475	(222)	28726	(219)	59618	205	0.37N ^{1.2}	
193	Rendip	SG	rendip	000	2021-05-21	0	416	107	2048	-	229	890	81	9	(60)	249	(86)	368	(69)	697	(70)	1452	(65)	2926	158	0.08N ^{1.1}	
194	Reveal Media Ltd	UK	revealmedia	000	2022-02-02	287	196	207	2052	-	50	383	88	10	(209)	2322	(209)	2019	(182)	3838	(180)	7816	(182)	16559	129	0.78N ^{1.0}	
195	SQISoft	KR	sqisoft	001	2021-12-20	271	377	219	2056	-	77	462	78	9	(180)	1310	(179)	1319	(148)	2456	(144)	4906	(146)	9755	37	0.90N ^{1.0}	
196	SQISoft	KR	sqisoft	002	2022-10-26	354	593	217	2056	-	128	661	125	13	(185)	1480	(186)	1456	(158)	2712	(154)	5487	(161)	12210	121	0.59N ^{1.0}	
197	Samsung S1 Corp	KR	s1	000	2021-06-03	257	196	256	4096	-	216	865	193	20	(257)	6715	(262)	6794	(224)	13032	(219)	26372	(217)	55723	119	2.82N ^{1.0}	
198	Samsung S1 Corp	KR	s1	001	2021-11-01	240	198	131	2048	-	193	813	62	8	(211)	2415	(223)	2491	(193)	4718	(192)	9614	(196)	24472	162	0.53N ^{1.1}	
199	Samsung S1 Corp	KR	s1	002	2022-05-04	244	93	142	2048	-	266	958	169	16	(173)	1234	(179)	1285	(145)	2411	(143)	4805	(147)	9705	63	0.77N ^{1.0}	
200	Samsung S1 Corp	KR	s1	003	2022-09-27	471	93	189	2048	-	269	977	135	13	(190)	1620	(195)	1697	(169)	3187	(165)	6400	(164)	12792	69	0.99N ^{1.0}	
201	Samsung S1 Corp	KR	s1	004	2023-02-03	471	58	154	2048	-	250	955	124	13</													

	DEVELOPER FULL NAME	DEVELOPER LOCATION	SHORT NAME	SEQ. NUM.	VALIDATION DATE	CONFIG ¹ DATA (MB)	LIB ¹ DATA (MB)	TEMPLATE GENERATION SIZE (B) MULT ³ TIME (MS) ⁴	FINALIZE ² TIME (S)	SEARCH DURATION ⁵ MILLISEC							
										L=1		L=50		L=50			
										N=1.6M	N=1.6M	N=1.6M	N=3M	N=6M	N=12M		
209	Sensetime Group	CN	sensetime	005	2020-12-17	631	39	72 1032 - 270 980	98 11	(215) 2459	(237) 3939	(203) 7398	(201) 14768	(191) 19016	22 14.03N ^{0.9}		
210	Sensetime Group	CN	sensetime	006	2021-07-26	526	54	73 1032 - 244 929	48 7	(210) 2414	(218) 2422	(187) 4527	(186) 6128	(186) 18640	81 1.35N ^{1.0}		
211	Sensetime Group	CN	sensetime	007	2022-01-15	526	37	66 1032 - 247 935	63 8	(212) 2432	(216) 2406	(185) 4513	(183) 8998	(189) 18796	89 1.28N ^{1.0}		
212	Sensetime Group	CN	sensetime	008	2022-08-17	567	37	74 1032 - 249 937	74 9	(213) 2444	(217) 2419	(186) 4525	(185) 6114	(184) 18279	68 1.43N ^{1.0}		
213	Sensetime Group	CN	sensetime	009	2023-01-04	883	59	70 1032 - 277 994	64 9	(214) 2446	(215) 2398	(188) 4540	(184) 9040	(183) 18167	67 1.42N ^{1.0}		
214	Shaman Software	US	shaman	6	2018-10-26	0	200	164 2048	k	151 706	131 14	(126) 603	(125) 612	-	-		
215	Shaman Software	US	shaman	7	2018-10-26	0	200	147 2048	k	150 707	154 14	(125) 602	(126) 614	(97) 1187	(102) 2448	(97) 5083	124 0.25N ^{1.0}
216	Shanghai Yitu Technology	CN	yitu	4	2018-10-30	2119	136	230 2070	1	233 897	237 45	(178) 1288	(173) 1203	(147) 2440	(151) 5241	(142) 9671	118 0.52N ^{1.0}
217	Shanghai Yitu Technology	CN	yitu	5	2018-10-30	2043	136	229 2070	1	219 853	236 44	(174) 1237	(172) 1199	(152) 2513	(146) 5013	(141) 9620	114 0.55N ^{1.0}
218	Smilart	DE	smilart	4	2018-10-30	65	89	42 512	k	8 167	26 4	(265) 16137	(270) 15633	-	-		
219	Smilart	DE	smilart	5	2018-10-30	562	89	12 2048	k	70 450	148 14	-	-	-	-		
220	Staqu Technologies	IN	st aqu	000	2021-08-30	1018	690	248 4096	-	199 826	205 24	(242) 4950	(245) 4933	-	-		
221	Synesis	RU	synesis	3	2018-10-30	237	150	246 4096	k	59 99	214 29	(142) 789	(144) 801	(133) 1941	(127) 3888	(128) 8810	192 0.07N ^{1.1}
222	Synesis	RU	synesis	003	2019-07-04	143	17	113 2048	k	19 211	110 12	(110) 507	(110) 502	(142) 2297	(137) 4564	(137) 9452	225 0.00N ^{1.4}
223	Synesis	RU	synesis	005	2020-09-08	494	24	260 4104	-	171 756	203 24	(153) 877	(151) 865	(168) 3182	(140) 4658	(145) 9750	209 0.06N ^{1.2}
224	T4iSB	BR	t4isb	000	2022-08-17	228	15	130 2048	-	168 741	131 13	(61) 250	(62) 250	-	-		
225	Tech5 SA	CH	tech5	001	2019-08-19	1394	116	93 1536	k	228 887	87 10	(87) 383	(141) 766	(159) 2767	(162) 6149	(111) 6178	183 0.12N ^{1.1}
226	Tech5 SA	CH	tech5	002	2021-04-07	727	112	45 513	-	259 940	24 4	(240) 4682	(260) 6689	(221) 12541	(216) 25145	(214) 50239	51 4.18N ^{1.0}
227	Tencent Deepsea Lab	CN	deepsea	001	2019-07-29	250	323	151 2048	1	167 737	113 12	(162) 1021	(162) 1020	(160) 2774	(158) 5767	(162) 12341	214 0.06N ^{1.2}
228	Tevian	RU	tevian	5	2018-10-30	773	15	130 2048	1	59 405	160 15	(93) 405	(94) 408	(76) 854	(81) 1757	(76) 3380	145 0.14N ^{1.0}
229	Tevian	RU	tevian	006	2021-04-16	769	19	71 1032	-	105 597	86 10	(76) 295	(74) 295	(58) 578	(58) 1187	(61) 2741	159 0.06N ^{1.1}
230	Tevian	RU	tevian	007	2021-10-12	703	19	79 1032	-	178 777	30 4	(77) 297	(75) 298	(59) 579	(57) 1179	(52) 2418	137 0.11N ^{1.0}
231	Thales Group	US	cogent	2	2018-10-30	681	39	79 1043	k	256 945	208 27	(206) 2017	(213) 2144	(184) 4298	(181) 8472	(181) 16429	96 1.08N ^{1.0}
232	Thales Group	US	cogent	3	2018-10-30	681	39	78 1043	k	252 940	83 9	(171) 1230	(178) 1311	(157) 2687	(152) 5398	(149) 10184	109 0.62N ^{1.0}
233	Thales Group	US	cogent	004	2021-02-10	1376	59	214 2053	-	256 947	140 14	(224) 2903	(205) 1911	(174) 3566	(177) 7498	(180) 16370	144 0.64N ^{1.0}
234	Thales Group	US	cogent	005	2021-09-13	1043	56	80 1062	-	176 769	34 5	(155) 912	(158) 996	(128) 1872	(126) 3845	(121) 7555	111 0.44N ^{1.0}
235	Thales Group	US	cogent	006	2022-05-14	508	70	54 550	-	208 843	58 8	(124) 587	(142) 820	(120) 1564	(126) 3173	(125) 8290	166 0.16N ^{1.1}
236	Thales Group	US	cogent	007	2023-01-30	597	72	53 550	-	271 984	20 3	(149) 843	(152) 868	(123) 1631	(177) 1649	(174) 3341	17 25.73N ^{0.7}
237	TigerIT Americas LLC	US	tiger	2	2018-10-29	416	518	196 2052	k	76 461	164 15	(201) 1816	(206) 1921	(181) 3833	(178) 7526	(179) 14820	116 0.83N ^{1.0}
238	TigerIT Americas LLC	US	tiger	3	2018-10-30	416	518	209 2052	k	76 461	273 37431	(49) 191	(47) 189	-	-	-	-
239	Toshiba	JP	toshiba	0	2018-10-30	961	105	98 1548	k	227 876	105 12	(254) 6153	(256) 6236	(218) 12221	(217) 25355	(213) 49448	200 0.36N ^{1.2}
240	Toshiba	JP	toshiba	1	2018-10-30	961	105	227 2060	k	227 875	274 44701	(253) 6007	(256) 6355	-	-	-	-
241	Tripleize	JP	aize	001	2021-08-06	262	150	157 2048	-	56 402	79 9	(228) 3087	(231) 3080	-	-	-	-
242	Trueface.ai	US	trueface	000	2021-01-27	247	119	105 2000	-	42 363	119 13	(64) 271	(82) 327	(62) 614	(61) 1239	(55) 2678	106 0.15N ^{1.0}
243	TuringTech.vip	CN	turingtechvip	001	2022-09-29	151	161	108 2048	-	198 817	137 13	(267) 22085	(222) 22044	-	-	-	-
244	Veridas Digital Authentication Solutions S.L.	ES	veridas	001	2021-03-05	347	875	153 2048	-	219 872	120 13	(245) 5493	(250) 5469	(213) 10350	(211) 20655	(207) 41264	55 3.40N ^{1.0}
245	Veridas Digital Authentication Solutions S.L.	ES	veridas	002	2021-07-06	347	870	193 2048	-	224 877	96 10	(80) 322	(80) 325	(68) 685	(67) 1365	(59) 2730	152 0.09N ^{1.1}
246	Veridas Digital Authentication Solutions S.L.	ES	veridas	003	2021-11-09	346	870	12 2048	-	21 867	66 9	(101) 440	(81) 327	(70) 699	(68) 1401	(83) 3954	203 0.02N ^{1.2}
247	Veridas Digital Authentication Solutions S.L.	ES	veridas	004	2023-02-03	1074	608	143 2048	-	213 856	133 13	(102) 466	(104) 474	(85) 951	(48) 953	(81) 3881	29 0.49N ^{1.0}
248	Verijelas	ID	verijelas	000	2022-10-11	248	11	161 2048	-	36 334	142 14	(9 20)	(10) 27	-	-	-	-
249	Vietnam Posts and Telecommunications Group	VN	vnpt	001	2022-05-05	361	235	175 2048	-	231 892	194 20	(145) 813	(145) 804	(804 117) 1514	(117) 3037	(109) 6128	53 0.50N ^{1.0}
250	Vietnam Posts and Telecommunications Group	VN	vnpt	002	2022-09-08	547	235	112 2048	-	198 808	178 16	(151) 857	(148) 835	(121) 1576	(121) 3183	(116) 6412	88 0.44N ^{1.0}
251	Viettel Group	VN	vts	000	2021-03-12	250	257	183 2048	-	86 492	256 2295	(3) 4	(2) 6	(4) 11	-	15 0.61N ^{0.6}	
252	Viettel Group	VN	vts	001	2021-07-16	352	600	135 2048	-	230 891	199 21	(216) 2477	(222) 2487	(189) 4644	(188) 6313	(188) 18713	57 1.53N ^{1.0}
253	Viettel Group	VN	vts	002	2022-02-08	244	600	159 2048	-	230 903	215 29	(218) 2485	(221) 2485	(189) 4678	(190) 9370	(190) 18833	66 1.49N ^{1.0}
254	Viettel Group	VN	vts	003	2022-07-14	493	468	150 2048	-	151 702	225 34	(217) 2482	(220) 2480	(190) 4649	(187) 9302	(187) 18651	58 1.52N ^{1.0}
255	Vigilant Solutions	US	vigilant	5	2018-10-30	335	122	98 1544	k	176 762	189 19	-	(198) 1720	-	-	-	-
256	Vigilant Solutions	US	vigilant	6	2018-10-30	337	122	95 1544	k	194 816	197 21	-	(197) 1713	-	-	-	-
257	Vigilant Solutions	US	vigilantsolutions	007	2021-01-08	340	51	97 1544	-	116 616	177 16	(183) 1354	(182) 1352	(162) 2911	(160) 5966	(159) 11466	165 0.27N ^{1.1}
258	Vigilant Solutions	US	vigilantsolutions	008	2021-07-23	340	51	94 1544	-	97 403	130 13	(165) 1062	(164) 1061	(144) 2330	(156) 5520	(158) 9499	188 0.11N ^{1.1}
259	Visidon	FI	visidon	1	2018-10-30	166	42	21 2052	k	131 667	166 15	(235) 4370	(242) 4472	(206) 8454	(207) 17262	(202) 34288	87 2.40N ^{1.0}
260	Visidon	FI	vd	002	2021-05-18	248	42	198 2052	-	143 687	67 9	(207) 2089	(214) 2336	-	-	-	-

Notes
 1 Configuration size does not capture static data present in libraries. Libraries are included but the size also includes any ancillary libraries for image processing (e.g. openCV) or numerical computation (e.g. blas).
 2 Finalization is the processing of converting $N = 1600000$ templates into a searchable data structure an operation which can be a simple copy, or the building of an index or tree, for example. The duration of the operation may be data dependent, and may not be linear in the number of input templates.
 3 This multiplier expresses the increase in template size when k images are passed to the template generation function.
 4 All durations are measured on Intel®/Xeon®@CPU E5-2630 v4 @ 2.20GHz processors. Estimates are made by wrapping the API function call in calls to std::chrono::high_resolution_clock which on the machine in (3) counts 1ns clock ticks. Precision is somewhat worse than that however.
 5 Search durations are measured as in the prior note. The power-law model in the final column mostly fits the empirical results in Figure 151. However in certain cases the model is not correct and should not be used numerically.

Table 6: Summary of algorithms and properties included in this report. The blue superscripts give ranking for the quantity in that column. Missing search durations, denoted by “-”, are absent because those runs were not executed, usually because we did not run on the larger galleries. Caution: The power-law model is sometimes an incorrect model. It is included here only to show broad sublinear behavior, which is flagged in green. The models should not be used for prediction.

2023/04/04
07:31:47FNIR(N, R, T) = False neg. identification rate
FPFR(N, T) = False pos. identification rate
N = Num. enrolled subjects
R = Num. candidates examined

T = Threshold

T = 0 → Investigation
T > 0 → Identification

ID	DEVELOPER	DEVELOPER	SHORT	SEQ. NUM.	VALIDATION DATE	CONFIG ¹ DATA (MB)	LIB ¹ DATA (MB)	TEMPLATE GENERATION SIZE (B) MULT ³	FINALIZE ² TIME (S)	SEARCH DURATION ⁵ MILLISEC					POWER LAW (μ s)	
										L=1		L=50		L=50		
										N=1.6M	N=1.6M	N=1.6M	N=3M	N=6M	N=12M	
261	Visidon	FI	vd	003	2021-10-12	497	43	197 2052	-	146 692	57 8	2085	2082	-	-	20.46N ^{0.8}
262	Vision-Box	PT	visionbox	000	2021-09-17	252	274	229 2059	-	84 481	176 16	422	359	855	631	2096
263	VisionLabs	RU	visionlabs	6	2018-10-30	360	17	34 512	1	31 289	270 20290	36	36	39	44	3211.93N ^{0.2}
264	VisionLabs	RU	visionlabs	7	2018-10-30	360	17	37 512	1	29 289	272 34666	21 63	19 63	15 72	15 80	2076.32N ^{0.2}
265	VisionLabs	RU	visionlabs	008	2019-06-18	348	17	32 512	1	27 272	267 12747	23 24	24 26	29 29	33 61N ^{0.2}	
266	VisionLabs	RU	visionlabs	009	2020-08-04	689	20	40 512	-	79 467	268 13245	23 29	9 34	14 61	145 8.88N ^{0.6}	
267	VisionLabs	RU	visionlabs	010	2021-02-05	1042	20	33 512	-	161 731	263 11837	21 21	14 32	11 36	43 3183.79N ^{0.2}	
268	VisionLabs	RU	visionlabs	011	2021-10-20	1042	20	38 512	-	163 735	266 12255	21 23	8 26	7 34	51 301.26N ^{0.3}	
269	Vixvizion	AU	vixvizion	009	2022-11-28	580	460	128 2048	-	239 907	139 14	389	312	714	1530	0.02N ^{1.2}
270	Vocord	RU	vocord	5	2018-10-30	1035	185	57 768	k	181 780	46 7	158	204	383	767	0.12N ^{1.0}
271	Vocord	RU	vocord	6	2018-10-30	1035	185	275 10240	k	182 785	259 243	170 170	216 216	-	-	-
272	Xforward AI Technology	CN	xforwardai	000	2020-07-24	236	171	144 2048	-	170 753	134 13	4603	7647	15723	23900	53729 0.56N ^{1.1}
273	Xforward AI Technology	CN	xforwardai	001	2021-01-21	332	50	188 2048	-	137 677	174 16	5887	4384	8798	18553	48993 0.32N ^{1.1}
274	Xforward AI Technology	CN	xforwardai	002	2021-05-24	691	50	247 4096	-	245 930	187 18	6957	6400	12659	31077	65158 0.52N ^{1.1}
275	verihubs-inteligensia	ID	verihubs-inteligensia	000	2022-09-29	204	75	160 2048	-	101 575	149 14	9715	9670	18711	38110	79675 4.77N ^{1.0}

Notes

- Configuration size does not capture static data present in libraries. Libraries are included but the size also includes any ancillary libraries for image processing (e.g. openCV) or numerical computation (e.g. blas).
- Finalization is the processing of converting N = 1600000 templates into a searchable data structure an operation which can be a simple copy, or the building of an index or tree, for example. The duration of the operation may be data dependent, and may not be linear in the number of input templates.
- This multiplier expresses the increase in template size when k images are passed to the template generation function.
- All durations are measured on Intel®Xeon®CPU E5-2630 v4 @ 2.20GHz processors. Estimates are made by wrapping the API function call in calls to std::chrono::high_resolution_clock which on the machine in (3) counts 1ns clock ticks. Precision is somewhat worse than that however.
- Search durations are measured as in the prior note. The power-law model in the final column mostly fits the empirical results in Figure 151. However in certain cases the model is not correct and should not be used numerically.

Table 7: Summary of algorithms and properties included in this report. The blue superscripts give ranking for the quantity in that column. Missing search durations, denoted by “-”, are absent because those runs were not executed, usually because we did not run on the larger galleries. Caution: The power-law model is sometimes an incorrect model. It is included here only to show broad sublinear behavior, which is flagged in green. The models should not be used for prediction.

#	ALGORITHM	INVESTIGATION, FNIR(N, R = 1, T = 0)								IDENTIFICATION, FNIR(N, R = L, T ≥ 0) FOR FPIR = 0.001							
		(0, 2]	(2, 4]	(4, 6]	(6, 8]	(8, 10]	(10, 12]	(12, 14]	(14, 18]	(0, 2]	(2, 4]	(4, 6]	(6, 8]	(8, 10]	(10, 12]	(12, 14]	(14, 18]
1	3DIVI-005	⁹⁷ 0.0207	⁹⁷ 0.0304	⁹⁷ 0.0415	⁹⁷ 0.0533	⁹⁷ 0.0646	¹⁵⁵ 0.0735	¹⁵⁵ 0.0884	¹⁵⁶ 0.1148	¹⁰⁷ 0.1580	⁹⁸ 0.2316	⁹⁸ 0.3033	⁹⁸ 0.3740	⁹⁸ 0.4285	¹⁵³ 0.4742	¹⁵³ 0.5329	¹⁵³ 0.5975
2	ANKE-000	⁹⁵ 0.0162	⁹⁵ 0.0245	⁹⁵ 0.0333	⁹⁵ 0.0428	⁹⁵ 0.0515	¹⁵³ 0.0615	¹⁵³ 0.0780	¹⁵² 0.1028	⁹⁶ 0.1132	⁹⁶ 0.1761	⁹⁶ 0.2402	⁹⁵ 0.3057	⁹⁵ 0.3640	¹⁵¹ 0.4200	¹⁵¹ 0.4928	¹⁵¹ 0.5680
3	ANKE-002	⁴⁷ 0.0055	⁵⁰ 0.0074	⁵⁰ 0.0090	⁴⁹ 0.0103	⁴⁸ 0.0116	¹⁰⁴ 0.0135	¹⁰³ 0.0162	¹⁰² 0.0202	⁵⁴ 0.0329	⁵⁴ 0.0560	⁵⁶ 0.0843	⁵⁷ 0.1169	⁵⁷ 0.1481	¹¹² 0.1820	¹¹¹ 0.2280	¹¹¹ 0.2831
4	AWARE-005	¹⁰⁶ 0.0328	¹⁰⁶ 0.0519	¹⁰⁶ 0.0712	¹⁰⁴ 0.0910	¹⁰⁴ 0.1078	¹⁶² 0.1235	¹⁶² 0.1457	¹⁶³ 0.1831	¹⁰⁸ 0.3605	¹⁰⁷ 0.4949	¹⁰⁷ 0.5948	¹⁰⁷ 0.6783	¹⁰⁸ 0.7393	¹⁶⁴ 0.7905	¹⁶⁴ 0.8408	¹⁶⁵ 0.8831
5	AWARE-006	¹¹⁰ 0.0702	¹¹¹ 0.1110	¹¹¹ 0.1502	¹¹¹ 0.1899	¹¹¹ 0.2253	¹⁷¹ 0.2614	¹⁷⁰ 0.3045	¹⁷⁰ 0.3659								
6	AYONIX-002	¹¹³ 0.3360	¹¹⁴ 0.4389	¹¹⁴ 0.5144	¹¹⁴ 0.5814	¹¹⁴ 0.6340	¹⁷⁴ 0.6818	¹⁷⁴ 0.7297	¹⁷⁵ 0.7774	¹¹⁶ 0.8288	¹¹¹ 0.9013	¹¹¹ 0.9375	¹¹¹ 0.9603	¹¹¹ 0.9744	¹⁶⁹ 0.9837	¹⁶⁹ 0.9893	¹⁶⁹ 0.9927
7	CAMVI-004	¹⁰⁹ 0.0623	¹⁰⁹ 0.0944	¹⁰⁹ 0.1243	¹⁰⁸ 0.1548	¹⁰⁸ 0.1812	¹⁶⁸ 0.2056	¹⁶⁸ 0.2344	¹⁶⁶ 0.2672	⁹¹ 0.0810	⁹¹ 0.1267	⁸⁸ 0.1721	⁸⁸ 0.2203	⁸⁸ 0.2619	¹⁴² 0.3040	¹⁴¹ 0.3543	¹³⁷ 0.4124
8	CAMVI-005	¹¹¹ 0.0849	¹¹¹ 0.1255	¹¹¹ 0.1631	¹¹¹ 0.1989	¹¹¹ 0.2298	¹⁷⁰ 0.2585	¹⁶⁹ 0.2915	¹⁶⁹ 0.3246								
9	CANON-001									⁴⁸ 0.0052	⁴⁷ 0.0057	⁴¹ 0.0042					
10	CANON-002									⁶³ 0.0066	⁶³ 0.0070	⁶² 0.0070					
11	CIB-000	¹⁴ 0.0022	¹⁴ 0.0030	¹⁵ 0.0037	¹⁵ 0.0044	¹⁷ 0.0049	³⁸ 0.0057	⁶¹ 0.0069	⁶⁰ 0.0062	²⁵ 0.0139	²⁶ 0.0240	²⁷ 0.0373	²⁸ 0.0525	²⁸ 0.0689	⁷³ 0.0859	⁷⁴ 0.1109	⁷⁴ 0.1454
12	CLEARVIEW1-000	⁴ 0.0017	⁴ 0.0023	⁴ 0.0028	⁹ 0.0034	¹¹ 0.0039	³⁸ 0.0046	⁴⁶ 0.0056	⁵⁰ 0.0047	¹⁶ 0.0066	¹⁸ 0.0121	¹⁸ 0.0194	¹⁹ 0.0287	¹⁹ 0.0385	⁵⁹ 0.0493	⁶⁰ 0.0662	⁶⁰ 0.0873
13	CLOUDWALK-MT-000	¹ 0.0019	² 0.0024	⁸ 0.0029	⁶ 0.0032	⁵ 0.0032	⁸ 0.0036	¹² 0.0041	⁸ 0.0020	¹ 0.0029	¹ 0.0041	¹ 0.0054	¹ 0.0064	² 0.0073	⁹ 0.0085	⁹ 0.0102	⁹ 0.0112
14	CLOUDWALK-MT-000																
15	CLOUDWALK-MT-001									¹⁰ 0.0037	² 0.0037	² 0.0012					
16	CLOUDWALK-MT-002									⁹ 0.0036	⁴ 0.0038	³ 0.0012					
17	COGENT-000	⁹⁰ 0.0128	⁹¹ 0.0184	⁹³ 0.0250	⁹³ 0.0327	⁹³ 0.0407	¹⁴⁸ 0.0488	¹⁴⁶ 0.0611	¹⁴⁶ 0.0794	⁷⁷ 0.0559	⁷⁹ 0.0923	⁷⁶ 0.1342	⁷⁶ 0.1812	⁷⁶ 0.2243	¹³¹ 0.2675	¹³⁰ 0.3240	¹³³ 0.3992
18	COGENT-001	⁹¹ 0.0128	⁹⁰ 0.0184	⁹² 0.0250	⁹² 0.0327	⁹² 0.0407	¹⁴⁷ 0.0488	¹⁴⁷ 0.0611	¹⁴⁵ 0.0794	⁷⁸ 0.0559	⁷⁸ 0.0923	⁷⁷ 0.1342	⁷⁷ 0.1812	⁷⁷ 0.2243	¹³⁰ 0.2675	¹³⁰ 0.3240	¹³⁰ 0.3992
19	COGENT-002	⁶⁹ 0.0081	⁶⁶ 0.0105	⁶³ 0.0123	⁶⁴ 0.0137	⁶² 0.0157	¹¹⁸ 0.0175	¹¹⁶ 0.0215	¹¹⁶ 0.0280	⁶⁹ 0.0499	⁶⁸ 0.0827	⁶⁷ 0.1207	⁶⁷ 0.1639	⁶⁷ 0.2037	¹²² 0.2432	¹²³ 0.2972	¹²⁴ 0.3638
20	COGENT-003	⁷¹ 0.0082	⁶⁷ 0.0108	⁶⁵ 0.0128	⁶⁷ 0.0145	⁶⁶ 0.0168	¹²⁴ 0.0191	¹²⁵ 0.0239	¹²² 0.0312	⁸⁰ 0.0582	⁸⁰ 0.0971	⁸¹ 0.1417	⁸¹ 0.1918	⁸⁰ 0.2380	¹³⁷ 0.2836	¹³⁴ 0.3440	¹⁴⁰ 0.4207
21	COGENT-004	⁵⁹ 0.0066	⁵³ 0.0080	⁴⁵ 0.0085	³⁹ 0.0080	³¹ 0.0083	⁸² 0.0092	⁸² 0.0106	⁸⁶ 0.0130	⁶³ 0.0410	⁶⁵ 0.0720	⁶⁵ 0.1099	⁶⁵ 0.1539	⁶⁴ 0.1974	¹²³ 0.2443	¹²⁶ 0.3043	¹²⁶ 0.3757
22	COGENT-006								³⁴ 0.0045	²⁴ 0.0049	³⁰ 0.0038						
23	COGENT-007								³¹ 0.0044	³⁰ 0.0049	³³ 0.0036						
24	COGNITEC-000	¹⁰⁵ 0.0265	¹⁰³ 0.0423	¹⁰³ 0.0588	¹⁰³ 0.0757	¹⁰² 0.0894	¹⁶⁰ 0.1014	¹⁶⁰ 0.1169	¹⁵⁹ 0.1381	¹⁰⁰ 0.1522	⁹⁹ 0.2330	⁹⁹ 0.3051	⁹⁹ 0.3751	⁹⁹ 0.4300	¹⁵² 0.4779	¹⁵² 0.5307	¹⁵² 0.5913
25	COGNITEC-001	⁹³ 0.0149	⁹⁴ 0.0228	⁹⁴ 0.0312	⁹⁴ 0.0399	⁹⁴ 0.0479	¹⁵⁰ 0.0546	¹⁴⁹ 0.0656	¹⁴⁷ 0.0806	⁹³ 0.0963	⁹³ 0.1562	⁹³ 0.2157	⁹³ 0.2771	⁹³ 0.3287	¹⁴⁹ 0.3771	¹⁴⁸ 0.4343	¹⁴⁷ 0.4959
26	COGNITEC-002	⁷¹ 0.0101	⁸⁶ 0.0138	⁸¹ 0.0170	⁸¹ 0.0201	⁸¹ 0.0237	¹³⁶ 0.0264	¹³⁴ 0.0309	¹³³ 0.0389	⁷² 0.0517	⁷¹ 0.0879	⁷² 0.1269	⁷¹ 0.1707	⁷¹ 0.2098	¹²⁴ 0.2463	¹²² 0.2919	¹²² 0.3535
27	COGNITEC-003	⁷⁰ 0.0104	⁸¹ 0.0140	⁸² 0.0174	⁸² 0.0205	⁸² 0.0238	¹³⁷ 0.0266	¹³⁵ 0.0311	¹³⁵ 0.0401	⁷¹ 0.0504	⁷⁰ 0.0855	⁶⁹ 0.1235	⁶⁹ 0.1662	⁶⁹ 0.2045	¹²² 0.2403	¹²³ 0.2854	¹²³ 0.3451
28	COGNITEC-004	⁶⁴ 0.0073	⁶³ 0.0099	⁶² 0.0118	⁵⁹ 0.0130	⁵⁹ 0.0147	¹¹² 0.0163	¹¹² 0.0189	¹¹² 0.0239	⁵³ 0.0325	⁵³ 0.0548	⁵² 0.0798	⁵¹ 0.1074	⁵¹ 0.1325	¹⁰³ 0.1591	¹⁰¹ 0.1952	⁹⁹ 0.2414
29	COGNITEC-006								⁷⁵ 0.0081	⁷³ 0.0086	⁷¹ 0.0090						
30	CUBOX-000	⁷ 0.0019	⁵ 0.0024	⁵ 0.0028	⁴ 0.0031	⁴ 0.0032	¹¹ 0.0037	¹⁹ 0.0044	¹⁹ 0.0027	⁶ 0.0039	⁶ 0.0059	⁷ 0.0083	⁸ 0.0111	⁸ 0.0141	²³ 0.0185	²⁴ 0.0252	²⁵ 0.0339
31	CYBERLINK-002	⁵¹ 0.0055	⁴⁸ 0.0068	⁴¹ 0.0075	³⁵ 0.0078	³² 0.0084	⁸³ 0.0094	⁸³ 0.0107	⁸ 0.0114	³² 0.0180	³³ 0.0302	³³ 0.0460	³³ 0.0643	³³ 0.0837	⁸² 0.1058	⁸¹ 0.1370	⁸¹ 0.1787
32	CYBERLINK-003	³⁵ 0.0041	³⁴ 0.0052	²⁷ 0.0057	²⁵ 0.0058	²⁵ 0.0061	⁷¹ 0.0068	⁶⁸ 0.0078	⁷⁰ 0.0078	¹⁹ 0.0109	¹⁹ 0.0175	²⁰ 0.0259	²¹ 0.0356	²¹ 0.0468	⁶³ 0.0594	⁶⁶ 0.0787	⁶⁸ 0.1072
33	DAHUA-002	³ 0.0035	²⁸ 0.0047	²⁸ 0.0058	²⁷ 0.0067	²⁸ 0.0074	⁷⁶ 0.0082	⁷⁹ 0.0100	⁷⁸ 0.0108	³⁰ 0.0169	³² 0.0294	³¹ 0.0449	³⁰ 0.0635	³⁰ 0.0817	⁷⁹ 0.1013	⁷⁸ 0.1291	⁷⁷ 0.1638
34	DAHUA-003	¹⁹ 0.0026	¹⁹ 0.0036	¹⁹ 0.0043	²⁰ 0.0050	²⁰ 0.0055	⁶² 0.0062	⁷⁰ 0.0080	⁶⁵ 0.0073	²⁹ 0.0160	³⁰ 0.0280	²⁹ 0.0432	²⁹ 0.0615	²⁹ 0.0794	⁷⁷ 0.0987	⁷⁷ 0.1270	⁷⁵ 0.1587
35	DEEPEGLINT-001	¹ 0.0024	¹⁶ 0.0032	¹⁴ 0.0037	¹³ 0.0040	¹³ 0.0043	⁴⁴ 0.0049	⁵³ 0.0060	⁵³ 0.0052	¹² 0.0058	¹⁰ 0.0087	¹¹ 0.0119	¹¹ 0.0155	¹¹ 0.0199	²⁹ 0.0249	³¹ 0.0338	³¹ 0.0463
36	DEEPSA-001	⁷⁰ 0.0081	⁷⁰ 0.0116	⁷³ 0.0149	⁷⁶ 0.0182	⁷⁶ 0.0216	¹³⁵ 0.0260	¹³⁷ 0.0332	¹³⁷ 0.0432	⁶⁶ 0.0458	⁶⁶ 0.0752	⁶⁴ 0.1086	⁶³ 0.1460	⁶³ 0.1812	¹¹⁹ 0.2186	¹¹⁹ 0.2663	¹¹⁸ 0.3213
37	DERMALOG-006	⁸ 0.0113	⁸² 0.0142	⁷⁸ 0.0163	⁷⁷ 0.0183	⁷⁴ 0.0200	¹²⁹ 0.0218	¹²⁷ 0.0251	¹²⁵ 0.0329	⁷⁵ 0.0545	⁷³ 0.0889	⁷³ 0.1271	⁷² 0.1697	⁷¹ 0.2090	¹²⁶ 0.2498	¹²⁶ 0.3028	¹²⁵ 0.3670
38	DERMALOG-007	⁸⁸ 0.0125	⁸⁸ 0.0170	⁸⁸ 0.0214	⁸⁸ 0.0264	⁸⁷ 0.0309	¹⁴² 0.0356	¹⁴³ 0.0432	¹⁴³ 0.0579	⁹² 0.0910	⁹² 0.1453	⁹² 0.2009	⁹² 0.2602	⁹² 0.3134	¹⁴⁸ 0.3649	¹⁴⁷ 0.4289	¹⁴⁸ 0.5007
39	DERMALOG-008	⁵³ 0.0057	⁵² 0.0077	⁵⁴ 0.0095	⁵⁴ 0.0110	⁵³ 0.0128	¹¹⁰ 0.0148	¹¹⁰ 0.0									

MISS RATES		INVESTIGATION, FNIR(N, R = 1, T = 0)								IDENTIFICATION, FNIR(N, R = L, T ≥ 0) FOR FPIR = 0.001									
#	ALGORITHM	(0, 2]	(2, 4]	(4, 6]	(6, 8]	(8, 10]	(10, 12]	(12, 14]	(14, 18]	(0, 2]	(2, 4]	(4, 6]	(6, 8]	(8, 10]	(10, 12]	(12, 14]	(14, 18]		
45	FUJITSULAB-001																		
46	GORILLA-002	100.0213	108.0359	101.0528	102.0716	103.0895	101.0898	101.1367	101.1765	103.1828	104.2787	104.3654	104.4485	104.5168	108.5823	108.6508	108.7180		
47	GORILLA-005	38.0044	47.0070	38.0102	62.0136	6.0170	127.0204	130.0272	13.0373	70.0566	81.0973	82.1432	81.1937	81.2398	139.2862	138.3437	138.4150		
48	GORILLA-007															114.1862	112.2198	108.2716	
49	GORILLA-008															101.1557	98.1847	97.2340	
50	GRIAULE-001															45.0402	43.0487	41.0636	
51	HZAILU-001															60.0524	57.0630	53.0791	
52	HZAILU-002															33.0488	32.0597	48.0728	
53	IDEMIA-003	81.0110	86.0151	86.0196	82.0238	84.0281	140.0313	140.0368	139.0504	87.0717	86.1147	86.1614	86.2113	85.2553	141.2976	140.3537	141.4334		
54	IDEMIA-004	80.0107	84.0148	85.0192	84.0233	80.0277	139.0312	139.0367	140.0512	86.0373	86.0587	86.0833	83.1100	82.1340	102.1580	99.1911	100.2482		
55	IDEMIA-005	84.0118	87.0167	90.0218	89.0270	88.0317	143.0357	142.0425	142.0579	65.0440	64.0689	60.0964	59.1254	58.1513	105.1762	104.2113	107.2698		
56	IDEMIA-006	87.0124	89.0171	89.0218	80.0263	80.0302	141.0321	138.0356	138.0471	67.0409	59.0620	57.0850	52.1097	49.1309	95.1486	92.1738	91.2200		
57	IDEMIA-007	47.0050	48.0071	48.0089	50.0106	51.0124	106.0142	108.0171	108.0220	36.0202	36.0335	34.0491	33.0663	31.0825	78.0999	75.1240	78.1645		
58	IDEMIA-008	5.0018	6.0024	6.0029	7.0032	7.0035	12.0039	23.0046	29.0033	3.0034	3.0051	5.0069	5.0087	5.0102	14.0123	13.0146	13.0186		
59	IDEMIA-009															10.0094	10.0103	10.0123	
60	IDEMIA-010									4.0034	1.0036	1.0011					4.0045	3.0052	3.0043
61	IMAGUS-005	33.0039	33.0052	31.0061	29.0067	30.0077	79.0088	80.0103	79.0109	39.0212	39.0357	40.0539	40.0755	38.0967	87.01183	86.1485	84.1893		
62	IMAGUS-008																		
63	IMPERIAL-000	34.0040	35.0054	36.0067	38.0079	40.0093	93.0112	92.0139	96.0178	48.0286	51.0503	51.0779	54.1116	56.1455	113.1844	116.2341	115.2951		
64	INCODE-003	94.0155	96.0247	96.0348	94.0463	96.0571	154.0674	154.0856	154.1114	102.1627	102.2507	103.3322	103.4122	108.4772	157.5368	157.6059	157.6766		
65	INCODE-004	56.0061	59.0087	59.0110	61.0136	61.0161	120.0185	123.0236	121.0309	79.0532	79.0908	75.1809	77.2245	132.2675	131.3249	130.3932			
66	INNOVATRICS-004	113.3594	113.3629	113.3688	112.3754	112.3813	172.3870	172.3960	172.4135	107.4243	105.4642	106.5073	106.5522	107.5902	161.6274	159.6736	159.7253		
67	INNOVATRICS-005	41.0046	41.0063	42.0078	45.0092	45.0106	96.0124	97.0149	97.0178	39.0343	50.0590	58.0886	58.1222	59.1544	116.1881	115.2321	113.2874		
68	INNOVATRICS-008									42.0047	31.0049	26.0031					34.0309	31.0353	30.0463
69	INTELLIVISION-002																		
70	INTEMA-000									21.0040	16.0043	16.0024					24.0193	23.0235	23.0294
71	INTEMA-001									15.0039	8.0040	9.0020					18.0157	18.0194	18.0246
72	IREX-000	24.0031	24.0042	25.0051	26.0060	26.0068	74.0080	76.0095	77.0107	52.0313	52.0539	53.0815	56.1137	55.1442	108.1755	111.2181	109.2718		
73	ISYSTEMS-002	76.0101	79.0135	80.0169	79.0197	80.0228	133.0256	133.0304	133.0398	90.0779	90.1258	91.1759	90.2299	90.2758	145.3204	145.3763	143.4401		
74	ISYSTEMS-003	75.0089	69.0115	69.0139	69.0158	70.0177	126.0198	123.0234	119.0303	84.0647	84.1056	84.1502	84.1986	83.2402	133.2819	134.3351	132.3976		
75	KAKAO-001									18.0039	17.0043	14.0022					21.0182	21.0220	21.0291
76	KEDACOM-001	83.0116	78.0130	67.0135	60.0133	57.0135	105.0141	98.0151	95.0176	41.0241	41.0360	39.0513	34.0689	34.0866	83.1060	79.1327	79.1694		
77	LINECLOVA-002									36.0045	29.0049	22.0030					33.0307	34.0374	35.0497
78	LINECLOVA-003									29.0044	28.0048	24.0030					39.0356	38.0443	38.0586
79	LOOKMAN-003	86.0123	83.0144	77.0158	70.0168	71.0178	122.0188	115.0212	116.0260	64.0438	62.0687	61.0978	61.1296	60.1581	115.1879	114.2294	111.2756		
80	LOOKMAN-005	85.0118	77.0134	70.0142	66.0144	61.0150	115.0160	107.0176	105.0213	51.0310	49.0480	46.0698	46.0954	46.1216	96.1491	98.1890	98.2381		
81	MAXVISION-000									96.0128	96.0146	94.0169					10.1706	101.2023	101.2550
82	MAXVISION-001									39.0046	32.0049	31.0033					37.0351	37.0435	36.0581
83	MICROFOCUS-005	113.4269	113.5527	115.6355	116.7024	116.7503	176.7876	172.8234	172.8601	111.8338	112.9113	112.9468	112.9667	112.9771	168.9836	168.9880	168.9924		
84	MICROSOFT-003	28.0034	32.0050	33.0064	36.0078	38.0092	89.0107	91.0135	93.0166	50.0288	50.0503	50.0763	50.1067	54.1359	108.1680	108.2116	105.2644		
85	MICROSOFT-004	25.0032	27.0047	29.0060	32.0075	33.0087	84.0103	90.0131	91.0159	47.0268	48.0470	45.0716	48.1007	48.1291	104.1610	103.2052	102.2590		
86	MICROSOFT-005	22.0031	29.0047	35.0066	43.0084	41.0103	101.0131	104.0164	100.0185	41.0243	41.0432	44.0658	44.0913	45.1172	93.1476	97.1874	95.2272		
87	MICROSOFT-006	26.0032	31.0049	34.0065	42.0081	42.0096	91.0117	93.0144	92.0160	24.0134	24.0233	23.0346	23.0462	22.0578	69.0713	69.0903	69.1156		
88	MUKH-002									163.0394	164.01754	164.02335					160.9761	160.9840	160.9899

Table 9: **Accuracy for the FRVT 2018 mugshot sets under ageing.** The second row shows the time lapse between gallery and subsequent probe images, in years. The first two columns identify the algorithm. The next 8 values give rank-based FNIR with $R = 1$, $T = 0$ and $FPIR = 1$. All these are relevant to investigational uses where candidates from all searches would need human review. The second 8 values give threshold-based FNIR with $T \geq 0$, $FPIR = 0.001$ and no rank criterion. The shaded cells indicate the three most accurate algorithms for that elapsed time. The gallery size is 3068801. The total number of searches is 10951064.

2023 / 04 / 04

FNIR(N, R, T) = False neg. identification rate

FPIR(N, T) = False pos. identification rate

N = Num. enrolled subjects

T = Threshold

T = 0 → Investigation

T > 0 → Identification

#	ALGORITHM	INVESTIGATION, FNIR(N, R = 1, T = 0)								IDENTIFICATION, FNIR(N, R = L, T ≥ 0) FOR FPIR = 0.001							
		(0, 2]	(2, 4]	(4, 6]	(6, 8]	(8, 10]	(10, 12]	(12, 14]	(14, 18]	(0, 2]	(2, 4]	(4, 6]	(6, 8]	(8, 10]	(10, 12]	(12, 14]	(14, 18]
89	NEC-000	⁹⁷ 0.0195	⁹⁹ 0.0316	⁹⁹ 0.0445	⁹⁹ 0.0581	⁹⁸ 0.0699	¹⁰⁰ 0.0817	¹⁰⁰ 0.0998	¹⁰⁰ 0.1237	⁸⁹ 0.0759	⁸⁹ 0.1245	⁸⁹ 0.1729	⁸⁹ 0.2240	⁸⁹ 0.2671	¹⁴⁴ 0.3117	¹⁴² 0.3639	¹⁴² 0.4348
90	NEC-001	¹⁰⁴ 0.0246	¹⁰² 0.0382	¹⁰⁰ 0.0524	¹⁰⁰ 0.0672	¹⁰¹ 0.0793	¹⁰⁰ 0.0904	¹⁰⁰ 0.1076	¹⁰⁰ 0.1317	⁹⁴ 0.1019	⁹⁴ 0.1623	⁹⁴ 0.2214	⁹⁴ 0.2834	⁹⁴ 0.3341	¹⁵⁰ 0.3844	¹⁵⁰ 0.4440	¹⁴⁹ 0.5183
91	NEC-002	²⁹ 0.0033	²² 0.0041	¹⁸ 0.0043	¹⁶ 0.0044	¹⁵ 0.0045	⁴³ 0.0049	⁴⁵ 0.0056	⁴⁰ 0.0041	¹⁵ 0.0066	¹¹ 0.0090	¹⁰ 0.0111	¹⁰ 0.0131	⁹ 0.0149	¹⁸ 0.0171	²⁰ 0.0207	²⁰ 0.0267
92	NEC-003	³¹ 0.0036	²⁶ 0.0046	²⁴ 0.0051	²⁴ 0.0055	²⁴ 0.0059	⁶⁶ 0.0067	⁶⁶ 0.0077	⁶⁸ 0.0073	⁹ 0.0056	⁹ 0.0076	⁹ 0.0091	⁷ 0.0105	⁶ 0.0119	¹⁷ 0.0137	¹⁵ 0.0162	¹⁵ 0.0209
93	NEC-004	³² 0.0039	²⁵ 0.0045	²² 0.0047	¹⁸ 0.0046	¹⁴ 0.0044	⁴¹ 0.0046	⁴² 0.0052	³⁵ 0.0036	⁷ 0.0046	⁵ 0.0057	² 0.0063	² 0.0066	¹ 0.0069	⁷ 0.0076	⁷ 0.0090	⁷ 0.0105
94	NEC-005														⁸ 0.0080	⁸ 0.0091	⁸ 0.0107
95	NEC-006														¹ 0.0030	¹ 0.0033	² 0.0012
96	NEC-007														¹ 0.0027	¹ 0.0031	¹ 0.0010
97	NEUROTECHNOLOGY-003	¹⁰¹ 0.0234	¹⁰¹ 0.0379	¹⁰² 0.0549	¹⁰¹ 0.0682	¹⁰⁰ 0.0720	¹⁵⁶ 0.0747	¹⁵⁶ 0.0886	¹⁵⁴ 0.1066	¹⁰⁹ 0.6802	¹⁰⁹ 0.8187	¹¹⁰ 0.8920	¹¹⁰ 0.9355	¹¹⁰ 0.9594	¹⁶⁶ 0.9738	¹⁶⁶ 0.9828	¹⁶⁶ 0.9885
98	NEUROTECHNOLOGY-004	⁷⁹ 0.0104	⁷⁸ 0.0134	⁷⁹ 0.0156	⁷³ 0.0173	⁷² 0.0195	¹²⁹ 0.0212	¹²⁶ 0.0245	¹²³ 0.0320	⁸³ 0.0642	⁸² 0.1015	⁸¹ 0.1426	⁷⁹ 0.1881	⁷⁸ 0.2299	¹³³ 0.2722	¹³² 0.3269	¹³³ 0.3943
99	NEUROTECHNOLOGY-005	⁷⁴ 0.0089	⁷¹ 0.0116	⁶⁸ 0.0136	⁶⁸ 0.0152	⁶⁹ 0.0173	¹²⁵ 0.0196	¹²¹ 0.0233	¹²⁰ 0.0306	⁷⁶ 0.0556	⁷⁶ 0.0913	⁷⁴ 0.1315	⁷⁴ 0.1766	⁷⁴ 0.2192	¹²⁹ 0.2617	¹²⁸ 0.3174	¹²⁸ 0.3843
100	NEUROTECHNOLOGY-007	⁶⁶ 0.0078	⁶⁵ 0.0103	⁶⁹ 0.0124	⁶⁹ 0.0140	⁶³ 0.0161	¹¹⁸ 0.0185	¹¹⁸ 0.0225	¹¹⁷ 0.0290	⁸² 0.0641	⁸⁵ 0.1069	⁸⁵ 0.1546	⁸⁵ 0.2075	⁸⁶ 0.2572	¹⁴⁵ 0.3081	¹⁴⁴ 0.3713	¹⁴⁴ 0.4421
101	NEUROTECHNOLOGY-010														⁷⁴ 0.0863	⁷² 0.1050	⁷² 0.1333
102	NEUROTECHNOLOGY-012														⁶⁹ 0.0638	⁶⁹ 0.0783	⁶⁶ 0.1027
103	NEUROTECHNOLOGY-013														⁴⁶ 0.0406	⁴⁶ 0.0498	⁴³ 0.0654
104	NOBLIS-002	¹¹² 0.1520	¹¹² 0.2419	¹¹² 0.3296	¹¹³ 0.4114	¹¹³ 0.4855	¹⁷³ 0.5528	¹⁷³ 0.6061	¹⁷³ 0.6532	¹¹³ 0.9984	¹¹³ 0.9996	¹¹³ 0.9998	¹¹³ 0.9999	¹¹³ 0.9999	¹⁷⁰ 1.0000	¹⁷⁶ 1.0000	¹⁷² 1.0000
105	NTECHLAB-003	⁶⁵ 0.0078	⁷⁶ 0.0131	⁸⁹ 0.0202	⁹⁰ 0.0295	⁹¹ 0.0405	¹⁴⁷ 0.0543	¹⁵⁰ 0.0761	¹⁵³ 0.1035	⁶⁸ 0.0491	⁷² 0.0881	⁷⁹ 0.1384	⁸³ 0.1985	⁸⁷ 0.2594	¹⁴⁶ 0.3270	¹⁴⁶ 0.4065	¹⁴⁶ 0.4891
106	NTECHLAB-004	⁶² 0.0068	⁶⁸ 0.0110	⁷⁹ 0.0167	⁸⁶ 0.0239	⁸⁹ 0.0330	¹⁴⁶ 0.0447	¹⁴⁸ 0.0641	¹⁵⁰ 0.0891	⁶¹ 0.0379	⁶³ 0.0688	⁶⁶ 0.1108	⁶⁶ 0.1629	⁷³ 0.2192	¹³⁸ 0.2846	¹⁴³ 0.3657	¹⁴⁵ 0.4524
107	NTECHLAB-006	⁸¹ 0.0056	⁶⁹ 0.0095	⁷⁷ 0.0148	⁸³ 0.0218	⁸⁵ 0.0301	¹⁴⁴ 0.0413	¹⁴⁵ 0.0591	¹⁴⁸ 0.0814	⁵⁶ 0.0349	⁶⁰ 0.0636	⁶³ 0.1023	⁶⁴ 0.1506	⁶⁶ 0.2024	¹²⁸ 0.2617	¹³⁵ 0.3374	¹³⁵ 0.4185
108	NTECHLAB-007	³⁷ 0.0044	⁴³ 0.0066	⁴⁹ 0.0089	⁵⁷ 0.0118	⁶⁰ 0.0150	¹²⁹ 0.0189	¹²⁸ 0.0255	¹²⁸ 0.0342	⁴⁵ 0.0256	⁴⁶ 0.0450	⁴⁸ 0.0705	⁴⁹ 0.1012	⁵¹ 0.1334	¹⁰⁶ 0.1692	¹⁰⁸ 0.2170	¹¹⁰ 0.2752
109	NTECHLAB-008	¹⁸ 0.0025	²¹ 0.0038	²⁹ 0.0052	³¹ 0.0074	⁴⁴ 0.0104	¹⁰ 0.0146	¹²⁴ 0.0236	¹²⁹ 0.0348	²⁶ 0.0143	²⁸ 0.0267	³² 0.0459	³⁷ 0.0733	⁴⁰ 0.1062	⁹² 0.1469	¹⁰² 0.2044	¹⁰⁶ 0.2698
110	NTECHLAB-009	¹³ 0.0022	¹⁵ 0.0031	¹⁶ 0.0038	¹⁷ 0.0045	¹⁹ 0.0055	⁶⁸ 0.0067	⁷⁴ 0.0088	⁷⁶ 0.0100	¹⁸ 0.0073	¹⁷ 0.0117	¹⁷ 0.0170	¹⁷ 0.0238	¹⁸ 0.0319	⁴⁸ 0.0419	⁴⁹ 0.0577	⁵⁷ 0.0833
111	NTECHLAB-011														³⁹ 0.0351	⁴¹ 0.0475	⁴¹ 0.0724
112	PANGIAM-000														³⁹ 0.0503	³⁶ 0.0617	³⁹ 0.0810
113	PANGIAM-001														⁶⁹ 0.0545	⁶⁹ 0.0685	⁶² 0.0894
114	PARAVISION-002	⁵³ 0.0058	⁵⁸ 0.0083	⁶⁹ 0.0111	⁶³ 0.0137	⁶⁵ 0.0162	¹²¹ 0.0187	¹²⁰ 0.0229	¹¹⁸ 0.0295								
115	PARAVISION-003	⁴⁴ 0.0048	⁴⁴ 0.0067	⁵¹ 0.0090	⁵² 0.0109	⁵⁴ 0.0128	¹⁰⁸ 0.0148	¹⁰⁸ 0.0178	¹⁰⁶ 0.0219	⁵⁷ 0.0354	⁵⁸ 0.0618	⁵⁹ 0.0931	⁶⁰ 0.1290	⁶¹ 0.1625	¹¹⁷ 0.1964	¹¹⁷ 0.2408	¹¹⁴ 0.2924
116	PARAVISION-004	¹⁶ 0.0024	¹⁷ 0.0032	¹⁹ 0.0040	¹⁹ 0.0047	¹⁸ 0.0053	⁶¹ 0.0061	⁶⁴ 0.0073	⁶⁴ 0.0072	²⁰ 0.0118	²³ 0.0209	²⁴ 0.0327	²⁴ 0.0465	²⁴ 0.0613	⁷¹ 0.0779	⁷¹ 0.1008	⁷¹ 0.1285
117	PARAVISION-005	¹² 0.0021	¹³ 0.0028	¹³ 0.0035	¹⁴ 0.0041	¹⁶ 0.0046	⁵³ 0.0054	⁵⁹ 0.0067	⁶³ 0.0070	¹¹ 0.0057	¹² 0.0093	¹² 0.0144	¹⁴ 0.0207	¹⁵ 0.0278	⁴² 0.0368	⁴⁶ 0.0508	⁴⁶ 0.0715
118	PARAVISION-007	⁴ 0.0019	⁸ 0.0025	⁷ 0.0029	⁸ 0.0033	⁸ 0.0036	²⁵ 0.0042	³³ 0.0049	²⁵ 0.0030	¹⁰ 0.0057	¹³ 0.0094	¹⁴ 0.0144	¹⁵ 0.0206	¹⁴ 0.0275	⁴⁹ 0.0357	⁴⁸ 0.0485	⁴² 0.0652
119	PARAVISION-009														³¹ 0.0283	³³ 0.0371	³⁴ 0.0525
120	PARAVISION-012														¹⁸ 0.0137	¹⁸ 0.0167	¹⁶ 0.0219
121	PIXELLALL-002	⁷² 0.0085	⁷³ 0.0119	⁷¹ 0.0147	⁷² 0.0172	⁷³ 0.0198	¹³⁰ 0.0225	¹²⁹ 0.0270	¹³⁰ 0.0349	⁹⁷ 0.1193	⁹⁷ 0.1900	⁹⁷ 0.2601	⁹⁷ 0.3332	⁹⁷ 0.3955	¹⁵³ 0.4565	¹⁵³ 0.5268	¹⁵⁴ 0.6030
122	PIXELLALL-003	⁴⁶ 0.0050	⁴² 0.0063	³⁹ 0.0072	³⁴ 0.0077	³³ 0.0085	⁸⁴ 0.0095	⁸⁵ 0.0113	⁸² 0.0119	⁴⁴ 0.0248	⁴³ 0.0418	⁴³ 0.0622	⁴³ 0.0861	⁴³ 0.1104	⁸⁹ 0.1364	⁸⁹ 0.1723	⁸⁹ 0.2167
123	PIXELLALL-004	⁴⁵ 0.0049	⁴⁰ 0.0063	⁴⁰ 0.0072	³⁷ 0.0079	³⁶ 0.0089	⁸⁸ 0.0103	⁸⁸ 0.0127	⁸⁸ 0.0146	³⁸ 0.0211	⁴⁰ 0.0360	⁴² 0.0553	⁴² 0.0792	³⁹ 0.1045	⁸⁸ 0.1317	⁸⁹ 0.1700	⁹² 0.2246
124	PTAKURATSATU-000	⁵⁴ 0.0061	⁵⁶ 0.0082	⁵⁶ 0.0097	⁵³ 0.0109	⁴⁵ 0.0120	¹⁰⁸ 0.0131	⁹⁵ 0.0146	⁹⁵ 0.0146	⁵⁹ 0.0375	⁵⁷ 0.0596	⁵⁵ 0.0842	⁵⁵ 0.1116	⁵³ 0.1357	¹⁰⁰ 0.1553	⁹⁵ 0.1820	⁹⁶ 0.2326
125	RANKONE-002	⁹⁹ 0.0212	⁹⁸ 0.0313	⁹⁸ 0.0431	⁹⁸ 0.0562	⁹⁹ 0.0712	¹⁵⁹ 0.0881	¹⁵⁹ 0.1130	¹⁶⁰ 0.1543	⁹⁵ 0.1111	⁹⁵ 0.1707	⁹⁵ 0.2305	⁹⁵ 0.2968	⁹⁶ 0.3646	¹⁵² 0.4345	¹⁵² 0.5172	¹⁵⁵ 0.6110
126	RANKONE-004	¹⁰⁸ 0.0424	¹⁰⁷ 0.0643	¹⁰⁷ 0.0875	¹⁰⁷ 0.1127	¹⁰⁷ 0.1364	¹⁶⁴ 0.1579	¹⁶⁴ 0.1914	¹⁶⁵ 0.2378	¹⁰⁴ 0.1855	¹⁰³ 0.2681	¹⁰¹ 0.4341	¹⁰¹ 0.4785	¹⁵⁶ 0.5350	¹⁵⁶ 0.5980	¹⁵⁶ 0.6722	
127	RANKONE-005	⁹² 0.0136	⁹³ 0.0192	⁹¹ 0.0246	⁹¹ 0.0303	⁹⁰ 0.0362	¹⁴⁴ 0.0422	¹⁴⁴ 0.0521	¹⁴⁴ 0.0694	⁸¹ 0.0582	⁷⁵ 0.0910	⁷¹ 0.1260	⁶⁸ 0.1645	⁶⁵ 0.2005	¹²⁰ 0.2353	¹²⁰ 0.2816	¹²² 0.3522
128	RANKONE-007	⁶⁷ 0.0078	⁶⁴ 0.0099	⁶¹ 0.0113	⁵⁸ 0.0123	⁵⁸ 0.0139	¹¹⁴ 0.0156	¹¹⁴ 0.0191	¹¹³ 0.0242	⁴² 0.0242	⁴² 0.03						

MISS RATES		INVESTIGATION, FNIR(N, R = 1, T = 0)								IDENTIFICATION, FNIR(N, R = L, T ≥ 0) FOR FPIR = 0.001								
#	ALGORITHM	(0, 2]	(2, 4]	(4, 6]	(6, 8]	(8, 10]	(10, 12]	(12, 14]	(14, 18]	(0, 2]	(2, 4]	(4, 6]	(6, 8]	(8, 10]	(10, 12]	(12, 14]	(14, 18]	
133	RANKONE-013						47	0.0051	39	0.0051						32	0.0306	
134	RANKONE-014						30	0.0044	24	0.0047	21	0.0029				29	0.0222	
135	REALNETWORKS-002	107	0.0381	108	0.0687	108	0.1062	108	0.1495	109	0.1963	169	0.2513	171	0.3206	171	0.3927	
136	REALNETWORKS-003	103	0.0245	105	0.0437	105	0.0686	106	0.0975	108	0.1312	167	0.1719	167	0.2294	168	0.2907	
137	REALNETWORKS-004	102	0.0244	104	0.0428	104	0.0663	105	0.0939	105	0.1251	166	0.1634	166	0.2170	167	0.2785	
138	REALNETWORKS-006							72	0.0069	67	0.0077	71	0.0080				89	0.1022
139	REALNETWORKS-008							45	0.0049	43	0.0054	49	0.0047				30	0.0462
140	RECOGNITO-000							26	0.0042	26	0.0047	25	0.0030				29	0.0176
141	S1-002							40	0.0046	38	0.0051	38	0.0038				32	0.0482
142	S1-003							57	0.0057	55	0.0063	58	0.0056				67	0.0681
143	S1-004							23	0.0042	20	0.0045	28	0.0032				41	0.0360
144	SCANOVATE-001	68	0.0079	72	0.0117	75	0.0151	78	0.0185	78	0.0221	134	0.0259	136	0.0321	136	0.0427	
145	SENSETIME-002	96	0.0186	92	0.0191	81	0.0183	75	0.0179	68	0.0173	105	0.0133	75	0.0089	59	0.0059	
146	SENSETIME-003	11	0.0021	12	0.0028	11	0.0031	7	0.0033	6	0.0035	19	0.0040	22	0.0047	30	0.0033	
147	SENSETIME-004	70	0.0016	70	0.0022	3	0.0025	3	0.0028	30	0.0030	7	0.0035	18	0.0043	17	0.0025	
148	SENSETIME-005	2	0.0015	2	0.0020	2	0.0024	2	0.0026	2	0.0029	6	0.0035	15	0.0043	20	0.0028	
149	SENSETIME-006	10	0.0015	10	0.0019	10	0.0022	10	0.0025	10	0.0027	1	0.0033	9	0.0040	12	0.0021	
150	SENSETIME-007											5	0.0035	5	0.0038	5	0.0015	
151	SENSETIME-008											4	0.0034	7	0.0039	7	0.0017	
152	SIAT-002	117	0.8309	117	0.8310	117	0.8311	117	0.8306	117	0.8296	170	0.8302	170	0.8300	112	0.8340	
153	SYNESIS-003	89	0.0125	85	0.0151	83	0.0174	80	0.0199	79	0.0223	131	0.0240	131	0.0279	126	0.0331	
154	SYNESIS-005	40	0.0044	37	0.0058	37	0.0070	40	0.0080	37	0.0091	87	0.0103	87	0.0125	89	0.0152	
155	T4ISB-000											152	0.0606	151	0.0748	151	0.0970	
156	TECH5-001	37	0.0061	61	0.0093	66	0.0128	71	0.0171	77	0.0221	135	0.0289	141	0.0412	141	0.0560	
157	TOSHIBA-001	73	0.0086	74	0.0119	74	0.0150	74	0.0178	72	0.0209	132	0.0241	132	0.0292	131	0.0365	
158	TRUEFACE-000	36	0.0043	36	0.0057	36	0.0061	28	0.0067	27	0.0073	77	0.0084	77	0.0097	75	0.0099	
159	VERIDAS-001	58	0.0063	56	0.0083	56	0.0099	56	0.0113	56	0.0132	109	0.0148	110	0.0184	61	0.0219	
160	VERIDAS-004											49	0.0052	52	0.0059	45	0.0043	
161	VISIONLABS-004	43	0.0048	46	0.0069	52	0.0091	53	0.0111	53	0.0130	112	0.0152	111	0.0187	114	0.0242	
162	VISIONLABS-005	30	0.0044	30	0.0063	41	0.0081	46	0.0095	46	0.0109	97	0.0125	99	0.0151	101	0.0187	
163	VISIONLABS-006	29	0.0035	30	0.0048	30	0.0061	30	0.0069	29	0.0077	78	0.0087	81	0.0105	84	0.0120	
164	VISIONLABS-008	21	0.0028	20	0.0037	21	0.0047	22	0.0053	23	0.0058	67	0.0067	72	0.0081	27	0.0143	
165	VISIONLABS-009	10	0.0020	10	0.0026	10	0.0030	10	0.0034	10	0.0038	32	0.0044	41	0.0052	47	0.0046	
166	VISIONLABS-010	9	0.0020	9	0.0025	9	0.0030	11	0.0034	9	0.0036	28	0.0043	36	0.0051	48	0.0047	
167	VISIONLABS-011										24	0.0042	22	0.0046	34	0.0036		
168	VIXVIZION-009										116	0.0161	113	0.0190	111	0.0238		
169	VNPT-002										51	0.0053	51	0.0059	45	0.0044		
170	VTS-000	116	0.5878	116	0.6312	116	0.6602	115	0.6863	115	0.7073	175	0.7246	173	0.7458	174	0.7747	
171	VTS-003										52	0.0054	48	0.0059	56	0.0054		
172	XFORWARDAI-000	20	0.0027	18	0.0034	20	0.0044	21	0.0052	21	0.0058	70	0.0067	69	0.0079	28	0.0157	
173	XFORWARDAI-001	15	0.0023	14	0.0028	15	0.0034	12	0.0037	12	0.0039	35	0.0045	40	0.0052	44	0.0043	
174	YITU-002	90	0.0066	97	0.0083	53	0.0094	48	0.0101	50	0.0121	111	0.0150	112	0.0223	124	0.0328	
175	YITU-003	63	0.0072	68	0.0089	51	0.0107	52	0.0125	111	0.0153	115	0.0226	127	0.0334	34	0.0194	
176	YITU-004	85	0.0061	51	0.0075	44	0.0081	41	0.0081	39	0.0092	90	0.0107	102	0.0154	104	0.0207	

Table 11: **Accuracy for the FRVT 2018 mugshot sets under ageing.** The second row shows the time lapse between gallery and subsequent probe images, in years. The first two columns identify the algorithm. The next 8 values give rank-based FNIR with $R = 1$, $T = 0$ and FPIR = 1. All these are relevant to investigational uses where candidates from all searches would need human review. The second 8 values give threshold-based FNIR with $T \geq 0$, FPIR = 0.001 and no rank criterion. The shaded cells indicate the three most accurate algorithms for that elapsed time. The gallery size is 3068801. The total number of searches is 10951064.

MISS RATES		INVESTIGATION, FNIR(N, R = 1, T = 0)								IDENTIFICATION, FNIR(N, R = L, T ≥ 0) FOR FPIR = 0.001							
#	ALGORITHM	(0, 2]	(2, 4]	(4, 6]	(6, 8]	(8, 10]	(10, 12]	(12, 14]	(14, 18]	(0, 2]	(2, 4]	(4, 6]	(6, 8]	(8, 10]	(10, 12]	(12, 14]	(14, 18]
177	YITU-005	⁶¹ 0.0067	³⁴ 0.0080	⁴⁷ 0.0087	⁴⁴ 0.0085	⁴¹ 0.0094	⁹¹ 0.0108	¹⁰⁰ 0.0151	¹⁰³ 0.0204	²¹ 0.0124	²¹ 0.0198	²² 0.0308	²² 0.0462	²⁵ 0.0667	⁷⁸ 0.0953	⁸¹ 0.1418	⁸⁸ 0.1930

Table 12: **Accuracy for the FRVT 2018 mugshot sets under ageing.** The second row shows the time lapse between gallery and subsequent probe images, in years. The first two columns identify the algorithm. The next 8 values give rank-based FNIR with $R = 1$, $T = 0$ and FPIR = 1. All these are relevant to investigational uses where candidates from all searches would need human review. The second 8 values give threshold-based FNIR with $T \geq 0$, FPIR = 0.001 and no rank criterion. The shaded cells indicate the three most accurate algorithms for that elapsed time. The gallery size is 3068801. The total number of searches is 10951064.

2023/04/04
07:31:47FNIR(N, R, T) = False neg. identification rate
FPIR(N, T) = False pos. identification rateN = Num. enrolled subjects
R = Num. candidates examined

T = Threshold

T = 0 → Investigation
T > 0 → Identification

#	ALGORITHM	INVESTIGATION MODE						IDENTIFICATION MODE						FAILURE TO EXTRACT FEATURES						
		RANK ONE MISS RATE, FNIR(N, 0, 1)						HIGH T → FPIR = 0.001, FNIR(N, T, L)												
		N=1.6M						N=1.6M												
GALLERY	MUGSHOT	MUGSHOT	MUGSHOT	VISA	BORDER	VISA		MUGSHOT	MUGSHOT	MUGSHOT	VISA	BORDER	VISA	MUGSHOT	MUGSHOT	MUGSHOT	VISA	BORDER	KIOSK	
PROBE	MUGSHOT	WEBCAM	PROFILE	BORDER	BOR ₁ 10YR	KIOSK		MUGSHOT	WEBCAM	PROFILE	BORDER	BOR ₁ 10YR	KIOSK	MUGSHOT	WEBCAM	PROFILE	BORDER	BOR ₁ 10YR	KIOSK	
1	20FACE-000	29 ^{0.055}	28 ^{0.085}	19 ^{0.736}	22 ^{0.056}	15 ¹ 0.239	219 ^{0.243}	29 ⁰ 0.348	28 ⁰ 0.450	258 ¹ 0.000	22 ⁰ 0.424	13 ¹ 0.772	21 ⁰ 0.938	0.000	0.000	0.000	0.000	0.000		
2	3DIVI-003	30 ^{0.083}	30 ^{0.206}	23 ⁰ 0.141	24 ⁰ 0.474	30 ³ 0.400	30 ² 0.626	23 ⁰ 0.605	20 ⁰ 0.821	0.002	0.005									
3	3DIVI-004	26 ^{0.018}	27 ^{0.062}	21 ⁰ 0.035	22 ⁰ 0.279	27 ⁰ 0.169	27 ⁵ 0.343	21 ⁰ 0.277	17 ² 0.607	0.002	0.005									
4	3DIVI-005	26 ⁷ 0.018	27 ³ 0.062	24 ⁶ 0.930	25 ⁷ 0.821	22 ⁴ 0.279	27 ⁰ 0.166	27 ³ 0.339	18 ² 0.996	24 ⁸ 0.864	17 ¹ 0.597	0.002	0.005	0.442						
5	3DIVI-006	27 ^{0.024}	28 ¹ 0.074	22 ⁰ 0.047	23 ⁰ 0.312	27 ⁰ 0.168	27 ⁴ 0.342	21 ⁵ 0.283	17 ¹ 0.615	0.002	0.005									
6	ACER-000	24 ⁵ 0.011	23 ⁶ 0.036	22 ⁶ 0.827	20 ⁰ 0.025	20 ⁶ 0.209	26 ⁰ 0.146	25 ² 0.246	13 ¹ 0.981	20 ⁸ 0.201	15 ⁵ 0.490	0.000	0.000	0.042						
7	ACER-001	19 ⁰ 0.005	18 ² 0.020	14 ² 0.422	16 ⁰ 0.008	12 ⁸ 0.050	10 ⁵ 0.098	20 ⁰ 0.056	17 ⁷ 0.109	22 ¹ 0.999	16 ⁷ 0.068	11 ⁵ 0.406	15 ⁴ 0.479	0.001	0.001	0.041	0.000			
8	AIZE-001	20 ⁰ 0.006	19 ⁶ 0.022	18 ⁹ 0.683	19 ⁰ 0.016	13 ⁰ 0.050	18 ⁹ 0.165	22 ⁰ 0.077	20 ⁷ 0.143	16 ⁰ 0.994	17 ⁵ 0.101	10 ⁸ 0.364	13 ⁵ 0.387	0.001	0.001	0.047				
9	ALCHERA-000	26 ² 0.016	26 ¹ 0.047	23 ³ 0.870	21 ⁰ 0.046	22 ⁹ 0.292	25 ⁰ 0.138	23 ⁶ 0.216	20 ⁰ 0.999	20 ² 0.176	19 ⁹ 0.803	0.006	0.014	0.328						
10	ALCHERA-001	33 ⁷ 0.987	33 ³ 1.000	25 ⁹ 1.000	32 ⁸ 1.000	33 ⁹ 0.999	32 ⁸ 1.000	30 ⁶ 1.000	28 ³ 1.000	0.006	0.013	0.324								
11	ALCHERA-002	31 ⁰ 0.095	30 ⁰ 0.166	26 ⁰ 0.954	25 ⁴ 0.668	24 ² 0.446	31 ⁰ 0.486	29 ⁷ 0.591	22 ⁹ 1.000	24 ⁷ 0.827	19 ⁷ 0.811	0.001	0.002	0.106						
12	ALCHERA-003	24 ⁹ 0.010	23 ⁴ 0.035	20 ⁰ 0.741	19 ¹ 0.016	20 ⁴ 0.206	26 ¹ 0.155	24 ⁸ 0.239	21 ⁴ 0.999	20 ⁷ 0.172	13 ⁵ 0.464	0.001	0.002	0.106						
13	ALCHERA-004	24 ⁶ 0.011	24 ⁰ 0.038	13 ⁴ 0.345	19 ² 0.017	14 ¹ 0.088	17 ⁸ 0.144	30 ² 0.394	29 ² 0.529	15 ² 0.991	22 ⁰ 0.424	12 ³ 0.708	16 ⁶ 0.546	0.001	0.001	0.046	0.000			
14	ALLGOVISION-000	24 ⁹ 0.011	23 ⁰ 0.033	23 ⁶ 0.894	19 ⁶ 0.021	22 ⁶ 0.282	23 ⁹ 0.088	22 ³ 0.166	14 ⁹ 0.990	18 ⁵ 0.117	16 ³ 0.526	0.002	0.003	0.122						
15	ALLGOVISION-001	22 ⁹ 0.009	24 ⁶ 0.038	18 ⁵ 0.661	19 ⁷ 0.021	21 ⁷ 0.241	24 ¹ 0.102	24 ⁰ 0.221	13 ⁸ 0.986	19 ⁵ 0.150	15 ⁶ 0.491	0.001	0.001	0.042						
16	ALLGOVISION-002	21 ⁰ 0.007	20 ⁵ 0.023	17 ⁷ 0.585	16 ⁸ 0.008	14 ⁶ 0.161	16 ⁸ 0.132	21 ⁸ 0.068	21 ¹ 0.520	10 ⁰ 0.950	21 ⁰ 0.232	24 ⁹ 1.000	18 ⁷ 0.716	0.000	0.000	0.041	0.000			
17	ANKE-000	25 ⁷ 0.013	24 ² 0.038	24 ⁹ 0.931	23 ⁹ 1.000	28 ⁸ 1.000	24 ⁶ 0.117	25 ⁹ 0.220	15 ⁹ 0.994	26 ¹ 0.1000	33 ⁰ 1.000	0.000	0.001	0.080						
18	ANKE-001	25 ⁹ 0.013	24 ¹ 0.038	25 ⁵ 0.946	29 ¹ 0.000	33 ⁰ 1.000	25 ⁹ 0.119	25 ⁰ 0.220	16 ⁶ 0.994	30 ⁸ 1.000	28 ¹ 0.1000	0.000	0.001	0.080						
19	ANKE-002	15 ² 0.003	15 ⁵ 0.016	16 ¹ 0.522	12 ⁰ 0.005	14 ⁹ 0.119	16 ¹ 0.032	14 ² 0.079	9 ⁹ 0.948	12 ⁵ 0.034	9 ⁸ 0.245	0.001	0.001	0.049						
20	AWARE-003	28 ⁵ 0.031	28 ⁷ 0.090	27 ² 0.966	24 ⁴ 0.316	22 ⁸ 0.290	25 ⁴ 0.128	26 ⁷ 0.298	13 ⁵ 0.984	22 ⁷ 0.428	16 ⁴ 0.530	0.004	0.003	0.874						
21	AWARE-004	30 ⁵ 0.068	30 ² 0.176	28 ¹ 0.976	23 ⁹ 0.122	24 ⁰ 0.414	28 ⁰ 0.269	29 ⁰ 0.509	23 ² 1.000	22 ⁷ 0.397	19 ⁸ 0.816	0.003	0.003	0.776						
22	AWARE-005	28 ⁶ 0.031	27 ⁵ 0.067	28 ² 0.978	22 ² 0.048	23 ² 0.308	29 ⁷ 0.364	25 ⁴ 0.253	23 ⁶ 1.000	21 ³ 0.255	21 ³ 0.916	0.001	0.002	0.189						
23	AWARE-006	30 ⁰ 0.070	29 ⁶ 0.128	28 ⁴ 0.983	23 ¹ 0.111	24 ¹ 0.421	28 ⁷ 0.276	27 ⁸ 0.398	22 ³ 0.999	22 ⁸ 0.368	18 ⁷ 0.749	0.001	0.002	0.189						
24	AYONIX-000	33 ⁰ 0.450	32 ⁸ 0.685	29 ³ 0.996	25 ² 0.607	25 ⁶ 0.867	32 ⁸ 0.811	32 ¹ 0.939	19 ¹ 0.998	24 ⁹ 0.954	22 ⁸ 0.982	0.010	0.031	0.939						
25	AYONIX-001	32 ⁷ 0.341	31 ⁸ 0.527	28 ⁸ 0.993	25 ⁹ 0.994	25 ³ 0.778	32 ¹ 0.824	31 ⁶ 0.920	22 ⁰ 0.999	25 ⁹ 0.999	22 ⁷ 0.969	0.010	0.031	0.939						
26	AYONIX-002	32 ⁵ 0.341	31 ⁹ 0.527	28 ⁹ 0.993	24 ⁸ 0.464	25 ² 0.778	32 ³ 0.824	31 ⁷ 0.920	21 ⁹ 0.999	24 ⁶ 0.915	22 ⁴ 0.969	0.010	0.031	0.939						
27	CAMVI-003	29 ⁶ 0.052	28 ⁸ 0.090	23 ⁹ 0.911	23 ⁹ 0.093	23 ⁷ 0.360	21 ⁸ 0.071	19 ⁹ 0.132	11 ¹ 0.970	18 ¹ 0.114	13 ⁴ 0.402	0.006	0.013	0.675						
28	CAMVI-004	29 ⁶ 0.047	28 ² 0.077	20 ² 0.744	22 ⁹ 0.072	23 ¹ 0.296	22 ⁰ 0.072	20 ¹ 0.136	17 ¹ 0.999	17 ⁰ 0.100	19 ⁴ 0.787	0.000	0.000	0.000						
29	CAMVI-005	30 ⁶ 0.065	29 ⁴ 0.103	20 ⁴ 0.746	23 ⁹ 0.098	23 ⁶ 0.341	24 ⁹ 0.099	23 ⁰ 0.179	22 ⁸ 1.000	19 ⁶ 0.156	23 ⁹ 0.999	0.000	0.000	0.000						
30	CANON-001	25 ¹ 0.001	8 ⁰ 0.006	54 ⁴ 0.088	39 ⁰ 0.001	29 ⁰ 0.007	33 ¹ 0.062	36 ⁰ 0.005	38 ⁰ 0.023	29 ⁰ 0.365	41 ¹ 0.008	30 ⁰ 0.068	30 ¹ 0.139	0.001	0.000	0.042	0.000			
31	CANON-002	32 ¹ 0.001	11 ⁰ 0.006	66 ¹⁰ 0.001	29 ¹ 0.001	33 ⁰ 0.007	29 ⁰ 0.059	40 ⁵ 0.005	33 ⁰ 0.020	33 ⁰ 0.407	61 ⁰ 0.013	47 ⁰ 0.075	83 ¹ 0.188	0.001	0.000	0.042	0.000			
32	CIB-000	72 ⁰ 0.002	39 ⁰ 0.008	64 ⁰ 1.000	69 ⁰ 0.002	63 ⁰ 0.011	46 ⁰ 0.069	92 ⁰ 0.012	85 ⁰ 0.045	24 ⁵ 1.000	81 ⁰ 0.017	62 ⁰ 1.411	21 ⁰ 0.894	0.000	0.000	0.000	0.000			
33	CLEARVIEWAI-000	22 ¹ 0.001	20 ⁰ 0.007	18 ⁰ 0.062	37 ¹ 0.001	23 ⁰ 0.006	22 ⁰ 0.056	39 ⁰ 0.006	46 ⁰ 0.025	11 ⁶ 0.974	42 ¹ 0.008	30 ⁰ 0.057	11 ⁰ 0.268	0.000	0.000	0.037	0.000			
34	CLOUDWALK-HR-000	66 ⁰ 0.001	67 ⁰ 0.010	22 ⁰ 0.644	30 ⁰ 0.002	27 ⁰ 0.006	23 ⁰ 0.057	18 ⁰ 0.002	18 ⁰ 0.013	6 ⁰ 1.133	21 ⁰ 0.005	15 ⁰ 0.033	28 ⁰ 0.099	0.001	0.000	0.042	0.000			
35	CLOUDWALK-MT-000	90 ⁰ 0.002	88 ⁰ 0.011	8 ⁰ 0.057	19 ⁰ 0.001	3 ⁰ 0.004	12 ⁰ 0.051	17 ⁰ 0.002	17 ⁰ 0.013	4 ⁰ 1.109	7 ⁰ 0.002	7 ⁰ 0.018	7 ⁰ 0.072	0.001	0.000	0.042	0.000			
36	CLOUDWALK-MT-001	88 ⁰ 0.002	89 ⁰ 0.011	5 ⁰ 0.053	2 ⁰ 0.001	2 ⁰ 0.003	2 ⁰ 0.042	18 ⁰ 0.002	9 ⁰ 0.012	2 ⁰ 0.012	2 ⁰ 0.070	7 ⁰ 0.001	10 ⁰ 0.015	2 ⁰ 0.056	0.001	0.000	0.042	0.000		
37	CLOUDWALK-MT-002	88 ⁰ 0.002	87 ⁰ 0.011	2 ⁰ 0.052	1 ⁰ 0.001	1 ⁰ 0.002	1 ⁰ 0.041	13 ⁰ 0.002	7 ⁰ 0.011	1 ⁰ 0.063	1 ⁰ 0.001	2 ⁰ 0.013	1 ⁰ 0.055	0.001	0.000	0.042</				

#	ALGORITHM	INVESTIGATION MODE										IDENTIFICATION MODE										FAILURE TO EXTRACT FEATURES										
		RANK ONE MISS RATE, FNIR(N, 0, 1)					N=1.6M					HIGH T → FPIR = 0.001, FNIR(N, T, L)					N=1.6M															
		GALLERY	MUGSHOT	MUGSHOT	MUGSHOT	VISA	BORDER	BOR _L 10YR	KIOSK	MUGSHOT	MUGSHOT	MUGSHOT	VISA	BORDER	BOR _L 10YR	KIOSK	MUGSHOT	MUGSHOT	MUGSHOT	VISA	BORDER	BOR _L 10YR	KIOSK									
47	COGNITEC-001	250	0.012	232	0.034	263	0.958			242	0.102	244	0.230	314	1.000						0.003	0.002	0.924									
48	COGNITEC-002	207	0.006	210	0.025	257	0.949			196	0.053	229	0.178	243	1.000						0.003	0.002	0.924									
49	COGNITEC-003	205	0.006	213	0.025	248	0.930			192	0.053	221	0.162	246	1.000						0.004	0.002	0.878									
50	COGNITEC-004	161	0.003	151	0.016	223	0.813	182	0.013	134	0.057	177	0.143	163	0.031	161	0.097	149	0.990	164	0.068	105	0.316	112	0.288	0.002	0.001	0.635	0.006			
51	COGNITEC-005	79	0.002	73	0.010	196	0.713	199	0.021	125	0.037	147	0.115	78	0.010	81	0.041	284	1.000	136	0.041	72	0.157	78	0.179	0.002	0.001	0.614	0.017			
52	COGNITEC-006	74	0.002	63	0.010	193	0.703	135	0.007	103	0.024	137	0.111	69	0.008	77	0.040	320	1.000	112	0.030	78	0.171	182	0.681	0.002	0.001	0.568	0.003			
53	CUBOX-000	58	0.001	70	0.010	12	0.058	42	0.002	12	0.004	8	0.049	27	0.003	29	0.019	10	0.168	17	0.004	14	0.028	7	0.073	0.001	0.000	0.042	0.000			
54	CYBERLINK-000	174	0.004	181	0.020	197	0.717	158	0.007	171	0.134	204	0.056	183	0.116	175	0.995	162	0.063	122	0.339	0.001	0.001	0.663								
55	CYBERLINK-001	166	0.004	167	0.018	198	0.731	151	0.007	169	0.133	197	0.054	180	0.109	179	0.995	159	0.062	178	0.652	0.000	0.000	0.040								
56	CYBERLINK-002	143	0.003	144	0.012	175	0.577	106	0.004	129	0.107	102	0.015	101	0.053	144	0.988	99	0.024	113	0.288	0.001	0.000	0.042								
57	CYBERLINK-003	75	0.002	50	0.009	182	0.474	86	0.003	64	0.012	77	0.082	70	0.008	69	0.035	114	0.972	65	0.012	53	0.100	130	0.368	0.000	0.000	0.039	0.000			
58	CYBERLINK-004	81	0.002	100	0.011	143	0.423	83	0.003	61	0.011	120	0.104	66	0.007	69	0.036	269	1.000	67	0.013	54	0.109	221	0.954	0.000	0.000	0.111	0.000			
59	CYBERLINK-005	93	0.002	81	0.011	96	0.209	65	0.002	54	0.010	108	0.098	82	0.010	78	0.041	234	1.000	71	0.014	49	0.089	218	0.926	0.000	0.000	0.034	0.000			
60	DAHUA-000	233	0.009	217	0.026					232	0.086	200	0.135								0.004	0.003										
61	DAHUA-001	207	0.007	206	0.024	184	0.703			222	0.073	191	0.122	127	0.980						0.002	0.002	0.346									
62	DAHUA-002	98	0.002	103	0.012	122	0.304	81	0.003	80	0.084	103	0.015	87	0.046	57	0.638	78	0.017	66	0.159	0.001	0.000	0.099								
63	DAHUA-003	37	0.001	23	0.007	94	0.206	57	0.002	50	0.009	53	0.073	97	0.014	80	0.041	52	0.579	66	0.013	46	0.081	48	0.134	0.000	0.000	0.000	0.000			
64	DAHUA-004	21	0.001	27	0.008	29	0.144	43	0.002	35	0.007	44	0.069	65	0.007	48	0.026	45	0.485	49	0.008	26	0.051	39	0.113	0.000	0.000	0.000	0.000			
65	DAON-000	177	0.004	162	0.017	164	0.530	127	0.005	92	0.020	156	0.125	134	0.023	115	0.061	233	1.000	100	0.025	80	0.173	205	0.846	0.002	0.002	0.108	0.001			
66	DECATUR-000	119	0.002	107	0.011	104	0.229	116	0.004	89	0.019	130	0.109	137	0.023	121	0.066	62	0.675	104	0.027	79	0.173	96	0.239	0.001	0.000	0.044				
67	DEEPLINT-001	62	0.001	19	0.007	92	0.200	73	0.002	54	0.073	33	0.003	19	0.014	225	1.000	31	0.006	63	0.159	0.000	0.000	0.038								
68	DEEPSEA-001	182	0.004	152	0.016	224	0.814	169	0.010	170	0.140	184	0.046	171	0.101	136	0.985	169	0.077	177	0.099	169	0.557	0.001	0.002	0.102						
69	DERMALOG-003	314	0.126	305	0.217	247	0.296	247	0.560	307	0.482	304	0.655	233	0.677	208	0.870	0.002	0.002	0.103												
70	DERMALOG-004	312	0.125	304	0.215	247	0.930	237	0.135	247	0.467	308	0.480	305	0.657	176	0.995	237	0.603	206	0.856	0.001	0.002	0.107								
71	DERMALOG-005	261	0.015	239	0.037	192	0.701	242	0.242	239	0.384	235	0.088	214	0.154	147	0.990	216	0.300	174	0.614	0.001	0.002	0.102								
72	DERMALOG-006	223	0.008	217	0.024	182	0.619	170	0.010	188	0.155	191	0.052	171	0.105	137	0.981	157	0.059	122	0.318	0.003	0.006	0.181								
73	DERMALOG-007	232	0.009	219	0.027	187	0.675	186	0.014	191	0.170	233	0.086	212	0.152	148	0.990	177	0.099	169	0.557	0.001	0.002	0.102								
74	DERMALOG-008	154	0.003	140	0.015	159	0.516	148	0.007	117	0.029	178	0.139	182	0.045	161	0.094	265	1.000	154	0.057	112	0.382	220	0.940	0.000	0.000	0.002	0.000			
75	DERMALOG-009	153	0.003	139	0.014	87	0.167	156	0.007	159	0.999	123	0.106	126	0.021	122	0.066	247	1.000	114	0.031	148	0.999	203	0.840	0.001	0.001	0.018	0.003			
76	DERMALOG-010	122	0.002	97	0.011	31	0.666	217	0.038	145	0.124	143	0.113	64	0.007	105	0.055	209	0.999	175	0.089	146	1.000	161	0.522	0.001	0.001	0.018	0.003			
77	DERMALOG-011	76	0.002	70	0.010	62	0.096	95	0.003	119	0.031	99	0.092	129	0.022	151	0.087	196	0.998	185	0.129	142	0.991	191	0.764	0.000	0.000	0.013	0.000			
78	DIGIDATA-000	333	0.590	320	0.548	237	0.895	253	0.642	153	0.707	258	0.813	315	0.610	296	0.577	164	0.994	241	0.646	132	0.789	201	0.824	0.002	0.001	0.070	0.001			
79	DILUSENSE-000	123	0.002	102	0.012	120	0.297	161	0.008	118	0.028	119	0.099	161	0.030	144	0.078	88	0.655	131	0.039	122	0.664	87	0.203	0.001	0.001	0.219	0.006			
80	DILUSENSE-001	61	0.001	60	0.010	110	0.250	141	0.006	80	0.016	87	0.088	72	0.009	67	0.034	38	0.456	74	0.015	119	0.511	49	0.137	0.001	0.001	0.219	0.007			
81	EYEDEA-003	307	0.080	298	0.148	266	0.960	234	0.101	239	0.379	299	0.388	294	0.543	169	0.994	235	0.570	199	0.792	0.001	0.003	0.161								
82	F8-001	254	0.012			186	0.669	297	1.000	269	1.000	269	0.166			199	0.998					0.004	1.000	0.158								
83	FINCORE-000	245	0.011	233	0.034	210	0.767	210	0.032	144	0.117	209	0.191	238	0.134	237	0.217	231	1.000	203	0.187	121	0.598	147	0.458	0.000	0.001	0.043	0.000			
84	FIRSTCREDITZ-001	39	0.001	42	0.008	61	0.094	58	0.002	55	0.010	37	0.065	29	0.003	24	0.019	24	0.291	38	0.007	34	0.061	23	0.097	0.000	0.001	0.047	0.001			
85	FUJITSULAB-000	126	0.002	132	0.014	146	0.440	111	0.004	96	0.023	107	0.098	127	0.021	108																

#	ALGORITHM	INVESTIGATION MODE						IDENTIFICATION MODE						FAILURE TO EXTRACT						
		RANK ONE MISS RATE, FNIR(N, 0, 1)						HIGH T → FPIR = 0.001, FNIR(N, T, L)						FEATURES						
		N=1.6M						N=1.6M												
GALLERY	MUGSHOT	MUGSHOT	MUGSHOT	VISA	BORDER	BOR ₂ 10YR	KIOSK	MUGSHOT	MUGSHOT	MUGSHOT	VISA	BORDER	BOR ₂ 10YR	KIOSK	MUGSHOT	MUGSHOT	MUGSHOT	VISA	BORDER	KIOSK
PROBE	MUGSHOT	WEBCAM	PROFILE	BORDER	BOR ₂ 10YR	KIOSK	MUGSHOT	WEBCAM	PROFILE	BORDER	BOR ₂ 10YR	KIOSK	MUGSHOT	WEBCAM	PROFILE	BORDER	BOR ₂ 10YR	KIOSK		
93	GORILLA-005	160.003	170.018	99.209	140.006	158.124	208.058	206.042	64.700	174.088	130.315	0.000	0.000	0.040						
94	GORILLA-006	87.002	108.012	71.122	94.003	84.018	122.015	152.027	153.089	50.531	105.028	76.166	96.218	0.000	0.000	0.041			0.000	
95	GORILLA-007	83.002	80.011	69.114	70.002	82.016	86.088	150.027	146.077	51.534	101.026	95.264	78.178	0.000	0.000	0.041			0.000	
96	GORILLA-008	67.001	64.010	52.085	48.002	68.012	78.082	138.024	147.083	39.463	111.030	107.319	74.178	0.000	0.000	0.041			0.000	
97	GRIAULE-000	143.002	126.014	128.327	173.011	122.031	158.126	124.020	118.063	171.095	121.033	85.185	80.198	0.000	0.002	0.090			0.001	
98	GRIAULE-001	36.001	35.008	76.132	15.001	98.023	38.065	49.005	53.028	85.865	35.007	143.995	26.099	0.000	0.000	0.000			0.000	
99	HIK-003	251.012	222.027	198.689	178.012	182.151	243.103	216.158	169.069	192.042	147.445	0.000	0.000	0.048						
100	HIK-004	248.011	220.027	201.743	176.012	184.152	239.099	213.153	117.976	190.037	142.434	0.000	0.000	0.048						
101	HIK-005	186.005	157.017	166.535	153.007	136.111	177.044	139.077	22.999	163.068	168.541	0.000	0.000	0.000						
102	HIK-006	187.005	156.017	167.535				186.047	150.086	260.1000		0.000	0.000	0.000						
103	HYPERVERGE-001	54.001	92.011	38.067	41.002	30.007	31.061	44.004	66.031	18.220	36.007	28.053	31.101	0.001	0.000	0.041			0.000	
104	HYPERVERGE-002	51.001	86.011	19.063	31.001	25.006	28.058	35.004	51.027	16.210	25.006	25.048	20.093	0.001	0.000	0.041			0.000	
105	HZAILU-000	124.002	124.013	108.244	87.003	78.015	90.090	125.020	92.051	107.967	88.020	104.316	69.153	0.001	0.001	0.054			0.001	
106	HZAILU-001	108.002	90.011	69.106	66.002	142.113	93.092	73.009	23.183	141.986	207.096	260.1000	181.679	0.000	0.000	0.039			0.000	
107	HZAILU-002	111.002	91.011	72.122	52.002	56.010	60.076	71.008	76.039	65.704	63.012	38.066	125.330	0.001	0.000	0.041			0.000	
108	IDEMIA-003	213.007	231.034	26.098	195.018	20.210	187.047	222.165		183.0123	197.0766	0.000	0.000	0.041						
109	IDEMIA-004	208.007	229.032	256.947	194.018	208.210	173.037	187.118	115.973	184.0123	192.766	0.000	0.000	0.041						
110	IDEMIA-005	223.008	247.039	259.954	201.021	212.217	179.044	211.150	128.978	186.130	209.879	0.000	0.000	0.041						
111	IDEMIA-006	237.010	279.072	275.969	206.030	220.253	176.043	242.226	132.982	193.144	187.733	0.000	0.000	0.041						
112	IDEMIA-007	144.003	149.015	318.100	142.006	124.036	165.131	115.018	104.055	28.1000	148.052	83.182	30.1000	0.000	0.000	0.040			0.000	
113	IDEMIA-008	20.001	13.007	48.079	40.001	34.007	59.075	14.002	16.013	15.204	20.005	19.036	34.106	0.000	0.000	0.040			0.000	
114	IDEMIA-009	9.001	12.006	28.065	17.001	17.005	15.051	7.002	9.011	7.141	10.003	12.027	10.074	0.000	0.000	0.040			0.000	
115	IDEMIA-010	7.001	9.006	19.058	7.001	8.004	7.049	1.001	2.008	5.131	5.002	12.028	3.070	0.000	0.000	0.037			0.000	
116	IMAGUS-002	321.0220	309.301	286.988				319.079	311.816	256.1000		0.004	0.008	0.550						
117	IMAGUS-003	327.0356	316.513	299.993				321.807	319.090	248.1000		0.004	0.008	0.550						
118	IMAGUS-005	106.002	108.012	125.319	139.006	94.022	167.132	119.018	130.066	83.838	107.029	75.161	93.231	0.000	0.000	0.000			0.000	
119	IMAGUS-006	115.002	129.014	118.293	114.004	91.019	139.112	122.019	126.069	93.897	106.028	74.161	108.260	0.000	0.000	0.000			0.000	
120	IMAGUS-007	116.002	122.013	126.321	107.004	95.022	147.117	136.023	132.073	91.893	115.031	77.169	109.265	0.000	0.000	0.000			0.000	
121	IMAGUS-008	309.086	289.093	126.305	200.021	140.081	150.119	329.074	308.0774	178.0996	233.0520	147.1000	168.0518	0.000	0.000	0.000			0.000	
122	IMPERIAL-000	142.002	146.015	116.280	122.004		102.097	144.026	124.068	204.999	137.042	99.245	0.000	0.000	0.000					
123	INCODE-000	297.049	292.100	259.951				290.310	281.420	194.998		0.001	0.004	0.173						
124	INCODE-001	264.017	260.046	207.762				279.212	268.296	252.1000		0.001	0.004	0.173						
125	INCODE-002	268.018	262.048	228.843				275.184	262.269	158.993		0.000	0.001	0.066						
126	INCODE-003	256.013	249.040	208.764				271.167	258.264	222.999		0.000	0.001	0.066						
127	INCODE-004	167.004	167.017	153.475	166.008		172.135	200.054	198.120	168.995	161.063	118.313	0.000	0.001	0.066					
128	INCODE-005	80.002	98.011	84.147	72.002	71.013	71.079	86.011	83.043	48.0528	80.017	66.145	63.155	0.000	0.000	0.042		0.000		
129	INNOVATRICS-002	295.045	280.074	231.853				284.234	269.310	257.1000		0.000	0.001	0.046						
130	INNOVATRICS-003	281.026	265.055	238.845				280.221	268.297	231.1000		0.000	0.001	0.046						
131	INNOVATRICS-004	258.012	251.040	262.958				256.132	241.222	125.980		0.000	0.001	0.046						
132	INNOVATRICS-005	140.002	138.014	144.407	125.005		132.109	166.034	154.089	84.846	144.047	101.251	0.000	0.001	0.041					
133	INNOVATRICS-007	84.002	96.011	109.248	74.002	73.013	62.077	93.013	92.051	68.743	79.017	51.093	61.154	0.000	0.001	0.041			0.000	
134	INNOVATRICS-008	45.001	46.008	51.082	47.002	93.021	52.072	53.005	70.036	261.1000	68.013	135.886	51.139	0.000	0.004	0.000			0.000	
135	INTELIGENSIJA-000	115.002	113.012	97.210	120.004	123.033	151.124	139.024	138.077	75.786	152.053	93.235	108.255	0.001	0.000	0.046			0.001	
136	INTELLIVISION-001	288.036	293.102	277.972	225.057	150.222	233.033	288.279	240.404	237.1000	218.328	128.749	183.685	0.001	0.000	0.044			0.000	
137	INTELLIVISION-002	244.011	228.031	259.942	193.018	139.080	202.200	263.154	235.196	207.099	188.0134	117.437	148.460	0.001	0.000	0.043			0.000	
138	INTEMA-000	27.001	43.008	10.058	20.001	22.005	11.051	21.002	24.017	259.1000	22.005	101.288	13.081	0.000	0.000	0.040			0.000	

Table 15: **Miss rates by dataset**: At left, rank 1 miss rates relevant to investigations; at right, with threshold set to target FPIR = 0.01 for higher volume, low prior, uses. Yellow indicates most accurate algorithm. Throughout blue superscripts indicate the rank of the algorithm for that column.

2023/04/04
07:31:47

$\text{FNIR}(N, k, l) =$ False neg. identification rate
 $\text{FPIR}(N, T) =$ False pos. identification rate

N = Num. enrolled subjects
 R = Num. candidates examined
 I = I threshold

$T = 0 \rightarrow$ Investigation
 $T > 0 \rightarrow$ Identification

#	ALGORITHM	INVESTIGATION MODE										IDENTIFICATION MODE										FAILURE TO EXTRACT FEATURES														
		RANK ONE MISS RATE, FNIR(N, 0, 1)										HIGH T → FPIR = 0.001, FNIR(N, T, L)										N=1.6M														
		GALLERY	MUGSHOT	MUGSHOT	MUGSHOT	VISA	BORDER	BOR;10YR	KIOSK	MUGSHOT	MUGSHOT	MUGSHOT	VISA	BORDER	VISA	MUGSHOT	MUGSHOT	MUGSHOT	VISA	BORDER	KIOSK	MUGSHOT	MUGSHOT	WEBCAM	PROFILE	BORDER	BOR;10YR	KIOSK								
139	INTEMA-001	¹ 0.001	³² 0.601	⁴ 0.052	⁸ 0.001	⁶⁵ 0.012	⁴ 0.046			⁵ 0.001	²⁹ 0.603	³ 0.103	¹⁴ 0.004	¹²⁴ 0.715	¹¹ 0.076	0.001	0.000	0.041				0.000	0.000													
140	INTSYSMSU-000	³¹⁶ 0.146	²⁰⁶ 0.023	¹⁷ 0.562	²³⁰ 0.072			¹⁶⁶ 0.132		³³² 0.998	³²⁶ 1.000	²³¹ 1.000	²⁵ 0.999			²³⁷ 0.999							0.000	0.000	0.050											
141	IREX-000	¹⁸³ 0.004	⁵⁷ 0.010	¹⁸⁸ 0.681	⁷¹ 0.002	⁶⁶ 0.012	⁷⁵ 0.082			¹⁵⁶ 0.028	¹¹⁴ 0.060	¹⁰¹ 0.957	¹⁴⁰ 0.044	¹⁰³ 0.302	⁷² 0.170	0.000	0.000	0.042				0.000	0.000													
142	ISYSTEMS-002	²⁰⁷ 0.006	²¹⁶ 0.026	²² 0.844						²²⁶ 0.078	¹⁹⁴ 0.126	¹⁸⁷ 0.998					0.002	0.002	0.142																	
143	ISYSTEMS-003	¹⁹⁵ 0.005	²⁰² 0.023	²¹³ 0.791						²⁰⁹ 0.059	¹⁷⁸ 0.107	²³⁸ 1.000					0.002	0.002	0.142																	
144	KAKAO-000	⁶⁵ 0.001	⁷⁹ 0.011	⁷⁰ 0.119	⁷⁶ 0.002	⁷⁰ 0.013	⁶⁶ 0.078			¹⁰⁵ 0.015	¹⁰⁷ 0.056	⁴¹ 0.468	⁸⁵ 0.019	⁶¹ 0.141	⁶⁴ 0.158	0.000	0.000	0.041				0.000	0.000													
145	KAKAO-001	³⁵ 0.001	⁵¹ 0.009	⁹ 0.058	¹² 0.001	¹⁴ 0.004	⁵ 0.047			²⁴ 0.003	²⁶ 0.017	⁹ 0.159	¹⁶ 0.004	²² 0.042	⁹ 0.074	0.000	0.000	0.040				0.000	0.000													
146	KEDACOM-001	²¹⁹ 0.008	²³⁵ 0.036	²⁷ 0.972	²¹² 0.034			²¹⁴ 0.237	¹³⁵ 0.023	¹³⁰ 0.072	¹⁴⁶ 0.986	¹⁵ 0.055					0.000	0.000	0.000				0.000	0.000												
147	KNERON-000	²⁰² 0.006	²²¹ 0.027	¹⁷² 0.552	²⁰⁵ 0.028			²⁰¹ 0.195															0.000	0.000												
148	KNERON-001	²⁸⁴ 0.030	³² 0.621	¹⁰ 0.237	²³⁹ 0.144	¹⁴⁹ 0.207	²²⁵ 0.280																0.000	0.000	0.000											
149	LINE-000	¹²⁷ 0.002	¹³⁰ 0.014	¹⁰³ 0.223	¹³² 0.005	¹¹⁵ 0.029	¹²⁷ 0.107	¹⁶² 0.031	¹⁶⁴ 0.095		¹⁴² 0.046	⁹⁸ 0.278	²⁷⁰ 1.000											0.000	0.000	0.000										
150	LINE-001	²⁶ 0.001	²⁴ 0.007	²¹ 0.603	³⁰ 0.002	⁴⁴ 0.008	⁸⁵ 0.085		³⁰ 0.005	⁴⁹ 0.027	²⁷⁰ 1.000	⁵⁰ 0.009	⁴¹ 0.072	²⁸¹ 1.000										0.000	0.000	0.000										
151	LINECLOVA-002	⁴⁷ 0.001	²⁶ 0.008	³⁹ 0.070	⁴⁵ 0.002	⁶² 0.011	²⁷ 0.058		³⁶ 0.004	¹⁹⁶ 0.130	¹²⁹ 0.981	¹³⁴ 0.040	¹⁴⁸ 1.000	¹⁸⁴ 0.700										0.000	0.001	0.040										
152	LINECLOVA-003	¹¹ 0.001	³²⁵ 0.601	⁶ 0.099	¹⁸ 0.001	⁴⁶ 0.009	⁸⁴ 0.085		²⁵ 0.003	³⁰⁰ 0.606		²⁴ 0.006	¹⁴⁰ 0.974	³⁶ 0.110										0.000	0.000	0.024										
153	LOOKMAN-003	²²⁸ 0.009	²⁴⁵ 0.038		²¹⁵ 0.035			²¹⁶ 0.239		¹⁷⁸ 0.044	¹⁸² 0.112		¹⁷³ 0.084										0.000	0.000												
154	LOOKMAN-004	²³⁰ 0.009	²⁴⁸ 0.039	²⁸ 0.973						¹⁸¹ 0.045	¹⁷⁶ 0.105	¹¹⁸ 0.977											0.000	0.000												
155	LOOKMAN-005	²²² 0.008	²³⁸ 0.036	²⁷ 0.972	²¹⁴ 0.035			²¹⁵ 0.237		¹⁶⁰ 0.030	¹⁴⁹ 0.086	¹²¹ 0.978	¹⁶⁰ 0.062										0.000	0.000												
156	MANTRA-000	⁸⁶ 0.002	⁷¹ 0.010	¹⁹ 0.709	¹⁵⁹ 0.007	¹⁰³ 0.024	¹³⁸ 0.112		⁸³ 0.010	⁷⁹ 0.041	³⁰⁸ 1.000	¹⁰⁸ 0.029	⁷⁰ 0.152	²⁴⁰ 1.000									0.002	0.001	0.591		^{0.003}									
157	MAXVISION-000	¹³⁹ 0.002	¹⁴² 0.015	¹² 0.327	¹¹ 0.004	¹³¹ 0.051	¹¹² 0.101		¹⁵⁷ 0.028	²⁴⁵ 0.237	⁷² 0.767	¹⁹ 0.149	¹⁴⁴ 0.997	¹⁶⁸ 0.557									0.000	0.000	0.042											
158	MAXVISION-001	³⁸ 0.001	²⁸ 0.008	²⁷ 0.064	²² 0.001	⁸⁷ 0.018	²⁵ 0.057		⁴¹ 0.004	⁴⁴ 0.025	¹⁷ 0.219	³⁴ 0.007	¹³⁷ 0.951	³⁰ 0.100									0.000	0.000	0.042											
159	MEGVII-001	²⁵² 0.012	¹⁶⁶ 0.017	²⁸⁷ 1.000						²²¹ 0.072	¹⁶⁸ 0.097												0.002	0.000												
160	MEGVII-002	²⁵³ 0.012	¹⁶⁸ 0.017	¹⁴⁷ 0.450	³¹⁷ 1.000					²²⁵ 0.077	¹⁶⁶ 0.096	¹⁹⁸ 0.998											0.002	0.000	0.033											
161	MICROFOCUS-003	³³⁵ 0.594	³³¹ 0.781		²⁵ 0.708			²⁵⁸ 0.907	³² 0.931	³²⁵ 0.979		²⁵ 0.982											0.001	0.005												
162	MICROFOCUS-004	³³² 0.576	³³⁰ 0.758		²⁵⁵ 0.701			²⁵⁷ 0.904	³³³ 0.999	³²³ 0.975		²⁵⁰ 0.974											0.001	0.005												
163	MICROFOCUS-005	³²⁸ 0.424	³²⁴ 0.601		²⁵⁹ 0.494			²⁵¹ 0.777	³²⁵ 0.835	³¹⁹ 0.928		²⁴⁸ 0.935											0.001	0.005												
164	MICROFOCUS-006	³²⁹ 0.427	³²² 0.583		²⁴⁹ 0.490			²⁵⁴ 0.782	³³⁰ 0.978	³¹⁸ 0.923		²⁴⁷ 0.923											0.001	0.005												
165	MICROSOFT-003	⁷⁷ 0.002	¹¹⁰ 0.012		¹⁰⁴ 0.004			¹³⁴ 0.109	¹⁵⁴ 0.028	¹⁵⁸ 0.091		¹² 0.036	⁹⁵ 0.233										0.000	0.001												
166	MICROSOFT-004	⁶⁸ 0.001	¹⁰⁹ 0.012		⁹⁸ 0.004			¹³⁵ 0.109	¹⁴⁵ 0.026	¹⁵² 0.087		¹²² 0.033	⁹¹ 0.222										0.000	0.001												
167	MICROSOFT-005	¹⁰² 0.002	⁸⁵ 0.011	⁸⁰ 0.144	⁹¹ 0.003			¹⁰⁸ 0.099	¹⁴² 0.026	¹²⁸ 0.070	⁵³ 0.587	¹⁰³ 0.027	⁷⁹ 0.180										0.000	0.001	0.049											
168	MICROSOFT-006	¹¹⁰ 0.002	¹⁰¹ 0.011	⁸⁰ 0.150	¹⁰² 0.004			¹¹¹ 0.100	⁸⁸ 0.012	⁷¹ 0.037	³¹ 0.386	¹¹⁰ 0.032	⁷⁵ 0.178										0.000	0.001	0.049											
169	MUKH-002	²⁸⁰ 0.026	²³⁷ 0.036	¹⁸³ 0.638	¹⁷⁴ 0.012	¹³⁸ 0.079			¹⁶¹ 0.129	³¹³ 0.594	²⁵¹ 0.242	²⁴⁴ 1.000	¹⁹⁹ 0.170	¹²⁷ 0.741	¹³⁴ 0.389									0.000	0.000	0.042		^{0.000}								
170	NEC-000	²⁶⁵ 0.017	²⁵³ 0.041	²⁶ 0.959	²⁰² 0.025			²¹⁸ 0.243	²²⁸ 0.079	²⁰⁵ 0.140	¹²⁴ 0.979												¹⁵³ 0.474		0.001	0.002	^{0.890}									
171	NEC-001	²⁷⁴ 0.021	²⁶⁶ 0.056	²³⁷ 0.967	²¹¹ 0.033			²²² 0.277	²⁴⁵ 0.106	²³⁴ 0.197	¹³⁹ 0.986	¹⁸⁷ 0.133											¹⁵¹ 0.468		0.005	0.003	^{0.934}									
172	NEC-002	¹⁸ 0.001	⁴⁸ 0.009	¹³ 0.363	⁹ 0.003			¹⁴⁶ 0.117	²¹ 0.003	³² 0.020																										

#	ALGORITHM	INVESTIGATION MODE						IDENTIFICATION MODE						FAILURE TO EXTRACT FEATURES					
		RANK ONE MISS RATE, FNIR(N, 0, 1)						HIGH T → FPIR = 0.001, FNIR(N, T, L)						N=1.6M					
		GALLERY		MUGSHOT	MUGSHOT	MUGSHOT	VISA	BORDER	VISA	MUGSHOT	MUGSHOT	MUGSHOT	VISA	BORDER	VISA	MUGSHOT	MUGSHOT	MUGSHOT	VISA
	PROBE	MUGSHOT	WEBCAM	PROFILE	BORDER	BOR;10YR	KIOSK	MUGSHOT	WEBCAM	PROFILE	BORDER	BOR;10YR	KIOSK	MUGSHOT	WEBCAM	PROFILE	BORDER	BOR;10YR	KIOSK
185	NEUROTECHNOLOGY-010	40.001	56.009	40.070	34.001	39.007	43.068	81.010	74.037	23.277	60.010	45.075	43.126	0.000	0.000	0.041	0.000	0.000	0.000
186	NEUROTECHNOLOGY-012	15.001	33.008	20.063	10.001	20.005	24.057	63.007	64.032	105.059	50.008	33.061	214.016	0.000	0.000	0.039	0.000	0.000	0.000
187	NEUROTECHNOLOGY-013	16.001	32.008	11.058	9.001	15.004	21.056	42.004	37.023	28.324	29.006	23.046	177.641	0.000	0.000	0.039	0.000	0.000	0.000
188	NEWLAND-002	306.079	295.117	259.936				306.0438	287.466	210.999				0.007	0.012	0.200			
189	NOBLIS-001	323.249	312.522	297.993				335.1000	327.1000	266.1000				0.000	0.000	0.000			
190	NOBLIS-002	319.179	314.392	287.982				331.0977	335.1000	251.1000				0.000	0.000	0.000			
191	NOTIONTAG-000	141.002	111.012	93.204	110.004	79.016	99.095	110.017	113.059	59.611	92.021	69.150	73.176	0.000	0.000	0.000	0.000	0.000	
192	NTECHLAB-003	203.006	199.023	151.504				199.054	185.118	82.837				0.000	0.000	0.040			
193	NTECHLAB-004	190.005	178.019	158.506	160.008			162.129	174.041	175.105	81.833	151.053		106.263	0.000	0.000	0.040		
194	NTECHLAB-005	188.005	171.018	137.367	164.008			148.118	175.042	173.102	73.771	161.073		114.294	0.000	0.000	0.040		
195	NTECHLAB-006	178.004	161.017	137.347	157.007			144.113	169.037	161.094	71.754	159.057		105.260	0.000	0.000	0.040		
196	NTECHLAB-007	146.003	114.012	127.326	121.004			126.107	141.026	123.067	70.750	119.032		92.223	0.000	0.000	0.042		
197	NTECHLAB-008	85.002	58.010	80.157	50.003			81.084	99.014	86.045	49.529	12.033		80.183	0.000	0.000	0.044		
198	NTECHLAB-009	43.001	34.008	77.138	62.002	74.013	57.074	52.005	36.022	39.430	73.015	55.109	54.142	0.000	0.000	0.041	0.001		
199	NTECHLAB-010	25.001	41.008	51.085	40.002	43.008	26.057	22.003	22.015	22.252	37.007	32.059	24.098	0.001	0.001	0.043	0.000		
200	NTECHLAB-011	17.001	16.007	41.072	36.001	42.007	14.051	28.003	21.015	19.228	54.009	43.074	17.091	0.000	0.000	0.040			
201	PANGIAM-000	34.001	30.008	40.074	36.002	41.007	39.065	60.006	58.030	27.318	57.009	60.136	33.105	0.000	0.001	0.044	0.001		
202	PANGIAM-001	214.007	119.013	40.078	23.001	32.009	36.064	87.011	57.030	30.383	58.009	134.860	53.141	0.003	0.000	0.040	0.000		
203	PARAVISION-000	270.019	244.038	167.534	249.423			246.529	237.089	24.170	210.999	23.470	217.926	0.000	0.000	0.000			
204	PARAVISION-001	171.004	185.020	139.329	246.414			245.484	188.049	195.128	201.999	22.444		188.739	0.000	0.000	0.000		
205	PARAVISION-002	176.004	192.022	131.335	188.015			193.175	189.050	188.119	133.983	170.080		157.497	0.000	0.000	0.032		
206	PARAVISION-003	159.003	177.019	111.252	189.015			190.167	167.035	165.096	165.994	159.058		115.296	0.000	0.000	0.032		
207	PARAVISION-004	78.002	74.010	67.104	137.006			140.112	85.010	75.038	264.1000	82.018	212.908	0.000	0.000	0.032			
208	PARAVISION-005	71.002	62.010	47.079	152.007			124.106	40.004	40.024	126.980	61.011		46.132	0.000	0.000	0.038		
209	PARAVISION-007	31.001	37.008	30.066	130.005	57.010	113.101	38.004	43.025	262.1000	53.009	56.113	263.1000	0.000	0.000	0.000	0.000		
210	PARAVISION-009	14.001	23.007	37.067	33.001	11.004	18.054	25.003	30.019	67.735	11.003	16.033	8.073	0.000	0.001	0.025	0.000		
211	PARAVISION-012	8.001	18.007	17.061	30.001	10.004	15.052	6.002	13.012	42.475	8.002	10.025	4.068	0.000	0.001	0.025	0.000		
212	PIXELALL-002	185.005	195.022	227.810	172.011			198.187	244.105	277.388	268.1000	23.062		271.1000	0.000	0.000	0.000		
213	PIXELALL-003	120.002	136.014	150.515	147.006			181.151	131.022	131.073	227.1000	130.037		167.554	0.000	0.000	0.000		
214	PIXELALL-004	117.002	143.015	162.523	134.005			183.152	118.018	143.079	240.1000	146.051		233.994	0.000	0.000	0.000		
215	PIXELALL-005	104.002	84.011	111.264	177.012	111.028	179.146	90.012	90.050	262.1000	107.027	87.203	239.1000	0.000	0.000	0.000	0.000		
216	PTAKURATSATU-000	157.003	160.017	179.605	133.005	108.027	121.105	168.037	193.124	96.924	143.046	89.206	94.232	0.000	0.001	0.039	0.000		
217	QNAP-000	220.008	224.027	166.522	184.013	132.054	186.158	255.129	247.238	273.1000	201.191	120.539	235.998	0.001	0.000	0.054	0.000		
218	QNAP-001	179.004	193.022	153.498	145.006	127.041	141.112	198.054	202.137	92.928	171.081	110.368	126.0331	0.000	0.000	0.044	0.000		
219	QNAP-002	191.005	187.021	89.172	115.004	121.031	157.125	146.026	177.106	74.772	159.052	99.281	111.0272	0.001	0.004	0.057	0.001		
220	QNAP-003	151.003	164.017	85.152	162.008	135.061	97.093	121.019	313.835	154.992	232.502	240.1000	207.865	0.000	0.001	0.002	0.001		
221	QUANTASOFT-001	320.218	329.727					318.639						0.000	0.000				
222	RANKONE-002	272.019	278.071					249.118	256.261					0.000	0.000				
223	RANKONE-003	271.019	276.068					248.118	255.255					0.000	0.000				
224	RANKONE-004	294.041	297.141					277.193	282.426					0.000	0.000				
225	RANKONE-005	234.009	252.041	283.986				210.059	227.173	192.998				0.000	0.000	0.489			
226	RANKONE-006	193.005	214.019	215.797				170.037		119.977				0.002	0.000	0.167			
227	RANKONE-007	163.003	174.019	215.796				133.022	162.095	106.967				0.001	0.001	0.102			
228	RANKONE-009	135.002	116.013	167.549	126.006	171.134	113.018	135.076	116.969	158.062		124.328	0.000	0.000	0.000				
229	RANKONE-010	128.002	65.010	139.374	128.005	106.027	159.126	96.014	111.058	78.802	149.052	90.208	103.0259	0.000	0.000	0.000	0.000		
230	RANKONE-011	69.002	99.011	103.223	100.004	88.019	79.082	74.009	88.048	12.037	82.0182	227.977	0.000	0.000	0.000	0.000			

Table 17: **Miss rates by dataset:** At left, rank 1 miss rates relevant to investigations; at right, with threshold set to target FPIR = 0.01 for higher volume, low prior, uses. Yellow indicates most accurate algorithm. Throughout blue superscripts indicate the rank of the algorithm for that column.

2023 / 04 / 04 07:31:47

FNIR(N, R, T) = False neg. identification rate

N = Num. enrolled subjects

T = Threshold

T = 0 → Investigation

T > 0 → Identification

#	ALGORITHM	INVESTIGATION MODE										IDENTIFICATION MODE										FAILURE TO EXTRACT FEATURES										
		RANK ONE MISS RATE, FNIR(N, 0, 1)					HIGH T → FPIR = 0.001, FNIR(N, T, L)					N=1.6M					N=1.6M					N=1.6M										
		GALLERY	MUGSHOT	MUGSHOT	MUGSHOT	VISA	BORDER	VISA	MUGSHOT	MUGSHOT	MUGSHOT	VISA	BORDER	VISA	MUGSHOT	MUGSHOT	MUGSHOT	VISA	BORDER	BOR _T 10YR	KIOSK											
231	RANKONE-012	⁵² 0.001	⁷⁸ 0.010	²⁰ 0.127	⁹¹ 0.003	⁷⁶ 0.014	⁴⁵ 0.069	⁵⁸ 0.008	¹⁰² 0.053	¹⁰³ 0.029	¹⁰⁵ 0.144	¹⁵⁰ 0.465	0.000	0.000	0.000	0.000	0.000	0.000	0.000	0.000	0.000	0.000										
232	RANKONE-013	¹⁹ 0.001	¹⁵ 0.007	⁴⁸ 0.076	²³ 0.001	⁴⁵ 0.008	¹⁷ 0.054	⁴² 0.005	⁶⁶ 0.034	¹⁸¹ 0.996	⁸ 0.018	⁶³ 0.141	³⁵ 0.142	0.000	0.000	0.033	0.000	0.000	0.000	0.000	0.000	0.000	0.000	0.000	0.000	0.000						
233	RANKONE-014	¹⁰ 0.001	⁷ 0.006	³⁶ 0.067	¹⁴ 0.001	²¹ 0.005	¹⁰ 0.050	³¹ 0.003	⁴¹ 0.024	⁵⁷ 0.009	⁴⁷ 0.081	²⁹⁸ 1.000	0.000	0.000	0.000	0.006	0.000	0.000	0.000	0.000	0.000	0.000	0.000	0.000	0.000	0.000	0.000					
234	REALNETWORKS-000	²⁹³ 0.040	²⁸⁵ 0.078					²⁸ 0.234	²⁷² 0.319										0.001	0.000												
235	REALNETWORKS-001	²⁹² 0.040	²⁸⁴ 0.078					²⁸³ 0.234	²⁷¹ 0.319										0.001	0.000												
236	REALNETWORKS-002	²⁸⁹ 0.039	²⁸³ 0.078					²⁸¹ 0.231	²⁷⁰ 0.315										0.001	0.000												
237	REALNETWORKS-003	²⁷⁸ 0.024	²⁷² 0.062	²¹ 0.771	²⁰⁹ 0.031		²⁰⁵ 0.209	²⁶⁷ 0.159	²⁵⁹ 0.266	¹⁹⁷ 0.998	¹⁹⁸ 0.164	¹⁵⁸ 0.500	0.001	0.000	0.009																	
238	REALNETWORKS-004	²⁷⁶ 0.024	²⁶⁹ 0.059	²¹⁷ 0.797	²⁰⁸ 0.031		²¹⁰ 0.213	²⁶⁶ 0.158	²⁵⁷ 0.263	²¹⁵ 0.999	²⁰⁰ 0.170	¹⁷³ 0.613	0.001	0.000	0.009																	
239	REALNETWORKS-005	¹³¹ 0.002	¹²³ 0.013	¹⁴³ 0.433	¹¹⁸ 0.004	⁹⁷ 0.023	¹¹⁷ 0.102	¹⁵³ 0.028	¹³³ 0.074	¹¹² 0.971	¹²⁴ 0.037	⁹¹ 0.223	⁸⁹ 0.215	0.000	0.000	0.006	0.000	0.000	0.000	0.000	0.000	0.000	0.000	0.000	0.000	0.000	0.000	0.000				
240	REALNETWORKS-006	⁵⁷ 0.001	⁶⁶ 0.010	¹¹⁸ 0.287	⁷⁸ 0.002	³⁸ 0.010	⁶⁷ 0.078	¹⁰⁹ 0.015	⁹⁹ 0.053	¹²⁸ 0.980	⁷⁵ 0.016	⁵⁷ 0.120	⁶² 0.154	0.000	0.000	0.009	0.000	0.000	0.000	0.000	0.000	0.000	0.000	0.000	0.000	0.000	0.000	0.000				
241	REALNETWORKS-007	⁴⁸ 0.001	⁵⁵ 0.009	¹¹⁴ 0.267	⁴⁹ 0.002	⁴⁷ 0.009	⁵¹ 0.072	⁷⁰ 0.010	⁸⁴ 0.043	¹²³ 0.979	⁶¹ 0.012	¹¹⁸ 0.463	⁵² 0.140	0.000	0.000	0.009	0.000	0.000	0.000	0.000	0.000	0.000	0.000	0.000	0.000	0.000	0.000	0.000				
242	REALNETWORKS-008	³⁰ 0.001	³¹ 0.008	⁵⁹ 0.089	⁵⁰ 0.002	³⁷ 0.007	⁹¹ 0.091	⁶¹ 0.006	⁵⁶ 0.029	¹⁰⁸ 0.968	⁵⁰ 0.008	⁴⁰ 0.068	⁴⁴ 0.129	0.000	0.000	0.042	0.000	0.000	0.000	0.000	0.000	0.000	0.000	0.000	0.000	0.000	0.000	0.000				
243	RECOGNITO-000	¹⁶⁹ 0.004	¹⁰ 0.006	²³ 0.064	⁸ 0.001	¹⁰⁹ 0.028	³ 0.045	⁴ 0.005	⁸ 0.012	¹² 0.184	³ 0.007	¹²⁵ 0.730	¹⁸ 0.092	0.000	0.000	0.040	0.000	0.000	0.000	0.000	0.000	0.000	0.000	0.000	0.000	0.000	0.000	0.000				
244	REMARKAI-000	¹⁶⁵ 0.003	¹⁷² 0.018	¹⁸¹ 0.660	¹⁵⁹ 0.008		¹⁸⁰ 0.148	²⁰² 0.055	¹⁸⁹ 0.120	²¹¹ 0.999	¹⁶⁶ 0.069	¹⁸⁶ 0.717	0.000	0.000	0.000																	
245	REMARKAI-000	²² 0.009	²² 0.030					²⁵ 0.128	²³⁵ 0.203										0.000	0.001												
246	REMARKAI-002	²²⁵ 0.008	²²⁶ 0.029	²¹⁹ 0.802				²⁵² 0.124	²³³ 0.196	¹⁵¹ 0.991									0.000	0.001	0.017											
247	RENDIP-000	⁷³ 0.002	¹⁴⁴ 0.015	¹⁴⁴ 0.424	¹⁴³ 0.006	¹¹⁰ 0.028	⁸² 0.084	⁸⁹ 0.012	¹¹² 0.059	⁹² 0.894	⁹³ 0.022	⁸⁴ 0.185	⁷⁰ 0.167	0.000	0.000	0.041	0.000	0.000	0.000	0.000	0.000	0.000	0.000	0.000	0.000	0.000	0.000	0.000	0.000			
248	REVEALMEDIA-000	¹⁰⁰ 0.002	⁶¹ 0.010	¹¹⁵ 0.275	⁶³ 0.002	⁶⁷ 0.012	⁵⁶ 0.074	⁹¹ 0.012	⁸² 0.042	⁶³ 0.680	⁹ 0.021	⁵² 0.093	⁵⁶ 0.143	0.000	0.000	0.041	0.000	0.000	0.000	0.000	0.000	0.000	0.000	0.000	0.000	0.000	0.000	0.000	0.000			
249	S1-000	¹³⁷ 0.002	¹⁵⁹ 0.017	¹¹² 0.258	¹³⁵ 0.005	¹⁰⁴ 0.025	⁸⁹ 0.090	¹⁵⁵ 0.028	¹⁴⁸ 0.085	²⁷² 1.000	¹⁴⁵ 0.047	²⁶⁹ 1.000	³²¹ 1.000	0.000	0.000	0.040	0.000	0.000	0.000	0.000	0.000	0.000	0.000	0.000	0.000	0.000	0.000	0.000	0.000			
250	S1-001	¹⁵⁸ 0.003	¹³³ 0.014	¹⁰⁸ 0.215	⁸⁰ 0.003	⁸⁵ 0.018	⁶¹ 0.077	¹⁰⁷ 0.016	⁹⁶ 0.052	¹³⁷ 0.985	⁸ 0.019	⁹⁹ 0.136	³⁸ 0.148	0.001	0.000	0.035	0.000	0.000	0.000	0.000	0.000	0.000	0.000	0.000	0.000	0.000	0.000	0.000	0.000			
251	S1-002	⁵⁹ 0.001	⁵³ 0.009	⁶⁰ 0.093	²¹ 0.001	⁵⁹ 0.010	²⁰ 0.055	⁵⁷ 0.006	⁵⁹ 0.031	¹⁴ 0.196	³⁷ 0.007	¹³³ 0.792	²⁰⁴ 0.841	0.000	0.000	0.028	0.000	0.000	0.000	0.000	0.000	0.000	0.000	0.000	0.000	0.000	0.000	0.000	0.000			
252	S1-003	⁶⁴ 0.001	⁵⁹ 0.010	⁶⁸ 0.114	³⁶ 0.001	³⁶ 0.007	³⁰ 0.060	⁷² 0.009	⁷² 0.037	²⁴⁰ 1.000	⁷¹ 0.014	¹¹³ 0.396	²⁵⁶ 1.000	0.000	0.000	0.033	0.000	0.000	0.000	0.000	0.000	0.000	0.000	0.000	0.000	0.000	0.000	0.000	0.000			
253	S1-004	⁴⁹ 0.001	⁵² 0.009	²⁴ 0.064	¹⁵ 0.001	¹⁸ 0.005	⁸ 0.049	³⁹ 0.004	⁴² 0.025	¹⁸⁴ 0.997	²⁷ 0.006	³⁶ 0.064	²⁴⁹ 1.000	0.000	0.000	0.033	0.000	0.000	0.000	0.000	0.000	0.000	0.000	0.000	0.000	0.000	0.000	0.000	0.000			
254	SCANOVATE-000	¹⁹² 0.005	²⁵⁶ 0.045	¹⁷³ 0.560	²¹³ 0.035		²⁰⁹ 0.211	²¹⁷ 0.067	²⁵⁰ 0.240	⁹⁰ 0.893	²⁰¹ 0.215	¹⁵⁶ 0.400	0.000	0.001	0.057																	
255	SCANOVATE-001	¹⁹⁶ 0.005	²⁵⁰ 0.040	¹⁷⁸ 0.585	²⁰⁷ 0.031		¹⁹⁶ 0.178	²²⁹ 0.081	²⁴³ 0.227	⁹⁵ 0.911	²⁰⁵ 0.192	¹³⁹ 0.404	0.000	0.001	0.044																	
256	SENSETIME-000	¹³³ 0.002	¹⁵¹ 0.016	¹⁶³ 0.528				¹²⁸ 0.021	¹¹⁷ 0.063	³³³ 1.000							0.004	0.000	0.042													
257	SENSETIME-001	¹³⁴ 0.002	¹⁵⁰ 0.016					¹³² 0.022	¹¹⁹ 0.064									0.004	0.000	0.040												
258	SENSETIME-002	¹⁵⁹ 0.014	¹⁷⁸ 0.020	¹⁴⁰ 0.384	¹⁷¹ 0.011		¹¹⁹ 0.104	¹⁰¹ 0.015	⁵⁴ 0.028	¹⁶² 0.994	¹¹⁷ 0.032	¹⁶² 0.523	0.009	0.000	0.040																	
259	SENSETIME-003	¹³ 0.001	¹⁴ 0.007	⁸³ 0.150	⁸² 0.003		⁹² 0.091	¹² 0.002	¹¹ 0.012	⁴³ 0.477	⁴⁰ 0.008	⁴⁷ 0.133	0.000	0.000	0.041																	
260	SENSETIME-004	¹² 0.001	¹⁷ 0.007	⁴² 0.072	⁶⁹ 0.002		⁸³ 0.084	⁹ 0.002	¹⁴ 0.013	²⁰ 0.229	²⁶ 0.006	³⁸ 0.113	0.000	0.000	0.041																	
261	SENSETIME-005	⁶ 0.001	⁶ 0.006	¹⁶ 0.059	⁶⁸ 0.002	³⁵ 0.007	⁷⁴ 0.082	¹⁹ 0.002	²⁰ 0.014	¹¹ 0.173	³ 0.007	²⁷ 0.051	³² 0.104	0.000	0.000	0.041	0.000	0.000	0.000	0.000	0.000	0.000	0.000	0.000	0.000	0.000	0.000	0.000	0.000			
262	SENSETIME-006	⁵ 0.001	^{4</sup}																													

#	ALGORITHM	INVESTIGATION MODE										IDENTIFICATION MODE										FAILURE TO EXTRACT FEATURES															
		RANK ONE MISS RATE, FNIR(N, 0, 1)										HIGH T → FPIR = 0.001, FNIR(N, T, L)																									
		N=1.6M					N=1.6M					N=1.6M					N=1.6M					N=1.6M					N=1.6M										
GALLERY	PROBE	MUGSHOT	MUGSHOT	WEBCAM	PROFILE	VISA	BORDER	BOR _L 10YR	KIOSK	MUGSHOT	MUGSHOT	WEBCAM	PROFILE	BORDER	BOR _L 10YR	KIOSK	MUGSHOT	MUGSHOT	WEBCAM	PROFILE	BORDER	BOR _L 10YR	KIOSK	MUGSHOT	MUGSHOT	WEBCAM	PROFILE	BORDER	BOR _L 10YR	KIOSK							
277	SYNESIS-003	263.016	203.023	227.0827	180.013			173.0136		215.065	192.0123	104.0960	168.075			119.0314		0.000	0.001	0.063																	
278	SYNESIS-003	317.0170	306.0235							312.0582	303.0646																										
279	SYNESIS-005	226.009	118.013	203.0744	93.003			95.0092		140.025	129.072	134.0984	120.032			88.0214		0.001	0.000	0.135																	
280	T4ISB-000	239.010	207.023	159.0462	79.003	143.0115	73.0081			108.016	100.0053	46.0510	89.0021	129.0759	67.0161		0.000	0.000	0.000																		
281	TECH5-001	175.004	158.017	171.0584	147.0007			128.0107		205.0057	320.0935	274.1.000	21.0244			234.0994		0.000	0.006																		
282	TECH5-002	147.003	83.011	121.0312	92.0003	116.029	88.0089			149.027	127.070	79.0805	132.039	88.0205	144.0440		0.001	0.000	0.041																		
283	TEVIAN-003	260.015	263.052							274.0177	266.0298																										
284	TEVIAN-004	247.011	243.038							247.0117	228.0176																										
285	TEVIAN-005	217.007	225.028	151.0467						234.0087	208.0144	105.0962																									
286	TEVIAN-006	138.002	94.011	71.0123	84.0003	75.013	49.0071			80.010	62.0032	34.0425	76.016	50.0093	221.0951		0.001	0.000	0.062																		
287	TEVIAN-007	92.002	54.009	59.093	59.0002	53.0009	42.0067			55.0005	35.022	26.301	58.0009	37.0065	41.0122		0.000	0.000	0.062																		
288	TIGER-000	301.062	291.095							301.0390	289.500																										
289	TIGER-002	199.006	200.023	157.0514						231.0086	217.0158	206.0999																									
290	TIGER-003	198.006	201.023							230.0086	218.0158																										
291	TONGYITRANS-000	211.007	197.022							223.0074	181.0112																										
292	TONGYITRANS-001	212.007	198.022							216.0066	172.0101																										
293	TOSHIBA-000	184.004	190.022	208.0766						212.0062	186.0118	174.0995																									
294	TOSHIBA-001	189.005	194.022							207.0058	159.0092																										
295	TRUEFACE-000	162.003	127.014	108.0230	154.0007	101.024	96.0092			117.018	116.0062	87.0882	110.030	86.0194	82.0188		0.001	0.001	0.047																		
296	TURINGTECHVIP-001	235.009	218.026	43.0801	218.045	148.0199	213.0220			292.0345	314.0850	156.0993	251.0978	222.1000	238.0999		0.001	0.003	0.044																		
297	VD-000	331.0474	321.0551							326.0917	322.0946																										
298	VD-001	283.028	264.053							278.0201	263.0281																										
299	VD-002	236.010	223.027	231.0893	183.0013	129.0050	194.0176			227.0079	210.0148	177.0996	109.0095	109.0367	131.0372		0.004	0.003	0.156																		
300	VD-003	218.008	191.022	212.0773	163.0008	118.030	174.0137			183.0046	170.100	208.0999	147.0051	94.0244	121.0315		0.003	0.003	0.144																		
301	VERIDAS-001	150.003	138.014	171.0550	146.0006	112.028	163.0131			171.0037	146.0082	142.0987	138.0044	96.0266	108.0264		0.000	0.002	0.093																		
302	VERIDAS-002	149.003	134.014	171.0550	144.0006	113.028	164.0131			172.0037	145.0082	143.0987	139.0044	97.0266	107.0264		0.000	0.002	0.093																		
303	VERIDAS-003	95.002	93.011	121.0297	108.0004	81.016	131.0108			109.0017	106.005	105.005	181.0997	80.020	68.0150	77.0178		0.000	0.002	0.093																	
304	VERIDAS-004	50.001	36.008	91.0186	80.0003	51.0009	40.0097			58.0006	45.0025	122.0979	44.0008	31.0058	40.0118		0.000	0.002	0.094																		
305	VERIELAS-000	326.0355	313.0369	271.0968	231.086	147.0191	230.0292			320.0799	310.0813	205.0999	217.0324	136.0933	170.0589		0.002	0.001	0.070																		
306	VIGILANTSOLUTIONS-003	304.069	299.0151	284.0958						305.0408	306.0660	202.0999																									
307	VIGILANTSOLUTIONS-004	312.0125	307.0244	26.0965						311.0549	312.0817	180.0996																									
308	VIGILANTSOLUTIONS-005	231.009	241.0920							300.0388		251.0000																									
309	VIGILANTSOLUTIONS-006	238.010	242.0921							295.0353		271.0000																									
310	VIGILANTSOLUTIONS-007	164.003	163.0017	241.0925	181.0013	136.0068	192.0175			158.0208	153.0088	178.0996	172.0081	111.0371	135.0391		0.000	0.001	0.127																		
311	VIGILANTSOLUTIONS-008	156.003	165.0017	240.0913	185.0014	137.0072	195.0178			125.0021	137.0077	203.0999	110.0104	114.0398	139.0511		0.000	0.001	0.127																		
312	VISIONBOX-000	105.002	95.0011	207.0752	124.0005	83.0017	68.0078			114.0018	109.0057	150.0990	98.0023	67.0146	68.0162		0.000	0.001	0.043																		
313	VISIONLABS-004	148.003	179.020	133.0343						206.0058	219.0159	89.0890																									
314	VISIONLABS-005	136.002	173.019	131.0334						190.0050	209.0147	88.0888																									
315	VISIONLABS-006	97.002	148.0015	97.0211	103.0004					101.0096	148.0027	157.0090	59.0672																								
316	VISIONLABS-007	91.002	147.0015	97.0211	97.0004					100.0095	147.0027	156.0090	60.0672	116.0301	81.0185		0.001	0.001	0.051				</														

#	ALGORITHM	INVESTIGATION MODE										IDENTIFICATION MODE										FAILURE TO EXTRACT FEATURES										
		RANK ONE MISS RATE, FNIR(N, 0, 1)										HIGH T → FPIR = 0.001, FNIR(N, T, L)																				
		N=1.6M					N=1.6M					N=1.6M					N=1.6M					N=1.6M					N=1.6M					
		GALLERY	MUGSHOT	MUGSHOT	MUGSHOT	VISA	BORDER	BOR _i 10YR	KIOSK	MUGSHOT	MUGSHOT	MUGSHOT	VISA	BORDER	BOR _i 10YR	KIOSK	MUGSHOT	MUGSHOT	WEBCAM	PROFILE	BORDER	BOR _i 10YR	KIOSK	MUGSHOT	MUGSHOT	WEBCAM	PROFILE	BORDER	BOR _i 10YR	KIOSK		
323	VNPT-002	103	0.002	112	0.012	37	0.068	24	0.001	28	0.006	19	0.054	62	0.007	61	0.032	25	0.292	40	0.007	42	0.072	22	0.096	0.001	0.000	0.042	0.000	0.000	0.000	
324	VCORD-003	204	0.006	210	0.024	225	0.804	227	0.061	199	0.188	251	0.122	215	0.155	197	0.998	197	0.157	138	0.404	0.001	0.011	0.425								
325	VCORD-004	221	0.008	186	0.021	214	0.792	179	0.012	160	0.127	296	0.355	225	0.173	241	1.000	206	0.193	231	0.991	0.000	0.000	0.000								
326	VCORD-005	215	0.007	204	0.023	222	0.812	223	0.055	205	0.206	265	0.158	198	0.130	187	0.997	191	0.138	132	0.381	0.001	0.009	0.554								
327	VCORD-006	338	1.000	338	1.000	303	1.000	338	1.000	289	1.000	338	1.000	337	1.000	304	1.000	262	1.000	332	1.000	0.001	0.009	0.554								
328	VTS-000	334	0.594	322	0.608	239	0.909	251	0.607	154	0.724	250	0.739	314	0.598	301	0.619	219	0.999	239	0.613	130	0.760	190	0.761	0.000	0.001	0.047	0.000			
329	VTS-001	70	0.002	69	0.010	88	0.167	138	0.006	86	0.018	64	0.077	95	0.013	94	0.051	161	0.994	94	0.022	64	0.141	84	0.192	0.000	0.000	0.040	0.000			
330	VTS-002	107	0.002	120	0.013	106	0.233	187	0.014	126	0.038	135	0.125	145	0.026	134	0.075	228	1.000	141	0.045	92	0.231	140	0.417	0.000	0.000	0.029	0.000			
331	VTS-003	29	0.001	27	0.007	44	0.074	44	0.002	48	0.009	16	0.053	67	0.007	65	0.033	249	1.000	70	0.014	138	0.954	176	0.635	0.000	0.001	0.029	0.000			
332	XFORWARDAI-000	130	0.002	131	0.014	56	0.089	105	0.004	77	0.015	98	0.094	104	0.015	103	0.053	36	0.440	90	0.021	73	0.159	71	0.169	0.000	0.000	0.000	0.000			
333	XFORWARDAI-001	118	0.002	117	0.013	34	0.067	88	0.003	49	0.009	76	0.082	51	0.005	55	0.028	37	0.448	47	0.008	35	0.062	42	0.123	0.000	0.000	0.000	0.000			
334	XFORWARDAI-002	109	0.002	107	0.012	14	0.059	75	0.002	31	0.007	61	0.077	30	0.003	23	0.016	47	0.525	23	0.005	21	0.041	22	0.099	0.000	0.000	0.000	0.000			
335	YISHENG-001	282	0.027	277	0.060	226	0.058	227	0.287	293	0.346	309	0.808	242	0.666	215	0.919	0.002	0.005													
336	YITU-002	99	0.002	72	0.010							112	0.018	89	0.049										0.000	0.000						
337	YITU-003	155	0.003	151	0.016							120	0.019	98	0.052										0.003	0.001						
338	YITU-004	44	0.001	44	0.008	232	0.866					77	0.010	50	0.027	98	0.936								0.000	0.000	0.000	0.000				
339	YITU-005	132	0.002	147	0.014							84	0.010	63	0.032										0.003	0.001						

Table 20: **Miss rates by dataset:** At left, rank 1 miss rates relevant to investigations; at right, with threshold set to target FPIR = 0.01 for higher volume, low prior, uses. Yellow indicates most accurate algorithm. Throughout blue superscripts indicate the rank of the algorithm for that column.

2023 / 04 / 04 07:31:47

FNIR(N, R, T) = False neg. identification rate
FPIR(N, T) = False pos. identification rateN = Num. enrolled subjects
R = Num. candidates examinedT = Threshold
T = 0 → Investigation

T > 0 → Identification

#	ALGORITHM	MISSES BELOW THRESHOLD, T					ENROL, MOST RECENT				
		FNIR(N, T > 0, R > L)					DATASET: FRVT 2018 MUGSHOTS				
		N=0.64M	N=1.6M	N=3.0M	N=6.0M	N=12.0M					
1	3DIVI-005	²⁷⁰ 0.1358	²⁷⁰ 0.1664	²⁴⁹ 0.1915	²³⁰ 0.2370	²²² 0.3054					
2	ACER-000	²⁶³ 0.1185	²⁶² 0.1455	²³⁴ 0.1714	²²³ 0.2074	²¹⁵ 0.2537					
3	ALCHERA-003	²⁶¹ 0.1176	²⁶⁴ 0.1553	²³⁹ 0.1853	²³¹ 0.2409	²³¹ 0.3553					
4	ALLGOVISION-000	²³⁵ 0.0688	²³⁶ 0.0881	²¹⁷ 0.1084	²⁰⁸ 0.1389	¹⁹⁵ 0.2129					
5	ALLGOVISION-001	²⁴¹ 0.0785	²⁴¹ 0.1017	²²³ 0.1218	²¹⁵ 0.1584	²⁰² 0.2273					
6	ANKE-000	²⁴⁸ 0.0942	²⁴⁶ 0.1169	²²⁹ 0.1404	²²⁰ 0.1776	²¹⁶ 0.2559					
7	ANKE-002	¹⁶⁴ 0.0229	¹⁶⁴ 0.0318	¹⁶⁷ 0.0406	¹⁵⁶ 0.0605	¹⁴⁴ 0.1466					
8	AWARE-003	²⁵⁸ 0.1098	²⁵⁴ 0.1283	²³⁰ 0.1447	²¹⁸ 0.1768	²⁰⁷ 0.2364					
9	AWARE-005	²⁵⁹ 0.3389	²⁹⁷ 0.3643	²⁴⁷ 0.3993	²³⁹ 0.4526	²¹⁵ 0.2531					
10	AYONIX-002	³²³ 0.7862	³²³ 0.8242	²⁵⁴ 0.8508	²⁴⁵ 0.8704	²³⁹ 0.8939					
11	CAMVI-004	¹⁹⁰ 0.0367	²²⁰ 0.0716	²¹¹ 0.0983	²³³ 0.2508	²¹⁷ 0.2701					
12	CANON-001	⁵⁵ 0.0039	⁵⁶ 0.0054	⁵⁶ 0.0074	⁵¹ 0.0158	⁶¹ 0.0924					
13	CANON-002	⁴⁹ 0.0036	⁴⁸ 0.0047	⁴⁷ 0.0061	⁴² 0.0124	⁴⁹ 0.0808					
14	CIB-000	⁸⁸ 0.0086	⁹² 0.0125	⁹² 0.0160	⁹⁵ 0.0303	¹¹⁴ 0.1251					
15	CLEARVIEWAI-000	⁹⁵ 0.0040	⁵⁹ 0.0058	⁵⁹ 0.0078	⁵³ 0.0159	⁶¹ 0.0971					
16	CLOUDWALK-HR-000	¹⁸ 0.0019	¹⁸ 0.0020	¹³ 0.0023	²⁰ 0.0072	²⁹ 0.0701					
17	CLOUDWALK-MT-000	¹⁸ 0.0019	¹⁷ 0.0020	¹² 0.0022	⁸ 0.0049	¹⁴ 0.0466					
18	CLOUDWALK-MT-001	¹⁶ 0.0018	¹⁵ 0.0019	⁹ 0.0020	¹⁰ 0.0052	²¹ 0.0555					
19	CLOUDWALK-MT-002	¹⁷ 0.0018	¹⁵ 0.0019	³⁶ 0.0045	²³ 0.0077	²⁵ 0.0612					
20	COGENT-000	²⁰⁹ 0.0430	¹⁹³ 0.0527	¹⁹⁴ 0.0695	¹⁹⁴ 0.1133	¹⁸³ 0.1960					
21	COGENT-001	²⁰⁸ 0.0430	¹⁹⁴ 0.0527	¹⁹⁴ 0.0695	¹⁹³ 0.1133	¹⁸⁴ 0.1960					
22	COGENT-002	¹⁷⁶ 0.0322	¹⁸⁰ 0.0444	¹⁷⁹ 0.0610	¹⁹¹ 0.1116	¹⁹⁷ 0.2180					
23	COGENT-003	¹⁷⁷ 0.0328	¹⁸⁵ 0.0463	¹⁹¹ 0.0683	²⁰¹ 0.1294	²⁰⁹ 0.2445					
24	COGENT-004	¹⁶ 0.0210	¹⁶⁵ 0.0331	¹⁷⁴ 0.0527	¹⁹⁶ 0.1138	¹⁹⁴ 0.2119					
25	COGENT-005	⁷⁶ 0.0064	⁷⁶ 0.0091	⁷⁶ 0.0123	⁹⁶ 0.0303	¹¹⁰ 0.1233					
26	COGENT-006	⁴⁹ 0.0032	⁴⁵ 0.0044	⁴⁹ 0.0057	³⁸ 0.0120	⁴¹ 0.0830					
27	COGENT-007	³⁵ 0.0028	³⁴ 0.0036	³⁷ 0.0049	³⁹ 0.0049	¹⁰ 0.0111					
28	COGNITEC-000	²⁷² 0.1377	²⁶⁸ 0.1606	²³⁹ 0.1870	²²⁵ 0.2176	²²¹ 0.2831					
29	COGNITEC-001	²⁴³ 0.0807	²⁴² 0.1017	²²³ 0.1214	²¹¹ 0.1513	²⁰⁸ 0.2238					
30	COGNITEC-002	²⁰¹ 0.0406	¹⁹⁶ 0.0531	¹⁸⁷ 0.0666	¹⁷⁹ 0.0935	¹⁷⁹ 0.1874					
31	COGNITEC-003	¹⁹⁸ 0.0400	¹⁹² 0.0526	¹⁸⁷ 0.0650	¹⁷⁴ 0.0895	¹⁷⁷ 0.1772					
32	COGNITEC-004	¹⁶³ 0.0222	¹⁶³ 0.0313	¹⁵⁹ 0.0388	¹⁴⁷ 0.0540	⁸⁸ 0.1103					
33	COGNITEC-005	⁷⁹ 0.0063	⁷⁸ 0.0096	⁸⁶ 0.0144	⁸⁹ 0.0287	⁶⁹ 0.0967					
34	COGNITEC-006	⁶⁷ 0.0053	⁶⁹ 0.0077	⁷² 0.0117	⁷⁶ 0.0254	⁵⁷ 0.0919					
35	CYBERLINK-000	²⁶³ 0.0414	²⁰⁴ 0.0565	¹⁹⁸ 0.0707	¹⁸⁷ 0.1031	¹⁹⁴ 0.2050					
36	CYBERLINK-001	¹⁹⁴ 0.0392	¹⁹⁷ 0.0536	¹⁹³ 0.0695	¹⁸⁴ 0.0973	¹⁷³ 0.1794					
37	CYBERLINK-002	⁹⁹ 0.0105	¹⁰² 0.0148	¹⁰⁷ 0.0202	¹¹⁸ 0.0399	¹¹⁵ 0.1255					
38	CYBERLINK-003	⁶⁹ 0.0056	⁷⁰ 0.0077	⁶⁷ 0.0100	⁷² 0.0235	¹¹ 0.1237					
39	CYBERLINK-004	⁶³ 0.0051	⁶⁶ 0.0071	⁷⁰ 0.0102	⁶¹ 0.0199	¹¹⁸ 0.1269					
40	CYBERLINK-005	⁷⁹ 0.0067	⁸² 0.0099	⁸¹ 0.0138	¹¹⁵ 0.0394	¹⁵ 0.1566					
41	DAHUA-001	²²⁴ 0.0569	²²² 0.0727	²⁰⁶ 0.0878	¹⁹⁷ 0.1148	¹⁷⁸ 0.1867					
42	DAHUA-002	¹⁰⁴ 0.0108	¹⁰³ 0.0151	¹⁰⁵ 0.0191	⁹¹ 0.0291	¹⁰¹ 0.1153					
43	DAHUA-003	⁹⁶ 0.0100	⁹⁷ 0.0139	⁹⁸ 0.0180	⁹² 0.0296	⁹⁴ 0.1130					
44	DAHUA-004	⁶⁹ 0.0048	⁶⁵ 0.0069	⁶⁴ 0.0090	⁵⁶ 0.0164	⁴⁹ 0.0853					
45	DAON-000	¹³⁴ 0.0161	¹³⁴ 0.0226	¹³⁸ 0.0293	¹³⁵ 0.0562	¹⁶⁶ 0.1702					
46	DECATUR-000	¹³⁷ 0.0173	¹³⁷ 0.0229	¹³⁸ 0.0305	¹²⁹ 0.0464	¹⁴⁰ 0.1433					
47	DEEPLINT-001	³³ 0.0027	³³ 0.0033	³⁰ 0.0043	⁴⁰ 0.0121	⁶⁰ 0.0922					
48	DEEPSSEA-001	¹⁸⁶ 0.0347	¹⁸⁴ 0.0462	¹⁷⁸ 0.0586	¹⁷² 0.0802	¹⁶⁶ 0.1708					
49	DERMALOG-005	²³⁹ 0.0700	²³⁸ 0.0880	²¹⁹ 0.1144	²¹⁴ 0.1578	²¹⁰ 0.2451					
50	DERMALOG-006	¹⁹² 0.0395	¹⁹¹ 0.0517	¹⁸⁹ 0.0659	¹⁸³ 0.0973	¹⁷² 0.1745					
51	DERMALOG-007	²³⁶ 0.0691	²³³ 0.0863	²¹⁹ 0.1107	²¹⁰ 0.1504	²⁰³ 0.2299					
52	DERMALOG-008	¹⁸² 0.0338	¹⁸² 0.0455	¹⁸¹ 0.0626	¹⁸⁸ 0.1060	²⁰³ 0.2276					
53	DERMALOG-009	¹²⁶ 0.0148	¹²⁶ 0.0206	¹²⁹ 0.0268	¹²² 0.0416	¹³² 0.1374					
54	DERMALOG-010	⁶⁶ 0.0052	⁶⁴ 0.0069	⁶³ 0.0088	⁶³ 0.0207	⁶⁵ 0.0971					
55	DERMALOG-011	¹²⁸ 0.0149	¹²⁹ 0.0215	¹³⁶ 0.0279	¹²⁸ 0.0461	¹⁰⁷ 0.1192					
56	DILUSENSE-000	¹⁶⁰ 0.0208	¹⁶¹ 0.0305	¹⁵⁷ 0.0377	¹⁵¹ 0.0543	¹³⁸ 0.1429					
57	DILUSENSE-001	⁷⁷ 0.0061	⁷² 0.0085	⁷⁷ 0.0109	⁷⁰ 0.0161	¹⁰ 0.1161					
58	FIRSTCREDITKZ-001	²⁷ 0.0023	²⁹ 0.0030	²⁷ 0.0039	²⁹ 0.0093	³⁶ 0.0760					
59	FUJITSULAB-000	¹² 0.0148	¹²⁷ 0.0206	¹³⁰ 0.0277	¹⁴⁹ 0.0541	¹⁷¹ 0.1739					
60	FUJITSULAB-001	¹⁰⁹ 0.0126	¹¹⁶ 0.0182	¹²¹ 0.0251	¹⁵⁹ 0.0646	¹⁹¹ 0.2079					
61	GORILLA-002	²⁷⁶ 0.1539	²⁷⁶ 0.1880	²⁴³ 0.2184	²³⁴ 0.2596	²²⁹ 0.3398					
62	GORILLA-004	²³⁸ 0.0699	²³⁸ 0.0892	²¹⁷ 0.1048	²⁰⁶ 0.1370	¹⁸ 0.1969					
63	GORILLA-005	²¹³ 0.0453	²⁰⁸ 0.0583	¹⁹⁷ 0.0704	¹⁸⁵ 0.0974	¹⁴⁴ 0.1474					
64	GORILLA-006	¹⁵² 0.0196	¹⁵² 0.0275	¹⁴⁷ 0.0331	¹³⁹ 0.0516	⁹¹ 0.1113					
65	GORILLA-007	¹⁴⁹ 0.0190	¹⁵⁰ 0.0271	¹⁴⁹ 0.0348	¹⁴³ 0.0520	⁹³ 0.1129					
66	GORILLA-008	¹³⁶ 0.0170	¹³⁸ 0.0238	¹³⁰ 0.0308	¹³⁰ 0.0469	⁹² 0.1120					
67	GRIAULE-000	¹²³ 0.0145	¹²⁴ 0.0201	¹²² 0.0253	¹²⁰ 0.0407	¹⁴¹ 0.1440					
68	GRIAULE-001	⁴⁹ 0.0033	⁴⁹ 0.0047	⁵¹ 0.0064	⁴⁷ 0.0153	³⁸ 0.0910					
69	HIK-003	²⁴⁸ 0.0828	²⁴³ 0.1028	²²² 0.1202	²¹³ 0.1525	²¹² 0.2480					
70	HIK-004	²⁴ 0.0796	²³⁹ 0.0988	²²³ 0.1147	²⁰⁹ 0.1474	²¹ 0.2483					
71	HIK-005	¹⁷⁴ 0.0312	¹⁷⁷ 0.0436	¹⁷⁷ 0.0560	¹⁷⁶ 0.0911	¹⁹⁶ 0.2129					
72	HYPERVERGE-001	⁴³ 0.0033	⁴⁴ 0.0045	⁴⁵ 0.0059	³⁵ 0.0117	⁴⁸ 0.0872					

Table 21: Identification-mode: Effect of N on FNIR at high threshold. Values are threshold-based miss rates i.e. FNIR at FPIR = 0.001 for five enrollment population sizes, N. The right six columns apply for enrollment of one image. Missing entries usually apply because another algorithm from the same developer was run instead. Some developers are missing because less accurate algorithms were not run on galleries with $N \geq 3\,000\,000$. Throughout blue superscripts indicate the rank of the algorithm for that column.

#	ALGORITHM	MISSES BELOW THRESHOLD, T					ENROL MOST RECENT				
		FNIR(N, T > 0, R > L)					DATASET: FRVT 2018 MUGSHOTS				
		N=0.64M	N=1.6M	N=3.0M	N=6.0M	N=12.0M					
73	HYPERVERGE-002	³⁶ 0.0028	³⁵ 0.0037	³³ 0.0046	¹⁶ 0.0064	¹⁷ 0.0538					
74	HZAILU-000	¹²² 0.0143	¹²³ 0.0197	¹²² 0.0255	¹²¹ 0.0411	¹⁰⁴ 0.1174					
75	HZAILU-001	⁷⁸ 0.0066	⁷³ 0.0086	⁷¹ 0.0109	⁶⁴ 0.0207	⁸⁰ 0.1052					
76	HZAILU-002	⁷² 0.0061	⁷¹ 0.0080	⁶⁹ 0.0101	⁵⁹ 0.0187	⁵⁵ 0.0914					
77	IDEMIA-003	¹⁸⁴ 0.0346	¹⁸⁷ 0.0471	²⁰⁹ 0.0892	²³⁶ 0.2789	²³³ 0.4311					
78	IDEMIA-004	¹⁷⁰ 0.0300	¹⁷³ 0.0373	¹⁶⁶ 0.0447	¹⁵⁷ 0.0617	¹⁶⁵ 0.1635					
79	IDEMIA-005	¹⁸⁹ 0.0360	¹⁷⁹ 0.0440	¹⁷⁷ 0.0537	¹⁷¹ 0.0764	¹⁸⁰ 0.1915					
80	IDEMIA-006	¹⁸⁷ 0.0351	¹⁷⁶ 0.0433	¹⁷³ 0.0525	¹⁵⁷ 0.0734	¹⁹⁸ 0.2201					
81	IDEMIA-007	¹¹⁷ 0.0136	¹¹⁵ 0.0181	¹⁰⁹ 0.0228	¹⁰⁷ 0.0357	¹⁵⁶ 0.1402					
82	IDEMIA-008	¹³ 0.0016	¹⁴ 0.0019	¹⁵ 0.0024	¹¹ 0.0053	¹⁵ 0.0470					
83	IDEMIA-009	¹⁰ 0.0013	⁷ 0.0016	³ 0.0018	¹⁵ 0.0061	²⁰ 0.0550					
84	IDEMIA-010	² 0.0010	¹ 0.0011	¹ 0.0012	² 0.0027	² 0.0193					
85	IMAGUS-005	¹¹⁸ 0.0137	¹¹⁹ 0.0185	¹¹⁵ 0.0237	¹¹⁹ 0.0368	⁸¹ 0.1067					
86	IMAGUS-006	¹¹⁹ 0.0137	¹²² 0.0190	¹¹⁹ 0.0244	¹¹⁶ 0.0396	¹⁰¹ 0.1159					
87	IMAGUS-007	¹³ 0.0160	¹³⁶ 0.0228	¹³⁰ 0.0284	¹²⁵ 0.0444	¹⁶⁵ 0.1179					
88	IMPERIAL-000	¹⁴⁵ 0.0187	¹⁴⁴ 0.0259	¹⁵⁵ 0.0358	¹⁶⁶ 0.0733	¹⁷⁴ 0.1794					
89	INCODE-003	²⁶ 0.1324	²⁷ 0.1672	²⁴ 0.1961	²⁸ 0.2345	²² 0.3123					
90	INCODE-004	¹⁹⁹ 0.0403	²⁰⁰ 0.0538	¹⁸⁸ 0.0662	¹⁷⁸ 0.0917	¹⁶² 0.1619					
91	INCODE-005	⁸⁶ 0.0083	⁸⁶ 0.0113	⁸⁰ 0.0145	⁷³ 0.0247	⁵⁴ 0.0912					
92	INNOVATRICS-007	⁹² 0.0093	⁹³ 0.0125	⁹¹ 0.0159	⁷⁸ 0.0259	⁸⁴ 0.1092					
93	INNOVATRICS-008	⁵¹ 0.0037	⁵³ 0.0050	⁵³ 0.0066	⁶² 0.0206	⁸⁵ 0.1093					
94	INTEMA-000	²⁰ 0.0019	²¹ 0.0024	²⁹ 0.0032	³⁰ 0.0098	³⁴ 0.0745					
95	INTEMA-001	⁷ 0.0014	⁵ 0.0014	³⁵ 0.0049	³² 0.0098	³⁰ 0.0703					
96	INTSYSMSU-000	³³⁴ 0.9982	³³² 0.9984	²⁵⁸ 0.9985	²⁴⁸ 0.9987	²⁴ 0.9988					
97	IREX-000	¹⁵⁰ 0.0190	¹⁵⁶ 0.0280	¹⁶⁰ 0.0391	¹⁶² 0.0677	¹⁴⁷ 0.1479					
98	ISYSTEMS-002	²²⁶ 0.0584	²²⁶ 0.0783	²¹⁷ 0.0973	²⁰⁷ 0.1373	²⁰⁴ 0.2295					
99	ISYSTEMS-003	²¹¹ 0.0438	²⁰⁹ 0.0590	²⁰⁴ 0.0807	¹⁹⁹ 0.1259	²⁰⁶ 0.2357					
100	KAKAO-000	¹⁰ 0.0109	¹⁰⁵ 0.0151	¹⁰⁸ 0.0196	¹⁰² 0.0324	⁷¹ 0.1010					
101	KAKAO-001	²⁵ 0.0021	²⁴ 0.0026	²¹ 0.0032	²⁷ 0.0085	²⁸ 0.0693					
102	KEDACOM-001	¹⁴ 0.0181	¹³⁵ 0.0227	¹²⁴ 0.0265	¹²⁴ 0.0422	¹² 0.1340					
103	LINECLOVA-002	³⁴ 0.0028	³⁶ 0.0040	³⁶ 0.0049	³⁹ 0.0120	⁴¹ 0.0824					
104	LINECLOVA-003	³¹ 0.0026	²⁶ 0.0026	³⁴ 0.0049	³² 0.0158	⁶⁹ 0.0989					
105	LOOKMAN-003	¹⁸⁵ 0.0346	¹⁷⁸ 0.0437	¹⁷¹ 0.0514	¹⁶⁵ 0.0724	¹⁶³ 0.1620					
106	LOOKMAN-005	¹⁶ 0.0240	¹⁶⁰ 0.0301	¹⁵⁴ 0.0356	¹³⁸ 0.0512	¹²⁰ 0.1334					
107	MANTRA-000	⁷⁷ 0.0065	⁸³ 0.0101	⁸⁷ 0.0151	⁹⁷ 0.0308	⁷⁶ 0.1035					
108	MAXVISION-000	¹⁵⁹ 0.0206	¹⁵⁷ 0.0282	¹⁵¹ 0.0355	¹⁴⁰ 0.0517	¹²⁶ 0.1340					
109	MAXVISION-001	⁴⁰ 0.0031	⁴¹ 0.0043	³⁹ 0.0055	⁴¹ 0.0122	³² 0.0895					
110	MEGVI-001	²² 0.0562	²²¹ 0.0722	²⁰⁹ 0.0872	²¹³ 0.1309	²²⁰ 0.2713					
111	MICROFOCUS-005	³³¹ 0.9732	³²⁵ 0.8354	²⁵⁸ 0.8555	²⁴⁶ 0.8755	²⁴⁰ 0.8954					
112	MICROSOFT-003	¹⁵ 0.0198	¹⁵⁴ 0.0278	¹⁵⁰ 0.0356	¹⁴⁶ 0.0538	¹⁵ 0.1539					
113	MICROSOFT-004	¹⁴⁵ 0.0185	¹⁴⁵ 0.0259	¹⁴⁴ 0.0333	¹⁴¹ 0.0517	¹⁵¹ 0.1510					
114	MICROSOFT-005	¹⁴¹ 0.0181	¹⁴² 0.0256	¹⁴² 0.0320	¹³⁷ 0.0512	¹⁴⁹ 0.1491					
115	MICROSOFT-006	⁹¹ 0.0091	⁸⁸ 0.0120	⁹⁰ 0.0162	⁹⁴ 0.0301	¹⁴⁸ 0.1482					
116	MUKH-002	³¹³ 0.5041	³¹³ 0.5942	²⁵² 0.6674	²⁴³ 0.7314	²³⁸ 0.8276					
117	NEC-000	²³⁰ 0.0637	²²⁸ 0.0789	²¹⁹ 0.0933	¹⁹⁸ 0.1163	¹⁸⁶ 0.1941					
118	NEC-001	²⁴⁵ 0.0863	²⁴⁵ 0.1055	²²⁷ 0.1249	²¹² 0.1519	²⁰¹ 0.2253					
119	NEC-002	²⁹ 0.0020	²³ 0.0026	²⁵ 0.0033	⁴⁵ 0.0135	²⁵ 0.0653					
120	NEC-003	²⁴ 0.0021	²⁰ 0.0024	¹⁷ 0.0028	¹⁴ 0.0059	¹⁸ 0.0540					
121	NEC-004	¹⁴ 0.0017	¹⁰ 0.0018	⁸ 0.0020	⁵ 0.0037	⁹ 0.0329					
122	NEC-005	³ 0.0015	⁸ 0.0017	⁷ 0.0019	¹⁷ 0.0065	⁷ 0.0307					
123	NEC-006	¹⁵ 0.0018	¹⁶ 0.0020	¹⁶ 0.0026	³³ 0.0103	²² 0.0573					
124	NEC-007	³⁴ 0.0039	³⁷ 0.0040	²⁹ 0.0041	¹⁵ 0.0055	¹⁰ 0.0294					
125	NEUROTECHNOLOGY-003	³¹⁶ 0.5698	³¹⁷ 0.6362	²⁵³ 0.7035	²⁴⁴ 0.7602	²³⁷ 0.8224					
126	NEUROTECHNOLOGY-004	²¹⁷ 0.0466	²¹⁴ 0.0629	¹⁹⁹ 0.0779	¹⁹⁵ 0.1135	¹⁹³ 0.2102					
127	NEUROTECHNOLOGY-005	¹⁹⁶ 0.0396	²⁰¹ 0.0538	¹⁸⁹ 0.0675	¹⁸² 0.0950	¹⁸⁶ 0.1966					
128	NEUROTECHNOLOGY-007	²¹⁰ 0.0436	²¹³ 0.0623	²⁰⁸ 0.0802	²⁰⁴ 0.1320	²⁰⁶ 0.2393					
129	NEUROTECHNOLOGY-008	¹⁸³ 0.0339	¹⁹⁵ 0.0530	²⁰⁸ 0.0893	²¹⁹ 0.1769	²²⁷ 0.3288					
130	NEUROTECHNOLOGY-009	¹⁰ 0.0108	¹⁰⁶ 0.0152	¹⁰⁸ 0.0196	¹⁰⁰ 0.0324	⁸¹ 0.1102					
131	NEUROTECHNOLOGY-010	⁸² 0.0069	⁸¹ 0.0099	⁸⁰ 0.0138	¹²⁷ 0.0449	¹⁶⁹ 0.1727					
132	NEUROTECHNOLOGY-012	⁶² 0.0047	⁶³ 0.0068	⁶⁶ 0.0097	⁸² 0.0265	¹³⁰ 0.1343					
133	NEUROTECHNOLOGY-013	³⁷ 0.0029	⁴² 0.0043	⁴⁸ 0.0057	⁶⁵ 0.0208	¹⁰⁸ 0.1202					
134	NOTIONTAG-000	¹¹⁰ 0.0128	¹¹⁰ 0.0175	¹¹⁰ 0.0228	¹⁰⁸ 0.0357	¹¹⁹ 0.1270					
135	NTECHLAB-003	²⁰ 0.0421	¹⁹⁹ 0.0537	¹⁸⁸ 0.0674	¹⁷⁵ 0.0907	¹⁵⁹ 0.1582					
136	NTECHLAB-004	¹⁷³ 0.0312	¹⁷⁴ 0.0405	¹⁷² 0.0519	¹⁶⁴ 0.0722	¹⁵⁰ 0.1503					
137	NTECHLAB-005	¹⁷ 0.0334	¹⁷⁵ 0.0424	¹⁷⁸ 0.0537	¹⁷⁰ 0.0760	¹⁵⁹ 0.1543					
138	NTECHLAB-006	¹⁷¹ 0.0288	¹⁶⁹ 0.0367	¹⁶⁹ 0.0471	¹⁶¹ 0.0670	¹⁵² 0.1523					
139	NTECHLAB-007	¹⁴⁶ 0.0188	¹⁴¹ 0.0256	¹³⁹ 0.0317	¹³⁵ 0.0495	¹²² 0.1306					
140	NTECHLAB-008	¹⁰² 0.0107	⁹⁹ 0.0145	¹⁰⁸ 0.0187	⁸⁸ 0.0286	⁶⁹ 0.0995					
141	NTECHLAB-009	⁵⁰ 0.0037	⁵² 0.0049	⁵⁶ 0.0062	⁴³ 0.0125	³² 0.0735					
142	NTECHLAB-010	²¹ 0.0020	²² 0.0025	¹⁹ 0.0030	²⁴ 0.0077	³² 0.0710					
143	NTECHLAB-011	²⁶ 0.0022	²⁸ 0.0030	²⁶ 0.0038	²¹ 0.0075	²⁴ 0.0625					
144	PANGIAM-000	⁵⁹ 0.0042	⁶⁰ 0.0060	⁶⁰ 0.0080	⁵⁴ 0.0160	⁵⁰ 0.0876					

Table 22: Identification-mode: Effect of N on FNIR at high threshold. Values are threshold-based miss rates i.e. FNIR at FPIR = 0.001 for five enrollment population sizes, N. The right six columns apply for enrollment of one image. Missing entries usually apply because another algorithm from the same developer was run instead. Some developers are missing because less accurate algorithms were not run on galleries with $N \geq 3\,000\,000$. Throughout blue superscripts indicate the rank of the algorithm for that column.

MISSES BELOW THRESHOLD, T FNIR(N, T > 0, R > L)		ENROL MOST RECENT DATASET: FRVT 2018 MUGSHOTS				
#	ALGORITHM	N=0.64M	N=1.6M	N=3.0M	N=6.0M	N=12.0M
145	PANGIAM-001	⁹⁵ 0.0098	⁸⁷ 0.0113	⁸⁰ 0.0134	⁶⁸ 0.0232	⁴⁷ 0.0865
146	PARAVISION-003	¹⁶⁷ 0.0260	¹⁶⁷ 0.0351	¹⁶⁷ 0.0447	¹⁶⁰ 0.0657	¹⁶⁴ 0.1630
147	PARAVISION-004	⁸³ 0.0074	⁸⁵ 0.0101	⁸² 0.0136	⁸³ 0.0267	¹¹⁶ 0.1256
148	PARAVISION-005	⁴¹ 0.0032	⁴⁰ 0.0041	⁴⁵ 0.0057	³⁸ 0.0174	⁷⁷ 0.1037
149	PARAVISION-007	³⁸ 0.0030	³⁸ 0.0040	⁴⁰ 0.0055	⁶⁶ 0.0211	⁸⁶ 0.1097
150	PARAVISION-009	²⁷ 0.0020	²⁵ 0.0026	²⁵ 0.0038	³¹ 0.0098	⁴⁸ 0.0857
151	PARAVISION-012	⁵ 0.0013	⁶ 0.0015	⁸ 0.0018	¹⁸ 0.0065	³⁷ 0.0770
152	PIXELALL-002	²⁴ 0.0716	²⁴⁴ 0.1052	²³⁶ 0.1475	²³² 0.2489	²³² 0.3904
153	PIXELALL-003	¹³¹ 0.0158	¹³¹ 0.0218	¹³⁴ 0.0288	¹³¹ 0.0474	⁹⁸ 0.1138
154	PIXELALL-004	¹¹³ 0.0129	¹¹⁸ 0.0183	¹²⁰ 0.0245	¹¹⁰ 0.0378	¹³³ 0.1375
155	PIXELALL-005	⁸⁰ 0.0087	⁹⁰ 0.0121	⁹⁹ 0.0171	⁷⁵ 0.0250	⁷⁹ 0.1052
156	PTAKURATSATU-000	¹⁶⁸ 0.0275	¹⁶⁸ 0.0366	¹⁶⁸ 0.0458	¹⁴⁴ 0.0523	¹⁶ 0.0523
157	QNAP-001	²⁰⁰ 0.0404	¹⁹⁸ 0.0536	¹⁸⁷ 0.0661	¹⁷⁷ 0.0916	¹⁶⁰ 0.1595
158	QNAP-002	¹⁵⁴ 0.0200	¹⁴⁶ 0.0265	¹⁴² 0.0327	¹³³ 0.0490	¹²⁹ 0.1341
159	QNAP-003	¹² 0.0139	¹²¹ 0.0189	¹¹⁷ 0.0239	¹¹¹ 0.0379	¹³ 0.1414
160	QUANTASOFT-001	³¹⁸ 0.6387	³¹⁸ 0.6387	²⁵¹ 0.6387		²³⁵ 0.6387
161	RANKONE-002	²⁵ 0.0973	²⁴⁹ 0.1175	²²⁹ 0.1359	²¹⁶ 0.1718	²¹⁷ 0.2613
162	RANKONE-003	²⁵³ 0.0973	²⁴⁸ 0.1175	²²⁷ 0.1359	²¹⁷ 0.1718	²¹⁸ 0.2613
163	RANKONE-005	²¹ 0.0473	²¹⁰ 0.0592	¹⁹⁷ 0.0700	¹⁸⁰ 0.0944	¹⁸ 0.1998
164	RANKONE-007	¹³⁵ 0.0168	¹³³ 0.0222	¹²⁸ 0.0266	¹¹³ 0.0381	⁹⁵ 0.1132
165	RANKONE-009	¹¹⁴ 0.0132	¹¹⁵ 0.0177	¹¹² 0.0230	¹⁰⁴ 0.0344	⁸⁹ 0.0921
166	RANKONE-010	¹⁰⁰ 0.0106	⁹⁶ 0.0136	⁹⁶ 0.0174	⁸¹ 0.0265	³⁸ 0.0785
167	RANKONE-011	⁷⁴ 0.0063	⁷⁴ 0.0087	⁷³ 0.0115	⁸⁴ 0.0269	⁹⁷ 0.1135
168	RANKONE-012	⁷⁰ 0.0058	⁶⁸ 0.0077	⁶⁸ 0.0100	⁶⁷ 0.0220	⁹⁹ 0.1111
169	RANKONE-013	⁴⁶ 0.0034	⁴⁵ 0.0046	⁴⁶ 0.0059	⁴⁴ 0.0127	⁴⁹ 0.0875
170	RANKONE-014	²⁸ 0.0025	³¹ 0.0033	²⁹ 0.0043	³⁴ 0.0106	²⁸ 0.0656
171	REALNETWORKS-002	²⁸² 0.1943	²⁸¹ 0.2314	²⁴⁶ 0.2656	²³⁸ 0.3134	²²⁶ 0.3208
172	REALNETWORKS-003	²⁶ 0.1300	²⁶⁷ 0.1594	²³⁸ 0.1858	²²⁶ 0.2246	²² 0.3076
173	REALNETWORKS-004	²⁶⁷ 0.1279	²⁶⁶ 0.1581	²³⁷ 0.1857	²²⁷ 0.2329	²² 0.3179
174	REALNETWORKS-005	¹⁵⁵ 0.0202	¹⁵³ 0.0277	¹⁵² 0.0355	¹⁵⁴ 0.0560	¹³⁹ 0.1431
175	REALNETWORKS-006	⁹¹ 0.0097	¹⁰⁰ 0.0145	⁹⁹ 0.0182	⁹⁸ 0.0308	⁶⁸ 0.0991
176	REALNETWORKS-007	⁸¹ 0.0068	⁷⁹ 0.0097	⁷⁷ 0.0125	⁷⁰ 0.0233	⁵⁶ 0.0917
177	REALNETWORKS-008	⁶¹ 0.0044	⁶¹ 0.0062	⁶¹ 0.0082	⁴⁶ 0.0139	⁴² 0.0824
178	RECOGNITO-000	⁶⁰ 0.0043	⁴⁷ 0.0047	³⁸ 0.0053	²⁶ 0.0083	¹⁹ 0.0545
179	REMARKAI-000	²⁰² 0.0406	²⁰² 0.0552	¹⁹⁶ 0.0676	¹⁸⁶ 0.1028	¹⁸ 0.2003
180	RENDIP-000	⁸⁷ 0.0085	⁸⁹ 0.0121	⁸⁹ 0.0156	⁸⁷ 0.0277	¹⁰⁶ 0.1182
181	REVEALMEDIA-000	⁹⁰ 0.0090	⁹¹ 0.0122	⁹⁶ 0.0158	⁸⁶ 0.0277	⁷³ 0.1019
182	S1-000	¹⁵⁸ 0.0204	¹⁵⁵ 0.0279	¹⁵⁸ 0.0382	¹⁵⁸ 0.0630	¹⁶⁷ 0.1707
183	S1-001	¹⁶ 0.0115	¹⁰⁷ 0.0156	¹⁰⁸ 0.0199	¹¹⁴ 0.0392	¹¹ 0.1256
184	S1-002	⁵⁶ 0.0040	⁵⁷ 0.0056	⁵⁷ 0.0077	⁸⁰ 0.0264	¹²¹ 0.1285
185	S1-003	⁷³ 0.0061	⁷⁵ 0.0088	⁷¹ 0.0116	⁸⁵ 0.0277	¹²³ 0.1298
186	S1-004	³⁹ 0.0030	³⁹ 0.0040	⁴¹ 0.0056	³⁵ 0.0162	⁶⁷ 0.0989
187	SCANOVATE-000	²¹⁷ 0.0498	²¹⁷ 0.0667	²⁰² 0.0804	¹⁹⁰ 0.1097	⁸⁹ 0.1109
188	SCANOVATE-001	²² 0.0630	²²⁹ 0.0815	²¹⁷ 0.0993	²⁰⁰ 0.1292	¹⁸ 0.1960
189	SENSETIME-000	¹³⁰ 0.0158	¹²⁸ 0.0208	¹²⁸ 0.0270	¹¹⁷ 0.0398	¹⁰⁹ 0.1232
190	SENSETIME-001	¹³ 0.0161	¹³² 0.0219	¹³¹ 0.0277	¹²³ 0.0420	¹² 0.1304
191	SENSETIME-002	¹²⁴ 0.0146	¹⁰¹ 0.0148	⁸⁸ 0.0153	⁷¹ 0.0234	²⁷ 0.0657
192	SENSETIME-003	¹¹ 0.0016	¹² 0.0018	¹¹ 0.0021	¹² 0.0054	¹² 0.0451
193	SENSETIME-004	¹⁰ 0.0015	⁹ 0.0018	¹⁰ 0.0021	⁶ 0.0040	¹⁰ 0.0354
194	SENSETIME-005	¹² 0.0016	¹⁹ 0.0022	¹⁹ 0.0031	²⁸ 0.0089	¹² 0.0454
195	SENSETIME-006	³ 0.0014	¹¹ 0.0018	¹⁴ 0.0023	⁷ 0.0047	¹¹ 0.0372
196	SENSETIME-007	⁴ 0.0012	⁴ 0.0014	⁴ 0.0016	⁴ 0.0036	⁸ 0.0316
197	SENSETIME-008	³ 0.0011	³ 0.0013	³ 0.0015	³ 0.0031	³ 0.0288
198	SENSETIME-009	¹ 0.0010	² 0.0011	² 0.0012	¹ 0.0024	⁴ 0.0238
199	SHAMAN-007	²⁶ 0.1212	²⁶¹ 0.1413	²³¹ 0.1587	²²¹ 0.1879	²¹ 0.2460
200	SIAT-001	¹¹⁶ 0.0136	¹¹¹ 0.0176	¹¹³ 0.0230	¹⁰³ 0.0344	⁷⁵ 0.1035
201	SIAT-002	¹² 0.0154	¹³⁰ 0.0216	¹²⁸ 0.0273	¹¹⁹ 0.0404	¹² 0.1283
202	SQISOFT-001	²⁴⁶ 0.0921	²⁵⁷ 0.1322	²³⁸ 0.1781	²²⁹ 0.2348	²⁴¹ 0.9271
203	SQISOFT-002	¹³ 0.0177	¹⁵⁹ 0.0290	¹⁶¹ 0.0415	¹⁶⁸ 0.0739	¹³ 0.1351
204	SYNESIS-003	²¹⁸ 0.0499	²¹⁵ 0.0652	²⁰³ 0.0804	¹⁸⁹ 0.1095	¹⁸¹ 0.1916
205	SYNESIS-003	³¹⁴ 0.5341	³¹² 0.5821	²⁵⁹ 0.6113	²⁴² 0.6479	²³⁶ 0.6822
206	SYNESIS-005	¹³⁹ 0.0181	¹⁴⁰ 0.0248	¹⁴⁶ 0.0319	¹⁴² 0.0518	¹⁵⁸ 0.1580
207	TECH5-001	²⁰⁴ 0.0420	²⁰⁵ 0.0574	²⁰⁸ 0.0911	²²⁴ 0.2106	²³¹ 0.3725
208	TECH5-002	¹⁵ 0.0194	¹⁴⁹ 0.0269	¹⁴⁸ 0.0346	¹⁴⁵ 0.0537	¹⁶ 0.1607
209	TEVIAN-005	²³⁷ 0.0692	²³⁴ 0.0873	²¹⁶ 0.1066	²⁰² 0.1301	¹⁷⁶ 0.1840
210	TEVIAN-006	⁸¹ 0.0078	⁸⁰ 0.0098	⁷⁹ 0.0130	⁷⁹ 0.0261	¹² 0.1305
211	TEVIAN-007	⁵³ 0.0038	⁵⁵ 0.0052	⁵² 0.0065	⁵⁰ 0.0154	⁶² 0.0957
212	TIGER-002	²³² 0.0647	²³¹ 0.0861	²¹⁸ 0.1036	²⁰⁵ 0.1332	¹⁹ 0.2231
213	TOSHIBA-000	²¹⁴ 0.0460	²¹² 0.0620	²⁰⁰ 0.0780	¹⁹² 0.1117	¹⁹² 0.2082
214	TRUEFACE-000	¹¹⁵ 0.0134	¹¹⁷ 0.0182	¹¹⁸ 0.0238	¹¹² 0.0380	¹³ 0.1385
215	VD-001	²⁷⁸ 0.1642	²⁷⁸ 0.2015	²⁴⁵ 0.2351	²³⁵ 0.2736	²²⁸ 0.3293
216	VERIDAS-001	¹⁶⁹ 0.0278	¹⁷¹ 0.0373	¹⁷⁰ 0.0491	¹⁶⁹ 0.0753	¹⁵⁴ 0.1541

Table 23: **Identification-mode: Effect of N on FNIR at high threshold.** Values are threshold-based miss rates i.e. FNIR at FPIR = 0.001 for five enrollment population sizes, N. The right six columns apply for enrollment of one image. Missing entries usually apply because another algorithm from the same developer was run instead. Some developers are missing because less accurate algorithms were not run on galleries with $N \geq 3\ 000\ 000$. Throughout blue superscripts indicate the rank of the algorithm for that column.

#	ALGORITHM	MISSES BELOW THRESHOLD, T						ENROL MOST RECENT					
		FNIR(N, T > 0, R > L)		DATASET: FRVT 2018 MUGSHOTS									
		N=0.64M	N=1.6M	N=3.0M	N=6.0M	N=12.0M							
217	VERIDAS-002	¹²⁰ 0.0278	¹⁷² 0.0373	¹⁵⁶ 0.0373	¹³⁴ 0.0491	¹³⁵ 0.0753							
218	VERIDAS-003	¹⁰ 0.0117	¹⁰⁹ 0.0166	¹⁰⁸ 0.0219	¹²⁶ 0.0446	¹⁵⁵ 0.1543							
219	VERIDAS-004	³⁸ 0.0042	³⁸ 0.0058	³⁸ 0.0077	²² 0.0077	³ 0.0232							
220	VIGILANTSOLUTIONS-008	¹²⁰ 0.0146	¹²⁵ 0.0205	¹² 0.0269	¹³² 0.0489	¹⁰³ 0.1164							
221	VISIONBOX-000	¹⁰⁸ 0.0122	¹¹⁴ 0.0177	¹¹⁸ 0.0239		²⁴² 0.9538							
222	VISIONLABS-004	²⁰ 0.0427	²⁰⁶ 0.0578	¹⁹⁸ 0.0703	¹⁸¹ 0.0949	¹⁷ 0.1853							
223	VISIONLABS-005	¹⁹² 0.0369	¹⁹⁰ 0.0502	¹⁸⁰ 0.0626	¹⁷³ 0.0847	¹⁷⁵ 0.1815							
224	VISIONLABS-006	¹⁴⁷ 0.0188	¹⁴⁸ 0.0267	¹⁴⁶ 0.0336	¹⁵⁰ 0.0542	¹⁴⁵ 0.1478							
225	VISIONLABS-007	¹⁴⁸ 0.0188	¹⁴⁷ 0.0266	¹⁴⁸ 0.0335	¹⁴⁸ 0.0540	¹⁴⁶ 0.1479							
226	VISIONLABS-008	⁹³ 0.0096	⁹⁴ 0.0131	⁹⁴ 0.0166	⁹⁰ 0.0291	¹¹³ 0.1247							
227	VISIONLABS-009	⁴⁷ 0.0034	⁴⁶ 0.0046	⁴⁷ 0.0060	⁴⁷ 0.0140	³¹ 0.0881							
228	VISIONLABS-010	⁵² 0.0038	⁵⁴ 0.0051	⁵⁵ 0.0070	⁴⁸ 0.0149	⁵⁸ 0.0920							
229	VISIONLABS-011	³⁰ 0.0025	³² 0.0033	³¹ 0.0044	³⁷ 0.0120	⁴³ 0.0825							
230	VIXVIZION-009	¹⁵⁷ 0.0203	¹⁵¹ 0.0273	¹⁵⁰ 0.0348	¹⁵² 0.0545	¹³⁴ 0.1377							
231	VNPT-001	⁹⁸ 0.0104	⁹⁸ 0.0143	¹⁰¹ 0.0190	⁹³ 0.0296	⁷⁴ 0.1028							
232	VNPT-002	⁶⁴ 0.0051	⁶² 0.0065	⁶² 0.0083	⁵⁷ 0.0172	⁷⁰ 0.1005							
233	VCORD-005	²⁶² 0.1179	²⁶⁵ 0.1577	²⁴ 0.2183	²³⁷ 0.3122	²³¹ 0.4490							
234	VTS-001	⁹⁷ 0.0102	⁹⁵ 0.0133	⁹⁷ 0.0175	⁹⁹ 0.0322	¹¹² 0.1243							
235	VTS-002	¹⁴ 0.0185	¹⁴³ 0.0259	¹⁴ 0.0344	¹³⁵ 0.0549	¹⁴ 0.1447							
236	VTS-003	⁶⁸ 0.0053	⁶⁷ 0.0073	⁶⁹ 0.0096	⁶⁰ 0.0188	⁷² 0.1017							
237	XFORWARDAI-000	¹⁰¹ 0.0107	¹⁰⁴ 0.0151	¹⁰³ 0.0195	¹⁰¹ 0.0324	⁸¹ 0.1057							
238	XFORWARDAI-001	⁴⁹ 0.0037	⁵¹ 0.0049	⁴⁸ 0.0060	³⁶ 0.0120	³⁹ 0.0800							
239	XFORWARDAI-002	³² 0.0026	³⁰ 0.0030	²⁴ 0.0035	²⁵ 0.0078	³¹ 0.0706							
240	YITU-002	¹¹² 0.0129	¹¹² 0.0177	¹¹¹ 0.0228	¹⁰⁵ 0.0345	⁹⁶ 0.1133							
241	YITU-003	¹²⁰ 0.0138	¹²⁰ 0.0185	¹¹⁴ 0.0236	¹⁰⁶ 0.0353	⁹⁹ 0.1148							
242	YITU-004	³⁸ 0.0067	⁷⁷ 0.0096	⁷⁸ 0.0129	⁶⁹ 0.0232	⁷⁸ 0.1046							
243	YITU-005	⁸⁴ 0.0074	⁸⁴ 0.0101	⁸¹ 0.0135	⁷⁷ 0.0255	⁸² 0.1057							

Table 24: Identification-mode: Effect of N on FNIR at high threshold. Values are threshold-based miss rates i.e. FNIR at FPIR = 0.001 for five enrollment population sizes, N. The right six columns apply for enrollment of one image. Missing entries usually apply because another algorithm from the same developer was run instead. Some developers are missing because less accurate algorithms were not run on galleries with $N \geq 3\,000\,000$. Throughout blue superscripts indicate the rank of the algorithm for that column.

MISSES AT GIVEN RANK		ENROL MOST RECENT													
#	ALGORITHM	RANK 1					aN^b	RANK 50					aN^b		
		N=0.64M	N=1.6M	N=3.0M	N=6.0M	N=12.0M		N=0.64M	N=1.6M	N=3.0M	N=6.0M	N=12.0M			
1	3DIVI-005	²⁶⁹ 0.0137	²⁶⁷ 0.0176	²³³ 0.0210	²²⁶ 0.0253	²²¹ 0.0302	¹⁶⁹ 0.0004 N ^{0.271} 202	²⁴⁶ 0.0040	²⁴⁷ 0.0049	²²² 0.0057	²¹⁸ 0.0068	²¹³ 0.0081	⁵¹ 0.0002 N ^{-0.240} 206		
2	ACER-000	²³⁵ 0.0081	²⁴³ 0.0106	²²¹ 0.0128	²¹⁸ 0.0157	²¹³ 0.0195	⁶⁹ 0.0001 N ^{0.299} 226	¹⁸⁸ 0.0020	²⁰⁷ 0.0026	¹⁹⁵ 0.0031	¹⁹⁷ 0.0037	¹⁹⁴ 0.0045	²¹ 0.0000 N ^{0.284} 220		
3	ALCHERA-003	²³¹ 0.0079	²⁴⁰ 0.0104	²¹⁹ 0.0123	²¹⁷ 0.0147	²¹³ 0.0180	¹⁰¹ 0.0002 N ^{0.278} 213	²²⁵ 0.0027	²²³ 0.0032	²⁰³ 0.0035	²⁰⁹ 0.0042	¹⁹⁵ 0.0048	⁵⁶ 0.0002 N ^{-0.199} 196		
4	ALLGOVISION-000	²⁵¹ 0.0101	²⁴⁹ 0.0114	²²⁰ 0.0127	²¹⁶ 0.0145	²¹¹ 0.0166	²¹⁴ 0.0010 N ^{0.171} 132	²⁶⁸ 0.0063	²⁶³ 0.0067	²²⁸ 0.0071	²²¹ 0.0075	²¹² 0.0081	²²² 0.0020 N ^{0.086} 151		
5	ALLGOVISION-001	²²³ 0.0069	²²⁸ 0.0096	²¹⁴ 0.0107	²¹¹ 0.0128	²⁰⁸ 0.0157	⁸⁶ 0.0002 N ^{0.277} 211	²¹¹ 0.0023	²¹² 0.0027	¹⁹⁶ 0.0031	¹⁹¹ 0.0036	¹⁸⁷ 0.0043	⁴⁴ 0.0001 N ^{-0.211} 201		
6	ANKE-000	²⁵⁴ 0.0102	²⁵⁷ 0.0132	²²⁹ 0.0155	²²⁴ 0.0188	²¹⁷ 0.0225	¹⁴³ 0.0003 N ^{0.270} 204	²³⁴ 0.0032	²³⁸ 0.0040	²¹⁸ 0.0046	²¹⁰ 0.0056	²⁰³ 0.0066	⁴² 0.0001 N ^{-0.247} 208		
7	ANKE-002	¹⁵¹ 0.0024	¹⁵⁴ 0.0026	¹⁵¹ 0.0032	¹⁴⁸ 0.0037	¹⁴⁴ 0.0043	⁷⁹ 0.0002 N ^{0.203} 151	¹⁵⁷ 0.0016	¹⁵⁸ 0.0017	¹⁴⁴ 0.0017	¹⁴¹ 0.0019	¹³⁵ 0.0019	¹¹⁶ 0.0006 N ^{-0.057} 158		
8	AWARE-003	²⁸⁷ 0.0238	²⁸⁵ 0.0306	²⁴⁶ 0.0361	²³⁸ 0.0431	²³³ 0.0506	²¹¹ 0.0008 N ^{0.258} 196	²⁶² 0.0055	²⁷¹ 0.0075	²³⁹ 0.0092	²³³ 0.0113	²³² 0.0143	³² 0.0001 N ^{0.323} 230		
9	AWARE-005	²⁸⁸ 0.0245	²⁸⁶ 0.0311	²⁴⁶ 0.0366	²³⁹ 0.0434	²²³ 0.0312	²³⁰ 0.0056 N ^{0.118} 82	²⁶⁶ 0.0062	²⁷⁷ 0.0082	²⁴¹ 0.0101	²³⁸ 0.0128	²¹⁵ 0.0089	¹⁴⁶ 0.0007 N ^{-0.169} 191		
10	AYONIX-002	³²⁴ 0.2935	³²⁵ 0.3414	²⁵⁶ 0.3736	²⁴⁷ 0.4101	²⁴¹ 0.4465	²⁴¹ 0.0440 N ^{0.143} 103	³²³ 0.0950	³²⁵ 0.1274	²⁵⁶ 0.1524	²⁴⁸ 0.1828	²⁴⁰ 0.2150	²²² 0.0023 N ^{0.279} 217		
11	CAMVI-004	²⁶² 0.0124	²⁹⁴ 0.0463	²⁵⁰ 0.0719	²⁴⁶ 0.2363	²⁴⁰ 0.2367	³ 0.0000 N ^{0.055} 242	²⁹⁵ 0.0117	³¹⁰ 0.0464	²⁷² 0.0175	²⁴¹ 0.2361	²⁴¹ 0.2364	³ 0.0000 N ^{0.171} 242		
12	CANON-001	²⁵ 0.0011	²³ 0.0011	²⁵ 0.0012	²⁵ 0.0013	²² 0.0014	¹³² 0.0002 N ^{0.113} 73	²⁷ 0.0009	²⁷ 0.0009	²⁷ 0.0009	²⁷ 0.0009	²⁷ 0.0009	¹¹⁷ 0.0006 N ^{0.26} 76		
13	CANON-002	³⁰ 0.0011	³² 0.0012	³² 0.0013	³⁹ 0.0014	³⁸ 0.0016	⁷⁸ 0.0002 N ^{0.142} 102	²⁸ 0.0009	²⁶ 0.0009	²⁴ 0.0009	²⁴ 0.0009	²³ 0.0009	¹⁴⁷ 0.0007 N ^{0.105} 45		
14	CIB-000	⁷⁴ 0.0014	⁷² 0.0015	⁶⁹ 0.0017	⁷¹ 0.0019	²⁰⁹ 0.0131	⁵ 0.0000 N ^{0.035} 240	⁸³ 0.0012	⁷³ 0.0012	⁷² 0.0012	⁷¹ 0.0012	²² 0.0122	⁴ 0.0000 N ^{0.647} 241		
15	CLEARVIEW1-000	²¹ 0.0010	²² 0.0011	²² 0.0012	²⁷ 0.0013	²⁶ 0.0015	⁹¹ 0.0002 N ^{0.129} 93	³¹ 0.0009	²⁶ 0.0009	²⁶ 0.0009	²⁶ 0.0009	²⁵ 0.0009	¹³³ 0.0007 N ^{0.19} 62		
16	CLOUDWALK-HR-000	⁸⁰ 0.0015	⁶⁸ 0.0015	⁶⁹ 0.0015	⁵² 0.0016	⁴⁷ 0.0017	²⁰⁹ 0.0007 N ^{0.054} 16	¹³⁹ 0.0014	¹²⁷ 0.0014	¹¹⁵ 0.0014	¹⁰⁹ 0.0014	⁸⁸ 0.0014	²⁰³ 0.0012 N ^{0.012} 33		
17	CLOUDWALK-MT-000	¹¹⁰ 0.0018	⁹⁰ 0.0018	⁸⁹ 0.0018	⁶⁸ 0.0019	⁵⁹ 0.0020	²¹⁶ 0.0011 N ^{0.036} 9	¹⁷⁴ 0.0018	¹⁶⁸ 0.0018	¹⁵³ 0.0018	¹³⁷ 0.0018	¹²³ 0.0018	²¹⁸ 0.0017 N ^{0.002} 4		
18	CLOUDWALK-MT-001	¹⁰⁹ 0.0018	⁸⁸ 0.0018	⁷⁹ 0.0018	⁶⁴ 0.0018	⁵⁷ 0.0019	²¹⁸ 0.0012 N ^{0.029} 7	¹⁷² 0.0017	¹⁶⁷ 0.0018	¹⁵⁰ 0.0018	¹³⁸ 0.0018	¹²² 0.0018	²¹⁷ 0.0017 N ^{0.002} 10		
19	CLOUDWALK-MT-002	¹⁰⁸ 0.0018	⁸⁹ 0.0018	¹⁷³ 0.0044	¹⁵⁸ 0.0045	¹⁴⁸ 0.0045	⁸ 0.0000 N ^{0.388} 236	¹⁷³ 0.0018	¹⁶⁹ 0.0018	¹⁶⁶ 0.0044	¹⁶⁷ 0.0044	¹⁹² 0.0044	¹² 0.0000 N ^{0.380} 233		
20	COGENT-000	²⁵³ 0.0101	²⁴² 0.0105	²¹⁶ 0.0109	²⁰⁷ 0.0115	²⁰⁹ 0.0125	²³⁸ 0.0038 N ^{0.071} 29	¹⁹⁹ 0.0021	²⁰¹ 0.0024	¹⁹⁰ 0.0028	¹⁹⁰ 0.0036	¹⁸⁹ 0.0095	⁹ 0.0000 N ^{0.466} 237		
21	COGENT-001	²⁵² 0.0101	²⁴¹ 0.0105	²¹⁵ 0.0109	²⁰⁶ 0.0115	¹⁹⁹ 0.0125	²³³ 0.0038 N ^{0.071} 30	²⁰⁰ 0.0021	²⁰⁰ 0.0024	¹⁹¹ 0.0028	¹⁹⁵ 0.0036	¹⁸⁸ 0.0095	¹⁰ 0.0000 N ^{0.466} 236		
22	COGENT-002	¹⁶⁵ 0.0029	¹⁶⁸ 0.0036	¹⁶⁷ 0.0041	¹⁶⁵ 0.0049	¹⁶¹ 0.0059	⁴⁷ 0.0001 N ^{0.244} 187	¹³⁷ 0.0014	¹⁴⁸ 0.0015	¹⁴⁴ 0.0017	¹⁴⁰ 0.0019	¹⁴¹ 0.0021	⁵⁶ 0.0002 N ^{0.144} 185		
23	COGENT-003	¹⁷¹ 0.0031	¹⁷² 0.0038	¹⁷³ 0.0043	¹⁶⁸ 0.0051	¹⁶⁰ 0.0060	⁶⁵ 0.0001 N ^{0.230} 175	¹⁵¹ 0.0015	¹⁶¹ 0.0017	¹⁶⁵ 0.0018	¹⁶⁰ 0.0020	¹⁵⁴ 0.0022	⁶² 0.0002 N ^{0.143} 184		
24	COGENT-004	¹¹¹ 0.0018	¹⁰² 0.0020	¹⁰⁸ 0.0022	¹⁰⁷ 0.0025	¹⁰⁸ 0.0028	¹¹⁰ 0.0002 N ^{0.159} 120	¹²⁹ 0.0013	¹²⁴ 0.0014	¹²² 0.0014	¹¹⁶ 0.0015	¹¹² 0.0015	¹²² 0.0007 N ^{0.050} 117		
25	COGENT-005	⁸⁷ 0.0016	⁸² 0.0017	⁸¹ 0.0018	⁷⁶ 0.0020	⁶⁹ 0.0021	¹⁶⁸ 0.0004 N ^{0.108} 67	¹³¹ 0.0013	¹¹⁷ 0.0013	¹⁰⁸ 0.0014	⁹⁶ 0.0014	⁸⁷ 0.0014	¹⁹⁴ 0.0011 N ^{0.107} 81		
26	COGENT-006	⁴⁴ 0.0012	⁴¹ 0.0012	³⁸ 0.0013	³⁵ 0.0014	³² 0.0015	¹⁶⁷ 0.0004 N ^{0.088} 49	⁶⁰ 0.0011	⁶¹ 0.0011	⁵⁵ 0.0011	⁴⁵ 0.0011	⁴¹ 0.0011	¹⁶⁷ 0.0008 N ^{0.019} 59		
27	COGENT-007	²³ 0.0010	²⁴ 0.0011	²⁷ 0.0012	¹⁸ 0.0012	¹⁶ 0.0013	¹⁶⁸ 0.0004 N ^{0.081} 40	³⁹ 0.0009	³⁷ 0.0010	³⁴ 0.0010	³⁰ 0.0010	²⁸ 0.0010	¹⁶⁴ 0.0008 N ^{0.013} 40		
28	COGNITEC-000	²⁸⁰ 0.0195	²⁷⁹ 0.0252	²⁴¹ 0.0297	²³⁵ 0.0352	²²⁹ 0.0417	²⁰⁰ 0.0006 N ^{0.259} 197	²⁵⁷ 0.0050	²⁶¹ 0.0065	²³⁵ 0.0077	²³¹ 0.0097	²²⁶ 0.0122	³⁹ 0.0001 N ^{0.305} 224		
29	COGNITEC-001	²⁴⁶ 0.0090	²⁵⁹ 0.0117	²²⁶ 0.0139	²²¹ 0.0166	²¹⁵ 0.0199	¹³² 0.0002 N ^{0.271} 204	²³⁰ 0.0030	²²⁹ 0.0034	²¹¹ 0.0040	²⁰⁹ 0.0046	¹⁹⁵ 0.0054	⁵⁴ 0.0002 N ^{0.207} 200		
30	COGNITEC-002	²⁰³ 0.0048	²⁰¹ 0.0057	¹⁹³ 0.0067	¹⁸⁰ 0.0079	¹⁸⁶ 0.0094	¹¹³ 0.0002 N ^{0.232} 178	²¹³ 0.0024	²⁰⁹ 0.0026	¹⁹³ 0.0028	¹⁸⁴ 0.0030	¹⁷⁴ 0.0034	⁹⁵ 0.0005 N ^{0.117} 171		
31	COGNITEC-003	²⁰⁶ 0.0053	²⁰⁶ 0.0066	¹⁹⁷ 0.0072	¹⁹³ 0.0085	¹⁸⁷ 0.0100	¹³⁹ 0.0003 N ^{0.222} 165	²²⁷ 0.0028	²²¹ 0.0030	¹⁹⁸ 0.0032	¹⁸⁶ 0.0035	¹⁸⁵ 0.0037	⁹⁵ 0.0008 N ^{0.097} 159		
32	COGNITEC-004	¹⁶⁰ 0.0027	¹⁶¹ 0.0032	¹⁶³ 0.0037	¹⁶⁰ 0.0045	¹⁵⁸ 0.0056	³⁶ 0.0001 N ^{0.233} 193	¹²⁸ 0.0013	¹²⁸ 0.0014	¹²⁵ 0.0015	¹²⁰ 0.0017	¹²⁹ 0.0019	⁶⁵ 0.0002 N ^{0.123} 176		
33	COGNITEC-005	⁷⁷ 0.0014	⁸⁴ 0.0018	⁸¹ 0.0018	⁷⁹ 0.0021	⁷⁸ 0.0024	⁷⁰ 0.0001 N ^{0.169} 129	⁶⁸ 0.0011	⁶⁹ 0.0011	⁶⁴ 0.0012	⁶⁰ 0.0012	⁵⁹ 0.0012	¹²⁵ 0.0007 N ^{0.037} 92		
34	COGNITEC-006	⁷² 0.0014	⁷⁶ 0.0016	⁷⁰ 0.0017	⁶² 0.0018	⁶¹ 0.0020	¹⁵⁸ 0.0002 N ^{0.114} 112	⁷⁰ 0.0011	⁶⁵ 0.0011	⁶³ 0.0012	⁶¹ 0.0012	⁶¹ 0.0012	¹²⁶ 0.0007 N ^{0.036} 91		
35	CYBERLINK-000	¹⁷⁷ 0.0034	¹⁷⁴ 0.0040	¹⁷⁶ 0.0046	¹⁷¹ 0.0054	¹⁶⁷ 0.0063	¹⁰⁶ 0.0002 N ^{0.209} 158	¹⁹⁶ 0.0021	¹⁹¹ 0.0022	^{182</sup}					

MISSES AT GIVEN RANK		ENROL MOST RECENT											
#	ALGORITHM	RANK 1					RANK 50						
	FNIR(N, T= 0, r)	N=0.64M	N=1.6M	N=3.0M	N=6.0M	N=12.0M	aN ^b	N=0.64M	N=1.6M	N=3.0M	N=6.0M	N=12.0M	aN ^b
73	HYPERVERGE-002	61.00013	31.00014	40.00014	40.00015	31.00016	206.00007 N ^{0.047} 14	112.00013	96.00013	78.00013	69.00013	202.00011 N ^{0.008} 23	
74	HZAILU-000	125.00019	124.00022	123.00025	119.00028	119.00033	88.00002 N ^{0.185} 141	144.00014	134.00014	126.00015	117.00015	106.00016	184.00009 N ^{0.032} 87
75	HZAILU-001	116.00018	108.00020	103.00021	89.00022	89.00025	193.00005 N ^{0.095} 56	144.00014	143.00015	136.00016	125.00016	114.00016	155.00008 N ^{0.048} 113
76	HZAILU-002	115.00018	111.00020	104.00021	97.00023	90.00026	173.00004 N ^{0.114} 77	148.00014	144.00015	134.00015	128.00016	116.00017	154.00008 N ^{0.048} 115
77	IDEMIA-003	209.00054	213.00069	206.00084	204.00101	198.00122	57.00001 N ^{-0.281} 215	207.00023	215.00027	194.00031	192.00036	182.00041	48.00002 N ^{0.201} 197
78	IDEMIA-004	212.00054	208.00066	201.00079	205.00097	199.00117	67.00001 N ^{0.220} 206	181.00018	187.00021	187.00025	183.00030	179.00036	31.00001 N ^{0.241} 207
79	IDEMIA-005	218.00064	223.00081	211.00097	208.00118	205.00143	73.00002 N ^{-0.277} 212	206.00022	218.00030	206.00036	206.00044	200.00055	19.00000 N ^{0.301} 223
80	IDEMIA-006	228.00076	237.00096	218.00113	211.00135	210.00161	128.00002 N ^{-0.259} 198	226.00028	235.00037	217.00046	212.00059	209.00076	17.00000 N ^{0.341} 232
81	IDEMIA-007	135.00021	144.00026	144.00030	141.00036	145.00044	28.00001 N ^{0.250} 191	67.00011	78.00012	82.00012	100.00014	100.00015	66.00002 N ^{0.110} 168
82	IDEMIA-008	14.00010	20.00011	18.00011	19.00013	21.00014	98.00002 N ^{0.121} 86	26.00009	24.00009	22.00009	20.00009	18.00009	140.00007 N ^{0.016} 47
83	IDEMIA-009	9.00009	9.00010	9.00010	9.00011	9.00012	134.00002 N ^{0.097} 57	17.00008	15.00009	14.00009	14.00009	9.00009	158.00008 N ^{0.037} 18
84	IDEMIA-010	7.00009	7.00009	6.00009	9.00010	7.00010	172.00004 N ^{0.059} 20	15.00008	14.00009	12.00009	11.00009	7.00009	168.00008 N ^{0.002} 9
85	IMAGUS-005	107.00018	106.00019	108.00022	108.00025	98.00028	109.00002 N ^{0.158} 119	108.00013	118.00013	110.00014	105.00014	105.00016	99.00005 N ^{0.056} 137
86	IMAGUS-006	112.00018	113.00020	107.00022	104.00025	102.00029	115.00002 N ^{0.156} 113	136.00014	133.00014	127.00015	114.00015	110.00016	138.00007 N ^{0.049} 116
87	IMAGUS-007	103.00017	116.00020	110.00022	111.00026	108.00030	63.00001 N ^{0.189} 143	98.00012	95.00013	89.00013	87.00013	91.00015	98.00005 N ^{0.064} 135
88	IMPERIAL-000	143.00022	142.00024	136.00027	131.00030	124.00035	138.00003 N ^{0.157} 115	165.0016	159.0017	151.0017	140.0018	127.00018	185.00009 N ^{0.041} 101
89	INCODE-003	250.00098	256.00129	221.00154	221.00191	211.00233	97.00002 N ^{-0.296} 223	217.00024	222.00031	201.00036	206.00046	201.00056	21.00001 N ^{0.285} 221
90	INCODE-004	166.00029	167.00035	168.00041	166.00049	163.00060	46.00001 N ^{-0.244} 188	172.00018	174.00019	171.00020	166.00021	153.00022	116.00006 N ^{0.07} 148
91	INCODE-005	83.00015	80.00017	78.00018	77.00020	76.00023	124.00002 N ^{-0.140} 100	99.00012	93.00013	88.00013	85.00014	87.00017	87.00007 N ^{0.041} 98
92	INNOVATRICS-007	89.00016	84.00017	85.00019	81.00021	84.00024	120.00002 N ^{0.143} 105	96.00012	88.00012	85.00013	81.00013	78.00013	144.00007 N ^{0.037} 95
93	INNOVATRICS-008	47.00012	45.00013	42.00014	44.00015	44.00016	150.00003 N ^{0.102} 62	62.00011	57.00011	50.00111	46.00111	43.00011	171.00008 N ^{0.18} 55
94	INTEMA-000	28.00011	27.00011	25.00012	26.00013	25.00016	103.00002 N ^{0.124} 88	59.00100	52.00100	52.00101	52.00101	55.00013	77.00003 N ^{0.09} 146
95	INTEMA-001	1.00008	1.00008	1.00036	1.00037	1.00039	4.00000 N ^{0.636} 241	8.00008	6.00008	201.00035	181.00035	181.00037	0.00000 N ^{0.628} 240
96	INTSYSMSU-000	316.0.1395	316.0.1457	292.0.1498	240.0.1544	237.0.1591	243.0.0768 N ^{0.045} 12	323.0.1098	323.0.1163	235.0.1206	245.0.1252	239.0.1296	243.0.0519 N ^{0.056} 124
97	IREX-000	194.0.0043	183.0.0044	174.0.0044	167.0.0046	159.0.0048	228.0.0028 N ^{0.332} 8	250.0.0043	242.0.0043	215.0.0043	203.0.0043	188.0.0043	23.0.0042 N ^{0.002} 6
98	ISYSTEMS-002	207.0.0053	207.0.0064	198.0.0072	191.0.0083	187.0.0096	162.0.0003 N ^{0.204} 153	230.0.0033	230.0.0034	198.0.0038	186.0.0041	207.0.0013 N ^{0.07} 140	
99	ISYSTEMS-003	197.0.0046	195.0.0052	184.0.0057	180.0.0066	174.0.0076	184.0.0004 N ^{0.174} 134	232.0.0031	226.0.0033	199.0.0034	184.0.0035	208.0.0013 N ^{0.063} 134	
100	KAKAO-000	52.0.0013	65.0.0015	66.0.0016	70.0.0019	74.0.0022	41.0.0001 N ^{0.192} 147	36.0.0009	38.0.0010	36.0.0010	39.0.0010	38.0.0011	91.0.0005 N ^{0.050} 118
101	KAKAO-001	65.0.0014	55.0.0014	50.0.0015	45.0.0015	41.0.0016	197.0.0005 N ^{0.106} 22	115.0.0013	105.0.0013	99.0.0013	84.0.0013	73.0.0013	199.0.0011 N ^{0.012} 32
102	KEDACOM-001	229.0.0076	219.0.0077	203.0.0079	190.0.0083	180.0.0087	234.0.0040 N ^{0.047} 13	274.0.0071	267.0.0072	232.0.0072	219.0.0073	206.0.0073	237.0.0063 N ^{0.009} 26
103	KNERON-000	202.0.0048	202.0.0059	194.0.0067	188.0.0079	185.0.0093	125.0.0002 N ^{0.226} 171	254.0.0048	256.0.0059	226.0.0067	224.0.0079	217.0.0093	64.0.0002 N ^{0.226} 204
104	LINECLOVA-002	50.0.0013	47.0.0013	41.0.0014	43.0.0015	40.0.0016	178.0.0004 N ^{0.179} 39	88.0.0012	79.0.0012	71.0.0012	62.0.0012	55.0.0012	195.0.0011 N ^{0.018} 19
105	LINECLOVA-003	13.0.0010	11.0.0010	16.0.0011	17.0.0012	14.0.0013	102.0.0002 N ^{0.116} 79	12.0.0008	9.0.0008	11.0.0008	10.0.0009	11.0.0009	105.0.0005 N ^{0.028} 82
106	LOOKMAN-003	238.0.0083	228.0.0088	210.0.0091	201.0.0096	199.0.0104	230.0.0030 N ^{0.076} 35	270.0.0072	270.0.0074	234.0.0075	222.0.0076	210.0.0076	235.0.0054 N ^{0.022} 65
107	LOOKMAN-005	230.0.0078	222.0.0080	207.0.0083	194.0.0086	183.0.0092	231.0.0038 N ^{0.075} 15	276.0.0072	268.0.0072	233.0.0073	220.0.0073	207.0.0074	236.0.0060 N ^{0.013} 39
108	MANTRA-000	84.0.0015	86.0.0017	88.0.0019	87.0.0022	88.0.0025	79.0.0002 N ^{0.171} 131	89.0.0012	81.0.0012	79.0.0012	74.0.0013	72.0.0013	125.0.0007 N ^{0.042} 102
109	MAXVISION-000	134.0.0021	139.0.0024	137.0.0027	134.0.0032	135.0.0038	59.0.0001 N ^{0.206} 156	111.0.0013	121.0.0013	121.0.0014	119.0.0014	120.0.0015	73.0.0003 N ^{0.100} 161
110	MAXVISION-001	40.0.0012	38.0.0012	39.0.0013	36.0.0014	29.0.0015	160.0.0003 N ^{0.089} 50	67.0.0011	60.0.0011	54.0.0011	50.0.0011	42.0.0011	178.0.0009 N ^{0.014} 42
111	MEGVII-001	257.0.0105	252.0.0118	222.0.0128	215.0.0142	209.0.0161	222.0.0015 N ^{0.143} 104	280.0.0077	276.0.0080	229.0.0086	216.0.0089	231.0.0040 N ^{0.048} 114	
112	MICROFOCUS-005	328.0.3700	328.0.4242	257.0.4610	240.0.5000	245.0.5391	242.0.0647 N ^{0.128} 92	328.0.1300	328.0.1724	257.0.2046	248.0.2425	242.0.2810	239.0.0040 N ^{0.263} 214
113	MICROSOFT-003	49.0.0013	77.0.0016	83.0.0018	91.0.0022	99.0.0028	16.0.0000 N ^{0.271} 205	206.0.0006	206.0.0006	206.0.0007	206.0.0008	206.0.0009	30.0.0001 N ^{0.158} 190
114	MICROSOFT-004	45.0.0012	68.0.0015	76.0.0018	86.0.0021	97.0.0028	15.0.0000 N ^{0.281} 214	1.0.0006	1.0.0006	1.0.0007	1.0.0007	8.0.0009	40.0.0001 N ^{0.139} 182
115	MICROSOFT-005	82.0.0015	102.0.0019	117.0.0023	128.0.0030	130.0.0037	11.0.0000 N ^{0.320} 231	3.0.0006	3.0.0006	2.0.0007	2.0.0008	10.0.0009	41.0.0001 N ^{0.136} 181
116	MICROSOFT-006	86.0016	110.0020	120.0.0025	128.0.0030	130.0.0036	14.0.0000 N ^{0.305} 227	4.0.0006	4.0.0006	4.0.0007	4.0.0007	4.0.0010	24.0.0000 N ^{0.184} 193
117	MUKH-002	284.0.0204	280.0.0258	242.0.0303	236.0.0361	232.0.0430	209.0.0007 N ^{0.255} 194	264.0.0070	257.0.0070	232.0.0083	232.0.0101	228.0.0124	45.0.0001 N ^{0.288} 218
118	NEC-000	265.0.0131	265.0.0170	253.0.0203	224.0.0244	220.0.0294	156.0.0003 N ^{0.276} 210	225.0.0029	219.0.0048	219.0.0059	208.0.0074	208.0.0074	165.0.0008 N ^{0.025} 72
119	NEC-001	277.0.0180	274.0.0209	236.0.0233	222.0.0266	222.0.0304	223.0.0016 N ^{0.179} 137	297.0.0109	286.0.0113	242.0.0116	234.0.0121	229.0.0129	234.0.0051 N ^{0.056} 122
120	NEC-002	11.0.0009	18.0.0010										

#	ALGORITHM	ENROL MOST RECENT										
		RANK 1					aN^b	RANK 50				
		N=0.64M	N=1.6M	N=3.0M	N=6.0M	N=12.0M		N=0.64M	N=1.6M	N=3.0M	N=6.0M	N=12.0M
145	PANGIAM-000	³⁷ 0.0011	³⁴ 0.0012	³⁶ 0.0013	³³ 0.0014	³⁹ 0.0016	¹¹⁹ 0.0002 N ^{0.118} 83	⁴⁷ 0.0010	⁴⁸ 0.0010	⁴³ 0.0010	⁴⁰ 0.0011	³⁹ 0.0011
146	PANGIAM-001	²²¹ 0.0068	²¹⁴ 0.0069	¹⁹⁶ 0.0070	¹⁸³ 0.0071	¹⁷² 0.0073	²³⁵ 0.0052 N ^{0.020} 5	²⁷² 0.0068	²⁶⁴ 0.0068	²²⁷ 0.0068	²¹⁷ 0.0068	²⁰⁵ 0.0068
147	PARAVISION-003	¹⁵⁹ 0.0026	¹⁵⁹ 0.0031	¹⁵⁹ 0.0035	¹⁵⁹ 0.0042	¹⁵⁹ 0.0048	⁷⁶ 0.0002 N ^{0.210} 159	¹⁶¹ 0.0016	¹⁶⁴ 0.0017	¹⁶² 0.0018	¹⁵⁹ 0.0020	¹⁴⁶ 0.0021
148	PARAVISION-004	⁸⁵ 0.0015	⁷⁸ 0.0016	⁷⁴ 0.0017	⁶⁹ 0.0019	⁶⁷ 0.0021	¹⁵⁸ 0.0003 N ^{0.111} 71	¹¹⁹ 0.0013	¹⁰⁸ 0.0013	⁹⁸ 0.0013	⁸⁹ 0.0013	⁸⁴ 0.0014
149	PARAVISION-005	⁷⁹ 0.0015	⁷¹ 0.0015	⁶⁹ 0.0016	⁶⁰ 0.0018	⁵⁶ 0.0019	¹⁷⁵ 0.0004 N ^{0.094} 35	¹²⁵ 0.0013	¹¹² 0.0013	¹⁰⁵ 0.0013	⁹³ 0.0013	⁸² 0.0014
150	PARAVISION-007	³⁵ 0.0011	³¹ 0.0012	²⁹ 0.0012	²⁹ 0.0013	²⁵ 0.0015	¹⁵³ 0.0003 N ^{0.091} 52	⁵² 0.0010	⁴¹ 0.0010	³⁸ 0.0010	³⁶ 0.0011	¹⁶² 0.0008 N ^{0.018} 57
151	PARAVISION-009	¹⁶ 0.0010	¹⁴ 0.0010	¹³ 0.0011	¹⁵ 0.0012	¹⁸ 0.0014	¹⁶ 0.0002 N ^{0.118} 81	³² 0.0009	³³ 0.0009	³² 0.0009	³¹ 0.0010	³⁰ 0.0010
152	PARAVISION-012	¹⁰ 0.0009	⁸ 0.0009	⁷ 0.0010	⁷ 0.0012	¹⁵⁹ 0.0003 N ^{0.072} 32	³⁴ 0.0009	²⁸ 0.0009	²³ 0.0009	²² 0.0009	¹⁷ 0.0009	¹⁷⁵ 0.0009 N ^{0.003} 11
153	PIXELALL-002	¹⁸⁸ 0.0037	¹⁸⁵ 0.0045	¹⁸² 0.0052	¹⁷⁷ 0.0062	¹⁷⁴ 0.0075	⁷² 0.0002 N ^{0.238} 182	¹⁶⁹ 0.0017	¹⁸⁰ 0.0019	¹⁷⁶ 0.0021	¹⁷³ 0.0024	¹⁶⁵ 0.0027
154	PIXELALL-003	¹²⁰ 0.0019	¹²⁰ 0.0021	¹¹⁷ 0.0024	¹¹⁵ 0.0028	¹¹¹ 0.0032	⁸³ 0.0002 N ^{0.182} 140	¹³⁹ 0.0014	¹³⁰ 0.0014	¹²¹ 0.0014	¹¹³ 0.0015	¹⁰⁷ 0.0016
155	PIXELALL-004	¹⁰¹ 0.0017	¹¹⁷ 0.0020	¹¹⁴ 0.0023	¹⁰⁹ 0.0026	¹⁰⁷ 0.0030	⁶¹ 0.0001 N ^{0.192} 146	¹²³ 0.0013	¹¹⁴ 0.0013	¹¹² 0.0014	¹⁰⁴ 0.0014	¹³¹ 0.0007 N ^{0.046} 110
156	PIXELALL-005	¹⁰⁵ 0.0018	¹⁰⁴ 0.0019	⁹⁹ 0.0020	⁸⁹ 0.0021	⁸⁸ 0.0024	¹⁵⁸ 0.0005 N ^{0.098} 38	¹⁵⁹ 0.0015	¹⁵¹ 0.0016	¹³⁹ 0.0016	¹²⁴ 0.0016	¹¹³ 0.0016
157	PTAKURATSATU-000	¹⁵⁵ 0.0025	¹⁵⁷ 0.0030	¹⁶⁰ 0.0036	¹⁵³ 0.0040	¹³⁹ 0.0040	¹⁴⁴ 0.0003 N ^{0.167} 127	¹⁵⁴ 0.0015	¹⁵⁴ 0.0016	¹⁶⁶ 0.0018	¹⁵⁵ 0.0020	⁸⁵ 0.0004 N ^{0.096} 158
158	QNAP-001	¹⁷⁹ 0.0035	¹⁷⁹ 0.0041	¹⁷⁷ 0.0047	¹⁷⁶ 0.0054	¹⁶⁸ 0.0063	¹³⁰ 0.0002 N ^{0.200} 149	²⁰⁸ 0.0022	¹⁹⁹ 0.0023	¹⁸⁶ 0.0024	¹⁷⁹ 0.0025	¹⁶⁹ 0.0028
159	QNAP-002	²⁰¹ 0.0047	¹⁹¹ 0.0049	¹⁸¹ 0.0052	¹²² 0.0054	¹⁶² 0.0059	²²³ 0.0016 N ^{0.079} 38	²⁴⁸ 0.0041	²¹⁴ 0.0042	²⁰⁴ 0.0043	¹⁹¹ 0.0044	²²⁷ 0.0032 N ^{0.019} 63
160	QNAP-003	¹⁵⁴ 0.0025	¹⁵¹ 0.0028	¹⁴⁷ 0.0031	¹⁴⁶ 0.0035	¹⁴⁰ 0.0040	¹⁴⁵ 0.0003 N ^{0.161} 122	¹⁵⁰ 0.0014	¹⁴⁵ 0.0016	¹³⁵ 0.0018	¹⁴¹ 0.0020	⁷⁸ 0.0004 N ^{0.104} 162
161	QUANTASOFT-001	³²³ 0.2177	³²⁰ 0.2177	²⁵⁵ 0.2177	²³⁸ 0.2177	²⁴⁴ 0.2177 N ^{0.000} 1	³²⁰ 0.1116	³²² 0.1116	²⁵⁴ 0.1116	²³⁸ 0.1116	²⁴⁴ 0.1116 N ^{0.000} 1	
162	RANKONE-002	²⁷³ 0.0155	²⁷¹ 0.0194	²³⁴ 0.0224	²²⁹ 0.0262	²²² 0.0304	²⁰⁷ 0.0007 N ^{0.230} 173	²⁵⁶ 0.0048	²⁵⁸ 0.0060	²²⁹ 0.0071	²²⁷ 0.0085	²²³ 0.0102
163	RANKONE-003	²²⁷ 0.0155	²⁷¹ 0.0194	²³⁵ 0.0224	²²⁹ 0.0262	²²⁴ 0.0304	²⁰⁸ 0.0007 N ^{0.230} 174	²⁵⁸ 0.0048	²⁵⁹ 0.0060	²³⁰ 0.0071	²²⁸ 0.0085	²²² 0.0102
164	RANKONE-005	²²⁷ 0.0075	²³⁴ 0.0094	²¹⁷ 0.0110	²¹² 0.0132	²⁰⁷ 0.0156	¹³⁶ 0.0003 N ^{0.251} 192	²²² 0.0026	²²⁴ 0.0032	²¹⁰ 0.0036	²⁰⁶ 0.0043	¹⁹⁶ 0.0050
165	RANKONE-007	¹⁶³ 0.0028	¹⁶³ 0.0034	¹⁶⁴ 0.0038	¹⁵⁷ 0.0045	¹⁵⁹ 0.0053	⁸⁸ 0.0002 N ^{0.211} 160	¹⁵³ 0.0015	¹⁵⁷ 0.0017	¹⁶⁰ 0.0018	¹⁵¹ 0.0019	¹⁵⁰ 0.0021
166	RANKONE-009	¹²⁸ 0.0020	¹³⁵ 0.0027	¹³⁵ 0.0032	¹³² 0.0032	⁴⁷ 0.0001 N ^{0.219} 163	¹³² 0.0013	¹²⁶ 0.0014	¹²⁴ 0.0015	¹¹⁶ 0.0015	¹⁰⁹ 0.0016	¹¹² 0.0006 N ^{0.059} 128
167	RANKONE-010	¹³¹ 0.0020	¹²⁸ 0.0022	¹²² 0.0025	¹¹⁷ 0.0029	¹¹¹ 0.0032	¹⁰² 0.0002 N ^{0.164} 126	¹⁴⁴ 0.0014	¹³⁵ 0.0015	¹³⁰ 0.0015	¹²² 0.0016	¹¹⁷ 0.0017
168	RANKONE-011	⁶⁴ 0.0014	⁶⁹ 0.0015	⁶⁷ 0.0017	⁶³ 0.0018	⁶⁸ 0.0021	⁹³ 0.0002 N ^{0.150} 110	⁷⁸ 0.0011	⁷¹ 0.0012	⁶⁹ 0.0012	⁶⁴ 0.0012	⁵⁷ 0.0012
169	RANKONE-012	⁵¹ 0.0013	⁵² 0.0014	⁵⁹ 0.0015	⁵⁶ 0.0017	⁵⁸ 0.0020	⁹⁵ 0.0002 N ^{0.144} 106	⁶⁹ 0.0011	⁶⁷ 0.0011	⁶¹ 0.0011	⁵³ 0.0011	⁴⁷ 0.0012
170	RANKONE-013	¹⁷ 0.0010	¹⁹ 0.0011	¹⁹ 0.0012	²⁷ 0.0013	²⁷ 0.0015	⁶⁴ 0.0001 N ^{0.144} 107	²³ 0.0009	¹⁹ 0.0009	¹⁸ 0.0009	¹⁷ 0.0009	¹⁵ 0.0009
171	RANKONE-014	⁸ 0.0009	¹⁰ 0.0010	¹⁰ 0.0010	¹¹ 0.0011	¹² 0.0013	¹¹ 0.0002 N ^{0.109} 68	²⁶ 0.0009	²¹ 0.0009	¹⁷ 0.0009	¹⁶ 0.0009	¹⁵ 0.0009
172	REALNETWORKS-002	²⁹³ 0.0299	²⁸⁹ 0.0393	²⁴⁸ 0.0470	²⁴¹ 0.0562	²³⁶ 0.0580	²¹⁹ 0.0013 N ^{0.236} 181	²⁶⁸ 0.0054	²⁷² 0.0076	²⁴⁰ 0.0097	²³⁵ 0.0126	²³⁰ 0.0132
173	REALNETWORKS-003	²⁷⁸ 0.0183	²⁷⁸ 0.0242	²⁴⁹ 0.0291	²³⁴ 0.0352	²³¹ 0.0423	¹⁷⁴ 0.0004 N ^{0.287} 218	²⁴⁹ 0.0041	²⁵¹ 0.0054	²²¹ 0.0064	²²² 0.0080	²⁰¹ 0.0080
174	REALNETWORKS-004	²⁷⁵ 0.0175	²⁷⁶ 0.0236	²³⁹ 0.0284	²³³ 0.0347	²²⁹ 0.0416	¹⁶¹ 0.0003 N ^{0.295} 221	²⁴⁸ 0.0040	²⁴⁸ 0.0050	²²³ 0.0061	²²² 0.0078	²²⁰ 0.0099
175	REALNETWORKS-005	¹²⁷ 0.0020	¹³¹ 0.0023	¹³² 0.0026	¹²⁷ 0.0030	¹²⁷ 0.0037	⁵⁴ 0.0001 N ^{0.207} 157	⁸¹ 0.0012	⁸⁶ 0.0012	⁹⁴ 0.0013	⁹³ 0.0015	⁸³ 0.0004 N ^{0.081} 148
176	REALNETWORKS-006	⁵³ 0.0013	⁵⁷ 0.0014	⁶¹ 0.0016	⁶¹ 0.0018	⁶² 0.0021	⁶⁶ 0.0001 N ^{0.163} 125	⁴⁵ 0.0010	⁴² 0.0010	⁴⁵ 0.0010	⁴⁸ 0.0011	³⁸ 0.0004 N ^{0.069} 130
177	REALNETWORKS-007	⁴⁸ 0.0013	⁴⁸ 0.0013	⁴⁷ 0.0014	⁴⁵ 0.0014	⁵¹ 0.0016	¹²⁶ 0.0002 N ^{0.124} 180	⁴¹ 0.0010	³⁹ 0.0010	⁴² 0.0010	⁴⁴ 0.0011	⁴⁴ 0.0011
178	REALNETWORKS-008	²⁶ 0.0011	³⁰ 0.0011	³¹ 0.0013	³¹ 0.0014	³⁶ 0.0016	⁹⁴ 0.0002 N ^{0.131} 94	¹⁹ 0.0009	¹⁸ 0.0009	²⁵ 0.0009	²⁴ 0.0009	²² 0.0009
179	RECOGNITO-000	¹⁸¹ 0.0035	¹⁶⁹ 0.0036	¹⁶⁹ 0.0036	¹⁴⁸ 0.0037	¹³⁴ 0.0038	²²⁶ 0.0025 N ^{0.026} 6	²³⁹ 0.0035	²³¹ 0.0035	¹⁹⁸ 0.0035	¹⁹⁷ 0.0035	²²⁸ 0.0034 N ^{0.002} 7
180	REMARKAI-000	¹⁶¹ 0.0027	¹⁶⁵ 0.0034	¹⁶⁴ 0.0040	¹⁶⁴ 0.0048	¹⁶⁸ 0.0058	³⁵ 0.0001 N ^{0.177} 199	¹⁴⁶ 0.0014	¹⁴⁹ 0.0015	¹⁴² 0.0016	¹³⁹ 0.0018	¹³⁶ 0.0020
181	RENDIP-000	⁷³ 0.0014	⁷³ 0.0015	⁷³ 0.0017	⁷³ 0.0019	⁷³ 0.0022	⁸⁴ 0.0002 N ^{0.158} 117	⁸² 0.0012	⁸⁰ 0.0012	⁷⁵ 0.0012	⁶⁷ 0.0012	⁶⁴ 0.0013
182	REVEALMEDIA-000	⁹⁶ 0.0017	¹⁰⁰ 0.0019	⁹¹ 0.0020	⁹² 0.0023	⁸⁸ 0.0025	¹⁴⁴ 0.0003 N ^{0.134} 96	⁹¹ 0.0012	⁸⁷ 0.0012	⁸¹ 0.0012	⁷⁵ 0.0013	⁷¹ 0.0013
183	S1-000	¹³³ 0.0021	¹³⁷ 0.0024	¹⁴⁰ 0.0028	¹³⁷ 0.0032	¹³¹ 0.0037	⁶² 0.0001 N ^{0.203} 152	¹⁴⁹ 0.0014	¹⁴² 0.0015	¹³⁵ 0.0015	¹²⁷ 0.0016	¹²⁸ 0.0007 N ^{0.059} 121
184	S1-001	¹⁷² 0.0031	¹⁵⁸ 0.0031	¹⁴² 0.0034	¹⁴² 0.0040	¹⁴⁴ 0.0040	²⁰⁷ 0.0009 N ^{0.192} 94	²⁰⁸ 0.0023	¹⁸³ 0.0024	¹⁸² 0.0024	¹⁶² 0.0025	²¹⁶ 0.0017 N ^{0.023} 69
185	S1-002	⁶⁷ 0.0014	⁵⁹ 0.0014	⁵⁹ 0.0015	⁵⁹ 0.0016	⁵⁹ 0.0018	¹⁷⁹ 0.0008 N ^{0.085} 45	¹²² 0.0013	¹¹³ 0.0013	¹⁰¹ 0.0013	⁸⁵ 0.0013	⁷⁷ 0.0013
186	S1-003	⁶⁶ 0.0014	⁶⁴ 0.0015	⁶¹ 0.0015	⁵⁹ 0.0017	⁵⁵ 0.0019	¹⁶⁴ 0.0003 N ^{0.101} 61	¹⁰⁸ 0.0012	⁹¹ 0.0013	⁸⁶ 0.0013	⁷⁷ 0.0013	⁷⁶ 0.0013
187	S1-004	⁵⁸ 0.0013	⁴⁹ 0.0013	⁴⁹ 0.0014	<sup							

MISSES AT GIVEN RANK FNIR(N, T= 0, R)		ENROL MOST RECENT											
#	ALGORITHM	RANK 1					aN^b	RANK 50					aN^b
		N=0.64M	N=1.6M	N=3.0M	N=6.0M	N=12.0M		N=0.64M	N=1.6M	N=3.0M	N=6.0M	N=12.0M	
217	VERIDAS-001	¹⁴⁷ 0.0023	¹⁵⁰ 0.0028	¹⁵⁰ 0.0032	¹⁴⁸ 0.0037	¹⁴⁹ 0.0045	⁴¹ 0.0001 N ^{-0.231} ¹⁷⁶	¹⁴⁵ 0.0014	¹⁵⁷ 0.0015	¹³² 0.0015	¹²⁹ 0.0016	¹²⁵ 0.0018	⁸⁹ 0.0005 N ^{0.088} ¹⁴⁹
218	VERIDAS-002	¹⁴⁶ 0.0023	¹⁴⁹ 0.0028	¹⁵⁸ 0.0028	¹³³ 0.0032	¹²⁹ 0.0037	¹⁴² 0.0003 N ^{-0.158} ¹¹⁶	¹⁴⁰ 0.0014	¹³⁶ 0.0015	¹²³ 0.0015	¹¹⁸ 0.0015	¹¹² 0.0016	¹⁵¹ 0.0007 N ^{0.047} ¹¹²
219	VERIDAS-003	⁹⁵ 0.0017	⁹⁵ 0.0018	⁹⁶ 0.0020	⁹⁶ 0.0022	⁸⁹ 0.0026	¹¹¹ 0.0002 N ^{-0.150} ¹⁰⁹	¹¹⁰ 0.0013	¹⁰⁶ 0.0013	¹⁰² 0.0013	⁹⁵ 0.0014	⁸⁹ 0.0014	¹³⁴ 0.0007 N ^{0.043} ¹⁰⁵
220	VERIDAS-004	⁵⁷ 0.0013	⁵⁰ 0.0014	⁴⁵ 0.0014	³⁴ 0.0014	³¹ 0.0015	²⁰⁹ 0.0007 N ^{0.043} ¹¹	⁹³ 0.0012	⁸⁸ 0.0012	⁷⁸ 0.0012	⁶⁹ 0.0012	⁶² 0.0012	¹⁹⁷ 0.0011 N ^{0.008} ²²
221	VIGILANTSOLUTIONS-008	¹⁵³ 0.0025	¹⁵⁶ 0.0029	¹⁵⁵ 0.0034	¹⁵⁴ 0.0040	¹⁴⁹ 0.0047	⁵⁶ 0.0001 N ^{-0.224} ¹⁶⁸	⁸⁶ 0.0012	⁹⁹ 0.0013	¹¹⁷ 0.0014	¹²¹ 0.0015	¹¹⁹ 0.0017	⁸⁷ 0.0002 N ^{0.130} ¹⁸⁰
222	VISIONBOX-000	¹⁰⁴ 0.0017	¹⁰⁵ 0.0019	¹¹⁰ 0.0022	²⁸⁰ 1.0000	²⁴⁴ 0.9526	¹ 0.0000 N ^{-2.570} ²⁴⁴	¹⁰² 0.0012	⁹⁸ 0.0013	¹⁰⁴ 0.0013	²⁵⁰ 1.0000	²⁴⁴ 0.9525	¹ 0.0000 N ^{2.719} ²⁴⁴
223	VISIONLABS-004	¹⁴² 0.0022	¹⁴⁸ 0.0027	¹⁵² 0.0032	¹⁵⁶ 0.0044	¹⁷⁴ 0.0070	⁷ 0.0000 N ^{-0.387} ²³⁵	¹⁰⁵ 0.0012	¹²⁵ 0.0014	¹⁴⁵ 0.0017	¹⁷⁶ 0.0025	¹⁹³ 0.0045	⁷ 0.0000 N ^{0.45} ²³⁵
224	VISIONLABS-005	¹²⁶ 0.0020	¹³⁶ 0.0024	¹⁴³ 0.0029	¹⁴⁴ 0.0037	¹⁵⁶ 0.0051	¹³ 0.0000 N ^{-0.322} ²³²	⁹⁷ 0.0012	¹⁰⁴ 0.0013	¹³⁷ 0.0016	¹⁵² 0.0019	¹⁷² 0.0029	¹⁴ 0.0000 N ^{0.298} ²²²
225	VISIONLABS-006	⁹² 0.0016	⁹⁷ 0.0018	¹⁰ 0.0022	¹²⁸ 0.0028	¹⁴² 0.0041	¹² 0.0000 N ^{-0.314} ²³⁰	⁹³ 0.0012	¹⁰⁰ 0.0013	¹²⁵ 0.0015	¹⁴⁵ 0.0019	¹⁶⁷ 0.0027	¹⁵ 0.0000 N ^{0.275} ²¹⁵
226	VISIONLABS-007	⁹⁰ 0.0016	⁹¹ 0.0018	⁹³ 0.0020	⁹⁹ 0.0023	¹²¹ 0.0034	²² 0.0001 N ^{-0.248} ¹⁹⁰	⁸⁷ 0.0012	⁸⁵ 0.0012	⁸³ 0.0013	⁸³ 0.0013	¹³⁹ 0.0020	⁴⁶ 0.0001 N ^{0.152} ¹⁸⁶
227	VISIONLABS-008	¹¹⁷ 0.0019	¹¹⁴ 0.0020	¹⁰⁵ 0.0021	¹⁰⁸ 0.0025	¹⁰⁸ 0.0030	⁹⁶ 0.0002 N ^{-0.169} ¹²⁸	¹⁶⁷ 0.0016	¹⁶⁵ 0.0017	¹⁵⁶ 0.0020	¹⁵⁷ 0.0023	⁷⁶ 0.0003 N ^{0.114} ¹⁶⁹	
228	VISIONLABS-009	³² 0.0011	²⁸ 0.0011	²⁶ 0.0012	³⁶ 0.0014	⁴⁸ 0.0017	⁵⁷ 0.0001 N ^{-0.160} ¹²¹	⁴⁶ 0.0010	⁴⁰ 0.0010	⁴¹ 0.0010	³¹ 0.0011	⁸⁶ 0.0014	⁶² 0.0002 N ^{0.109} ¹⁶⁵
229	VISIONLABS-010	⁶³ 0.0014	⁵⁶ 0.0014	⁵⁶ 0.0015	⁵⁷ 0.0017	⁶³ 0.0021	¹⁰⁷ 0.0002 N ^{0.137} ⁹⁸	¹⁰⁹ 0.0013	⁹⁴ 0.0013	¹⁰⁵ 0.0013	¹⁰⁶ 0.0014	¹¹⁵ 0.0017	⁸⁹ 0.0004 N ^{0.090} ¹⁵⁸
230	VISIONLABS-011	³³ 0.0011	³⁵ 0.0012	³⁴ 0.0013	³⁶ 0.0014	³² 0.0018	⁵¹ 0.0001 N ^{-0.162} ¹²⁴	⁵⁶ 0.0010	⁵⁶ 0.0011	⁵⁹ 0.0011	⁶³ 0.0012	⁹⁸ 0.0015	³⁹ 0.0002 N ^{0.114} ¹⁷⁰
231	VIXVIZION-009	¹²³ 0.0019	¹²⁹ 0.0023	¹³³ 0.0026	¹³⁵ 0.0032	¹²⁶ 0.0037	⁴⁰ 0.0001 N ^{-0.226} ¹⁷⁰	⁶¹ 0.0011	⁸² 0.0012	⁹¹ 0.0013	⁹⁴ 0.0013	⁹² 0.0015	⁶⁸ 0.0003 N ^{0.106} ¹⁶³
232	VNPPT-001	¹³² 0.0020	¹²¹ 0.0022	¹¹⁵ 0.0023	¹⁰⁸ 0.0025	⁹⁶ 0.0028	¹⁹⁴ 0.0005 N ^{0.101} ⁶⁰	¹⁷⁶ 0.0018	¹⁷⁰ 0.0018	¹⁶³ 0.0018	¹⁴³ 0.0018	¹²⁸ 0.0019	²¹⁰ 0.0014 N ^{0.018} ⁵³
233	VNPPT-002	¹¹³ 0.0018	¹⁰³ 0.0019	⁸⁹ 0.0020	⁸⁴ 0.0021	⁷⁶ 0.0023	²⁰⁴ 0.0007 N ^{0.072} ³¹	¹⁷⁰ 0.0017	¹⁶⁶ 0.0017	¹⁵⁴ 0.0018	¹³⁶ 0.0018	¹²⁴ 0.0018	²¹⁴ 0.0015 N ^{0.009} ²⁸
234	VCORD-005	²¹⁴ 0.0060	²¹⁵ 0.0070	²⁰ 0.0082	²⁰ 0.0097	¹⁹ 0.0117	¹³⁸ 0.0003 N ^{-0.232} ¹⁷⁹	²³⁹ 0.0033	²⁵² 0.0035	²¹² 0.0037	¹⁹⁷ 0.0040	¹⁹⁰ 0.0043	¹⁸⁸ 0.0010 N ^{0.090} ¹⁵⁴
235	VTS-001	⁶² 0.0014	⁷⁰ 0.0015	⁷² 0.0017	⁷³ 0.0019	⁷⁹ 0.0023	⁵³ 0.0001 N ^{-0.179} ¹³⁸	⁴³ 0.0010	⁴³ 0.0010	⁴⁶ 0.0010	⁴¹ 0.0011	⁴⁶ 0.0011	⁹⁴ 0.0005 N ^{0.051} ¹¹⁹
236	VTS-002	⁹⁷ 0.0017	¹⁰⁷ 0.0019	¹¹⁷ 0.0022	¹¹¹ 0.0026	¹¹¹ 0.0032	³⁶ 0.0001 N ^{-0.215} ¹⁶²	⁶⁴ 0.0011	⁶⁶ 0.0011	⁷³ 0.0012	⁷² 0.0013	⁸¹ 0.0013	⁸² 0.0004 N ^{0.079} ¹⁴⁷
237	VTS-003	²⁹ 0.0011	²⁹ 0.0011	²⁶ 0.0012	²⁸ 0.0013	³³ 0.0015	¹⁰⁴ 0.0002 N ^{0.124} ⁸⁹	²¹ 0.0009	²⁰ 0.0009	¹⁹ 0.0009	¹⁹ 0.0009	²⁰ 0.0009	¹¹⁴ 0.0006 N ^{0.226} ⁷⁵
238	XFORWARDAI-000	¹³⁷ 0.0021	¹³⁰ 0.0023	¹¹⁸ 0.0024	¹¹³ 0.0027	¹⁰⁴ 0.0029	¹⁸⁶ 0.0005 N ^{0.111} ⁷²	¹⁸⁹ 0.0019	¹⁷⁹ 0.0019	¹⁷⁰ 0.0019	¹⁵⁸ 0.0020	¹⁴² 0.0020	²¹² 0.0015 N ^{0.18} ⁵⁶
239	XFORWARDAI-001	¹³⁰ 0.0020	¹¹⁸ 0.0020	¹⁰² 0.0021	⁸⁹ 0.0022	⁸¹ 0.0024	²¹³ 0.0009 N ^{0.058} ¹⁸	¹⁸⁰ 0.0019	¹⁷⁸ 0.0019	¹⁶⁸ 0.0019	¹⁵⁰ 0.0019	¹³⁴ 0.0019	²²⁰ 0.0018 N ^{0.004} ¹⁴
240	XFORWARDAI-002	¹²⁴ 0.0019	¹⁰⁹ 0.0020	⁹⁵ 0.0020	⁸⁹ 0.0021	⁷⁰ 0.0022	²¹⁷ 0.0011 N ^{0.038} ¹⁰	¹⁸¹ 0.0019	¹⁷⁶ 0.0019	¹⁶⁷ 0.0019	¹⁴⁹ 0.0019	¹³¹ 0.0019	²¹⁹ 0.0018 N ^{0.003} ¹²
241	YITU-002	⁸⁸ 0.0016	⁹⁹ 0.0018	¹⁰³ 0.0021	¹⁰⁸ 0.0024	¹⁰⁵ 0.0029	³⁷ 0.0001 N ^{-0.213} ¹⁶¹	⁴⁰ 0.0009	⁴⁶ 0.0010	⁴⁴ 0.0010	⁴³ 0.0011	⁵¹ 0.0012	⁷⁹ 0.0004 N ^{0.073} ¹⁴³
242	YITU-003	¹⁵⁸ 0.0026	¹⁵⁵ 0.0029	¹⁴⁸ 0.0031	¹³⁹ 0.0035	¹³⁸ 0.0039	¹⁷¹ 0.0004 N ^{0.141} ¹⁰¹	¹⁹⁴ 0.0020	¹⁸⁸ 0.0021	¹⁷⁹ 0.0022	¹⁷⁰ 0.0023	¹⁶⁰ 0.0024	¹⁸⁹ 0.0010 N ^{0.054} ¹²⁰
243	YITU-004	³⁴ 0.0011	⁴⁴ 0.0013	³⁹ 0.0015	³⁹ 0.0017	¹⁵ 0.0047	⁸ 0.0000 N ^{-0.438} ²³⁷	¹⁶ 0.0008	¹⁶ 0.0009	¹⁵ 0.0009	¹⁷⁸ 0.0036	⁸ 0.0000 N ^{0.395} ²³⁴	
244	YITU-005	¹⁴⁴ 0.0022	¹³² 0.0023	¹²³ 0.0025	¹¹⁴ 0.0027	¹⁰⁹ 0.0031	¹⁸⁹ 0.0005 N ^{0.113} ⁷⁴	¹⁸⁷ 0.0020	¹⁸² 0.0020	¹⁷³ 0.0020	¹⁵⁹ 0.0020	¹⁴⁴ 0.0020	²¹⁵ 0.0017 N ^{0.012} ³⁴

Table 28: Investigation-mode: Effect of N on FNIR on recent images For five enrollment population sizes, N, with $T = 0$ and FPIR = 1. The left five columns are rank 1 miss rates The right five columns are rank 50 miss rates Missing entries usually apply because another algorithm from the same developer was run instead. Some developers are missing because less accurate algorithms were not run on galleries with $N > 1\,600\,000$. Throughout blue superscripts indicate the rank of the algorithm for that column, and yellow highlighting indicates the most accurate value. Caution: The Power-low models are mostly intended to draw attention to the kind of behavior, not as a model to be used for prediction.

MISSES OUTSIDE RANK R		RESOURCE USAGE		ENROL MOST RECENT, N = 1.6M					
#	ALGORITHM	BYTES	MSEC	R=1	R=5	R=10	R=20	R=50	WORK=10
1	20FACE-000	19 ¹ 2048	41 ² 247	29 ³ 0.0552	29 ³ 0.0269	29 ³ 0.0198	28 ⁴ 0.0146	28 ² 0.0099	29 ⁴ 1.275
2	3DIVI-003	41 ¹ 512	153 ² 625	308 ³ 0.0833	303 ³ 0.0444	303 ³ 0.0349	299 ⁴ 0.0270	299 ⁴ 0.0191	304 ⁵ 1.447
3	3DIVI-004	305 ¹ 4096	154 ² 628	260 ³ 0.0175	257 ³ 0.0091	257 ³ 0.0075	251 ⁴ 0.0061	246 ⁵ 0.0049	263 ⁶ 1.092
4	3DIVI-005	316 ¹ 4096	165 ² 653	267 ³ 0.0176	258 ³ 0.0091	253 ³ 0.0074	250 ⁴ 0.0061	247 ⁵ 0.0049	263 ⁶ 1.092
5	3DIVI-006	63 ¹ 528	166 ² 653	27 ³ 0.0240	285 ³ 0.0171	280 ³ 0.0160	289 ⁴ 0.0154	295 ⁵ 0.0148	283 ⁶ 1.162
6	ACER-000	49 ¹ 512	31 ² 201	243 ³ 0.0106	223 ³ 0.0051	219 ³ 0.0041	215 ⁴ 0.0034	207 ⁵ 0.0026	223 ⁶ 1.053
7	ACER-001	186 ¹ 2048	22 ² 184	19 ³ 0.0051	194 ³ 0.0032	193 ³ 0.0028	192 ⁴ 0.0025	192 ⁵ 0.0022	193 ⁶ 1.031
8	AIZE-001	15 ¹ 2048	86 ² 403	20 ³ 0.0056	20 ³ 0.0037	20 ³ 0.0033	21 ⁴ 0.0030	211 ⁵ 0.0027	20 ⁶ 1.035
9	ALCHERA-000	20 ¹ 2048	46 ² 263	262 ³ 0.0161	271 ³ 0.0124	271 ³ 0.0117	282 ⁴ 0.0111	285 ⁵ 0.0105	270 ⁶ 1.116
10	ALCHERA-001	139 ¹ 2048	6 ² 66	33 ³ 0.9869	33 ³ 0.9782	33 ³ 0.9735	33 ⁴ 0.9679	33 ⁵ 0.9590	33 ⁶ 9.811
11	ALCHERA-002	146 ¹ 2048	14 ² 115	310 ³ 0.0949	308 ³ 0.0555	306 ³ 0.0443	306 ⁴ 0.0354	301 ⁵ 0.0254	308 ⁶ 1.544
12	ALCHERA-003	19 ¹ 2048	135 ² 548	240 ³ 0.0104	227 ³ 0.0054	227 ³ 0.0045	226 ⁴ 0.0038	223 ⁵ 0.0032	229 ⁶ 1.055
13	ALCHERA-004	238 ¹ 2048	267 ² 854	246 ³ 0.0110	222 ³ 0.0049	215 ³ 0.0038	207 ⁴ 0.0032	204 ⁵ 0.0025	223 ⁶ 1.051
14	ALLGOVISION-000	22 ¹ 2048	97 ² 425	240 ³ 0.0114	252 ³ 0.0084	250 ³ 0.0078	259 ⁴ 0.0073	263 ⁵ 0.0067	257 ⁶ 1.079
15	ALLGOVISION-001	212 ¹ 2048	237 ² 792	229 ³ 0.0090	220 ³ 0.0048	218 ³ 0.0040	214 ⁴ 0.0033	212 ⁵ 0.0027	220 ⁶ 1.048
16	ALLGOVISION-002	20 ¹ 2048	203 ² 712	21 ³ 0.0067	226 ³ 0.0052	230 ³ 0.0048	237 ⁴ 0.0046	245 ⁵ 0.0043	221 ⁶ 1.049
17	ANKE-000	282 ¹ 2072	99 ² 431	257 ³ 0.0132	243 ³ 0.0073	241 ³ 0.0060	240 ⁴ 0.0050	238 ⁵ 0.0040	248 ⁶ 1.072
18	ANKE-001	282 ¹ 2072	102 ² 433	259 ³ 0.0132	244 ³ 0.0073	241 ³ 0.0061	241 ⁴ 0.0050	239 ⁵ 0.0040	247 ⁶ 1.073
19	ANKE-002	27 ¹ 2056	159 ² 641	152 ³ 0.0028	151 ³ 0.0020	149 ³ 0.0018	157 ⁴ 0.0018	158 ⁵ 0.0017	151 ⁶ 1.019
20	AWARE-003	283 ¹ 2076	208 ² 716	285 ³ 0.0306	282 ³ 0.0162	279 ³ 0.0127	275 ⁴ 0.0100	271 ⁵ 0.0075	284 ⁶ 1.163
21	AWARE-004	29 ¹ 2076	92 ² 204	712 ³ 0.0679	300 ³ 0.0348	297 ³ 0.0274	297 ⁴ 0.0208	294 ⁵ 0.0145	300 ⁶ 1.354
22	AWARE-005	297 ¹ 3100	251 ² 827	286 ³ 0.0311	283 ³ 0.0167	281 ³ 0.0134	278 ⁴ 0.0107	277 ⁵ 0.0082	285 ⁶ 1.167
23	AWARE-006	3 ¹ 124	244 ² 818	30 ³ 0.6697	302 ³ 0.0369	299 ³ 0.0288	298 ⁴ 0.0223	296 ⁵ 0.0158	305 ⁶ 1.371
24	AYONIX-000	101 ¹ 1036	1 ² 10	330 ³ 0.4505	331 ³ 0.3540	331 ³ 0.3176	331 ⁴ 0.2834	330 ⁵ 0.2381	331 ⁶ 4.288
25	AYONIX-001	103 ¹ 1036	3 ² 12	32 ³ 0.3414	324 ³ 0.2338	322 ³ 0.1977	325 ⁴ 0.1652	324 ⁵ 0.1274	322 ⁶ 3.226
26	AYONIX-002	104 ¹ 1036	2 ² 11	325 ³ 0.3414	325 ³ 0.2338	322 ³ 0.1977	324 ⁴ 0.1652	325 ⁵ 0.1274	322 ⁶ 3.226
27	CAMVI-003	81 ¹ 1024	199 ² 707	29 ³ 0.0520	307 ³ 0.0057	306 ³ 0.0517	311 ⁴ 0.0517	311 ⁵ 0.0517	306 ⁶ 1.466
28	CAMVI-004	85 ¹ 1024	210 ² 718	296 ³ 0.0468	305 ³ 0.0465	307 ³ 0.0465	308 ⁴ 0.0464	310 ⁵ 0.0464	303 ⁶ 1.419
29	CAMVI-005	81 ¹ 1024	227 ² 769	30 ³ 0.0652	309 ³ 0.0648	312 ³ 0.0648	314 ⁴ 0.0648	316 ⁵ 0.0647	307 ⁶ 1.584
30	CANON-001	304 ¹ 4096	288 ² 893	23 ³ 0.0011	32 ³ 0.0010	29 ³ 0.0010	28 ⁴ 0.0009	27 ⁵ 0.0009	29 ⁶ 1.009
31	CANON-002	331 ¹ 6200	305 ² 932	32 ³ 0.0012	27 ³ 0.0010	29 ³ 0.0009	23 ⁴ 0.0009	26 ⁵ 0.0009	25 ⁶ 1.009
32	CIB-000	33 ¹ 8196	175 ² 674	7 ³ 0.0015	75 ³ 0.0013	69 ³ 0.0012	73 ⁴ 0.0012	73 ⁵ 0.0012	75 ⁶ 1.012
33	CLEARVIEWAI-000	302 ¹ 4096	224 ² 765	22 ³ 0.0011	30 ³ 0.0010	32 ³ 0.0010	26 ⁴ 0.0009	25 ⁵ 0.0009	25 ⁶ 1.009
34	CLOUDWALK-HR-000	20 ¹ 2048	296 ² 908	66 ³ 0.0015	97 ³ 0.0014	106 ³ 0.0014	117 ⁴ 0.0014	127 ⁵ 0.0014	91 ⁶ 1.013
35	CLOUDWALK-MT-000	154 ¹ 2048	275 ² 870	90 ³ 0.0018	132 ³ 0.0018	139 ³ 0.0018	151 ⁴ 0.0018	168 ⁵ 0.0018	125 ⁶ 1.016
36	CLOUDWALK-MT-001	141 ¹ 2048	315 ² 955	88 ³ 0.0018	131 ³ 0.0018	140 ³ 0.0018	149 ⁴ 0.0018	167 ⁵ 0.0018	124 ⁶ 1.016
37	CLOUDWALK-MT-002	177 ¹ 2048	328 ² 979	89 ³ 0.0018	129 ³ 0.0018	141 ³ 0.0018	155 ⁴ 0.0018	169 ⁵ 0.0018	126 ⁶ 1.016
38	COGENT-000	61 ¹ 525	136 ² 551	24 ³ 0.0105	263 ³ 0.0096	268 ³ 0.0095	206 ⁴ 0.0032	201 ⁵ 0.0024	259 ⁶ 1.088
39	COGENT-001	60 ¹ 525	137 ² 552	241 ³ 0.0105	264 ³ 0.0096	269 ³ 0.0095	209 ⁴ 0.0032	200 ⁵ 0.0024	269 ⁶ 1.088
40	COGENT-002	105 ¹ 1043	332 ² 987	168 ³ 0.0036	163 ³ 0.0022	166 ³ 0.0020	154 ⁴ 0.0018	148 ⁵ 0.0015	164 ⁶ 1.021
41	COGENT-003	106 ¹ 1043	320 ² 960	172 ³ 0.0038	174 ³ 0.0024	170 ³ 0.0021	171 ⁴ 0.0019	161 ⁵ 0.0017	172 ⁶ 1.023
42	COGENT-004	26 ¹ 2053	314 ² 952	11 ³ 0.0020	112 ³ 0.0016	113 ³ 0.0015	122 ⁴ 0.0015	124 ⁵ 0.0014	107 ⁶ 1.015
43	COGENT-005	109 ¹ 1062	220 ² 774	82 ³ 0.0017	95 ³ 0.0014	97 ³ 0.0014	108 ⁴ 0.0014	117 ⁵ 0.0013	94 ⁶ 1.013
44	COGENT-006	72 ¹ 550	265 ² 850	41 ³ 0.0012	47 ³ 0.0011	47 ³ 0.0011	53 ⁴ 0.0011	61 ⁵ 0.0011	46 ⁶ 1.010
45	COGENT-007	73 ¹ 550	333 ² 991	24 ³ 0.0011	33 ³ 0.0010	34 ³ 0.0010	35 ⁴ 0.0010	37 ⁵ 0.0010	31 ⁶ 1.009
46	COGNITEC-000	263 ¹ 2052	19 ² 176	279 ³ 0.0252	277 ³ 0.0136	275 ³ 0.0107	272 ⁴ 0.0085	261 ⁵ 0.0065	278 ⁶ 1.136
47	COGNITEC-001	25 ¹ 2052	32 ² 202	259 ³ 0.0117	235 ³ 0.0062	234 ³ 0.0051	234 ⁴ 0.0042	229 ⁵ 0.0034	239 ⁶ 1.062
48	COGNITEC-002	249 ¹ 2052	37 ² 227	201 ³ 0.0057	199 ³ 0.0037	198 ³ 0.0032	199 ⁴ 0.0029	209 ⁵ 0.0026	200 ⁶ 1.035
49	COGNITEC-003	26 ¹ 2052	297 ² 297	206 ³ 0.0062	208 ³ 0.0040	206 ³ 0.0036	213 ⁴ 0.0033	221 ⁵ 0.0030	170 ⁶ 1.039
50	COGNITEC-004	252 ¹ 2052	28 ² 192	161 ³ 0.0032	154 ³ 0.0020	144 ³ 0.0018	132 ⁴ 0.0015	128 ⁵ 0.0014	158 ⁶ 1.020
51	COGNITEC-005	250 ¹ 2052	73 ² 367	70 ³ 0.0016	69 ³ 0.0013	68 ³ 0.0012	68 ⁴ 0.0012	69 ⁵ 0.0011	79 ⁶ 1.012
52	COGNITEC-006	248 ¹ 2052	111 ² 463	70 ³ 0.0016	112 ³ 0.0015	112 ³ 0.0015	118 ⁴ 0.0014	129 ⁵ 0.0014	96 ⁶ 1.014
53	CUBOX-000	164 ¹ 2048	300 ² 918	58 ³ 0.0014	85 ³ 0.0014	98 ³ 0.0014	109 ⁴ 0.0014	120 ⁵ 0.0014	82 ⁶ 1.012
54	CYBERLINK-000	251 ¹ 2052	191 ² 699	174 ³ 0.0040	184 ³ 0.0028	188 ³ 0.0026	190 ⁴ 0.0024	191 ⁵ 0.0022	183 ⁶ 1.027
55	CYBERLINK-001	247 ¹ 2052	101 ² 433	166 ³ 0.0035	169 ³ 0.0023	168 ³ 0.0021	161 ⁴ 0.0018	163 ⁵ 0.0017	167 ⁶ 1.022
56	CYBERLINK-002	32 ¹ 4140	217 ² 738	14 ³ 0.0026	165 ³ 0.0023	174 ³ 0.0022	182 ⁴ 0.0021	186 ⁵ 0.0021	163 ⁶ 1.021
57	CYBERLINK-003	332 ¹ 6212	190 ² 696	75 ³ 0.0016	74 ³ 0.0013	74 ³ 0.			

MISSES OUTSIDE RANK R		RESOURCE USAGE		ENROL MOST RECENT, N = 1.6M					
#	ALGORITHM	BYTES	MSEC	R=1	R=5	R=10	R=20	R=50	WORK-10
73	DERMALOG-007	⁵ 128	⁹³ 413	²³² 0.0092	²³⁹ 0.0066	²⁴⁰ 0.0060	²⁴⁷ 0.0057	²⁵⁴ 0.0054	²⁵⁸ 1.062
74	DERMALOG-008	⁴¹ 512	⁷⁴ 370	¹⁵⁴ 0.0029	¹⁵⁰ 0.0020	¹⁴⁶ 0.0018	¹⁴² 0.0017	¹⁴⁵ 0.0015	¹⁵² 1.019
75	DERMALOG-009	⁵⁶ 512	⁷⁰ 347	¹⁵³ 0.0028	¹⁷² 0.0024	¹⁸¹ 0.0023	¹⁸⁵ 0.0023	¹⁹³ 0.0022	¹⁶⁶ 1.022
76	DERMALOG-010	³⁸ 512	¹⁵⁶ 634	¹²³ 0.0022	¹⁵⁸ 0.0021	¹⁶⁷ 0.0021	¹⁸⁰ 0.0020	¹⁸⁷ 0.0020	¹⁵¹ 1.019
77	DERMALOG-011	⁸ 128	⁶⁹ 343	⁷⁶ 0.0016	⁶² 0.0012	⁵⁹ 0.0012	⁵⁸ 0.0011	⁵⁹ 0.0011	⁶⁰ 1.011
78	DIGIDATA-000	¹⁵⁷ 2048	¹³⁸ 561	³³³ 0.5897	³³⁴ 0.5892	³³⁴ 0.5891	³³⁴ 0.5891	³³⁴ 0.5891	³³⁴ 6.303
79	DILUSENSE-000	¹⁴³ 2048	⁴² 249	¹²⁵ 0.0022	¹⁰⁸ 0.0015	¹⁰² 0.0014	¹⁰⁴ 0.0013	⁹⁰ 0.0013	¹¹⁰ 1.015
80	DILUSENSE-001	³¹¹ 4096	²⁸¹ 885	⁶³ 0.0015	⁶⁶ 0.0013	⁶⁷ 0.0012	⁷⁰ 0.0011	⁶⁵ 0.0011	⁶⁵ 1.011
81	EYEDEA-003	¹⁰² 1036	⁸⁰ 385	³⁰⁷ 0.0800	³⁰⁴ 0.0451	³⁰⁴ 0.0362	³⁰⁰ 0.0289	³⁰⁰ 0.0211	³⁰⁵ 1.448
82	F-001	²³⁴ 2048	²⁶⁶ 851	²⁵⁴ 0.0120	²⁶⁶ 0.0105	²⁷⁷ 0.0102	²⁷⁶ 0.0100	²⁸¹ 0.0099	²⁶⁶ 1.096
83	FINCORE-000	¹⁸⁸ 2048	¹¹⁶ 477	²⁴⁵ 0.0108	²²⁸ 0.0052	²²¹ 0.0042	²¹⁷ 0.0034	²¹⁰ 0.0026	²²⁷ 1.054
84	FIRSTCREDITKZ-001	³⁴ 288	²³⁸ 799	³⁹ 0.0012	⁵⁴ 0.0012	⁵⁶ 0.0012	⁷⁵ 0.0012	⁵¹ 0.0012	⁵¹ 1.011
85	FUJITSULAB-000	⁹² 1032	³¹⁵ 950	¹²⁶ 0.0022	¹¹⁹ 0.0016	¹²⁰ 0.0015	¹²⁰ 0.0015	¹¹⁹ 0.0014	¹¹⁹ 1.015
86	FUJITSULAB-001	⁹³ 1032	²⁸⁴ 890	¹⁰¹ 0.0019	¹⁰⁶ 0.0015	¹¹¹ 0.0015	¹¹⁴ 0.0014	¹²¹ 0.0014	¹⁰³ 1.014
87	GLORY-000	³⁹ 418	¹⁵ 160	³¹⁸ 0.1781	³²⁰ 0.1391	³²⁰ 0.1266	³²⁰ 0.1154	³²⁰ 0.1007	³¹⁸ 2.298
88	GLORY-001	¹³² 1726	⁸⁰ 405	³¹⁵ 0.1268	³¹⁵ 0.0967	³¹⁶ 0.0869	³¹⁶ 0.0778	³¹⁷ 0.0673	³¹⁷ 1.903
89	GORILLA-001	²⁸⁸ 2156	¹⁷ 169	³⁰⁰ 0.0603	²⁹⁵ 0.0304	²⁹⁴ 0.0230	²⁹⁴ 0.0174	²⁸⁷ 0.0117	²⁹⁵ 0.309
90	GORILLA-002	¹¹² 1132	⁶² 341	²⁷³ 0.0197	²⁵⁹ 0.0092	²⁴⁹ 0.0070	²⁴³ 0.0054	²⁴⁰ 0.0041	²⁶⁵ 1.096
91	GORILLA-003	²⁸⁷ 2156	¹⁴¹ 563	²⁸⁷ 0.0361	²⁸⁰ 0.0146	²⁷⁴ 0.0106	²⁶⁶ 0.0078	²⁵⁷ 0.0054	²⁸⁴ 1.158
92	GORILLA-004	²⁸⁹ 2192	⁸⁴ 395	²⁰⁶ 0.0063	¹⁹³ 0.0032	¹⁸⁹ 0.0026	¹⁸⁶ 0.0023	¹⁷⁷ 0.0018	¹⁹⁶ 1.033
93	GORILLA-005	³³⁵ 6288	¹¹⁹ 483	¹⁶⁰ 0.0032	¹³⁹ 0.0019	¹³⁷ 0.0017	¹²⁵ 0.0015	¹⁰² 0.0013	¹⁴⁷ 1.018
94	GORILLA-006	³³⁸ 8336	²²⁶ 768	⁸⁷ 0.0017	⁶⁵ 0.0013	⁶⁵ 0.0012	⁶² 0.0012	⁶² 0.0011	⁷⁴ 1.012
95	GORILLA-007	³³⁶ 6290	¹²² 527	⁸³ 0.0017	⁶⁰ 0.0012	⁵⁷ 0.0012	⁵¹ 0.0011	⁵⁵ 0.0011	⁶⁵ 1.012
96	GORILLA-008	³²⁹ 4242	³¹¹ 940	⁶⁷ 0.0015	⁵² 0.0012	⁵¹ 0.0011	⁴⁹ 0.0011	⁵³ 0.0011	⁵³ 1.011
97	GRIAULE-000	²⁵⁷ 2052	⁹⁶ 419	¹⁴³ 0.0025	¹⁴⁸ 0.0020	¹⁵⁰ 0.0019	¹⁵⁸ 0.0018	¹⁵⁵ 0.0017	¹⁴⁶ 1.018
98	GRIAULE-001	²⁶⁰ 2052	³³⁷ 1103	³⁶ 0.0012	³⁸ 0.0011	⁴² 0.0011	⁴³ 0.0010	⁵⁰ 0.0010	³⁹ 1.010
99	HIK-003	¹²⁰ 1408	¹⁵³ 633	²⁵¹ 0.0117	²³¹ 0.0060	²³¹ 0.0048	²³¹ 0.0039	²¹⁹ 0.0030	²³⁴ 1.061
100	HIK-004	¹¹³ 1152	¹²⁴ 510	²⁴⁸ 0.0113	²³¹ 0.0059	²³⁰ 0.0047	²²⁴ 0.0037	²¹⁶ 0.0030	²³³ 1.060
101	HIK-005	¹¹⁹ 1408	¹⁵² 619	¹⁸⁶ 0.0046	¹⁷⁷ 0.0025	¹⁶³ 0.0020	¹⁴⁶ 0.0017	¹³⁸ 0.0015	¹⁷⁷ 1.025
102	HIK-006	¹²¹ 1408	¹⁴⁸ 610	¹⁸⁷ 0.0046	¹⁷⁶ 0.0025	¹⁶⁷ 0.0020	¹⁴⁵ 0.0017	¹³⁹ 0.0015	¹⁷⁷ 1.025
103	HYPERVERGE-001	⁸⁶ 1024	²⁶³ 846	⁵⁴ 0.0014	⁷² 0.0013	⁸⁰ 0.0013	⁸⁹ 0.0013	¹⁰² 0.0013	⁶⁹ 1.012
104	HYPERVERGE-002	⁸⁰ 1024	³⁰² 935	⁵¹ 0.0014	⁷¹ 0.0013	⁷⁸ 0.0013	⁸⁸ 0.0013	⁹⁶ 0.0013	⁶⁵ 1.012
105	HZAILU-000	⁸⁸ 1024	¹⁶² 650	¹²⁴ 0.0022	¹¹² 0.0016	¹²² 0.0015	¹²³ 0.0015	¹³³ 0.0014	¹¹⁷ 1.015
106	HZAILU-001	²¹⁴ 2048	²³² 778	¹¹⁸ 0.0020	¹²⁶ 0.0017	¹³¹ 0.0016	¹³⁹ 0.0016	¹⁴¹ 0.0015	¹²² 1.016
107	HZAILU-002	²³³ 2048	²⁶⁴ 847	¹¹¹ 0.0020	¹²⁵ 0.0017	¹²⁹ 0.0016	¹³⁶ 0.0016	¹⁴⁴ 0.0015	¹²² 1.016
108	IDEMIA-003	⁶¹ 528	¹⁸² 689	²¹³ 0.0069	²¹⁶ 0.0045	²¹⁸ 0.0039	²¹⁶ 0.0034	²¹⁵ 0.0027	²¹³ 1.043
109	IDEMIA-004	⁶² 528	¹⁷³ 669	²⁰⁸ 0.0066	²⁰⁵ 0.0038	¹⁹⁸ 0.0032	¹⁹⁸ 0.0027	¹⁸⁷ 0.0021	²⁰³ 1.038
110	IDEMIA-005	³⁷ 352	⁷⁷ 374	²²³ 0.0081	²¹⁵ 0.0044	²¹⁰ 0.0036	²¹⁰ 0.0032	²¹⁰ 0.0030	²¹⁶ 1.044
111	IDEMIA-006	³⁸ 352	⁷⁶ 373	²³⁷ 0.0096	²²⁴ 0.0052	²²⁴ 0.0042	²³⁰ 0.0039	²³³ 0.0037	²²⁴ 1.052
112	IDEMIA-007	⁷⁷ 860	²⁴¹ 807	¹⁴⁴ 0.0026	¹¹⁵ 0.0016	¹⁰⁵ 0.0014	⁸⁷ 0.0013	⁷⁰ 0.0012	¹²⁰ 1.015
113	IDEMIA-008	³⁶ 300	¹⁰⁵ 451	²⁰ 0.0011	¹⁶ 0.0009	²¹ 0.0009	²⁵ 0.0009	²⁴ 0.0009	¹⁶ 1.009
114	IDEMIA-009	⁷⁵ 636	²⁷⁸ 874	⁹ 0.0010	⁹ 0.0009	¹² 0.0009	¹⁵ 0.0009	¹⁵ 0.0009	⁹ 1.008
115	IDEMIA-010	³⁶ 300	³¹⁷ 957	⁹ 0.0009	⁷ 0.0009	¹¹ 0.0009	¹³ 0.0009	¹⁴ 0.0009	⁷ 1.008
116	IMAGUS-002	⁴⁸ 512	⁷ 76	³²¹ 0.2203	³¹⁹ 0.1342	³¹⁸ 0.1090	³¹⁷ 0.0871	³¹⁹ 0.0632	³²⁰ 2.308
117	IMAGUS-003	³⁶ 512	⁵⁷ 37	³²⁷ 0.3559	³²⁶ 0.2491	³²⁶ 0.2132	³²⁶ 0.1791	³²² 0.1397	³²² 3.363
118	IMAGUS-005	²⁰⁵ 2048	²³⁶ 788	¹⁰⁶ 0.0019	¹¹⁶ 0.0016	¹¹¹ 0.0014	¹¹² 0.0013	¹¹¹ 0.0013	¹¹¹ 1.015
119	IMAGUS-006	¹⁹⁶ 2048	²⁹⁴ 905	¹¹³ 0.0020	¹²¹ 0.0016	¹²⁴ 0.0015	¹²⁴ 0.0015	¹³³ 0.0014	¹¹⁵ 1.015
120	IMAGUS-007	²²¹ 2048	¹⁴⁵ 590	¹¹⁶ 0.0020	¹⁰³ 0.0015	¹⁰³ 0.0014	⁹² 0.0013	⁹⁵ 0.0013	¹⁰¹ 1.014
121	IMAGUS-008	¹⁴² 2048	¹⁰⁰ 432	³⁰⁹ 0.0860	³¹⁰ 0.0701	³¹² 0.0646	³¹² 0.0590	³¹² 0.0518	³¹⁰ 1.648
122	IMPERIAL-000	¹⁷⁴ 2048	¹⁶⁸ 654	¹⁴² 0.0024	¹⁴¹ 0.0019	¹⁴⁶ 0.0018	¹⁵⁶ 0.0018	¹⁵⁹ 0.0017	¹⁴¹ 1.018
123	INCODE-000	⁸⁷ 1024	²⁵ 190	²⁹⁷ 0.0489	²⁹² 0.0261	²⁹³ 0.0204	²⁹¹ 0.0160	²⁸⁸ 0.0117	²⁹² 1.262
124	INCODE-001	²²⁶ 2048	¹⁸⁴ 690	²⁶⁴ 0.0166	²⁵³ 0.0084	²⁴⁸ 0.0067	²⁴⁵ 0.0055	²⁴⁷ 0.0043	²⁵⁹ 1.086
125	INCODE-002	²²⁹ 2048	⁵³ 291	²⁶⁸ 0.0178	²⁵⁰ 0.0090	²⁵⁰ 0.0070	²⁴⁶ 0.0056	²⁴⁷ 0.0043	²⁶¹ 1.092
126	INCODE-003	¹⁴⁸ 2048	¹⁹⁶ 704	²⁵⁶ 0.0129	²³⁷ 0.0064	²³⁹ 0.0051	²³² 0.0040	²²⁷ 0.0031	²⁴² 1.066
127	INCODE-004	¹⁶¹ 2048	¹²³ 508	¹⁶⁷ 0.0035	¹⁷⁰ 0.0024	¹⁷² 0.0021	¹⁷⁴ 0.0020	¹⁷⁵ 0.0019	¹⁶⁹ 1.023
128	INCODE-005	¹⁷⁶ 2048	¹²² 500	⁸⁰ 0.0017	⁸⁶ 0.0014	⁹⁵ 0.0014	⁹⁰ 0.0013	⁹³ 0.0013	⁸⁶ 1.013
129	INNOVATRICS-002	⁶⁶ 530	⁴⁴ 255	²⁹⁵ 0.0451	²⁹⁸ 0.0342	³⁰¹ 0.0322	³⁰² 0.0308	³⁰⁴ 0.0297	²⁹⁹ 1.321
130	INNOVATRICS-003	⁶⁵ 530	⁴³ 255	²⁸¹ 0.0263	²⁷² 0.0126	²⁶⁷ 0.0095	²⁶¹ 0.0074	²⁵⁸ 0.0053	²⁷⁵ 1.129
131	INNOVATRICS-004	¹⁰⁸ 1076	⁴⁰⁶	²⁸⁵ 0.0123	²³⁶ 0.0063	²³³ 0.0050	²³³ 0.0040	²²⁷ 0.0032	²⁴¹ 1.064
132	INNOVATRICS-005	⁶⁷ 538	²⁶⁰ 842	¹⁴⁰ 0.0024	¹³³ 0.0018	¹³³ 0.0017	¹³⁵ 0.0016	¹³² 0.0014	¹³⁵ 1.017
133	INNOVATRICS-007	⁶⁸ 538	²³⁵ 785	⁸⁴ 0.0017	⁹² 0.0014	⁸⁷ 0.0013	⁸² 0.0013	⁸⁹ 0.0012	⁸⁹ 1.013
134	INNOVATRICS-008	³²⁵ 4136	³³¹ 982	⁴⁵ 0.0013	⁴⁶ 0.0011	⁴⁸ 0.0011	⁵² 0.0011	⁵⁷ 0.0011	⁴⁷ 1.010
135	INTELLIGENSIA-000	¹⁵² 2048	¹⁴³ 576	¹¹⁵ 0.0020	⁹⁸ 0.0015	⁹⁶ 0.0013	⁸⁹ 0.0013	⁷⁶ 0.0012	⁹⁹ 1.014
136	INTELLIVISION-001	²⁶³ 2056	⁹⁹ 417	²⁸⁸ 0.0365	²⁹⁰ 0.0199	²⁸⁶ 0.0160	²⁸⁵ 0.0126	²⁸⁸ 0.0095	²⁸⁸ 1.199
137	INTELLIVISION-002	²⁷⁰ 2056	⁶³ 333	²⁴⁴ 0.0107	²²⁹ 0.0055	²²⁵ 0			

MISSES OUTSIDE RANK R		RESOURCE USAGE		ENROL MOST RECENT, N = 1.6M FRVT 2018 MUGSHOTS					
#	ALGORITHM	BYTES	MSEC	R=1	R=5	R=10	R=20	R=50	WORK-10
145	KAKAO-001	¹⁶ 2048	³² 976	⁵⁵ 0.0014	⁷⁹ 0.0013	⁸⁵ 0.0013	⁹⁶ 0.0013	¹⁰⁵ 0.0013	⁷³ 1.012
146	KEDACOM-001	³³ 292	¹³¹ 537	²¹⁹ 0.0077	²⁴⁵ 0.0074	²⁵¹ 0.0073	²⁵⁸ 0.0072	²⁶⁷ 0.0072	²⁴³ 1.067
147	KNERON-000	²⁰ 2048	¹² 530	²⁰² 0.0059	²³⁹ 0.0059	²³⁹ 0.0059	²⁴⁹ 0.0059	²⁵⁹ 0.0059	²²⁶ 1.053
148	KNERON-001	²² 2048	¹¹ 468	²⁸⁴ 0.0295	²⁹⁹ 0.0295	²⁹⁹ 0.0295	³⁰¹ 0.0295	³⁰³ 0.0295	²⁹³ 1.266
149	LINE-000	¹⁴ 2048	¹¹⁸ 482	¹²⁷ 0.0022	¹⁰² 0.0015	⁹⁹ 0.0014	⁷⁹ 0.0013	²⁴ 0.0012	¹⁰⁸ 1.015
150	LINE-001	¹⁵ 2048	²⁹ 910	²⁶ 0.0011	³¹ 0.0010	³³ 0.0010	²⁹ 0.0009	³¹ 0.0009	²⁹ 1.009
151	LINECLOVA-002	²³ 2048	²⁴ 825	⁴⁷ 0.0013	⁵⁹ 0.0012	⁶¹ 0.0012	⁷¹ 0.0012	²⁹ 0.0012	⁵⁶ 1.011
152	LINECLOVA-003	¹⁷ 2048	²³ 801	¹¹ 0.0010	⁸ 0.0009	¹⁰ 0.0008	¹² 0.0008	¹⁰ 0.0008	⁸ 1.008
153	LOOKMAN-003	³⁴ 292	⁶⁸ 342	²²⁸ 0.0088	²⁴⁹ 0.0078	²⁵⁹ 0.0076	²⁶¹ 0.0075	²⁷⁰ 0.0074	²⁴⁶ 1.071
154	LOOKMAN-004	⁷¹ 548	⁶ 325	²³⁰ 0.0091	²⁵⁹ 0.0079	²⁵⁶ 0.0076	²⁶² 0.0075	²⁶⁷ 0.0073	²⁴⁷ 1.072
155	LOOKMAN-005	⁷⁰ 548	¹² 514	²²² 0.0080	²⁴⁷ 0.0075	²⁵⁴ 0.0074	²⁶⁰ 0.0073	²⁶⁸ 0.0072	²⁴⁴ 1.068
156	MANTRA-000	²⁵ 2052	⁹ 412	⁸⁶ 0.0017	⁸¹ 0.0013	⁸¹ 0.0013	⁷⁸ 0.0012	⁸⁴ 0.0012	⁸¹ 1.013
157	MAXVISION-000	¹⁷ 2048	²¹ 184	¹³⁹ 0.0024	¹²⁷ 0.0017	¹²⁵ 0.0016	¹²⁹ 0.0015	¹²¹ 0.0014	¹³² 1.016
158	MAXVISION-001	²¹ 2048	¹⁰ 458	³⁸ 0.0012	⁴⁸ 0.0011	⁵² 0.0011	⁵⁶ 0.0011	⁶⁰ 0.0011	⁴⁵ 1.010
159	MEGVII-001	³⁰ 4096	¹⁶ 652	²⁵² 0.0118	²⁶⁰ 0.0093	²⁶⁰ 0.0087	²⁷⁰ 0.0084	²⁷⁶ 0.0080	²⁵⁶ 1.086
160	MEGVII-002	³¹ 4096	¹⁶ 656	²⁵³ 0.0118	²⁶¹ 0.0093	²⁶² 0.0088	²⁶⁹ 0.0084	²⁷⁷ 0.0080	²⁵⁷ 1.087
161	MICROFOCUS-003	²¹ 256	⁴⁹ 269	³³⁵ 0.5942	³³³ 0.4692	³³³ 0.4204	³³³ 0.3724	³³³ 0.3095	³³³ 5.361
162	MICROFOCUS-004	¹⁷ 256	⁵ 270	³³² 0.5763	³³⁸ 0.4519	³³² 0.4026	³³² 0.3560	³³⁸ 0.2957	³³² 5.199
163	MICROFOCUS-005	²³ 256	⁴⁸ 266	³²⁸ 0.4242	³²⁸ 0.3028	³²⁷ 0.2606	³²² 0.2209	³²⁸ 0.1724	³²⁸ 3.861
164	MICROFOCUS-006	²⁵ 256	⁴⁷ 265	³²⁹ 0.4268	³²⁹ 0.3049	³²⁸ 0.2623	³²⁹ 0.2233	³²⁹ 0.1746	³²⁹ 3.880
165	MICROSOFT-003	⁸ 1024	⁸ 404	⁷⁷ 0.0016	²⁹ 0.0010	¹³ 0.0009	³ 0.0008	¹ 0.0006	³³ 1.009
166	MICROSOFT-004	²³ 2048	²³ 773	⁶⁸ 0.0015	¹⁸ 0.0009	¹ 0.0008	¹ 0.0007	¹ 0.0006	³⁰ 1.009
167	MICROSOFT-005	⁸ 1024	¹⁷ 673	¹⁰² 0.0019	¹⁹ 0.0010	⁹ 0.0008	² 0.0008	³ 0.0006	⁴⁰ 1.010
168	MICROSOFT-006	⁸ 1024	¹⁸ 695	¹¹⁰ 0.0020	⁴⁸ 0.0011	²⁹ 0.0010	⁵ 0.0008	⁴ 0.0007	⁵⁷ 1.011
169	MUKH-002	¹⁷ 2048	³³ 1283	²⁸⁰ 0.0258	²⁷⁷ 0.0139	²⁷⁶ 0.0112	²⁷³ 0.0090	²⁶⁷ 0.0070	²⁷⁹ 1.140
170	NEC-000	²⁹ 2592	⁸ 82	²⁶⁵ 0.0170	²⁵⁸ 0.0086	²⁴⁵ 0.0066	²⁴² 0.0052	²³⁷ 0.0038	²⁵⁸ 1.087
171	NEC-001	²⁹ 2592	⁹ 88	²⁷⁴ 0.0209	²⁷⁷ 0.0141	²⁸⁰ 0.0128	²⁸³ 0.0119	²⁸⁰ 0.0113	²⁷⁷ 1.135
172	NEC-002	¹³ 1616	¹⁶ 553	¹⁸ 0.0010	¹¹ 0.0009	⁸ 0.0008	⁶ 0.0008	⁵ 0.0008	¹⁰ 1.008
173	NEC-003	¹³ 1712	¹⁸ 690	⁵³ 0.0014	⁶⁹ 0.0012	⁶⁷ 0.0012	⁷⁵ 0.0012	⁷⁷ 0.0012	⁵⁹ 1.011
174	NEC-004	¹⁰ 1104	³² 967	⁶⁰ 0.0014	⁸⁹ 0.0013	⁹¹ 0.0013	⁹³ 0.0013	¹⁰¹ 0.0013	⁸⁰ 1.012
175	NEC-005	¹¹ 1104	³² 964	³³ 0.0012	⁴⁵ 0.0011	⁴⁹ 0.0011	⁵⁴ 0.0011	⁵⁸ 0.0011	⁴⁴ 1.010
176	NEC-006	¹¹ 1104	³⁰ 940	⁴² 0.0013	⁵⁸ 0.0012	⁶² 0.0012	⁶⁴ 0.0012	⁶⁸ 0.0011	⁵⁴ 1.011
177	NEC-007	⁷ 560	³³ 992	¹⁷⁰ 0.0037	¹⁹⁷ 0.0036	²⁰⁹ 0.0036	²²⁰ 0.0036	²³³ 0.0036	¹⁹⁵ 1.033
178	NEUROTECHNOLOGY-003	¹⁸ 2048	¹³ 547	²⁷⁵ 0.0225	²⁷⁷ 0.0126	²⁷⁰ 0.0100	²⁶⁷ 0.0078	²⁵⁵ 0.0057	²⁷⁴ 1.125
179	NEUROTECHNOLOGY-004	¹⁸ 2048	¹³ 543	¹⁹⁷ 0.0056	¹⁹⁸ 0.0036	²⁰¹ 0.0032	²⁰³ 0.0029	²⁰² 0.0025	¹⁹⁹ 1.035
180	NEUROTECHNOLOGY-005	²⁴ 256	⁹ 412	¹⁸¹ 0.0043	¹⁸⁰ 0.0029	¹⁹⁰ 0.0027	¹⁹¹ 0.0024	¹⁹⁶ 0.0023	¹⁸⁷ 1.028
181	NEUROTECHNOLOGY-006	²⁰ 256	²² 746	²⁶⁹ 0.0180	²⁵¹ 0.0079	²³⁸ 0.0059	²³⁸ 0.0046	²²⁷ 0.0033	²⁵³ 1.083
182	NEUROTECHNOLOGY-007	¹⁶ 256	¹⁸ 169	¹⁷³ 0.0039	¹⁸⁷ 0.0027	¹⁸⁶ 0.0025	¹⁸⁷ 0.0023	¹⁸⁷ 0.0022	¹⁷⁹ 1.026
183	NEUROTECHNOLOGY-008	⁵⁹ 514	²⁴⁰ 804	¹²² 0.0022	¹⁰⁸ 0.0015	¹⁰⁹ 0.0014	¹¹⁰ 0.0014	¹¹¹ 0.0013	¹⁰⁷ 1.015
184	NEUROTECHNOLOGY-009	⁵⁷ 513	¹⁸⁰ 686	⁶¹ 0.0014	⁵⁷ 0.0012	⁶⁰ 0.0012	⁶⁰ 0.0011	⁶⁴ 0.0011	⁵⁸ 1.011
185	NEUROTECHNOLOGY-010	¹⁵ 256	¹⁷ 663	⁴⁰ 0.0012	³⁶ 0.0011	³⁸ 0.0010	³⁹ 0.0010	⁴⁰ 0.0010	³⁸ 1.010
186	NEUROTECHNOLOGY-012	¹⁹ 256	²⁰ 711	¹⁵⁰ 0.0010	²⁶ 0.0010	²⁷ 0.0010	³¹ 0.0009	³⁴ 0.0009	²⁰ 1.009
187	NEUROTECHNOLOGY-013	¹⁸ 256	³³ 980	¹⁶ 0.0010	²⁸ 0.0010	²⁸ 0.0010	³³ 0.0010	³⁶ 0.0010	¹⁹ 1.009
188	NEWLAND-002	¹⁹ 2048	²⁷ 868	³⁰⁶ 0.0786	³⁰⁶ 0.0480	³⁰⁵ 0.0397	³⁰⁵ 0.0332	³⁰² 0.0263	³⁰⁷ 1.468
189	NOBLIS-001	¹⁷ 2048	²¹ 211	³²⁴ 0.2492	³² 0.1772	³²⁵ 0.1542	³²³ 0.1339	³² 0.1112	³²³ 2.679
190	NOBLIS-002	³³ 6144	¹³⁰ 535	³¹⁹ 0.1794	³¹⁶ 0.1108	³¹⁶ 0.0903	³¹⁵ 0.0722	³¹⁴ 0.0535	³¹⁶ 2.077
191	NOTIONTAG-000	²⁸ 2120	¹¹ 461	¹⁴¹ 0.0024	¹⁶⁰ 0.0021	¹⁶⁶ 0.0021	¹⁷⁷ 0.0020	¹⁸ 0.0019	¹⁵⁵ 1.019
192	NTECHLAB-003	³⁰ 3484	²⁵ 831	²⁰³ 0.0062	¹⁸⁹ 0.0029	¹⁸² 0.0023	¹⁷² 0.0019	¹⁵² 0.0016	¹⁹² 1.030
193	NTECHLAB-004	²⁹ 3484	³⁰ 929	¹⁹⁰ 0.0048	¹⁶⁷ 0.0023	¹⁸⁵ 0.0019	¹⁴¹ 0.0016	¹¹⁷ 0.0013	¹⁰² 1.024
194	NTECHLAB-005	¹³ 1940	²⁰ 717	¹⁸⁸ 0.0047	¹⁶⁶ 0.0022	¹⁸² 0.0017	⁹⁹ 0.0013	⁸⁴ 0.0011	¹⁷⁰ 1.023
195	NTECHLAB-006	¹³ 1940	²⁵ 841	¹⁷⁸ 0.0041	¹⁴⁹ 0.0019	¹¹⁵ 0.0015	⁷⁰ 0.0012	²⁹ 0.0009	¹⁵⁷ 1.019
196	NTECHLAB-007	²⁹ 3348	²⁵ 834	¹⁴⁶ 0.0027	¹²⁴ 0.0017	¹⁰⁷ 0.0014	¹⁰³ 0.0013	⁸⁴ 0.0012	¹²⁸ 1.016
197	NTECHLAB-008	¹¹⁷ 1300	¹³⁹ 562	⁸⁵ 0.0017	⁵⁶ 0.0012	⁵⁶ 0.0012	⁵³ 0.0011	⁴⁹ 0.0010	⁶⁴ 1.012
198	NTECHLAB-009	¹¹⁸ 1300	²⁹ 900	⁴³ 0.0013	⁴⁸ 0.0011	³⁹ 0.0010	³⁶ 0.0010	³⁵ 0.0009	⁴² 1.010
199	NTECHLAB-010	¹¹⁵ 1280	²⁷ 875	²⁵ 0.0011	³⁴ 0.0010	³⁶ 0.0010	³⁸ 0.0010	⁴⁵ 0.0010	³² 1.009
200	NTECHLAB-011	¹¹⁶ 1280	²⁷ 865	¹⁷ 0.0010	¹⁵ 0.0009	¹⁸ 0.0009	²⁰ 0.0009	²⁷ 0.0009	¹⁵ 1.008
201	PANGIAM-000	²³ 2048	¹⁵ 637	³⁴ 0.0012	⁴² 0.0011	⁴⁴ 0.0011	⁴² 0.0010	⁴⁸ 0.0010	⁴¹ 1.010
202	PANGIAM-001	²⁴ 2048	³² 968	²¹⁴ 0.0069	²⁴⁹ 0.0068	²⁴⁸ 0.0068	²⁵⁴ 0.0068	²⁶⁷ 0.0068	²³⁵ 1.061
203	PARAVISION-000	¹⁵ 2048	¹⁰⁴ 438	²⁷⁰ 0.0188	²⁸⁹ 0.0171	²⁹⁰ 0.0167	²⁹¹ 0.0165	²⁹⁸ 0.0164	²⁸¹ 1.156
204	PARAVISION-001	²⁰ 2048	¹⁴⁶ 590	¹⁷¹ 0.0038	¹⁷³ 0.0024	¹⁷³ 0.0022	¹⁷⁸ 0.0020	¹⁷⁵ 0.0019	¹⁷³ 1.023
205	PARAVISION-002	¹⁶ 2048	⁷⁸ 577	¹⁷⁶ 0.0040	¹⁷⁸ 0.0025	¹⁷⁸ 0.0022	¹⁸¹ 0.0021	¹⁷⁷ 0.0019	¹⁷⁶ 1.025
206	PARAVISION-003	²² 2048	²¹³ 735	¹⁵⁹ 0.0031	¹⁶¹ 0.0022	¹⁶⁵ 0.0020	¹⁶⁸ 0.0019	¹⁶⁴ 0.0017	¹⁶¹ 1.021
207	PARAVISION-004	³⁰ 4096	²¹ 720	⁷⁸ 0.0016	⁸⁹ 0.0014	⁹⁴ 0.0013	¹⁰¹ 0.0013	⁸⁸ 0.0013	¹⁰³ 1.013
208	PARAVISION-005	³⁰ 4096	²⁶⁹ 858	⁷¹ 0.0015	⁸⁷ 0.0014	⁹² 0.0013	¹⁰² 0.0013	¹¹² 0.0013	⁸³ 1.013
209	PARAVISION-007	³⁰ 4096	¹⁹⁸ 706	³¹ 0.0012	⁴¹ 0.0011	⁴⁰ 0.0010	⁴¹ 0.0010	³⁷ 0.0010</	

MISSES OUTSIDE RANK R		RESOURCE USAGE		ENROL MOST RECENT, N = 1.6M					
#	ALGORITHM	BYTES	MSEC	R=1	R=5	R=10	R=20	R=50	WORK-10
217	QNAP-000	¹⁸ 2048	¹⁰ 457	²² 0.0078	²¹ 0.0044	²³ 0.0037	²¹ 0.0033	²¹ 0.0028	²¹ 0.0043
218	QNAP-001	²³ 2048	¹⁴ 615	¹⁷ 0.0041	¹⁸ 0.0029	¹⁹ 0.0027	¹⁹ 0.0025	¹⁹ 0.0023	¹⁸ 0.028
219	QNAP-002	²³ 2048	²⁴ 825	¹⁹ 0.0049	²¹ 0.0044	²² 0.0043	²³ 0.0043	²⁴ 0.0042	²¹ 0.040
220	QNAP-003	¹⁶ 2048	⁸³ 387	¹⁵ 0.0028	¹⁵ 0.0021	¹⁵ 0.0019	¹⁴ 0.0017	¹⁵ 0.0015	¹⁵ 0.019
221	QUANTASOFT-001	²² 2048	⁸⁷ 396	³² 0.2177	³² 0.1643	³² 0.1468	³² 0.1312	³² 0.1116	³² 0.239
222	RANKONE-002	⁹ 133	¹² 113	²⁷ 0.0194	²⁶ 0.0112	²⁶ 0.0093	²⁶ 0.0077	²⁸ 0.0060	²⁶ 0.111
223	RANKONE-003	¹¹ 133	¹³ 114	²⁷ 0.0194	²⁶ 0.0112	²⁶ 0.0093	²⁶ 0.0077	²⁹ 0.0060	²⁶ 0.111
224	RANKONE-004	¹ 85	⁴ 36	²⁹ 0.0415	²⁹ 0.0226	²⁹ 0.0177	²⁸ 0.0141	²⁸ 0.0102	²⁹ 0.125
225	RANKONE-005	¹⁰ 133	¹⁰ 94	²⁴ 0.0094	²² 0.0054	²² 0.0046	²² 0.0039	²² 0.0032	²² 0.054
226	RANKONE-006	¹³ 165	⁴² 261	¹⁹ 0.0050	¹⁹ 0.0030	¹⁹ 0.0027	¹⁸ 0.0024	¹⁸ 0.0021	¹⁹ 0.030
227	RANKONE-007	¹² 165	⁵² 278	¹⁶ 0.0034	¹⁶ 0.0023	¹⁶ 0.0021	¹⁶ 0.0018	¹⁵ 0.0017	¹⁶ 0.022
228	RANKONE-009	²⁶ 260	²⁷ 191	¹³ 0.0024	¹² 0.0016	¹² 0.0015	¹² 0.0015	¹² 0.0014	¹² 0.105
229	RANKONE-010	²⁷ 261	³⁰ 200	¹² 0.0022	¹³ 0.0018	¹³ 0.0016	¹³ 0.0015	¹³ 0.0015	¹³ 0.106
230	RANKONE-011	³⁰ 261	¹⁴ 567	⁶⁹ 0.0015	⁶⁷ 0.0012	⁶⁶ 0.0012	⁶⁸ 0.0012	⁷⁰ 0.0012	⁶³ 0.101
231	RANKONE-012	²⁸ 261	¹⁴⁰ 563	⁵² 0.0014	⁵³ 0.0012	⁵⁵ 0.0011	⁵⁹ 0.0011	⁶⁷ 0.0011	⁵¹ 0.101
232	RANKONE-013	²⁹ 261	¹⁷ 680	¹⁹ 0.0011	¹⁸ 0.0009	¹⁸ 0.0009	¹⁸ 0.0009	¹⁹ 0.0009	¹⁴ 0.008
233	RANKONE-014	³¹ 261	¹⁹³ 702	¹⁰ 0.0010	¹² 0.0009	¹⁵ 0.0009	¹⁷ 0.0009	²¹ 0.0009	¹² 0.008
234	REALNETWORKS-000	³¹⁸ 4100	³⁹ 244	²⁹ 0.0402	²⁸ 0.0195	²⁸ 0.0149	²⁸ 0.0111	²⁷ 0.0077	²⁹ 0.120
235	REALNETWORKS-001	³² 4104	³⁸ 243	²⁹ 0.0402	²⁸ 0.0195	²⁸ 0.0149	²⁸ 0.0111	²⁷ 0.0077	²⁸ 0.120
236	REALNETWORKS-002	³² 4104	⁴⁰ 245	²⁸ 0.0393	²⁸ 0.0189	²⁸ 0.0142	²⁷ 0.0108	²⁷ 0.0076	²⁸ 0.195
237	REALNETWORKS-003	¹³⁸ 1848	²⁸ 178	²⁸ 0.0242	²⁷ 0.0117	²⁶ 0.0090	²⁵ 0.0070	²⁵ 0.0054	²⁷ 1.120
238	REALNETWORKS-004	¹³⁴ 1848	²³ 185	²⁶ 0.0236	²⁶ 0.0112	²⁶ 0.0087	²⁵ 0.0068	²⁸ 0.0050	²⁶ 0.116
239	REALNETWORKS-005	²⁶ 2056	⁶³ 337	¹³¹ 0.0023	¹¹¹ 0.0016	¹⁰¹ 0.0014	¹⁰⁶ 0.0013	⁸ 0.0012	¹¹³ 0.105
240	REALNETWORKS-006	²⁶ 2056	⁷¹ 350	⁵⁷ 0.0014	⁵³ 0.0012	⁵³ 0.0011	⁴⁷ 0.0011	⁴² 0.0010	⁵² 0.101
241	REALNETWORKS-007	²⁷ 2056	¹⁶ 645	⁴⁸ 0.0013	⁵⁰ 0.0012	⁴⁶ 0.0011	⁴⁵ 0.0011	⁵ 0.0010	⁴⁹ 0.101
242	REALNETWORKS-008	²⁷ 2056	³² 977	³⁰ 0.0011	²⁹ 0.0010	²⁴ 0.0009	²⁷ 0.0009	¹⁸ 0.0009	²² 0.009
243	RECOGNITO-000	¹¹ 1280	³⁰¹ 925	¹⁶⁹ 0.0036	¹⁹⁶ 0.0035	²⁰⁴ 0.0035	²¹⁹ 0.0035	²¹ 0.0035	¹⁹⁴ 0.032
244	REMARKAI-000	²¹ 2048	¹⁸ 691	¹⁶⁵ 0.0034	¹⁵⁹ 0.0021	¹⁵¹ 0.0019	¹⁴⁴ 0.0017	¹⁴⁹ 0.0015	¹⁶⁰ 0.102
245	REMARKAI-000	²² 2048	¹⁵⁰ 615	²²⁷ 0.0086	²¹⁵ 0.0044	²⁰⁶ 0.0036	²⁰⁶ 0.0031	²⁰³ 0.0025	²¹⁷ 0.045
246	REMARKAI-002	¹⁸ 2048	¹⁰ 434	²²⁵ 0.0081	²⁰⁷ 0.0040	¹⁹⁷ 0.0031	¹⁹⁴ 0.0026	¹⁸⁴ 0.0021	²¹¹ 0.041
247	RENDIP-000	¹⁴⁵ 2048	²⁸⁹ 894	⁷³ 0.0015	⁷³ 0.0013	⁷⁰ 0.0012	⁷⁴ 0.0012	⁸⁰ 0.0012	⁷⁶ 0.102
248	REVEALMEDIA-000	²⁵ 2052	⁸¹ 385	¹⁰⁰ 0.0019	⁷⁹ 0.0013	⁸⁴ 0.0013	⁸³ 0.0013	⁸ 0.0012	⁸⁷ 0.103
249	S1-000	³¹³ 4096	²⁷² 865	¹³⁷ 0.0024	¹²⁸ 0.0018	¹³² 0.0017	¹³⁷ 0.0016	¹⁴² 0.0015	¹³⁴ 0.107
250	S1-001	¹⁹ 2048	²⁴ 814	¹⁵⁸ 0.0031	¹⁷⁵ 0.0025	¹⁸⁵ 0.0024	¹⁸⁹ 0.0024	¹⁹ 0.0023	¹⁷¹ 0.103
251	S1-002	¹⁵⁶ 2048	³²¹ 960	⁵⁹ 0.0014	⁸⁰ 0.0013	⁸⁶ 0.0013	⁹⁸ 0.0013	¹¹³ 0.0013	⁷⁸ 0.102
252	S1-003	¹⁶ 2048	³² 979	⁶⁴ 0.0015	⁷⁷ 0.0013	⁷⁹ 0.0013	⁸⁵ 0.0013	⁹ 0.0013	⁷⁷ 0.102
253	S1-004	¹⁸⁵ 2048	³¹⁸ 957	⁴⁹ 0.0013	⁷⁰ 0.0013	⁷⁵ 0.0013	⁸⁶ 0.0013	⁹² 0.0013	⁶⁷ 0.102
254	SCANOVATE-000	¹³⁸ 2048	⁷¹² 712	¹⁹² 0.0050	¹⁸⁰ 0.0026	¹⁷⁵ 0.0022	¹⁶² 0.0018	¹⁴⁷ 0.0015	¹⁸² 0.106
255	SCANOVATE-001	²⁰ 2048	¹⁷⁶ 675	¹⁹⁶ 0.0053	¹⁸⁷ 0.0027	¹⁷⁹ 0.0022	¹⁶³ 0.0018	¹⁴⁶ 0.0015	¹⁸⁶ 0.108
256	SENSETIME-000	³² 4104	²⁰⁷ 715	¹³³ 0.0023	¹⁵⁹ 0.0020	¹⁵⁷ 0.0019	¹⁵⁹ 0.0018	¹⁶² 0.0017	¹⁴⁷ 0.108
257	SENSETIME-001	³² 4104	¹⁷ 656	¹³⁴ 0.0023	¹⁴⁹ 0.0020	¹⁵⁴ 0.0019	¹⁴⁸ 0.0017	¹⁵³ 0.0016	¹⁴⁴ 0.108
258	SENSETIME-002	²⁶ 2056	¹⁶³ 650	²⁵⁹ 0.0137	²⁷⁶ 0.0136	²⁸² 0.0136	²⁸⁶ 0.0136	²⁹² 0.0136	²⁷³ 1.122
259	SENSETIME-003	²⁷ 2056	³⁰ 940	¹³ 0.0010	²⁴ 0.0010	³¹ 0.0010	³⁰ 0.0009	³⁰ 0.0009	¹⁷ 1.009
260	SENSETIME-004	⁹⁶ 1032	²⁰¹ 710	¹² 0.0010	¹⁰ 0.0009	¹⁴ 0.0009	¹⁴ 0.0009	¹³ 0.0009	¹¹ 1.008
261	SENSETIME-005	⁹⁷ 1032	³³⁵ 1007	⁶ 0.0009	⁹ 0.0008	⁵ 0.0008	⁷ 0.0008	⁷ 0.0008	⁵ 1.008
262	SENSETIME-006	⁹⁷ 1032	³¹⁶ 956	⁵ 0.0009	⁷ 0.0008	⁷ 0.0008	¹¹ 0.0008	¹¹ 0.0008	⁶ 1.008
263	SENSETIME-007	¹⁰⁰ 1032	³¹⁹ 958	⁴ 0.0008	⁴ 0.0008	⁶ 0.0008	⁹ 0.0008	¹² 0.0008	⁴ 1.007
264	SENSETIME-008	⁹⁹ 1032	³²² 969	³ 0.0008	³ 0.0008	⁴ 0.0008	⁸ 0.0008	¹⁰ 0.0008	² 1.007
265	SENSETIME-009	⁹⁴ 1032	³³⁶ 1023	² 0.0008	⁵ 0.0008	⁵ 0.0008	¹⁰ 0.0008	⁷ 0.0008	³ 1.007
266	SHAMAN-003	²¹ 2048	¹⁹ 704	³¹¹ 0.1243	³¹¹ 0.0823	³¹⁴ 0.0708	³¹³ 0.0616	³¹ 0.0518	³¹⁴ 1.789
267	SHAMAN-004	²³ 2048	¹⁶⁰ 642	³²² 0.2221	³²¹ 0.1473	³¹⁹ 0.1241	³¹⁹ 0.1049	³¹⁸ 0.0825	³²¹ 2.411
268	SHAMAN-006	¹⁶ 2048	¹⁹ 706	²⁹¹ 0.0398	²⁹⁹ 0.0344	³⁰² 0.0332	³⁰⁴ 0.0323	³⁰ 0.0315	²⁹⁸ 1.316
269	SHAMAN-007	¹⁵³ 2048	²⁰⁰ 709	²⁹⁰ 0.0396	²⁹⁷ 0.0342	³⁰¹ 0.0331	³⁰³ 0.0322	³⁰⁶ 0.0314	²⁹⁶ 1.315
270	SIAT-001	²⁴ 2052	²⁶ 842	⁹⁴ 0.0018	⁷⁷ 0.0014	⁶⁹ 0.0012	⁶⁹ 0.0012	⁸⁴ 0.0011	⁹⁰ 0.103
271	SIAT-002	²⁴ 2052	²⁹⁵ 906	⁹⁶ 0.0018	⁸⁹ 0.0014	⁹³ 0.0013	⁹¹ 0.0013	⁸⁴ 0.0012	⁹³ 0.103
272	SMILART-004	⁵⁰ 512	¹⁶ 167	³³⁶ 0.9648	³³⁶ 0.9641	³³⁶ 0.9640	³³⁶ 0.9639	³³ 0.9638	³³⁶ 9.678
273	SMILART-005	²⁰ 2048	¹¹ 464	³³⁶ 0.9648	³³⁶ 0.9641	³³⁶ 0.9640	³³⁶ 0.9639	³³ 0.9638	³³ 10.000
274	SQISOFT-001	²⁶ 2056	¹⁰⁹ 460	¹⁸⁰ 0.0042	⁹⁶ 0.0014	⁷³ 0.0013	⁶¹ 0.0012	⁵¹ 0.0010	¹²⁹ 0.106
275	SQISOFT-002	²⁷ 2056	¹⁷ 661	⁴⁶ 0.0013	³⁹ 0.0010	³⁵ 0.0010	³⁴ 0.0010	³⁰ 0.0009	³⁵ 0.1010
276	STAQU-000	³¹⁰ 4096	²⁵⁰ 827	²¹⁶ 0.0071	²³⁴ 0.0060	²³⁶ 0.0057	²⁴⁴ 0.0055	²⁴⁹ 0.0053	²³¹ 0.056
277	SYNESIS-003	²¹ 2048	³⁶ 215	²⁶³ 0.0162	²⁸¹ 0.0160	²⁸⁷ 0.0160	²⁹² 0.0160	²⁹ 0.0160	²⁸⁰ 1.144
278	SYNESIS-003	³¹² 4096	¹¹ 103	³¹⁷ 0.1700	³¹⁷ 0.1172	³¹⁷ 0.1047	³¹⁸ 0.0953	³¹⁷ 0.0869	³¹⁷ 2.120
279	SYNESIS-005	³² 4104	²² 772	²²⁶ 0.0085	²⁵⁹ 0.0085	²⁵⁹ 0.0085	²⁷¹ 0.0085	²⁷³ 0.0085	²⁵¹ 1.076
280	T4ISB-000	¹⁴⁰ 2048	²²² 752	²³⁹ 0.0104	²⁶⁵ 0.0103	²⁷³ 0.0103	²⁷¹ 0.0103	²⁸⁴ 0.0103	²⁶⁴ 1.093
281	TECH5-001	¹²² 1536	²⁹ 898	¹⁷⁵ 0.0040	¹⁷⁷ 0.0024	¹⁷¹ 0.0021	¹⁶⁵ 0.0018	¹⁶⁰ 0.0017	¹⁷⁴ 1.024
282	TECH5-002	⁵⁸ 513	³¹² 941	¹⁴⁷ 0.0027	⁹⁴ 0.0014	⁷² 0.0012	⁵⁷ 0.00		

MISSES OUTSIDE RANK R FNIR(N, T=0, R)		RESOURCE USAGE TEMPLATE		ENROL MOST RECENT, N = 1.6M FRVT 2018 MUGSHOTS					
#	ALGORITHM	BYTES	MSEC	R=1	R=5	R=10	R=20	R=50	WORK-10
289	TIGER-002	²⁵⁰ 2052	¹¹² 464	¹⁹⁹ 0.0056	¹⁹⁰ 0.0029	¹⁸⁴ 0.0024	¹⁶⁸ 0.0019	¹⁴⁰ 0.0015	¹⁸⁹ 1.030
290	TIGER-003	²⁵⁶ 2052	¹¹² 464	¹⁹⁸ 0.0056	¹⁹¹ 0.0029	¹⁸³ 0.0024	¹⁶⁷ 0.0019	¹⁴¹ 0.0015	¹⁹⁰ 1.030
291	TONGYITRANS-000	²⁸⁰ 2070	²⁶ 190	²¹¹ 0.0069	²⁰⁵ 0.0038	²⁰² 0.0032	²⁰² 0.0029	²⁰⁶ 0.0026	²⁰⁴ 1.038
292	TONGYITRANS-001	²⁸¹ 2070	²⁴ 189	²¹² 0.0069	²⁰³ 0.0038	²⁰⁰ 0.0032	²⁰¹ 0.0029	²⁰⁸ 0.0026	²⁰⁵ 1.038
293	TOSHIBA-000	¹²⁹ 1548	³⁰ 930	¹⁸⁴ 0.0045	¹⁷⁸ 0.0026	¹⁷⁷ 0.0022	¹⁷⁵ 0.0020	¹⁷³ 0.0018	¹⁸⁰ 1.026
294	TOSHIBA-001	²⁷⁷ 2060	³⁰⁴ 931	¹⁸⁹ 0.0048	¹⁸³ 0.0027	¹⁸⁰ 0.0023	¹⁷⁹ 0.0020	¹⁷² 0.0018	¹⁸⁴ 1.027
295	TRUEFACE-000	¹³⁷ 2000	⁷ 365	¹⁶² 0.0033	¹⁸⁸ 0.0028	¹⁹⁴ 0.0028	¹⁹⁶ 0.0026	²⁰⁰ 0.0026	¹⁸¹ 1.026
296	TURINGTECHVIP-001	¹⁵⁹ 2048	²⁴⁶ 823	²³⁵ 0.0095	²⁶² 0.0093	²⁶⁶ 0.0093	²⁷⁴ 0.0093	²⁵⁹ 0.0093	²⁵⁴ 1.084
297	VD-000	⁹⁰ 1028	⁶⁹ 337	³³¹ 0.4737	³⁵⁸ 0.3204	³²⁹ 0.2695	³²⁸ 0.2215	³² 0.1678	³³⁰ 4.058
298	VD-001	²⁴³ 2052	¹⁸⁹ 695	²⁸³ 0.0276	²⁸⁶ 0.0181	²⁸⁹ 0.0162	²⁸⁸ 0.0146	²⁹¹ 0.0130	²⁸⁶ 1.174
299	VD-002	²⁴⁸ 2052	¹⁸³ 689	²³⁶ 0.0095	²⁴⁸ 0.0077	²⁵² 0.0073	²⁵⁰ 0.0070	²⁶⁵ 0.0068	²⁴⁵ 1.071
300	VD-003	²⁴¹ 2052	¹⁸⁷ 693	²¹⁸ 0.0076	²⁴¹ 0.0069	²⁴⁷ 0.0067	²⁵¹ 0.0066	²⁶² 0.0066	²³⁹ 1.063
301	VERIDAS-001	²⁰³ 2048	²⁸² 885	¹⁵⁰ 0.0028	¹⁴⁹ 0.0019	¹³⁷ 0.0017	¹³⁴ 0.0015	¹³⁷ 0.0015	¹⁴⁵ 1.018
302	VERIDAS-002	¹⁷⁵ 2048	²⁸ 888	¹⁴⁹ 0.0028	¹⁴⁸ 0.0019	¹³⁴ 0.0017	¹³¹ 0.0015	¹³⁶ 0.0015	¹⁴³ 1.018
303	VERIDAS-003	¹⁶⁷ 2048	²⁸⁰ 877	⁹⁵ 0.0018	¹⁰¹ 0.0015	¹⁰³ 0.0014	¹⁰⁵ 0.0013	¹⁰⁶ 0.0013	⁹⁷ 1.014
304	VERIDAS-004	¹⁹⁴ 2048	²⁸⁶ 891	⁵⁰ 0.0014	⁶ 0.0013	⁷¹ 0.0012	⁷⁷ 0.0012	⁸⁸ 0.0012	⁶¹ 1.011
305	VERIJELAS-000	¹⁶⁸ 2048	⁶⁴ 335	³²⁶ 0.3547	³²⁷ 0.2975	³³⁰ 0.2805	³³⁰ 0.2655	³³¹ 0.2489	³²² 3.744
306	VIGILANTSOLUTIONS-003	¹²⁴ 1544	²⁵ 832	³⁰⁴ 0.0694	³⁰ 0.0349	²⁹⁶ 0.0262	²⁹⁹ 0.0201	²⁹³ 0.0140	³⁰¹ 1.355
307	VIGILANTSOLUTIONS-004	¹²³ 1544	²⁵² 830	³¹² 0.1249	³¹¹ 0.0706	³⁰⁹ 0.0557	³⁰⁷ 0.0434	³⁰⁵ 0.0305	³¹¹ 1.699
308	VIGILANTSOLUTIONS-005	¹²⁸ 1544	²³ 778	²³¹ 0.0092	²¹ 0.0045	²⁰⁷ 0.0036	²⁰⁶ 0.0029	¹⁹⁵ 0.0022	²¹⁸ 1.046
309	VIGILANTSOLUTIONS-006	¹²⁵ 1544	²⁵⁶ 834	²³⁸ 0.0099	²¹⁹ 0.0048	²¹⁴ 0.0038	²⁰⁹ 0.0030	¹⁹⁴ 0.0022	²²² 1.049
310	VIGILANTSOLUTIONS-007	¹²⁷ 1544	¹⁵¹ 618	¹⁶⁴ 0.0034	¹⁴⁷ 0.0020	¹³⁶ 0.0017	¹³⁰ 0.0015	¹¹⁰ 0.0013	¹⁵⁴ 1.019
311	VIGILANTSOLUTIONS-008	¹²⁶ 1544	⁸⁹ 405	¹⁵⁶ 0.0029	¹³⁸ 0.0018	¹²⁶ 0.0016	¹²¹ 0.0015	⁹⁹ 0.0013	¹⁴² 1.018
312	VISIONBOX-000	²⁷⁶ 2059	¹¹⁷ 482	¹⁰⁵ 0.0019	¹⁰⁵ 0.0015	¹¹⁰ 0.0014	¹⁰³ 0.0013	⁹⁸ 0.0013	¹⁰² 1.014
313	VISIONLABS-004	¹¹ 256	⁶⁹ 315	¹⁴⁸ 0.0027	¹³⁸ 0.0018	¹²⁸ 0.0016	¹²⁹ 0.0015	¹² 0.0014	¹³⁸ 1.017
314	VISIONLABS-005	⁴⁵ 512	⁵⁹ 300	¹³⁶ 0.0024	¹²³ 0.0017	¹¹⁸ 0.0015	¹¹¹ 0.0014	¹⁰⁴ 0.0013	¹²² 1.016
315	VISIONLABS-006	⁵¹ 512	⁵¹ 292	⁹⁷ 0.0018	⁹⁸ 0.0015	⁹⁶ 0.0014	¹⁰⁸ 0.0013	¹⁰⁰ 0.0013	⁹⁶ 1.014
316	VISIONLABS-007	⁴³ 512	⁵⁵ 293	⁹¹ 0.0018	⁹³ 0.0014	⁸³ 0.0013	⁸¹ 0.0013	⁸⁵ 0.0012	⁹² 1.013
317	VISIONLABS-008	⁵² 512	⁵¹ 277	¹¹⁴ 0.0020	¹³ 0.0018	¹⁴⁵ 0.0018	¹⁵² 0.0018	¹⁶⁵ 0.0017	¹³³ 1.017
318	VISIONLABS-009	⁴⁰ 512	¹²¹ 494	²⁸ 0.0011	³⁷ 0.0011	³⁷ 0.0010	⁴⁰ 0.0010	³⁴ 0.0010	³⁴ 1.010
319	VISIONLABS-010	⁴¹ 512	²¹⁴ 732	⁵⁶ 0.0014	⁷⁰ 0.0013	⁸² 0.0013	⁸⁴ 0.0013	⁹⁴ 0.0013	⁷² 1.012
320	VISIONLABS-011	³⁶ 512	²¹⁶ 736	³⁵ 0.0012	⁴³ 0.0011	⁵⁰ 0.0011	⁵⁰ 0.0011	⁵⁶ 0.0011	⁴³ 1.010
321	VIXVIZION-009	²³⁰ 2048	²⁹⁰ 896	¹²⁹ 0.0023	¹¹⁰ 0.0016	¹⁰⁴ 0.0014	⁹³ 0.0013	⁸² 0.0012	¹¹² 1.015
322	VNPT-001	¹⁹³ 2048	²⁸ 892	¹²¹ 0.0022	¹⁴² 0.0019	¹⁵⁰ 0.0018	¹⁶⁰ 0.0018	¹⁷⁰ 0.0018	¹³⁹ 1.017
323	VNPT-002	¹⁴⁹ 2048	²⁴² 810	¹⁰³ 0.0019	¹³⁴ 0.0018	¹⁴⁴ 0.0018	¹⁵⁰ 0.0018	¹⁶⁶ 0.0017	¹³⁰ 1.016
324	VOCORD-003	⁷ 896	²⁰⁶ 714	²⁰⁴ 0.0062	¹⁹⁸ 0.0035	¹⁹⁵ 0.0030	¹⁹⁹ 0.0026	¹⁹⁷ 0.0023	¹⁹⁸ 1.035
325	VOCORD-004	⁷⁹ 896	¹⁵² 538	²²¹ 0.0079	²²¹ 0.0049	²²³ 0.0043	²²⁸ 0.0038	²²⁸ 0.0034	²¹⁹ 1.048
326	VOCORD-005	⁷⁶ 768	²⁴ 822	²¹⁵ 0.0070	²¹⁸ 0.0046	²²⁰ 0.0041	²²⁷ 0.0038	²³² 0.0035	²¹⁵ 1.044
327	VOCORD-006	³³⁹ 10240	²⁴⁹ 825	³³⁸ 1.0000	³³⁹ 1.0000	³³⁸ 1.0000	³³⁸ 1.0000	³³⁸ 1.0000	³³⁸ 10.000
328	VTS-000	¹⁷² 2048	¹² 492	³³⁴ 0.5937	³³⁵ 0.5936	³³⁵ 0.5936	³³⁵ 0.5936	³³⁵ 0.5936	³³⁵ 6.343
329	VTS-001	²¹⁰ 2048	²⁸⁵ 891	⁷⁰ 0.0015	⁵¹ 0.0012	⁴⁵ 0.0011	⁴⁶ 0.0011	⁴³ 0.0010	³⁵ 1.011
330	VTS-002	¹⁸⁹ 2048	²⁹ 903	¹⁰⁷ 0.0019	⁹¹ 0.0014	⁷⁶ 0.0013	⁷⁶ 0.0012	⁶⁶ 0.0011	⁹⁵ 1.013
331	VTS-003	²¹⁹ 2048	¹⁹⁴ 703	²⁹ 0.0011	²⁹ 0.0010	²³ 0.0009	²¹ 0.0009	²⁰ 0.0009	²⁴ 1.009
332	XFORWARDAI-000	²³⁵ 2048	²²⁵ 768	¹³⁰ 0.0023	¹⁵³ 0.0020	¹⁶¹ 0.0020	¹⁷³ 0.0019	¹⁵⁹ 0.0019	¹⁴⁸ 1.018
333	XFORWARDAI-001	²¹⁶ 2048	¹⁷⁹ 681	¹¹⁸ 0.0020	¹⁴⁶ 0.0019	¹⁵⁸ 0.0019	¹⁷⁰ 0.0019	¹⁷⁸ 0.0019	¹⁴⁰ 1.018
334	XFORWARDAI-002	³⁰⁷ 4096	³⁰⁶ 935	¹⁰⁹ 0.0020	¹⁴³ 0.0019	¹⁵⁶ 0.0019	¹⁶⁹ 0.0019	¹⁷⁶ 0.0019	¹³⁷ 1.017
335	YISHENG-001	³⁰¹ 3704	⁸² 387	²⁸² 0.0265	²⁷⁹ 0.0130	²⁷¹ 0.0102	²⁶⁸ 0.0080	²⁵⁷ 0.0059	²⁶ 1.134
336	YITU-002	³²⁶ 4138	²⁷⁴ 870	⁹⁹ 0.0018	⁶¹ 0.0012	⁵⁴ 0.0011	⁴⁸ 0.0011	⁴⁶ 0.0010	⁷¹ 1.012
337	YITU-003	³²⁷ 4138	²⁷ 871	¹⁵⁵ 0.0029	¹⁶¹ 0.0023	¹⁷⁶ 0.0022	¹⁸⁷ 0.0021	¹⁸ 0.0021	¹⁶³ 1.021
338	YITU-004	²⁸² 2070	²⁹⁷ 910	⁴⁴ 0.0013	¹⁷ 0.0009	¹⁷ 0.0009	¹⁶ 0.0009	¹⁶ 0.0009	²⁷ 1.009
339	YITU-005	²⁹ 2070	²⁰ 861	¹³² 0.0023	¹⁵⁰ 0.0021	¹⁶² 0.0020	¹⁷⁸ 0.0020	¹⁸² 0.0020	¹⁵⁰ 1.019

Table 33: **Rank-based accuracy for the FRVT 2018 mugshot sets.** In columns 3 and 4 are template size and template generation duration. Thereafter values are rank-based FNIR with $T = 0$ and FPIR = 1. This is appropriate to investigational uses but not those with higher volumes where candidates from all searches would need review. The next column is a workload statistic, a small value shows an algorithm front-loads mates into the first 10 candidates. Throughout, blue superscripts indicate the rank of the algorithm for that column, and the best value is highlighted in yellow.

MISSES BELOW THRESHOLD, T		ENROL RECENT MUGSHOT, N = 1.6M												ENROL APPLICATION PORTRAIT, N = 1.6M																		
#	ALGORITHM	ENROL: MUGSHOT			ENROL: MUGSHOT			ENROL: WEBCAM			ENROL: PROFILE			ENROL: VISA			ENROL: BORDER			PROBE: BORDER			PROBE: BORDER 10+YR			PROBE: KIOSK						
		FPIR=0.0003	FPIR=0.001	FPIR=0.01	FPIR=0.0003	FPIR=0.001	FPIR=0.01	FPIR=0.0003	FPIR=0.001	FPIR=0.01	FPIR=0.0003	FPIR=0.001	FPIR=0.01	FPIR=0.0001	FPIR=0.001	FPIR=0.01	FPIR=0.0001	FPIR=0.001	FPIR=0.01	FPIR=0.0001	FPIR=0.001	FPIR=0.01	FPIR=0.0001	FPIR=0.001	FPIR=0.01							
1	20FACE-000	284	0.462	294	0.348	302	0.230	295	0.763	285	0.450	288	0.301	261	1.000	258	1.000	270	1.000	225	0.424	227	0.255	131	0.772	142	0.599	219	0.938	235	0.836	
2	3DIVI-003	286	0.482	303	0.400	308	0.282	289	0.685	302	0.626	304	0.497					238	0.605	239	0.445					200	0.821	229	0.717			
3	3DIVI-004	256	0.256	273	0.169	278	0.093	254	0.400	275	0.343	282	0.237					214	0.277	220	0.172					172	0.607	205	0.485			
4	3DIVI-005	253	0.255	270	0.166	277	0.093	253	0.395	277	0.339	281	0.234	171	0.998	182	0.996	201	0.990	245	0.864	248	0.846					171	0.597	204	0.484	
5	3DIVI-006	254	0.253	272	0.168	280	0.096	257	0.403	274	0.342	283	0.238					215	0.283	221	0.174					175	0.615	206	0.490			
6	ACER-000	240	0.208	262	0.146	267	0.074	257	0.300	252	0.246	256	0.157	115	0.987	131	0.981	163	0.955	208	0.201	219	0.114					155	0.490	186	0.363	
7	ACER-001	188	0.109	203	0.056	208	0.026	170	0.136	179	0.109	186	0.069	208	1.000	221	0.999	249	0.998	165	0.068	168	0.036	115	0.406	128	0.250	154	0.479	132	0.206	
8	AIZE-001	196	0.127	224	0.077	225	0.034	20	0.187	20	0.143	209	0.087	144	0.995	160	0.994	188	0.983	179	0.101	181	0.052	108	0.364	12	0.216	133	0.387	168	0.289	
9	ALCHERA-000	247	0.231	259	0.138	261	0.070	226	0.259	236	0.216	249	0.146	184	0.999	200	0.999	231	0.996	202	0.176	214	0.111					196	0.803	199	0.456	
10	ALCHERA-001	334	1.000	334	0.999	338	0.999	338	1.000	321	1.000	329	1.000					306	1.000	308	1.000					283	1.000	314	1.000			
11	ALCHERA-002	309	0.807	310	0.486	311	0.302	288	0.685	297	0.591	299	0.442	226	1.000	229	1.000	254	0.999	244	0.827	245	0.770					197	0.811	22	0.705	
12	ALCHERA-003	280	0.450	264	0.155	262	0.070	238	0.304	248	0.239	254	0.152	220	1.000	214	0.999	236	0.997	201	0.172	20	0.097					149	0.464	187	0.362	
13	ALCHERA-004	291	0.520	302	0.394	301	0.211	285	0.642	292	0.529	293	0.327	145	0.995	152	0.991	12	0.813	226	0.424	229	0.232	123	0.708	136	0.515	166	0.546	196	0.398	
14	ALLGOVISION-000	206	0.138	236	0.088	243	0.045	213	0.202	223	0.166	233	0.106	131	0.993	149	0.990	187	0.982	182	0.117	191	0.066					163	0.526	193	0.396	
15	ALLGOVISION-001	215	0.155	241	0.102	249	0.053	231	0.275	240	0.221	248	0.141	133	0.993	138	0.986	140	0.933	195	0.150	207	0.081					136	0.491	194	0.389	
16	ALLGOVISION-002	201	0.135	218	0.068	217	0.031	244	0.753	297	0.520	236	0.113	108	0.983	100	0.950	132	0.870	210	0.232	183	0.049	249	1.000	151	1.000	185	0.716	188	0.366	
17	ANKE-000	226	0.184	246	0.117	258	0.063	229	0.256	239	0.220	252	0.151	141	0.995	159	0.994	199	0.990	260	1.000	259	1.000					330	1.000	277	1.000	
18	ANKE-001	224	0.183	250	0.119	259	0.063	225	0.256	238	0.220	253	0.151	146	0.995	166	0.994	210	0.992	308	1.000	306	1.000					285	1.000	313	1.000	
19	ANKE-002	148	0.062	164	0.032	154	0.103	142	0.079	148	0.050	90	0.975	99	0.948	117	0.795	124	0.034	12	0.018					98	0.245	126	0.190			
20	AWARE-003	223	0.174	254	0.128	270	0.082	249	0.351	267	0.298	275	0.204	112	0.987	133	0.984	182	0.977	227	0.428	233	0.378					164	0.530	198	0.443	
21	AWARE-004	272	0.355	286	0.269	297	0.175	26	0.619	29	0.509	297	0.375	222	1.000	232	1.000	259	0.999	229	0.397	227	0.279					198	0.816	216	0.631	
22	AWARE-005	297	0.608	297	0.364	272	0.085	244	0.342	254	0.253	258	0.163	219	1.000	236	1.000	256	0.999	213	0.255	218	0.122					213	0.916	22	0.714	
23	AWARE-006	285	0.475	287	0.276	298	0.175	267	0.466	278	0.398	286	0.283	203	1.000	223	0.999	250	0.999	220	0.368	229	0.254					189	0.749	213	0.623	
24	AYONIX-000	313	0.846	322	0.811	328	0.724	309	0.956	321	0.939	323	0.892	173	0.998	191	0.998	220	0.995	249	0.954	250	0.891					228	0.982	241	0.959	
25	AYONIX-001	315	0.875	324	0.824	326	0.701	304	0.946	316	0.920	319	0.845	217	1.000	220	0.999	233	0.996	254	0.999	254	0.998					225	0.969	237	0.926	
26	AYONIX-002	316	0.876	323	0.824	322	0.702	305	0.946	317	0.920	318	0.845	216	1.000	219	0.999	232	0.996	246	0.915	246	0.821					224	0.969	238	0.926	
27	CAMVI-003	174	0.094	219	0.071	254	0.058	181	0.152	199	0.132	234	0.108	98	0.979	111	0.970	153	0.940	181	0.114	208	0.100					137	0.402	191	0.377	
28	CAMVI-004	183	0.107	220	0.072	257	0.054	227	0.240	201	0.136	223	0.100	206	1.000	217	0.999	249	0.998	178	0.100	20	0.081					194	0.787	207	0.507	
29	CAMVI-005	207	0.139	240	0.099	269	0.076	264	0.451	230	0.179	243	0.132	209	1.000	228	0.999	247	0.998	196	0.156	215	0.112					236	0.999	249	0.983	
30	CANON-001	46	0.012	56	0.005	38	0.031	38	0.023	39	0.015	41	0.633	29	0.365	40	0.217	41	0.008	40	0.004	39	0.068	43	0.034	50	0.139	45	0.092			
31	CANON-002	34	0.010	48	0.005	47	0.002	32	0.027	33	0.020	25	0.013	25	0.487	33	0.407	48	0.253	69	0.013	48	0.004	44	0.075	54	0.046	83	0.188	59	0.106	
32	CIB-000	112	0.044	92	0.012	88	0.005	103	0.077	85	0.045	84	0.025	249	1.000	245	1.000	26	1.000	81	0.017	79	0.008	62	0.141	66	0.068	210	0.894	208	0.521	
33	CLEARVIEWAI-000	50	0.013	59	0.006	52	0.002	15	0.015	18	0.013	210	0.012	50	0.188	6	0.133	10	0.095	21	0.005	20	0.003	15	0.033	19	0.018	28	0.099	17	0.075	
34	CLOUDWALK-HR-000	15	0.004	18	0.002	21	0.002	15	0.015	18	0.013	210	0.012	179	0.999	190	0.998	229	0.995													
35	CLOUDWALK-MT-000	10	0.003	17	0.002	31	0.002	11	0.015	17	0.013	23	0.012	40	0.169	4	0.109	5	0.077	7	0.002	11	0.002	5	0.018	7	0.009	6	0.072	10	0.063	
36	CLOUDWALK-MT-001	7	0.003	15	0.002	29	0.013	7	0.012	20	0.011	28	0.011	204	0.104	2	0.070	2														

MISSES BELOW THRESHOLD, T		ENROL RECENT MUGSHOT, N = 1.6M												ENROL APPLICATION PORTRAIT, N = 1.6M										
#	ALGORITHM	ENROL: MUGSHOT			ENROL: MUGSHOT			ENROL: WEBCAM			ENROL: MUGSHOT			ENROL: BORDER			ENROL: VISA		ENROL: BORDER		ENROL: BORDER 10+YR		ENROL: KIOSK	
		FPIR=0.0003	FPIR=0.001	FPIR=0.01	FPIR=0.0003	FPIR=0.001	FPIR=0.01	FPIR=0.0003	FPIR=0.001	FPIR=0.01	FPIR=0.0003	FPIR=0.001	FPIR=0.01	FPIR=0.001	FPIR=0.01	FPIR=0.001	FPIR=0.01	FPIR=0.001	FPIR=0.01	FPIR=0.001	FPIR=0.01	FPIR=0.001	FPIR=0.01	
47	COGNITEC-001	²³⁶ 0.192	²⁴² 0.102	²⁵⁰ 0.053	³²² 0.997	²⁴⁴ 0.230	²⁴⁵ 0.135	³³⁹ 1.000	³¹⁴ 1.000	¹⁶ 0.965	²⁷⁵ 1.000	²⁴³ 1.000	¹⁶⁴ 0.956	¹⁶⁴ 0.068	¹⁶⁹ 0.038	¹⁰⁵ 0.316	¹¹⁹ 0.196	¹¹² 0.288	¹⁴² 0.218					
48	COGNITEC-002	¹⁹² 0.122	¹⁹⁶ 0.053	²⁰³ 0.025	³¹⁹ 0.990	²²⁹ 0.178	²³⁰ 0.101	³⁰⁷ 1.000	²⁸⁴ 1.000	¹³ 0.878	¹³⁶ 0.041	¹⁵ 0.028	⁷² 0.157	⁸⁶ 0.092	⁷⁸ 0.179	⁹⁶ 0.145								
49	COGNITEC-003	¹⁷⁸ 0.099	¹⁹² 0.053	²⁰⁵ 0.025	²¹⁷ 0.222	²²¹ 0.162	²²⁴ 0.100	³⁰² 1.000	²⁴⁶ 1.000	¹⁵ 0.946	²⁷⁵ 1.000	²⁴¹ 1.000	¹¹² 0.030	¹⁰⁹ 0.013	⁷⁸ 0.171	⁷⁸ 0.081	¹⁸² 0.681	¹³⁹ 0.214						
50	COGNITEC-004	¹⁴⁰ 0.055	¹⁶³ 0.031	¹⁶⁵ 0.014	¹⁵⁸ 0.127	¹⁶⁷ 0.097	¹⁶⁶ 0.058	¹⁴³ 0.995	¹⁴⁶ 0.990	¹⁴¹ 0.919	¹⁶⁴ 0.068	¹⁶⁹ 0.038	¹⁰⁵ 0.316	¹¹⁹ 0.196	¹¹² 0.288	¹⁴² 0.218								
51	COGNITEC-005	¹⁴¹ 0.055	⁷⁸ 0.010	⁷¹ 0.004	⁷⁷ 0.058	⁸¹ 0.041	⁷³ 0.022	³⁰⁷ 1.000	²⁸⁴ 1.000	¹³ 0.878	¹³⁶ 0.041	¹⁵ 0.028	⁷² 0.157	⁸⁶ 0.092	⁷⁸ 0.179	⁹⁶ 0.145								
52	COGNITEC-006	⁸⁸ 0.029	⁶⁹ 0.008	⁶⁴ 0.003	⁸³ 0.065	⁷⁷ 0.040	⁷⁰ 0.022	²⁷² 1.000	³²⁰ 1.000	²⁵¹ 0.999	¹¹² 0.030	¹⁰⁹ 0.013	⁷⁸ 0.171	⁷⁸ 0.081	¹⁸² 0.681	¹³⁹ 0.214								
53	CUBOX-000	²⁰ 0.005	²⁷ 0.003	³¹ 0.002	²⁸ 0.022	²⁸ 0.019	³² 0.014	¹⁴ 0.276	¹⁰ 0.168	¹⁰ 0.104	¹⁷ 0.004	¹⁸ 0.003	¹⁴ 0.028	¹⁶ 0.014	⁷ 0.073	⁸ 0.062								
54	CYBERLINK-000	²⁰⁵ 0.137	²⁰⁴ 0.056	¹⁹⁵ 0.023	¹⁸⁷ 0.162	¹⁸³ 0.116	¹⁸⁹ 0.070	¹⁶³ 0.997	¹⁷⁵ 0.995	¹⁸⁶ 0.981	¹⁶² 0.063	¹⁶² 0.032	¹²⁷ 0.339	¹⁵⁰ 0.232										
55	CYBERLINK-001	¹⁷⁵ 0.096	¹⁹⁷ 0.054	¹⁹⁰ 0.022	¹⁷⁴ 0.138	¹⁸¹ 0.109	¹⁸² 0.067	¹⁶² 0.997	¹⁷⁰ 0.995	¹⁸⁹ 0.984	¹⁵⁹ 0.062	¹⁵⁹ 0.031	¹¹³ 0.288	¹⁰⁸ 0.157										
56	CYBERLINK-002	¹⁰³ 0.038	¹⁰² 0.015	¹⁰² 0.006	⁹⁵ 0.068	¹⁰¹ 0.053	¹⁰² 0.032	¹³⁷ 0.994	¹⁴⁴ 0.988	¹⁶⁵ 0.957	⁹⁹ 0.024	¹⁰² 0.013	¹¹³ 0.159	⁷⁶ 0.125										
57	CYBERLINK-003	¹¹⁶ 0.045	⁷⁰ 0.008	⁶⁹ 0.004	⁵⁹ 0.045	⁶⁸ 0.035	⁶⁵ 0.021	¹³⁸ 0.995	¹¹⁴ 0.972	¹²⁸ 0.845	⁶⁵ 0.012	⁷⁰ 0.007	⁵³ 0.100	⁵⁸ 0.051	¹³⁰ 0.368	⁷² 0.120								
58	CYBERLINK-004	²³⁴ 0.188	⁶⁶ 0.007	⁶⁵ 0.003	⁸¹ 0.063	⁶⁹ 0.036	⁷² 0.022	²⁶⁴ 1.000	²⁶⁹ 0.999	⁶⁷ 0.007	⁵⁴ 0.109	⁵⁹ 0.050	²²³ 0.954	¹⁷ 0.291										
59	CYBERLINK-005	²⁴¹ 0.208	⁸² 0.010	⁷⁷ 0.004	⁷² 0.054	⁷⁸ 0.041	⁸⁶ 0.026	²³⁴ 1.000	¹³⁶ 0.888	⁷¹ 0.014	⁴⁹ 0.089	⁵¹ 0.043	²¹⁸ 0.926	¹⁶ 0.266										
60	DAHUA-000	¹⁹⁸ 0.128	²³² 0.086	²⁴⁰ 0.045	¹⁹⁶ 0.179	²⁰⁰ 0.135	²⁰⁷ 0.083	¹¹⁴ 0.987	¹²⁷ 0.980	¹⁴⁷ 0.933	¹¹⁴ 0.013	¹¹⁴ 0.008	¹¹⁴ 0.013	¹¹⁴ 0.013	¹¹⁴ 0.013	¹¹⁴ 0.013	¹¹⁴ 0.013	¹¹⁴ 0.013	¹¹⁴ 0.013	¹¹⁴ 0.013	¹¹⁴ 0.013	¹¹⁴ 0.013		
61	DAHUA-001	¹⁸² 0.106	²²² 0.073	²²⁷ 0.037	¹⁸⁰ 0.151	¹⁹¹ 0.122	¹⁹⁸ 0.075	¹¹⁴ 0.987	¹²⁷ 0.980	¹⁴⁷ 0.933	¹¹⁴ 0.013	¹¹⁴ 0.008	¹¹⁴ 0.013	¹¹⁴ 0.013	¹¹⁴ 0.013	¹¹⁴ 0.013	¹¹⁴ 0.013	¹¹⁴ 0.013	¹¹⁴ 0.013	¹¹⁴ 0.013	¹¹⁴ 0.013	¹¹⁴ 0.013		
62	DAHUA-002	⁸¹ 0.026	¹⁰³ 0.015	¹⁰⁰ 0.006	⁷⁸ 0.060	⁸⁰ 0.046	⁹¹ 0.029	⁴⁷ 0.681	⁵⁷ 0.638	⁸¹ 0.522	⁷⁸ 0.017	⁷⁸ 0.008	⁶⁶ 0.159	⁷⁶ 0.125										
63	DAHUA-003	⁷⁹ 0.025	⁹⁷ 0.014	⁹⁰ 0.005	⁷¹ 0.054	⁸⁰ 0.041	⁸⁰ 0.024	⁴² 0.647	⁵² 0.579	⁷² 0.447	⁶⁶ 0.013	⁶⁸ 0.006	⁴⁶ 0.081	⁵² 0.043	⁴⁸ 0.134	⁵⁸ 0.109								
64	DAHUA-004	⁵³ 0.014	⁶⁵ 0.007	⁶⁰ 0.003	⁴⁴ 0.033	⁴⁶ 0.026	⁴⁶ 0.016	³¹ 0.552	⁴⁵ 0.485	⁶⁰ 0.345	⁴⁹ 0.008	⁵⁰ 0.004	²⁶ 0.051	³⁹ 0.027	³⁹ 0.113	⁴⁶ 0.094								
65	DAON-000	²⁰³ 0.135	¹³⁴ 0.023	¹³⁴ 0.009	¹⁰⁷ 0.079	¹¹⁵ 0.061	¹²⁰ 0.039	²²⁷ 1.000	²³¹ 1.000	²⁴⁶ 0.998	¹⁰³ 0.025	¹⁰³ 0.013	⁸⁰ 0.173	⁸⁰ 0.091	²⁰⁵ 0.846	¹¹³ 0.172								
66	DECATUR-000	¹⁰⁸ 0.043	¹³⁷ 0.023	¹³⁸ 0.010	¹¹² 0.085	¹²¹ 0.066	¹²³ 0.040	⁵⁰ 0.757	⁶² 0.675	⁷⁰ 0.509	¹⁰⁴ 0.027	¹¹¹ 0.014	⁷⁹ 0.173	⁹² 0.098	⁹⁶ 0.239	¹⁰³ 0.156								
67	DEEPLINT-001	³⁹ 0.010	³³ 0.003	³⁶ 0.002	¹⁹ 0.018	¹⁹ 0.014	¹⁴ 0.010	²⁵⁶ 1.000	²²⁵ 1.000	²⁷ 0.503	³¹ 0.006	⁴⁹ 0.004	¹⁶⁹ 0.557	¹⁷⁵ 0.497										
68	DEEPSEA-001	¹⁶⁰ 0.073	¹⁸⁴ 0.046	¹⁹⁴ 0.022	¹⁶¹ 0.129	¹⁷¹ 0.101	¹⁶⁹ 0.059	¹¹⁸ 0.988	¹³⁶ 0.985	¹⁷⁶ 0.973	¹⁶⁹ 0.077	¹⁷⁶ 0.041	¹²⁵ 0.326	¹⁵⁶ 0.251										
69	DERMALOG-003	²⁹³ 0.550	³⁰⁹ 0.482	³¹⁴ 0.360	²⁹² 0.715	³⁰⁴ 0.655	³⁰⁸ 0.526	¹⁵⁶ 0.997	¹⁷⁶ 0.995	²⁰⁹ 0.991	¹⁵⁶ 0.063	¹⁵⁶ 0.038	²⁴³ 0.677	²⁴¹ 0.554	²⁰⁸ 0.870	²³⁷ 0.791								
70	DERMALOG-004	²⁹⁵ 0.554	³⁰⁸ 0.480	³¹⁴ 0.358	²⁹¹ 0.711	³⁰⁶ 0.657	³⁰⁶ 0.526	¹⁵⁶ 0.997	¹⁷⁶ 0.995	²⁰⁹ 0.991	¹⁵⁶ 0.063	¹⁵⁶ 0.038	²⁴³ 0.677	²⁴¹ 0.554	²⁰⁸ 0.870	²³⁷ 0.791								
71	DERMALOG-005	²³⁸ 0.189	²³⁸ 0.088	²³⁵ 0.043	²⁰⁹ 0.201	²¹⁴ 0.154	²²⁰ 0.096	¹⁵³ 0.996	¹⁴⁷ 0.990	¹⁵⁸ 0.950	²¹⁶ 0.300	²²⁰ 0.267	¹⁷⁴ 0.614	²⁰⁶ 0.459										
72	DERMALOG-006	¹⁷⁷ 0.098	¹⁹¹ 0.052	²⁰⁷ 0.026	¹⁷² 0.137	¹⁷⁴ 0.105	¹⁸¹ 0.067	¹²⁰ 0.989	¹³⁰ 0.981	¹⁴⁸ 0.933	¹⁵⁷ 0.059	¹⁶⁰ 0.031	¹²² 0.318	¹⁴⁸ 0.230										
73	DERMALOG-007	²³² 0.188	²³³ 0.086	²³³ 0.040	²⁰⁸ 0.200	²¹² 0.152	²¹⁷ 0.093	¹⁵⁴ 0.996	¹⁴⁸ 0.990	¹⁵⁹ 0.950	¹⁷⁷ 0.059	¹⁸¹ 0.025	¹⁶⁹ 0.557	¹⁷⁵ 0.499										
74	DERMALOG-008	²⁵⁹ 0.268	¹⁸² 0.045	¹⁷⁴ 0.017	²¹⁸ 0.231	¹⁶⁰ 0.094	¹⁵⁹ 0.054	²⁴¹ 1.000	²⁶⁵ 1.000	²⁶⁷ 1.000	¹⁵⁴ 0.057	¹⁴⁹ 0.025	¹¹² 0.382	¹¹³ 0.158	²²⁰ 0.940	²¹⁰ 0.678								
75	DERMALOG-009	¹⁰⁷ 0.041	¹²⁶ 0.021	¹³⁴ 0.009	¹¹⁴ 0.086	¹²² 0.066	¹²⁶ 0.040	¹⁵¹ 0.997	¹⁶⁷ 0.994	¹⁹⁸ 0.990	¹¹⁴ 0.031	¹²⁰ 0.016	¹⁴⁵ 0.999	¹⁵⁹ 0.999	²⁰³ 0.840	¹⁴³ 0.422								
76	DERMALOG-010	⁶¹ 0.019	⁶⁴ 0.007	⁶⁸ 0.004	¹⁶⁸ 0.134	¹⁰⁵ 0.055	⁷⁵ 0.023	²⁰⁵ 1.000	²⁰⁹ 0.999	¹⁶⁰ 0.952	¹⁷⁸ 0.089	¹⁷⁶ 0.041	¹⁴⁶ 1.000	¹⁴⁸ 0.971	¹⁶¹ 0.522	¹³⁸ 0.211								
77	DERMALOG-011	¹¹⁹ 0.046	¹²⁹ 0.022	¹¹⁷ 0.007	²⁰⁹ 0.193	¹⁵¹ 0.087	¹²² 0.039	¹⁸⁷ 0.999	¹⁹⁶ 0.998</td															

MISSSES BELOW THRESHOLD, T		ENROL RECENT MUGSHOT, N = 1.6M												ENROL APPLICATION PORTRAIT, N = 1.6M												
		ENROL: MUGSHOT			ENROL: MUGSHOT			PROBE: WEBCAM			ENROL: MUGSHOT			PROBE: PROFILE			ENROL: VISA		ENROL: BORDER		ENROL: BORDER 10+YR		ENROL: KIOSP			
#	ALGORITHM	FPIR=0.0003	FPIR=0.001	FPIR=0.01	FPIR=0.0003	FPIR=0.001	FPIR=0.01	FPIR=0.0003	FPIR=0.001	FPIR=0.01	FPIR=0.0003	FPIR=0.001	FPIR=0.01	FPIR=0.001	FPIR=0.01	FPIR=0.001	FPIR=0.01	FPIR=0.001	FPIR=0.01	FPIR=0.001	FPIR=0.01	FPIR=0.001	FPIR=0.01	FPIR=0.001	FPIR=0.01	
93	GORILLA-005	17 ¹ 0.086	20 ⁶ 0.058	20 ⁹ 0.026	19 ⁵ 0.179	20 ⁶ 0.142	21 ¹ 0.088	33 ⁷ 0.770	64 ⁷ 0.700	88 ⁵ 0.553	17 ⁴ 0.088	17 ⁷ 0.040	105 ² 0.028	105 ³ 0.013	76 ¹ 0.166	89 ¹ 0.093	90 ² 0.218	101 ¹ 0.154	120 ¹ 0.315	144 ¹ 0.223						
94	GORILLA-006	12 ¹ 0.046	15 ² 0.027	14 ⁶ 0.011	14 ⁸ 0.118	15 ⁵ 0.089	15 ⁵ 0.053	37 ³ 0.602	50 ³ 0.531	65 ³ 0.369	101 ² 0.026	98 ² 0.012	95 ² 0.264	95 ³ 0.108	76 ¹ 0.178	98 ¹ 0.138										
95	GORILLA-007	11 ¹ 0.046	15 ⁰ 0.027	14 ³ 0.010	13 ¹ 0.101	14 ⁶ 0.077	13 ⁷ 0.045	40 ² 0.626	51 ² 0.534	66 ² 0.369	111 ¹ 0.030	96 ¹ 0.011	107 ² 0.319	84 ² 0.090	74 ¹ 0.178	84 ¹ 0.132										
96	GORILLA-008	11 ⁰ 0.044	15 ⁸ 0.024	12 ⁵ 0.009	14 ⁰ 0.111	14 ⁹ 0.083	14 ⁵ 0.048	29 ² 0.541	39 ² 0.463	55 ² 0.295	111 ¹ 0.030	96 ¹ 0.011	107 ² 0.319	84 ² 0.090	74 ¹ 0.178	84 ¹ 0.132										
97	GRIAULE-000	11 ¹ 0.044	12 ⁴ 0.020	12 ⁸ 0.009	11 ⁶ 0.082	11 ⁹ 0.038	16 ⁶ 0.997	17 ¹ 0.995	15 ⁹ 0.952	121 ¹ 0.033	13 ⁷ 0.020	85 ² 0.185	94 ¹ 0.107	85 ¹ 0.198	108 ¹ 0.166											
98	GRIAULE-001	49 ¹ 0.013	49 ¹ 0.005	42 ¹ 0.002	69 ¹ 0.051	53 ¹ 0.028	48 ¹ 0.016	75 ¹ 0.928	88 ¹ 0.865	96 ¹ 0.625	35 ¹ 0.007	26 ¹ 0.003	143 ¹ 0.995	143 ¹ 0.610	26 ¹ 0.099	22 ¹ 0.081	145 ¹ 0.445	183 ¹ 0.359								
99	HIK-003	22 ¹ 0.159	24 ¹ 0.103	25 ¹ 0.057	20 ⁴ 0.190	21 ⁶ 0.158	23 ² 0.105	100 ¹ 0.980	109 ¹ 0.969	141 ¹ 0.925	192 ¹ 0.142	20 ⁸ 0.080														
100	HIK-004	21 ⁷ 0.156	23 ⁹ 0.099	25 ¹ 0.054	19 ⁹ 0.182	21 ³ 0.153	22 ⁹ 0.101	108 ¹ 0.983	117 ¹ 0.976	156 ¹ 0.947	190 ¹ 0.137	199 ¹ 0.077														
101	HIK-005	18 ¹ 0.102	17 ⁷ 0.044	17 ⁹ 0.019	12 ⁵ 0.098	13 ⁷ 0.077	14 ⁶ 0.048	210 ¹ 1.000	224 ¹ 0.999	241 ¹ 0.998	163 ¹ 0.068	166 ¹ 0.036														
102	HIK-006	20 ⁹ 0.142	18 ⁶ 0.047	18 ² 0.020	13 ⁹ 0.111	15 ⁰ 0.086	15 ³ 0.052	236 ¹ 1.000	260 ¹ 0.999	261 ¹ 0.999																
103	HYPERVERGE-001	38 ¹ 0.009	44 ¹ 0.004	46 ¹ 0.002	53 ¹ 0.039	60 ¹ 0.031	64 ¹ 0.020	13 ¹ 0.275	18 ¹ 0.220	26 ¹ 0.146	36 ¹ 0.007	43 ¹ 0.004	28 ¹ 0.053	33 ¹ 0.027	31 ¹ 0.101	30 ¹ 0.083										
104	HYPERVERGE-002	31 ¹ 0.008	35 ¹ 0.004	38 ¹ 0.002	46 ¹ 0.034	51 ¹ 0.027	55 ¹ 0.018	16 ¹ 0.278	16 ¹ 0.210	21 ¹ 0.131	25 ¹ 0.006	24 ¹ 0.003	25 ¹ 0.048	23 ¹ 0.023	20 ¹ 0.093	20 ¹ 0.077										
105	HZAILU-000	9 ⁷ 0.035	12 ¹ 0.020	12 ⁹ 0.009	82 ¹ 0.064	92 ¹ 0.051	96 ¹ 0.031	108 ¹ 0.983	107 ¹ 0.967	124 ¹ 0.813	88 ¹ 0.020	89 ¹ 0.010	104 ¹ 0.316	73 ¹ 0.077	60 ¹ 0.153	75 ¹ 0.120										
106	HZAILU-001	58 ¹ 0.016	73 ¹ 0.009	82 ¹ 0.004	258 ¹ 0.414	231 ¹ 0.183	82 ¹ 0.024	176 ¹ 0.998	141 ¹ 0.986	53 ¹ 0.282	207 ¹ 0.196	140 ¹ 0.021	260 ¹ 1.000	149 ¹ 0.997	181 ¹ 0.160	184 ¹ 0.360										
107	HZAILU-002	56 ¹ 0.015	71 ¹ 0.008	80 ¹ 0.004	68 ¹ 0.050	76 ¹ 0.039	83 ¹ 0.024	123 ¹ 0.990	65 ¹ 0.704	56 ¹ 0.299	63 ¹ 0.012	63 ¹ 0.006	38 ¹ 0.066	44 ¹ 0.034	125 ¹ 0.330	59 ¹ 0.110										
108	IDEMIA-003	294 ¹ 0.552	187 ¹ 0.047	186 ¹ 0.021	32 ¹ 1.000	22 ¹ 0.165	20 ² 0.079				32 ¹ 1.000	183 ¹ 0.123	187 ¹ 0.061													
109	IDEMIA-004	139 ¹ 0.055	173 ¹ 0.037	185 ¹ 0.021	176 ¹ 0.144	181 ¹ 0.118	201 ¹ 0.079	94 ¹ 0.976	115 ¹ 0.973	166 ¹ 0.968	184 ¹ 0.123	186 ¹ 0.061														
110	IDEMIA-005	155 ¹ 0.066	179 ¹ 0.044	206 ¹ 0.026	198 ¹ 0.181	211 ¹ 0.150	231 ¹ 0.102	99 ¹ 0.979	120 ¹ 0.978	171 ¹ 0.973	186 ¹ 0.130	194 ¹ 0.070														
111	IDEMIA-006	153 ¹ 0.065	176 ¹ 0.043	204 ¹ 0.025	229 ¹ 0.266	242 ¹ 0.226	257 ¹ 0.161	111 ¹ 0.984	132 ¹ 0.982	189 ¹ 0.980	193 ¹ 0.144	205 ¹ 0.090														
112	IDEMIA-007	98 ¹ 0.035	115 ¹ 0.018	118 ¹ 0.008	101 ¹ 0.073	104 ¹ 0.055	105 ¹ 0.033	310 ¹ 1.000	287 ¹ 1.000	317 ¹ 1.000	148 ¹ 0.052	146 ¹ 0.022	83 ¹ 0.182	97 ¹ 0.109	307 ¹ 1.000	249 ¹ 0.982										
113	IDEMIA-008	12 ¹ 0.004	14 ¹ 0.002	14 ¹ 0.001	18 ¹ 0.016	16 ¹ 0.013	11 ¹ 0.009	15 ¹ 0.276	15 ¹ 0.204	23 ¹ 0.136	20 ¹ 0.005	21 ¹ 0.003	19 ¹ 0.036	21 ¹ 0.019	34 ¹ 0.106	42 ¹ 0.092										
114	IDEMIA-009	11 ¹ 0.004	7 ¹ 0.002	8 ¹ 0.001	7 ¹ 0.012	6 ¹ 0.011	6 ¹ 0.008	6 ¹ 0.202	7 ¹ 0.141	12 ¹ 0.099	10 ¹ 0.003	10 ¹ 0.002	12 ¹ 0.027	13 ¹ 0.013	10 ¹ 0.074	11 ¹ 0.064										
115	IDEMIA-010	3 ¹ 0.002	1 ¹ 0.001	2 ¹ 0.001	2 ¹ 0.009	2 ¹ 0.008	3 ¹ 0.007	8 ¹ 0.228	5 ¹ 0.131	6 ¹ 0.078	5 ¹ 0.002	5 ¹ 0.001	13 ¹ 0.028	6 ¹ 0.009	5 ¹ 0.070	5 ¹ 0.058										
116	IMAGUS-002	31 ¹⁸ 0.898	32 ¹ 0.807	32 ¹ 0.669	30 ⁸ 0.954	31 ⁹ 0.909	317 ¹ 0.809	255 ¹ 1.000	248 ¹ 1.000	268 ¹ 1.000																
117	IMAGUS-003	95 ¹ 0.034	119 ¹ 0.018	119 ¹ 0.008	115 ¹ 0.088	126 ¹ 0.066	124 ¹ 0.040	74 ¹ 0.926	83 ¹ 0.838	105 ¹ 0.647	107 ¹ 0.029	121 ¹ 0.016	75 ¹ 0.161	91 ¹ 0.094	93 ¹ 0.231	124 ¹ 0.189										
118	IMAGUS-006	104 ¹ 0.039	122 ¹ 0.019	121 ¹ 0.008	119 ¹ 0.093	128 ¹ 0.069	132 ¹ 0.042	102 ¹ 0.980	93 ¹ 0.897	94 ¹ 0.621	106 ¹ 0.028	115 ¹ 0.015	74 ¹ 0.161	87 ¹ 0.092	104 ¹ 0.260	120 ¹ 0.181										
119	IMAGUS-007	16 ¹ 0.044	136 ¹ 0.023	137 ¹ 0.010	132 ¹ 0.073	136 ¹ 0.045	87 ¹ 0.973	91 ¹ 0.893	104 ¹ 0.651	115 ¹ 0.031	118 ¹ 0.016	77 ¹ 0.169	95 ¹ 0.098	109 ¹ 0.265	119 ¹ 0.181											
120	IMAGUS-007	328 ¹ 0.995	329 ¹ 0.974	320 ¹ 0.923	310 ¹ 0.958	308 ¹ 0.774	287 ¹ 0.285	213 ¹ 1.000	178 ¹ 0.996	107 ¹ 0.700	233 ¹ 0.520	199 ¹ 0.071	147 ¹ 1.000	138 ¹ 0.540	160 ¹ 0.518	151 ¹ 0.246										
122	IMPERIAL-000	21 ¹ 0.154	14 ⁴ 0.026	13 ⁵ 0.009	11 ⁷ 0.089	12 ⁴ 0.068	12 ⁷ 0.041	242 ¹ 1.000	204 ¹ 0.999	229 ¹ 0.995	137 ¹ 0.042	136 ¹ 0.020														
123	INCODE-000	27 ⁸ 0.423	29 ⁰ 0.310	29 ⁹ 0.199	27 ⁰ 0.486	28 ¹ 0.420	29 ⁰ 0.304	214 ¹ 1.000	194 ¹ 0.998	217 ¹ 0.994																
124	INCODE-001	26 ¹ 0.319	27 ⁰ 0.212	26 ¹ 0.112	24 ¹ 0.348	26 ¹ 0.296	27 ¹ 0.198	251 ¹ 1.000	252 ¹ 1.000	261 ¹ 1.000																
125	INCODE-002	264 ¹ 0.285	275 ¹ 0.184	283 ¹ 0.100	242 ¹ 0.333	262 ¹ 0.269	267 ¹ 0.176	167 ¹ 0.998	158 ¹ 0.993	181 ¹ 0.976																
126	INCODE-003	265 ¹ 0.286	271 ¹ 0.16																							

Table 36: Threshold-based accuracy. Values are FNIR(N, T, L) with $N = 1.6$ million with thresholds set to produce FPIR = 0.0003, 0.001, and 0.01 in non-mate searches. Throughout blue superscripts indicate the rank of the algorithm for that column. Caution: The Power-low models are mostly intended to draw attention to the kind of behavior, not as a model to be used for prediction.

2023/04/04
07:31:47

$\text{FNIR}(N, R_1) = \text{False neg. identification rate}$
 $\text{FPIR}(N, T) = \text{False pos. identification rate}$

$N =$ Num. enrolled subjects
 $R =$ Num. candidates examined
 $T =$ Threshold

$T = 0 \rightarrow$ Investigation
 $T > 0 \rightarrow$ Identification

MISSES BELOW THRESHOLD, T		ENROL RECENT MUGSHOT, N = 1.6M												ENROL APPLICATION PORTRAIT, N = 1.6M													
#	ALGORITHM	ENROL: MUGSHOT			ENROL: MUGSHOT			ENROL: MUGSHOT			ENROL: VISA			ENROL: BORDER			ENROL: BORDER 10+YR			ENROL: KIOSK							
		FPIR=0.0003	FPIR=0.001	FPIR=0.01	FPIR=0.0003	FPIR=0.001	FPIR=0.01	FPIR=0.0003	FPIR=0.001	FPIR=0.01	FPIR=0.0001	FPIR=0.001	FPIR=0.01	FPIR=0.001	FPIR=0.01	FPIR=0.001	FPIR=0.01	FPIR=0.001	FPIR=0.01	FPIR=0.001	FPIR=0.01	FPIR=0.001	FPIR=0.01				
139	INTEMA-001	² 0.002	⁵ 0.001	⁴ 0.001	²⁹ 0.604	²⁹ 0.603	³⁰ 0.602	³ 0.137	³ 0.103	⁴ 0.073	¹⁴ 0.004	¹² 0.002	¹² 0.715	¹² 0.294	¹¹ 0.076	⁷ 0.062	²³ 0.999	²⁵ 0.988	²³ 0.999	²⁵ 0.988	²³ 0.999	²⁵ 0.988					
140	INTSYSMSU-000	³² 0.999	³³ 0.998	³³ 0.990	³² 1.000	³² 1.000	³² 0.998	²³ 1.000	²³ 1.000	²⁴ 0.998	²³ 0.999	²³ 0.989	¹⁰³ 0.302	⁶³ 0.062	⁷² 0.170	⁸⁸ 0.135											
141	IREX-000	¹⁵⁷ 0.068	¹⁵⁶ 0.028	¹¹⁷ 0.008	¹²⁸ 0.099	¹¹⁴ 0.060	¹⁰⁸ 0.032	¹¹⁷ 0.988	¹⁰¹ 0.957	¹⁰⁸ 0.680	¹⁴⁰ 0.044	⁹³ 0.011															
142	ISYSTEMS-002	²¹⁶ 0.155	²²⁶ 0.078	²²⁸ 0.032	¹⁸⁷ 0.161	¹⁹⁴ 0.126	²⁰⁴ 0.080	¹⁷⁵ 0.998	¹⁸⁷ 0.998	²¹² 0.993																	
143	ISYSTEMS-003	²³⁹ 0.204	²⁰⁹ 0.059	²⁰⁸ 0.024	¹⁶⁹ 0.135	¹⁷⁸ 0.107	¹⁸⁴ 0.068	²³⁴ 1.000	²³⁵ 1.000	²³⁹ 0.997																	
144	KAKAO-000	⁸⁶ 0.028	¹⁰⁵ 0.015	¹⁰⁴ 0.006	⁹⁹ 0.071	¹⁰⁷ 0.056	¹¹¹ 0.034	²⁸ 0.539	⁴¹ 0.468	⁶¹ 0.327	⁸⁵ 0.019	⁸³ 0.010	⁶¹ 0.141	⁷¹ 0.075	⁶⁴ 0.158	⁷³ 0.120											
145	KAKAO-001	²³ 0.006	²⁴ 0.003	²⁷ 0.002	²⁹ 0.022	²⁹ 0.017	²⁷ 0.013	⁷ 0.226	⁹ 0.159	¹⁴ 0.101	¹⁶ 0.004	¹⁴ 0.002	²² 0.042	¹⁶ 0.016	⁹ 0.074	⁹ 0.063											
146	KEDACOM-001	¹⁰⁶ 0.041	¹³⁸ 0.023	¹⁶³ 0.013	¹²² 0.096	¹³⁰ 0.072	¹⁵⁸ 0.054	¹²¹ 0.989	¹⁴⁰ 0.986	¹⁷⁷ 0.973	¹⁵³ 0.055	¹⁷⁷ 0.043										¹¹⁶ 0.305	¹⁶⁰ 0.264				
147	KNERON-000			²² 0.033			²³² 0.099																				
148	KNERON-001			²⁴ 0.052																							
149	LINE-000	¹⁴⁹ 0.062	¹⁶² 0.031	¹⁶⁰ 0.012	¹⁶⁵ 0.132	¹⁶⁴ 0.095	¹⁶⁰ 0.054			²⁷⁹ 1.000	¹⁴² 0.046	¹⁴¹ 0.021	⁹⁸ 0.278	¹¹¹ 0.151	²⁵⁰ 1.000	¹⁶² 0.268											
150	LINE-001	⁸⁹ 0.030	⁵⁰ 0.005	⁴¹ 0.002	⁸⁵ 0.066	⁴⁹ 0.027	⁴⁴ 0.015	²⁴⁷ 1.000	²⁷⁰ 1.000	²⁷⁸ 1.000	⁵⁶ 0.009	⁴⁷ 0.004	⁴¹ 0.072	⁴⁵ 0.034	²⁸¹ 1.000	²³⁶ 0.858											
151	LINECLOVA-002	³⁷ 0.010	³⁶ 0.004	³⁸ 0.002	²⁷ 0.508	¹⁹⁶ 0.130	³⁴ 0.014	¹²⁹ 0.992	¹²⁹ 0.981	⁹¹ 0.577	¹³⁴ 0.040	³³ 0.004	¹⁴⁸ 1.000	¹⁴⁴ 0.690	¹⁸ 0.700	⁴¹ 0.091											
152	LINECLOVA-003	¹⁶ 0.004	²⁶ 0.003	¹⁵ 0.001	²⁸⁰ 0.612	³⁰⁰ 0.606	³¹¹ 0.603			²⁷⁸ 1.000	²⁴ 0.006	¹⁸ 0.002	¹⁴⁰ 0.974	¹¹⁴ 0.158	³⁶ 0.110	⁴⁸ 0.097											
153	LOOKMAN-003	¹⁵⁴ 0.066	¹⁷⁸ 0.044	²⁰⁵ 0.025	¹⁶⁴ 0.131	¹⁸² 0.112	²⁰⁵ 0.082			¹⁷³ 0.084	¹⁸⁹ 0.061											¹²⁸ 0.355	¹⁷⁶ 0.304				
154	LOOKMAN-004	¹⁶¹ 0.074	¹⁸¹ 0.045	¹⁹⁸ 0.024	¹⁵⁴ 0.123	¹⁷⁶ 0.105	¹⁹⁶ 0.075	⁹⁷ 0.979	¹¹⁸ 0.977	¹⁷⁹ 0.974													¹¹⁷ 0.308	¹⁶⁴ 0.273			
155	LOOKMAN-005	¹²⁸ 0.050	¹⁶⁰ 0.030	¹⁷² 0.017	¹³² 0.102	¹⁴⁷ 0.086	¹⁷⁸ 0.063	¹⁰¹ 0.980	¹²¹ 0.978	¹⁷³ 0.973	¹⁶⁰ 0.062	¹⁷⁹ 0.047												¹²⁰ 1.000	⁹⁹ 0.151		
156	MANTRA-000	¹⁵⁶ 0.066	⁸³ 0.010	⁷² 0.004	⁷⁹ 0.063	⁷⁹ 0.041	⁷¹ 0.022	³³³ 1.000	³⁰⁸ 1.000	²⁵⁹ 0.999	¹⁰⁸ 0.029	¹¹⁰ 0.014	⁷⁰ 0.152	⁷⁹ 0.081	²⁴⁰ 1.000	²⁴⁰ 1.000											
157	MAXVISION-000	¹²⁴ 0.048	¹⁵⁷ 0.028	¹⁶¹ 0.013	²⁶⁸ 0.468	²⁴¹ 0.237	¹⁶¹ 0.054	⁶¹ 0.827	⁷² 0.767	⁹⁹ 0.631	¹⁹⁴ 0.149	¹⁴² 0.022	¹⁴⁴ 0.997	¹⁴⁷ 0.872	¹⁶ 0.557	¹⁵³ 0.245											
158	MAXVISION-001	³⁵ 0.010	⁴¹ 0.004	³⁹ 0.002	⁵⁸ 0.044	⁴⁴ 0.025	⁴³ 0.015	¹⁷ 0.282	¹⁷ 0.219	²² 0.136	³⁴ 0.007	²⁵ 0.003	¹³⁷ 0.951	¹³⁵ 0.485	³⁰ 0.100	²¹ 0.078											
159	MEGVII-001	²⁴³ 0.210	²²¹ 0.072	²²⁸ 0.037	¹⁵⁰ 0.119	¹⁶⁰ 0.097	¹⁷¹ 0.061																				
160	MEGVII-002	²⁵⁷ 0.258	²²⁵ 0.077	²²⁹ 0.037	¹⁵¹ 0.120	¹⁶⁶ 0.096	¹⁶⁸ 0.059	¹⁸³ 0.999	¹⁹⁸ 0.998	¹³⁴ 0.872																	
161	MICROFOCUS-003	³²² 0.958	³² 0.931	³¹ 0.866	³¹⁸ 0.988	³²⁵ 0.979	³²⁶ 0.948			²⁵² 0.982	²⁵² 0.945											²³² 0.991	²⁴⁴ 0.977				
162	MICROFOCUS-004	³³¹ 0.999	³³³ 0.999	³³⁷ 0.999	³¹⁷ 0.984	³²⁵ 0.975	³²⁵ 0.940			²⁵⁰ 0.974	²⁵¹ 0.935											²³⁹ 0.989	²⁴³ 0.976				
163	MICROFOCUS-005	³¹⁷ 0.883	³²⁵ 0.835	³²⁹ 0.736	³⁰⁷ 0.951	³¹⁹ 0.928	³²¹ 0.865			²⁴⁸ 0.935	²⁴⁹ 0.848											²²⁹ 0.985	²⁴² 0.965				
164	MICROFOCUS-006	³²⁶ 0.983	³³⁰ 0.978	³³² 0.963	³⁰⁶ 0.950	³¹⁹ 0.923	³²⁰ 0.858			²⁴⁷ 0.923	²⁴⁷ 0.843											²²³ 0.971	²³⁹ 0.939				
165	MICROSOFT-003	¹²⁶ 0.049	¹⁵⁴ 0.028	¹⁵³ 0.012	¹⁴⁵ 0.117	¹⁴⁸ 0.091	¹⁶⁴ 0.056			¹²⁷ 0.036	¹³³ 0.019											⁹⁵ 0.233	¹¹⁵ 0.176				
166	MICROSOFT-004	¹²⁰ 0.046	¹⁴⁵ 0.026	¹⁴⁴ 0.011	¹⁴¹ 0.111	¹⁵² 0.087	¹⁵⁷ 0.053			¹²² 0.033	¹³⁰ 0.018											⁹¹ 0.222	¹¹² 0.170				
167	MICROSOFT-005	¹²² 0.047	¹⁴² 0.026	¹⁴⁴ 0.010	¹¹⁸ 0.090	¹²⁰ 0.070	¹³⁰ 0.041	¹⁹⁷ 0.999	³³ 0.587	⁶⁴ 0.354	¹⁰² 0.027	¹⁰⁶ 0.013										²⁰ 0.180	⁸⁷ 0.134				
168	MICROSOFT-006	⁷⁷ 0.025	⁸⁸ 0.012	⁹⁶ 0.006	⁶⁴ 0.048	⁷¹ 0.037	⁸¹ 0.024	²⁴ 0.452	³¹ 0.386	⁵² 0.281	¹¹⁸ 0.032	¹¹⁶ 0.015										²⁰ 0.178	⁸⁹ 0.138				
169	MUKH-002	³³² 0.999	³¹³ 0.594	²⁸⁰ 0.110	²⁴⁰ 0.326	²⁵¹ 0.242	²⁵⁵ 0.153	²⁴³ 1.000	²⁴⁴ 1.000	¹⁹³ 0.987	¹⁹⁹ 0.170	²⁰⁴ 0.089	¹²⁷ 0.741	¹³¹ 0.382	¹³⁴ 0.389	¹⁶⁶ 0.286											
170	NEC-000	¹⁸⁸ 0.113	²²⁸ 0.079	²⁴⁴ 0.047	¹⁹⁶ 0.171	²⁰⁸ 0.140	²¹⁵ 0.093	¹⁰⁷ 0.983	¹²⁴ 0.979	¹⁷⁶ 0.969												¹⁵¹ 0.474	¹⁹² 0.377				
171	NEC-001	²¹³ 0.148	²⁴⁵ 0.106	²⁵⁷ 0.060	²²⁸ 0.238	²³⁴ 0.197	²⁴⁴ 0.133	¹²⁵ 0.991	¹³⁹ 0.986	¹⁷² 0.972	¹⁸⁷ 0.133	²⁰³ 0.082										¹⁵¹ 0.468	¹⁹³ 0.378				
172	NEC-002	³⁹ 0.018	²³ 0.003	²⁸ 0.002	³⁶ 0.029	³² 0.020	³⁰ 0.013	²⁰⁷ 1.000	²¹⁸ 0.999	²²² 0.995	⁴⁵ 0.008	⁶² 0.005										¹⁸⁰ 0.676	¹⁷² 0.292				
173	NEC-003	¹⁸ 0.005	²⁰ 0.002	³⁰ 0.002	²⁴ 0.021	²⁵ 0.017	²⁹ 0.013	⁷⁰ 0.902	⁸⁰ 0.824	⁹⁸ 0.628																	

MISSES BELOW THRESHOLD, T		ENROL RECENT MUGSHOT, N = 1.6M												ENROL APPLICATION PORTRAIT, N = 1.6M									
#	ALGORITHM	ENROL: MUGSHOT			ENROL: MUGSHOT			ENROL: WEBCAM			PROBE: PROFILE			ENROL: VISA		ENROL: BORDER		ENROL: 10+YR		ENROL: KIOSK			
		FPIR=0.0003	FPIR=0.001	FPIR=0.01	FPIR=0.0003	FPIR=0.001	FPIR=0.01	FPIR=0.0003	FPIR=0.001	FPIR=0.01	FPIR=0.0003	FPIR=0.001	FPIR=0.01	FPIR=0.001	FPIR=0.01	FPIR=0.001	FPIR=0.01	FPIR=0.001	FPIR=0.01	FPIR=0.001	FPIR=0.01		
185	NEUROTECHNOLOGY-010	²⁶⁹ 0.346	⁸¹ 0.010	⁶⁰ 0.003	⁶⁰ 0.047	⁷⁸ 0.037	⁷⁸ 0.023	²¹ 0.377	²³ 0.277	³⁴ 0.170	⁶⁰ 0.010	⁵⁶ 0.005	⁴⁵ 0.075	⁴⁹ 0.039	⁴³ 0.126	⁴⁹ 0.097							
186	NEUROTECHNOLOGY-012	¹⁷³ 0.092	⁶³ 0.007	⁵¹ 0.002	⁶⁰ 0.045	⁶¹ 0.032	⁵⁹ 0.019	²²⁸ 1.000	¹⁰³ 0.959	²⁷ 0.149	⁵² 0.008	³⁸ 0.004	³³ 0.061	³⁶ 0.028	²¹⁴ 0.916	³⁷ 0.088							
187	NEUROTECHNOLOGY-013	¹⁴⁵ 0.059	⁴² 0.004	²⁸ 0.002	³⁷ 0.030	³⁷ 0.023	³⁶ 0.014	⁹¹ 0.975	²⁸ 0.324	¹⁷ 0.117	²⁹ 0.006	²² 0.003	²⁵ 0.046	²³ 0.022	¹⁷⁷ 0.641	³² 0.083							
188	NEWLAND-002	²⁹² 0.523	³⁰⁶ 0.438	³⁰⁹ 0.294	²⁷² 0.535	²⁸⁷ 0.466	²⁹⁴ 0.335	¹⁹⁵ 0.999	²¹⁰ 0.999	²⁴⁴ 0.998													
189	NOBLIS-001	³³⁵ 1.000	³³⁵ 1.000	³³⁵ 0.991	³³⁹ 1.000	³²⁷ 1.000	³³¹ 1.000	²⁴⁴ 1.000	²⁶⁶ 1.000	²⁷ 1.000													
190	NOBLIS-002	³³³ 1.000	³³¹ 0.997	³¹⁸ 0.488	³³¹ 1.000	³³⁵ 1.000	²⁵⁰ 1.000	²⁵¹ 1.000	²⁸² 1.000														
191	NOTIONTAG-000	⁹³ 0.032	¹¹⁰ 0.017	¹¹⁴ 0.007	¹⁰⁵ 0.076	¹¹⁷ 0.059	¹¹⁷ 0.036	⁴⁶ 0.671	⁵⁵ 0.611	⁷⁴ 0.467	⁹² 0.021	⁹⁵ 0.011	⁶⁹ 0.150	⁸² 0.084	⁷³ 0.176	⁹¹ 0.140							
192	NTECHLAB-003	¹⁶⁵ 0.080	¹⁹⁹ 0.054	²¹² 0.028	¹⁷⁸ 0.148	¹⁸⁵ 0.118	¹⁹⁷ 0.075	⁶⁶ 0.873	⁸² 0.837	¹¹⁷ 0.752													
193	NTECHLAB-004	¹⁵¹ 0.063	¹⁷⁴ 0.041	¹⁸⁷ 0.021	¹⁶⁷ 0.131	¹⁷⁷ 0.105	¹⁸⁰ 0.065	⁶⁵ 0.868	⁸¹ 0.833	¹¹⁵ 0.746	¹⁵¹ 0.053	¹⁵⁷ 0.030									¹⁰⁶ 0.263	¹⁴¹ 0.214	
194	NTECHLAB-005	¹⁵⁰ 0.062	¹⁷⁵ 0.042	¹⁸⁸ 0.021	¹⁶² 0.130	¹⁷³ 0.102	¹⁷⁹ 0.063	⁵⁹ 0.816	⁷³ 0.771	¹⁰⁶ 0.661	¹⁶⁷ 0.073	¹⁷¹ 0.039									¹¹⁴ 0.294	¹⁴⁶ 0.227	
195	NTECHLAB-006	¹⁴² 0.056	¹⁶⁹ 0.037	¹⁷⁷ 0.018	¹⁵² 0.121	¹⁶¹ 0.094	¹⁶⁷ 0.059	⁵⁷ 0.802	⁷¹ 0.754	¹⁰¹ 0.635	¹⁵⁵ 0.057	¹⁶¹ 0.032									¹⁰⁶ 0.260	¹³⁴ 0.207	
196	NTECHLAB-007	¹⁰⁵ 0.040	¹⁴¹ 0.026	¹⁵⁴ 0.012	¹¹¹ 0.085	¹²² 0.067	¹²⁸ 0.041	⁵⁶ 0.796	⁷⁰ 0.750	¹⁰² 0.642	¹¹⁹ 0.032	¹²² 0.017									⁹² 0.223	¹¹⁴ 0.176	
197	NTECHLAB-008	⁷⁴ 0.024	⁹⁹ 0.014	¹⁰⁷ 0.007	⁷⁶ 0.057	⁸⁰ 0.045	⁹² 0.029	²⁶ 0.601	⁴⁹ 0.529	⁷⁰ 0.391	¹²³ 0.033	¹³¹ 0.018									⁸⁰ 0.183	⁹² 0.140	
198	NTECHLAB-009	³⁸ 0.010	⁵² 0.005	⁵⁷ 0.003	³⁹ 0.028	³⁶ 0.022	³⁵ 0.014	²⁷ 0.522	³⁵ 0.430	⁵⁷ 0.311	⁷³ 0.015	⁷⁶ 0.008	⁵⁵ 0.109	⁶² 0.061	⁵⁴ 0.142	⁶² 0.114							
199	NTECHLAB-010	²¹ 0.005	²² 0.003	¹⁷ 0.002	²¹ 0.018	²² 0.015	¹⁸ 0.011	²⁰ 0.334	²² 0.252	³³ 0.169	³² 0.007	⁴² 0.004	³² 0.059	³⁹ 0.031	²⁴ 0.098	¹⁹ 0.077							
200	NTECHLAB-011		²² 0.006	²⁸ 0.003	²¹ 0.002	²⁰ 0.018	²¹ 0.015	¹⁷ 0.010	¹⁸ 0.291	¹⁹ 0.228	³⁶ 0.150	³⁴ 0.009	⁵² 0.004	⁴¹ 0.074	⁴⁸ 0.038	¹⁷ 0.091	¹⁶ 0.075						
201	PANGIAM-000	⁵² 0.014	⁶⁰ 0.006	⁵³ 0.003	⁵⁵ 0.039	⁵⁸ 0.030	⁵⁶ 0.018	⁸⁹ 0.974	²⁷ 0.318	³³ 0.175	⁵⁹ 0.009	⁵⁴ 0.005	⁶⁰ 0.136	⁴² 0.033	³³ 0.105	³¹ 0.083							
202	PANGIAM-001	⁶⁷ 0.023	⁸⁷ 0.011	¹²⁰ 0.008	⁵² 0.039	⁵⁷ 0.030	⁶³ 0.020	⁴⁵ 0.650	³⁰ 0.383	³⁸ 0.180	²⁵ 0.009	⁴¹ 0.004	¹³⁴ 0.860	⁷⁷ 0.081	⁵⁵ 0.141	³³ 0.085							
203	PARAVISION-000	²⁶² 0.278	²³⁷ 0.089	²⁴⁵ 0.045	²⁶³ 0.447	²²⁴ 0.170	²²⁵ 0.100	²⁴⁶ 1.000	²¹² 0.999	²³⁸ 0.997	²³¹ 0.470	²³⁸ 0.443									²¹⁷ 0.926	²³⁰ 0.779	
204	PARAVISION-001	²⁰⁸ 0.140	¹⁸⁸ 0.049	¹⁸⁴ 0.020	²¹⁴ 0.207	¹⁹⁷ 0.128	¹⁹⁴ 0.074	²⁵⁷ 1.000	²⁰¹ 0.999	²¹⁸ 0.994	²²⁸ 0.444	²⁵⁷ 0.428									¹⁸⁸ 0.739	²¹² 0.573	
205	PARAVISION-002	¹⁷⁰ 0.085	¹⁸⁹ 0.050	¹⁹⁴ 0.022	¹⁸² 0.152	¹⁸⁸ 0.119	¹⁹⁹ 0.076	¹²⁸ 0.992	¹³³ 0.983	¹¹⁸ 0.748	¹⁷⁰ 0.080	¹⁷⁸ 0.043									¹⁵⁷ 0.497	¹⁶³ 0.268	
206	PARAVISION-003	¹⁵² 0.063	¹⁶⁷ 0.035	¹⁶⁸ 0.016	¹⁵⁷ 0.124	¹⁶⁷ 0.096	¹⁷⁰ 0.060	¹⁶¹ 0.997	¹⁶⁵ 0.994	¹¹¹ 0.733	¹⁵⁶ 0.058	¹⁶⁴ 0.034									¹¹⁷ 0.296	¹⁴⁹ 0.232	
207	PARAVISION-004	⁷⁶ 0.025	⁸⁸ 0.010	⁸³ 0.004	⁶⁶ 0.049	⁷⁹ 0.038	⁷⁹ 0.024	²³⁹ 1.000	²⁶⁴ 1.000	¹²¹ 0.797	⁸² 0.018	⁹¹ 0.011									²¹² 0.908	¹³⁷ 0.211	
208	PARAVISION-005	³⁵ 0.014	⁴⁰ 0.004	⁴⁶ 0.002	³⁹ 0.031	⁴⁰ 0.024	⁴⁹ 0.016	¹⁵⁹ 0.997	¹²⁶ 0.980	¹⁸¹ 0.081	⁶¹ 0.011	⁷⁷ 0.008									⁴⁶ 0.132	⁷¹ 0.120	
209	PARAVISION-007	¹²³ 0.048	³⁸ 0.004	³² 0.002	²⁷ 0.560	⁴⁵ 0.025	⁴² 0.015	²⁴⁵ 1.000	²⁶⁷ 1.000	²⁷⁶ 1.000	³³ 0.009	⁶⁷ 0.006	³⁶ 0.113	²⁷ 0.024	²⁶³ 1.000	³³¹ 1.000							
210	PARAVISION-009	²⁸ 0.007	²⁵ 0.003	¹² 0.001	³¹ 0.026	³⁰ 0.019	²² 0.012	³⁵ 0.778	⁶⁷ 0.735	⁸¹ 0.550	¹¹ 0.003	⁹ 0.002	¹⁶ 0.033	¹⁵ 0.015	⁸ 0.073	⁶ 0.061							
211	PARAVISION-012	¹⁵ 0.004	⁶ 0.002	⁶ 0.001	¹⁷ 0.16	¹⁵ 0.012	¹⁷ 0.006	⁸⁰ 0.999	³⁰ 0.546	⁴² 0.475	⁵¹ 0.272	⁸ 0.002	⁸ 0.002	¹⁰ 0.025	¹⁰ 0.012	⁴ 0.068	³ 0.057						
212	PIXELLALL-002	³⁰² 0.664	²⁴⁴ 0.105	²¹⁸ 0.030	³¹³ 0.974	²⁷⁷ 0.388	²³⁶ 0.083	²⁶⁸ 1.000	²²² 1.000	²³⁶ 0.602	¹⁸¹ 0.047										²⁷¹ 1.000	²³³ 1.000	
213	PIXELLALL-003	¹²⁵ 0.049	¹³¹ 0.022	¹³¹ 0.009	¹³³ 0.102	¹³¹ 0.073	¹³³ 0.043		²²⁷ 1.000	²⁴¹ 0.999	¹³⁰ 0.037	¹³⁶ 0.020									¹⁶ 0.554	¹⁵⁷ 0.255	
214	PIXELLALL-004	¹⁹¹ 0.120	¹¹⁸ 0.018	¹¹¹ 0.007	²⁹⁷ 0.783	¹⁴³ 0.079	¹¹⁸ 0.037		²⁸⁰ 1.000	²⁵³ 0.999	¹⁴⁶ 0.051	¹¹⁷ 0.015									²³³ 0.994	²⁴⁰ 0.942	
215	PIXELLALL-005	¹⁶⁴ 0.079	⁹⁰ 0.012	⁸³ 0.005	²⁶ 0.456	⁹⁶ 0.050	⁸⁹ 0.027		²⁶² 1.000	²⁶ 0.999	¹⁰³ 0.027	¹²³ 0.017	⁸⁷ 0.203	⁶⁷ 0.071							²³ 1.000	²⁴⁶ 0.983	
216	PTAKURATSATU-000	¹⁴⁴ 0.057	¹⁶⁸ 0.037	¹⁷³ 0.017	¹⁸⁸ 0.165	¹⁹³ 0.124	¹⁹¹ 0.071	⁸³ 0.947	⁹⁶ 0.924	¹³¹ 0.868	¹⁴³ 0.046	¹⁴³ 0.022	⁸⁹ 0.206	¹⁰¹ 0.120	⁹⁴ 0.232	¹¹⁸ 0.179							
217	QNAP-000	³²⁵ 0.972	²⁵⁵ 0.129	²⁴⁶ 0.052	³²² 0.998	²⁴¹ 0.238	²³⁸ 0.117	²⁶³ 1.000	²⁷³ 1.000	²⁷⁴ 1.000	²⁰⁴ 0.191	¹⁹³ 0.068	¹²⁰ 0.539	¹²⁷ 0.263	²³ 0.998	²⁴⁹ 0.985							
218	QNAP-001	¹⁶⁹ 0.083	¹⁹⁸ 0.054	²⁰⁷ 0.024	¹⁹⁴ 0.176	²⁰⁵ 0.137	²⁰⁸ 0.085	⁷⁹ 0.943	⁹⁷ 0.928	¹³³ 0.870	¹⁷¹ 0.081	¹⁷⁵ 0.041	¹¹⁰ 0.368	¹²² 0									

MISSES BELOW THRESHOLD, T		ENROL RECENT MUGSHOT, N = 1.6M												ENROL APPLICATION PORTRAIT, N = 1.6M														
#	ALGORITHM	ENROL: MUGSHOT			ENROL: MUGSHOT			ENROL: WEBCAM			ENROL: MUGSHOT			PROBE: PROFILE			ENROL: VISA			ENROL: BORDER			ENROL: BORDER 10+YR			ENROL: VISA		
		FPIR=0.0003	FPIR=0.001	FPIR=0.01	FPIR=0.0003	FPIR=0.001	FPIR=0.01	FPIR=0.0003	FPIR=0.001	FPIR=0.01	FPIR=0.0003	FPIR=0.001	FPIR=0.01	FPIR=0.0003	FPIR=0.001	FPIR=0.01	FPIR=0.001	FPIR=0.001	FPIR=0.01	FPIR=0.001	FPIR=0.001	FPIR=0.01	FPIR=0.001	FPIR=0.01	FPIR=0.001	FPIR=0.01		
231	RANKONE-012	64 ^{0.020}	68 ^{0.008}	70 ^{0.004}	100 ^{0.072}	102 ^{0.053}	94 ^{0.030}	62 ^{0.046}	66 ^{0.034}	62 ^{0.020}	172 ^{0.998}	181 ^{0.996}	45 ^{0.214}	109 ^{0.029}	111 ^{0.014}	65 ^{0.144}	66 ^{0.072}	130 ^{0.465}	80 ^{0.128}	138 ^{0.500}	187 ^{0.364}	173 ^{0.613}	189 ^{0.370}					
232	RANKONE-013	41 ^{0.010}	45 ^{0.005}	45 ^{0.002}	29 ^{0.003}	42 ^{0.033}	41 ^{0.024}	40 ^{0.015}																				
233	RANKONE-014	29 ^{0.008}	31 ^{0.003}	29 ^{0.002}																								
234	REALNETWORKS-000	27 ^{0.374}	28 ^{0.234}	29 ^{0.138}	26 ^{0.433}	27 ^{0.319}	28 ^{0.209}																					
235	REALNETWORKS-001	27 ^{0.374}	28 ^{0.234}	29 ^{0.138}	26 ^{0.433}	27 ^{0.319}	28 ^{0.209}																					
236	REALNETWORKS-002	27 ^{0.370}	28 ^{0.231}	29 ^{0.137}	25 ^{0.416}	27 ^{0.315}	28 ^{0.209}																					
237	REALNETWORKS-003	26 ^{0.273}	26 ^{0.159}	27 ^{0.090}	24 ^{0.342}	25 ^{0.266}	26 ^{0.172}	191 ^{0.999}	197 ^{0.998}	192 ^{0.987}	198 ^{0.164}	209 ^{0.103}																
238	REALNETWORKS-004	25 ^{0.242}	26 ^{0.158}	27 ^{0.090}	25 ^{0.353}	25 ^{0.263}	26 ^{0.169}	212 ^{1.000}	213 ^{0.999}	211 ^{0.992}	200 ^{0.170}	210 ^{0.103}																
239	REALNETWORKS-005	133 ^{0.052}	153 ^{0.028}	159 ^{0.012}	121 ^{0.094}	133 ^{0.074}	140 ^{0.047}	109 ^{0.984}	112 ^{0.971}	137 ^{0.896}	128 ^{0.037}	124 ^{0.017}	91 ^{0.223}	103 ^{0.123}	89 ^{0.215}	108 ^{0.165}												
240	REALNETWORKS-006	78 ^{0.025}	100 ^{0.015}	94 ^{0.006}	94 ^{0.068}	99 ^{0.053}	103 ^{0.032}	130 ^{0.993}	128 ^{0.980}	12 ^{0.838}	75 ^{0.016}	79 ^{0.008}	57 ^{0.120}	64 ^{0.063}	62 ^{0.154}	64 ^{0.116}												
241	REALNETWORKS-007	63 ^{0.019}	79 ^{0.010}	76 ^{0.004}	75 ^{0.057}	84 ^{0.043}	88 ^{0.027}	126 ^{0.992}	123 ^{0.979}	129 ^{0.855}	64 ^{0.012}	61 ^{0.005}	118 ^{0.463}	65 ^{0.063}	52 ^{0.140}	52 ^{0.100}												
242	REALNETWORKS-008	48 ^{0.012}	61 ^{0.006}	61 ^{0.003}	31 ^{0.037}	36 ^{0.029}	57 ^{0.018}	119 ^{0.988}	108 ^{0.968}	50 ^{0.271}	50 ^{0.008}	39 ^{0.004}	40 ^{0.068}	46 ^{0.035}	44 ^{0.129}	60 ^{0.110}												
243	RECOGNITO-000	26 ^{0.007}	42 ^{0.005}	29 ^{0.004}	12 ^{0.015}	8 ^{0.012}	9 ^{0.009}	12 ^{0.266}	12 ^{0.184}	19 ^{0.123}	39 ^{0.007}	32 ^{0.003}	125 ^{0.730}	134 ^{0.437}	18 ^{0.092}	11 ^{0.070}												
244	REMARKAI-000	195 ^{0.125}	202 ^{0.055}	196 ^{0.023}	191 ^{0.173}	189 ^{0.120}	188 ^{0.070}	202 ^{0.999}	211 ^{0.999}	223 ^{0.995}	166 ^{0.069}	163 ^{0.033}																
245	REMARKAI-000	237 ^{0.197}	253 ^{0.128}	256 ^{0.059}	228 ^{0.263}	235 ^{0.203}	241 ^{0.123}																					
246	REMARKAI-002	233 ^{0.188}	252 ^{0.124}	255 ^{0.059}	227 ^{0.248}	233 ^{0.196}	240 ^{0.122}	134 ^{0.993}	151 ^{0.991}	184 ^{0.980}																		
247	RENDIP-000	69 ^{0.023}	89 ^{0.012}	89 ^{0.005}	203 ^{0.189}	112 ^{0.059}	109 ^{0.034}	82 ^{0.945}	92 ^{0.894}	114 ^{0.744}	93 ^{0.022}	104 ^{0.013}	84 ^{0.185}	83 ^{0.089}	70 ^{0.167}	83 ^{0.130}												
248	REVEALMEDIA-000	70 ^{0.024}	91 ^{0.012}	93 ^{0.006}	73 ^{0.054}	82 ^{0.042}	85 ^{0.025}	49 ^{0.755}	63 ^{0.680}	88 ^{0.539}	91 ^{0.021}	92 ^{0.011}	52 ^{0.093}	56 ^{0.051}	56 ^{0.143}	66 ^{0.118}												
249	S1-000	204 ^{0.137}	155 ^{0.028}	148 ^{0.011}	160 ^{0.129}	148 ^{0.085}	144 ^{0.048}	265 ^{1.000}	272 ^{1.000}	92 ^{0.596}	145 ^{0.047}	132 ^{0.018}	269 ^{1.000}	102 ^{0.123}	321 ^{1.000}	217 ^{0.632}												
250	S1-001	138 ^{0.054}	107 ^{0.016}	106 ^{0.007}	86 ^{0.066}	96 ^{0.052}	108 ^{0.033}	127 ^{0.992}	137 ^{0.985}	16 ^{0.952}	84 ^{0.019}	88 ^{0.010}	59 ^{0.136}	77 ^{0.075}	58 ^{0.148}	66 ^{0.119}												
251	S1-002	146 ^{0.060}	57 ^{0.006}	53 ^{0.002}	115 ^{0.085}	59 ^{0.031}	53 ^{0.018}	73 ^{0.924}	14 ^{0.196}	10 ^{0.095}	37 ^{0.007}	28 ^{0.003}	133 ^{0.792}	117 ^{0.151}	204 ^{0.841}	94 ^{0.144}												
252	S1-003	130 ^{0.050}	75 ^{0.009}	67 ^{0.003}	20 ^{0.052}	72 ^{0.037}	69 ^{0.022}	240 ^{1.000}	240 ^{1.000}	197 ^{0.989}	72 ^{0.014}	65 ^{0.006}	113 ^{0.396}	47 ^{0.037}	256 ^{1.000}	136 ^{0.209}												
253	S1-004	72 ^{0.024}	39 ^{0.004}	40 ^{0.002}	44 ^{0.034}	42 ^{0.025}	47 ^{0.016}	229 ^{1.000}	184 ^{0.997}	41 ^{0.191}	27 ^{0.006}	29 ^{0.003}	36 ^{0.064}	249 ^{1.000}	30 ^{0.086}	31 ^{0.086}	30 ^{0.081}	136 ^{0.400}	174 ^{0.299}	170 ^{0.290}								
254	SCANOVATE-000	181 ^{0.103}	217 ^{0.067}	216 ^{0.030}	235 ^{0.296}	250 ^{0.240}	251 ^{0.150}	77 ^{0.931}	90 ^{0.893}	122 ^{0.803}	209 ^{0.215}	217 ^{0.118}																
255	SCANOVATE-001	197 ^{0.128}	229 ^{0.081}	222 ^{0.037}	231 ^{0.281}	241 ^{0.227}	247 ^{0.140}	78 ^{0.935}	95 ^{0.911}	128 ^{0.834}	205 ^{0.192}	211 ^{0.103}																
256	SENSETIME-000	99 ^{0.036}	128 ^{0.021}	132 ^{0.009}	105 ^{0.078}	117 ^{0.063}	125 ^{0.040}	288 ^{1.000}	333 ^{1.000}	194 ^{0.988}																		
257	SENSETIME-001	101 ^{0.036}	132 ^{0.022}	136 ^{0.010}	109 ^{0.080}	119 ^{0.064}	131 ^{0.041}																					
258	SENSETIME-002	102 ^{0.037}	101 ^{0.015}	167 ^{0.014}	156 ^{0.124}	54 ^{0.028}	76 ^{0.023}	158 ^{0.997}	162 ^{0.994}	183 ^{0.979}	117 ^{0.032}	128 ^{0.017}																
259	SENSETIME-003	14 ^{0.004}	12 ^{0.002}	11 ^{0.001}	11 ^{0.014}	11 ^{0.012}	10 ^{0.009}	38 ^{0.607}	43 ^{0.477}	58 ^{0.311}	46 ^{0.008}	69 ^{0.005}																
260	SENSETIME-004	9 ^{0.003}	9 ^{0.002}	10 ^{0.001}	15 ^{0.015}	14 ^{0.013}	15 ^{0.010}	19 ^{0.301}	20 ^{0.229}	29 ^{0.149}	26 ^{0.006}	36 ^{0.004}																
261	SENSETIME-005	43 ^{0.011}	19 ^{0.002}	7 ^{0.001}	23 ^{0.018}	20 ^{0.014}	13 ^{0.010}	11 ^{0.259}	11 ^{0.173}	13 ^{0.103}	33 ^{0.007}	40 ^{0.004}	27 ^{0.051}	26 ^{0.023}	32 ^{0.104}	44 ^{0.093}												
262	SENSETIME-006	17 ^{0.005}	11 ^{0.002}	7 ^{0.001}	16 ^{0.016}	12 ^{0.012}	7 ^{0.009}	180 ^{0.999}	195 ^{0.998}	10 ^{0.680}	15 ^{0.004}	14 ^{0.002}	17 ^{0.034}	17 ^{0.016}	19 ^{0.093}	24 ^{0.079}												
263	SENSETIME-007	8 ^{0.003}	4 ^{0.001}	5 ^{0.001}	5 ^{0.012}	5 ^{0.009}	4 ^{0.007}	211 ^{1.000}	216 ^{0.999}	85 ^{0.538}	9 ^{0.003}	7 ^{0.001}	9 ^{0.024}	9 ^{0.011}	14 ^{0.085}	15 ^{0.074}												
264	SENSETIME-008	4 ^{0.002}	3 ^{0.001}	3 ^{0.001} </td																								

MISSES BELOW THRESHOLD, T		ENROL RECENT MUGSHOT, N = 1.6M												ENROL APPLICATION PORTRAIT, N = 1.6M												
#	ALGORITHM	ENROL: MUGSHOT			ENROL: MUGSHOT			ENROL: MUGSHOT			ENROL: VISA			ENROL: BORDER			ENROL: VISA			ENROL: BORDER			PROBE: PROFILE			
		FPIR=0.0003	FPIR=0.001	FPIR=0.01	FPIR=0.0003	FPIR=0.001	FPIR=0.01	FPIR=0.0003	FPIR=0.001	FPIR=0.01	FPIR=0.0001	FPIR=0.01	FPIR=0.01	FPIR=0.0001	FPIR=0.01	FPIR=0.01	FPIR=0.0001	FPIR=0.01	FPIR=0.01	FPIR=0.0001	FPIR=0.01	FPIR=0.01	FPIR=0.0001	FPIR=0.01	FPIR=0.0001	FPIR=0.01
277	SYNESIS-003	187 0.111	215 0.065	218 0.032	183 0.155	192 0.123	200 0.078	88 0.973	104 0.960	139 0.911	168 0.075	170 0.039												119 0.314	151 0.235	
278	SYNESIS-003	300 0.648	312 0.582	316 0.443	299 0.708	305 0.646	305 0.524																		88 0.214	106 0.158
279	SYNESIS-005	127 0.050	140 0.025	152 0.011	116 0.088	129 0.072	134 0.043	142 0.995	134 0.984	118 0.795	120 0.032	119 0.016													67 0.161	77 0.125
280	T4ISB-000	83 0.027	108 0.016	147 0.011	92 0.068	108 0.053	110 0.034	33 0.566	46 0.510	73 0.463	89 0.021	88 0.010	129 0.759	117 0.177											234 0.994	234 0.817
281	TECH5-001	310 0.807	205 0.057	176 0.018	320 0.994	320 0.935	163 0.055	271 1.000	274 1.000	269 1.000	211 0.244	153 0.028												144 0.440	122 0.182	
282	TECH5-002	137 0.053	149 0.027	155 0.012	126 0.094	127 0.040	67 0.874	79 0.805	97 0.627	132 0.039	133 0.019	88 0.205	98 0.111													
283	TEVIAN-003	249 0.239	224 0.177	281 0.096	247 0.346	266 0.298	272 0.198																			
284	TEVIAN-004	222 0.170	247 0.117	266 0.063	218 0.216	228 0.176	237 0.115																			
285	TEVIAN-005	199 0.129	234 0.087	241 0.045	197 0.180	208 0.144	212 0.089	116 0.988	105 0.962	128 0.796															221 0.951	66 0.117
286	TEVIAN-006	73 0.024	80 0.010	86 0.005	57 0.041	62 0.032	67 0.021	32 0.562	34 0.425	54 0.291	76 0.016	80 0.009	50 0.093	56 0.050										41 0.033	54 0.102	
287	TEVIAN-007	44 0.011	35 0.005	36 0.003	34 0.028	35 0.022	38 0.015	26 0.504	26 0.301	40 0.183	38 0.009	37 0.005	41 0.065													
288	TIGER-000	283 0.462	301 0.390	308 0.261	274 0.565	289 0.500	296 0.366																			
289	TIGER-002	218 0.158	231 0.086	238 0.039	217 0.202	217 0.158	219 0.095	200 0.999	206 0.999	180 0.975																
290	TIGER-003	219 0.158	230 0.086	231 0.039	211 0.202	218 0.158	218 0.095																			
291	TONGYITRANS-000	184 0.107	223 0.074	239 0.038	177 0.141	181 0.112	187 0.069																			
292	TONGYITRANS-001	194 0.124	216 0.066	219 0.032	159 0.128	172 0.101	176 0.062																			
293	TOSHIBA-000	193 0.123	212 0.062	216 0.027	179 0.150	180 0.118	193 0.074	160 0.997	174 0.995	195 0.988																
294	TOSHIBA-001	244 0.225	207 0.058	178 0.019	167 0.133	159 0.092	162 0.054																			
295	TRUEFACE-000	118 0.046	117 0.018	122 0.008	106 0.079	118 0.062	121 0.039	147 0.995	87 0.882	76 0.499	110 0.030	122 0.016	86 0.194	99 0.111		82 0.188	95 0.145									
296	TURINGTECHVIP-001	314 0.865	292 0.345	149 0.011	311 0.967	314 0.850	266 0.173	201 0.999	156 0.993	44 0.205	251 0.978	248 0.754	222 1.000	153 1.000		238 0.999	248 0.984									
297	VD-000	321 0.950	326 0.917	336 0.827	311 0.968	322 0.946	322 0.871																			
298	VD-001	261 0.278	278 0.201	287 0.116	241 0.331	263 0.281	269 0.188																			
299	VD-002	212 0.144	227 0.079	225 0.036	208 0.188	218 0.148	213 0.092	169 0.998	177 0.996	191 0.987	176 0.095	182 0.048	109 0.367	121 0.220		131 0.372	165 0.280									
300	VD-003	248 0.234	183 0.046	181 0.020	168 0.133	171 0.100	175 0.061	199 0.999	208 0.999	218 0.994	147 0.051	152 0.027	94 0.244	104 0.133		121 0.315	129 0.203									
301	VERIDAS-001	166 0.080	171 0.037	171 0.016	136 0.106	146 0.082	150 0.051	133 0.993	142 0.987	150 0.938	138 0.044	147 0.023	96 0.266	107 0.146		168 0.264	130 0.204									
302	VERIDAS-002	167 0.080	172 0.037	170 0.016	137 0.106	144 0.082	149 0.051	132 0.993	143 0.987	151 0.938	139 0.044	148 0.023	97 0.266	108 0.146		107 0.264	131 0.204									
303	VERIDAS-003	158 0.072	109 0.017	101 0.006	97 0.071	106 0.055	106 0.033	177 0.998	183 0.997	144 0.927	86 0.020	90 0.011	68 0.150	74 0.078		77 0.178	93 0.142									
304	VERIDAS-004	80 0.026	38 0.006	56 0.003	47 0.034	47 0.025	50 0.017	124 0.990	122 0.979	125 0.822	44 0.008	55 0.005	31 0.058	40 0.029		41 0.118	56 0.107									
305	VERIJELAS-000	312 0.846	320 0.799	325 0.681	301 0.868	310 0.813	315 0.697	192 0.999	203 0.999	226 0.995	217 0.324	222 0.216	136 0.933	139 0.561		120 0.589	201 0.462									
306	VIGILANTSOLUTIONS-003	287 0.482	305 0.408	307 0.282	297 0.730	306 0.660	307 0.526	194 0.999	202 0.999	224 0.995																
307	VIGILANTSOLUTIONS-004	299 0.624	311 0.549	315 0.422	300 0.858	312 0.817	316 0.709	174 0.998	180 0.996	207 0.991																
308	VIGILANTSOLUTIONS-005	320 0.936	300 0.388	254 0.043							252 1.000	253 1.000	281 1.000													
309	VIGILANTSOLUTIONS-006	323 0.959	295 0.353	237 0.043							248 1.000	221 1.000	280 1.000													
310	VIGILANTSOLUTIONS-007	163 0.076	138 0.028	151 0.011	143 0.113	153 0.088	156 0.053	165 0.997	179 0.996	208 0.991	172 0.081	180 0.047	111 0.371	124 0.242		135 0.391	173 0.295									
311	VIGILANTSOLUTIONS-008	131 0.051	125 0.021	138 0.010	133 0.105	137 0.077	138 0.046	204 1.000	205 0.999	209 0.991	180 0.104	186 0.054	114 0.398	126 0.259		159 0.511	179 0.316									
312	VISIONBOX-000	159 0.073	114 0.018	110 0.007	98 0.071	109 0.057	114 0.035	139 0.995	150 0.990	178 0.974	96 0.023	103 0.012	67 0.146	76 0.081		68 0.162	78 0.126									
313	VISIONLABS-004	172 0.091	206 0.058	199 0.024	207 0.199	217 0.159	221 0.097	80 0.944	89 0.890	111 0.742																
314	VISIONLABS-005	168 0.080	190 0.050	183 0.020	208 0.183	209 0.147	210 0.087	81 0.945	88 0.888	112 0.736																
315	VISIONLABS-006	114 0.044	148 0.027	149 0.010	147 0.117	157 0.090	152 0.051	32 0.764	59 0.672	82 0.511																
316	VISIONLABS-007	113 0.044	142 0.027	137 0.010	146 0.117	156 0.090	151 0.051	31 0.764	60 0.672	81 0.511	116 0.031	114 0.014				81 0.185	97 0.145									
317	VISIONLABS-008	85 0.028	94 0.013	92 0.006	91 0.068	95 0.051	101 0.032	35 0.574	44 0.481	59 0.317	77 0.017	75 0.008				81 0.151	69 0.119									
318	VISIONLABS-009	47 0.012	46 0.005	37 0.002	40 0.032	47 0.025	51 0.017	76 0.930	77 0.799	43 0.196	51 0.008	51 0.004				37 0.113	45 0.093									
319	VISIONLABS-010	54 0.014	54 0.005	49 0.002	47 0.034	56 0.027	58 0.019				32 0.169	43 0.008	39 0.004	29 0.055	31 0.027		38 0.109	39 0.089		</td						

MISSES BELOW THRESHOLD, T		ENROL RECENT MUGSHOT, N = 1.6M												ENROL APPLICATION PORTRAIT, N = 1.6M															
#	ALGORITHM	ENROL: MUGSHOT			ENROL: MUGSHOT			ENROL: WEBCAM			ENROL: PROFILE			ENROL: VISA		ENROL: BORDER		ENROL: BORDER 10+YR		ENROL: VISA		ENROL: BORDER		ENROL: KIOSK					
		FPIR=0.0003	FPIR=0.001	FPIR=0.01	FPIR=0.0003	FPIR=0.001	FPIR=0.01	FPIR=0.0003	FPIR=0.001	FPIR=0.01	FPIR=0.0003	FPIR=0.001	FPIR=0.01	FPIR=0.001	FPIR=0.01	FPIR=0.001	FPIR=0.01	FPIR=0.001	FPIR=0.01	FPIR=0.001	FPIR=0.01	FPIR=0.001	FPIR=0.01	FPIR=0.001	FPIR=0.01				
323	VNPT-002	⁵¹ 0.013	⁶² 0.007	⁶⁵ 0.003	³⁶ 0.040	⁶¹ 0.032	⁶⁶ 0.021	³⁴ 0.568	²⁵ 0.292	³¹ 0.154	⁴⁰ 0.007	³⁰ 0.004	⁴² 0.072	⁴⁰ 0.031	²² 0.096	¹⁸ 0.075	¹³⁸ 0.404	¹⁶⁹ 0.289	²³¹ 0.991	²²⁹ 0.776	¹³² 0.381	¹⁶⁷ 0.287	³³² 1.000	²⁷⁵ 1.000					
324	VOCORD-003	²⁷⁰ 0.354	²⁵¹ 0.122	²⁴⁵ 0.048	²⁰⁵ 0.195	²¹⁵ 0.155	²¹⁶ 0.093	¹⁸¹ 0.999	¹⁹³ 0.998	²⁰² 0.991	¹⁹⁷ 0.157	²¹² 0.105																	
325	VOCORD-004	³¹¹ 0.826	²⁹⁶ 0.355	²⁴⁶ 0.051	²⁵⁵ 0.401	²²⁵ 0.173	²¹⁴ 0.093	²⁶² 1.000	²⁴¹ 1.000	²⁵² 0.999	²⁰⁶ 0.193	¹⁹⁰ 0.065																	
326	VOCORD-005	³⁰⁴ 0.689	²⁶⁵ 0.158	²³⁸ 0.044	¹⁸⁶ 0.161	¹⁹⁸ 0.130	²⁰³ 0.080	¹⁸⁹ 0.999	¹⁸⁵ 0.997	¹⁶⁹ 0.968	¹⁹¹ 0.138	²⁰⁶ 0.090																	
327	VOCORD-006	³³⁸ 1.000	³³⁸ 1.000	³³⁷ 1.000	³²⁷ 1.000	³³⁷ 1.000	³³³ 1.000	³²⁸ 1.000	³⁰⁴ 1.000	³³⁷ 1.000	²⁶² 1.000	²⁵⁷ 1.000																	
328	VTS-000	²⁹⁶ 0.605	³¹⁴ 0.598	³²² 0.595	²⁸² 0.624	³⁰¹ 0.619	³¹² 0.613	¹⁹⁸ 0.999	²¹⁵ 0.999	²⁴⁸ 0.998	²³⁹ 0.613	²⁴² 0.609	¹³⁰ 0.760	¹⁴⁶ 0.739	¹⁹⁰ 0.761	²²⁸ 0.749													
329	VTS-001	⁹⁶ 0.035	⁹⁵ 0.013	⁹⁰ 0.006	⁹⁴ 0.067	⁹⁵ 0.051	⁹⁵ 0.031	¹⁶⁸ 0.998	¹⁶¹ 0.994	⁸⁰ 0.510	⁹⁴ 0.022	¹⁰ 0.012	⁶⁴ 0.141	⁷⁵ 0.079	⁸⁴ 0.192	⁷⁹ 0.126													
330	VTS-002	¹³⁶ 0.053	¹⁴³ 0.026	¹⁴² 0.010	¹²⁷ 0.098	¹³⁴ 0.075	¹³⁹ 0.046	²¹⁵ 1.000	²²⁶ 1.000	¹⁶² 0.953	¹⁴¹ 0.045	¹⁵¹ 0.026	⁹² 0.231	¹⁰⁵ 0.133	¹⁴⁰ 0.417	¹²³ 0.187													
331	VTS-003	⁵⁷ 0.015	⁶⁷ 0.007	⁶² 0.003	⁶⁵ 0.048	⁶⁵ 0.033	⁶⁰ 0.019	²⁵⁹ 1.000	²⁴⁹ 1.000	¹⁰⁶ 0.632	⁷⁰ 0.014	⁵⁶ 0.005	¹³⁸ 0.954	⁶ 0.060	¹⁷⁶ 0.635	⁴⁶ 0.089													
332	XFORWARDAI-000	⁸⁷ 0.029	¹⁰⁴ 0.015	¹⁰⁵ 0.006	⁹⁵ 0.070	¹⁰³ 0.053	¹¹² 0.034	⁴⁸ 0.698	³⁶ 0.440	⁴⁷ 0.250	⁹⁰ 0.021	⁸⁹ 0.011	⁷³ 0.159	⁸⁰ 0.082	⁷¹ 0.169	⁸⁶ 0.134													
333	XFORWARDAI-001	⁴⁰ 0.010	⁵¹ 0.005	⁵⁰ 0.003	⁴⁹ 0.036	⁵² 0.028	⁶¹ 0.020	⁶² 0.838	³⁷ 0.448	²⁴ 0.143	⁴⁷ 0.008	³⁵ 0.005	³⁶ 0.062	³⁶ 0.030	⁴² 0.123	⁵³ 0.102													
334	XFORWARDAI-002	²⁵ 0.007	³⁰ 0.003	⁴⁴ 0.002	²² 0.018	²³ 0.016	³¹ 0.014	⁹² 0.975	⁴⁷ 0.525	⁹ 0.095	²³ 0.005	³⁰ 0.003	²¹ 0.041	²⁰ 0.018	²⁷ 0.099	³⁰ 0.089													
335	YISHENG-001	²⁸¹ 0.452	²⁹² 0.346	³⁰⁰ 0.206	³¹⁶ 0.983	³⁰⁹ 0.808	²⁸⁵ 0.269				²⁴² 0.666	²⁴⁶ 0.396										²¹⁵ 0.919	²²⁰ 0.695						
336	YITU-002	⁹¹ 0.031	¹¹² 0.018	¹¹⁶ 0.008	⁸⁰ 0.063	⁸⁹ 0.049	⁹⁰ 0.028																						
337	YITU-003	⁹² 0.032	¹²⁰ 0.019	¹²⁷ 0.009	⁸⁸ 0.067	⁹⁸ 0.052	¹⁰⁷ 0.033																						
338	YITU-004	⁶² 0.019	⁷⁷ 0.010	⁸¹ 0.004	⁴⁸ 0.035	⁵⁰ 0.027	⁵² 0.017	⁸⁴ 0.948	⁹⁸ 0.936	¹⁴⁰ 0.913																			
339	YITU-005	⁶⁶ 0.022	⁸⁴ 0.010	⁸⁷ 0.005	⁵⁴ 0.039	⁶³ 0.032	⁷⁴ 0.023																						

Table 41: **Threshold-based accuracy.** Values are FNIR(N, T, L) with N = 1.6 million with thresholds set to produce FPIR = 0.0003, 0.001, and 0.01 in non-mate searches. Throughout blue superscripts indicate the rank of the algorithm for that column. Caution: The Power-low models are mostly intended to draw attention to the kind of behavior, not as a model to be used for prediction.

2023 / 04 / 04 07:31:47

FNIR(N, R, T) = False neg. identification rate

N = Num. enrolled subjects

T = Threshold

T = 0 → Investigation

R = Num. candidates examined

T > 0 → Identification

Appendices

Appendix A Accuracy on large-population FRVT 2018 mugshots

2023/04/04 07:31:47	FNIR(N, R, T) = FPTR(N, T) =	False neg. identification rate False pos. identification rate	N = Num. enrolled subjects R = Num. candidates examined	T = Threshold	T = 0 → Investigation T > 0 → Identification
------------------------	---------------------------------	--	--	---------------	---

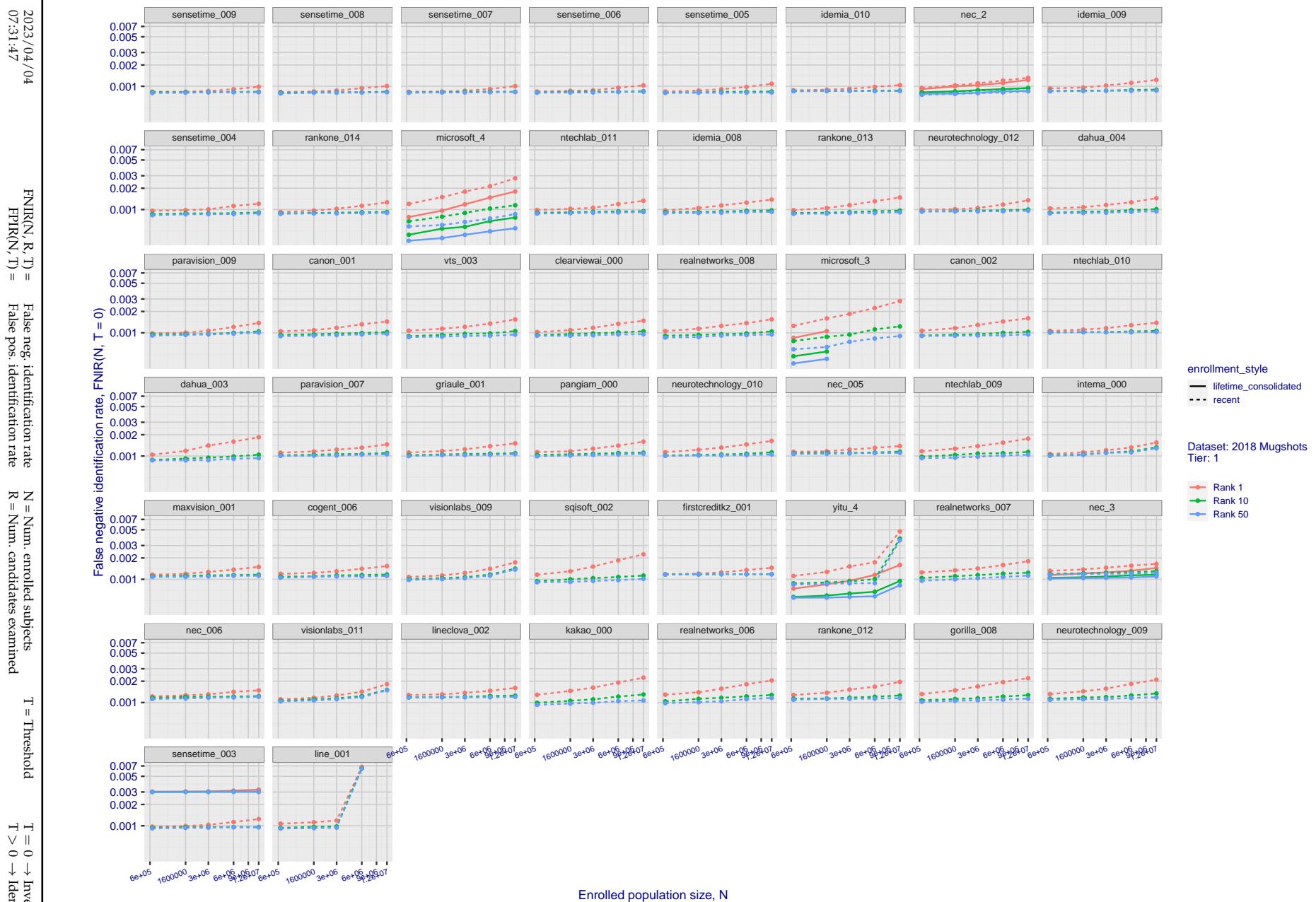


Figure 20: [FRVT-2018 Mugshot Dataset] Rank-based identification miss rates vs. number of enrolled subjects. The figure shows false negative identification rates, $\text{FNIR}(N, R)$, across various gallery sizes and ranks 1, 10 and 50. The threshold is set to zero, so this metric rewards even weak scoring rank 1 mates. This also means $\text{FPIR} = 1$, so any search without an enrolled mate will return non-mated candidates. For clarity, results are sorted and reported into tiers spanning multiple pages, the tiering criteria being rank 1 hit rate on a gallery size of 640 000.

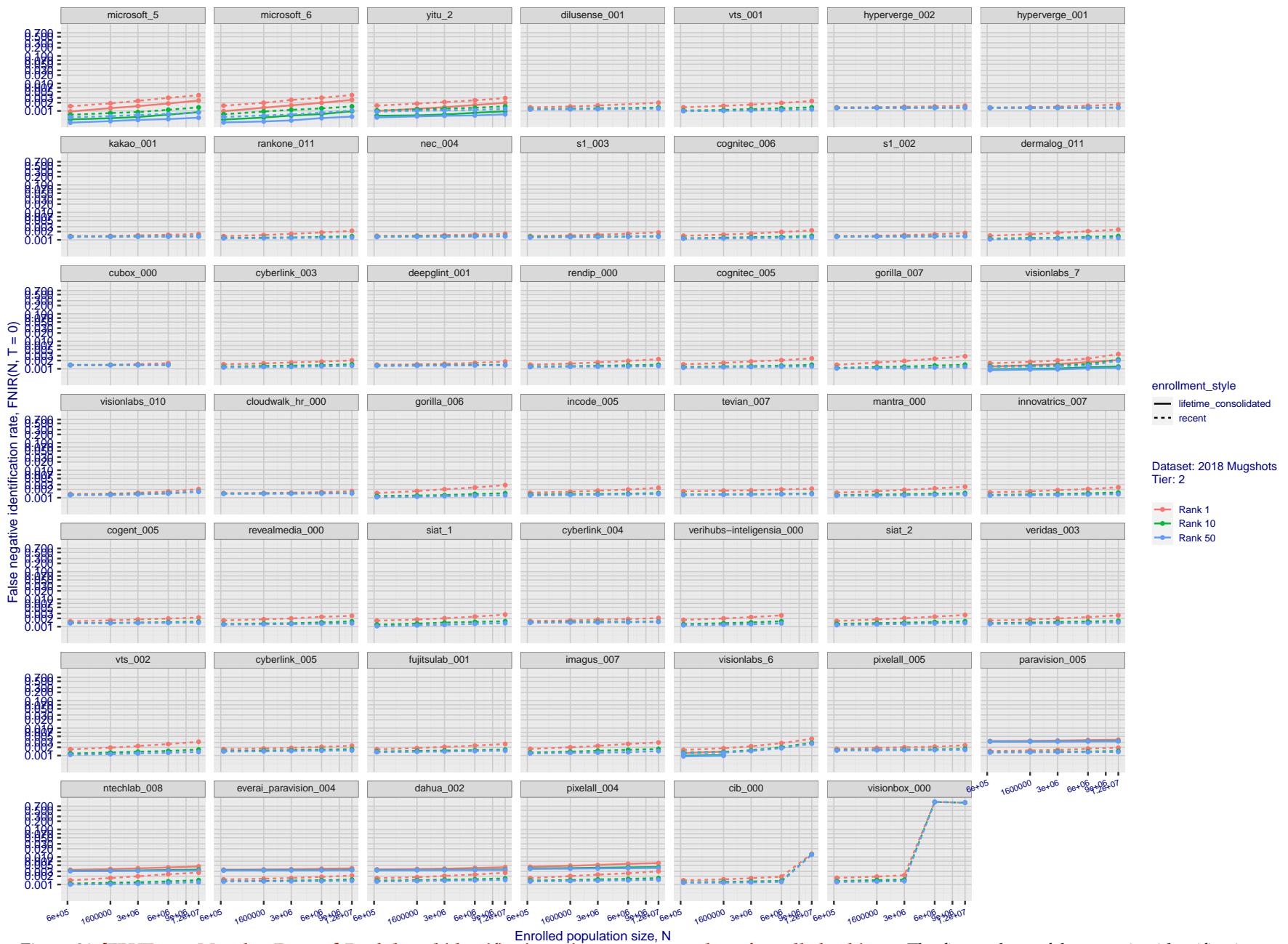


Figure 21: [FRVT-2018 Mugshot Dataset] Rank-based identification miss rates vs. number of enrolled subjects. The figure shows false negative identification rates, $\text{FNIR}(N, R)$, across various gallery sizes and ranks 1, 10 and 50. The threshold is set to zero, so this metric rewards even weak scoring rank 1 mates. This also means $\text{FPIR} = 1$, so any search without an enrolled mate will return non-mated candidates. For clarity, results are sorted and reported into tiers spanning multiple pages, the tiering criteria being rank 1 hit rate on a gallery size of 640 000.

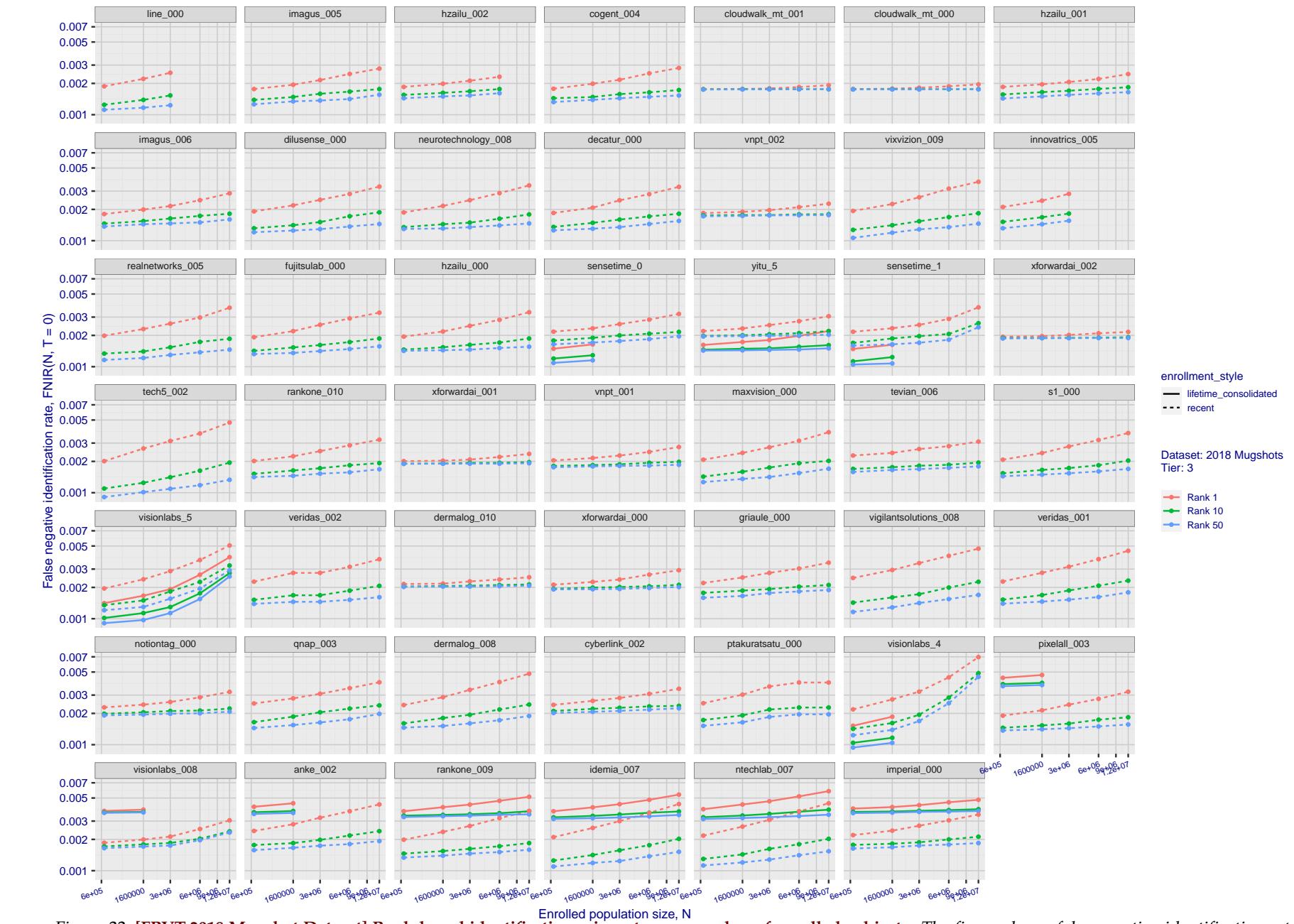


Figure 22: [FRVT-2018 Mugshot Dataset] Rank-based identification miss rates vs. number of enrolled subjects. The figure shows false negative identification rates, $FNIR(N, R)$, across various gallery sizes and ranks 1, 10 and 50. The threshold is set to zero, so this metric rewards even weak scoring rank 1 mates. This also means $FPIR = 1$, so any search without an enrolled mate will return non-mated candidates. For clarity, results are sorted and reported into tiers spanning multiple pages, the tiering criteria being rank 1 hit rate on a gallery size of 640 000.

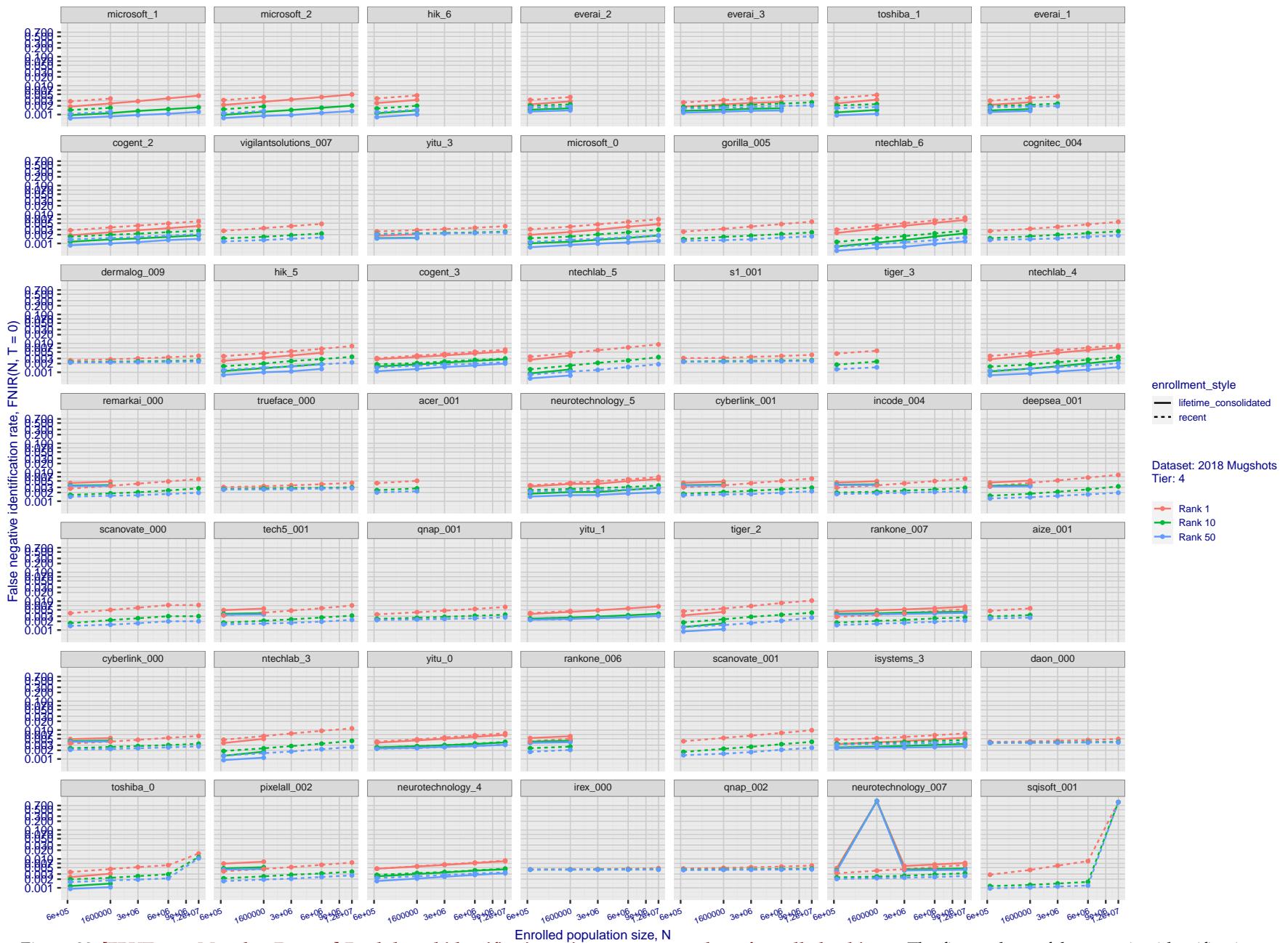


Figure 23: [FRVT-2018 Mugshot Dataset] Rank-based identification miss rates vs. number of enrolled subjects. The figure shows false negative identification rates, $\text{FNIR}(N, R)$, across various gallery sizes and ranks 1, 10 and 50. The threshold is set to zero, so this metric rewards even weak scoring rank 1 mates. This also means $\text{FPIR} = 1$, so any search without an enrolled mate will return non-mated candidates. For clarity, results are sorted and reported into tiers spanning multiple pages, the tiering criteria being rank 1 hit rate on a gallery size of 640 000.

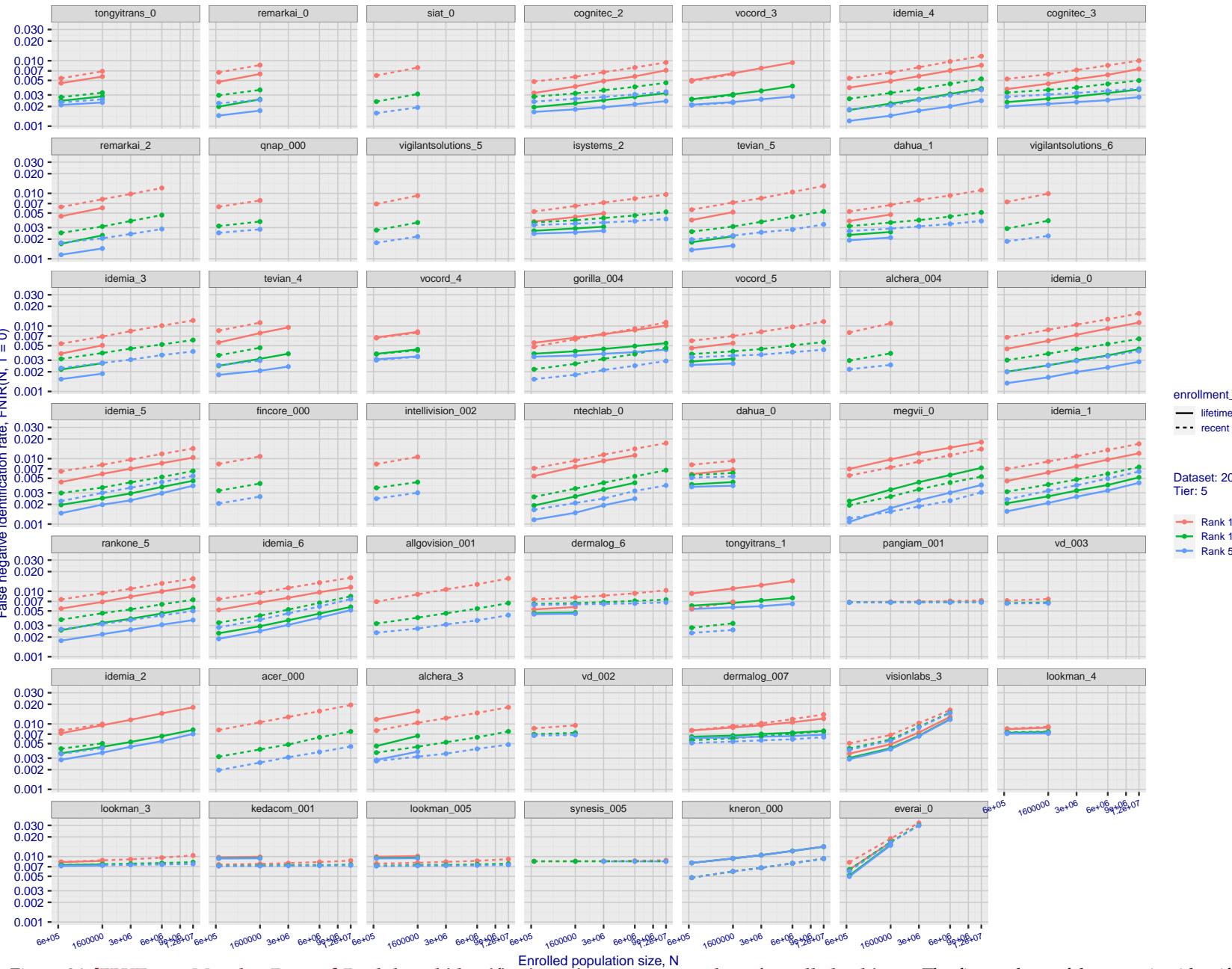
2023/04/04
07:31:47FNIR(N, R, T) = False neg. identification rate
FPIR(N, T) = False pos. identification rateN = Num. enrolled subjects
R = Num. candidates examined
T = ThresholdT = 0 → Investigation
T > 0 → Identification

Figure 24: [FRVT-2018 Mugshot Dataset] Rank-based identification miss rates vs. number of enrolled subjects. The figure shows false negative identification rates, FNIR(N, R), across various gallery sizes and ranks 1, 10 and 50. The threshold is set to zero, so this metric rewards even weak scoring rank 1 mates. This also means FPIR = 1, so any search without an enrolled mate will return non-mated candidates. For clarity, results are sorted and reported into tiers spanning multiple pages, the tiering criteria being rank 1 hit rate on a gallery size of 640 000.

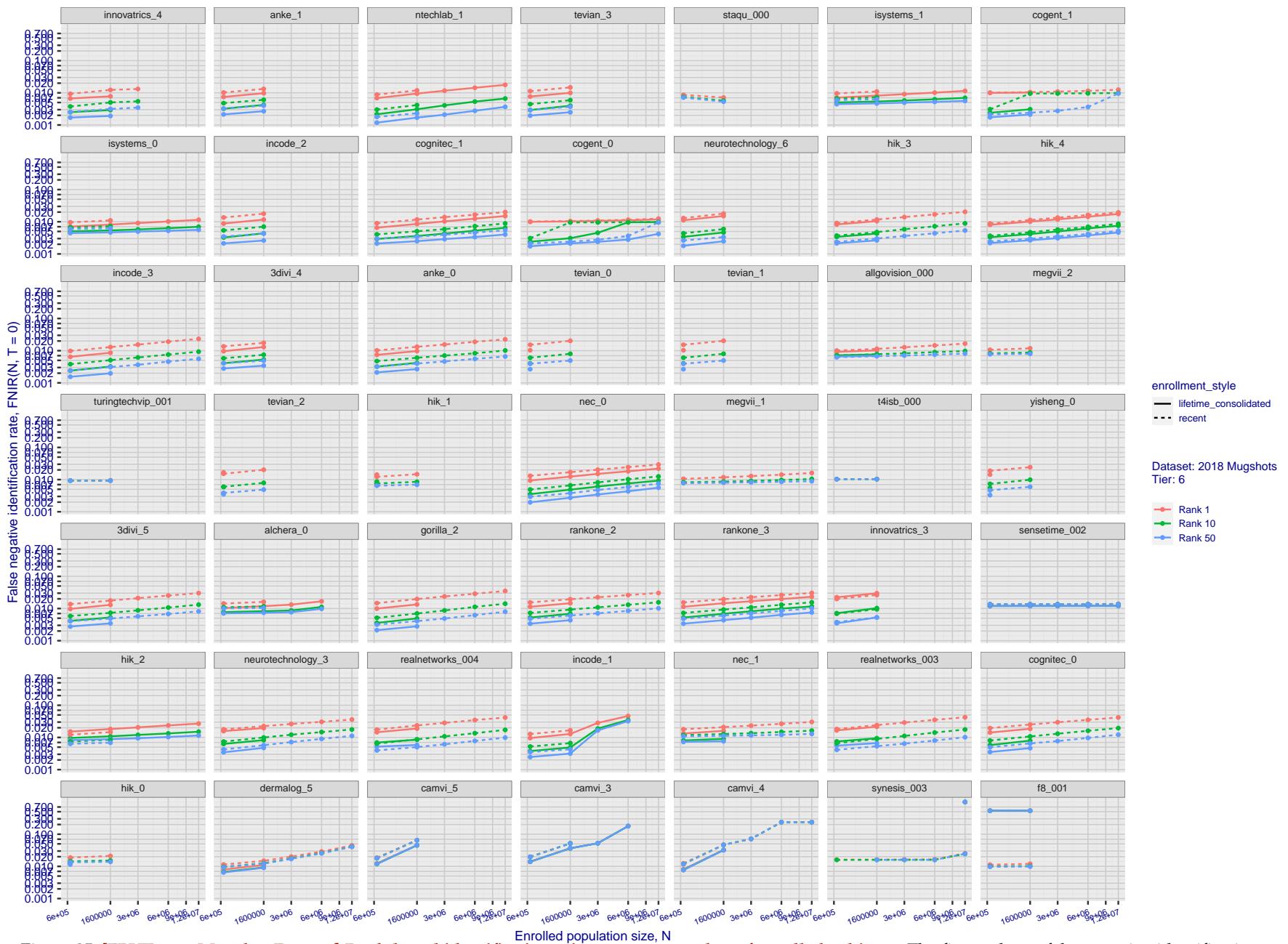


Figure 25: [FRVT-2018 Mugshot Dataset] Rank-based identification miss rates vs. number of enrolled subjects. The figure shows false negative identification rates, FNIR(N, R), across various gallery sizes and ranks 1, 10 and 50. The threshold is set to zero, so this metric rewards even weak scoring rank 1 mates. This also means FPIR = 1, so any search without an enrolled mate will return non-mated candidates. For clarity, results are sorted and reported into tiers spanning multiple pages, the tiering criteria being rank 1 hit rate on a gallery size of 640 000.

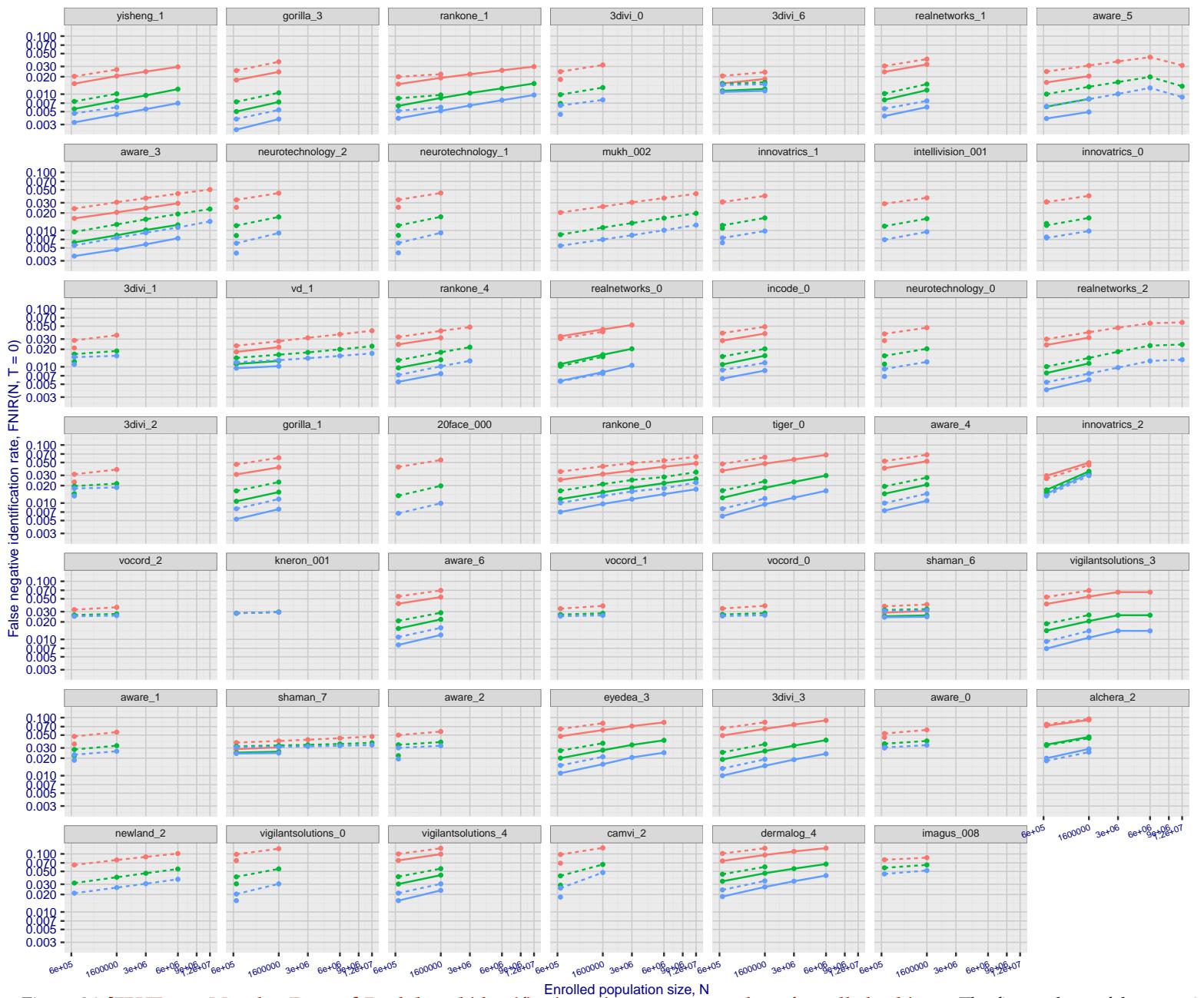


Figure 26: [FRVT-2018 Mugshot Dataset] Rank-based identification miss rates vs. number of enrolled subjects. The figure shows false negative identification rates, FNIR(N, R), across various gallery sizes and ranks 1, 10 and 50. The threshold is set to zero, so this metric rewards even weak scoring rank 1 mates. This also means FPIR = 1, so any search without an enrolled mate will return non-mated candidates. For clarity, results are sorted and reported into tiers spanning multiple pages, the tiering criteria being rank 1 hit rate on a gallery size of 640 000.

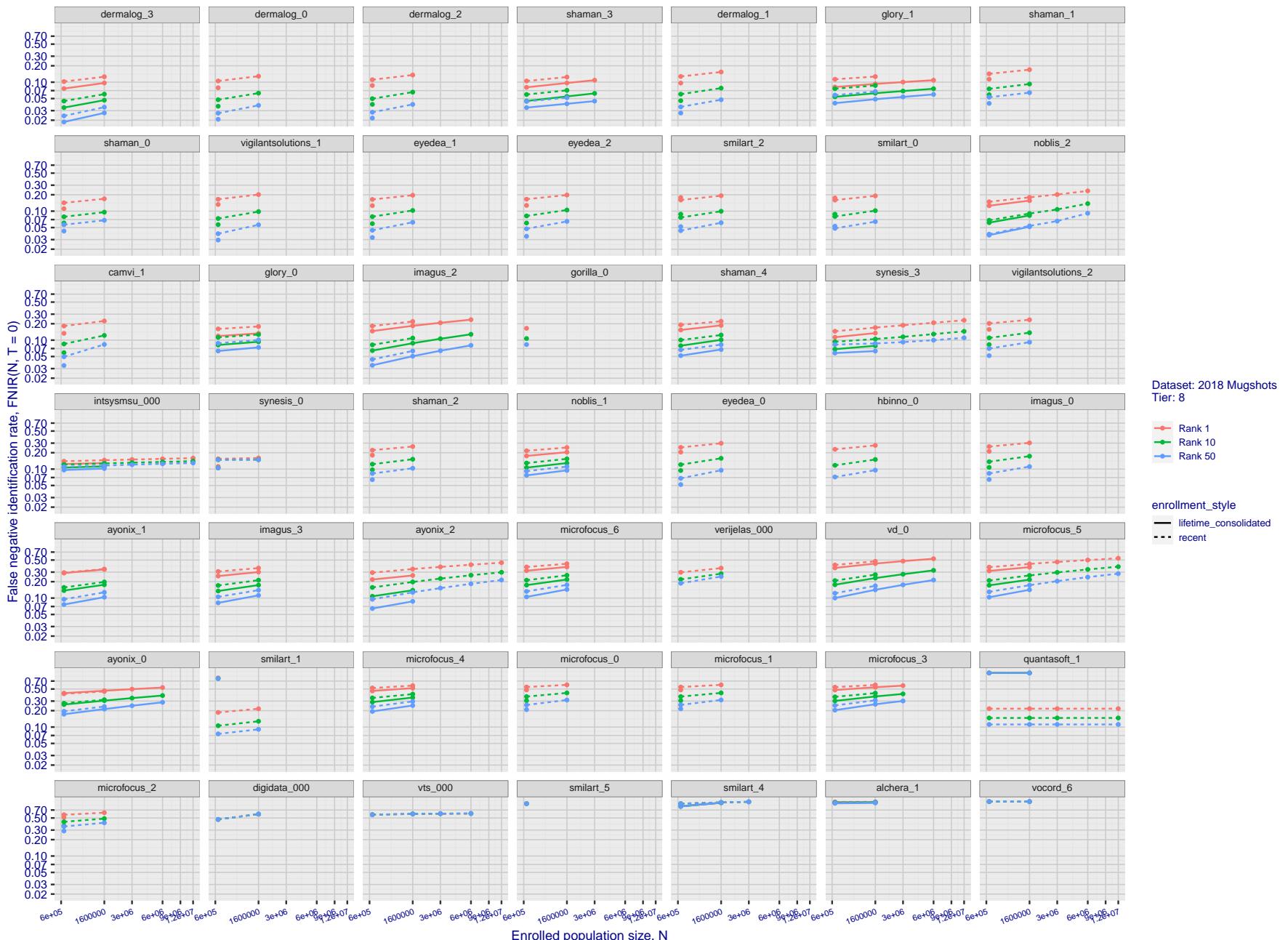


Figure 27: [FRVT-2018 Mugshot Dataset] Rank-based identification miss rates vs. number of enrolled subjects. The figure shows false negative identification rates, $\text{FNIR}(N, R)$, across various gallery sizes and ranks 1, 10 and 50. The threshold is set to zero, so this metric rewards even weak scoring rank 1 mates. This also means $\text{FPIR} = 1$, so any search without an enrolled mate will return non-mated candidates. For clarity, results are sorted and reported into tiers spanning multiple pages, the tiering criteria being rank 1 hit rate on a gallery size of 640 000.

2023/04/04 07:31:47	FNIR(N, R, T) = FPTR(N, T) =	False neg. identification rate False pos. identification rate	N = Num. enrolled subjects R = Num. candidates examined	T = Threshold T > 0 → Identification	T = 0 → Investigation
------------------------	---------------------------------	--	--	---	-----------------------

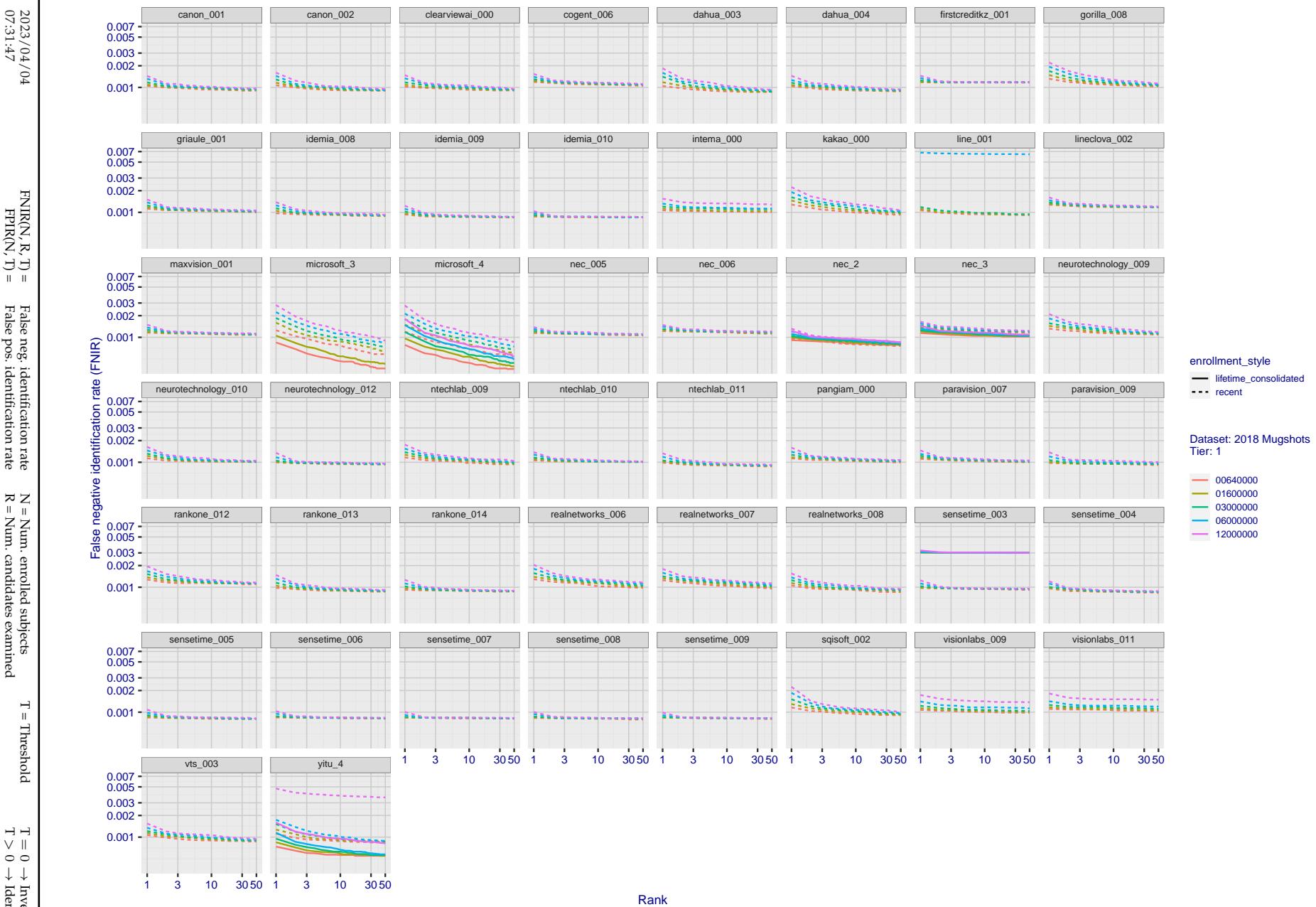


Figure 28: [FRVT-2018 Mugshot Dataset] Rank-based identification miss rates vs. rank. The figure shows false negative identification rates (FNIR) for ranks up to 50. This metric is appropriate to investigational applications where human reviewers will adjudicate sorted candidate lists. Note that with threshold set to zero, FPIR = 1, i.e. any search without an enrolled mate will return non-mated candidates. Results are sorted and reported into tiers for clarity, with the tiering criteria being rank 1 hit rate on a gallery size of N = 640 000 subjects.

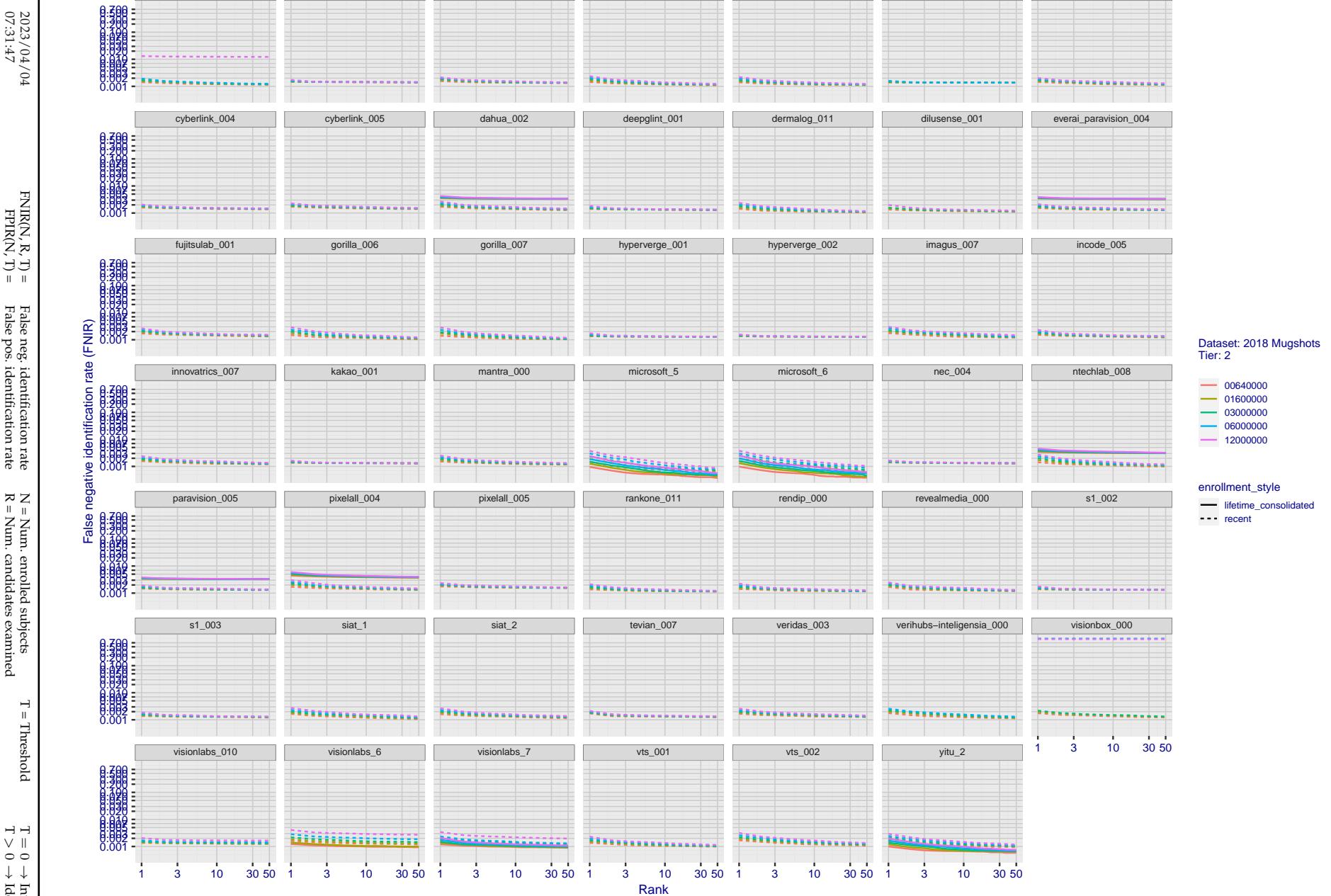


Figure 29: [FRVT-2018 Mugshot Dataset] Rank-based identification miss rates vs. rank. The figure shows false negative identification rates (FNIR) for ranks up to 50. This metric is appropriate to investigational applications where human reviewers will adjudicate sorted candidate lists. Note that with threshold set to zero, FPIR = 1, i.e. any search without an enrolled mate will return non-mated candidates. Results are sorted and reported into tiers for clarity, with the tiering criteria being rank 1 hit rate on a gallery size of N = 640 000 subjects.

2023/04/04
07:31:47FNIR(N, R, T) = False neg. identification rate
FPIR(N, T) = False pos. identification rateN = Num. enrolled subjects
R = Num. candidates examined

T = Threshold

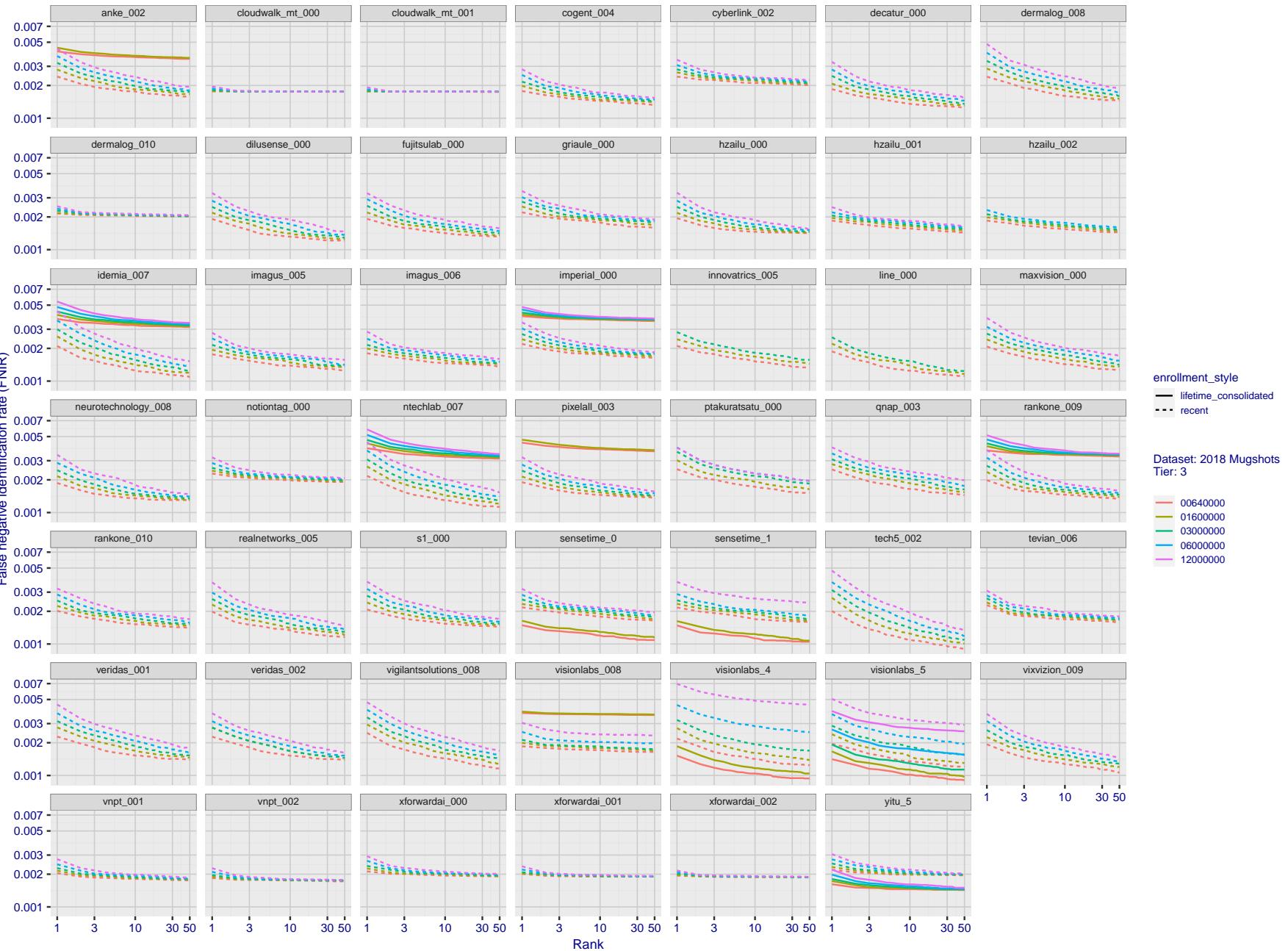
T = 0 → Investigation
T > 0 → Identification

Figure 30: [FRVT-2018 Mugshot Dataset] Rank-based identification miss rates vs. rank. The figure shows false negative identification rates (FNIR) for ranks up to 50. This metric is appropriate to investigational applications where human reviewers will adjudicate sorted candidate lists. Note that with threshold set to zero, FPIR = 1, i.e. any search without an enrolled mate will return non-mated candidates. Results are sorted and reported into tiers for clarity, with the tiering criteria being rank 1 hit rate on a gallery size of N = 640 000 subjects.

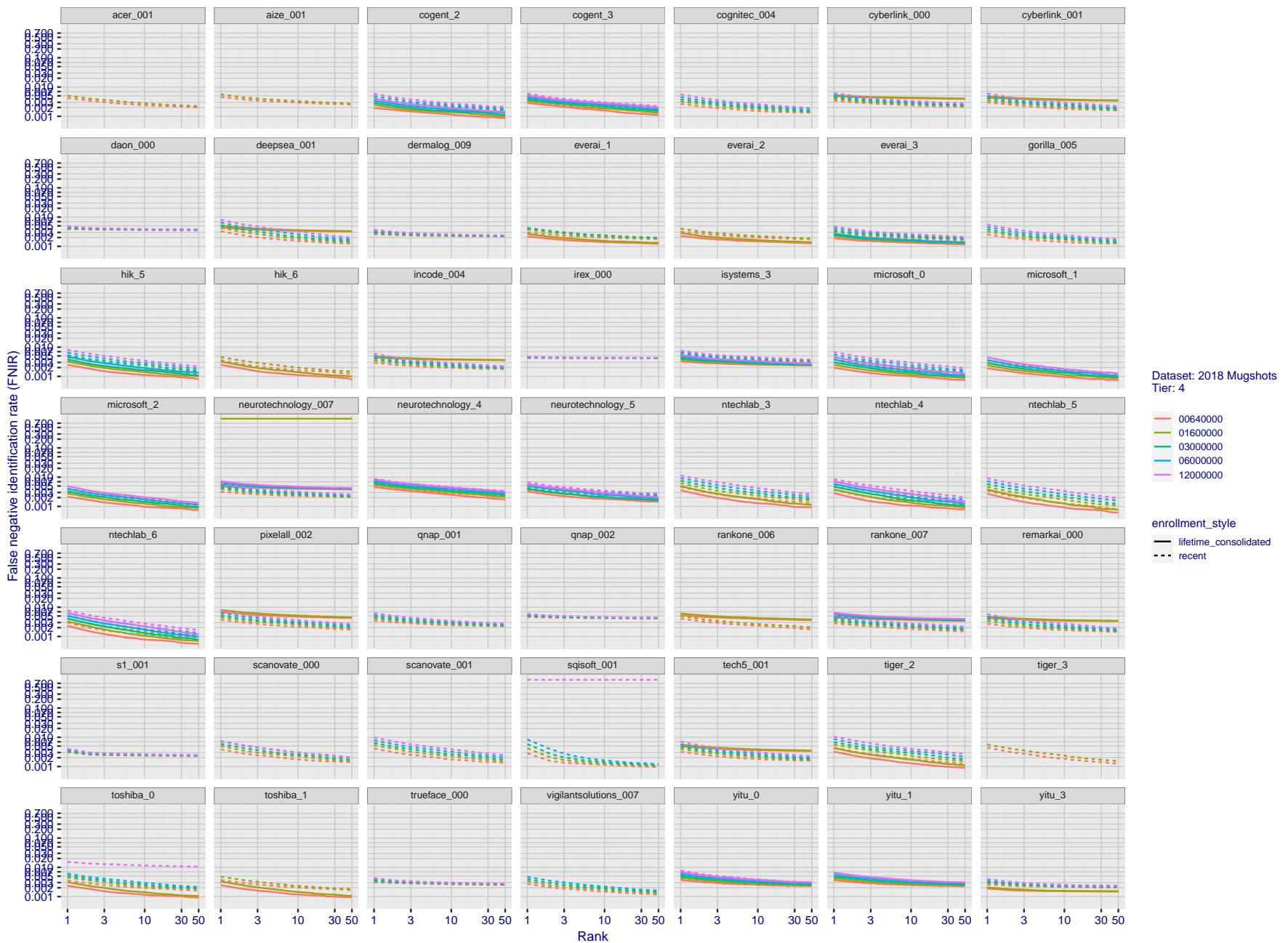


Figure 31: [FRVT-2018 Mugshot Dataset] Rank-based identification miss rates vs. rank. The figure shows false negative identification rates (FNIR) for ranks up to 50. This metric is appropriate to investigational applications where human reviewers will adjudicate sorted candidate lists. Note that with threshold set to zero, FPIR = 1, i.e. any search without an enrolled mate will return non-mated candidates. Results are sorted and reported into tiers for clarity, with the tiering criteria being rank 1 hit rate on a gallery size of $N = 640\,000$ subjects.

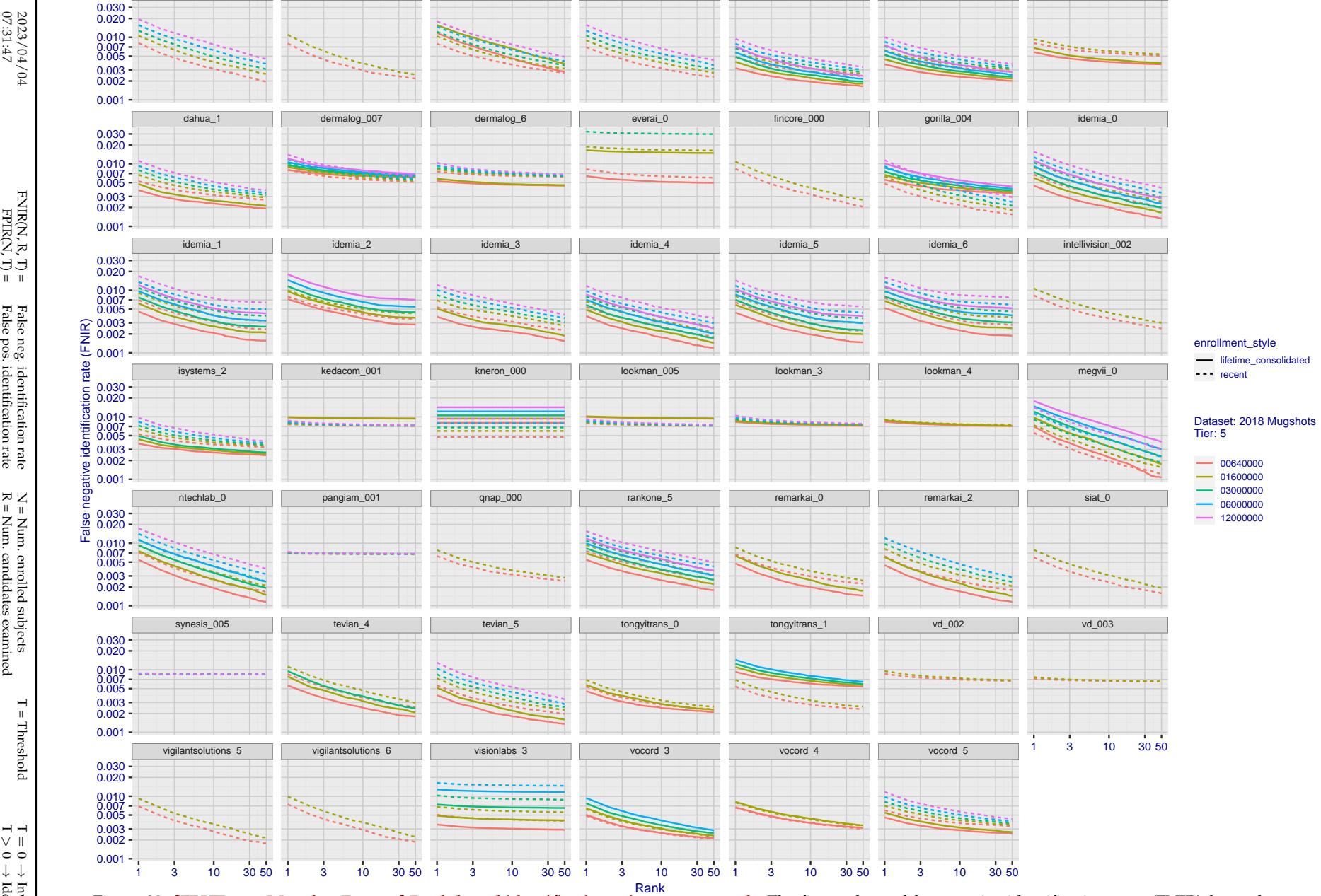


Figure 32: [FRVT-2018 Mugshot Dataset] Rank-based identification miss rates vs. rank. The figure shows false negative identification rates (FNIR) for ranks up to 50. This metric is appropriate to investigational applications where human reviewers will adjudicate sorted candidate lists. Note that with threshold set to zero, FPIR = 1, i.e. any search without an enrolled mate will return non-mated candidates. Results are sorted and reported into tiers for clarity, with the tiering criteria being rank 1 hit rate on a gallery size of N = 640 000 subjects.

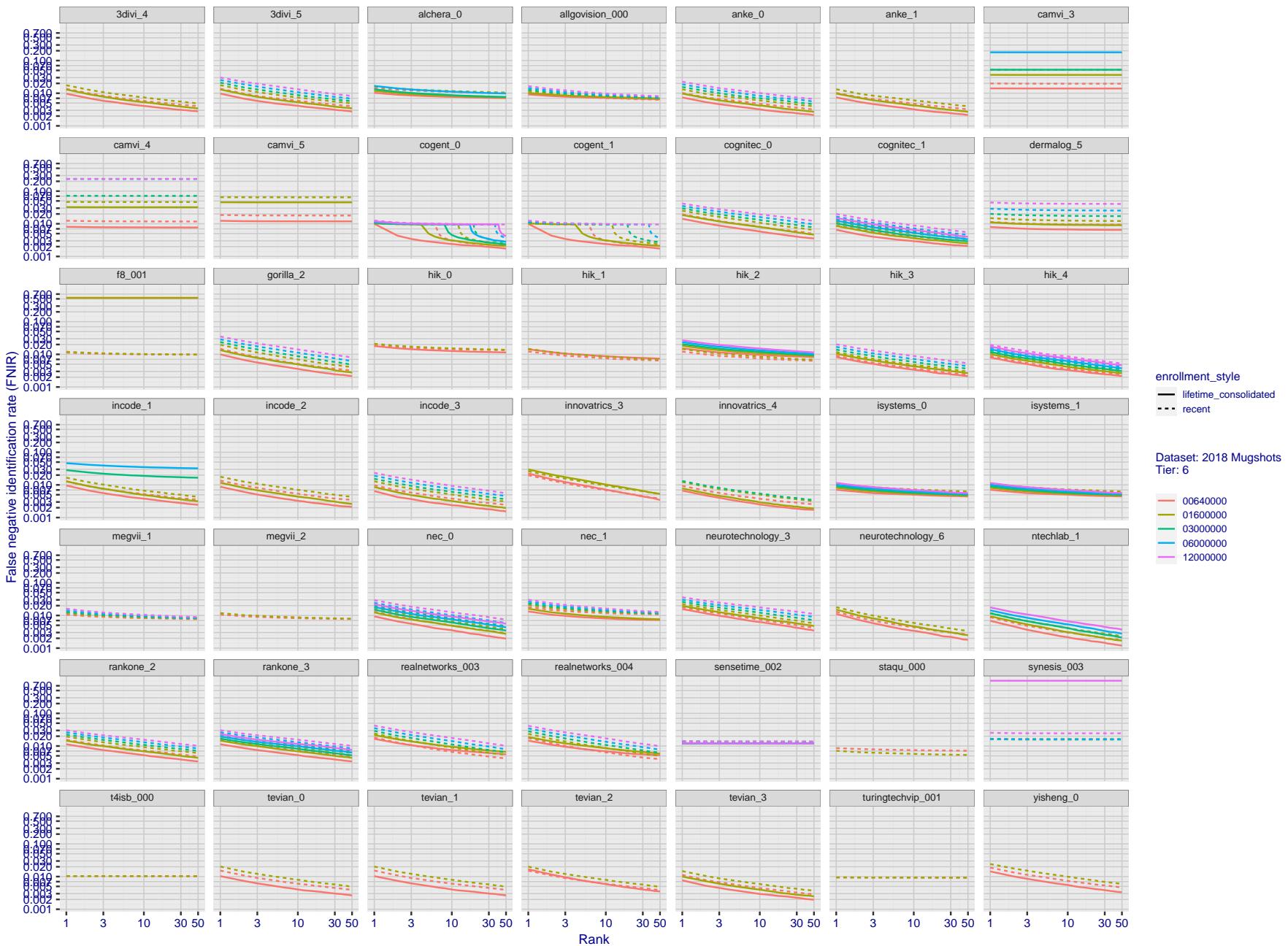


Figure 33: [FRVT-2018 Mugshot Dataset] Rank-based identification miss rates vs. rank. The figure shows false negative identification rates (FNIR) for ranks up to 50. This metric is appropriate to investigational applications where human reviewers will adjudicate sorted candidate lists. Note that with threshold set to zero, FPIR = 1, i.e. any search without an enrolled mate will return non-mated candidates. Results are sorted and reported into tiers for clarity, with the tiering criteria being rank 1 hit rate on a gallery size of $N = 640\,000$ subjects.

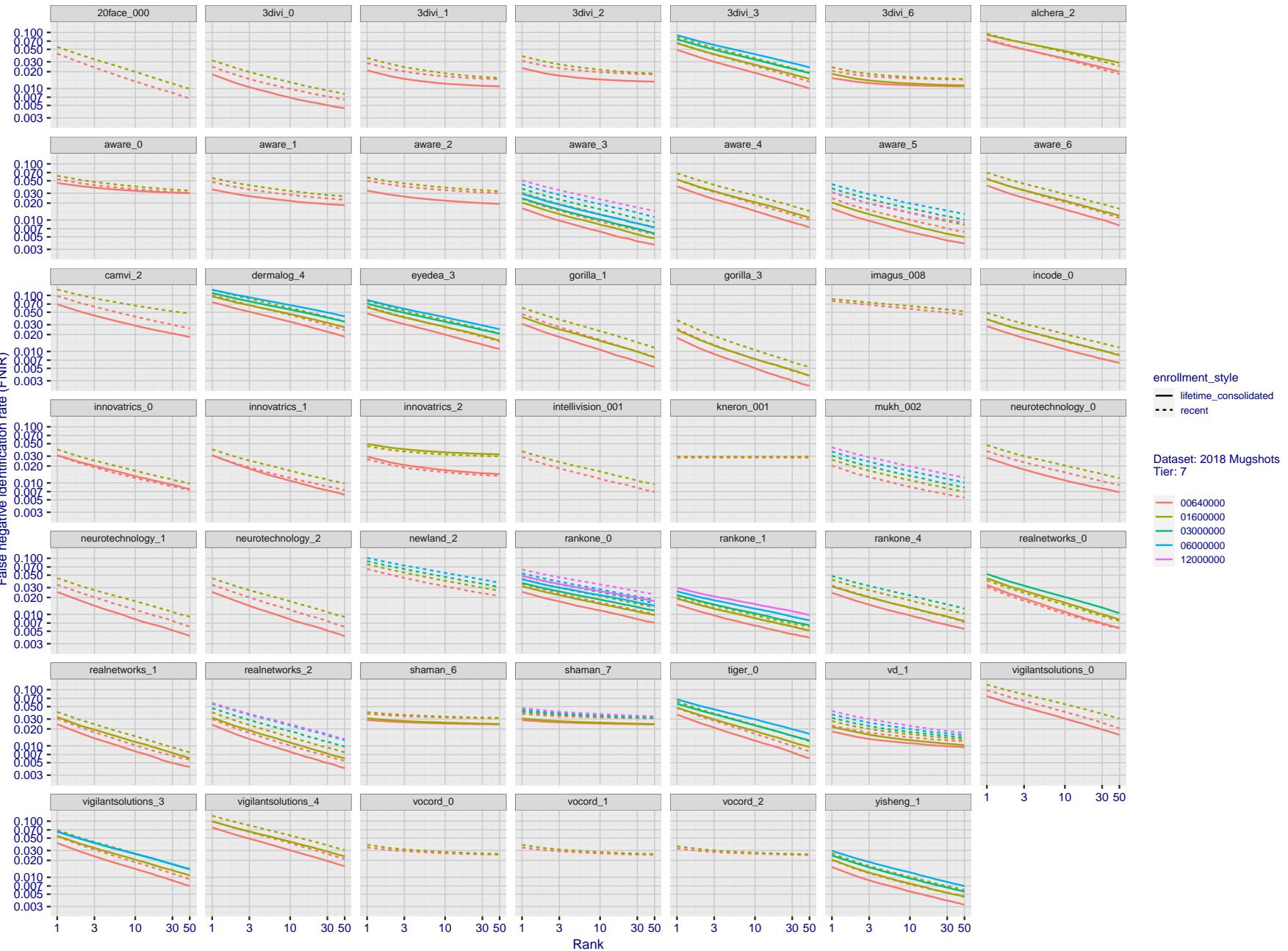
2023/04/04
07:31:47FNIR(N, R, T) = False neg. identification rate
FPIR(N, T) = False pos. identification rateN = Num. enrolled subjects
R = Num. candidates examined
T = ThresholdT = 0 → Investigation
T > 0 → Identification

Figure 34: [FRVT-2018 Mugshot Dataset] Rank-based identification miss rates vs. rank. The figure shows false negative identification rates (FNIR) for ranks up to 50. This metric is appropriate to investigational applications where human reviewers will adjudicate sorted candidate lists. Note that with threshold set to zero, FPIR = 1, i.e. any search without an enrolled mate will return non-mated candidates. Results are sorted and reported into tiers for clarity, with the tiering criteria being rank 1 hit rate on a gallery size of N = 640 000 subjects.

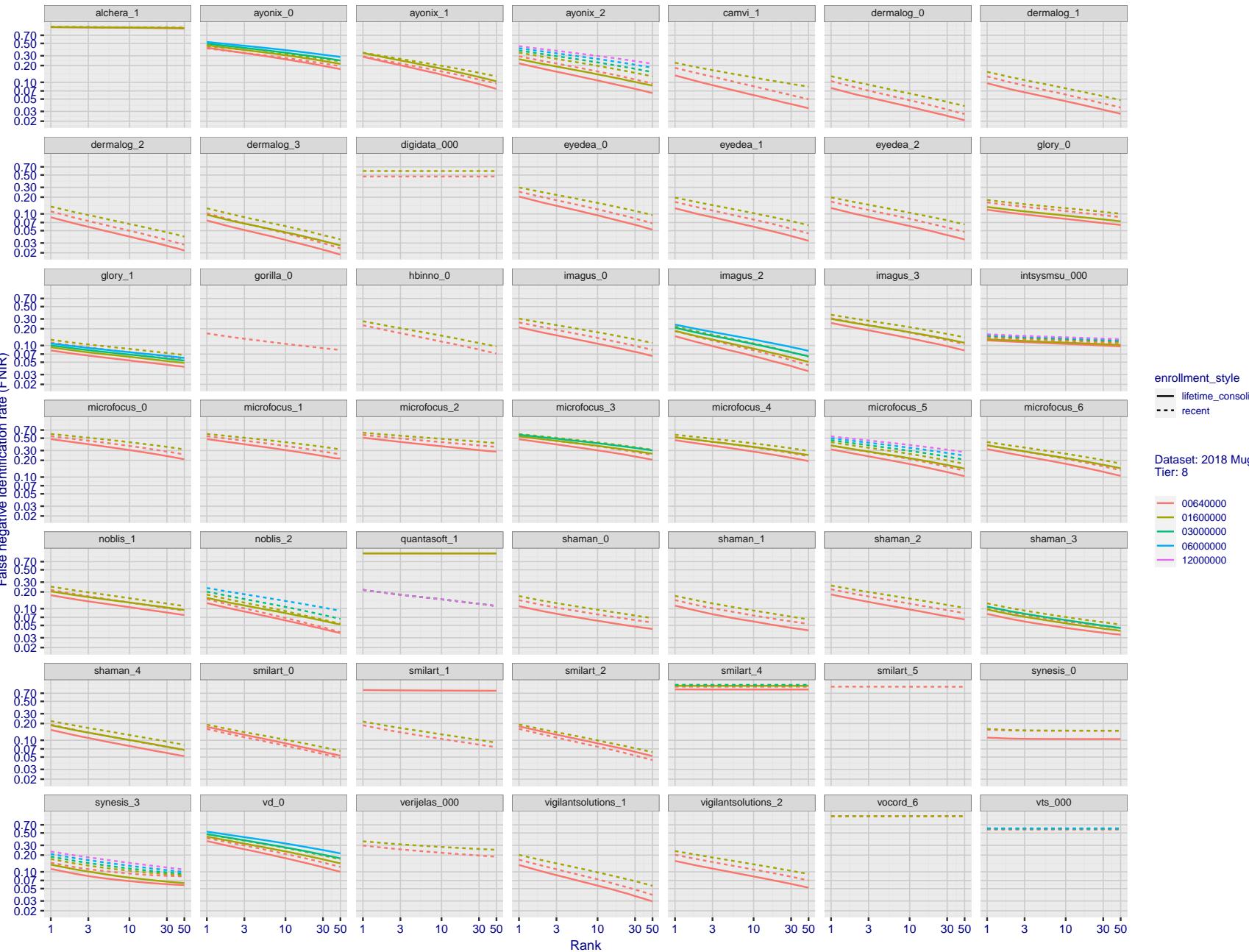
2023/04/04
07:31:47FNIR(N, R, T) = False neg. identification rate
FPIR(N, T) = False pos. identification rateN = Num. enrolled subjects
R = Num. candidates examinedT = Threshold
T = 0 → Investigation
T > 0 → Identification

Figure 35: [FRVT-2018 Mugshot Dataset] Rank-based identification miss rates vs. rank. The figure shows false negative identification rates (FNIR) for ranks up to 50. This metric is appropriate to investigational applications where human reviewers will adjudicate sorted candidate lists. Note that with threshold set to zero, FPIR = 1, i.e. any search without an enrolled mate will return non-mated candidates. Results are sorted and reported into tiers for clarity, with the tiering criteria being rank 1 hit rate on a gallery size of N = 640 000 subjects.

2023/04/04
07:31:47

FNIR(N, R, T) = False neg. identification rate
FPTR(N, T) = False pos. identification rate

N = Num. enrolled subjects
R = Num. candidates examined

T = Threshold
T = 0 → Investigation
T > 0 → Identification

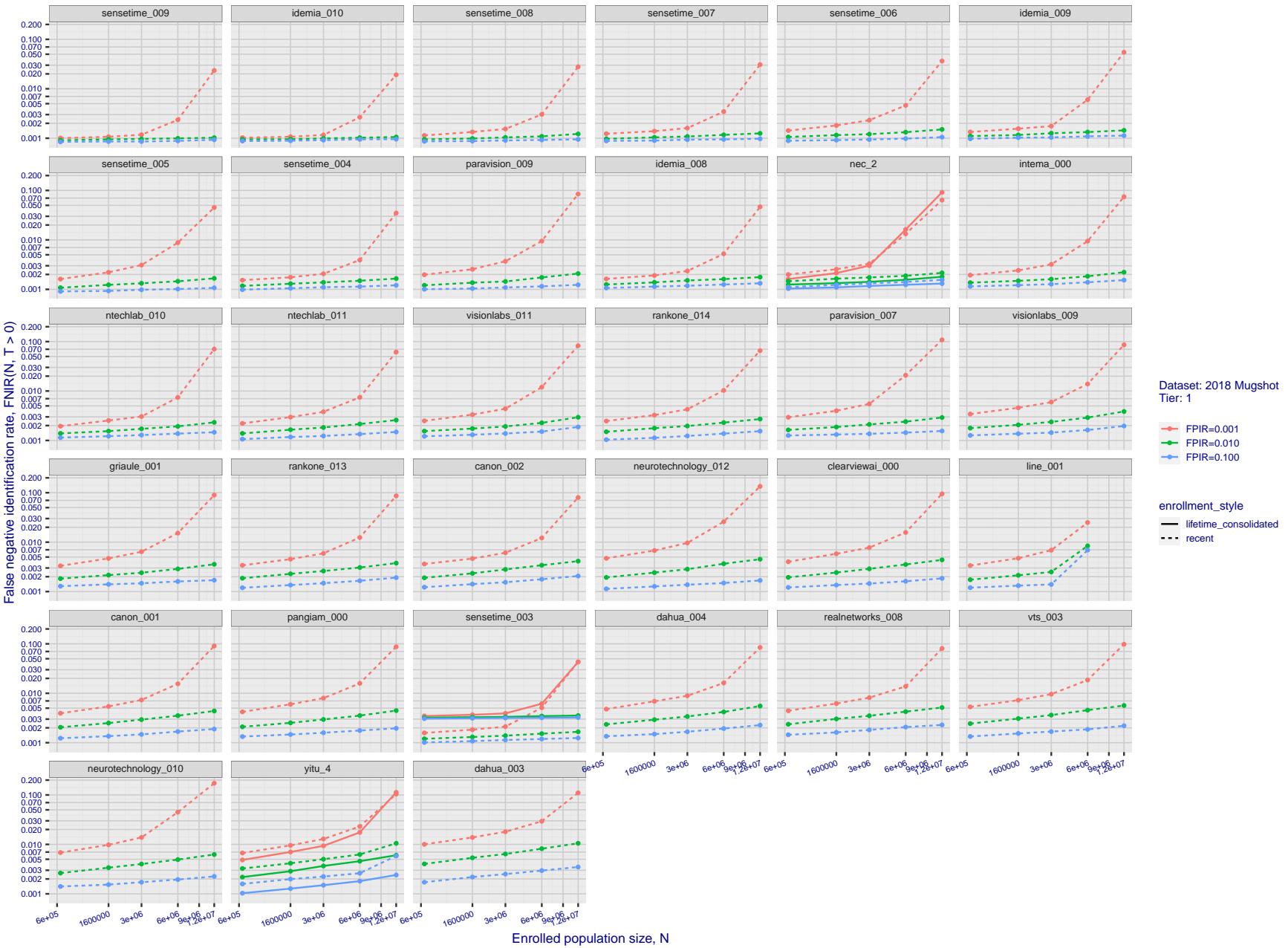
2023/04/04
07:31:47FNIR(N, R, T) = False neg. identification rate
FPIR(N, T) = False pos. identification rateN = Num. enrolled subjects
R = Num. candidates examined
T = ThresholdT = 0 → Investigation
T > 0 → Identification

Figure 36: [FRVT-2018 Mugshot Dataset] Threshold-based identification miss rates vs. number of enrolled subjects. The figure shows $\text{FNIR}(N, T)$ across various gallery sizes when the threshold is set to achieve the given FPIRs. The rank criterion is irrelevant at high thresholds as mates are always at rank 1. The results are computed from the trials listed in rows 1-10 of Table 1. Less accurate algorithms were not run on large N , so results are missing. For clarity, results are sorted and reported into tiers spanning multiple pages. The tiering criteria is complicated: First paging by $\text{FNIR}(N_b, 1, 0)$, then sorting by median $\text{FNIR}(N_b, T)$, $N_b = 640\,000$.

2023/04/04
07:31:47FNIR(N, R, T) = False neg. identification rate
FPFR(N, T) = False pos. identification rateN = Num. enrolled subjects
R = Num. candidates examined

T = Threshold

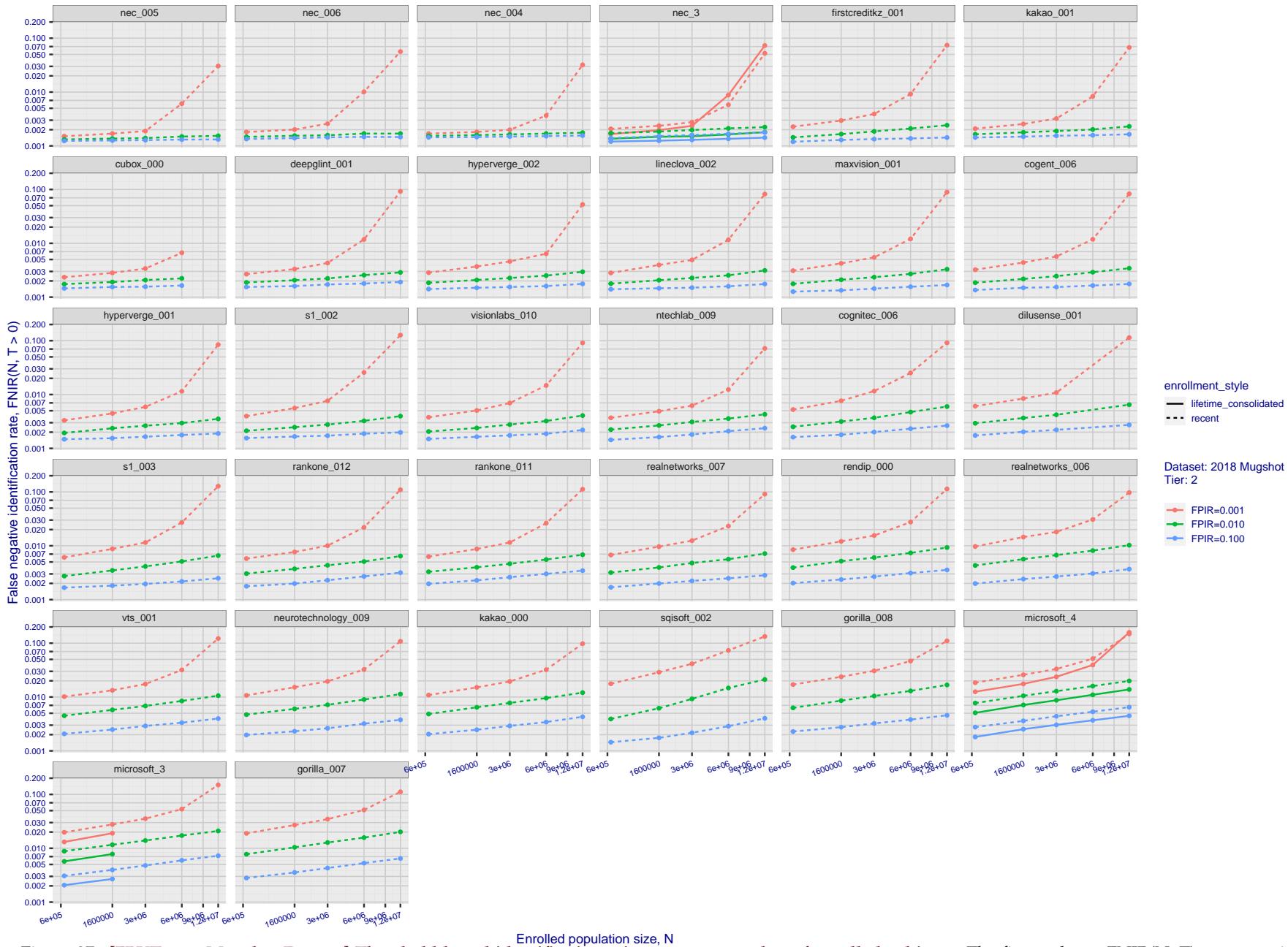
T = 0 → Investigation
T > 0 → Identification

Figure 37: [FRVT-2018 Mugshot Dataset] Threshold-based identification miss rates vs. number of enrolled subjects. The figure shows $\text{FNIR}(N, T)$ across various gallery sizes when the threshold is set to achieve the given FPIRs. The rank criterion is irrelevant at high thresholds as mates are always at rank 1. The results are computed from the trials listed in rows 1-10 of Table 1. Less accurate algorithms were not run on large N , so results are missing. For clarity, results are sorted and reported into tiers spanning multiple pages. The tiering criteria is complicated: First paging by $\text{FNIR}(N_b, 1, 0)$, then sorting by median $\text{FNIR}(N_b, T)$, $N_b = 640\,000$.

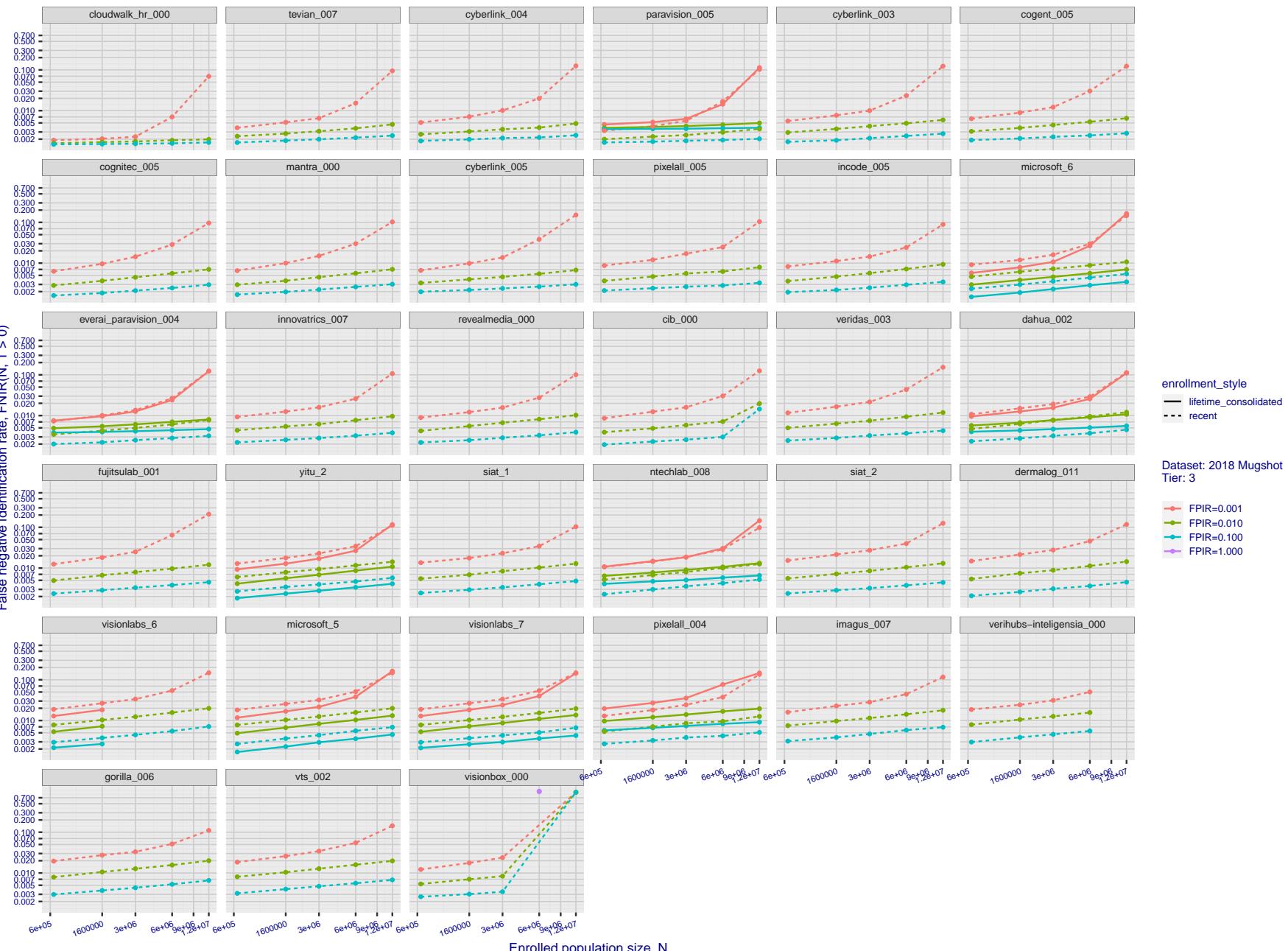
2023/04/04
07:31:47

Figure 38: [FRVT-2018 Mugshot Dataset] Threshold-based identification miss rates vs. number of enrolled subjects. The figure shows $\text{FNIR}(N, T)$ across various gallery sizes when the threshold is set to achieve the given FPIRs. The rank criterion is irrelevant at high thresholds as mates are always at rank 1. The results are computed from the trials listed in rows 1-10 of Table 1. Less accurate algorithms were not run on large N , so results are missing. For clarity, results are sorted and reported into tiers spanning multiple pages. The tiering criteria is complicated: First paging by $\text{FNIR}(N_b, 1, 0)$, then sorting by median $\text{FNIR}(N_b, T)$, $N_b = 640\,000$.

2023/04/04
07:31:47FNIR(N, R, T) = False neg. identification rate
FPFR(N, T) = False pos. identification rateN = Num. enrolled subjects
R = Num. candidates examined

T = Threshold

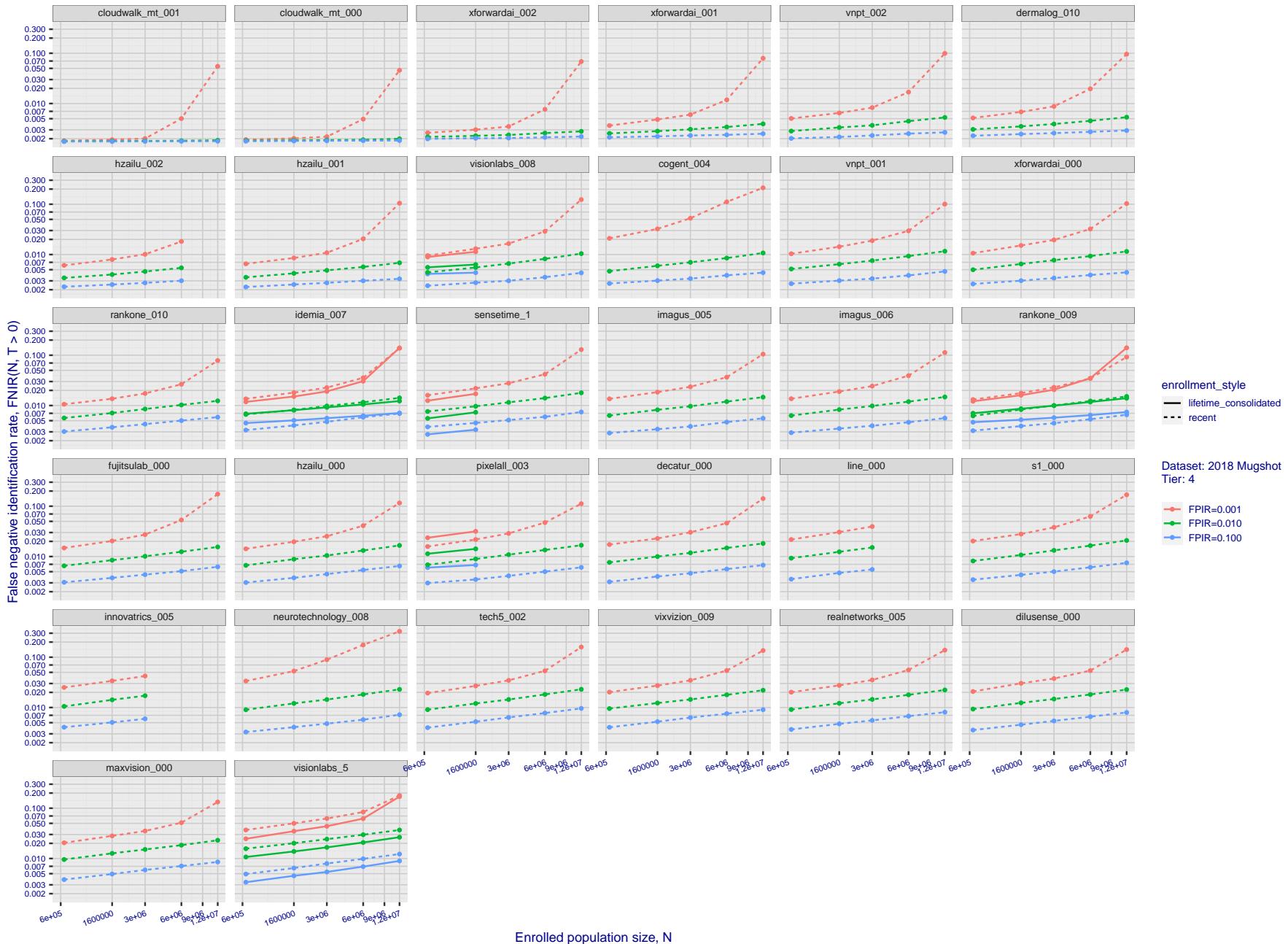
T = 0 → Investigation
T > 0 → Identification

Figure 39: [FRVT-2018 Mugshot Dataset] Threshold-based identification miss rates vs. number of enrolled subjects. The figure shows $\text{FNIR}(N, T)$ across various gallery sizes when the threshold is set to achieve the given FPIRs. The rank criterion is irrelevant at high thresholds as mates are always at rank 1. The results are computed from the trials listed in rows 1-10 of Table 1. Less accurate algorithms were not run on large N , so results are missing. For clarity, results are sorted and reported into tiers spanning multiple pages. The tiering criteria is complicated: First paging by $\text{FNIR}(N_b, 1, 0)$, then sorting by median $\text{FNIR}(N_b, T)$, $N_b = 640\,000$.

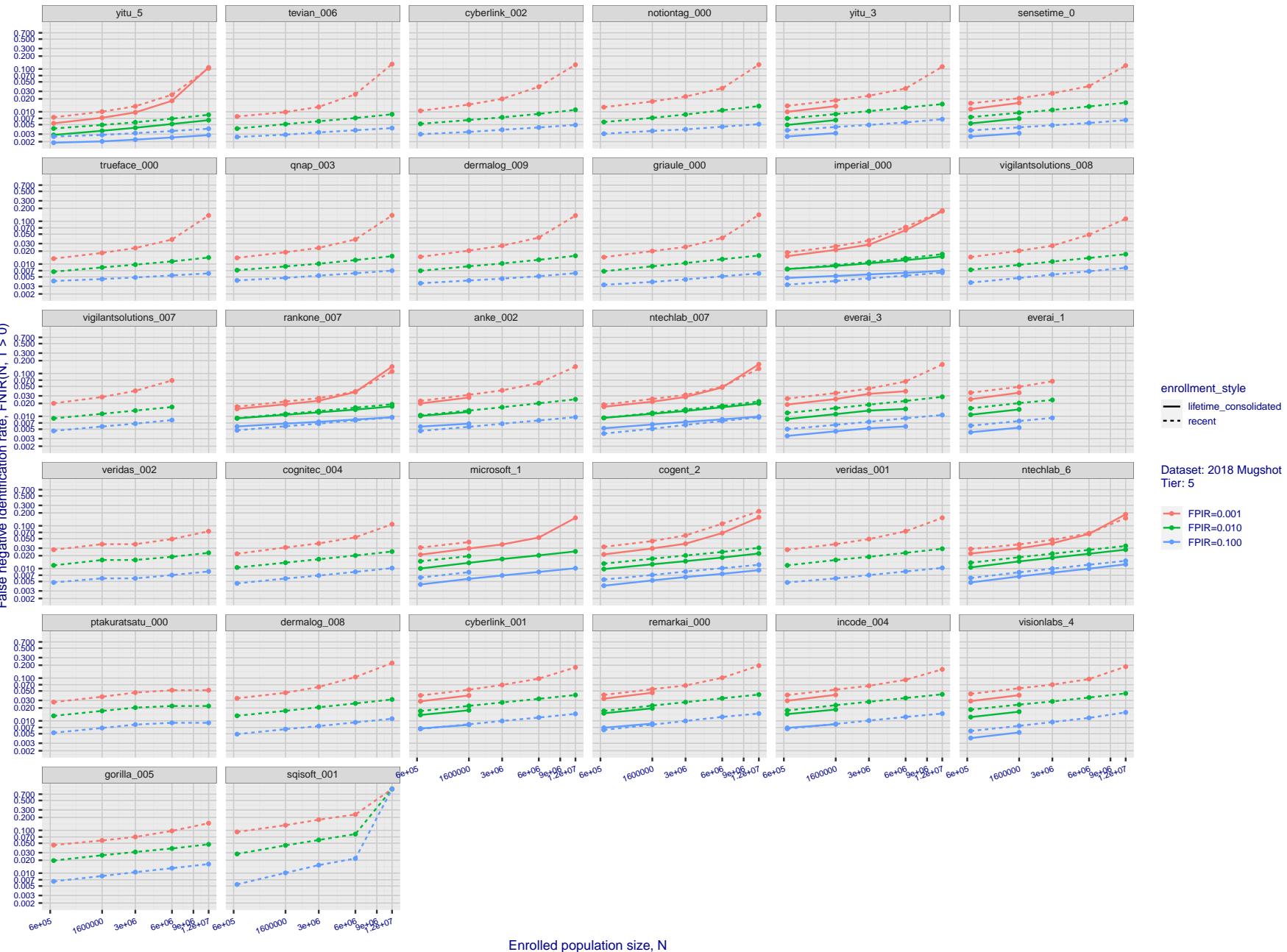
2023/04/04
07:31:47FNIR(N, R, T) = False neg. identification rate
FPIR(N, T) = False pos. identification rateN = Num. enrolled subjects
R = Num. candidates examined
T = ThresholdT = 0 → Investigation
T > 0 → Identification

Figure 40: [FRVT-2018 Mugshot Dataset] Threshold-based identification miss rates vs. number of enrolled subjects. The figure shows FNIR(N, T) across various gallery sizes when the threshold is set to achieve the given FPIRs. The rank criterion is irrelevant at high thresholds as mates are always at rank 1. The results are computed from the trials listed in rows 1-10 of Table 1. Less accurate algorithms were not run on large N, so results are missing. For clarity, results are sorted and reported into tiers spanning multiple pages. The tiering criteria is complicated: First paging by FNIR(N_b , 1, 0), then sorting by median FNIR(N_b , T), $N_b = 640\,000$.

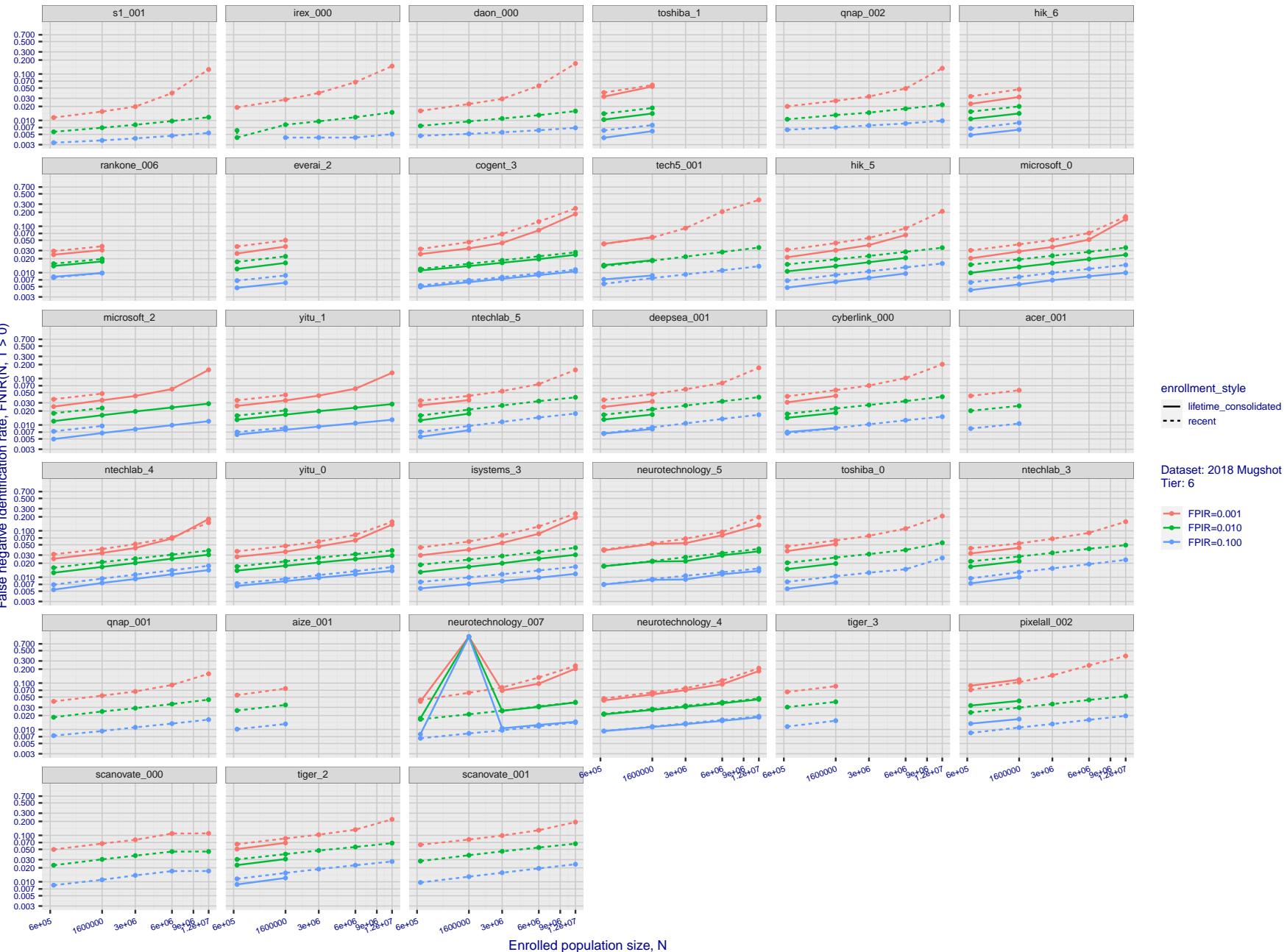
2023/04/04
07:31:47FNIR(N, R, T) = False neg. identification rate
FPFR(N, T) = False pos. identification rateN = Num. enrolled subjects
R = Num. candidates examined
T = ThresholdT = 0 → Investigation
T > 0 → Identification

Figure 41: [FRVT-2018 Mugshot Dataset] Threshold-based identification miss rates vs. number of enrolled subjects. The figure shows $\text{FNIR}(N, T)$ across various gallery sizes when the threshold is set to achieve the given FPIRs. The rank criterion is irrelevant at high thresholds as mates are always at rank 1. The results are computed from the trials listed in rows 1-10 of Table 1. Less accurate algorithms were not run on large N , so results are missing. For clarity, results are sorted and reported into tiers spanning multiple pages. The tiering criteria is complicated: First paging by $\text{FNIR}(N_b, 1, 0)$, then sorting by median $\text{FNIR}(N_b, T)$, $N_b = 640\,000$.

2023/04/04
07:31:47FNIR(N, R, T) = False neg. identification rate
FPFR(N, T) = False pos. identification rateN = Num. enrolled subjects
R = Num. candidates examined

T = Threshold

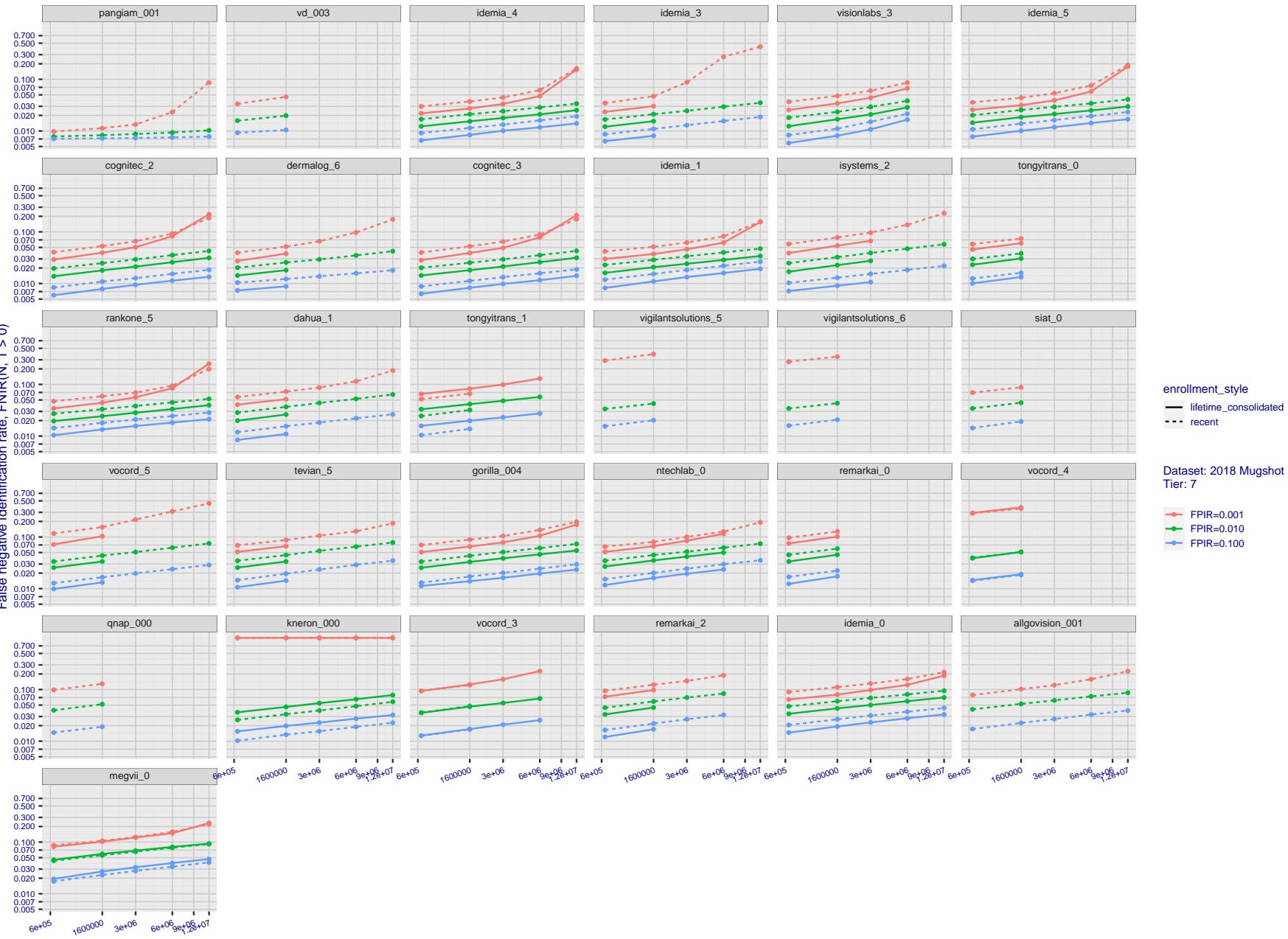
T = 0 → Investigation
T > 0 → Identification

Figure 42: [FRVT-2018 Mugshot Dataset] Threshold-based identification miss rates vs. number of enrolled subjects. The figure shows $\text{FNIR}(N, T)$ across various gallery sizes when the threshold is set to achieve the given FPIRs. The rank criterion is irrelevant at high thresholds as mates are always at rank 1. The results are computed from the trials listed in rows 1-10 of Table 1. Less accurate algorithms were not run on large N , so results are missing. For clarity, results are sorted and reported into tiers spanning multiple pages. The tiering criteria is complicated: First paging by $\text{FNIR}(N_b, 1, 0)$, then sorting by median $\text{FNIR}(N_b, T)$, $N_b = 640\,000$.

2023/04/04
07:31:47

$FNIR(N, K, I) =$ False neg. identification rate
 $FPIR(N, T) =$ False pos. identification rate

N = Num. enrolled subjects
R = Num. candidates examined

1 = 110.850

$I = 0 \rightarrow$ investigation
 $T > 0 \rightarrow$ identification

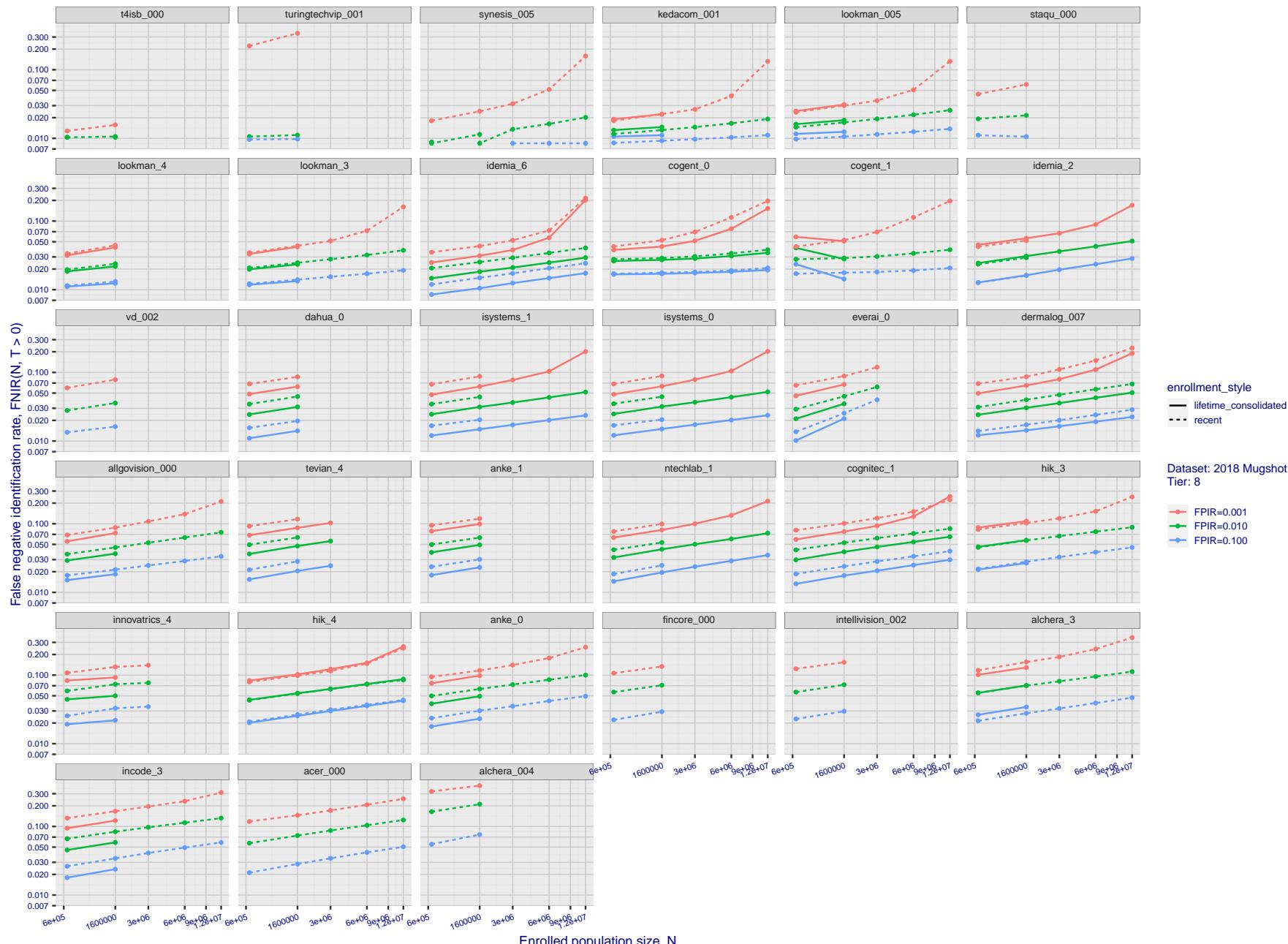


Figure 43: [FRVT-2018 Mugshot Dataset] Threshold-based identification miss rates vs. number of enrolled subjects. The figure shows FNIR(N, T) across various gallery sizes when the threshold is set to achieve the given FPIRs. The rank criterion is irrelevant at high thresholds as mates are always at rank 1. The results are computed from the trials listed in rows 1-10 of Table 1. Less accurate algorithms were not run on large N , so results are missing. For clarity, results are sorted and reported into tiers spanning multiple pages. The tiering criteria is complicated: First paging by $\text{FNIR}(N_b, 1, 0)$, then sorting by median $\text{FNIR}(N_b, T)$, $N_b = 640\,000$.

2023/04/04
07:31:47FNIR(N, R, T) = False neg. identification rate
FPIR(N, T) = False pos. identification rateN = Num. enrolled subjects
R = Num. candidates examined

T = Threshold

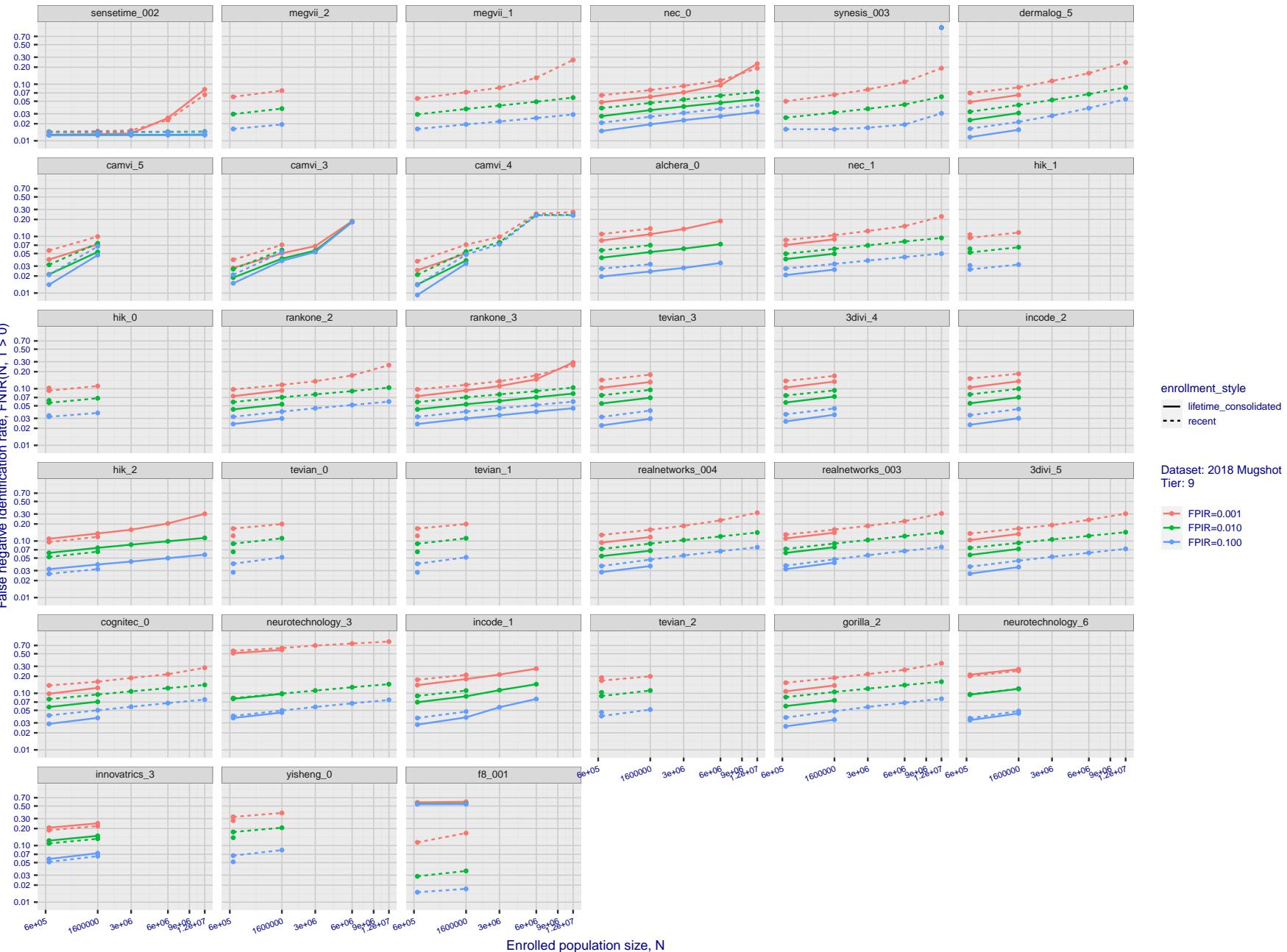
T = 0 → Investigation
T > 0 → Identification

Figure 44: [FRVT-2018 Mugshot Dataset] Threshold-based identification miss rates vs. number of enrolled subjects. The figure shows FNIR(N, T) across various gallery sizes when the threshold is set to achieve the given FPIRs. The rank criterion is irrelevant at high thresholds as mates are always at rank 1. The results are computed from the trials listed in rows 1-10 of Table 1. Less accurate algorithms were not run on large N , so results are missing. For clarity, results are sorted and reported into tiers spanning multiple pages. The tiering criteria is complicated: First paging by FNIR($N_b, 1, 0$), then sorting by median FNIR(N_b, T), $N_b = 640\,000$.

2023/04/04
07:31:47FNIR(N, R, T) = False neg. identification rate
FPFR(N, T) = False pos. identification rateN = Num. enrolled subjects
R = Num. candidates examined

T = Threshold

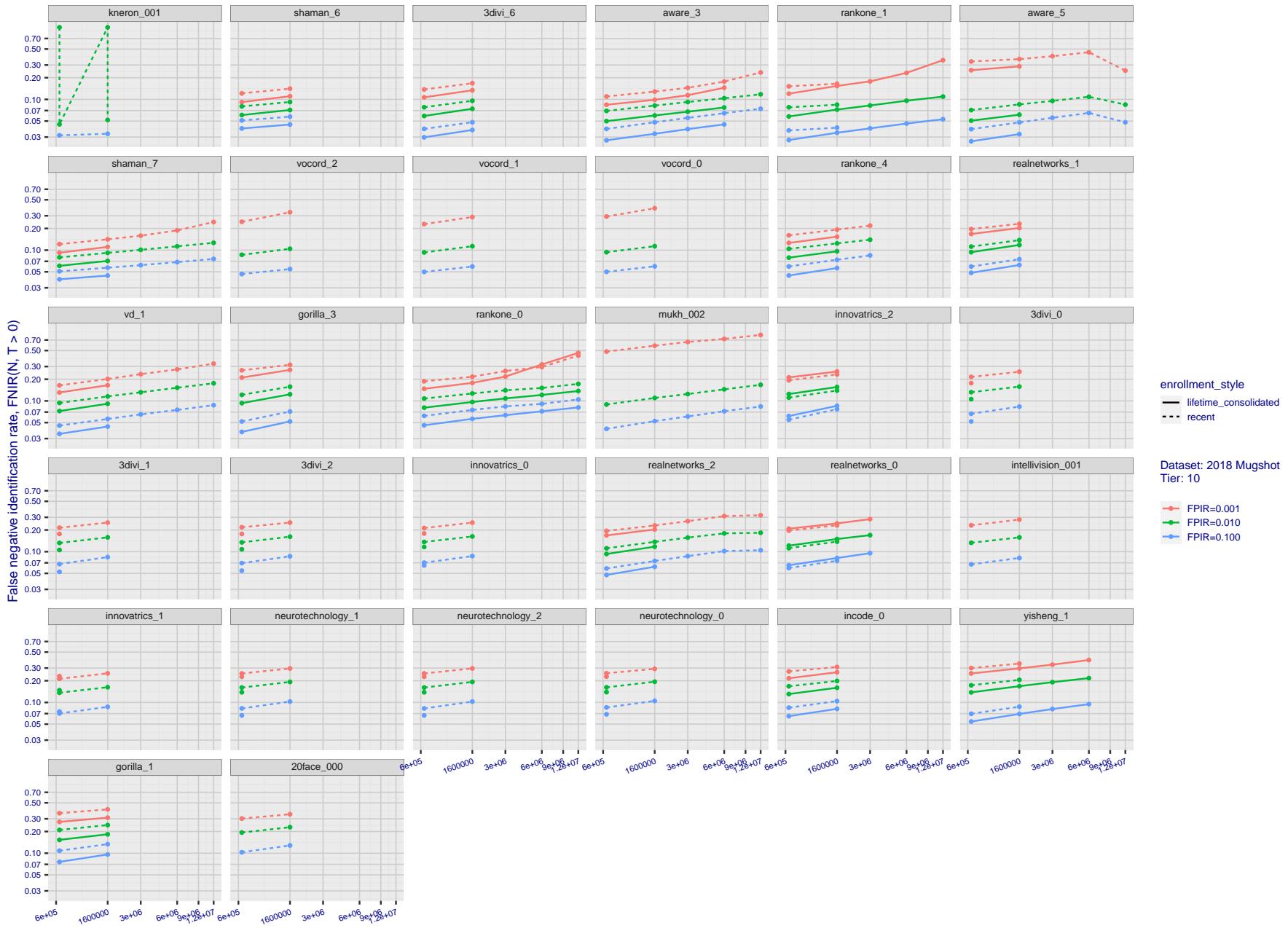
T = 0 → Investigation
T > 0 → Identification

Figure 45: [FRVT-2018 Mugshot Dataset] Threshold-based identification miss rates vs. number of enrolled subjects. The figure shows $\text{FNIR}(N, T)$ across various gallery sizes when the threshold is set to achieve the given FPIRs. The rank criterion is irrelevant at high thresholds as mates are always at rank 1. The results are computed from the trials listed in rows 1-10 of Table 1. Less accurate algorithms were not run on large N , so results are missing. For clarity, results are sorted and reported into tiers spanning multiple pages. The tiering criteria is complicated: First paging by $\text{FNIR}(N_b, 1, 0)$, then sorting by median $\text{FNIR}(N_b, T)$, $N_b = 640\,000$.

2023/04/04
07:31:47FNIR(N, R, T) = False neg. identification rate
FPFR(N, T) = False pos. identification rateN = Num. enrolled subjects
R = Num. candidates examined

T = Threshold

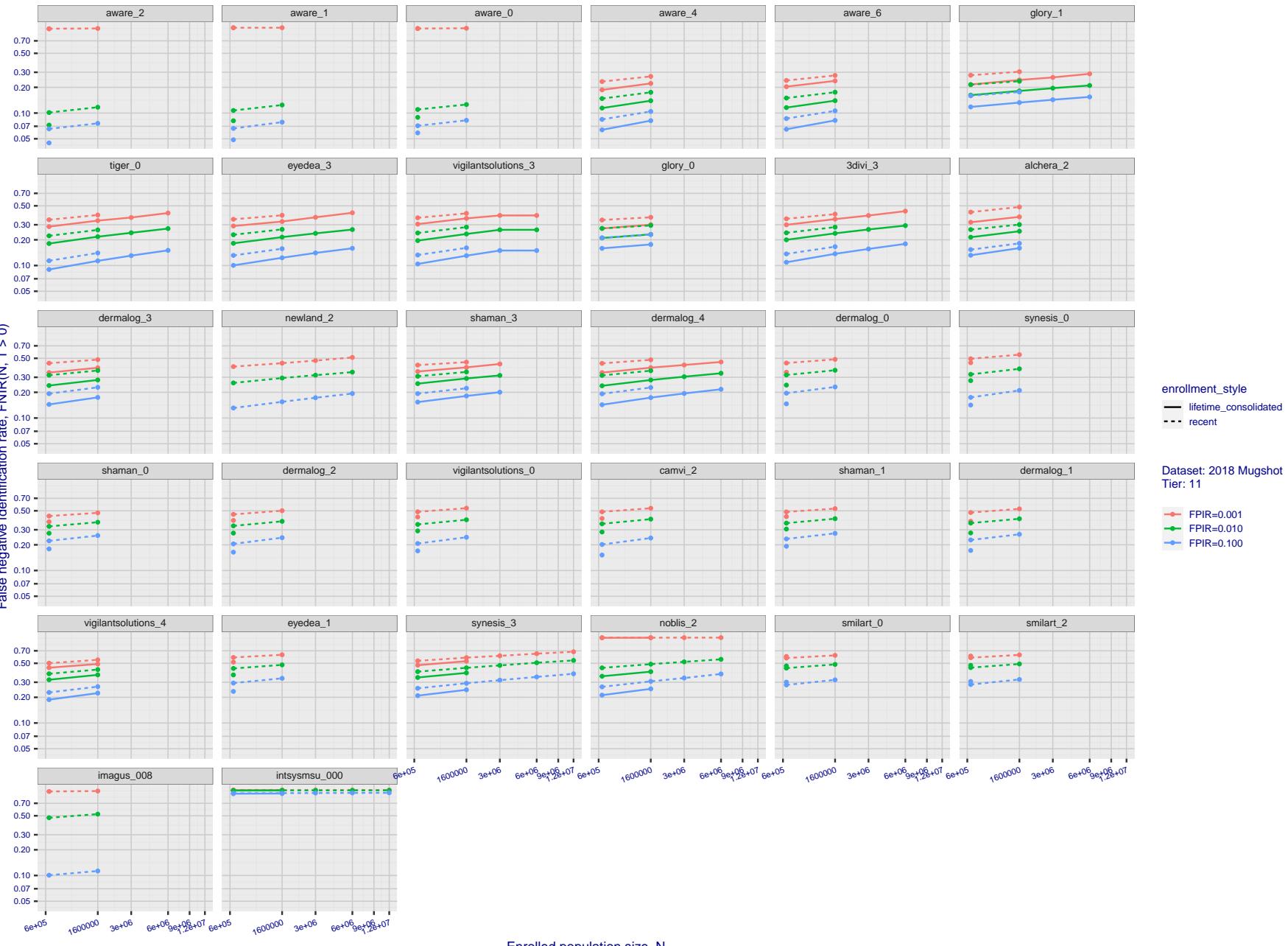
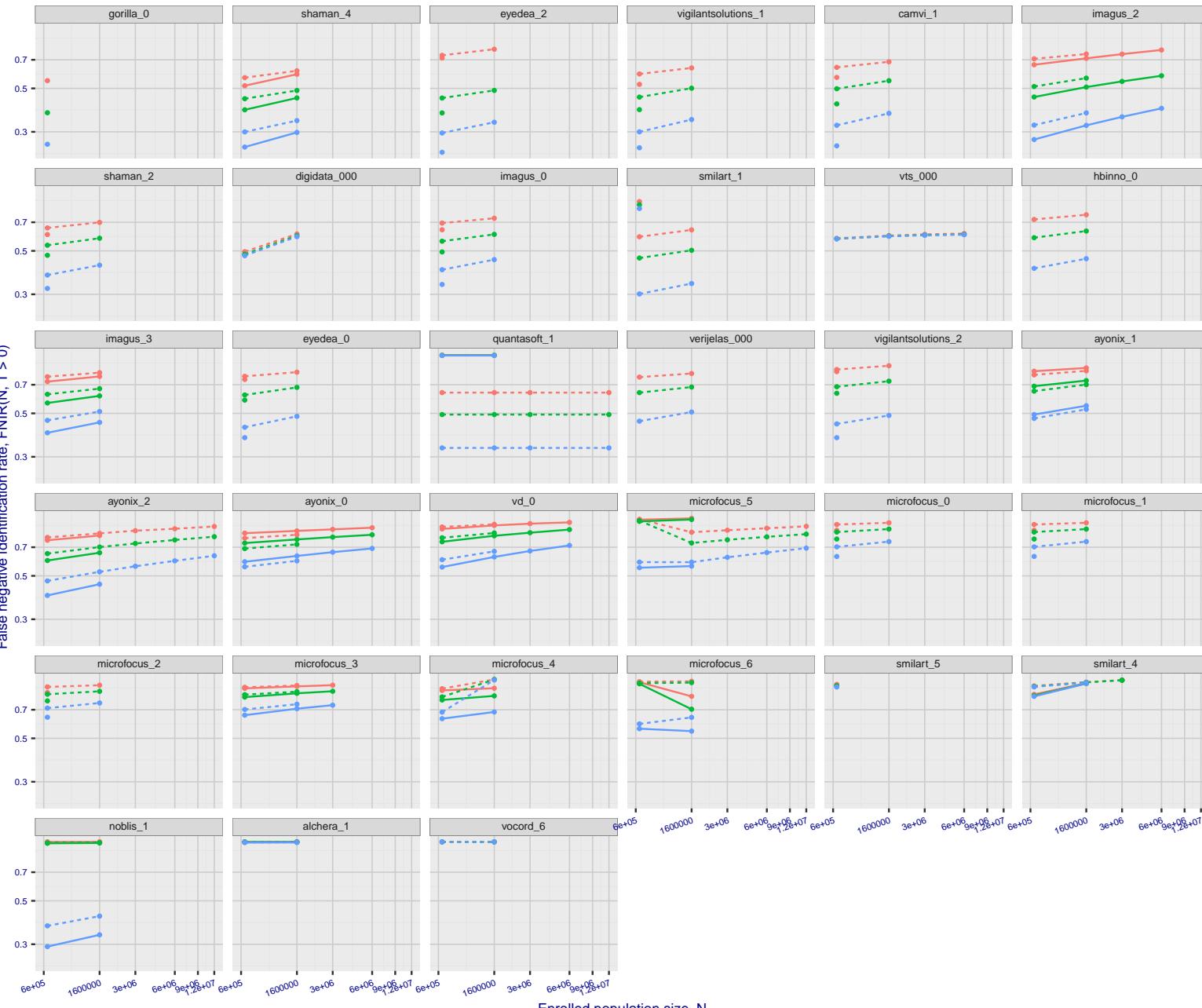
T = 0 → Investigation
T > 0 → Identification

Figure 46: [FRVT-2018 Mugshot Dataset] Threshold-based identification miss rates vs. number of enrolled subjects. The figure shows FNIR(N, T) across various gallery sizes when the threshold is set to achieve the given FPIRs. The rank criterion is irrelevant at high thresholds as mates are always at rank 1. The results are computed from the trials listed in rows 1-10 of Table 1. Less accurate algorithms were not run on large N, so results are missing. For clarity, results are sorted and reported into tiers spanning multiple pages. The tiering criteria is complicated: First paging by FNIR(N_b , 1, 0), then sorting by median FNIR(N_b , T), $N_b = 640\,000$.

2023/04/04

FNIR(N, R, T) = False neg. identification rate
FPIR(N, T) = False pos. identification rateN = Num. enrolled subjects
R = Num. candidates examined

T = Threshold

T = 0 → Investigation
T > 0 → IdentificationDataset: 2018 Mugshot
Tier: 12

- FPIR=0.001
- FPIR=0.010
- FPIR=0.100

- enrollment_style
- lifetime_consolidated
- recent

Figure 47: [FRVT-2018 Mugshot Dataset] Threshold-based identification miss rates vs. number of enrolled subjects. The figure shows $\text{FNIR}(N, T)$ across various gallery sizes when the threshold is set to achieve the given FPIRs. The rank criterion is irrelevant at high thresholds as mates are always at rank 1. The results are computed from the trials listed in rows 1-10 of Table 1. Less accurate algorithms were not run on large N , so results are missing. For clarity, results are sorted and reported into tiers spanning multiple pages. The tiering criteria is complicated: First paging by $\text{FNIR}(N_b, 1, 0)$, then sorting by median $\text{FNIR}(N_b, T)$, $N_b = 640\,000$.

2023/04/04
07:31:47

FNIR(N, R, T) = False neg. identification rate
FPTR(N, T) = False pos. identification rate

N = Num. enrolled subjects
R = Num. candidates examined

T = Threshold
T > 0 → Identification

T = 0 → Investigation

2023/04/04
07:31:47FNIR(N, R, T) = False neg. identification rate
FPIR(N, T) = False pos. identification rateN = Num. enrolled subjects
R = Num. candidates examined

T = Threshold

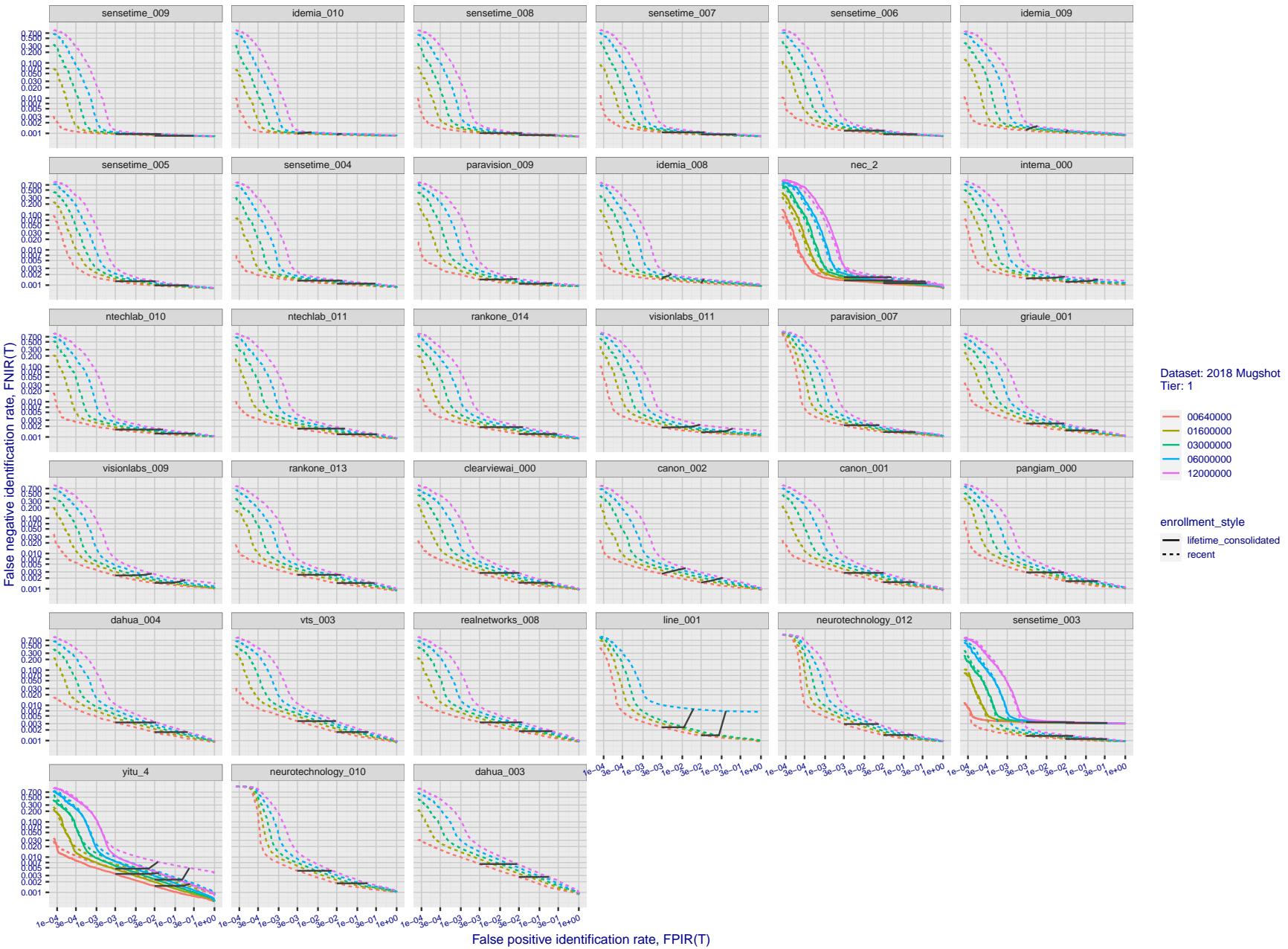
T = 0 → Investigation
 $T > 0 \rightarrow$ Identification

Figure 48: [FRVT-2018 Mugshot Dataset] Identification miss rates vs. false positive rates. The figure shows miss rates $\text{FNIR}(N, L, T)$ as a function of $\text{FPIR}(N, T)$, with N ranging from 640 000 to 12 000 000 as noted in rows 1-10 of Table 1. These error tradeoff characteristics are useful for applications where a threshold must be elevated to limit false positives, such as when human reviewer labor is not matched to the volume of searches. Dark lines join points of equal threshold: If horizontal, $\text{FPIR}(T)$ rises with N , and mate scores are independent of N . Other algorithms adjust scores in an attempt to make FPIR independent of N .

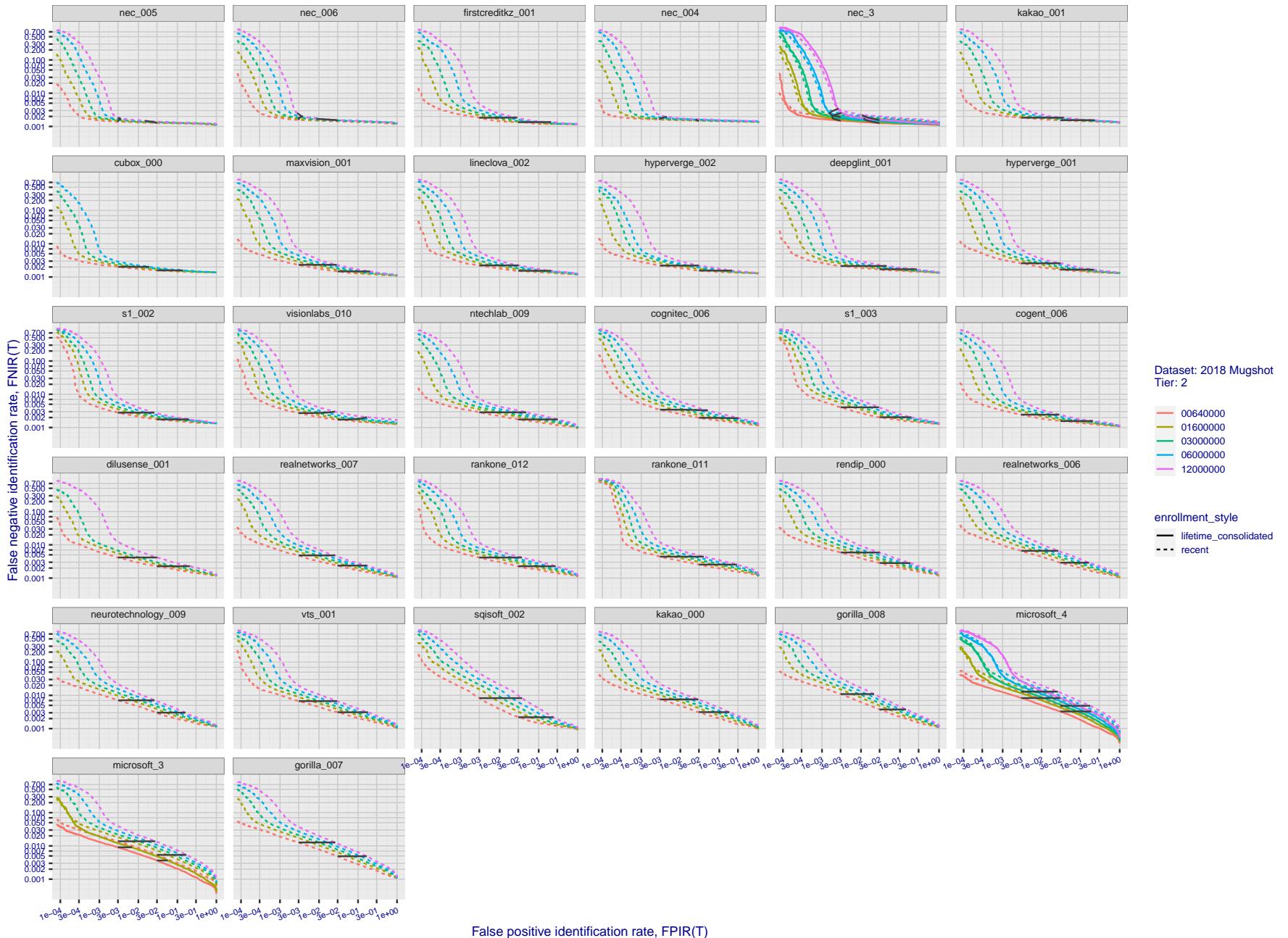


Figure 49: [FRVT-2018 Mugshot Dataset] Identification miss rates vs. false positive rates. The figure shows miss rates $\text{FNIR}(N, L, T)$ as a function of $\text{FPIR}(N, T)$, with N ranging from 640 000 to 12 000 000 as noted in rows 1-10 of Table 1. These error tradeoff characteristics are useful for applications where a threshold must be elevated to limit false positives, such as when human reviewer labor is not matched to the volume of searches. Dark lines join points of equal threshold: If horizontal, $\text{FPIR}(T)$ rises with N , and mate scores are independent of N . Other algorithms adjust scores in an attempt to make FPIR independent of N .

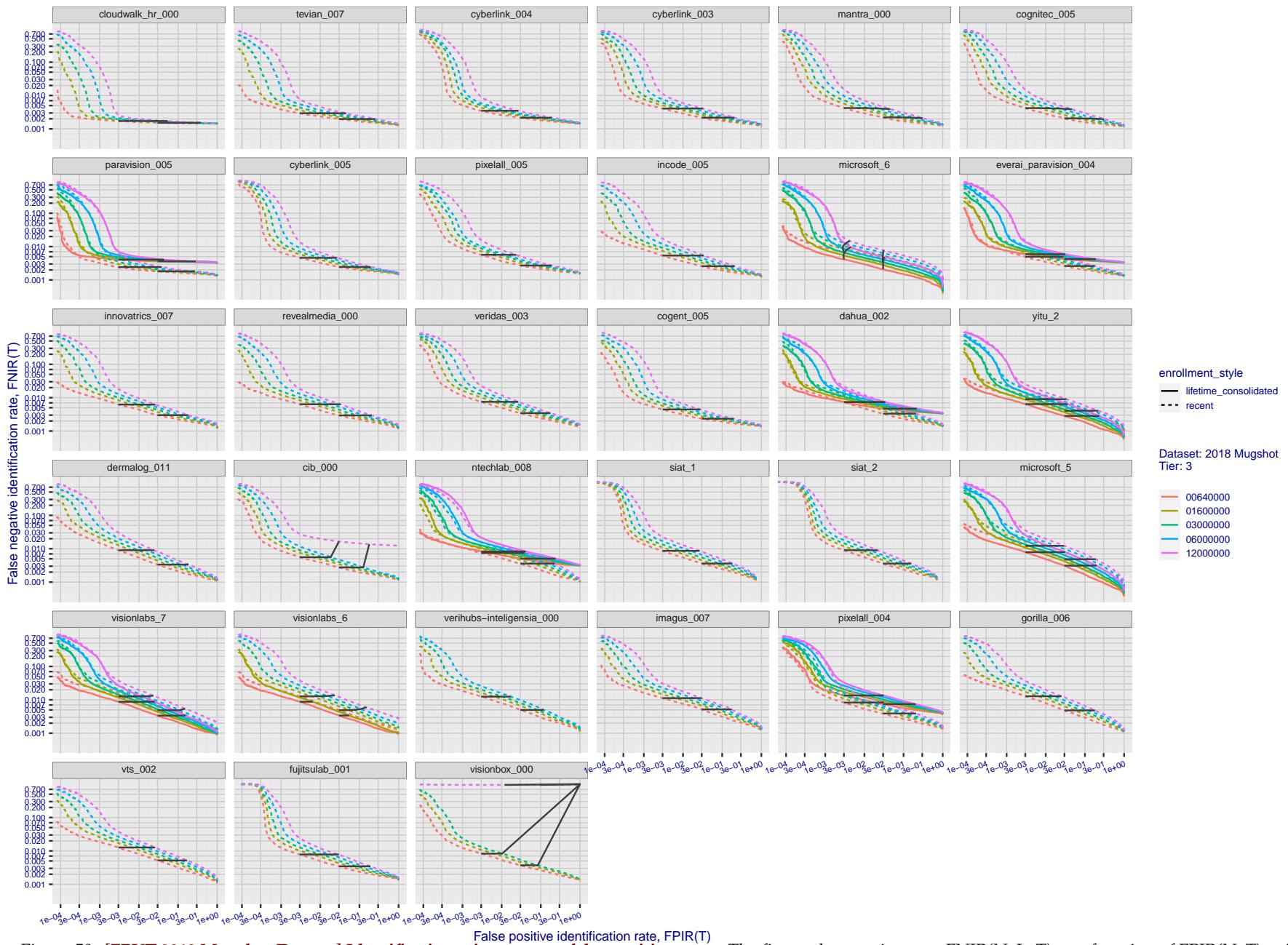


Figure 50: [FRVT-2018 Mugshot Dataset] Identification miss rates vs. false positive rates. The figure shows miss rates $\text{FNIR}(N, L, T)$ as a function of $\text{FPIR}(N, T)$, with N ranging from 640 000 to 12 000 000 as noted in rows 1-10 of Table 1. These error tradeoff characteristics are useful for applications where a threshold must be elevated to limit false positives, such as when human reviewer labor is not matched to the volume of searches. Dark lines join points of equal threshold: If horizontal, $\text{FPIR}(T)$ rises with N , and mate scores are independent of N . Other algorithms adjust scores in an attempt to make FPIR independent of N .

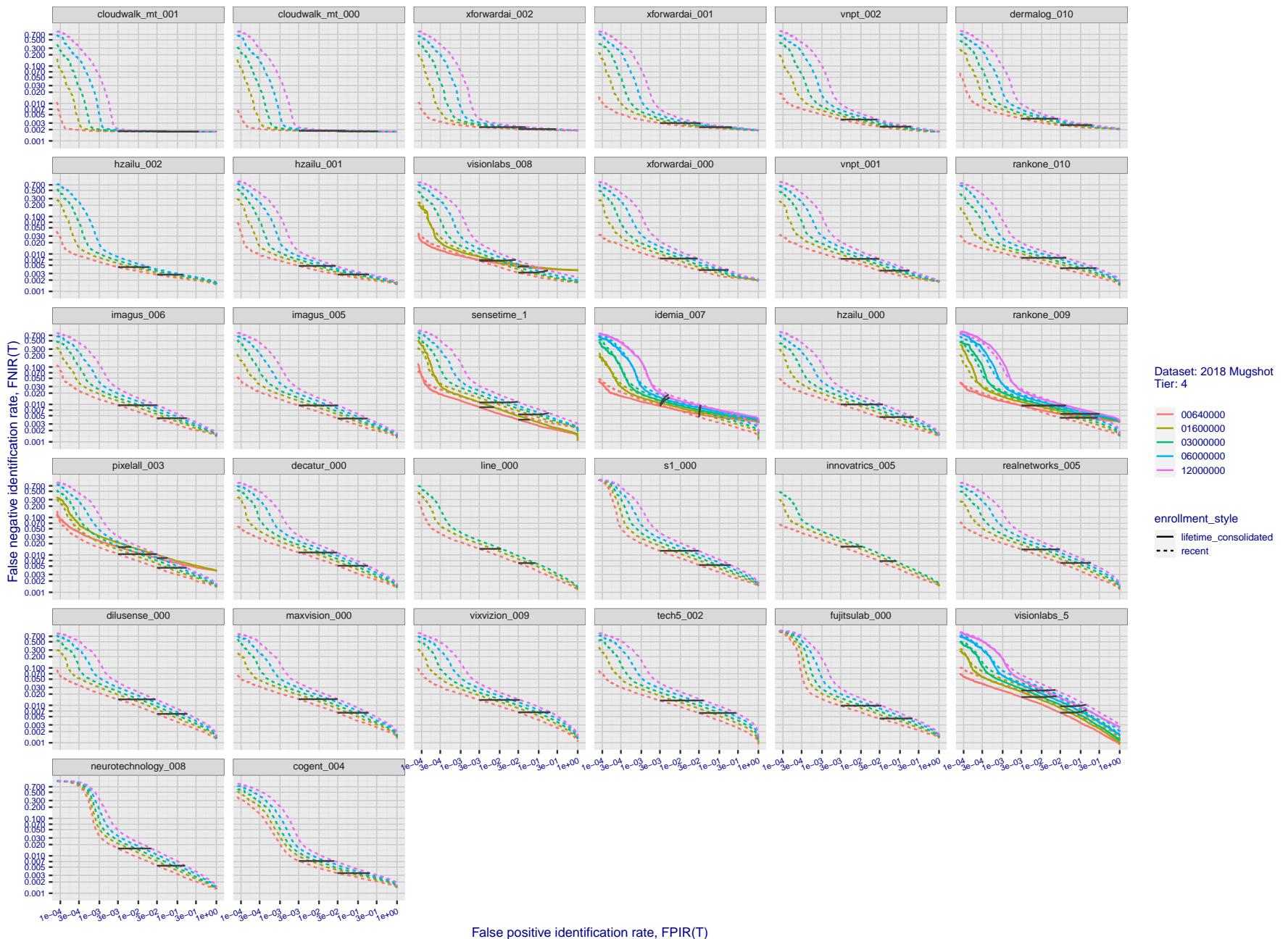


Figure 51: [FRVT-2018 Mugshot Dataset] Identification miss rates vs. false positive rates. The figure shows miss rates $\text{FNIR}(N, L, T)$ as a function of $\text{FPIR}(N, T)$, with N ranging from 64 000 to 12 000 000 as noted in rows 1-10 of Table 1. These error tradeoff characteristics are useful for applications where a threshold must be elevated to limit false positives, such as when human reviewer labor is not matched to the volume of searches. Dark lines join points of equal threshold: If horizontal, $\text{FPIR}(T)$ rises with N , and mate scores are independent of N . Other algorithms adjust scores in an attempt to make FPIR independent of N .

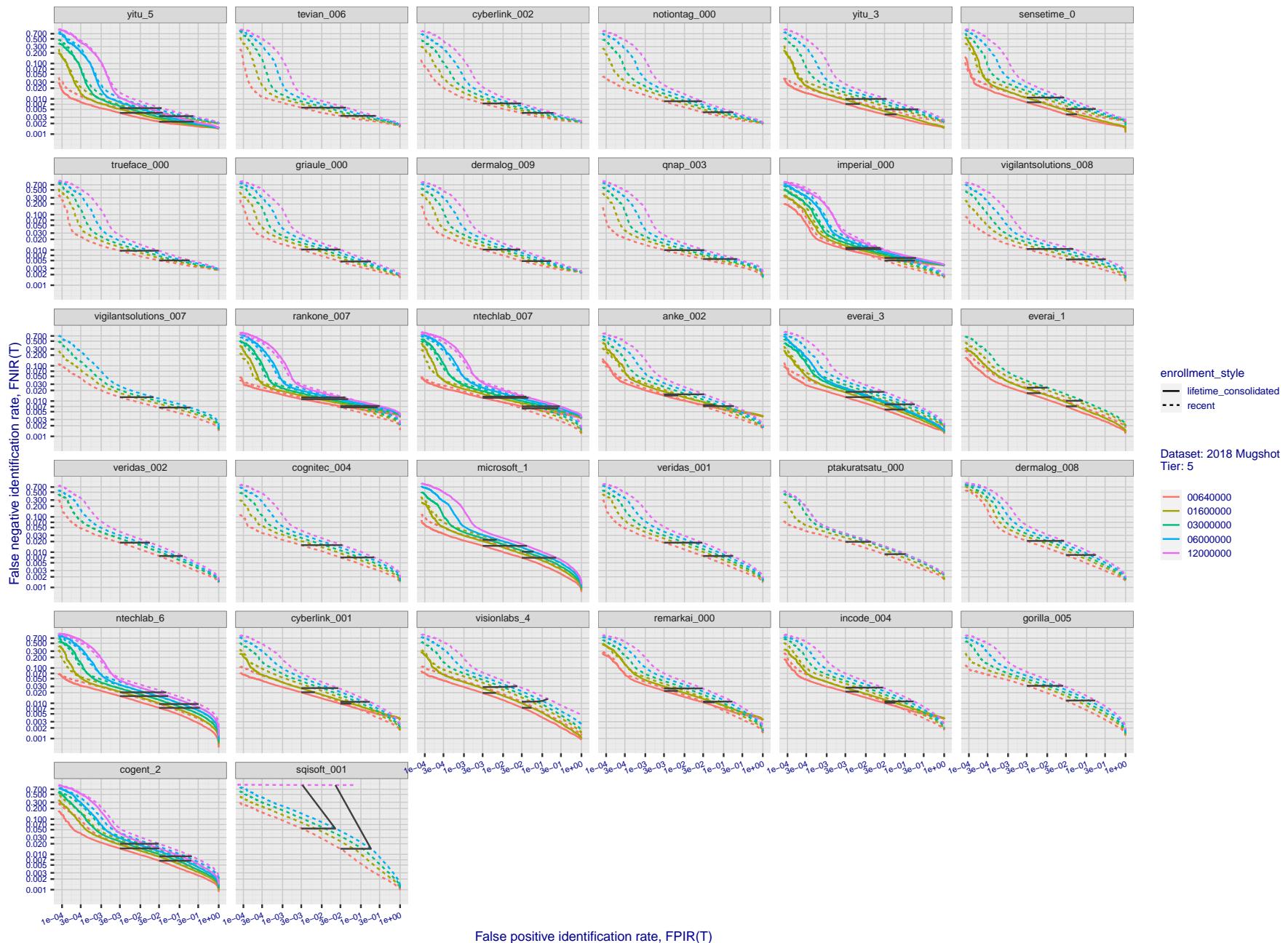


Figure 52: [FRVT-2018 Mugshot Dataset] Identification miss rates vs. false positive rates. The figure shows miss rates $\text{FNIR}(N, L, T)$ as a function of $\text{FPIR}(N, T)$, with N ranging from 640 000 to 12 000 000 as noted in rows 1-10 of Table 1. These error tradeoff characteristics are useful for applications where a threshold must be elevated to limit false positives, such as when human reviewer labor is not matched to the volume of searches. Dark lines join points of equal threshold: If horizontal, $\text{FPIR}(T)$ rises with N , and mate scores are independent of N . Other algorithms adjust scores in an attempt to make FPIR independent of N .

2023/04/04

07:31:47

 $\text{FNIR}(N, R, T) = \text{False neg. identification rate}$ $N = \text{Num. enrolled subjects}$ $T = \text{Threshold}$ $R = \text{Num. candidates examined}$ $\text{FPIR}(N, T) = \text{False pos. identification rate}$ $T = 0 \rightarrow \text{Investigation}$ $T > 0 \rightarrow \text{Identification}$

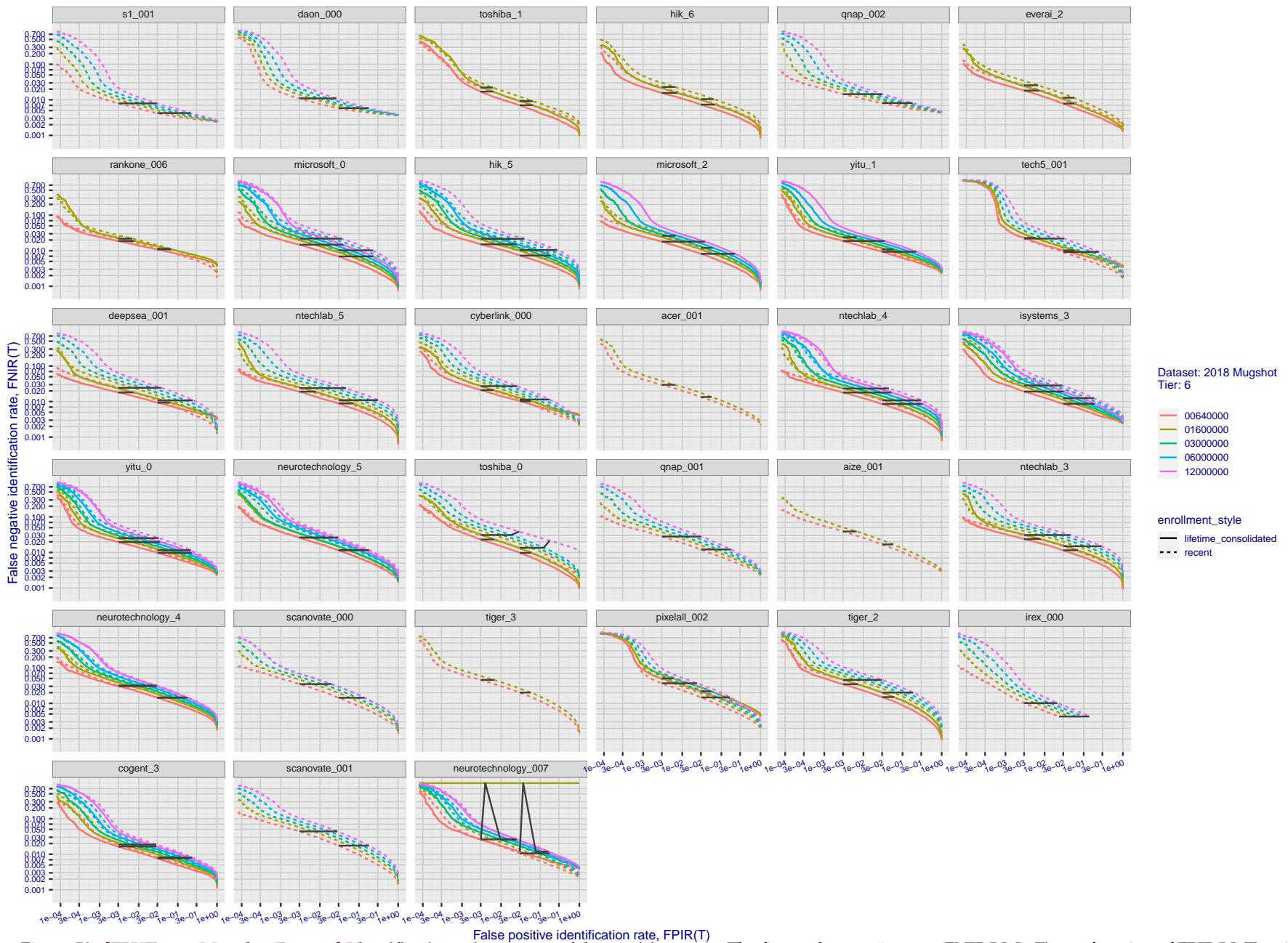


Figure 53: [FRVT-2018 Mugshot Dataset] Identification miss rates vs. false positive rates. The figure shows miss rates $\text{FNIR}(N, L, T)$ as a function of $\text{FPIR}(N, T)$, with N ranging from 640 000 to 12 000 000 as noted in rows 1-10 of Table 1. These error tradeoff characteristics are useful for applications where a threshold must be elevated to limit false positives, such as when human reviewer labor is not matched to the volume of searches. Dark lines join points of equal threshold: If horizontal, $\text{FPIR}(T)$ rises with N , and mate scores are independent of N . Other algorithms adjust scores in an attempt to make FPIR independent of N .

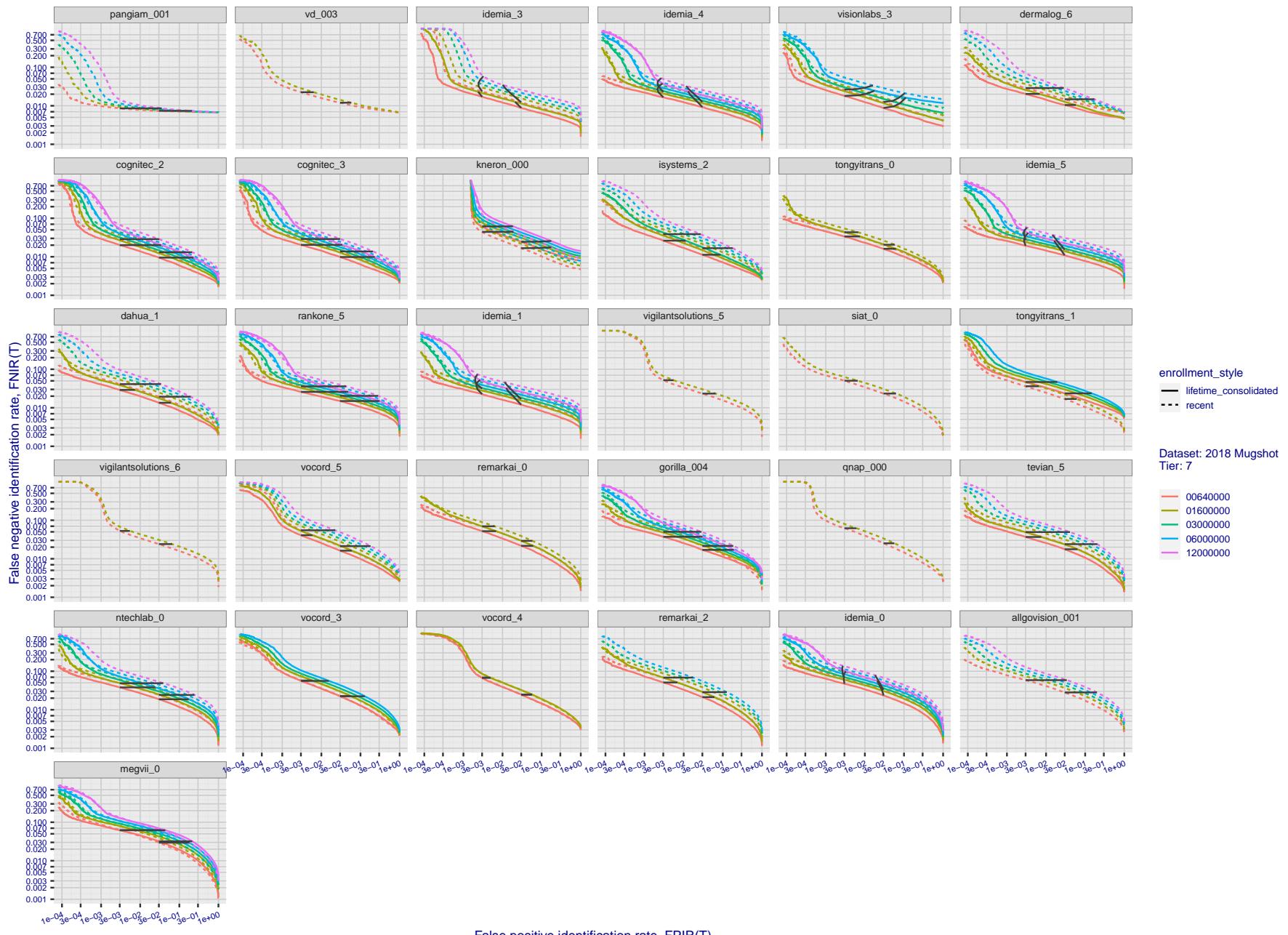


Figure 54: [FRVT-2018 Mugshot Dataset] Identification miss rates vs. false positive rates. The figure shows miss rates $\text{FNIR}(N, L, T)$ as a function of $\text{FPIR}(N, T)$, with N ranging from 640 000 to 12 000 000 as noted in rows 1-10 of Table 1. These error tradeoff characteristics are useful for applications where a threshold must be elevated to limit false positives, such as when human reviewer labor is not matched to the volume of searches. Dark lines join points of equal threshold: If horizontal, $\text{FPIR}(T)$ rises with N , and mate scores are independent of N . Other algorithms adjust scores in an attempt to make FPIR independent of N .

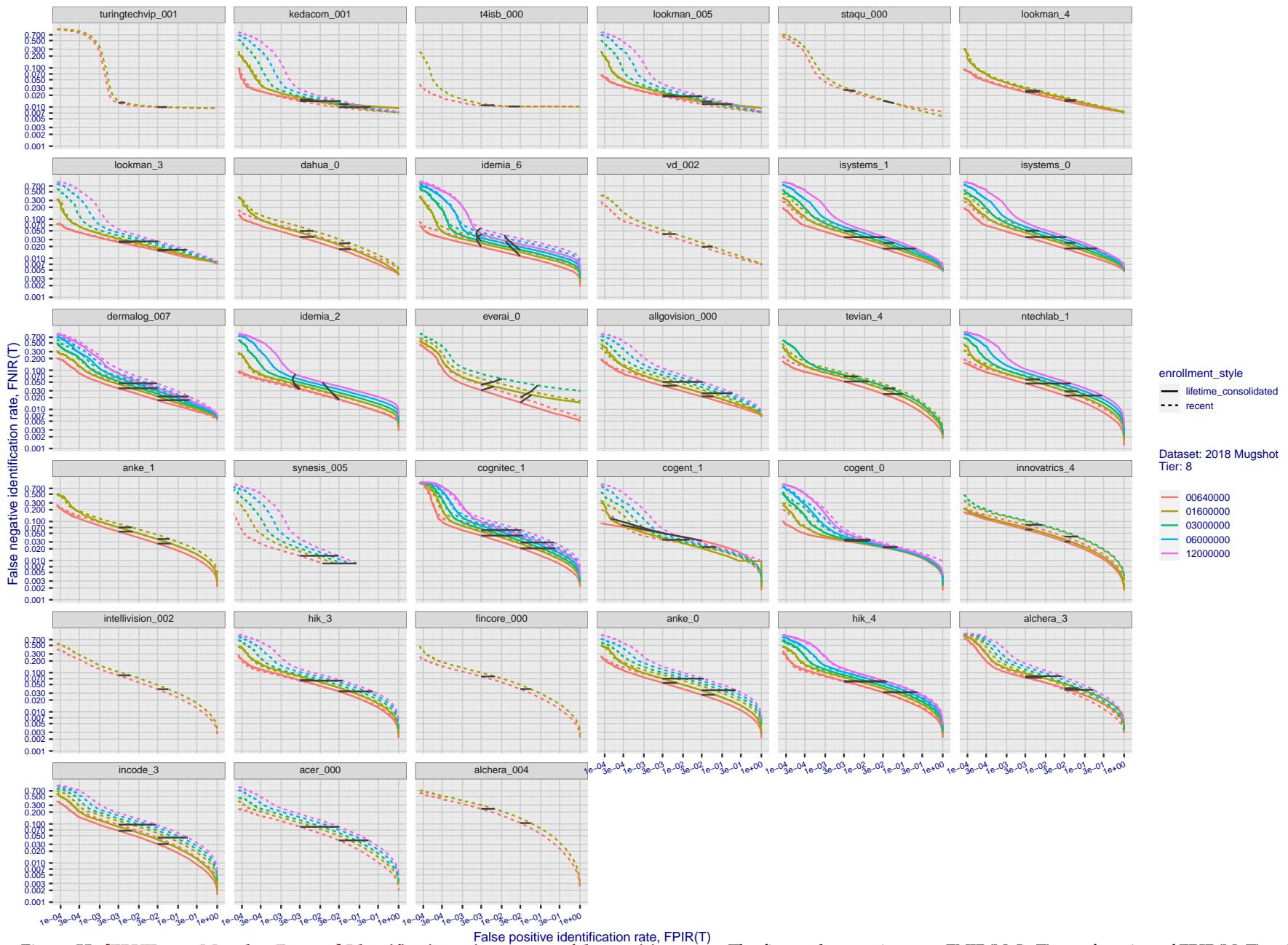


Figure 55: [FRVT-2018 Mugshot Dataset] Identification miss rates vs. false positive rates. The figure shows miss rates $\text{FNIR}(N, L, T)$ as a function of $\text{FPIR}(N, T)$, with N ranging from 640 000 to 12 000 000 as noted in rows 1-10 of Table 1. These error tradeoff characteristics are useful for applications where a threshold must be elevated to limit false positives, such as when human reviewer labor is not matched to the volume of searches. Dark lines join points of equal threshold: If horizontal, $\text{FPIR}(T)$ rises with N , and mate scores are independent of N . Other algorithms adjust scores in an attempt to make FPIR independent of N .

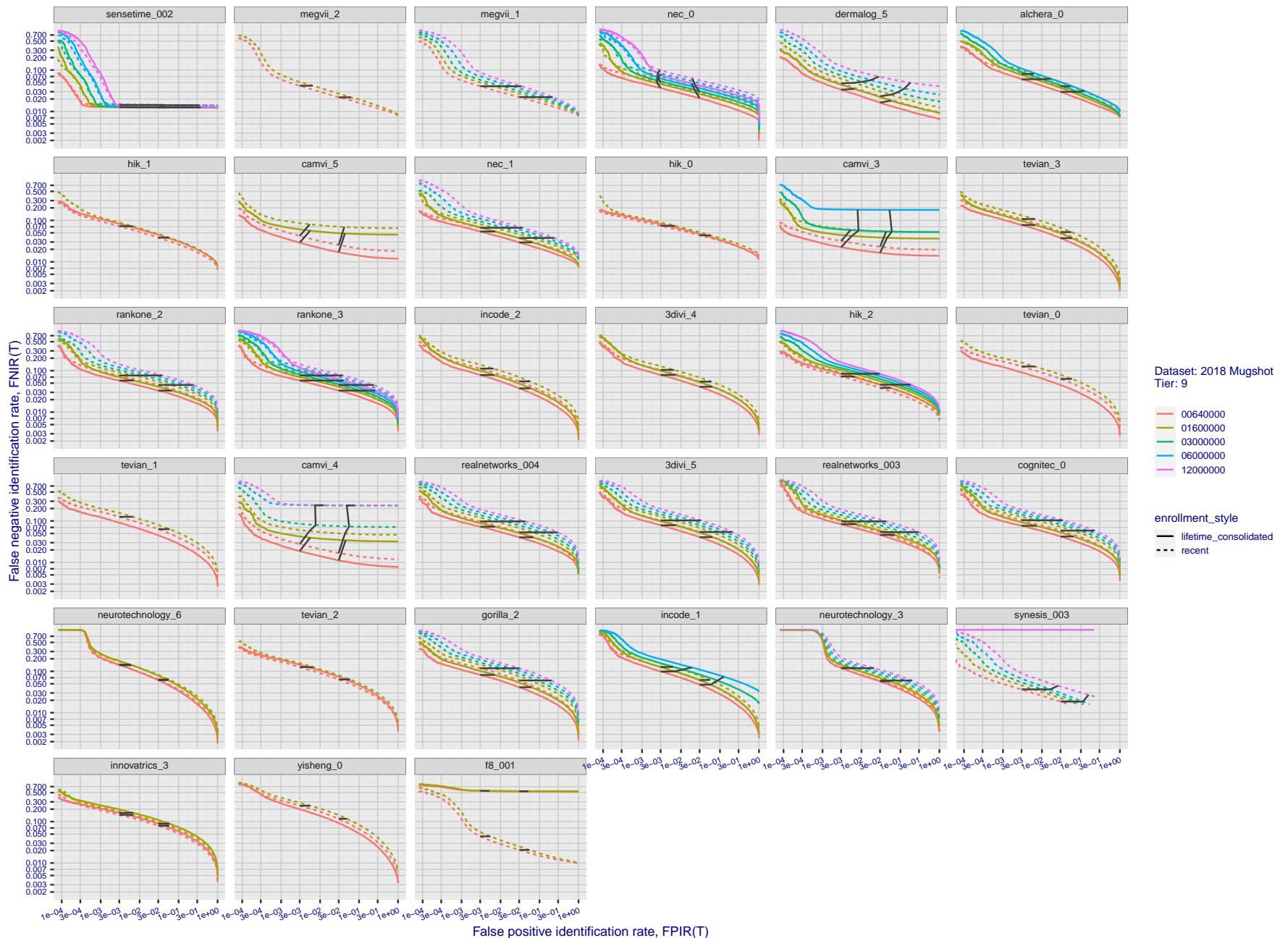


Figure 56: [FRVT-2018 Mugshot Dataset] Identification miss rates vs. false positive rates. The figure shows miss rates $\text{FNIR}(N, L, T)$ as a function of $\text{FPIR}(N, T)$, with N ranging from 640 000 to 12 000 000 as noted in rows 1-10 of Table 1. These error tradeoff characteristics are useful for applications where a threshold must be elevated to limit false positives, such as when human reviewer labor is not matched to the volume of searches. Dark lines join points of equal N . Other algorithms adjust scores in an attempt to make FPIR independent of N .

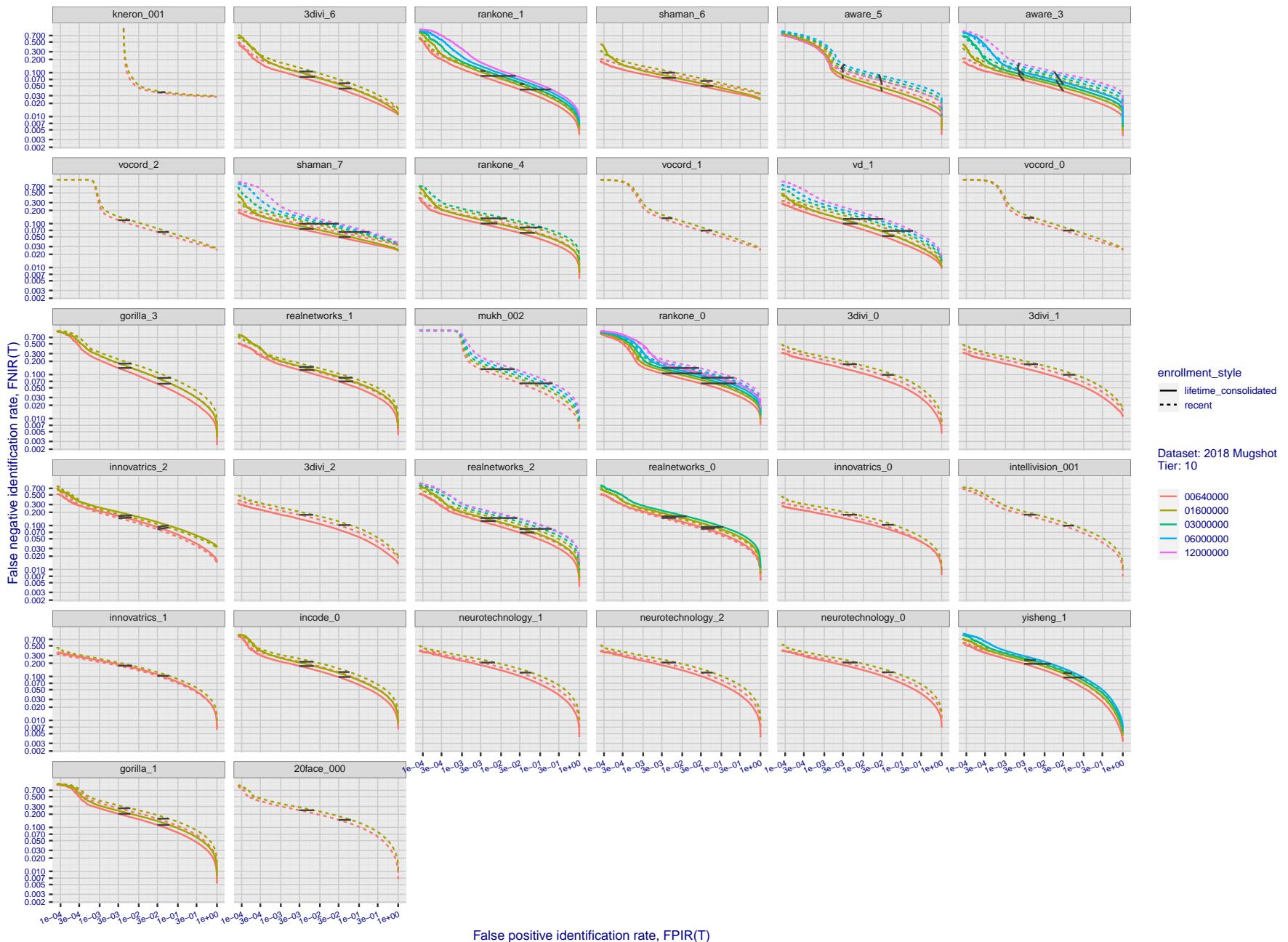


Figure 57: [FRVT-2018 Mugshot Dataset] Identification miss rates vs. false positive rates. The figure shows miss rates $\text{FNIR}(N, L, T)$ as a function of $\text{FPIR}(N, T)$, with N ranging from 640 000 to 12 000 000 as noted in rows 1-10 of Table 1. These error tradeoff characteristics are useful for applications where a threshold must be elevated to limit false positives, such as when human reviewer labor is not matched to the volume of searches. Dark lines join points of equal threshold: If horizontal, $\text{FPIR}(T)$ rises with N , and mate scores are independent of N . Other algorithms adjust scores in an attempt to make FPIR independent of N .

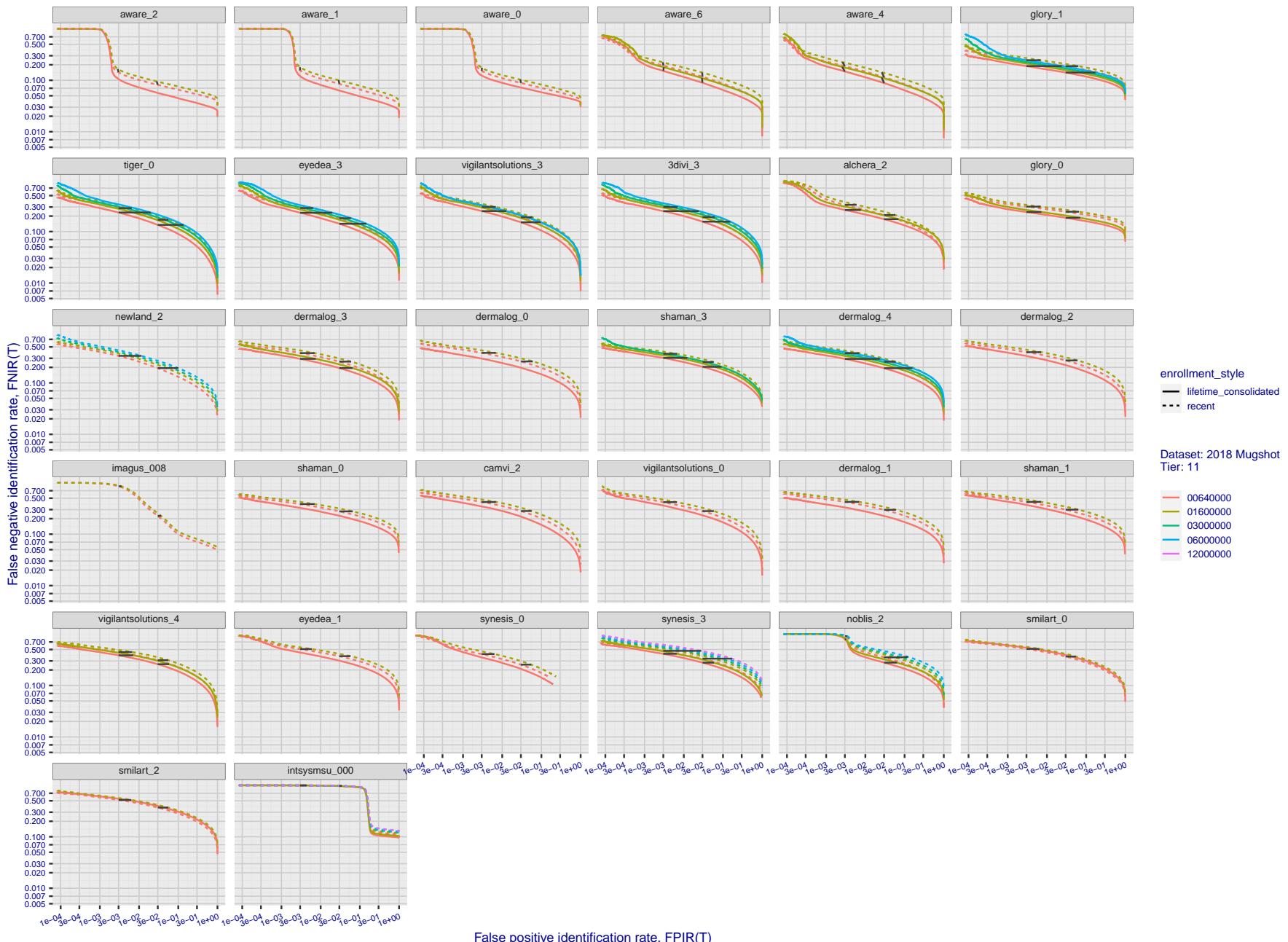


Figure 58: [FRVT-2018 Mugshot Dataset] Identification miss rates vs. false positive rates. The figure shows miss rates $\text{FNIR}(N, L, T)$ as a function of $\text{FPIR}(N, T)$, with N ranging from 640 000 to 12 000 000 as noted in rows 1-10 of Table 1. These error tradeoff characteristics are useful for applications where a threshold must be elevated to limit false positives, such as when human reviewer labor is not matched to the volume of searches. Dark lines join points of equal threshold: If horizontal, $\text{FPIR}(T)$ rises with N , and mate scores are independent of N . Other algorithms adjust scores in an attempt to make FPIR independent of N .

2023/04/04

07:31:47

FNIR(N, R, T) = False neg. identification rate
FPIR(N, T) = False pos. identification rateN = Num. enrolled subjects
R = Num. candidates examined

T = Threshold

T = 0 → Investigation
T > 0 → Identification

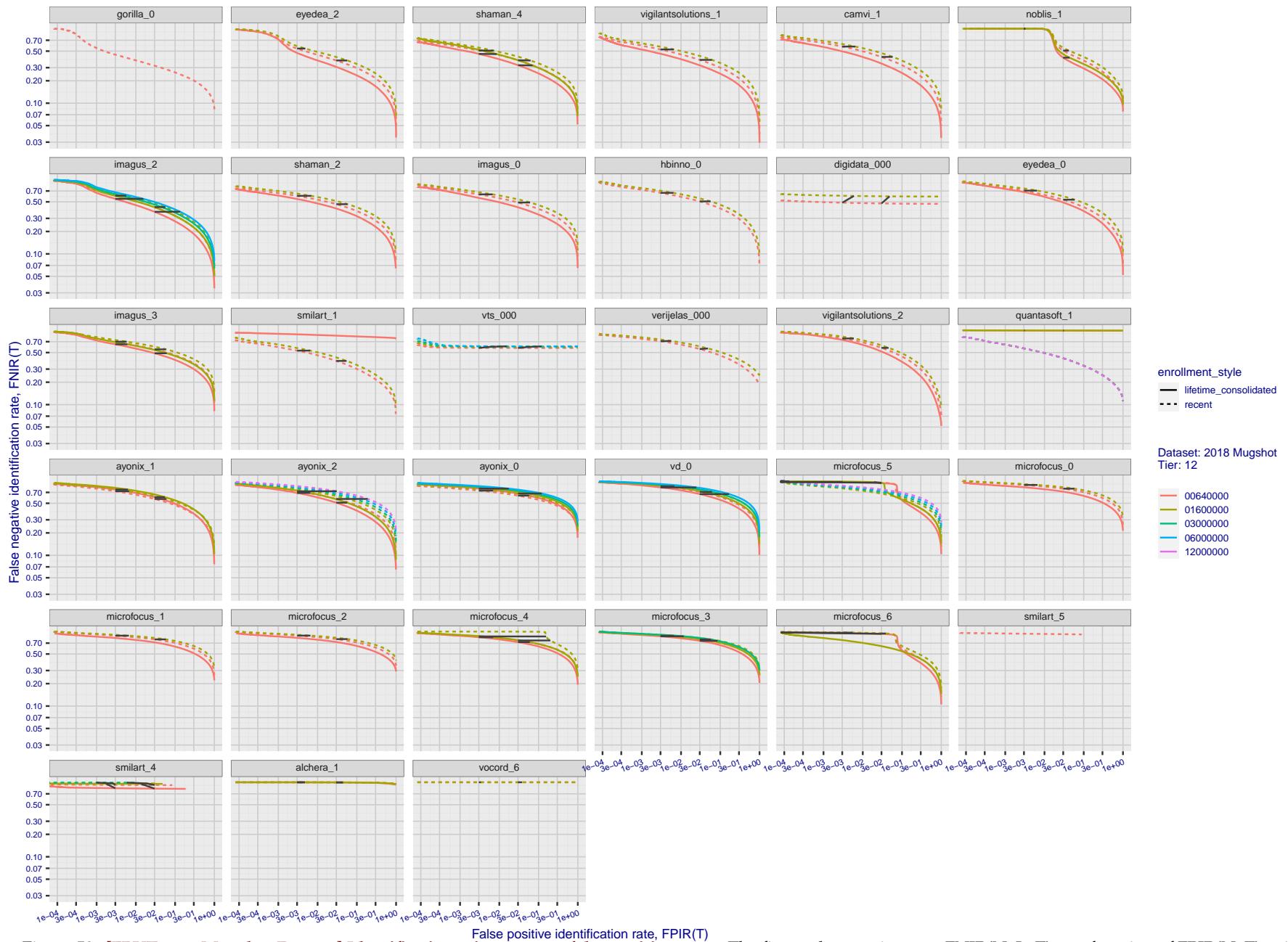


Figure 59: [FRVT-2018 Mugshot Dataset] Identification miss rates vs. false positive rates. The figure shows miss rates $\text{FNIR}(N, L, T)$ as a function of $\text{FPIR}(N, T)$, with N ranging from 640 000 to 12 000 000 as noted in rows 1-10 of Table 1. These error tradeoff characteristics are useful for applications where a threshold must be elevated to limit false positives, such as when human reviewer labor is not matched to the volume of searches. Dark lines join points of equal threshold: If horizontal, $\text{FPIR}(T)$ rises with N , and mate scores are independent of N . Other algorithms adjust scores in an attempt to make FPIR independent of N .

Appendix B Effect of time-lapse: Accuracy after face ageing

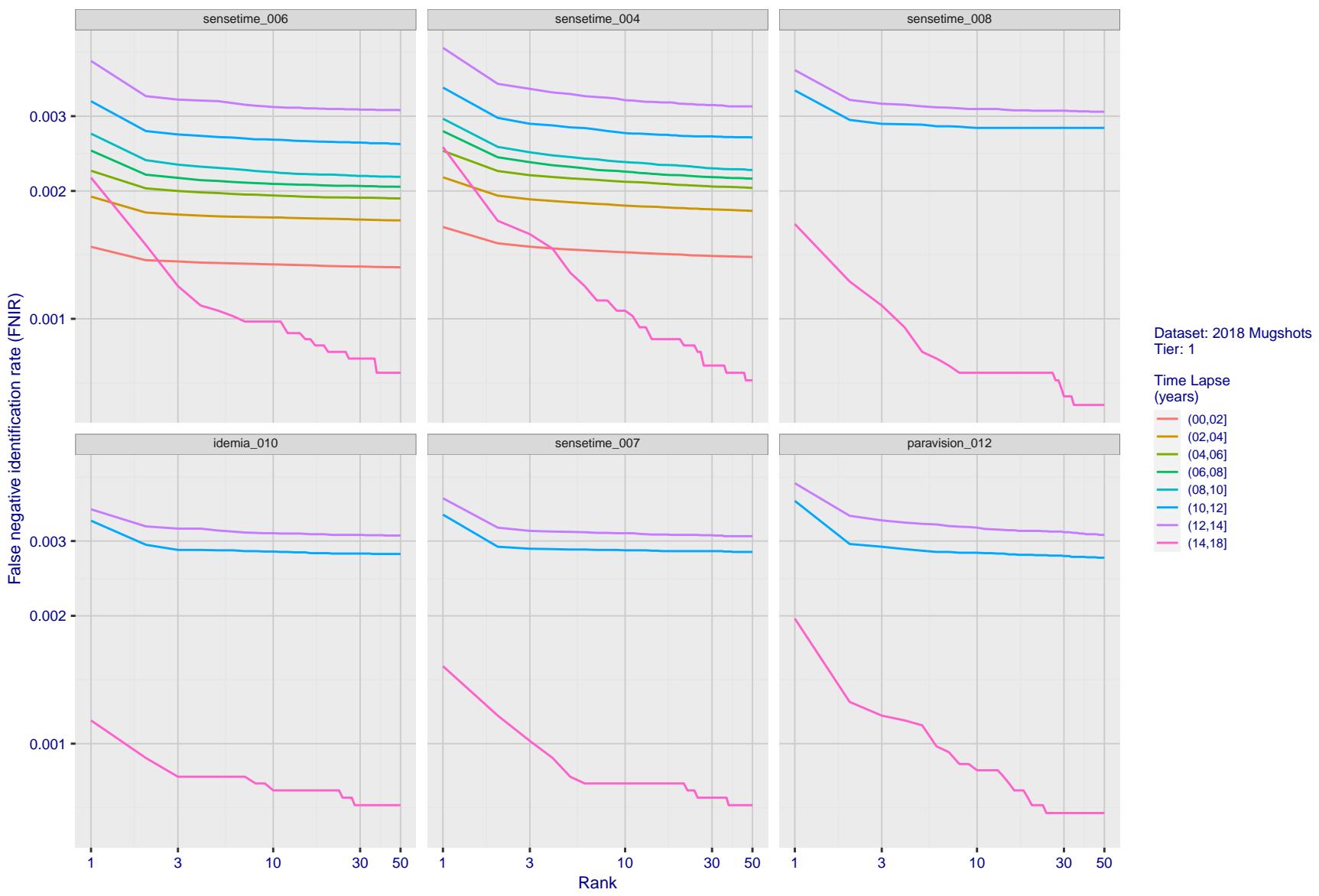


Figure 60: [FRVT-2018 Mugshot Ageing Dataset] Identification miss rates vs. rank by time-elapsed. The oldest image of each individual is enrolled. Thereafter, all more recent images are searched. Miss rates are computed over all searches noted in row 17 of Table 1 and binned by number of years between search and initial enrollment.

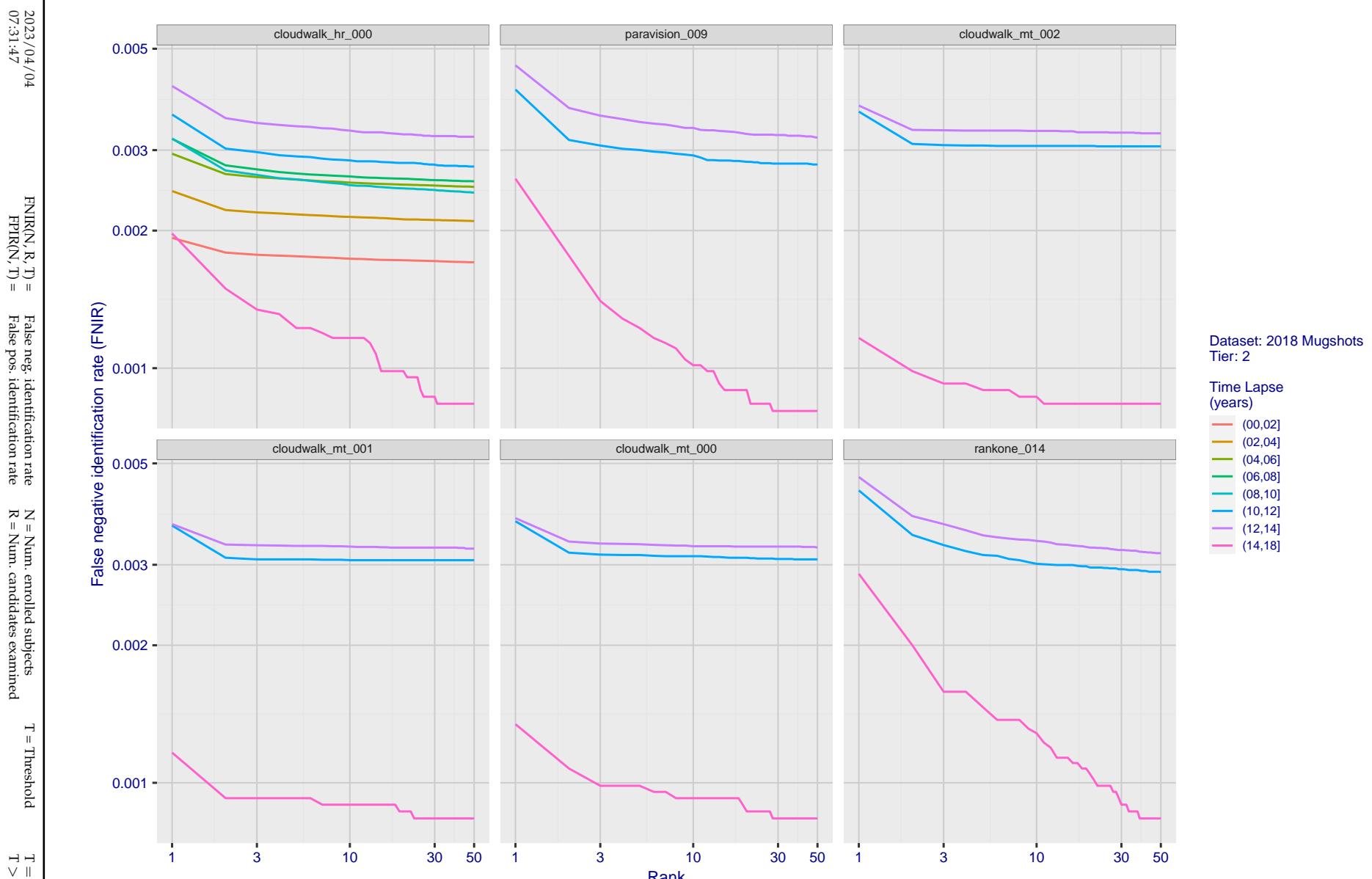


Figure 61: [FRVT-2018 Mugshot Ageing Dataset] Identification miss rates vs. rank by time-elapsed. The oldest image of each individual is enrolled. Thereafter, all more recent images are searched. Miss rates are computed over all searches noted in row 17 of Table 1 and binned by number of years between search and initial enrollment.

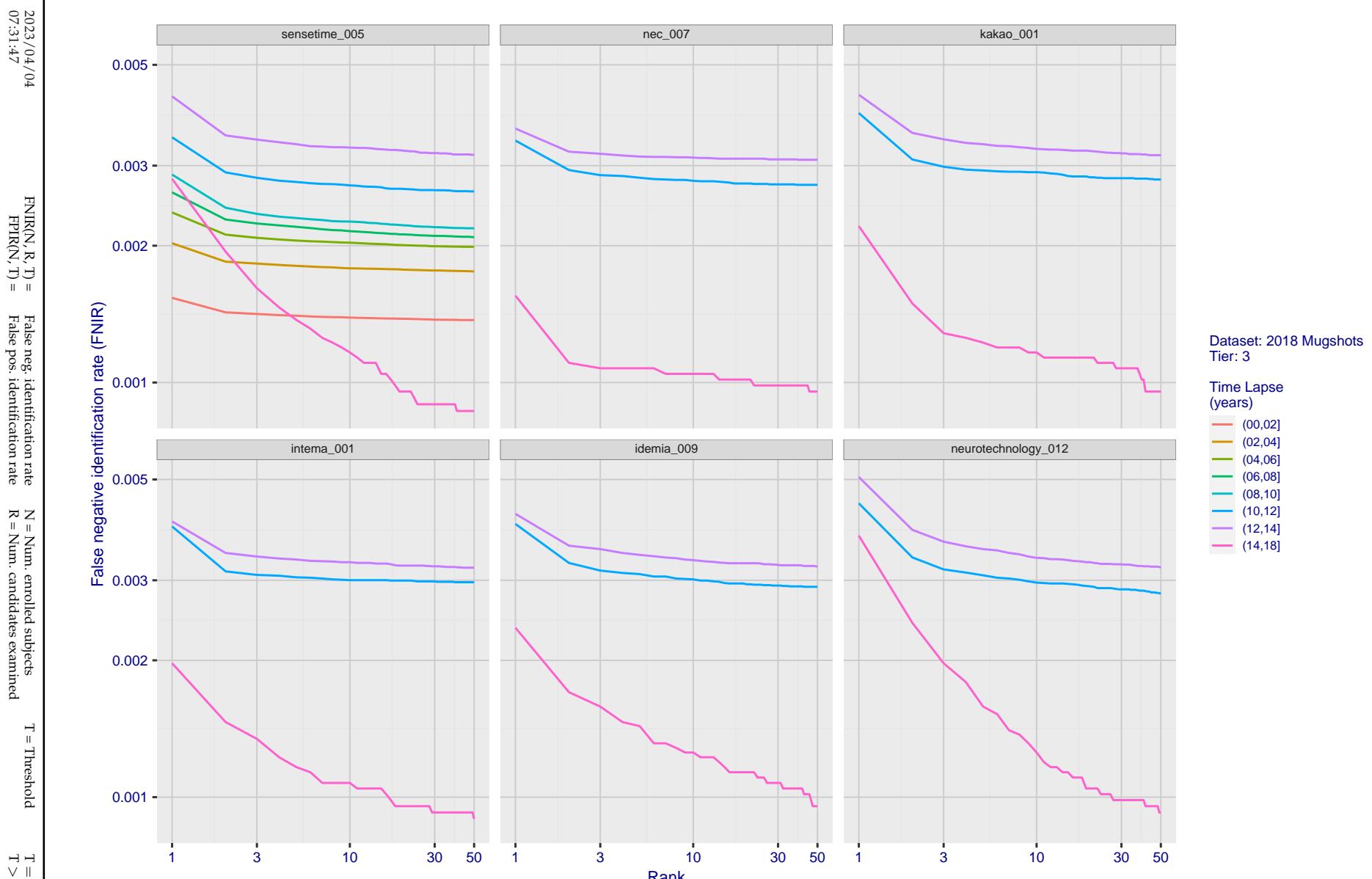


Figure 62: [FRVT-2018 Mugshot Ageing Dataset] Identification miss rates vs. rank by time-elapsed. The oldest image of each individual is enrolled. Thereafter, all more recent images are searched. Miss rates are computed over all searches noted in row 17 of Table 1 and binned by number of years between search and initial enrollment.

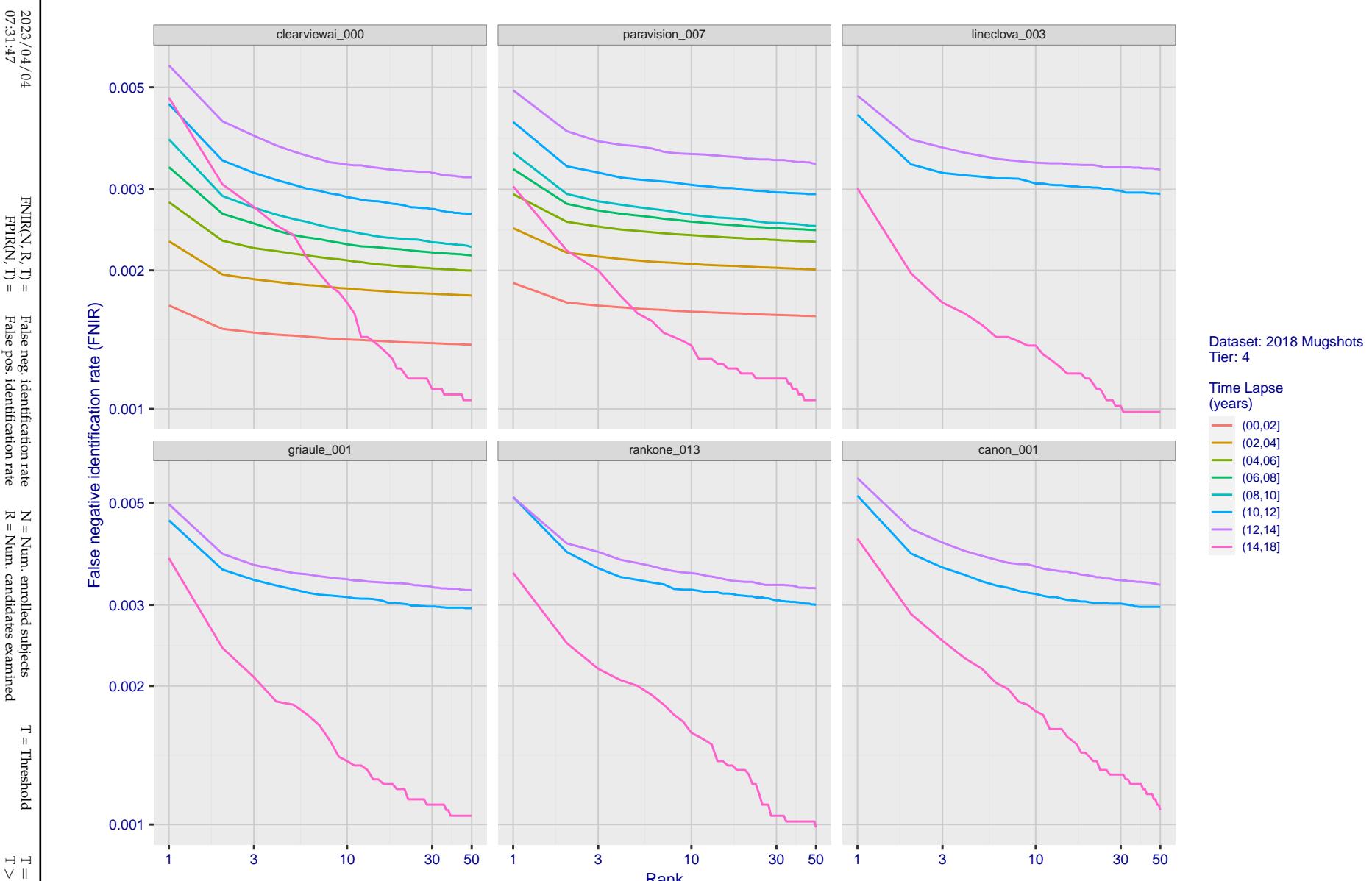


Figure 63: [FRVT-2018 Mugshot Ageing Dataset] Identification miss rates vs. rank by time elapsed. The oldest image of each individual is enrolled. Thereafter, all more recent images are searched. Miss rates are computed over all searches noted in row 17 of Table 1 and binned by number of years between search and initial enrollment.

2023/04/04
07:31:47FNIR(N, R, T) = False neg. identification rate
FPIR(N, T) = False pos. identification rateN = Num. enrolled subjects
R = Num. candidates examinedT = Threshold
T = 0 → Investigation

T > 0 → Identification

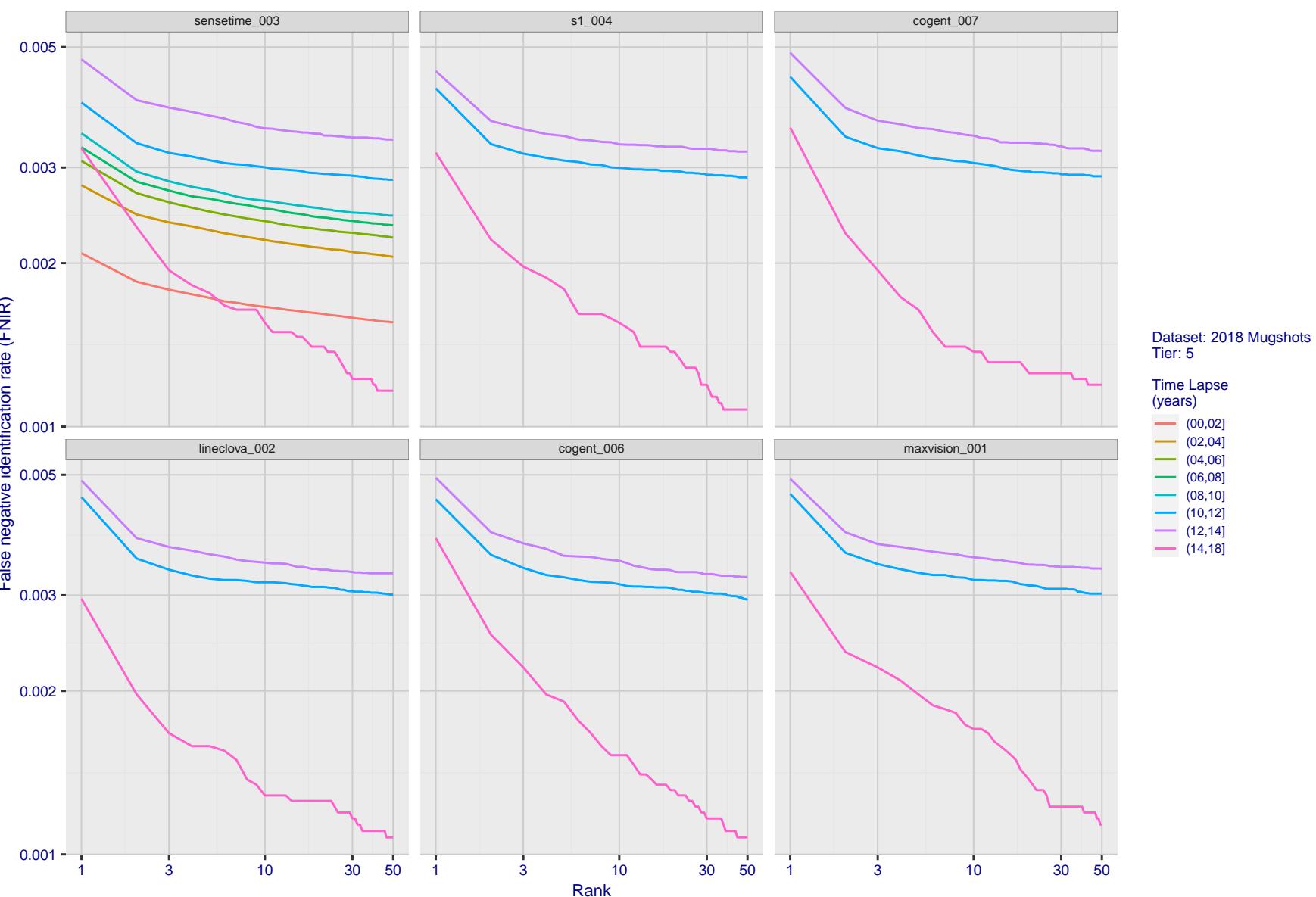


Figure 64: [FRVT-2018 Mugshot Ageing Dataset] Identification miss rates vs. rank by time-elapsed. The oldest image of each individual is enrolled. Thereafter, all more recent images are searched. Miss rates are computed over all searches noted in row 17 of Table 1 and binned by number of years between search and initial enrollment.

2023/04/04
07:31:47FNIR(N, R, T) = False neg. identification rate
FPIR(N, T) = False pos. identification rateN = Num. enrolled subjects
R = Num. candidates examinedT = Threshold
T = 0 → Investigation

T > 0 → Identification

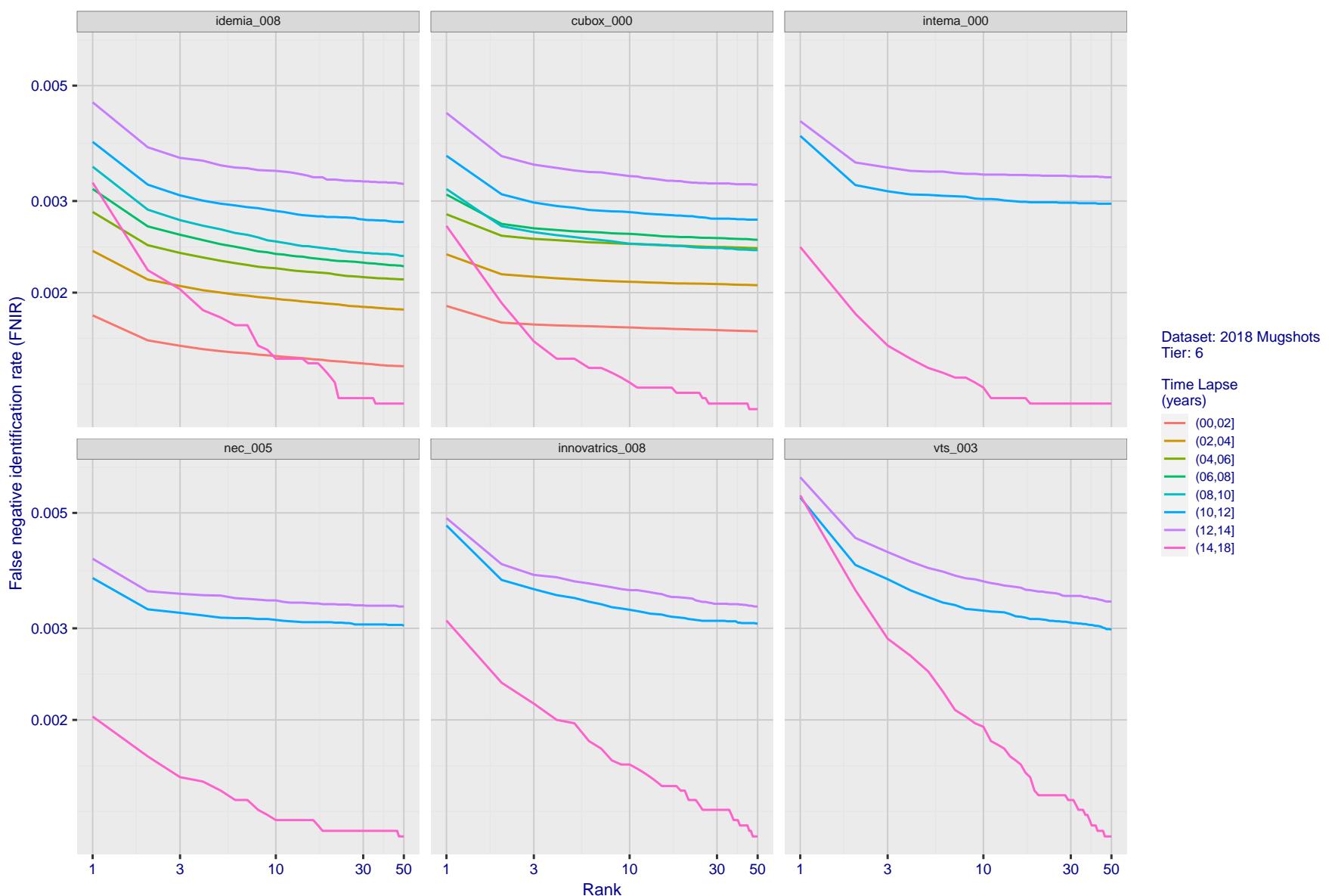


Figure 65: [FRVT-2018 Mugshot Ageing Dataset] Identification miss rates vs. rank by time-elapsed. The oldest image of each individual is enrolled. Thereafter, all more recent images are searched. Miss rates are computed over all searches noted in row 17 of Table 1 and binned by number of years between search and initial enrollment.

2023/04/04
07:31:47FNIR(N, R, T) = False neg. identification rate
FPIR(N, T) = False pos. identification rateN = Num. enrolled subjects
R = Num. candidates examinedT = Threshold
T = 0 → Investigation

T > 0 → Identification

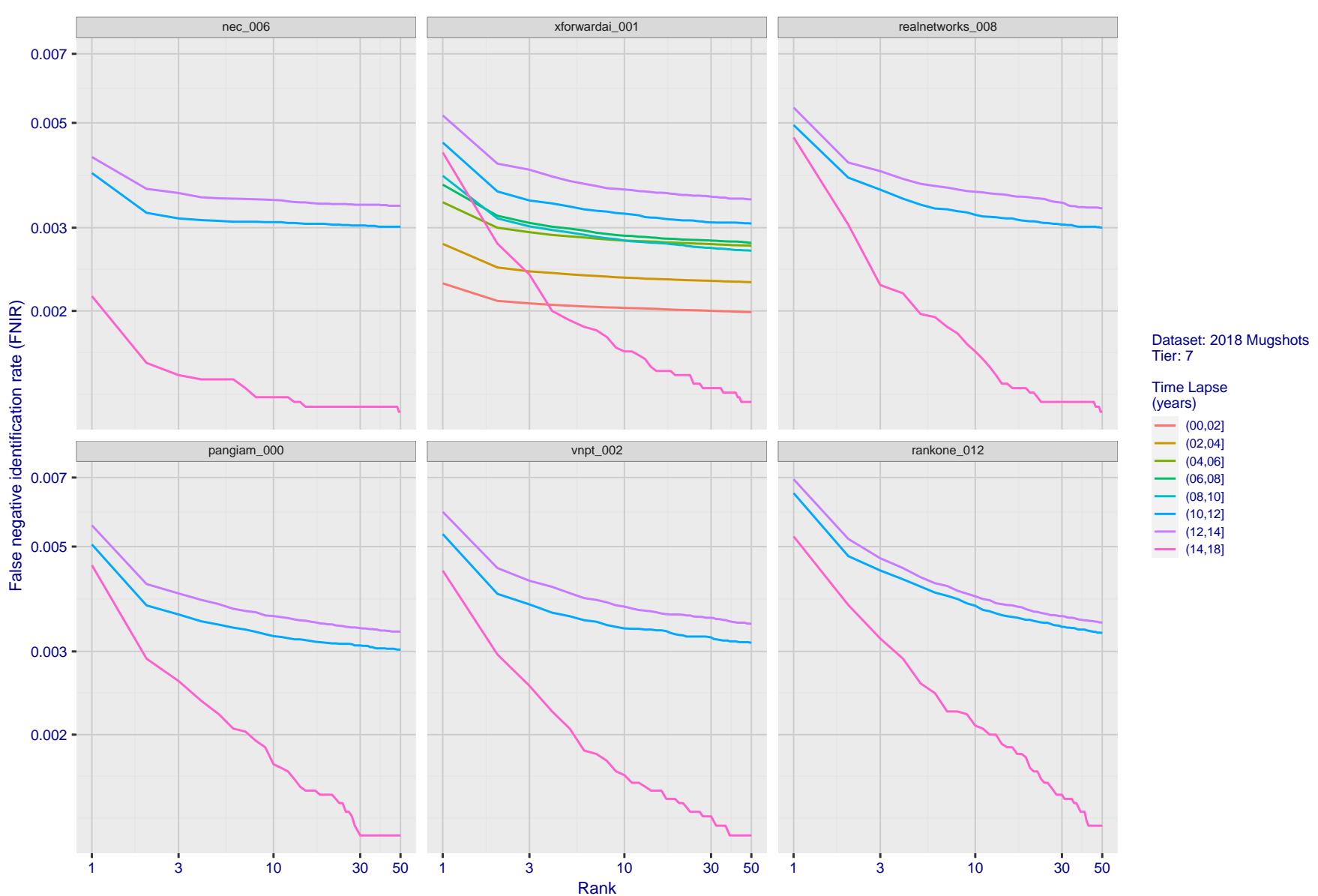


Figure 66: [FRVT-2018 Mugshot Ageing Dataset] Identification miss rates vs. rank by time elapsed. The oldest image of each individual is enrolled. Thereafter, all more recent images are searched. Miss rates are computed over all searches noted in row 17 of Table 1 and binned by number of years between search and initial enrollment.

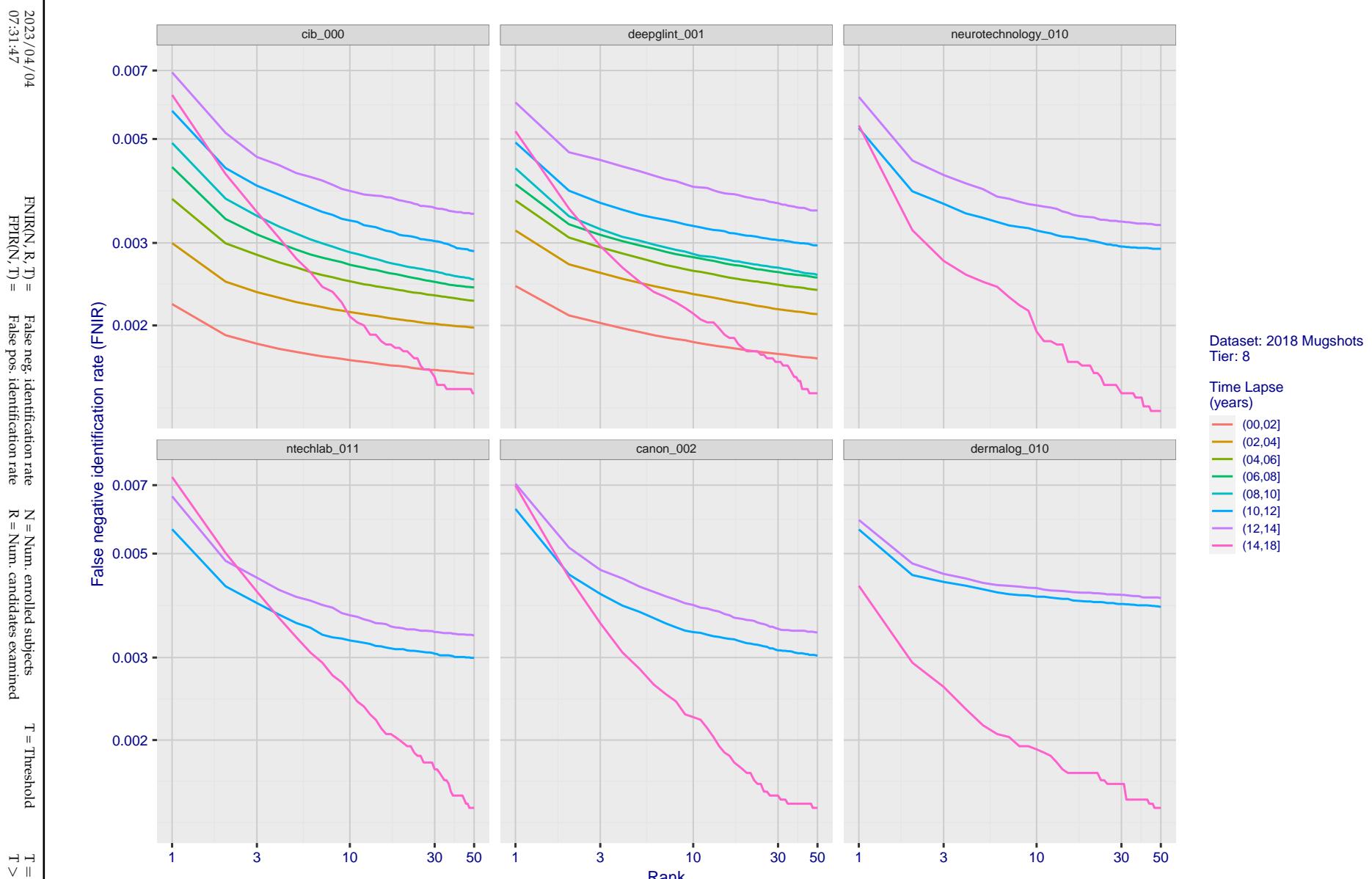


Figure 67: [FRVT-2018 Mugshot Ageing Dataset] Identification miss rates vs. rank by time-elapsed. The oldest image of each individual is enrolled. Thereafter, all more recent images are searched. Miss rates are computed over all searches noted in row 17 of Table 1 and binned by number of years between search and initial enrollment.

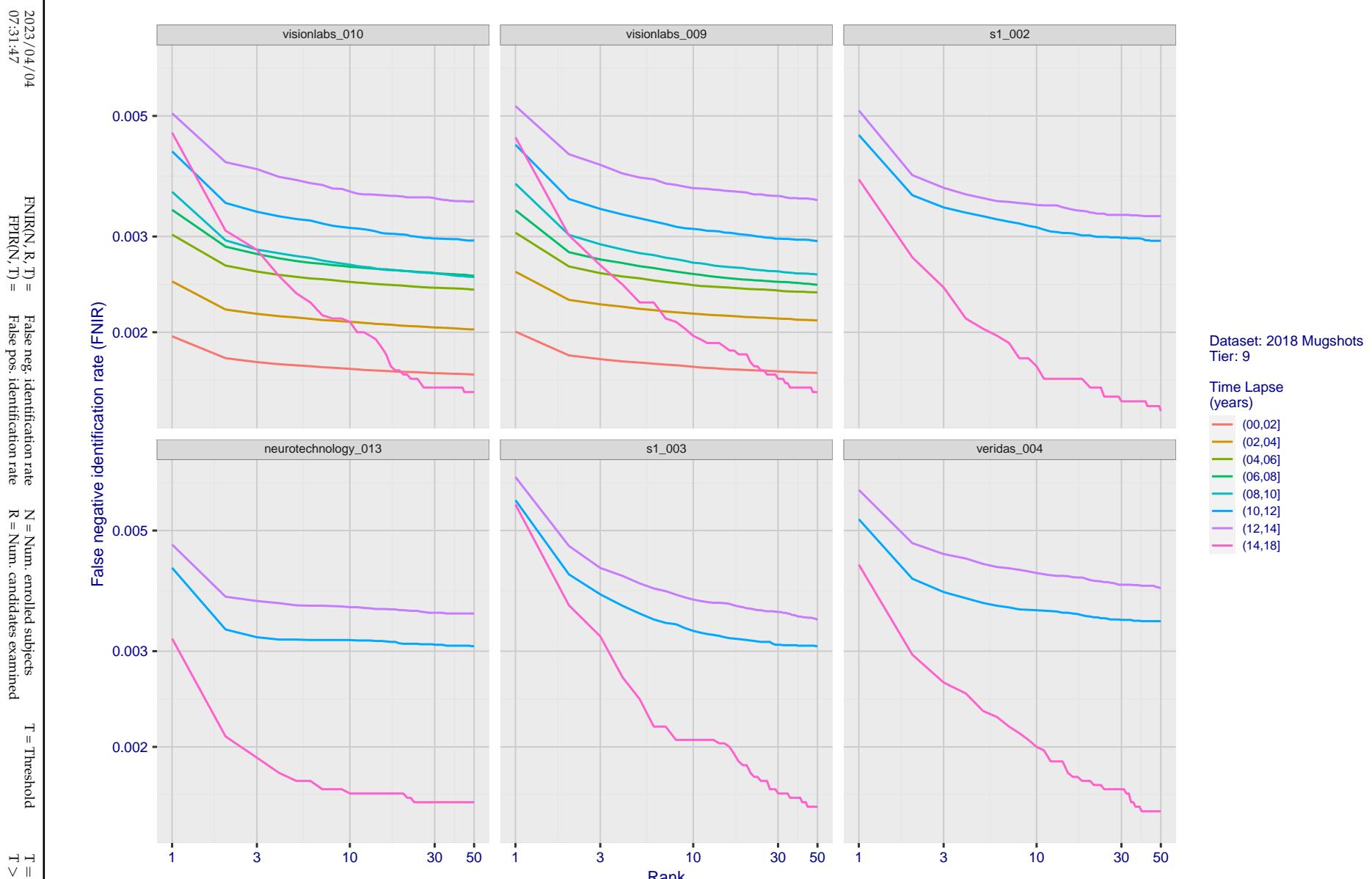


Figure 68: [FRVT-2018 Mugshot Ageing Dataset] Identification miss rates vs. rank by time-elapsed. The oldest image of each individual is enrolled. Thereafter, all more recent images are searched. Miss rates are computed over all searches noted in row 17 of Table 1 and binned by number of years between search and initial enrollment.

2023/04/04
07:31:47FNIR(N, R, T) = False neg. identification rate
FPIR(N, T) = False pos. identification rateN = Num. enrolled subjects
R = Num. candidates examinedT = Threshold
T = 0 → Investigation

T > 0 → Identification

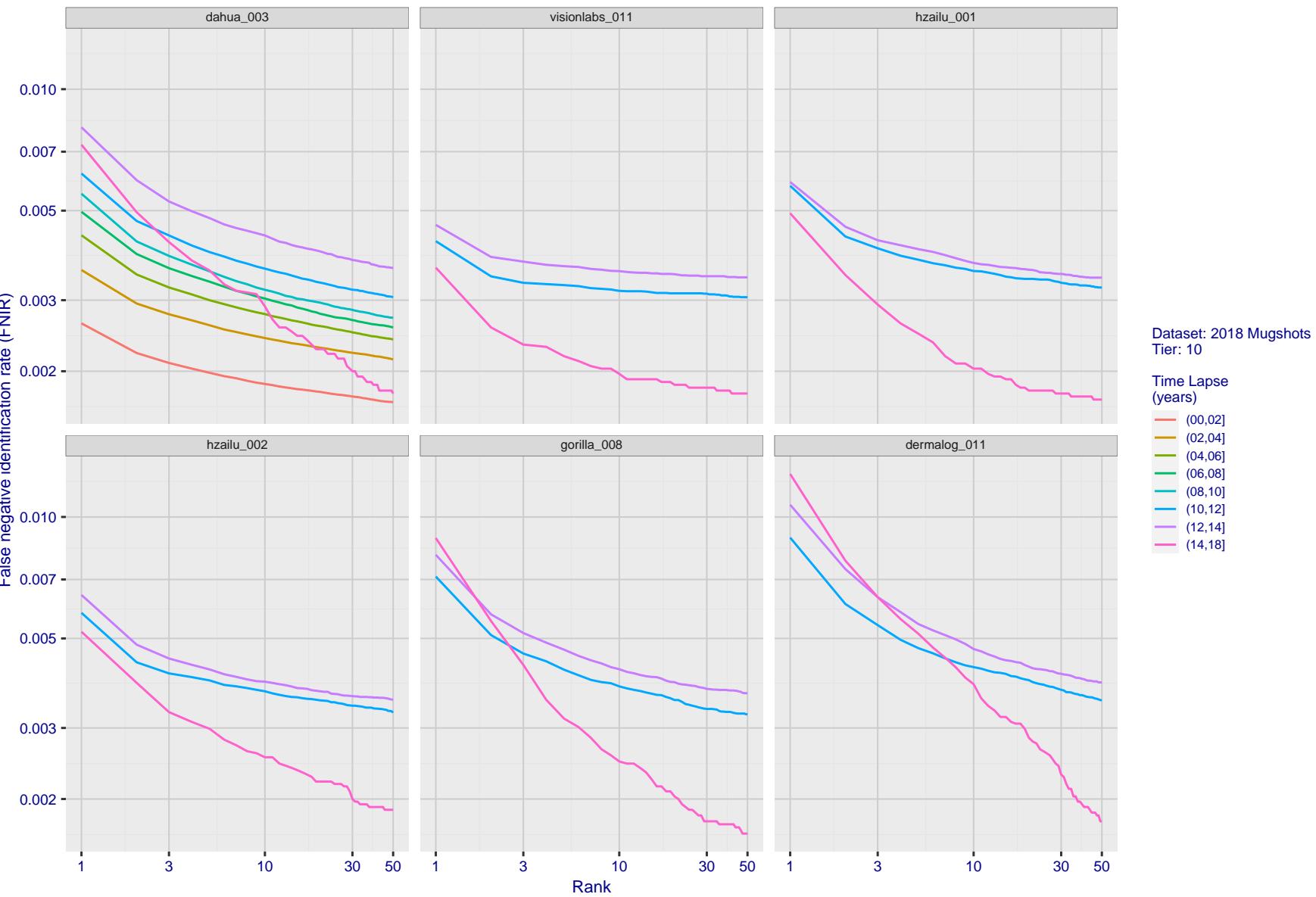


Figure 69: [FRVT-2018 Mugshot Ageing Dataset] Identification miss rates vs. rank by time-elapsed. The oldest image of each individual is enrolled. Thereafter, all more recent images are searched. Miss rates are computed over all searches noted in row 17 of Table 1 and binned by number of years between search and initial enrollment.

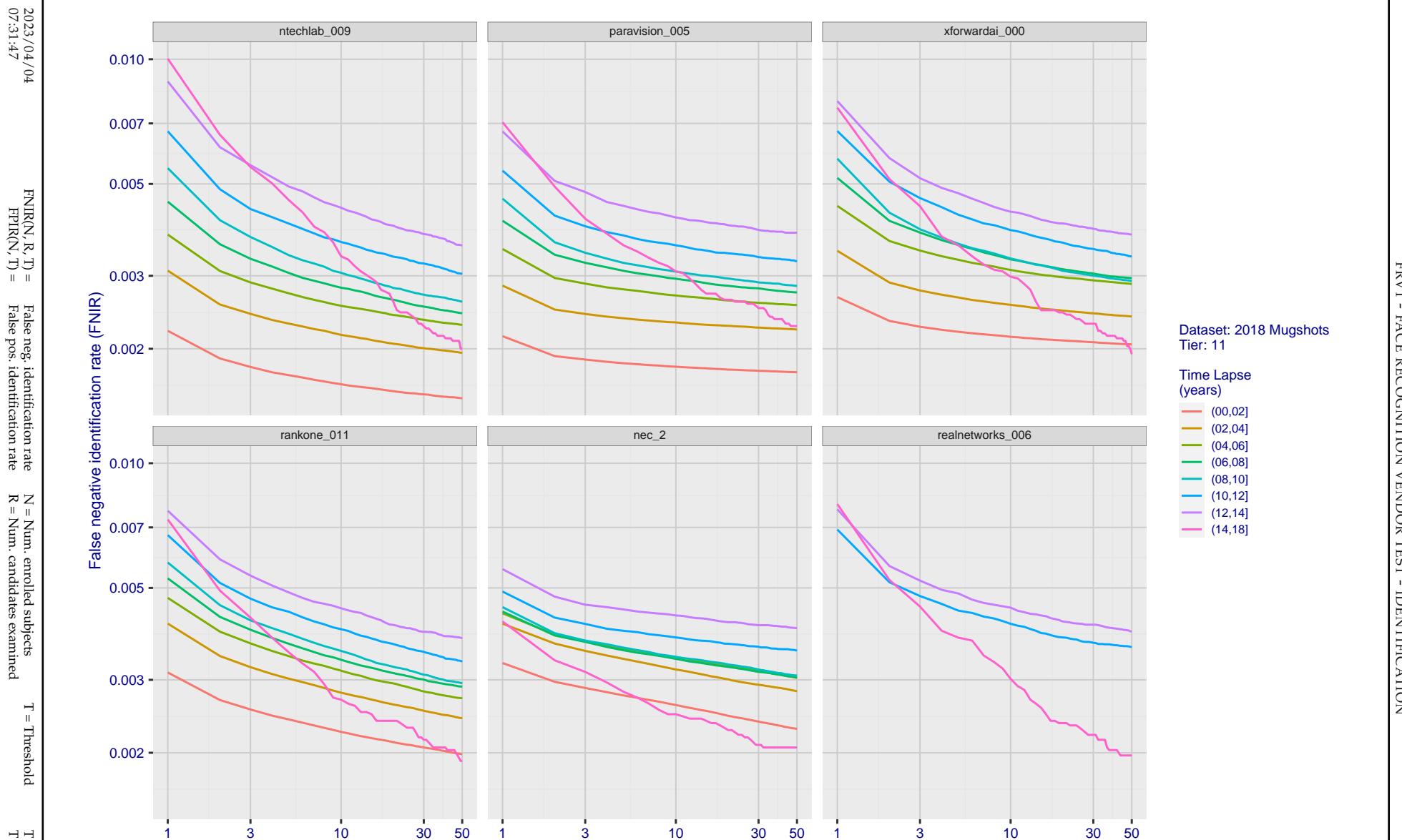


Figure 70: [FRVT-2018 Mugshot Ageing Dataset] Identification miss rates vs. rank by time-elapsed. The oldest image of each individual is enrolled. Thereafter, all more recent images are searched. Miss rates are computed over all searches noted in row 17 of Table 1 and binned by number of years between search and initial enrollment.

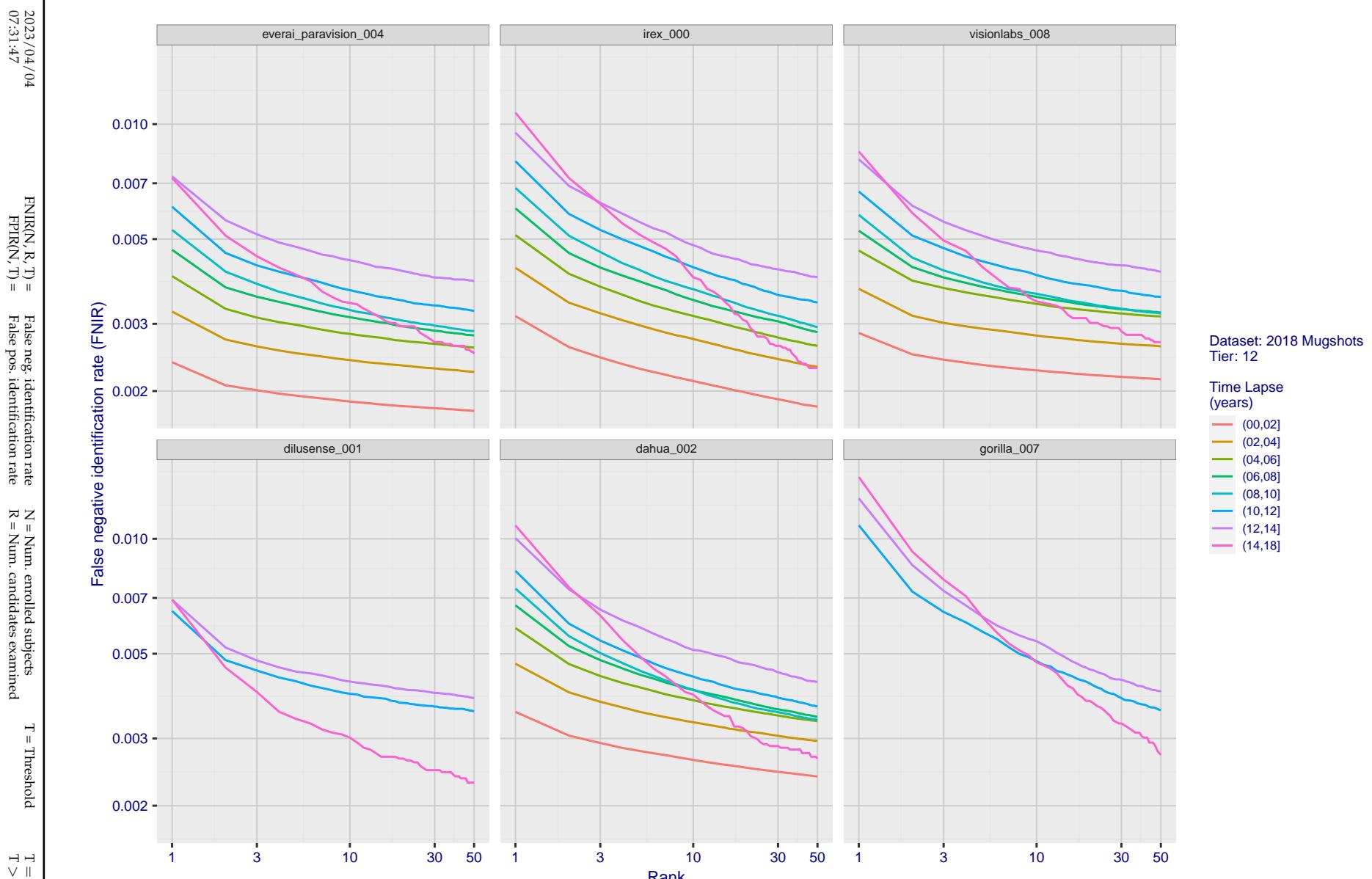


Figure 71: [FRVT-2018 Mugshot Ageing Dataset] Identification miss rates vs. rank by time-elapsed. The oldest image of each individual is enrolled. Thereafter, all more recent images are searched. Miss rates are computed over all searches noted in row 17 of Table 1 and binned by number of years between search and initial enrollment.

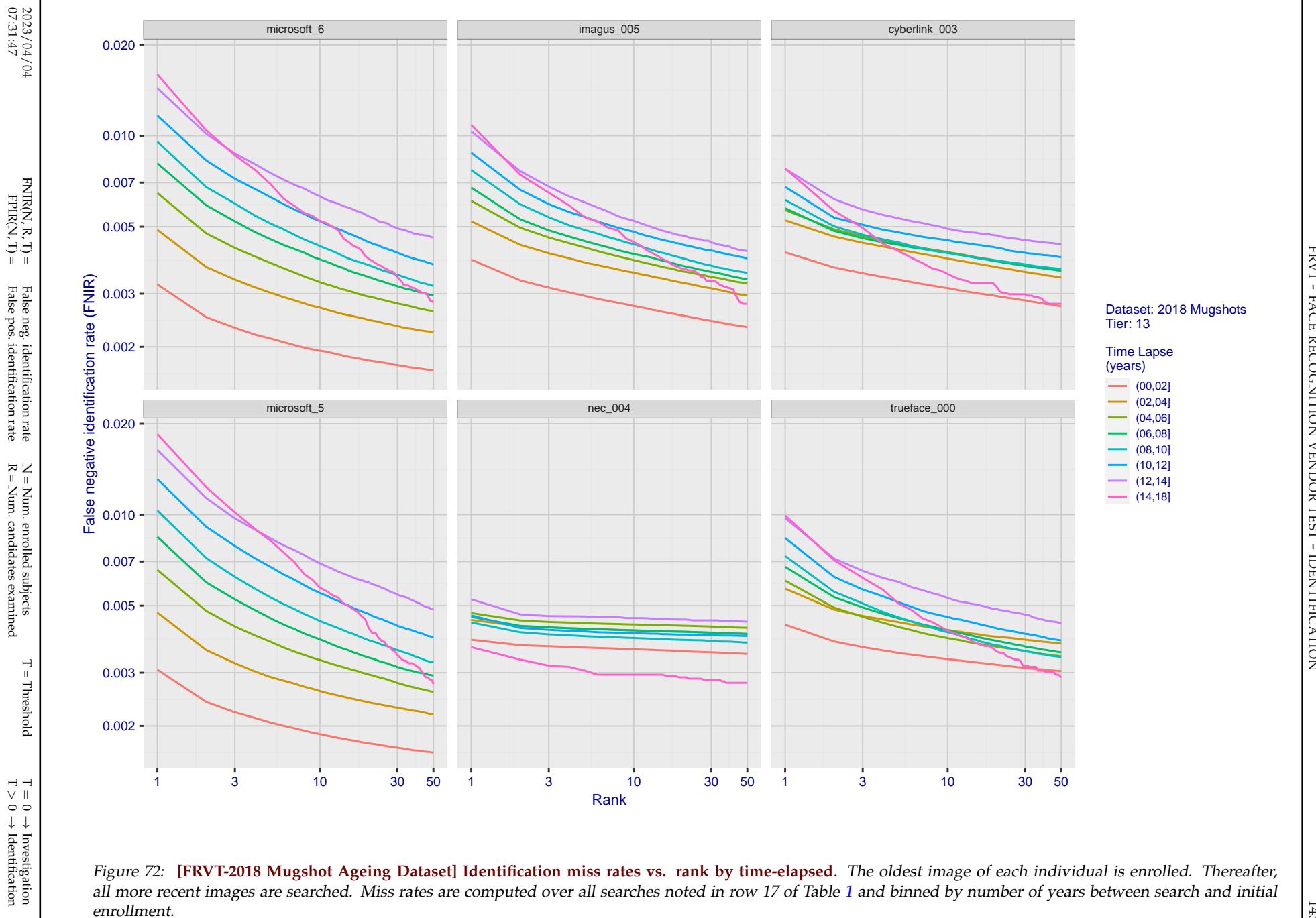


Figure 72: [FRVT-2018 Mugshot Ageing Dataset] Identification miss rates vs. rank by time-elapsed. The oldest image of each individual is enrolled. Thereafter, all more recent images are searched. Miss rates are computed over all searches noted in row 17 of Table 1 and binned by number of years between search and initial enrollment.

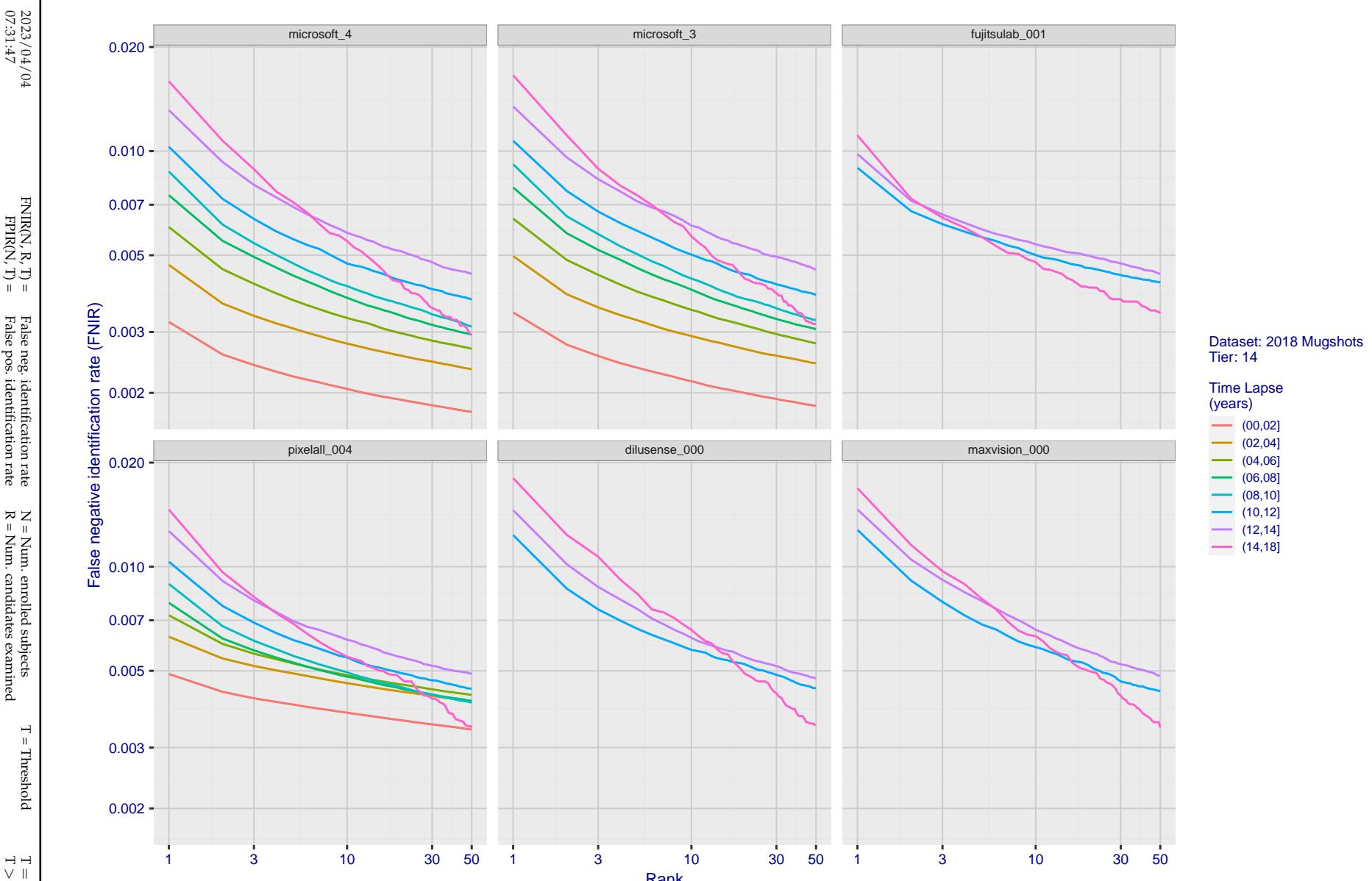


Figure 73: [FRVT-2018 Mugshot Ageing Dataset] Identification miss rates vs. rank by time-elapsed. The oldest image of each individual is enrolled. Thereafter, all more recent images are searched. Miss rates are computed over all searches noted in row 17 of Table 1 and binned by number of years between search and initial enrollment.

2023/04/04
07:31:47FNIR(N, R, T) = False neg. identification rate
FPIR(N, T) = False pos. identification rateN = Num. enrolled subjects
R = Num. candidates examinedT = Threshold
T = 0 → Investigation

T > 0 → Identification

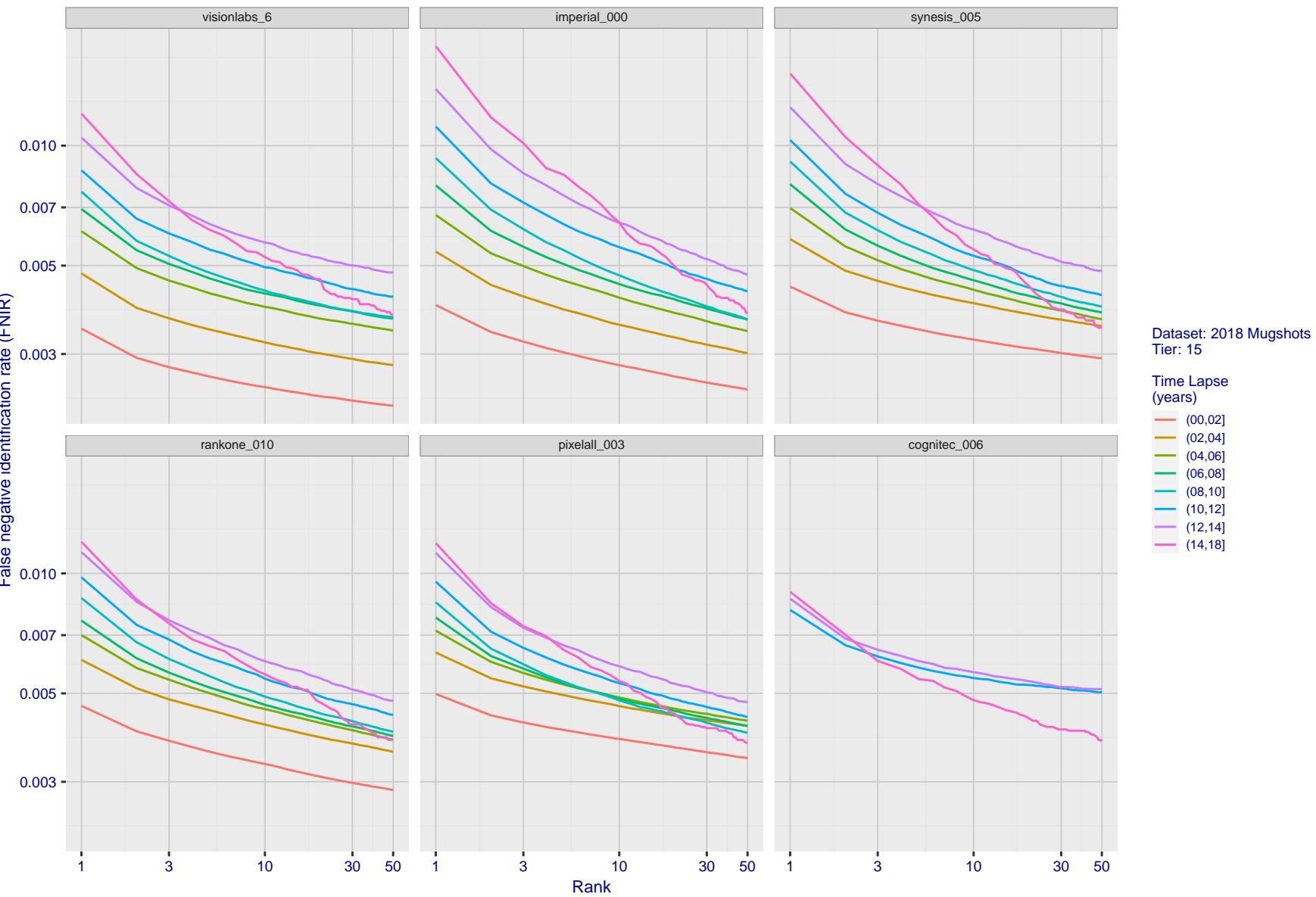


Figure 74: [FRVT-2018 Mugshot Ageing Dataset] Identification miss rates vs. rank by time-elapsed. The oldest image of each individual is enrolled. Thereafter, all more recent images are searched. Miss rates are computed over all searches noted in row 17 of Table 1 and binned by number of years between search and initial enrollment.

2023/04/04
07:31:47FNIR(N, R, T) = False neg. identification rate
FPIR(N, T) = False pos. identification rateN = Num. enrolled subjects
R = Num. candidates examinedT = Threshold
T = 0 → Investigation

T > 0 → Identification

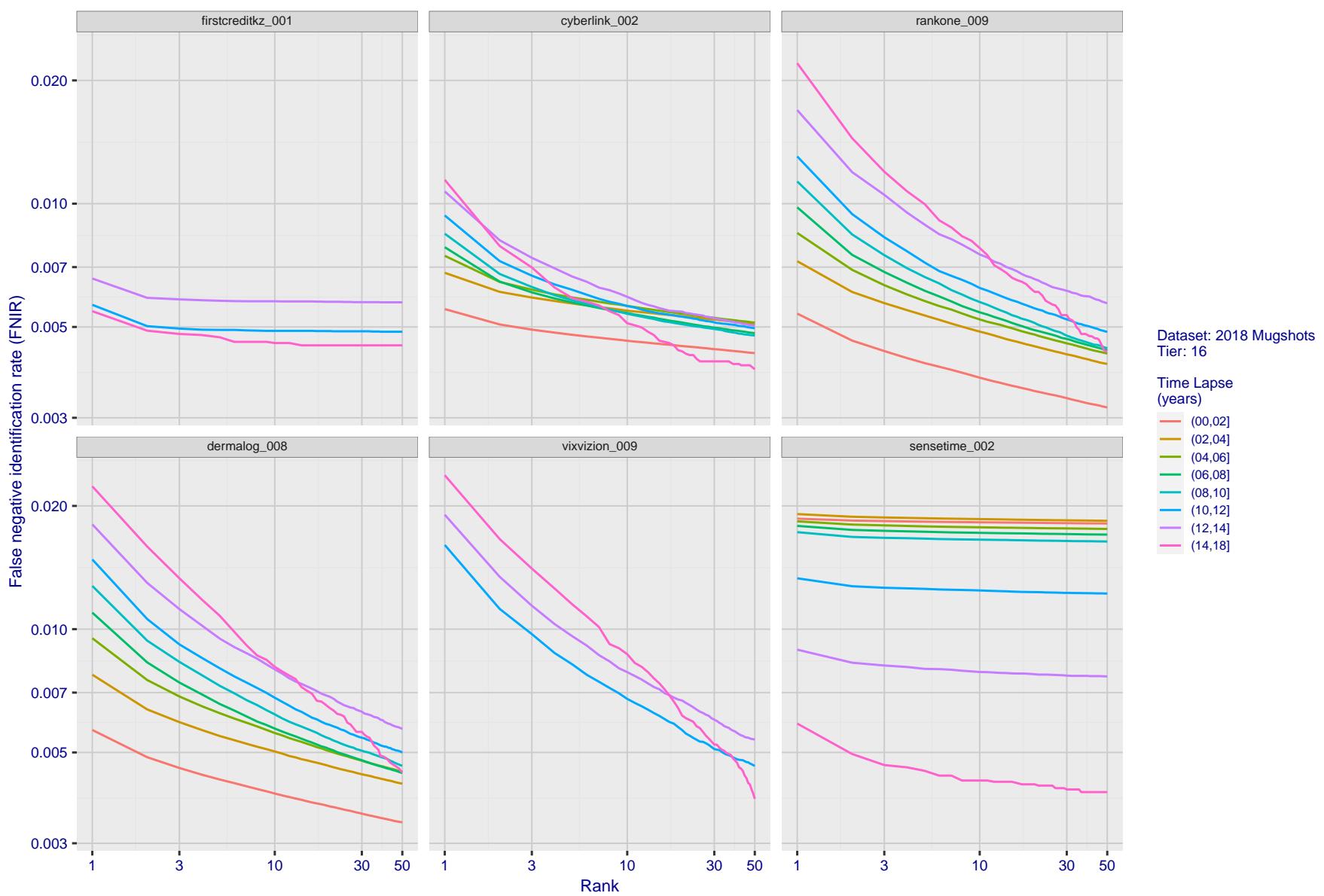


Figure 75: [FRVT-2018 Mugshot Ageing Dataset] Identification miss rates vs. rank by time-elapsed. The oldest image of each individual is enrolled. Thereafter, all more recent images are searched. Miss rates are computed over all searches noted in row 17 of Table 1 and binned by number of years between search and initial enrollment.

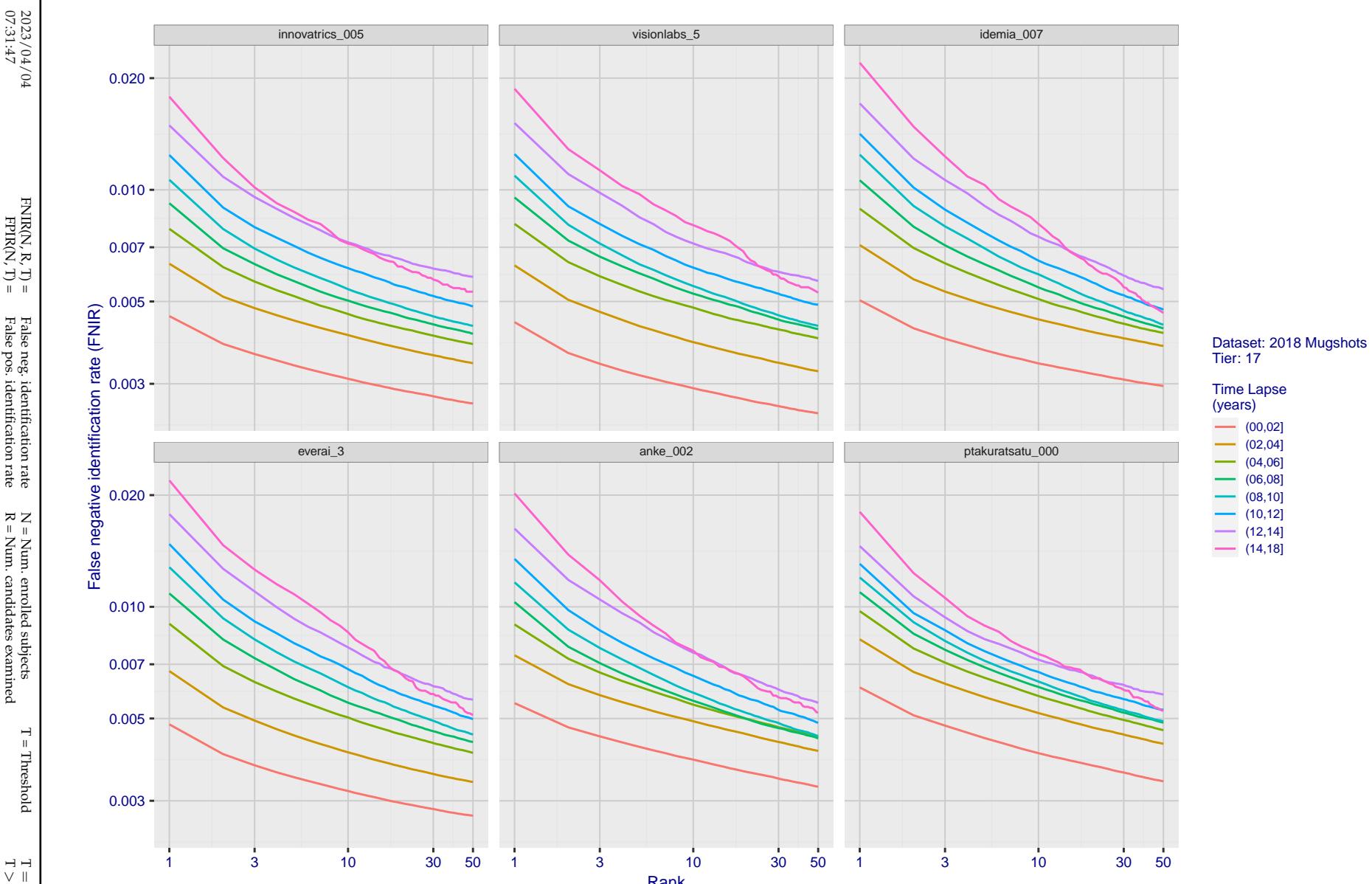


Figure 76: [FRVT-2018 Mugshot Ageing Dataset] Identification miss rates vs. rank by time-elapsed. The oldest image of each individual is enrolled. Thereafter, all more recent images are searched. Miss rates are computed over all searches noted in row 17 of Table 1 and binned by number of years between search and initial enrollment.

2023/04/04
07:31:47FNIR(N, R, T) = False neg. identification rate
FPFR(N, T) = False pos. identification rateN = Num. enrolled subjects
R = Num. candidates examinedT = Threshold
T = 0 → Investigation

T > 0 → Identification

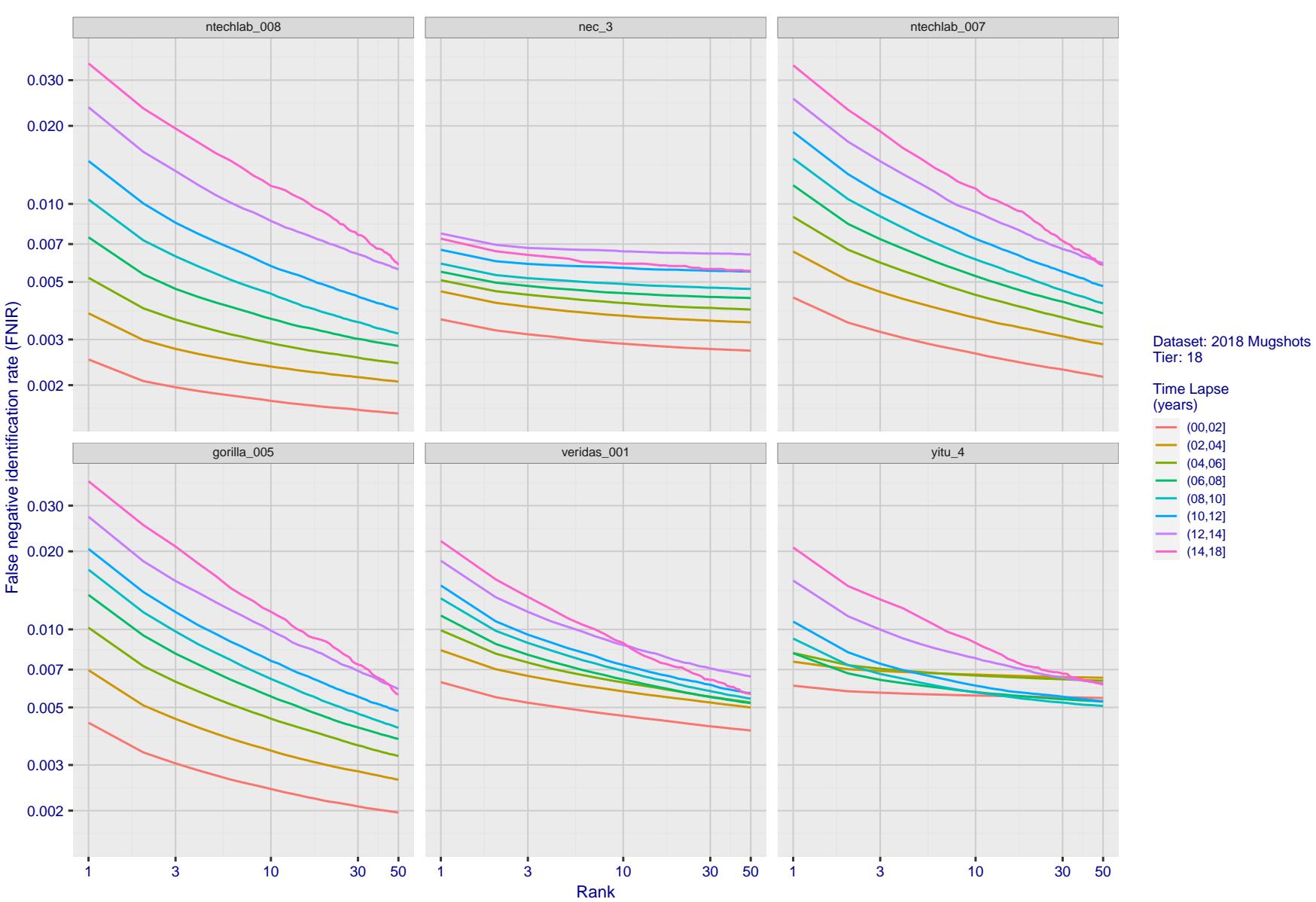


Figure 77: [FRVT-2018 Mugshot Ageing Dataset] Identification miss rates vs. rank by time-elapsed. The oldest image of each individual is enrolled. Thereafter, all more recent images are searched. Miss rates are computed over all searches noted in row 17 of Table 1 and binned by number of years between search and initial enrollment.

2023/04/04
07:31:47FNIR(N, R, T) = False neg. identification rate
FPIR(N, T) = False pos. identification rateN = Num. enrolled subjects
R = Num. candidates examined

T = Threshold

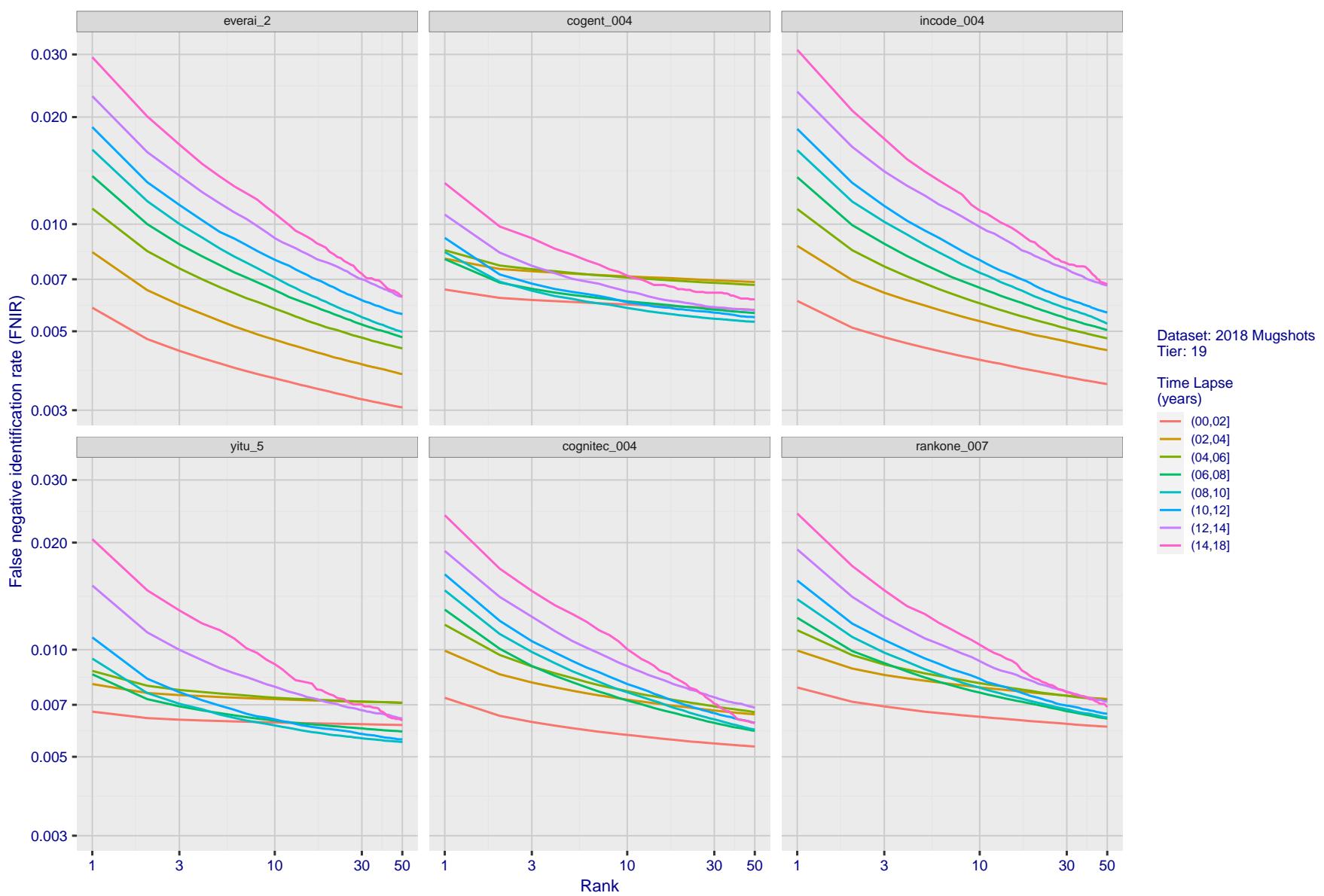
T = 0 → Investigation
T > 0 → Identification

Figure 78: [FRVT-2018 Mugshot Ageing Dataset] Identification miss rates vs. rank by time elapsed. The oldest image of each individual is enrolled. Thereafter, all more recent images are searched. Miss rates are computed over all searches noted in row 17 of Table 1 and binned by number of years between search and initial enrollment.

2023/04/04
07:31:47FNIR(N, R, T) = False neg. identification rate
FPIR(N, T) = False pos. identification rateN = Num. enrolled subjects
R = Num. candidates examinedT = Threshold
T = 0 → Investigation

T > 0 → Identification

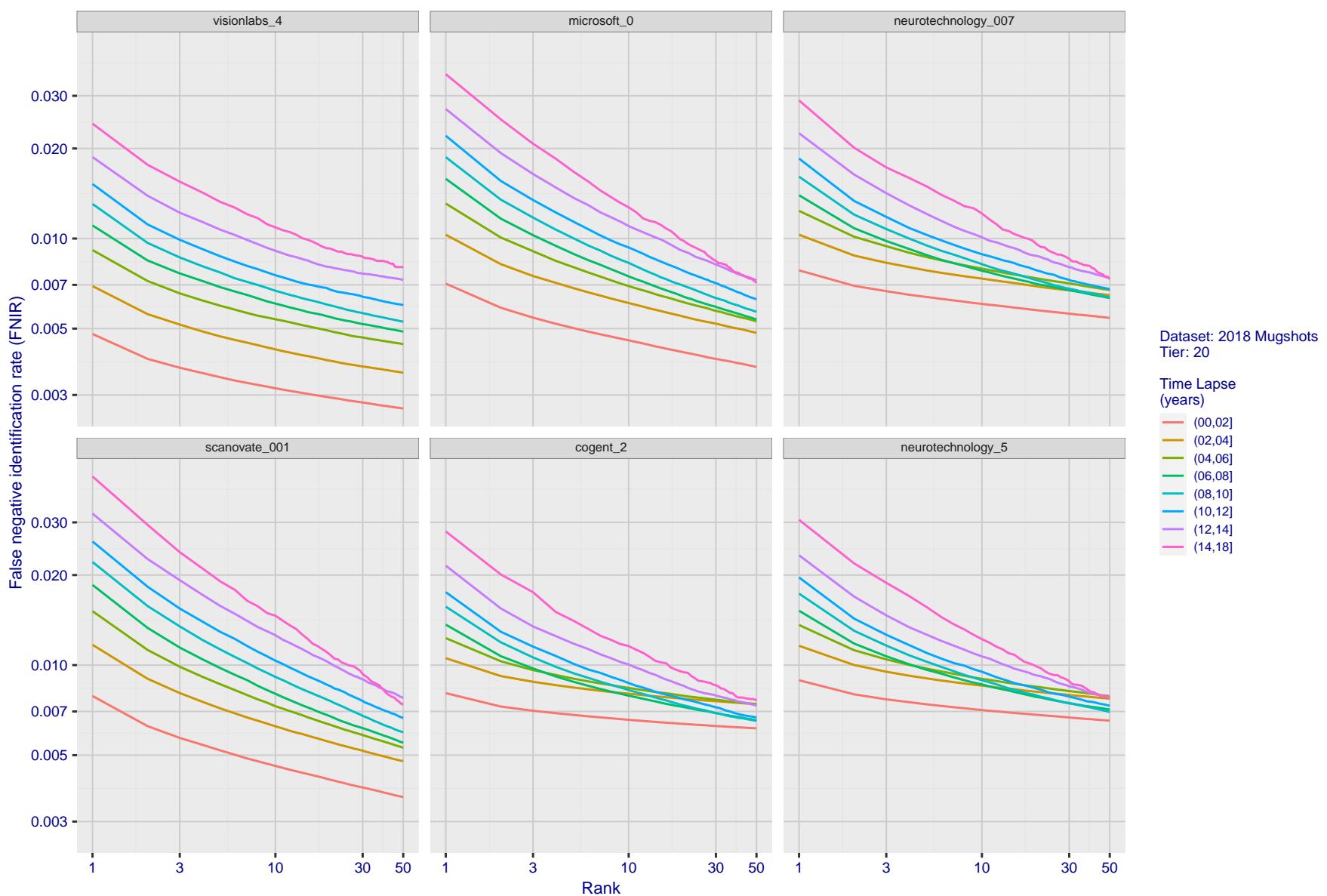


Figure 79: [FRVT-2018 Mugshot Ageing Dataset] Identification miss rates vs. rank by time elapsed. The oldest image of each individual is enrolled. Thereafter, all more recent images are searched. Miss rates are computed over all searches noted in row 17 of Table 1 and binned by number of years between search and initial enrollment.

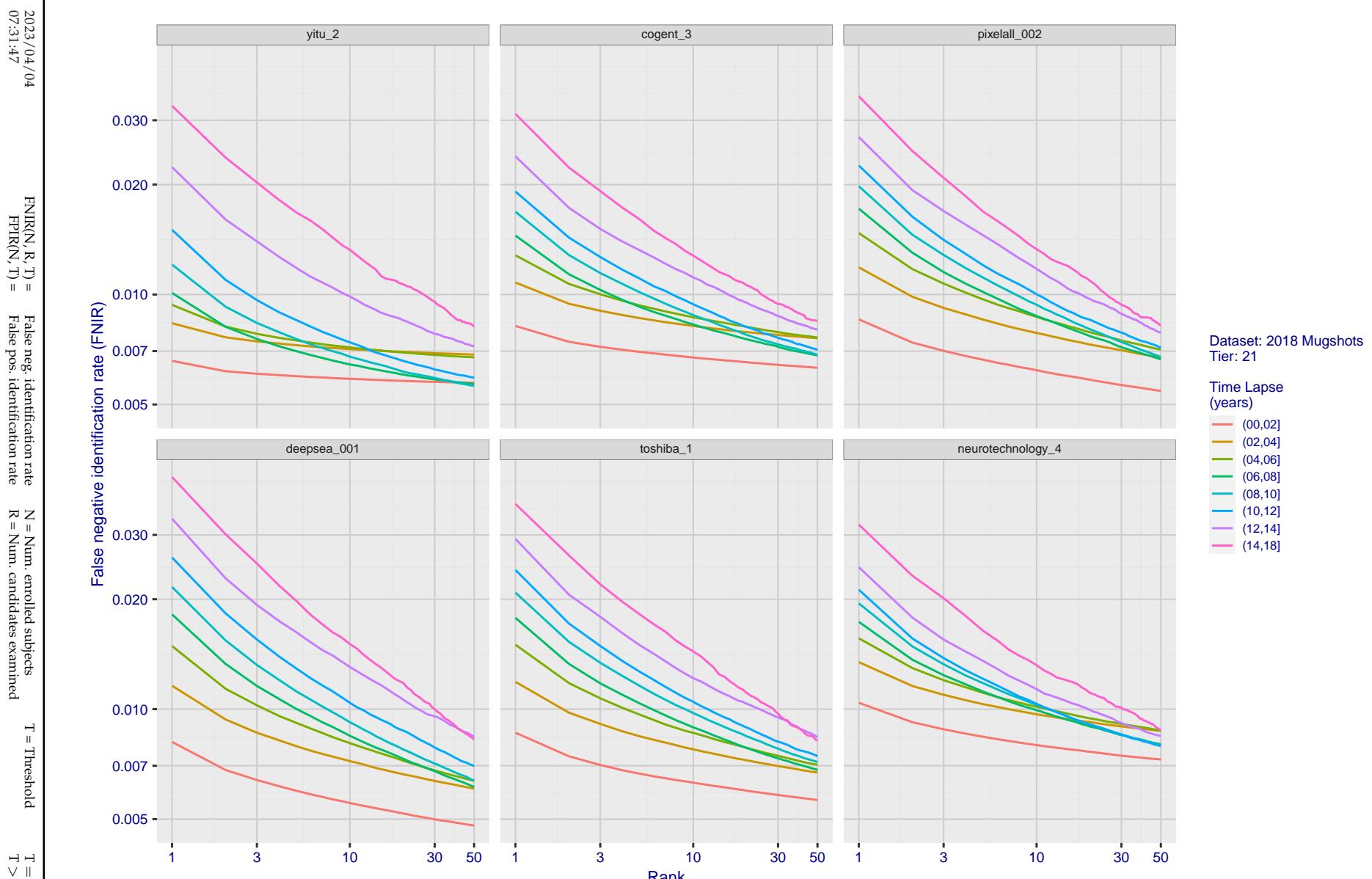


Figure 80: [FRVT-2018 Mugshot Ageing Dataset] Identification miss rates vs. rank by time elapsed. The oldest image of each individual is enrolled. Thereafter, all more recent images are searched. Miss rates are computed over all searches noted in row 17 of Table 1 and binned by number of years between search and initial enrollment.

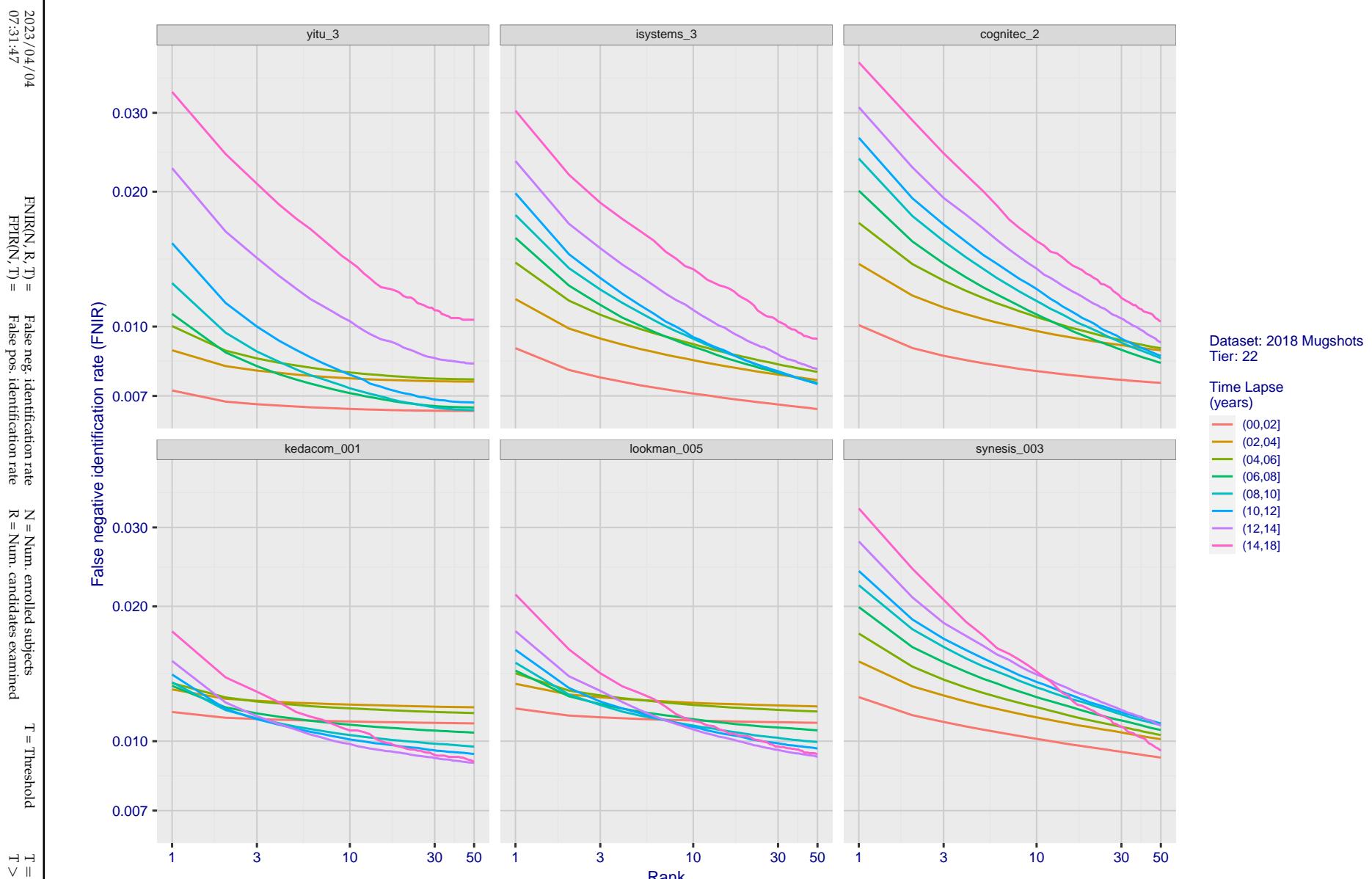


Figure 81: [FRVT-2018 Mugshot Ageing Dataset] Identification miss rates vs. rank by time-elapsed. The oldest image of each individual is enrolled. Thereafter, all more recent images are searched. Miss rates are computed over all searches noted in row 17 of Table 1 and binned by number of years between search and initial enrollment.

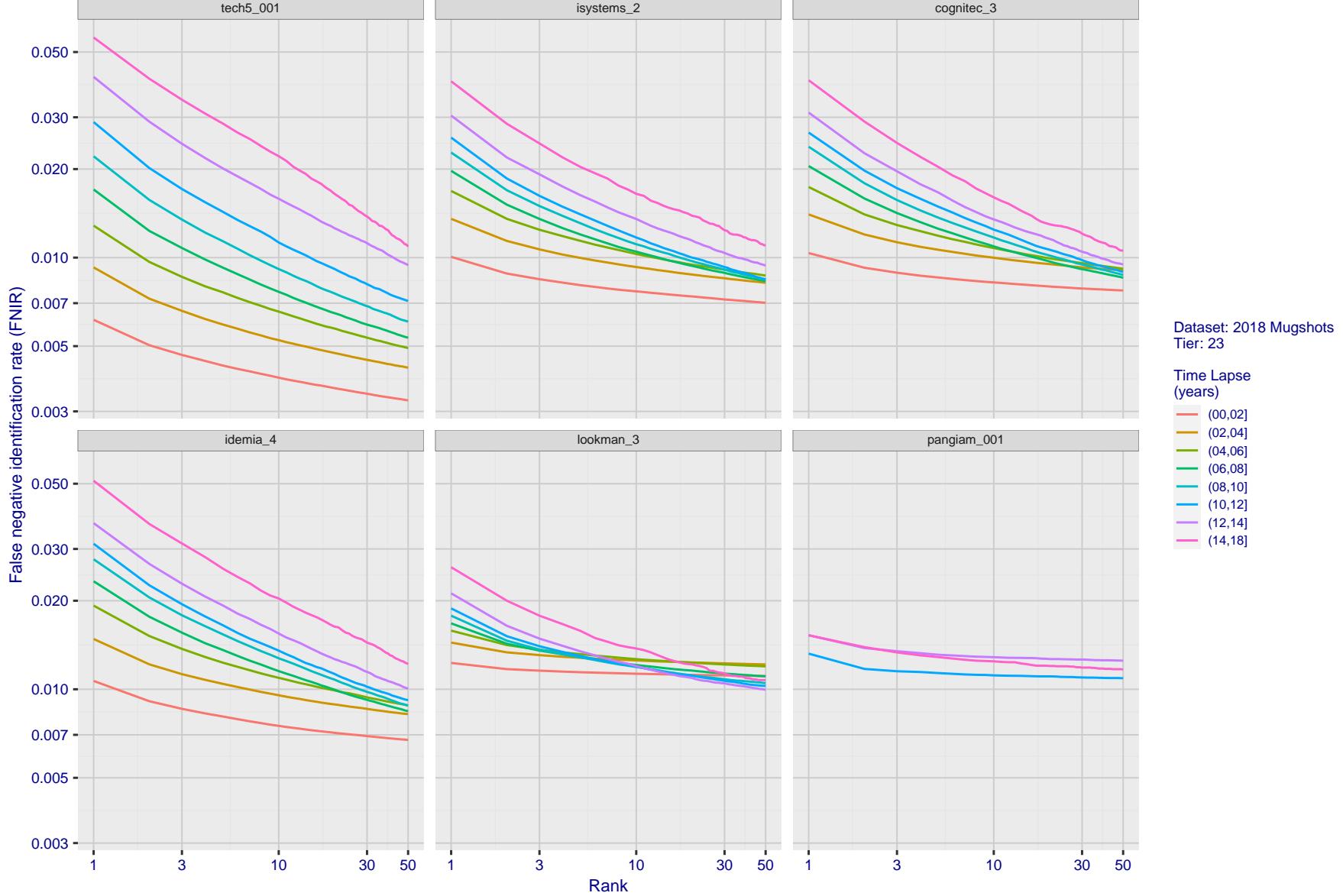


Figure 82: [FRVT-2018 Mugshot Ageing Dataset] Identification miss rates vs. rank by time-elapsed. The oldest image of each individual is enrolled. Thereafter, all more recent images are searched. Miss rates are computed over all searches noted in row 17 of Table 1 and binned by number of years between search and initial enrollment.

2023/04/04
07:31:47FNIR(N, R, T) = False neg. identification rate
FPIR(N, T) = False pos. identification rateN = Num. enrolled subjects
R = Num. candidates examinedT = Threshold
T = 0 → Investigation

T > 0 → Identification

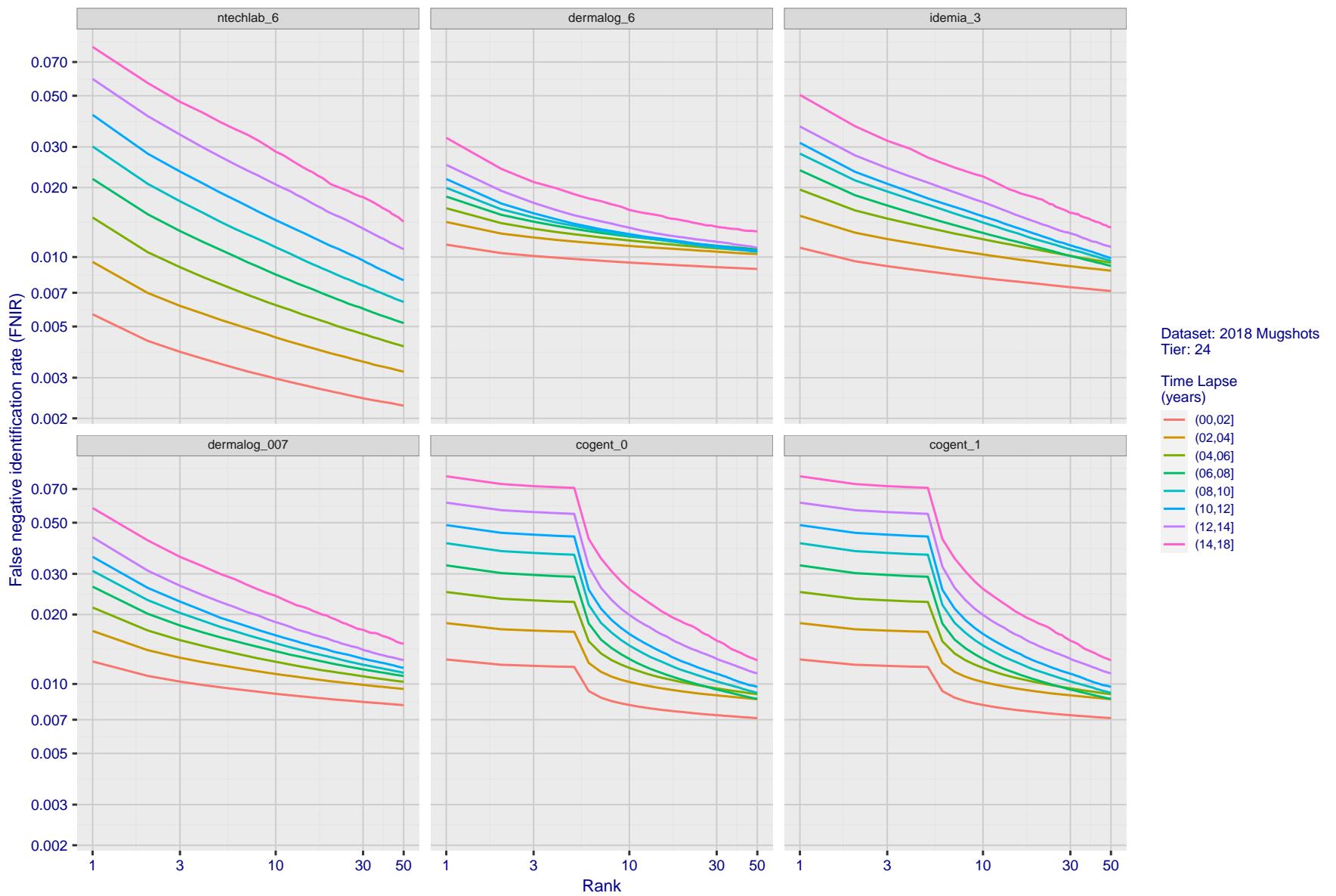


Figure 83: [FRVT-2018 Mugshot Ageing Dataset] Identification miss rates vs. rank by time-elapsed. The oldest image of each individual is enrolled. Thereafter, all more recent images are searched. Miss rates are computed over all searches noted in row 17 of Table 1 and binned by number of years between search and initial enrollment.

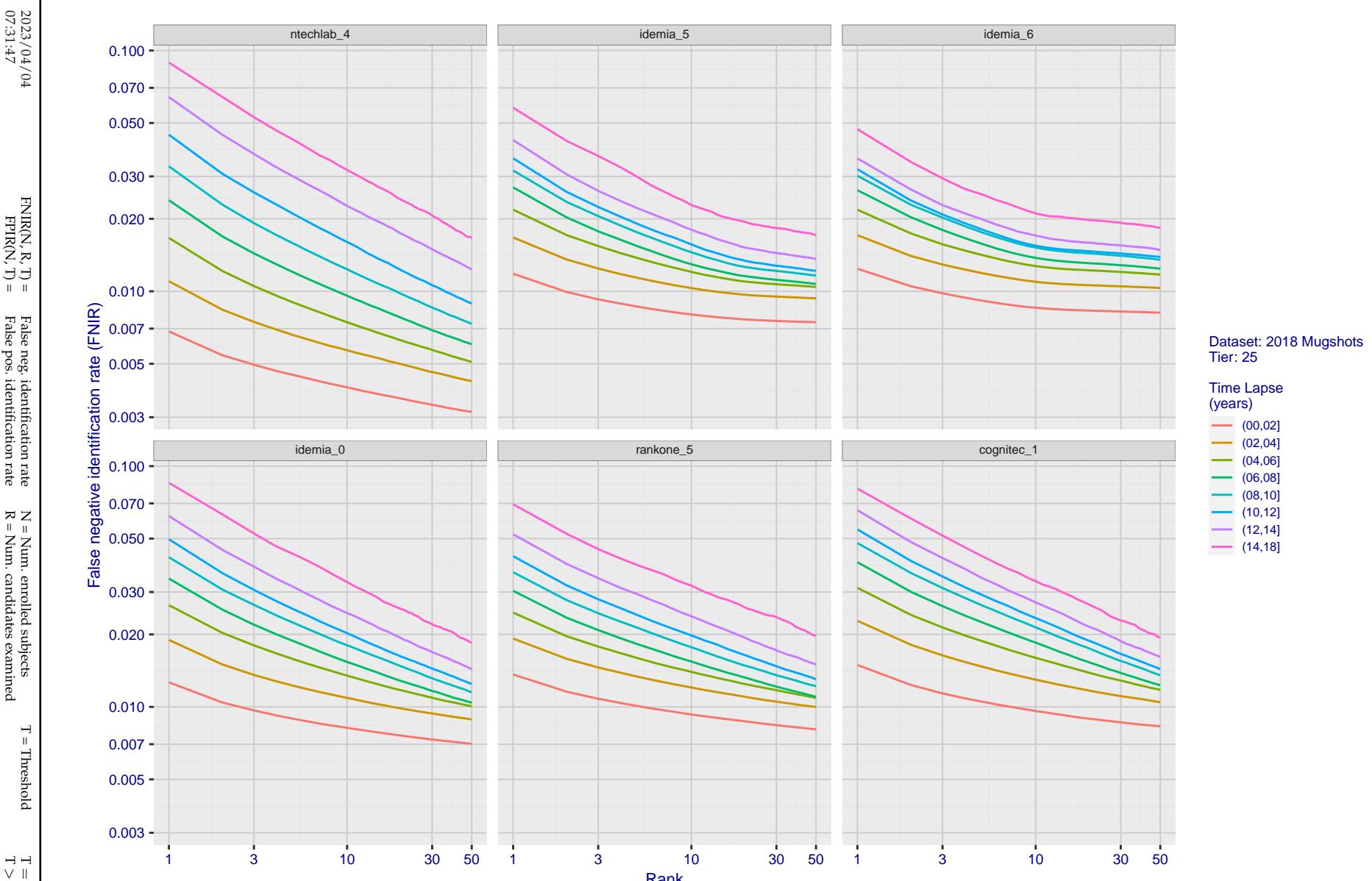


Figure 84: [FRVT-2018 Mugshot Ageing Dataset] Identification miss rates vs. rank by time-elapsed. The oldest image of each individual is enrolled. Thereafter, all more recent images are searched. Miss rates are computed over all searches noted in row 17 of Table 1 and binned by number of years between search and initial enrollment.

2023/04/04
07:31:47FNIR(N, R, T) = False neg. identification rate
FPFR(N, T) = False pos. identification rateN = Num. enrolled subjects
R = Num. candidates examinedT = Threshold
T = 0 → Investigation

T > 0 → Identification

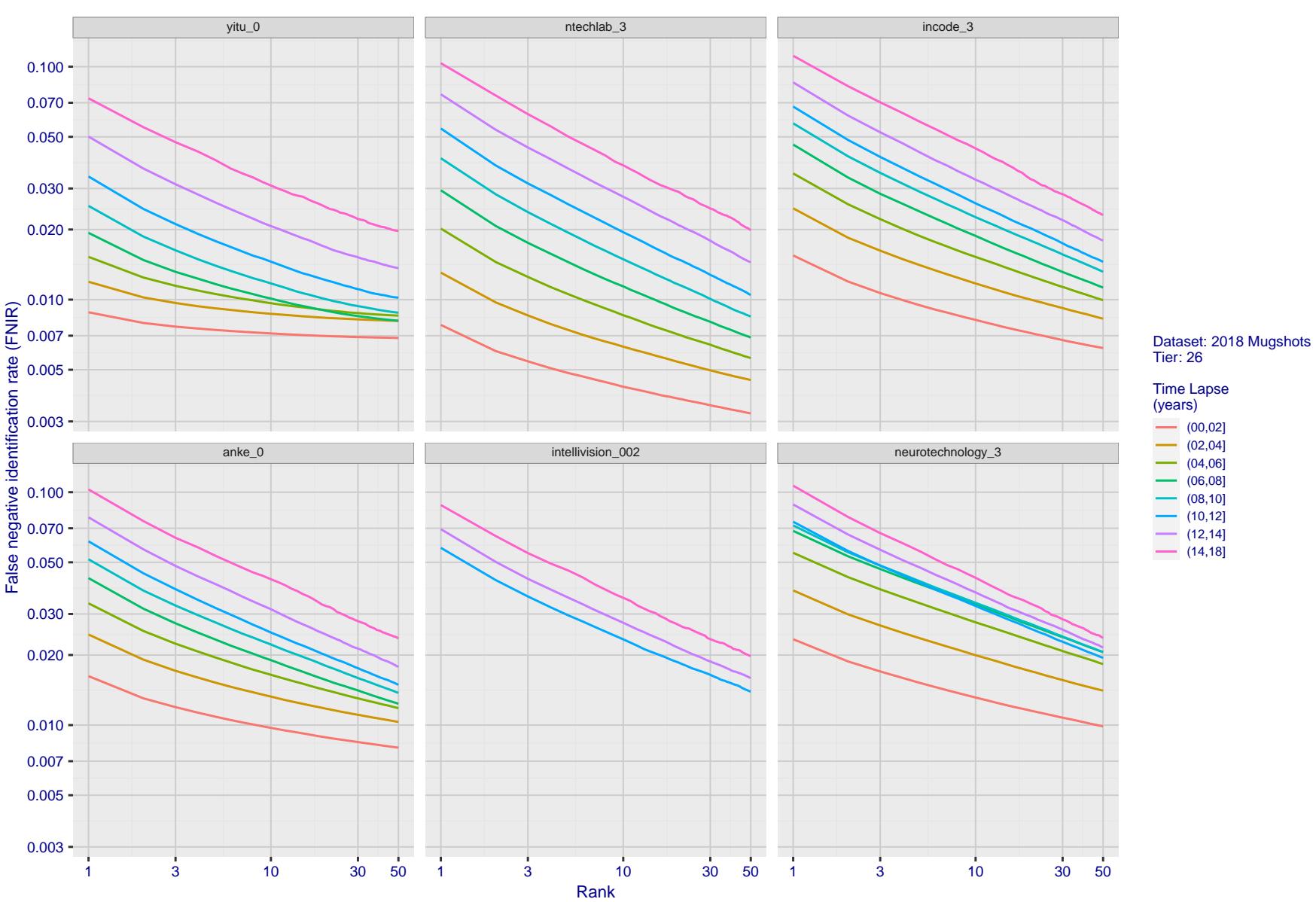


Figure 85: [FRVT-2018 Mugshot Ageing Dataset] Identification miss rates vs. rank by time elapsed. The oldest image of each individual is enrolled. Thereafter, all more recent images are searched. Miss rates are computed over all searches noted in row 17 of Table 1 and binned by number of years between search and initial enrollment.

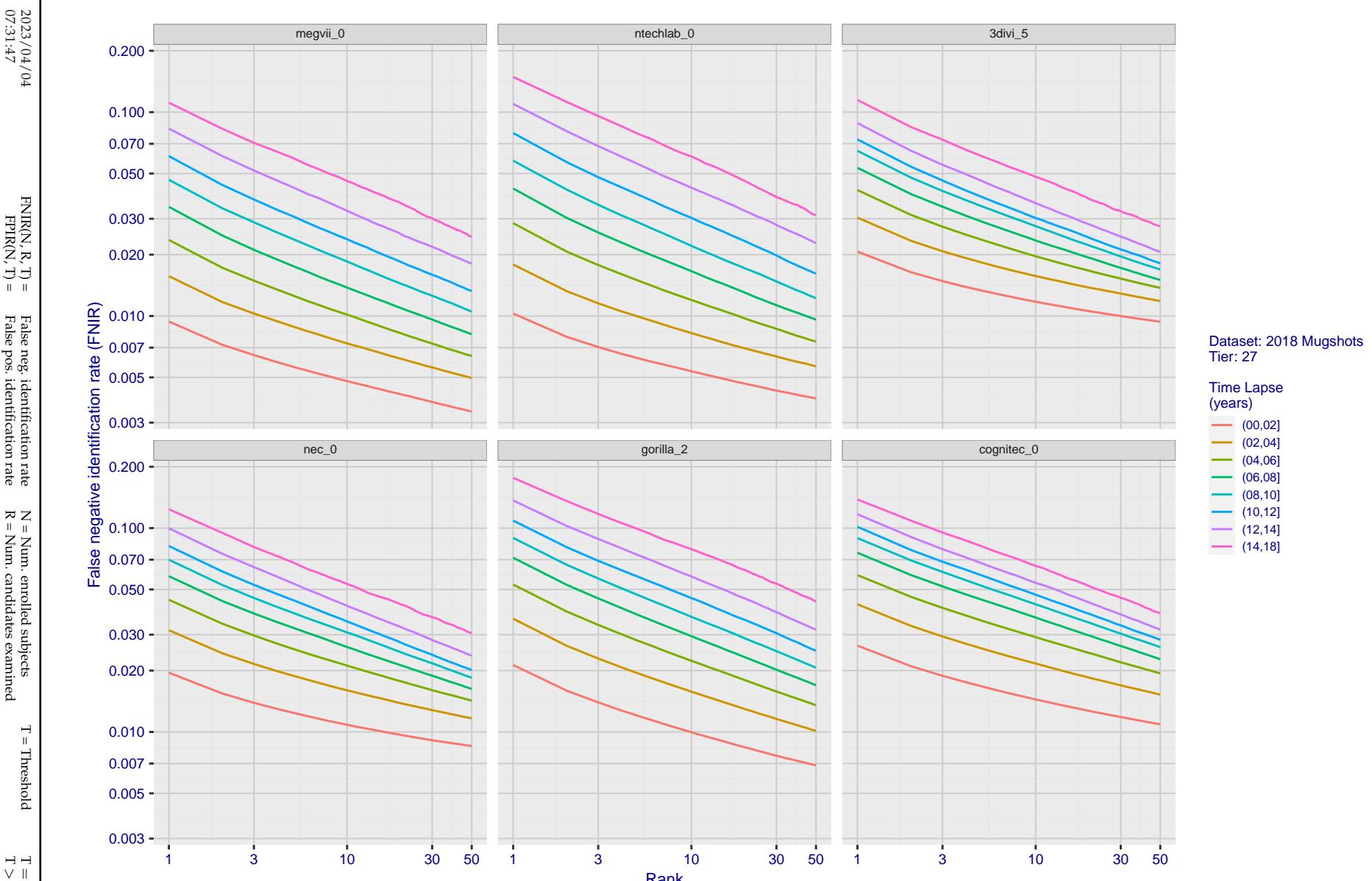


Figure 86: [FRVT-2018 Mugshot Ageing Dataset] Identification miss rates vs. rank by time-elapsed. The oldest image of each individual is enrolled. Thereafter, all more recent images are searched. Miss rates are computed over all searches noted in row 17 of Table 1 and binned by number of years between search and initial enrollment.

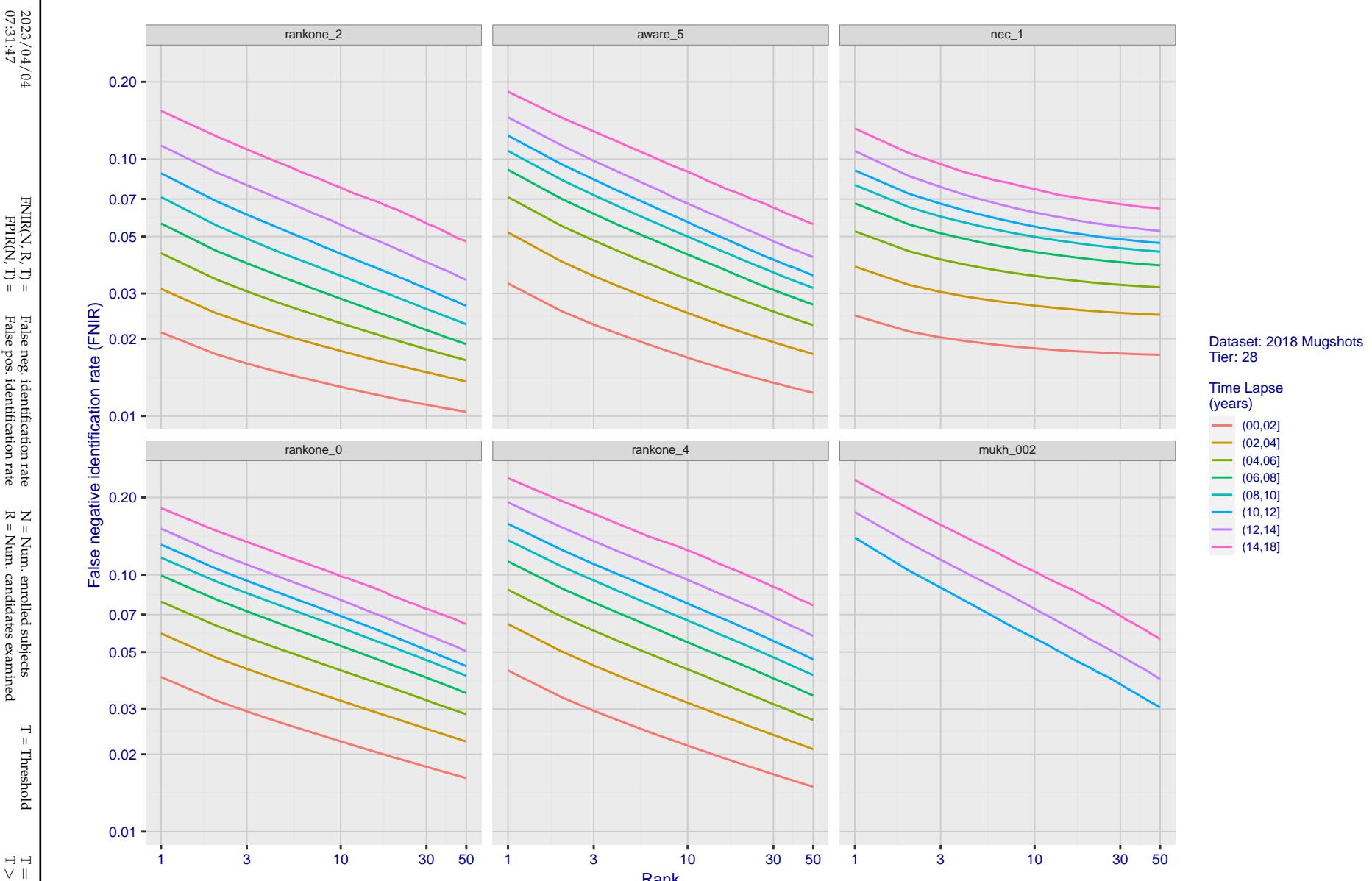


Figure 87: [FRVT-2018 Mugshot Ageing Dataset] Identification miss rates vs. rank by time elapsed. The oldest image of each individual is enrolled. Thereafter, all more recent images are searched. Miss rates are computed over all searches noted in row 17 of Table 1 and binned by number of years between search and initial enrollment.

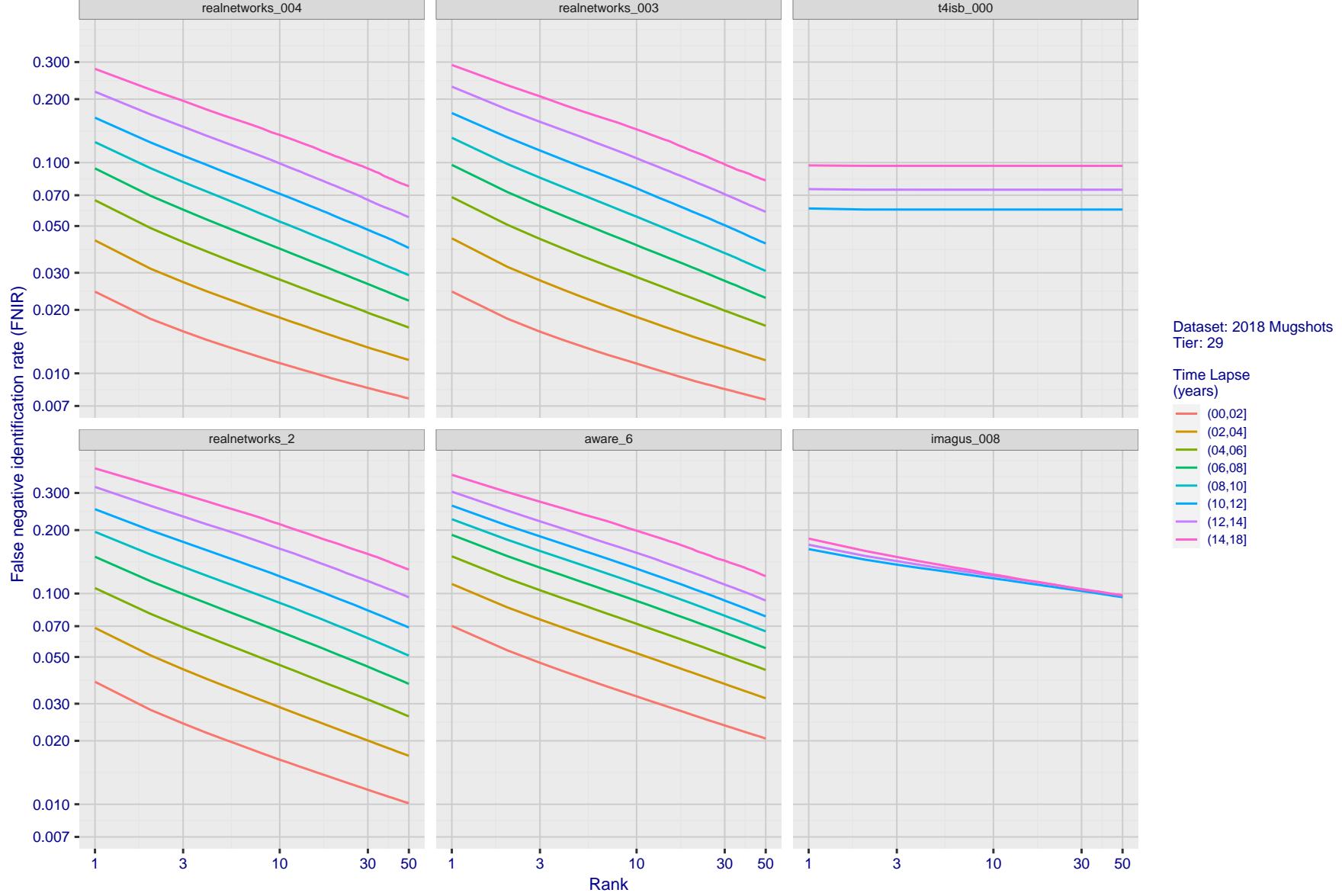


Figure 88: [FRVT-2018 Mugshot Ageing Dataset] Identification miss rates vs. rank by time-elapsed. The oldest image of each individual is enrolled. Thereafter, all more recent images are searched. Miss rates are computed over all searches noted in row 17 of Table 1 and binned by number of years between search and initial enrollment.

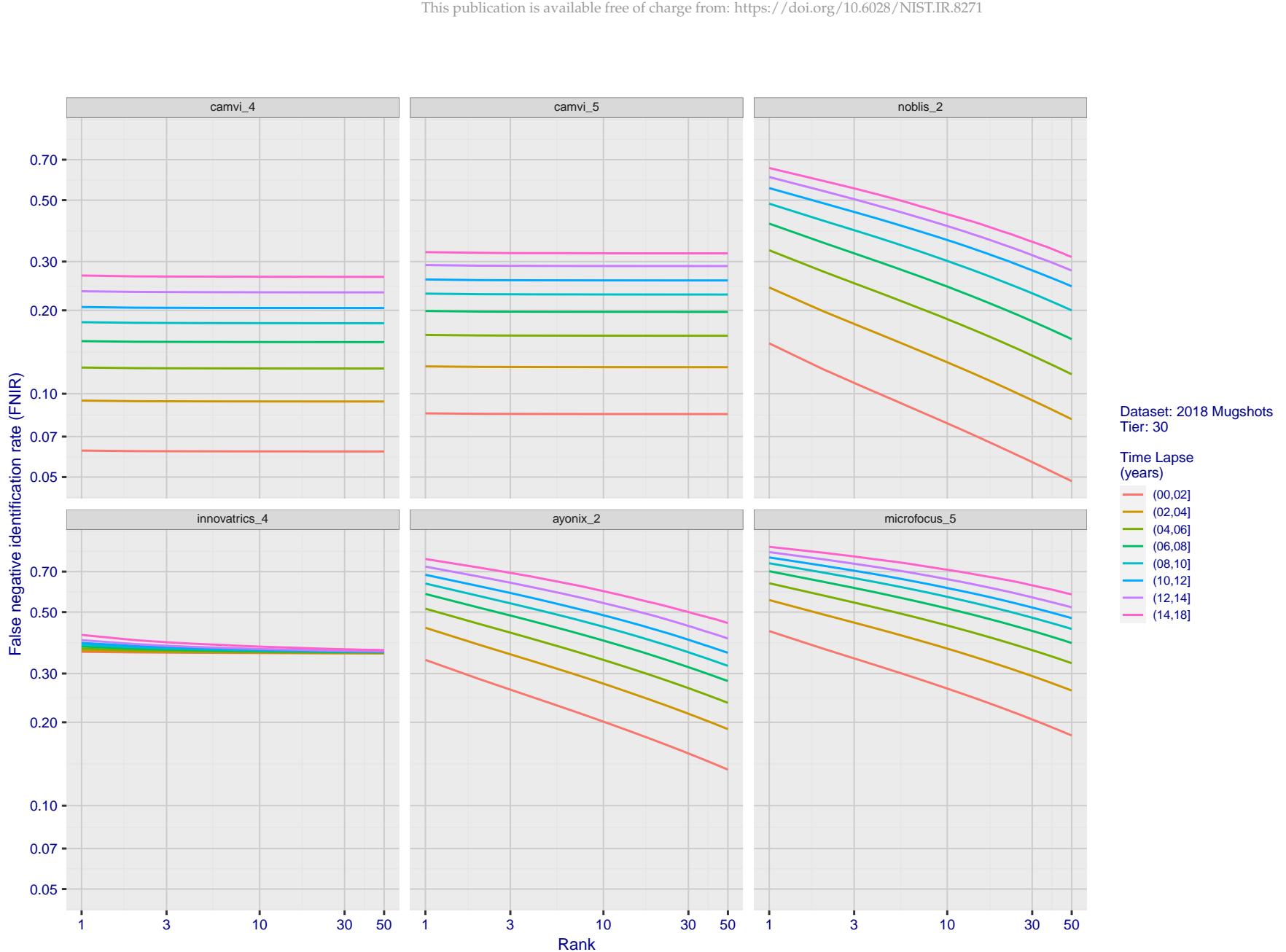


Figure 89: [FRVT-2018 Mugshot Ageing Dataset] Identification miss rates vs. rank by time-elapsed. The oldest image of each individual is enrolled. Thereafter, all more recent images are searched. Miss rates are computed over all searches noted in row 17 of Table 1 and binned by number of years between search and initial enrollment.

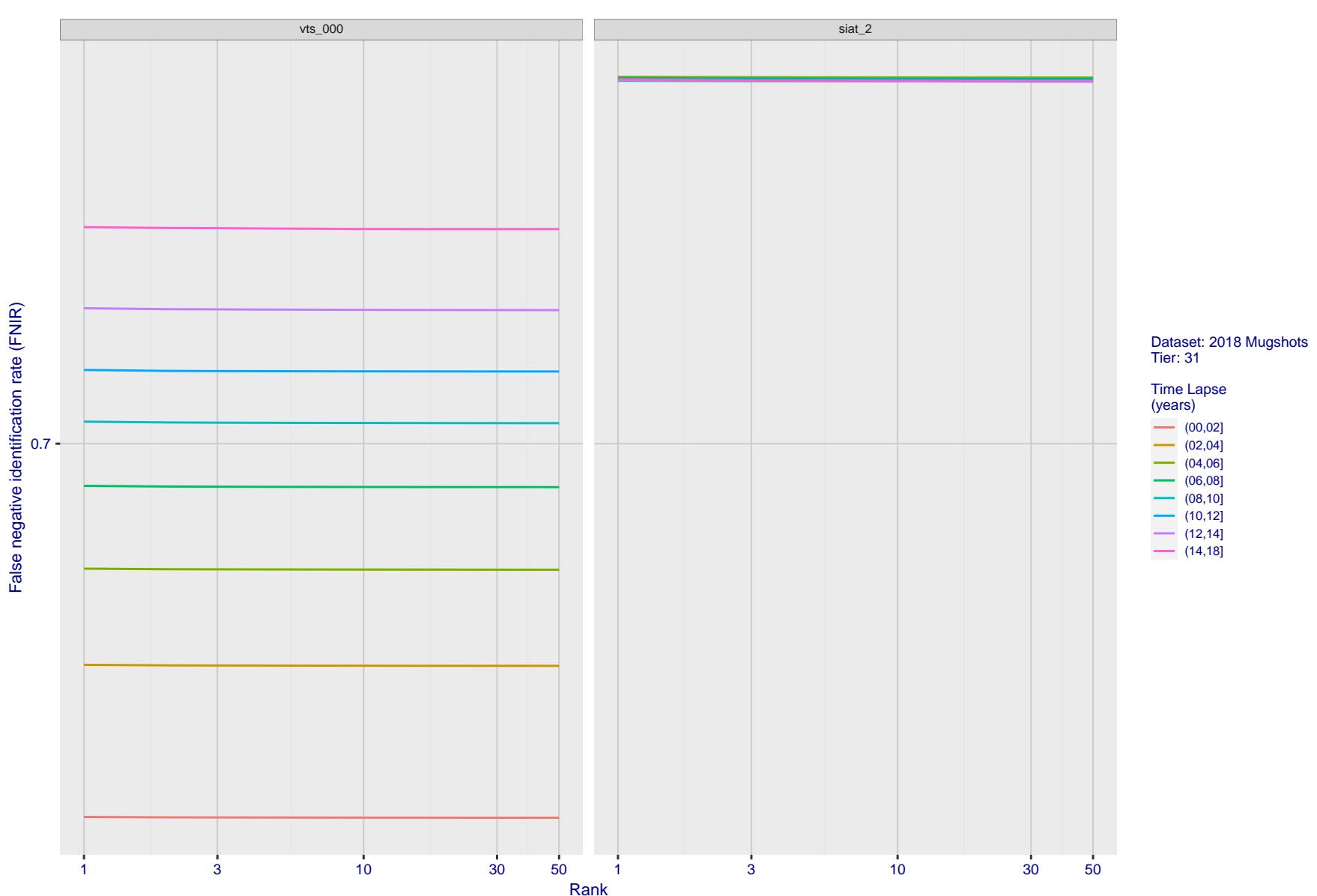


Figure 90: [FRVT-2018 Mugshot Ageing Dataset] Identification miss rates vs. rank by time-elapsed. The oldest image of each individual is enrolled. Thereafter, all more recent images are searched. Miss rates are computed over all searches noted in row 17 of Table 1 and binned by number of years between search and initial enrollment.

2023/04/04
07:31:47

FNIR(N, R, T) = False neg. identification rate
FPTR(N, T) = False pos. identification rate

N = Num. enrolled subjects
R = Num. candidates examined

T = Threshold
T = 0 → Investigation
T > 0 → Identification

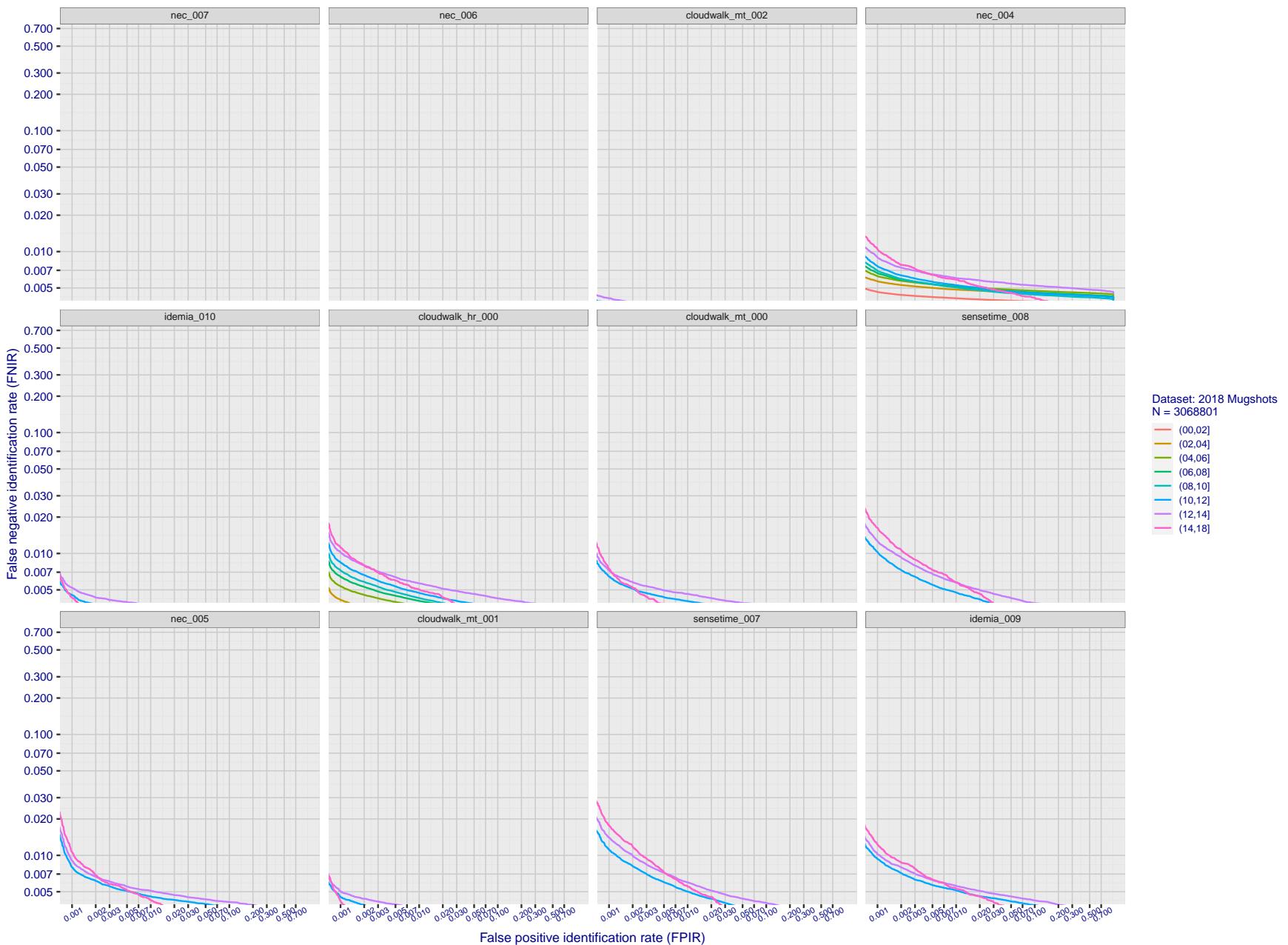


Figure 91: [FRVT-2018 Mugshot Ageing Dataset] Identification miss rates vs. FPIR by time-elapsed. The oldest image of each individual is enrolled. Thereafter, all more recent images are searched. Miss rates are computed over all searches noted in row 17 of Table 1 and binned by number of years between search and initial enrollment. FPIR is computed from the same FRVT 2018 non-mates noted in row 3 of Table 1 with $N = 3000\,000$.

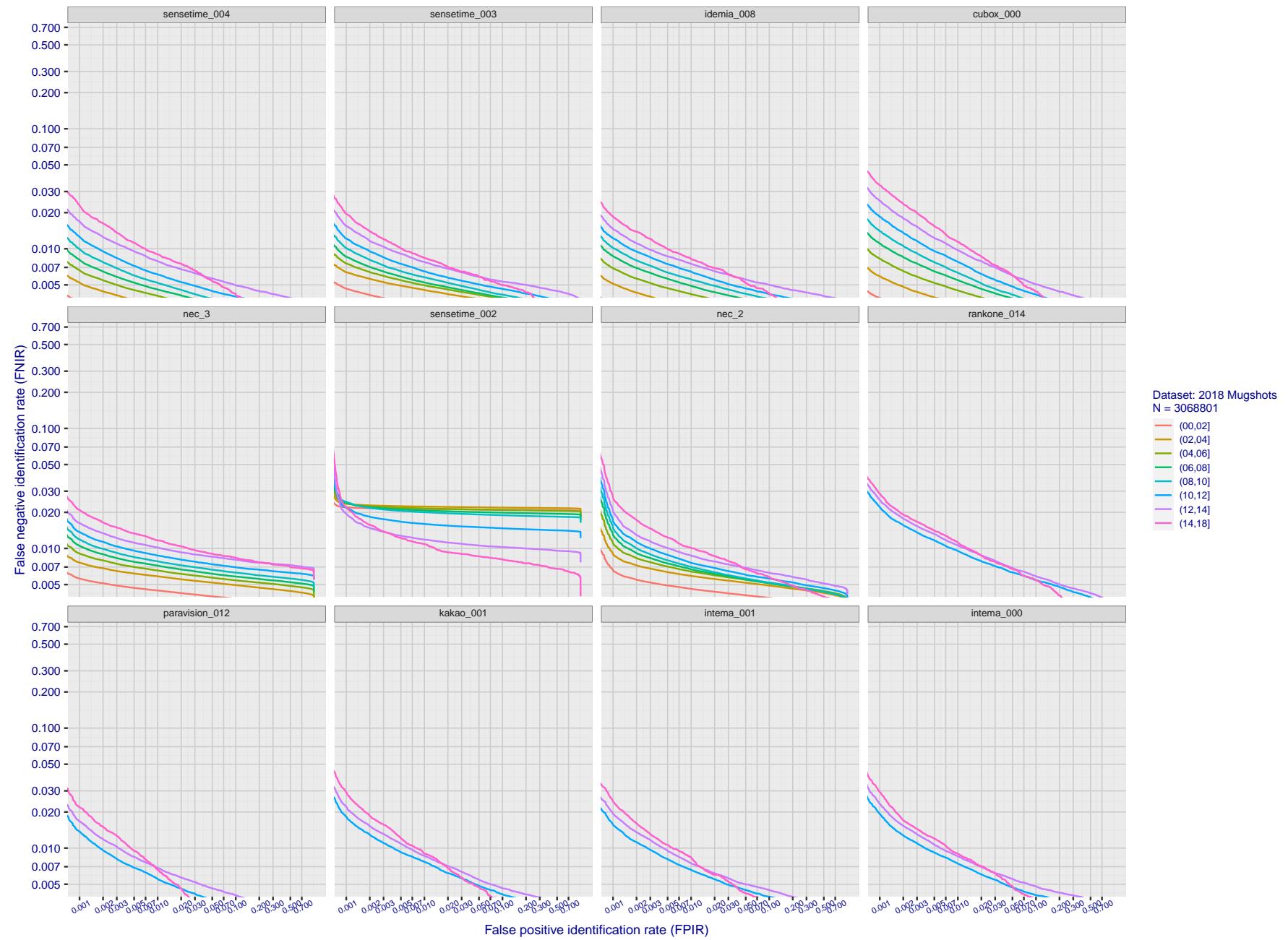


Figure 92: [FRVT-2018 Mugshot Ageing Dataset] Identification miss rates vs. FPIR by time-elapsed. The oldest image of each individual is enrolled. Thereafter, all more recent images are searched. Miss rates are computed over all searches noted in row 17 of Table 1 and binned by number of years between search and initial enrollment. FPIR is computed from the same FRVT 2018 non-mates noted in row 3 of Table 1 with $N = 3\,000\,000$.

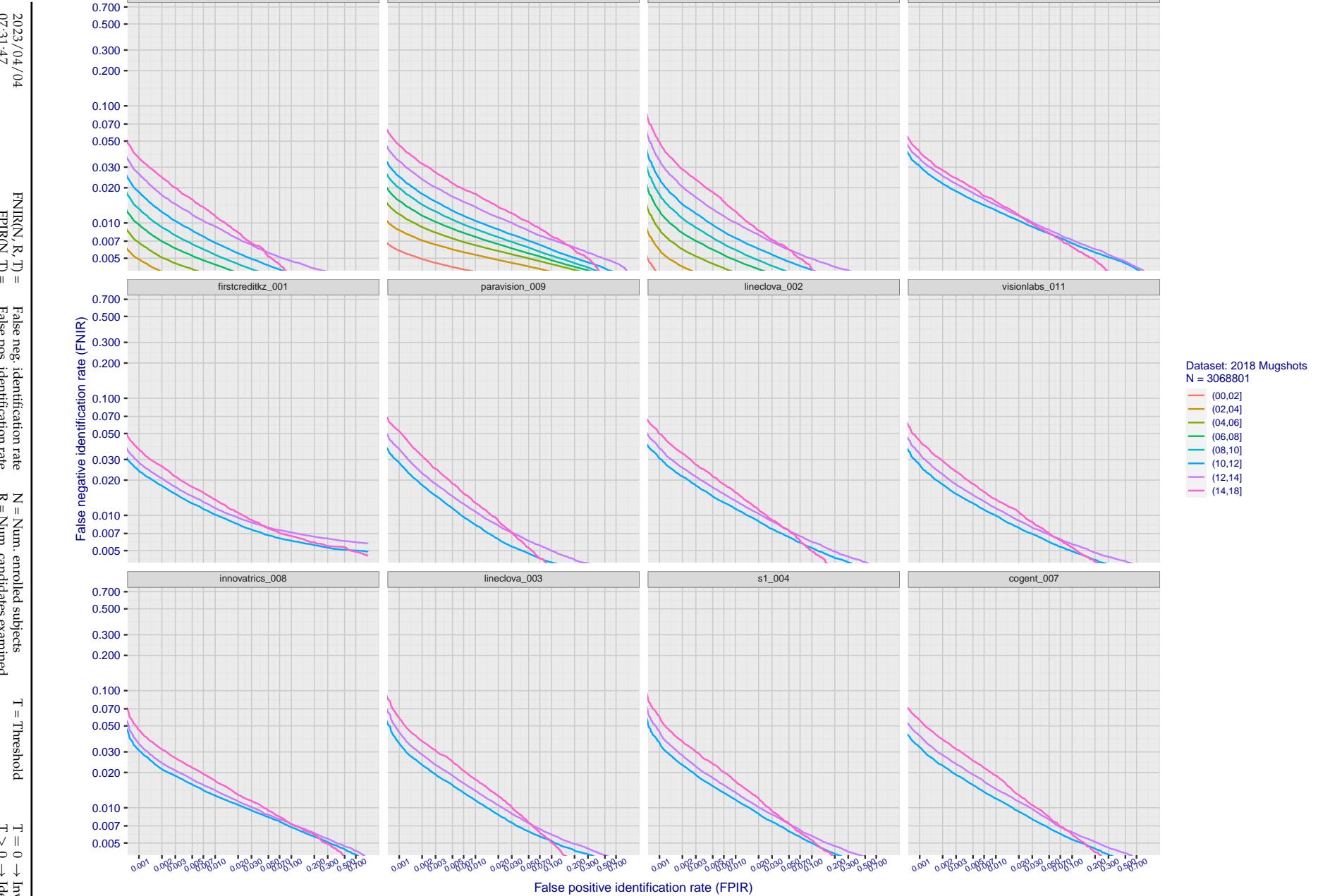


Figure 93: [FRVT-2018 Mugshot Ageing Dataset] Identification miss rates vs. FPIR by time-elapsed. The oldest image of each individual is enrolled. Thereafter, all more recent images are searched. Miss rates are computed over all searches noted in row 17 of Table 1 and binned by number of years between search and initial enrollment. FPIR is computed from the same FRVT 2018 non-mates noted in row 3 of Table 1 with $N = 3\,000\,000$.

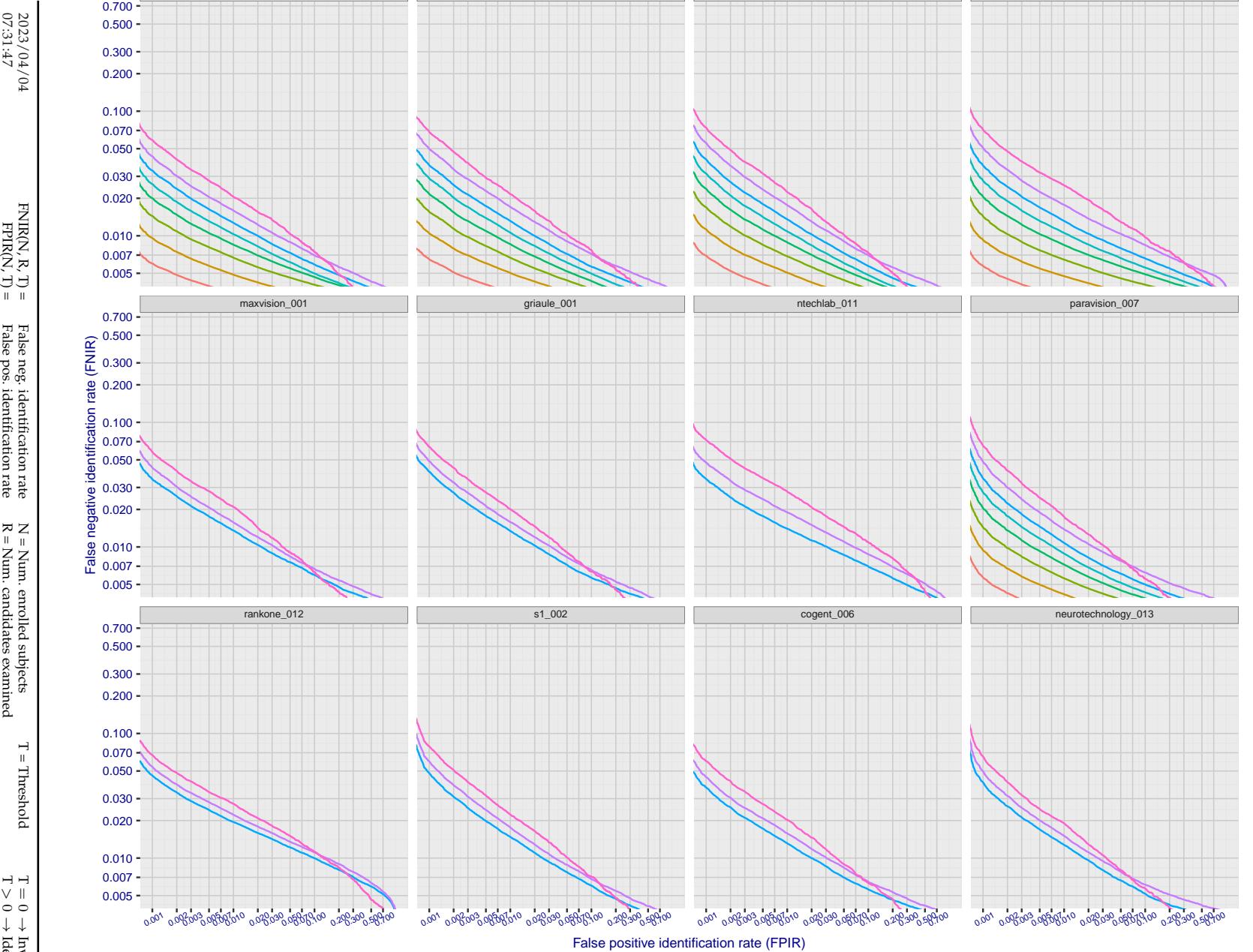


Figure 94: [FRVT-2018 Mugshot Ageing Dataset] Identification miss rates vs. FPIR by time-elapsed. The oldest image of each individual is enrolled. Thereafter, all more recent images are searched. Miss rates are computed over all searches noted in row 17 of Table 1 and binned by number of years between search and initial enrollment. FPIR is computed from the same FRVT 2018 non-mates noted in row 3 of Table 1 with $N = 3\,000\,000$.

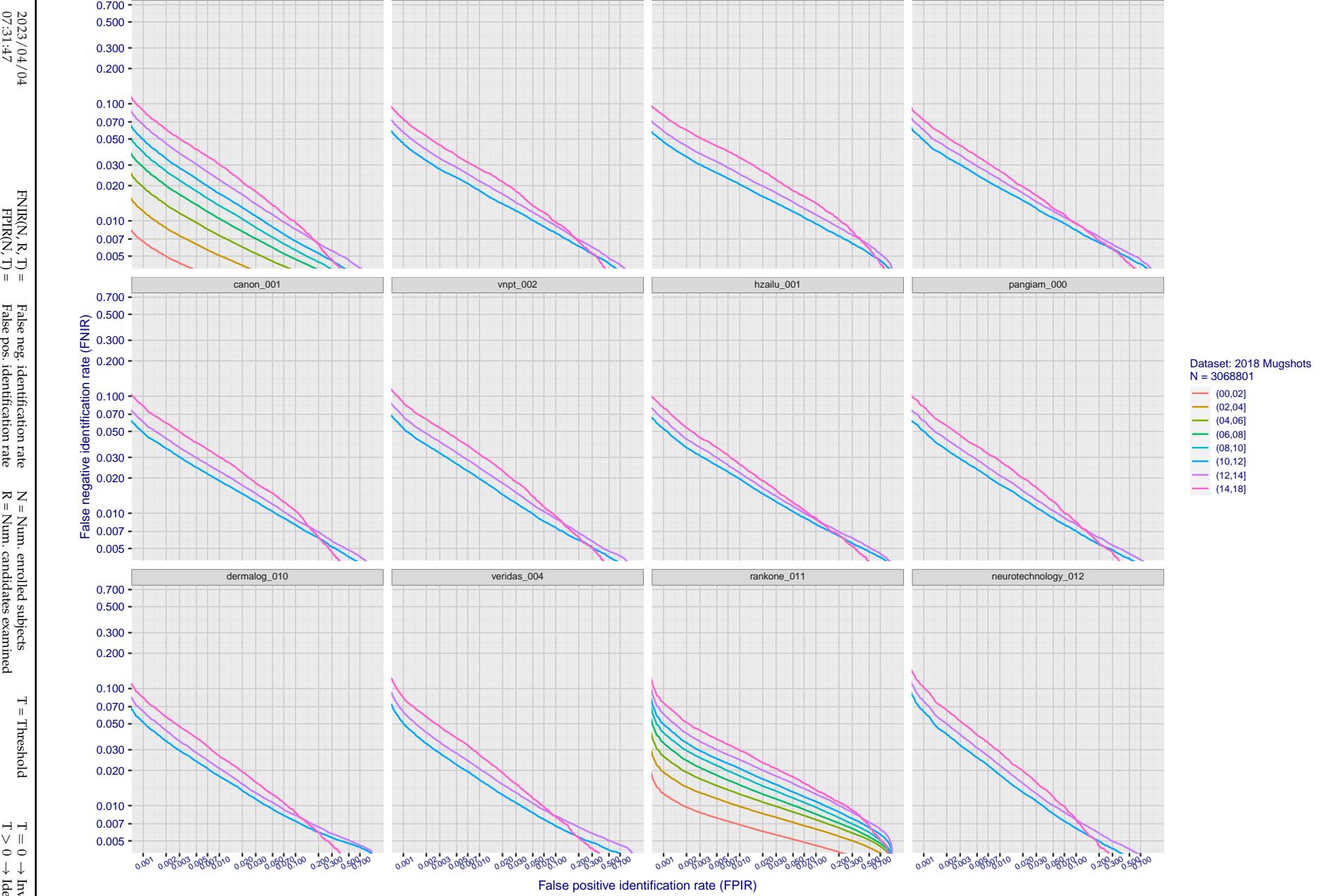


Figure 95: [FRVT-2018 Mugshot Ageing Dataset] Identification miss rates vs. FPIR by time-elapsed. The oldest image of each individual is enrolled. Thereafter, all more recent images are searched. Miss rates are computed over all searches noted in row 17 of Table 1 and binned by number of years between search and initial enrollment. FPIR is computed from the same FRVT 2018 non-mates noted in row 3 of Table 1 with $N = 3\,000\,000$.

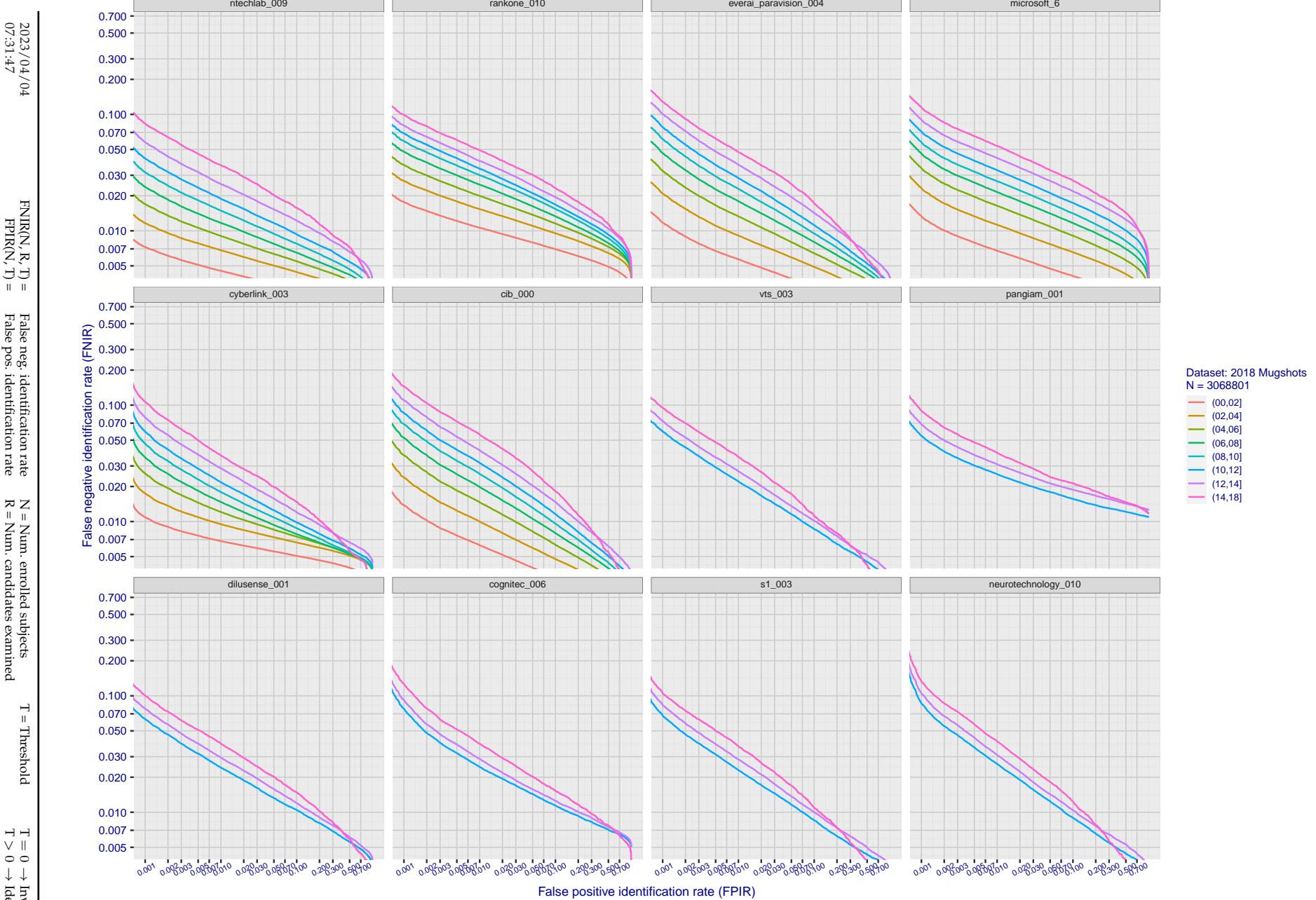


Figure 96: [FRVT-2018 Mugshot Ageing Dataset] Identification miss rates vs. FPIR by time-elapsed. The oldest image of each individual is enrolled. Thereafter, all more recent images are searched. Miss rates are computed over all searches noted in row 17 of Table 1 and binned by number of years between search and initial enrollment. FPIR is computed from the same FRVT 2018 non-mates noted in row 3 of Table 1 with $N = 3\,000\,000$.

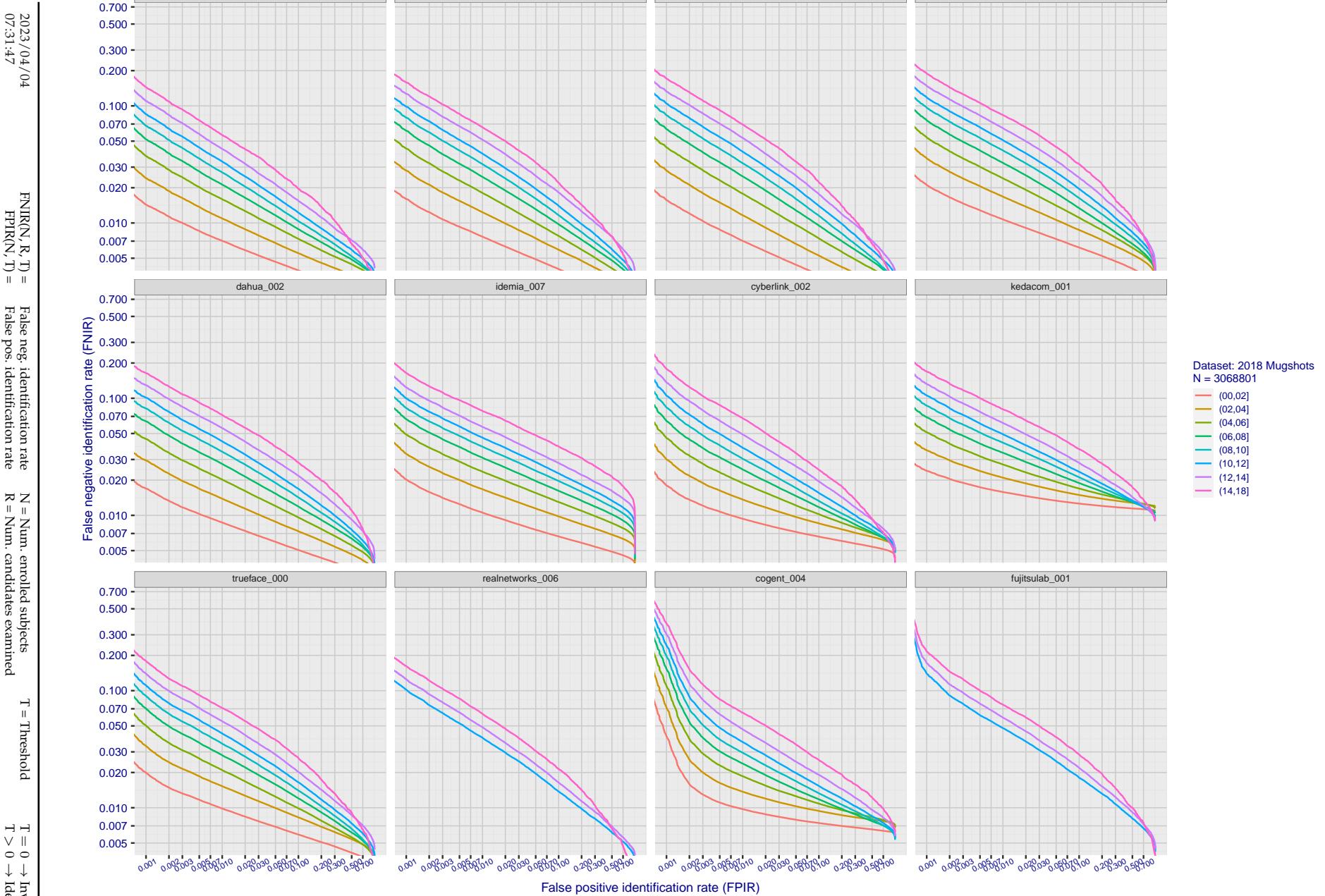


Figure 97: [FRVT-2018 Mugshot Ageing Dataset] Identification miss rates vs. FPIR by time-elapsed. The oldest image of each individual is enrolled. Thereafter, all more recent images are searched. Miss rates are computed over all searches noted in row 17 of Table 1 and binned by number of years between search and initial enrollment. FPIR is computed from the same FRVT 2018 non-mates noted in row 3 of Table 1 with N = 3 000 000.

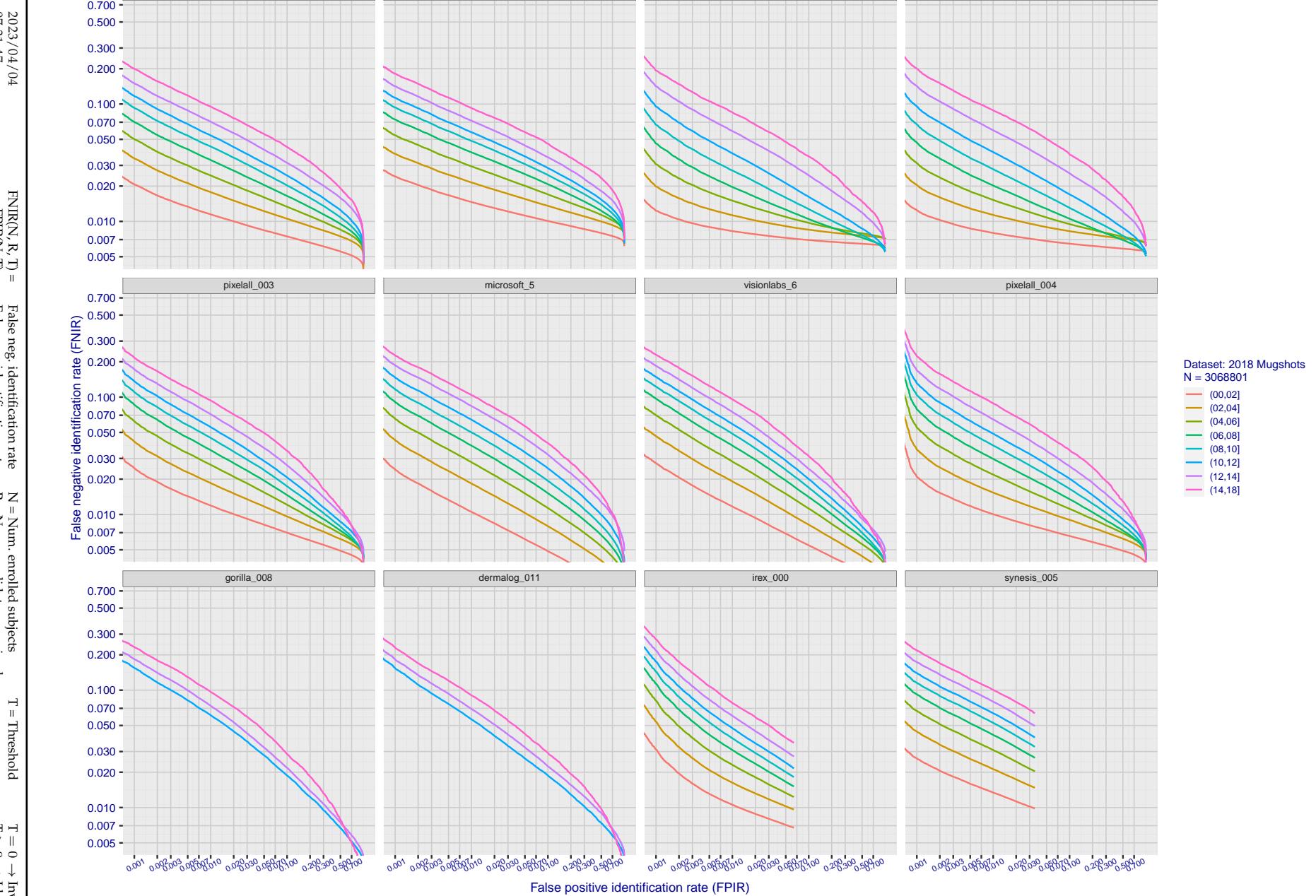


Figure 98: [FRVT-2018 Mugshot Ageing Dataset] Identification miss rates vs. FPIR by time-elapsed. The oldest image of each individual is enrolled. Thereafter, all more recent images are searched. Miss rates are computed over all searches noted in row 17 of Table 1 and binned by number of years between search and initial enrollment. FPIR is computed from the same FRVT 2018 non-mates noted in row 3 of Table 1 with $N = 3\,000\,000$.

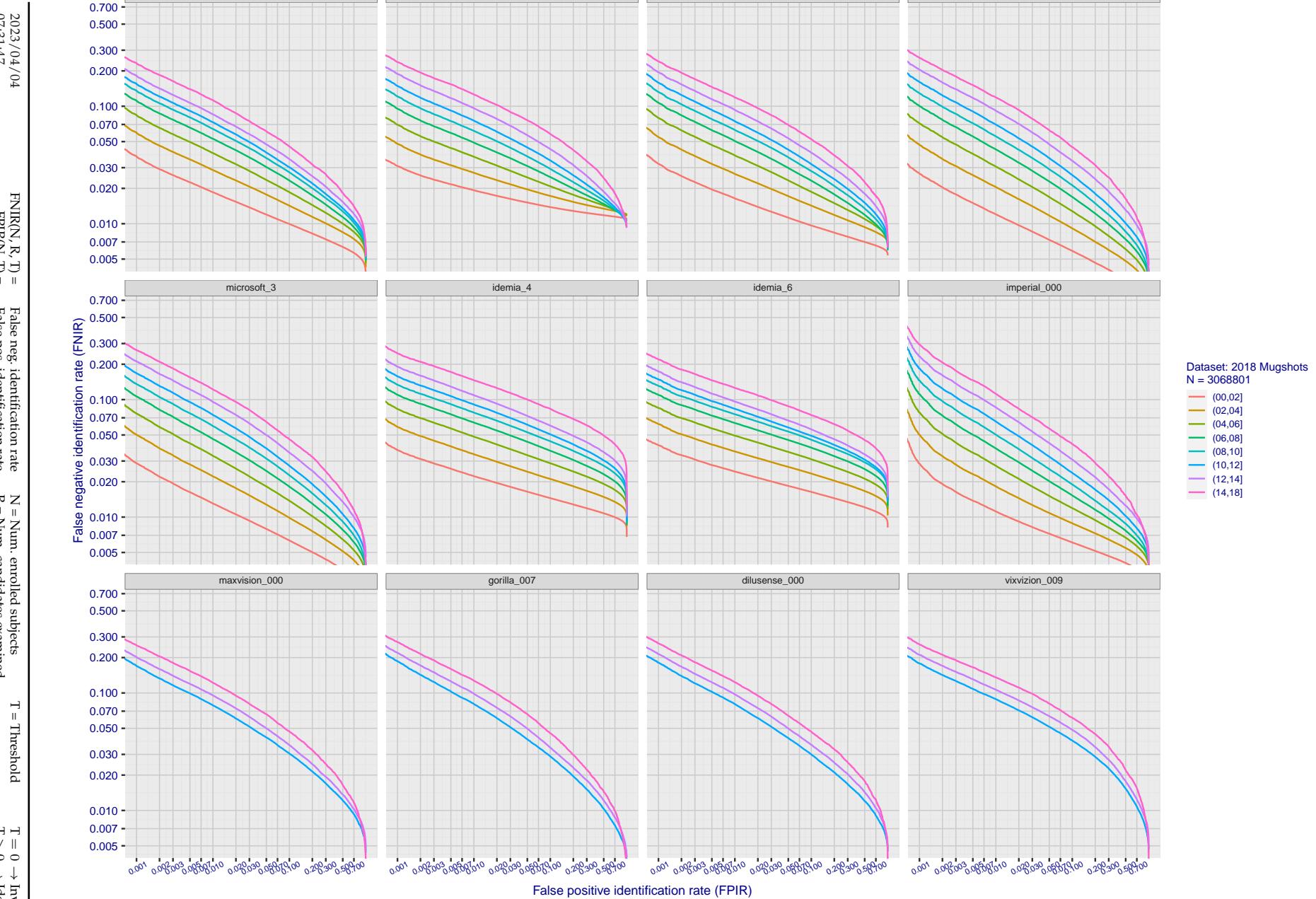


Figure 99: [FRVT-2018 Mugshot Ageing Dataset] Identification miss rates vs. FPIR by time elapsed. The oldest image of each individual is enrolled. Thereafter, all more recent images are searched. Miss rates are computed over all searches noted in row 17 of Table 1 and binned by number of years between search and initial enrollment. FPIR is computed from the same FRVT 2018 non-mates noted in row 3 of Table 1 with $N = 3000\,000$.

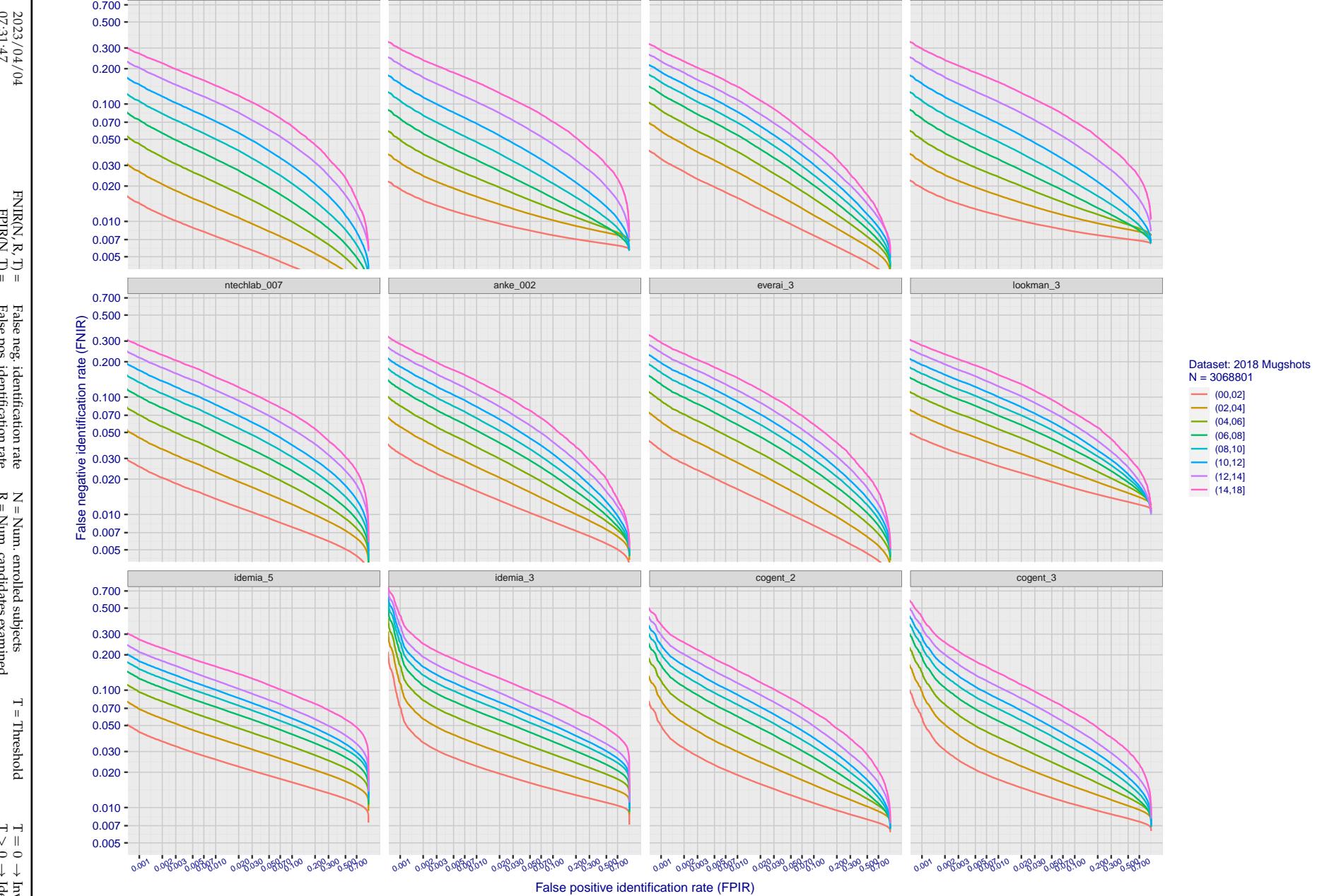


Figure 100: [FRVT-2018 Mugshot Ageing Dataset] Identification miss rates vs. FPIR by time-elapsed. The oldest image of each individual is enrolled. Thereafter, all more recent images are searched. Miss rates are computed over all searches noted in row 17 of Table 1 and binned by number of years between search and initial enrollment. FPIR is computed from the same FRVT 2018 non-mates noted in row 3 of Table 1 with $N = 3\,000\,000$.

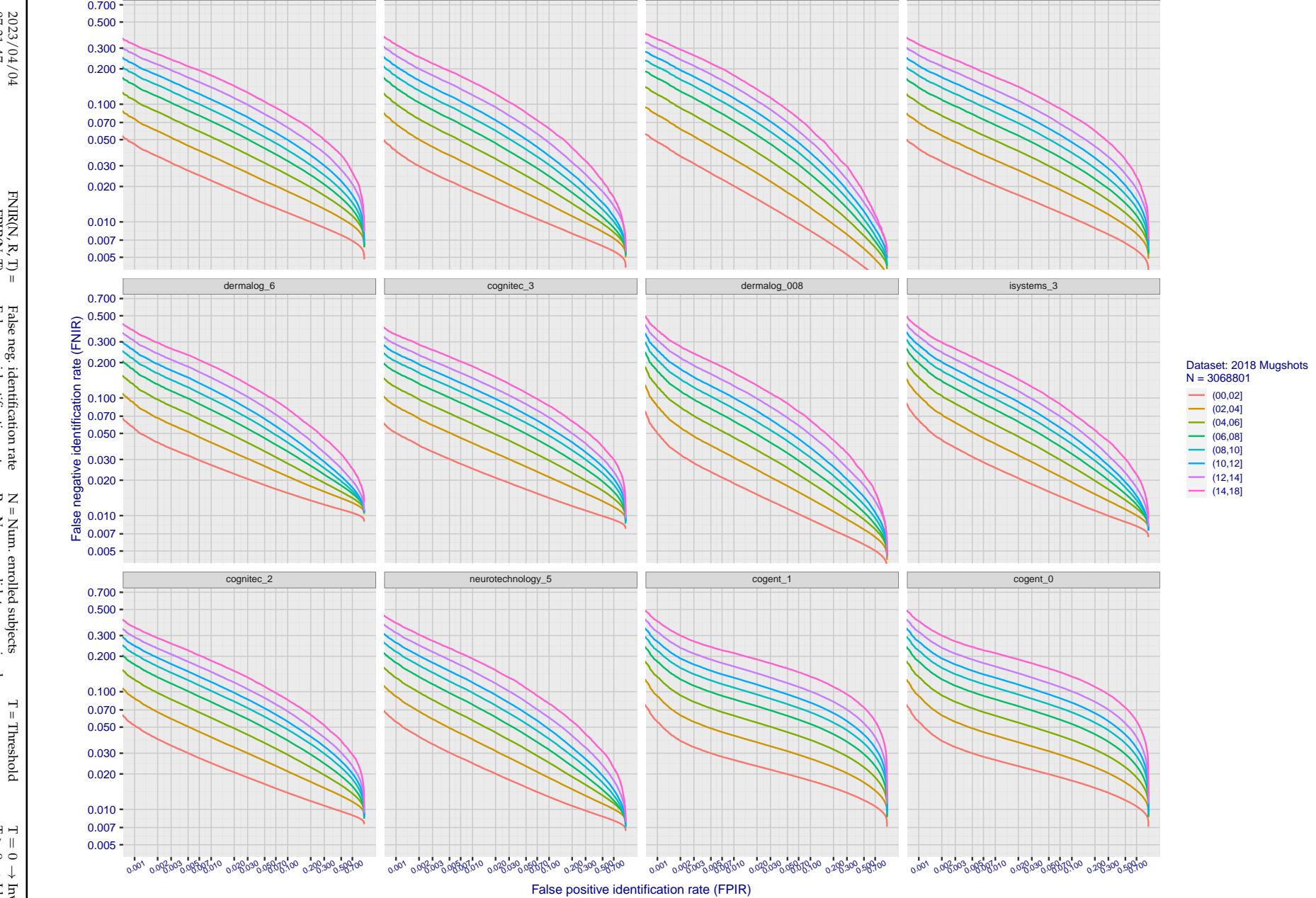


Figure 101: [FRVT-2018 Mugshot Ageing Dataset] Identification miss rates vs. FPIR by time-elapsed. The oldest image of each individual is enrolled. Thereafter, all more recent images are searched. Miss rates are computed over all searches noted in row 17 of Table 1 and binned by number of years between search and initial enrollment. FPIR is computed from the same FRVT 2018 non-mates noted in row 3 of Table 1 with N = 3 000 000.

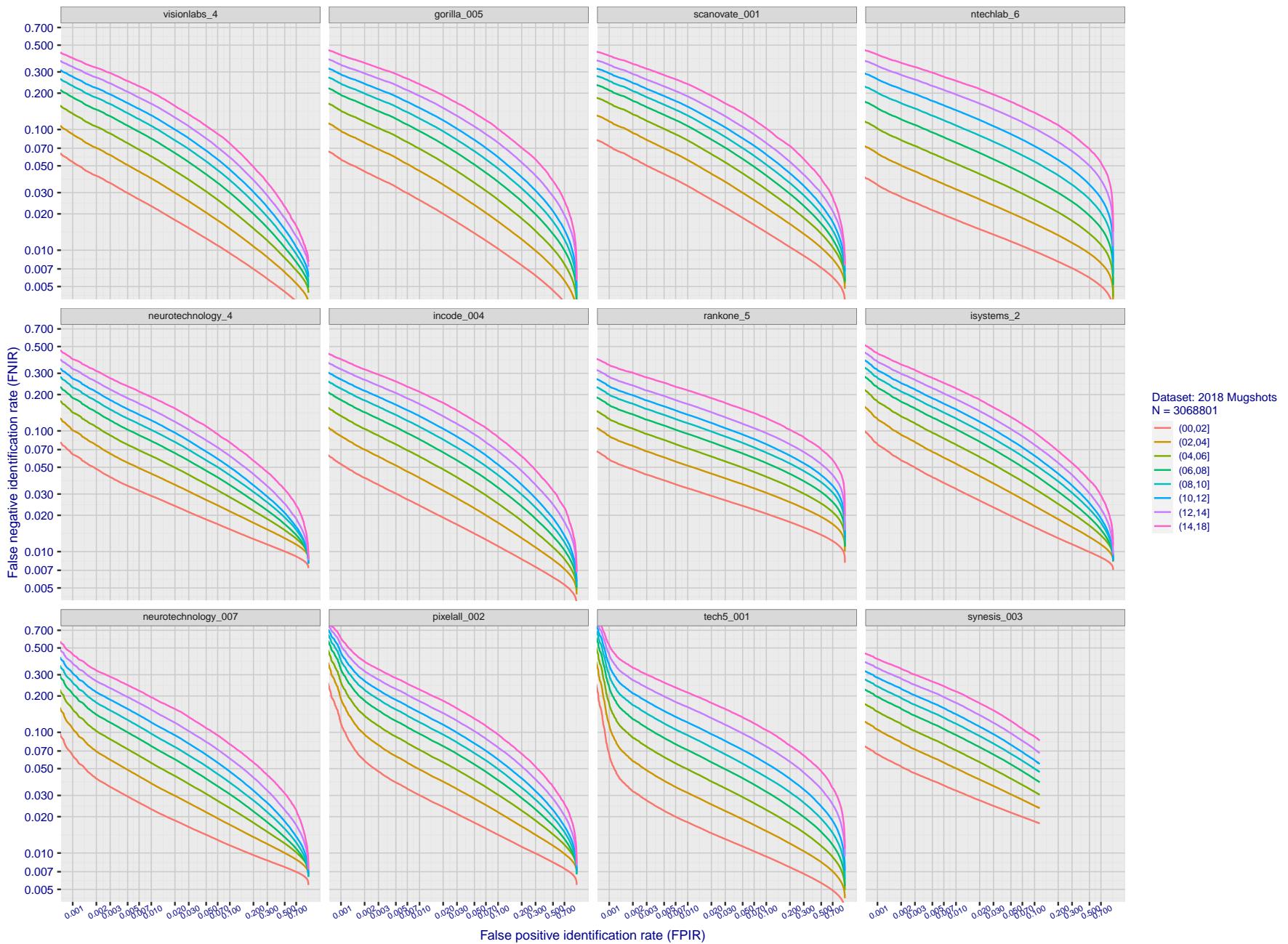


Figure 102: [FRVT-2018 Mugshot Ageing Dataset] Identification miss rates vs. FPIR by time-elapsed. The oldest image of each individual is enrolled. Thereafter, all more recent images are searched. Miss rates are computed over all searches noted in row 17 of Table 1 and binned by number of years between search and initial enrollment. FPIR is computed from the same FRVT 2018 non-mates noted in row 3 of Table 1 with $N = 3\,000\,000$.

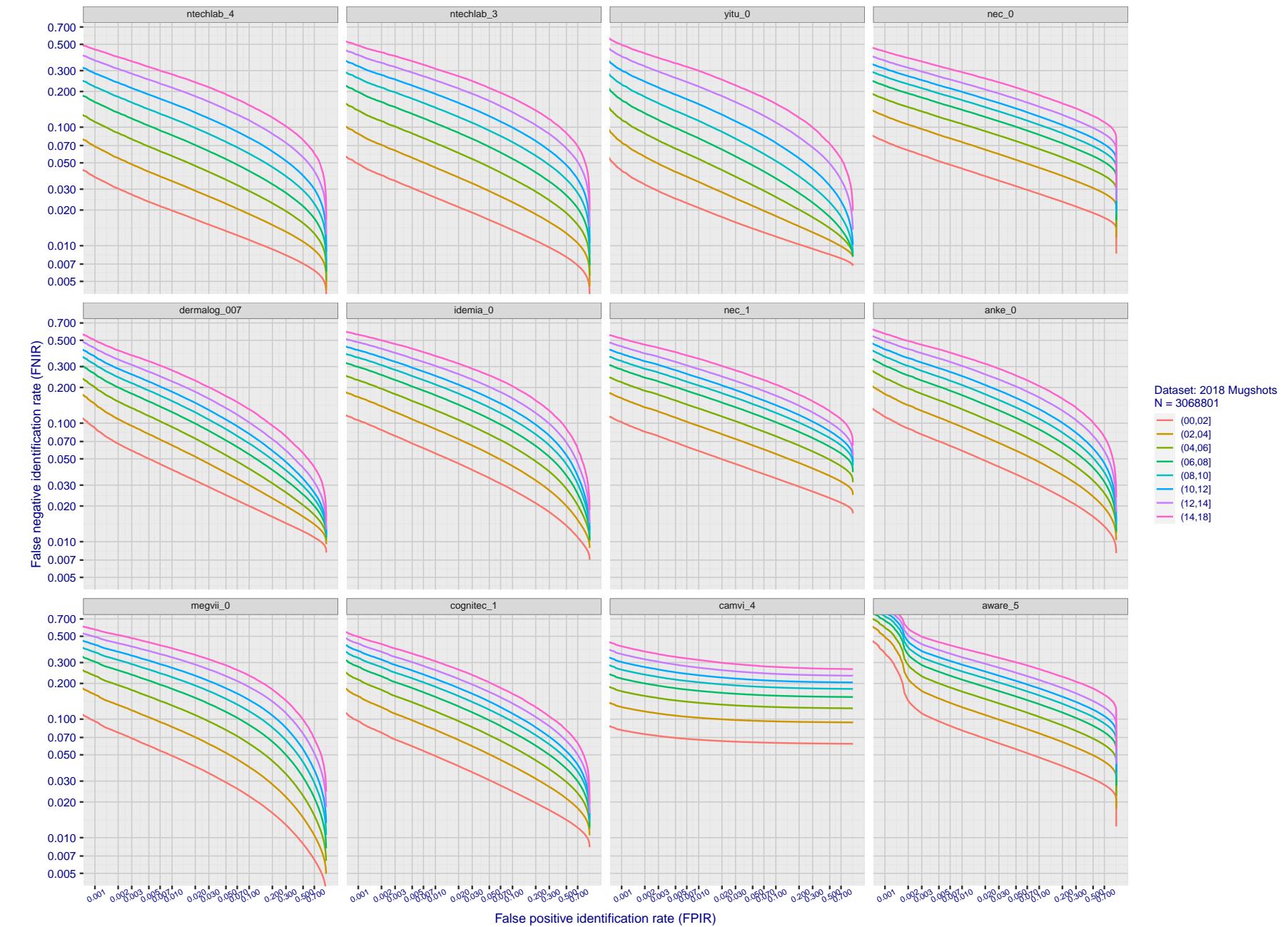


Figure 103: [FRVT-2018 Mugshot Ageing Dataset] Identification miss rates vs. FPIR by time-elapsed. The oldest image of each individual is enrolled. Thereafter, all more recent images are searched. Miss rates are computed over all searches noted in row 17 of Table 1 and binned by number of years between search and initial enrollment. FPIR is computed from the same FRVT 2018 non-mates noted in row 3 of Table 1 with N = 3 000 000.

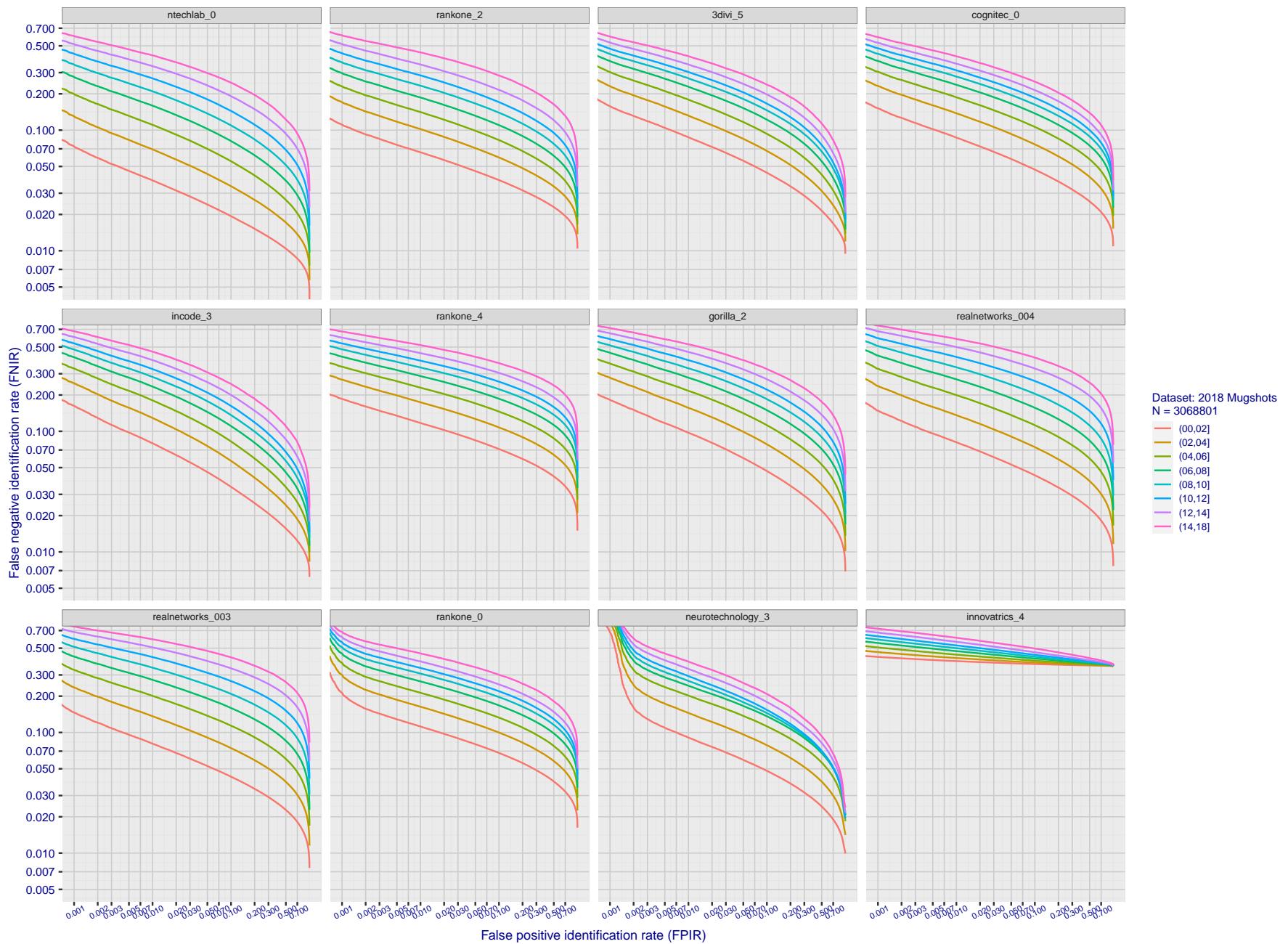


Figure 104: [FRVT-2018 Mugshot Ageing Dataset] Identification miss rates vs. FPIR by time-elapsed. The oldest image of each individual is enrolled. Thereafter, all more recent images are searched. Miss rates are computed over all searches noted in row 17 of Table 1 and binned by number of years between search and initial enrollment. FPIR is computed from the same FRVT 2018 non-mates noted in row 3 of Table 1 with $N = 3\,000\,000$.

2023/04/04
07:31:47FNIR(N, R, T) = False neg. identification rate
FPIR(N, T) = False pos. identification rateN = Num. enrolled subjects
R = Num. candidates examined

T = Threshold

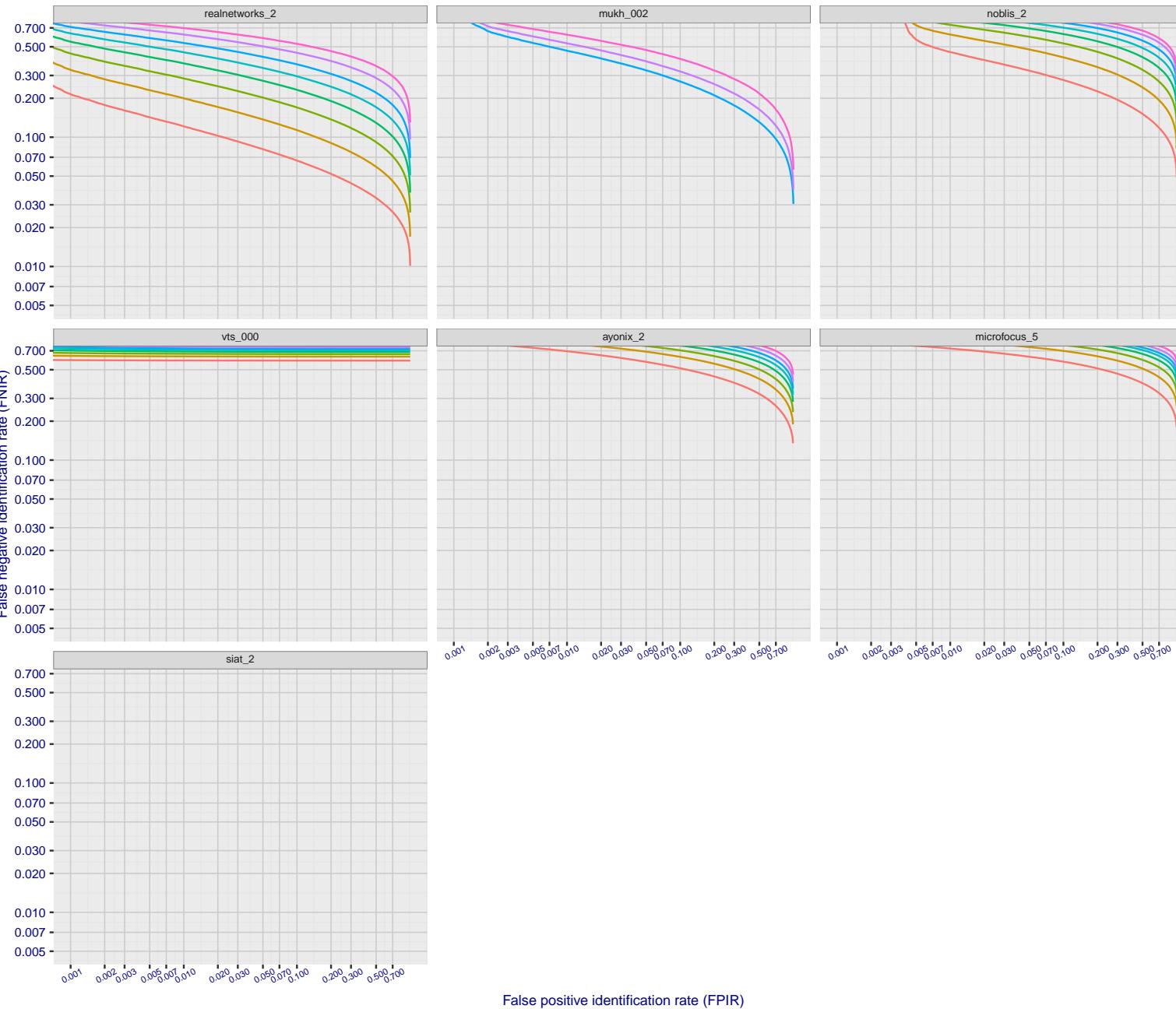
T = 0 → Investigation
T > 0 → Identification

Figure 105: [FRVT-2018 Mugshot Ageing Dataset] Identification miss rates vs. FPIR by time-elapsed. The oldest image of each individual is enrolled. Thereafter, all more recent images are searched. Miss rates are computed over all searches noted in row 17 of Table 1 and binned by number of years between search and initial enrollment. FPIR is computed from the same FRVT 2018 non-mates noted in row 3 of Table 1 with N = 3 000 000.

2023/04/04
07:31:47

FNIR(N, R, T) = False neg. identification rate
FPTR(N, T) = False pos. identification rate

N = Num. enrolled subjects
R = Num. candidates examined

T = Threshold
T > 0 → Identification

T = 0 → Investigation

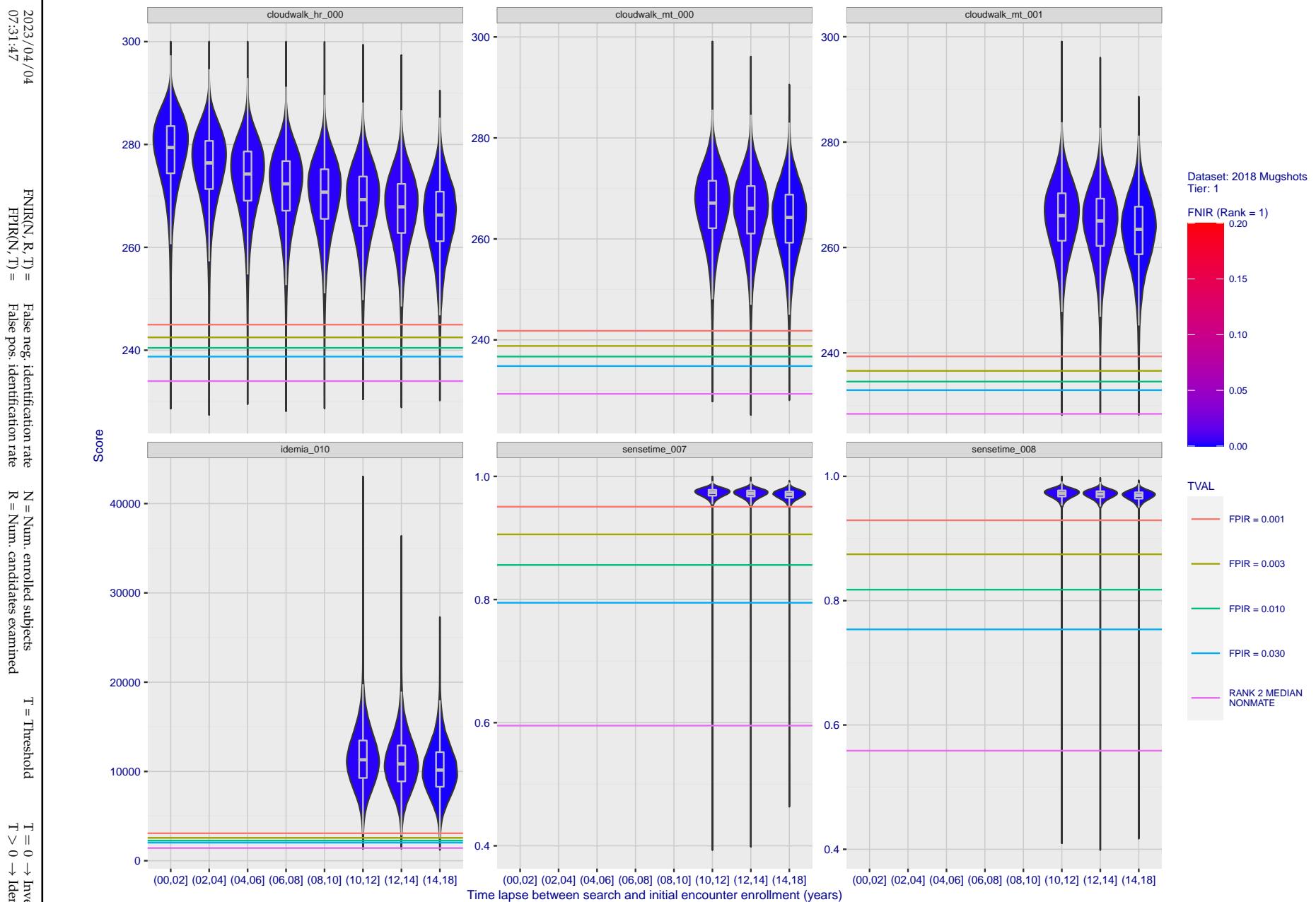


Figure 106: [FRVT-2018 Mugshot Ageing Dataset] Native mate scores vs. time-elapsed. The oldest image of each individual is enrolled. Thereafter, all more recent images are searched. Mated score distributions are computed over all searches noted in row 17 of Table 1 binned by number of years between search and initial enrollment.

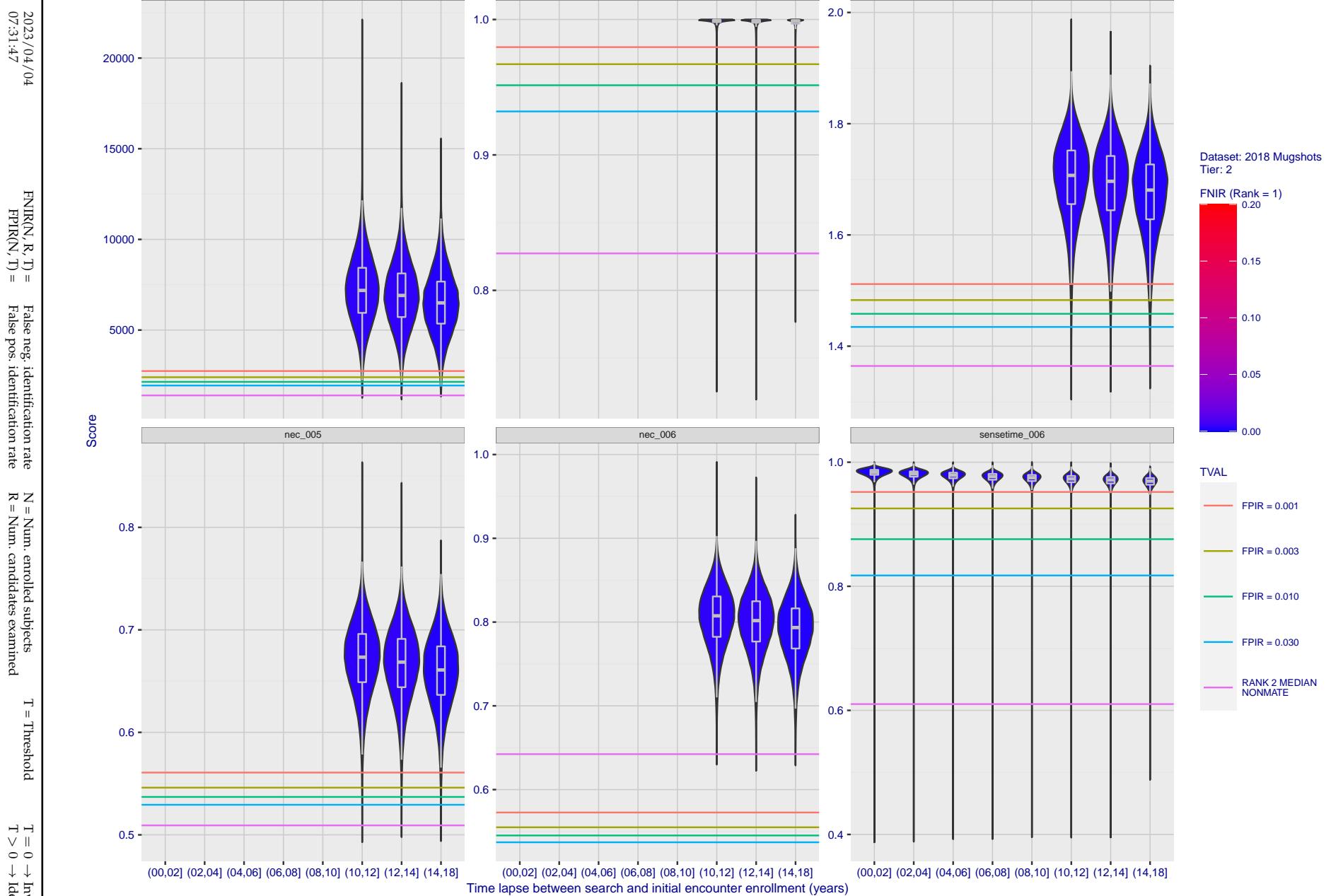


Figure 107: [FRVT-2018 Mugshot Ageing Dataset] Native mate scores vs. time-elapsed. The oldest image of each individual is enrolled. Thereafter, all more recent images are searched. Mated score distributions are computed over all searches noted in row 17 of Table 1 binned by number of years between search and initial enrollment.

2023/04/04

07:31:47

FNIR(N, R, T) = False neg. identification rate

FPIR(N, T) = False pos. identification rate

N = Num. enrolled subjects

R = Num. candidates examined

T = Threshold

T = 0 → Investigation

T > 0 → Identification

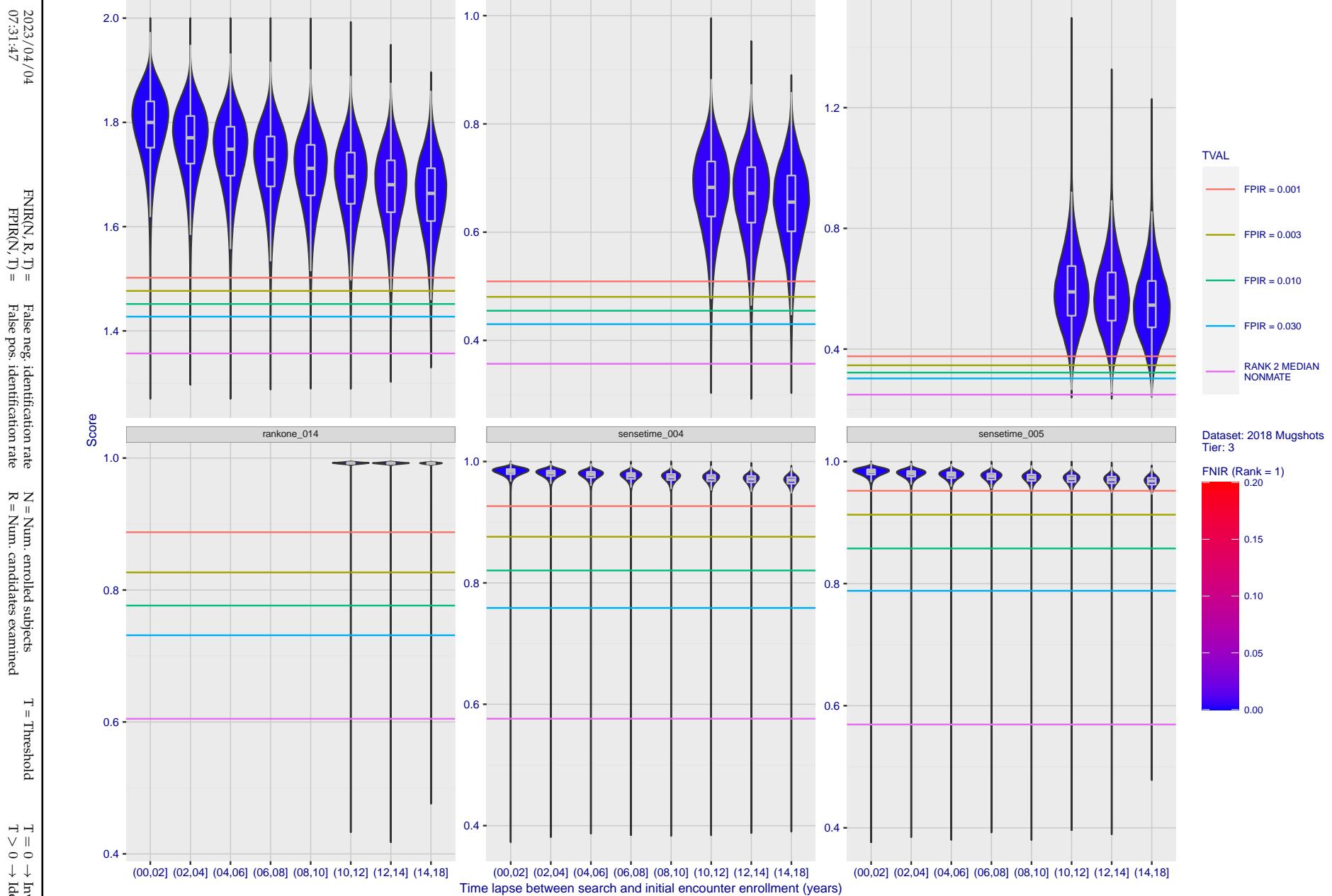


Figure 108: [FRVT-2018 Mugshot Ageing Dataset] Native mate scores vs. time-elapsed. The oldest image of each individual is enrolled. Thereafter, all more recent images are searched. Mated score distributions are computed over all searches noted in row 17 of Table 1 binned by number of years between search and initial enrollment.

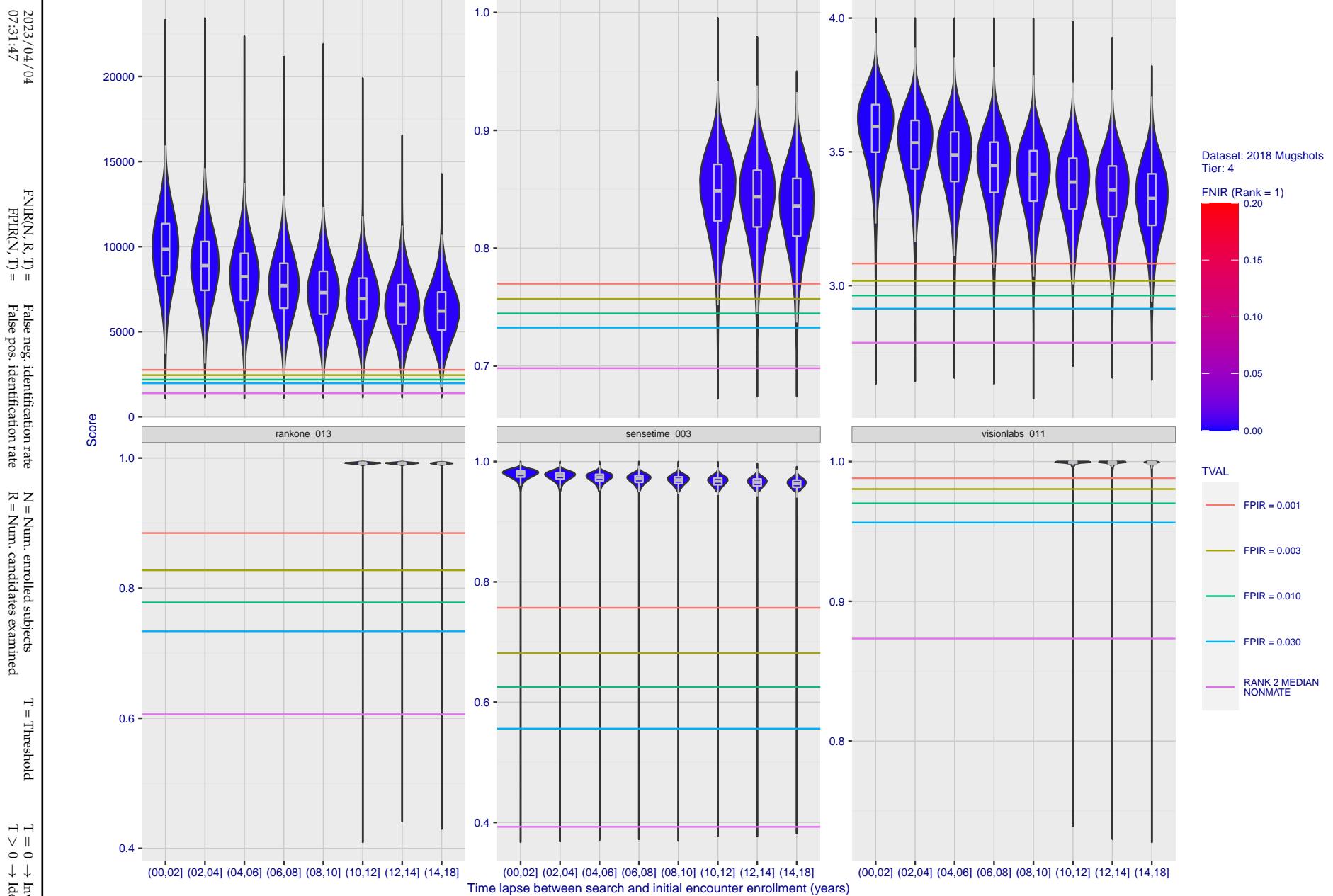


Figure 109: [FRVT-2018 Mugshot Ageing Dataset] Native mate scores vs. time-elapsed. The oldest image of each individual is enrolled. Thereafter, all more recent images are searched. Mated score distributions are computed over all searches noted in row 17 of Table 1 binned by number of years between search and initial enrollment.

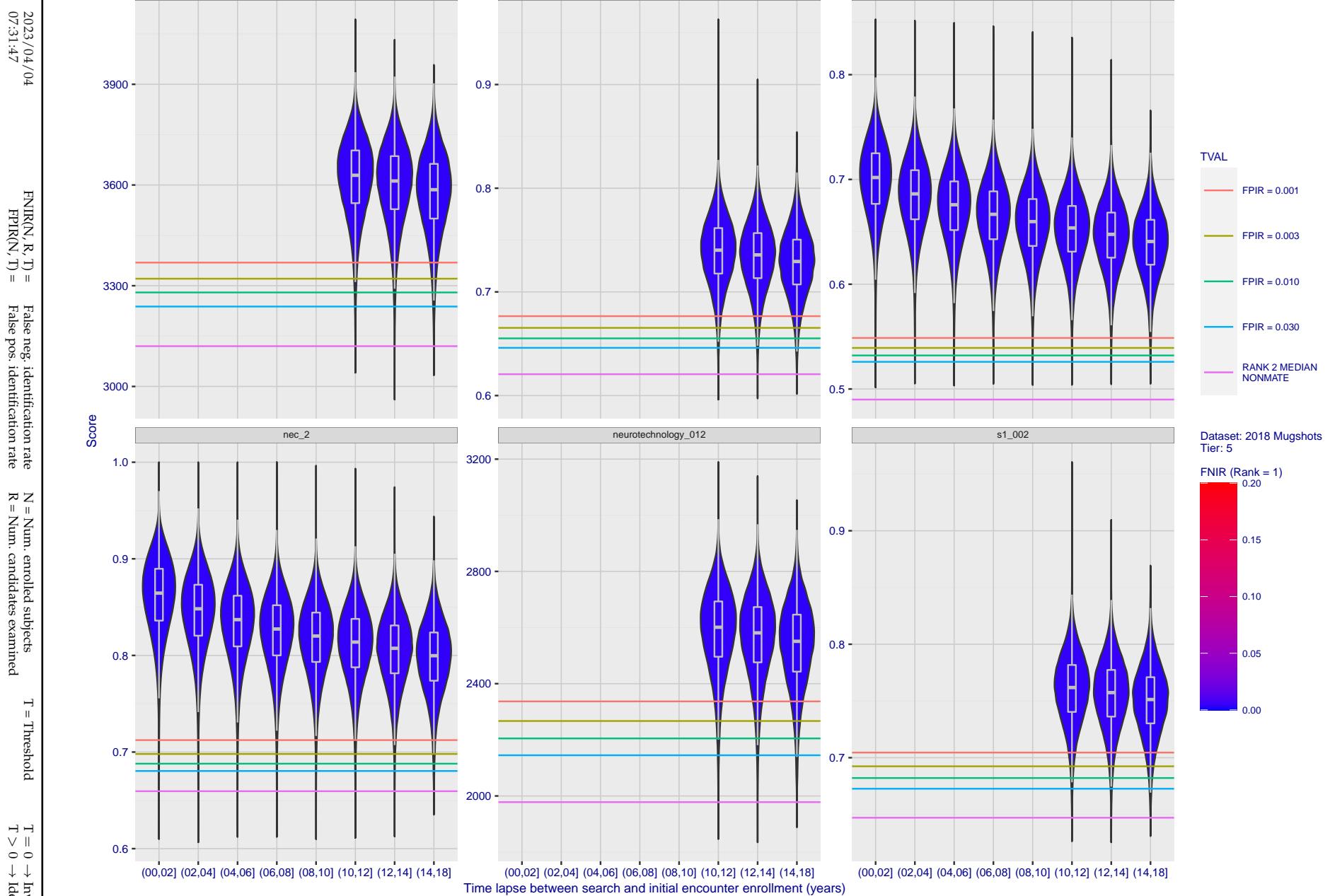


Figure 110: [FRVT-2018 Mugshot Ageing Dataset] Native mate scores vs. time-elapsed. The oldest image of each individual is enrolled. Thereafter, all more recent images are searched. Mated score distributions are computed over all searches noted in row 17 of Table 1 binned by number of years between search and initial enrollment.

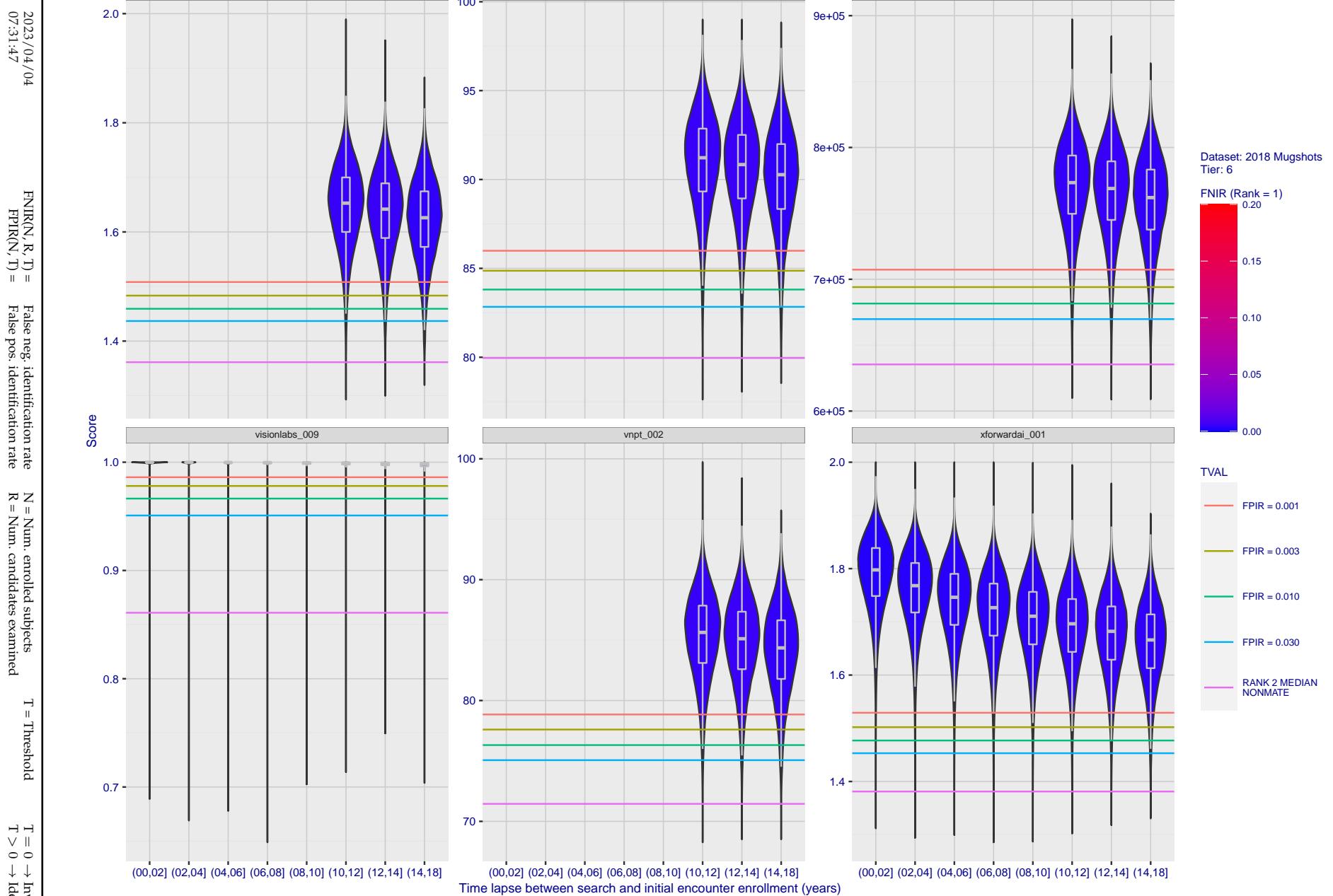


Figure 111: [FRVT-2018 Mugshot Ageing Dataset] Native mate scores vs. time-elapsed. The oldest image of each individual is enrolled. Thereafter, all more recent images are searched. Mated score distributions are computed over all searches noted in row 17 of Table 1 binned by number of years between search and initial enrollment.

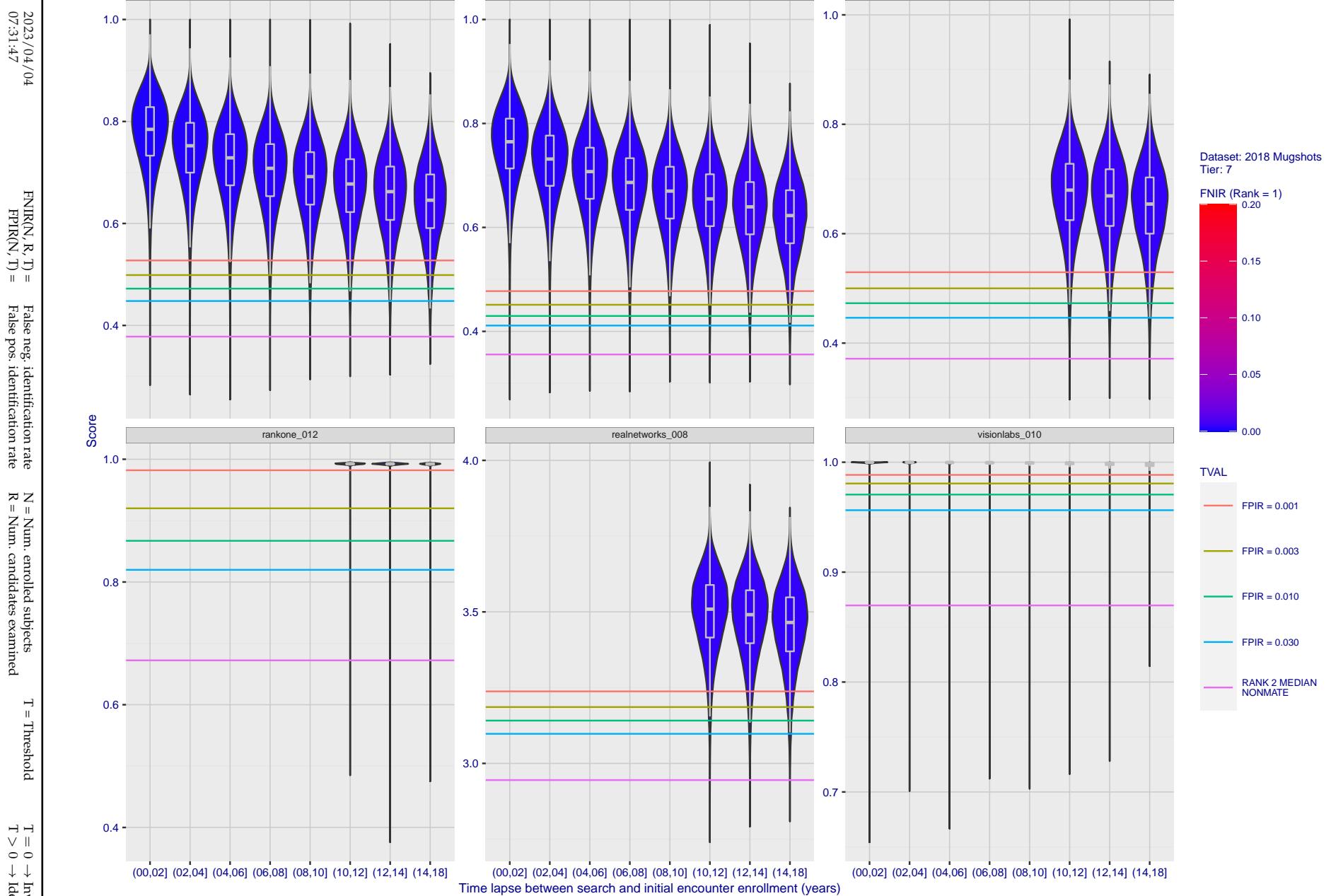


Figure 112: [FRVT-2018 Mugshot Ageing Dataset] Native mate scores vs. time-elapsed. The oldest image of each individual is enrolled. Thereafter, all more recent images are searched. Mated score distributions are computed over all searches noted in row 17 of Table 1 binned by number of years between search and initial enrollment.

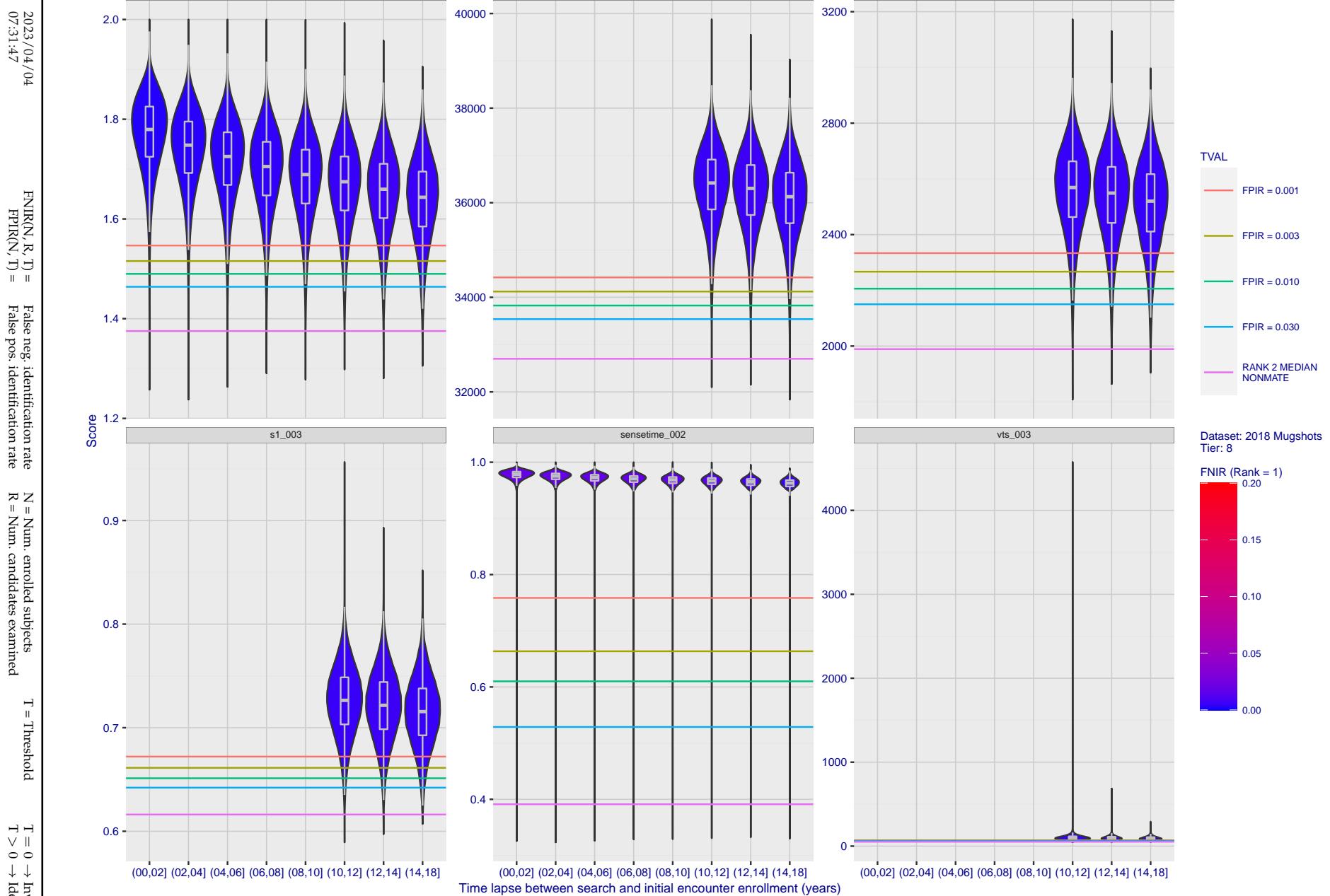


Figure 113: [FRVT-2018 Mugshot Ageing Dataset] Native mate scores vs. time-elapsed. The oldest image of each individual is enrolled. Thereafter, all more recent images are searched. Mated score distributions are computed over all searches noted in row 17 of Table 1 binned by number of years between search and initial enrollment.

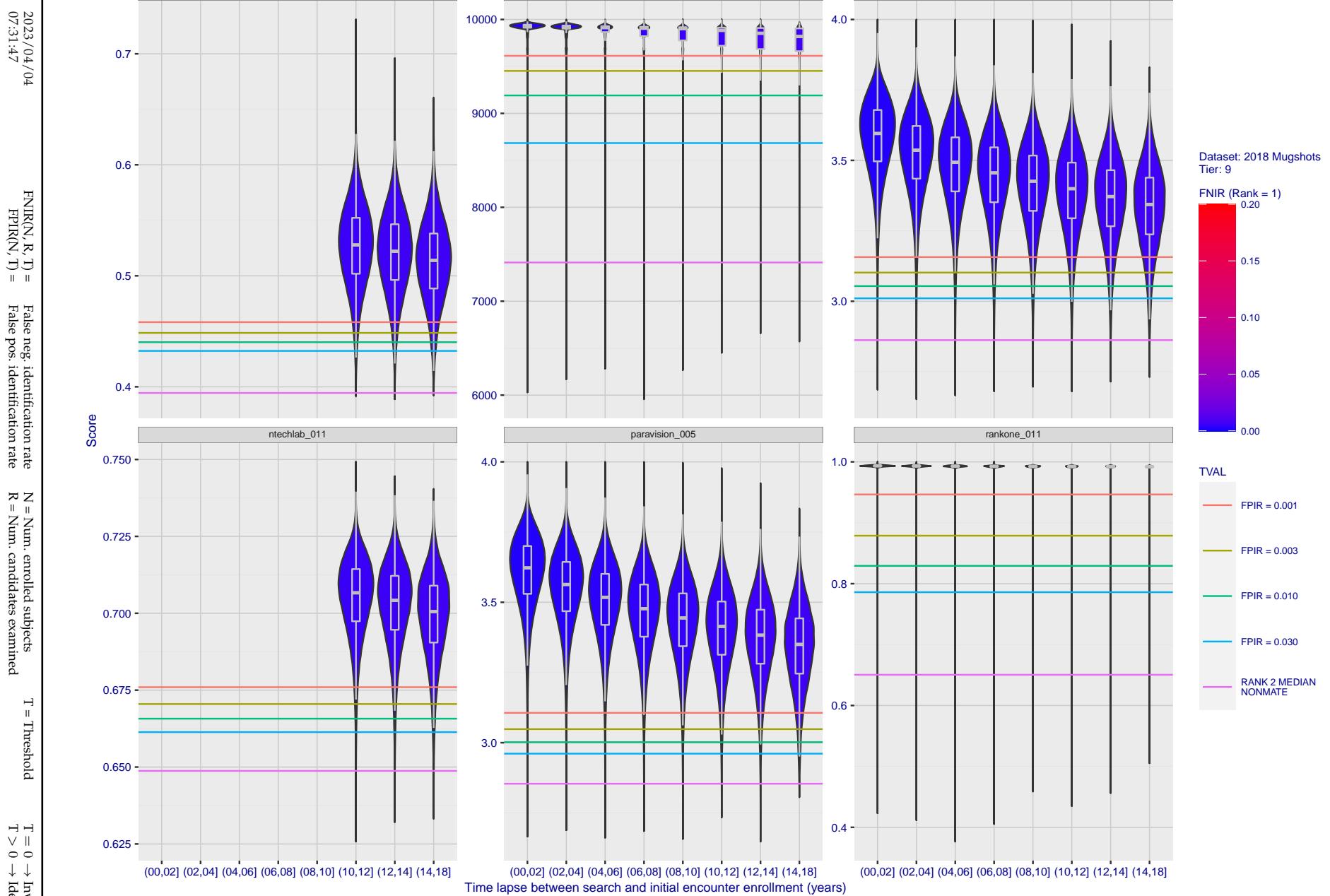


Figure 114: [FRVT-2018 Mugshot Ageing Dataset] Native mate scores vs. time-elapsed. The oldest image of each individual is enrolled. Thereafter, all more recent images are searched. Mated score distributions are computed over all searches noted in row 17 of Table 1 binned by number of years between search and initial enrollment.

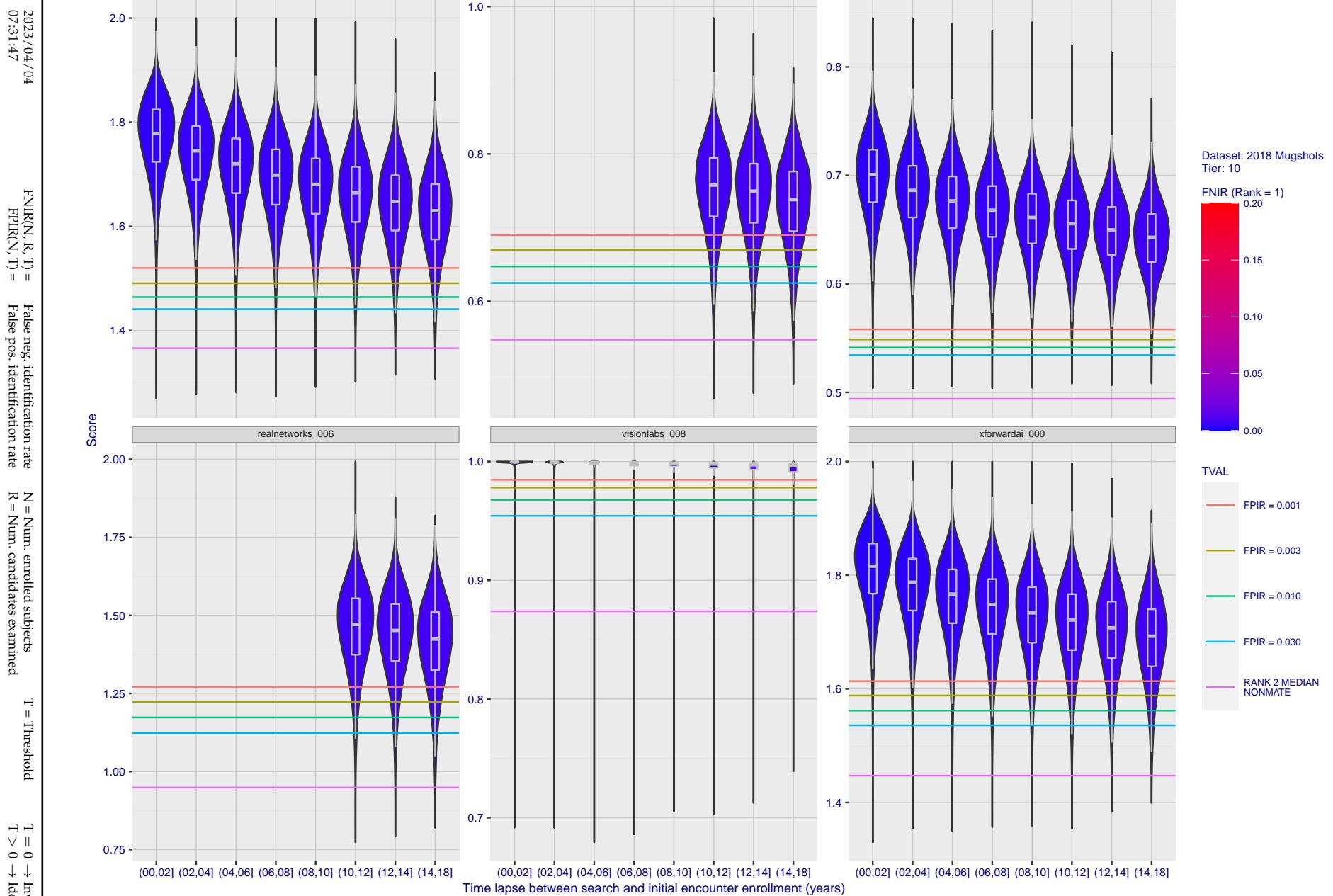


Figure 115: [FRVT-2018 Mugshot Ageing Dataset] Native mate scores vs. time-elapsed. The oldest image of each individual is enrolled. Thereafter, all more recent images are searched. Mated score distributions are computed over all searches noted in row 17 of Table 1 binned by number of years between search and initial enrollment.

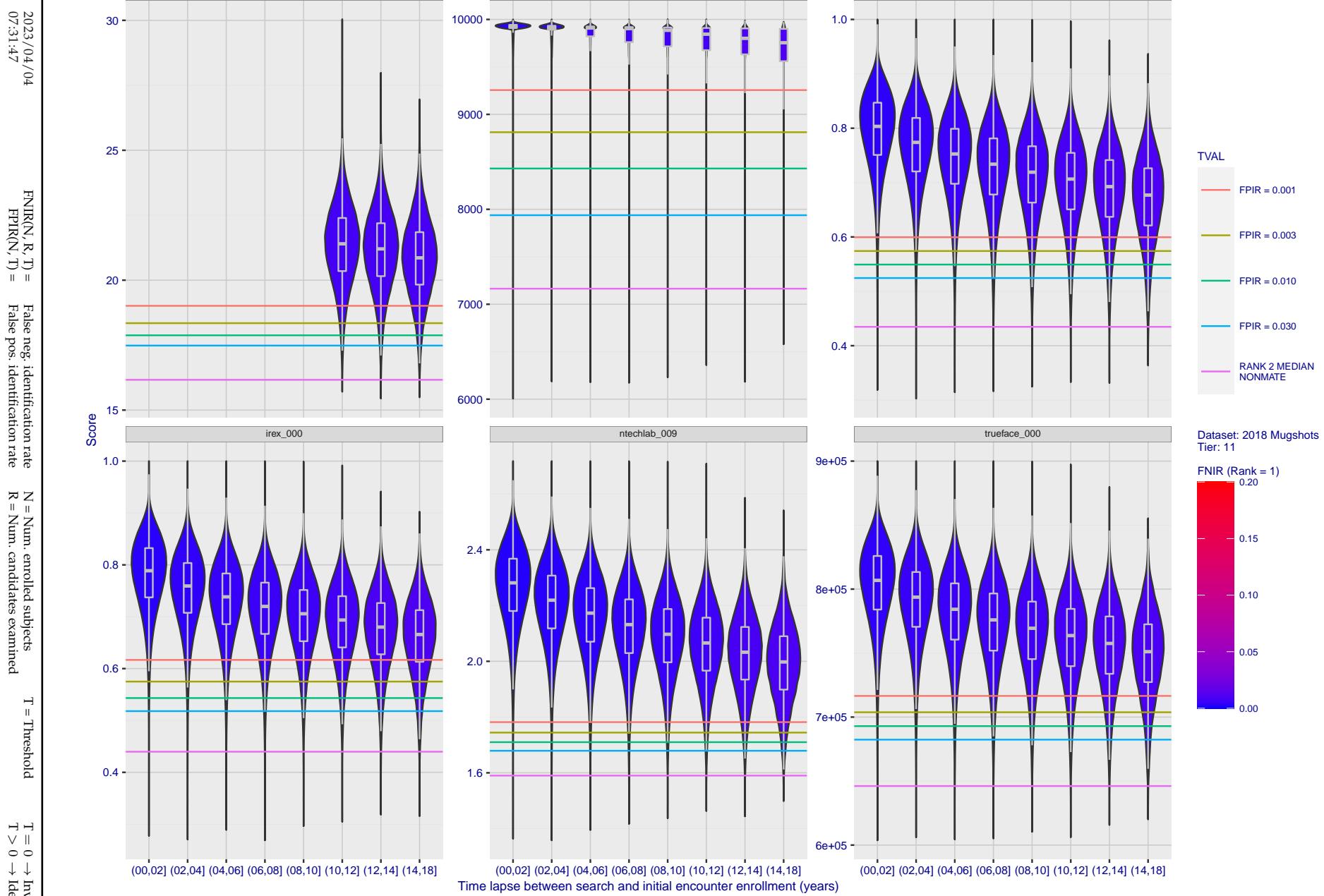


Figure 116: [FRVT-2018 Mugshot Ageing Dataset] Native mate scores vs. time-elapsed. The oldest image of each individual is enrolled. Thereafter, all more recent images are searched. Mated score distributions are computed over all searches noted in row 17 of Table 1 binned by number of years between search and initial enrollment.

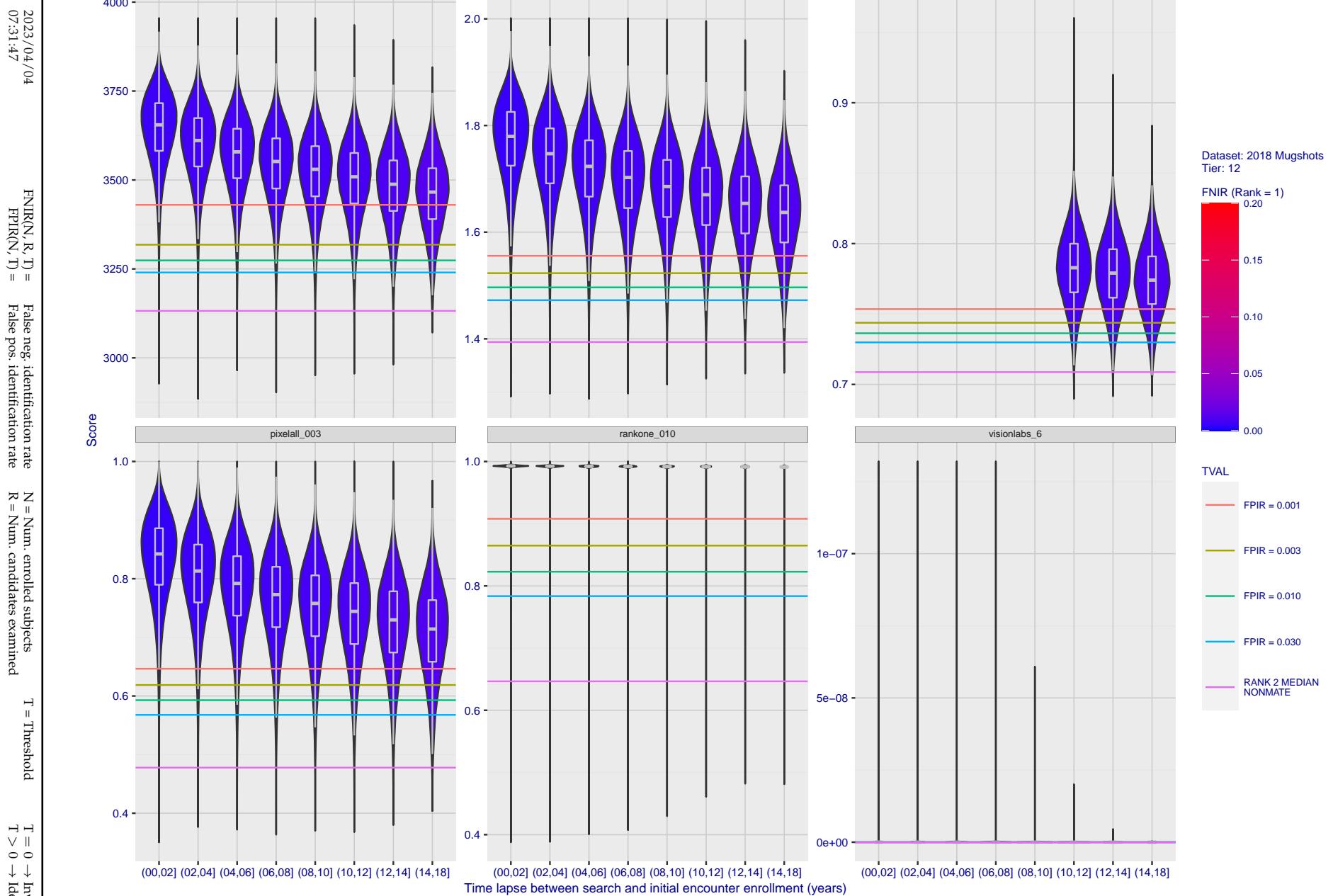


Figure 117: [FRVT-2018 Mugshot Ageing Dataset] Native mate scores vs. time-elapsed. The oldest image of each individual is enrolled. Thereafter, all more recent images are searched. Mated score distributions are computed over all searches noted in row 17 of Table 1 binned by number of years between search and initial enrollment.

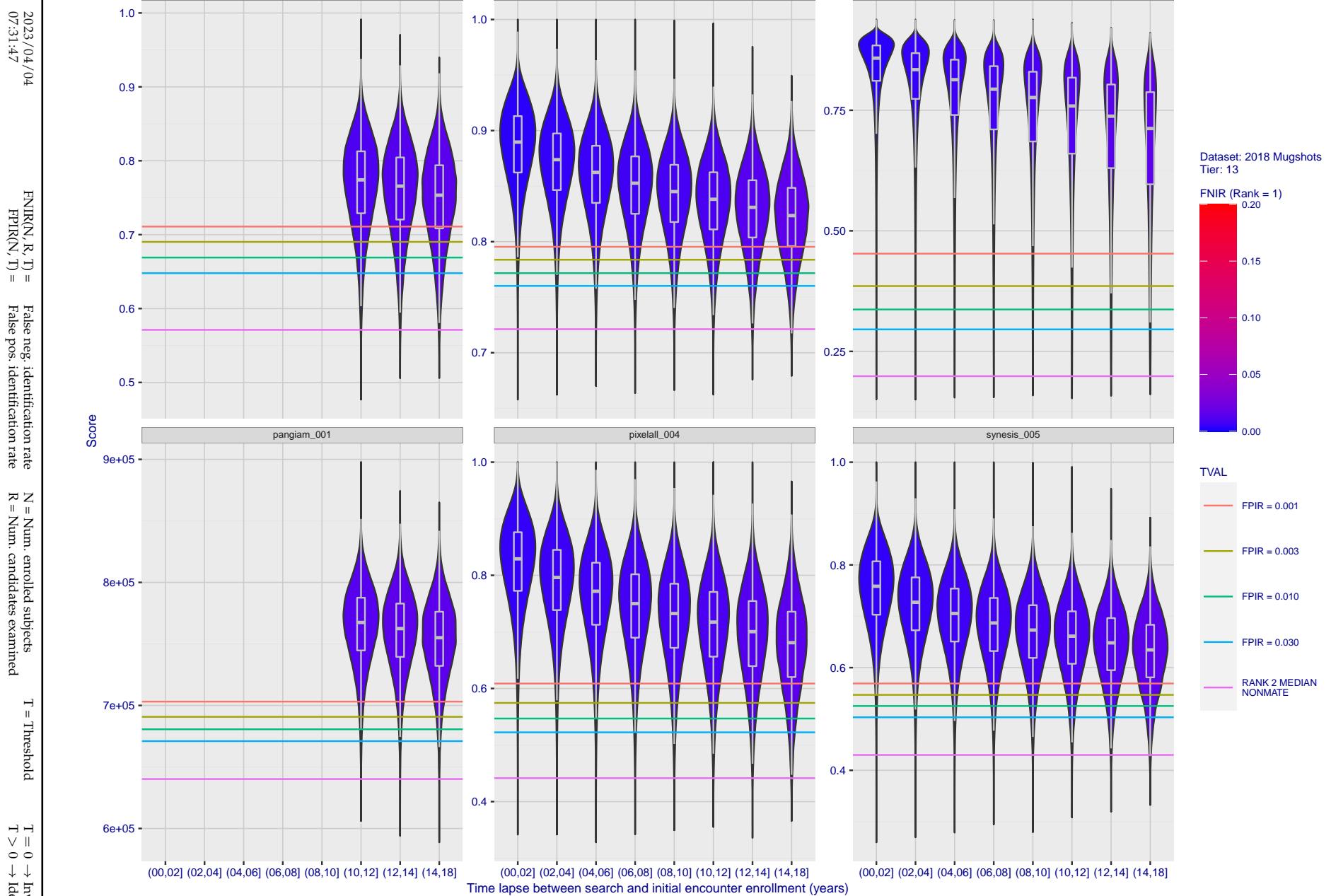


Figure 118: [FRVT-2018 Mugshot Ageing Dataset] Native mate scores vs. time-elapsed. The oldest image of each individual is enrolled. Thereafter, all more recent images are searched. Mated score distributions are computed over all searches noted in row 17 of Table 1 binned by number of years between search and initial enrollment.

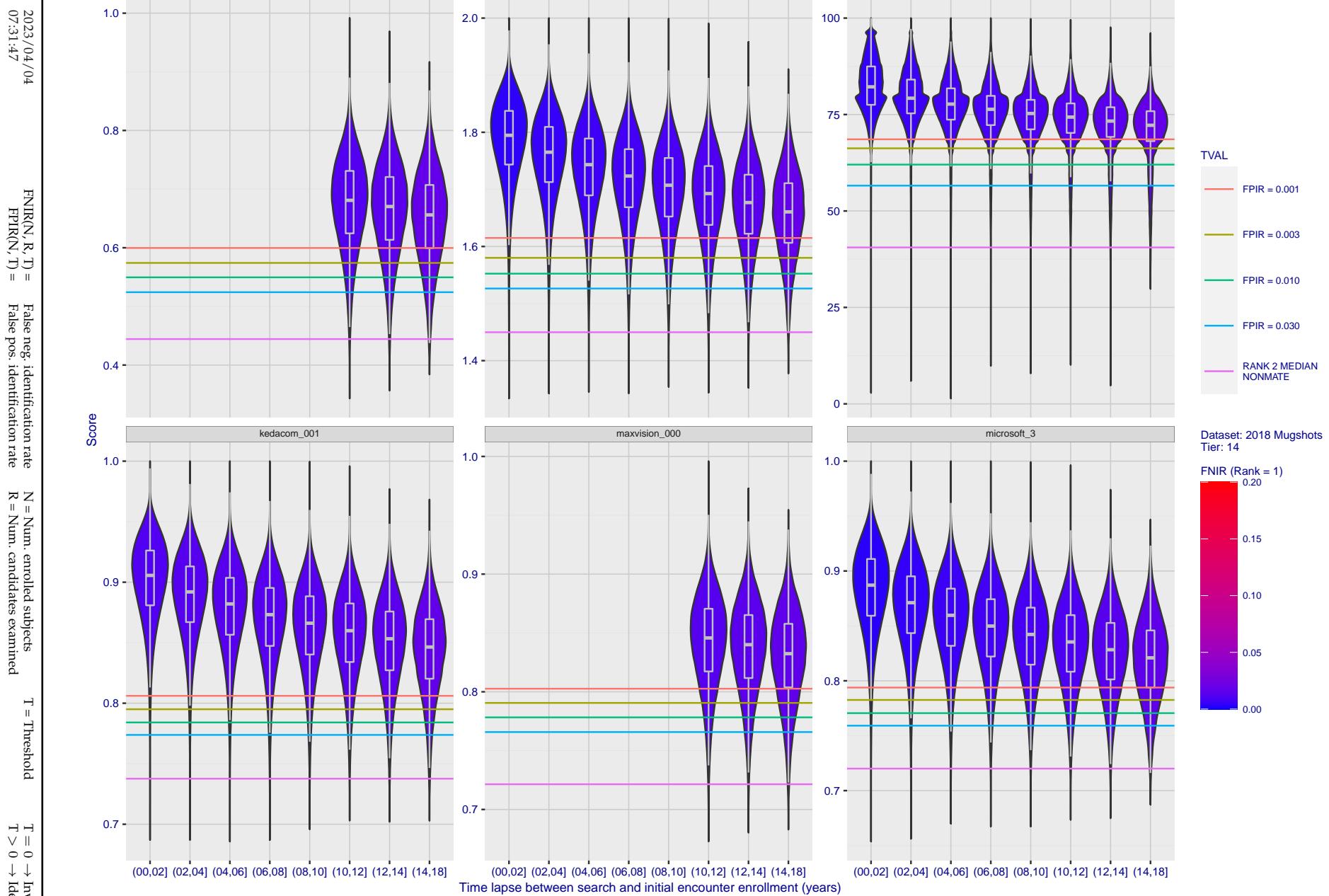


Figure 119: [FRVT-2018 Mugshot Ageing Dataset] Native mate scores vs. time-elapsed. The oldest image of each individual is enrolled. Thereafter, all more recent images are searched. Mated score distributions are computed over all searches noted in row 17 of Table 1 binned by number of years between search and initial enrollment.

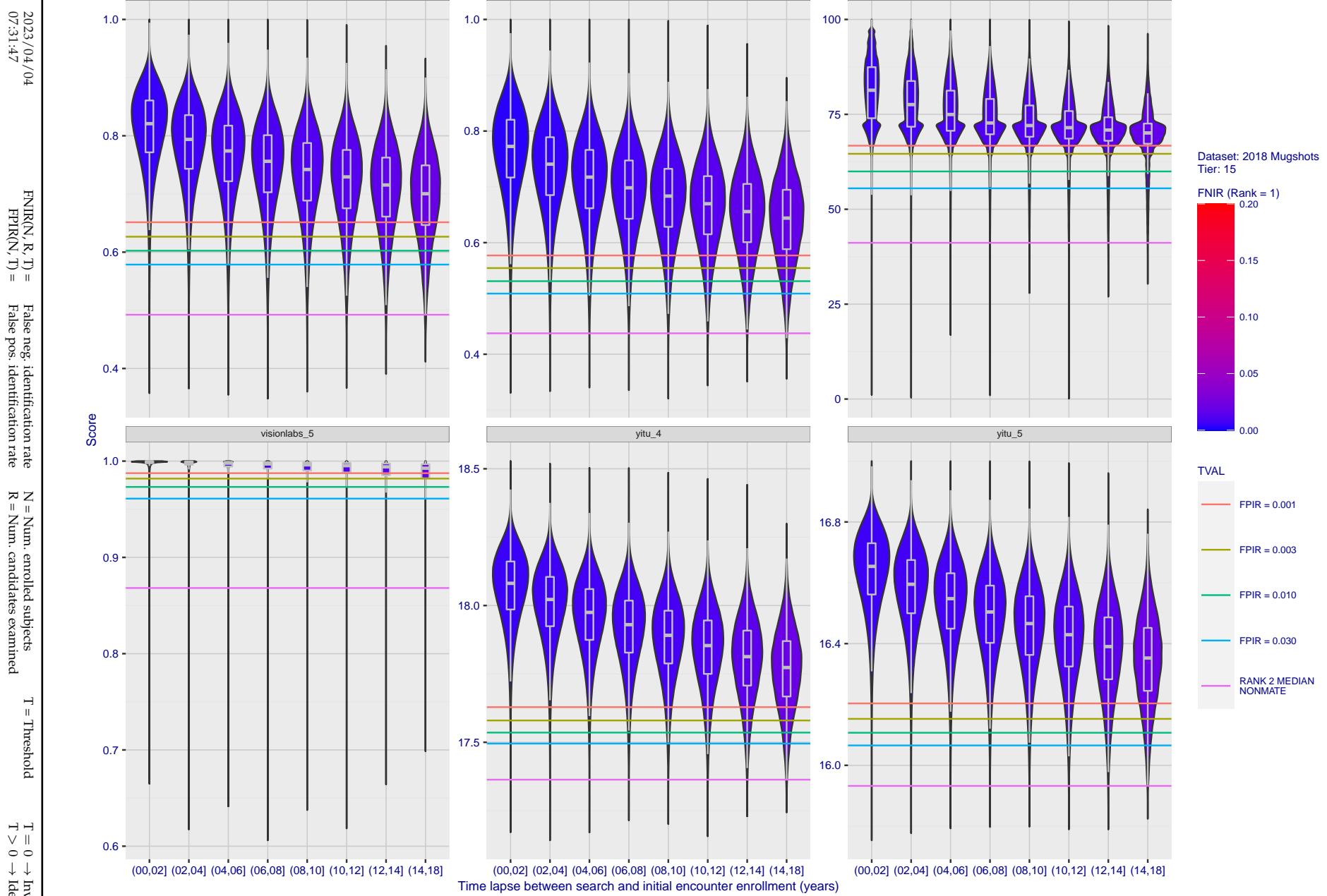


Figure 120: [FRVT-2018 Mugshot Ageing Dataset] Native mate scores vs. time-elapsed. The oldest image of each individual is enrolled. Thereafter, all more recent images are searched. Mated score distributions are computed over all searches noted in row 17 of Table 1 binned by number of years between search and initial enrollment.

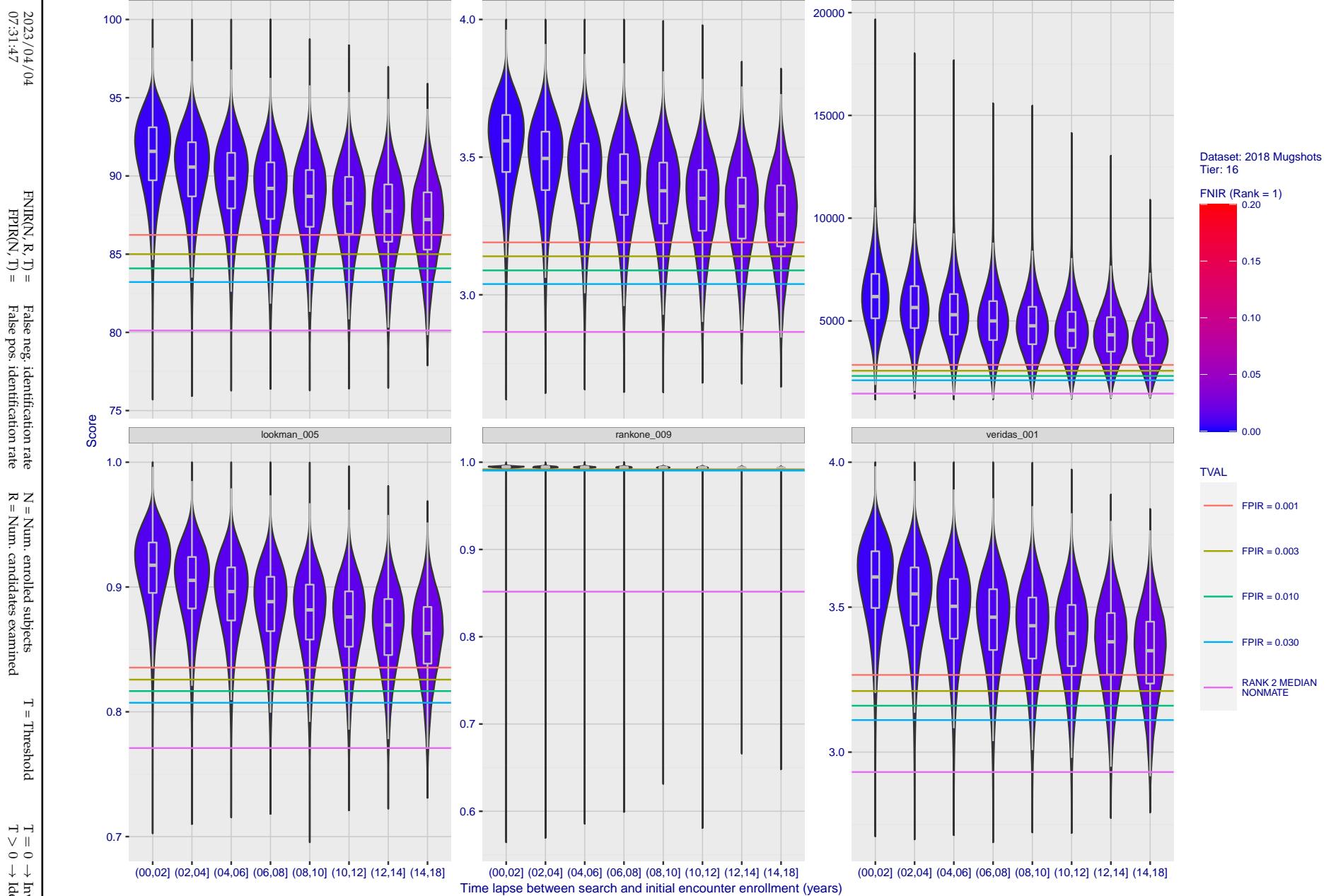


Figure 121: [FRVT-2018 Mugshot Ageing Dataset] Native mate scores vs. time-elapsed. The oldest image of each individual is enrolled. Thereafter, all more recent images are searched. Mated score distributions are computed over all searches noted in row 17 of Table 1 binned by number of years between search and initial enrollment.

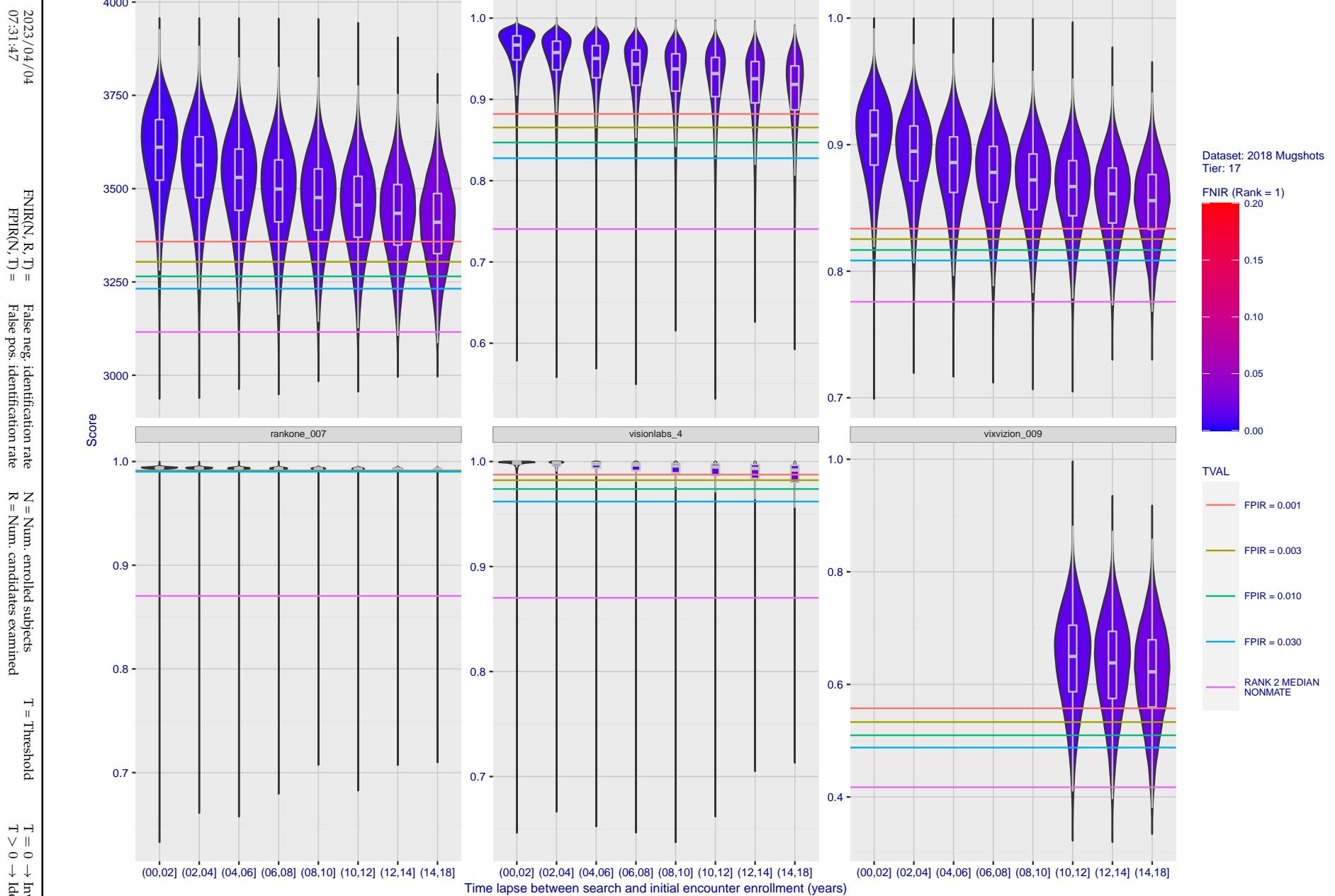


Figure 122: [FRVT-2018 Mugshot Ageing Dataset] Native mate scores vs. time-elapsed. The oldest image of each individual is enrolled. Thereafter, all more recent images are searched. Mated score distributions are computed over all searches noted in row 17 of Table 1 binned by number of years between search and initial enrollment.

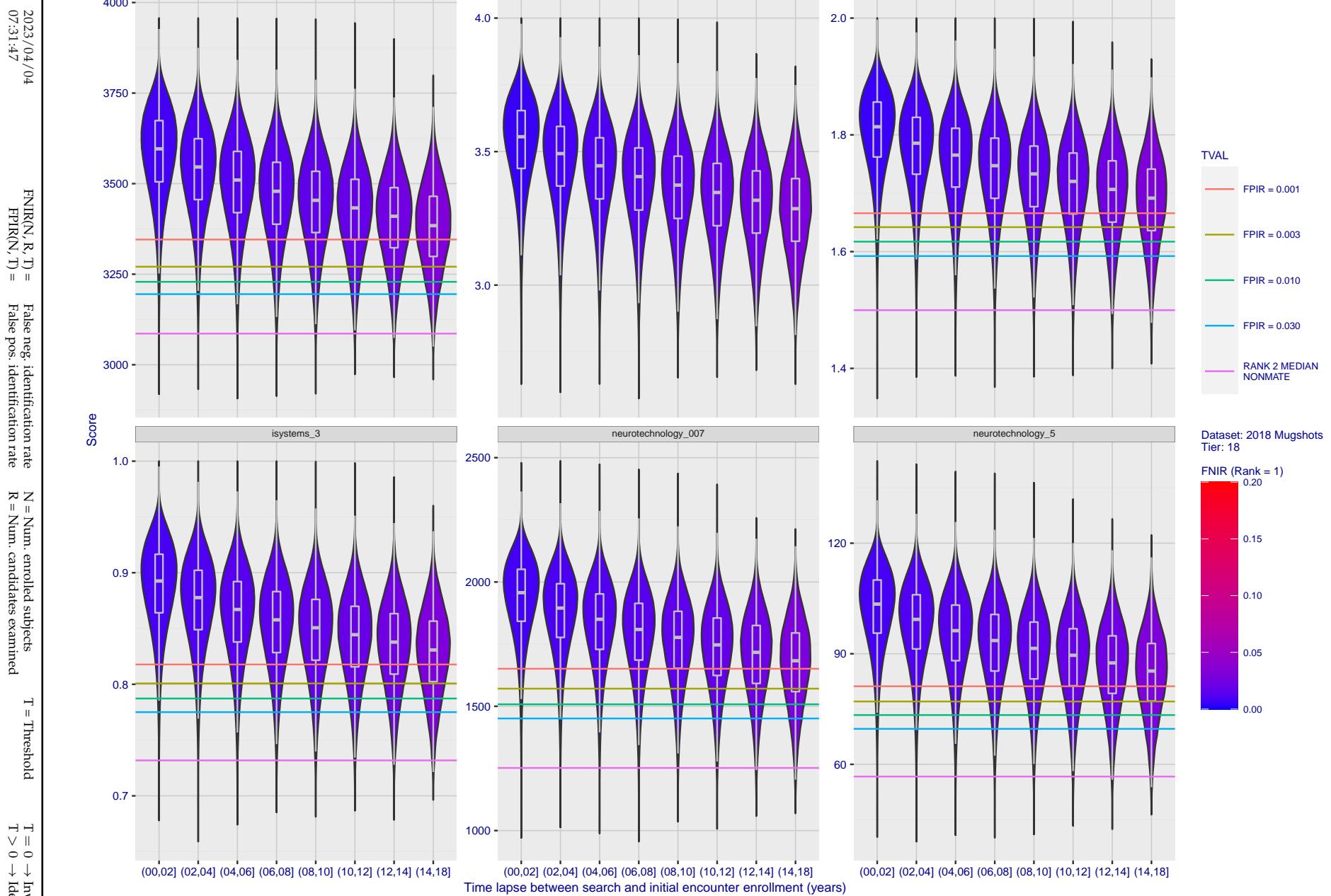


Figure 123: [FRVT-2018 Mugshot Ageing Dataset] Native mate scores vs. time-elapsed. The oldest image of each individual is enrolled. Thereafter, all more recent images are searched. Mated score distributions are computed over all searches noted in row 17 of Table 1 binned by number of years between search and initial enrollment.

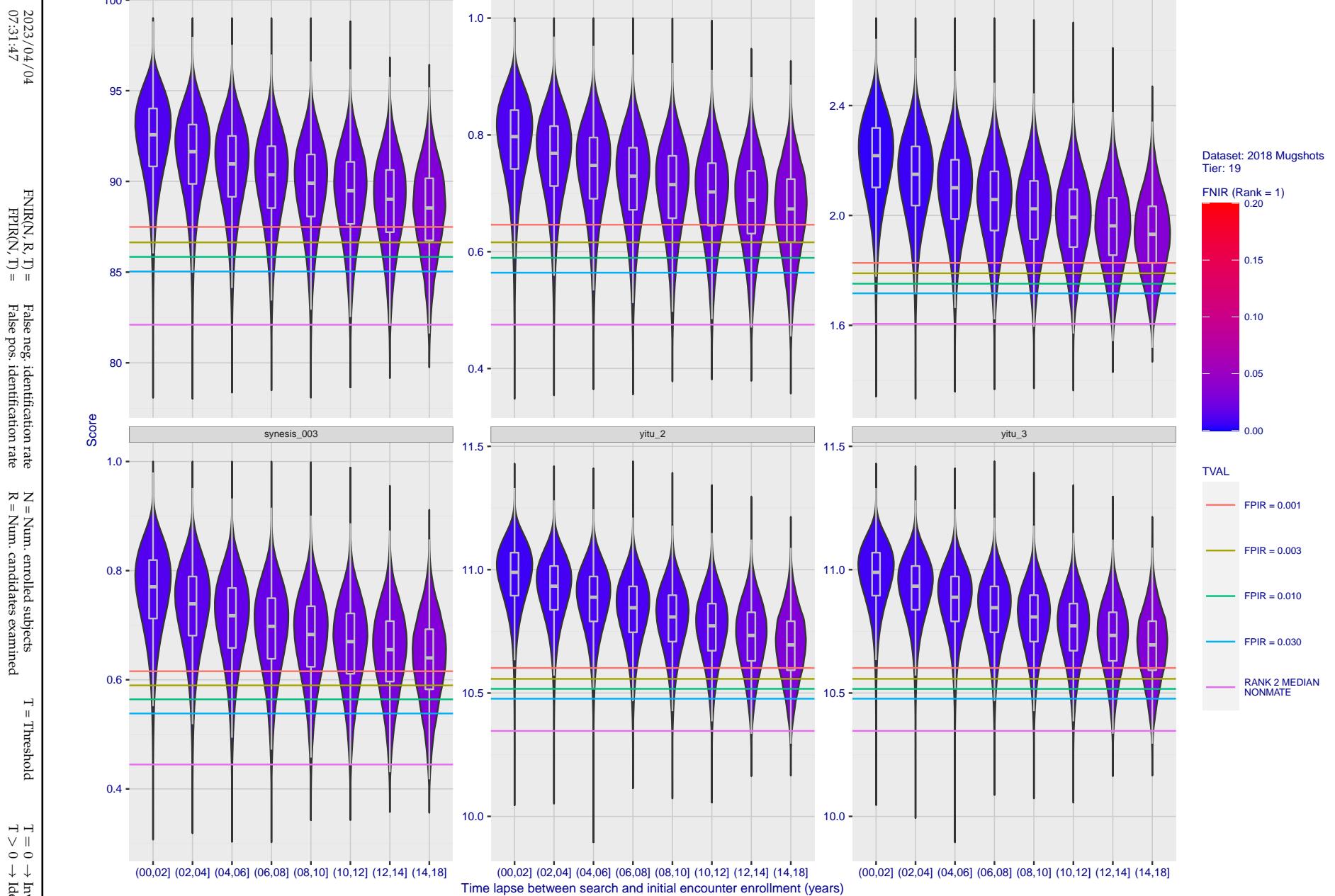


Figure 124: [FRVT-2018 Mugshot Ageing Dataset] Native mate scores vs. time-elapsed. The oldest image of each individual is enrolled. Thereafter, all more recent images are searched. Mated score distributions are computed over all searches noted in row 17 of Table 1 binned by number of years between search and initial enrollment.

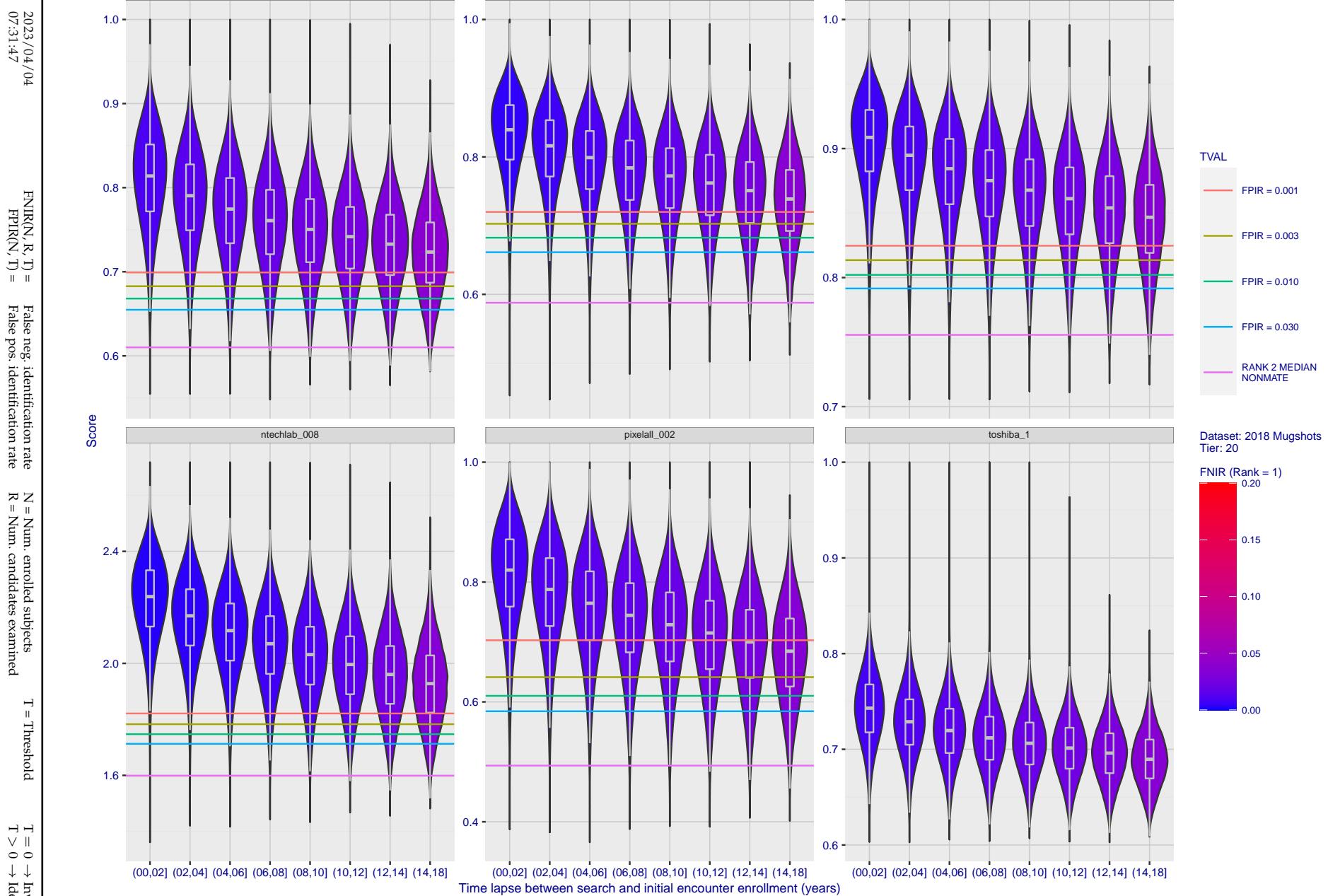


Figure 125: [FRVT-2018 Mugshot Ageing Dataset] Native mate scores vs. time-elapsed. The oldest image of each individual is enrolled. Thereafter, all more recent images are searched. Mated score distributions are computed over all searches noted in row 17 of Table 1 binned by number of years between search and initial enrollment.

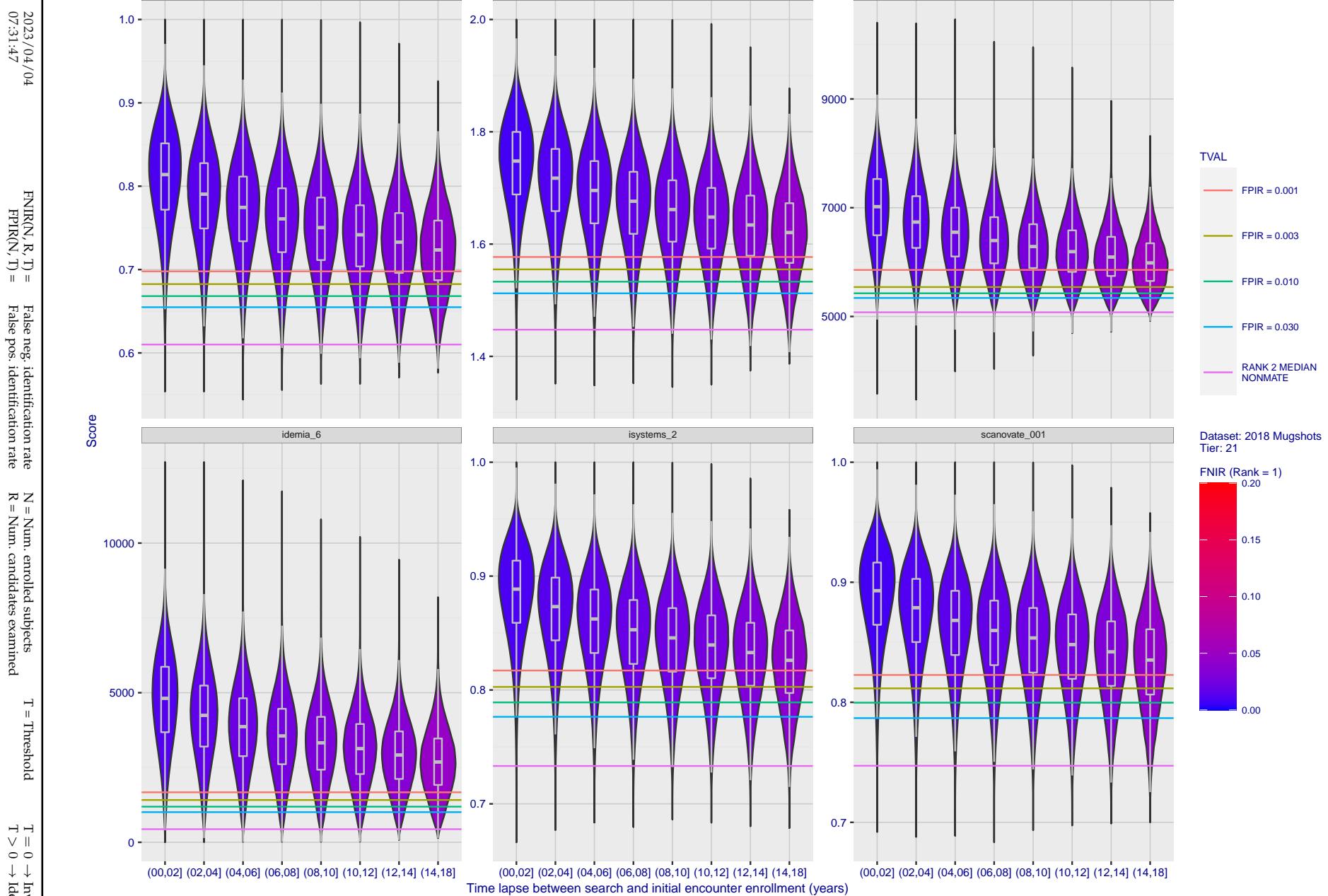


Figure 126: [FRVT-2018 Mugshot Ageing Dataset] Native mate scores vs. time-elapsed. The oldest image of each individual is enrolled. Thereafter, all more recent images are searched. Mated score distributions are computed over all searches noted in row 17 of Table 1 binned by number of years between search and initial enrollment.

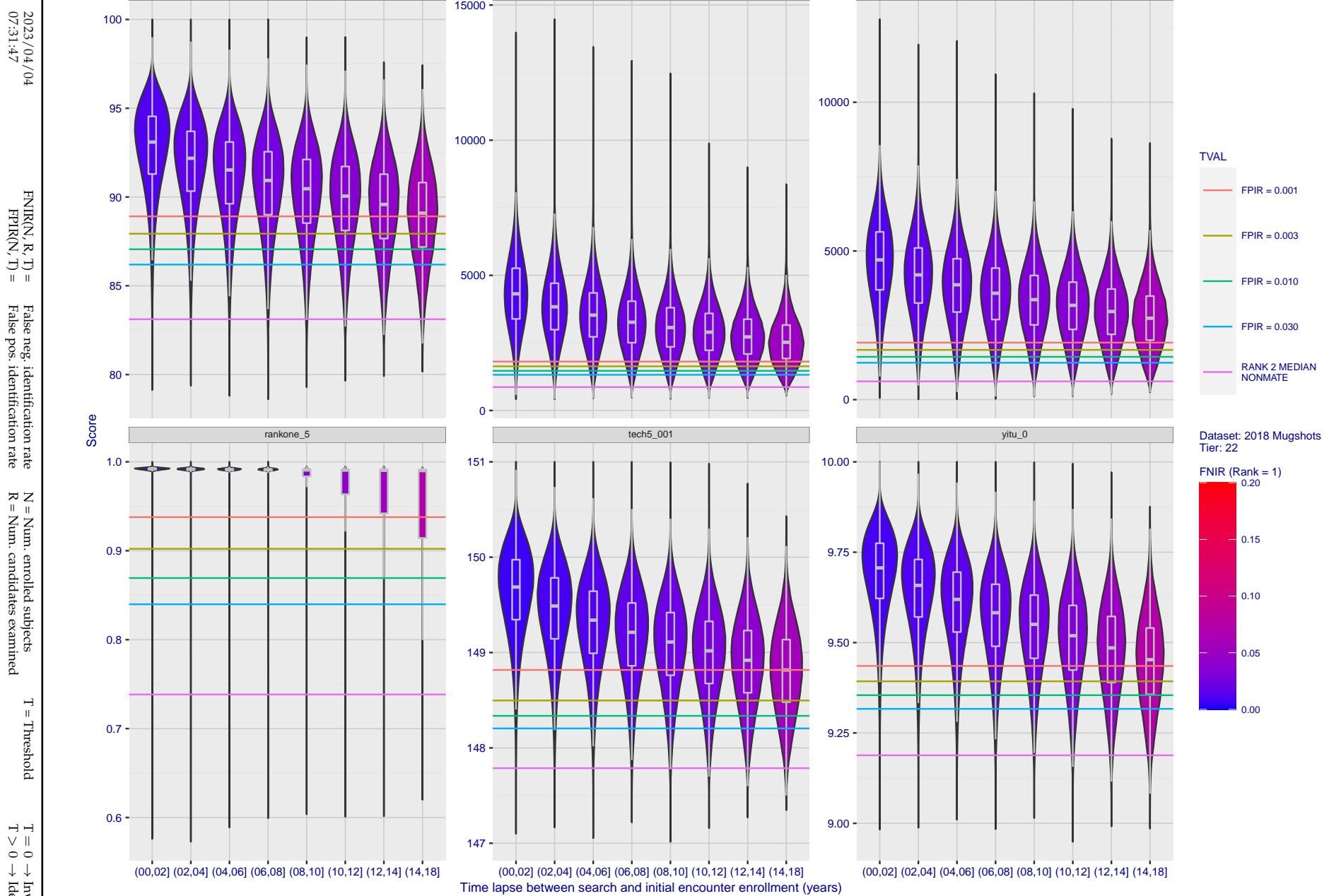


Figure 127: [FRVT-2018 Mugshot Ageing Dataset] Native mate scores vs. time-elapsed. The oldest image of each individual is enrolled. Thereafter, all more recent images are searched. Mated score distributions are computed over all searches noted in row 17 of Table 1 binned by number of years between search and initial enrollment.

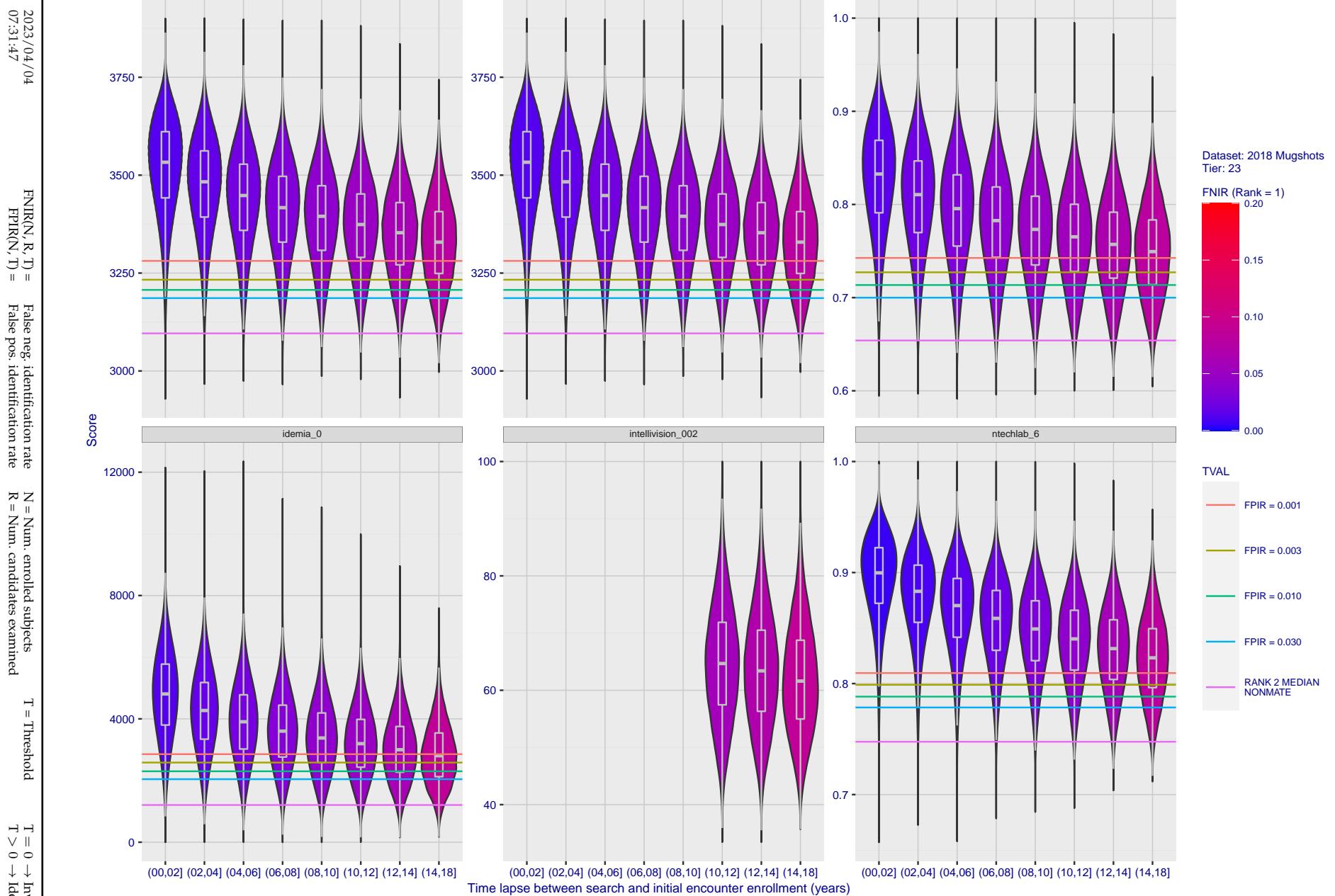


Figure 128: [FRVT-2018 Mugshot Ageing Dataset] Native mate scores vs. time-elapsed. The oldest image of each individual is enrolled. Thereafter, all more recent images are searched. Mated score distributions are computed over all searches noted in row 17 of Table 1 binned by number of years between search and initial enrollment.

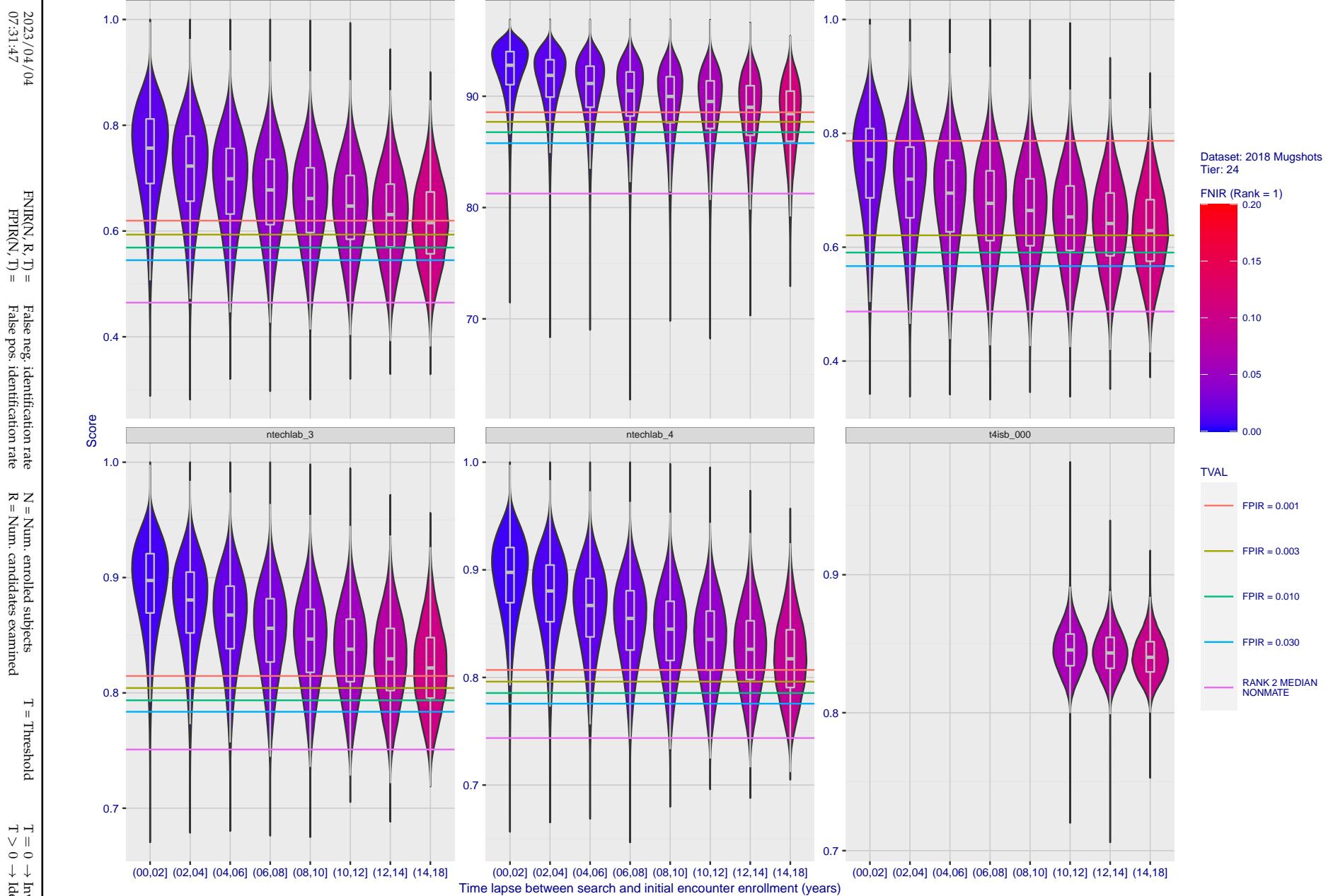


Figure 129: [FRVT-2018 Mugshot Ageing Dataset] Native mate scores vs. time-elapsed. The oldest image of each individual is enrolled. Thereafter, all more recent images are searched. Mated score distributions are computed over all searches noted in row 17 of Table 1 binned by number of years between search and initial enrollment.

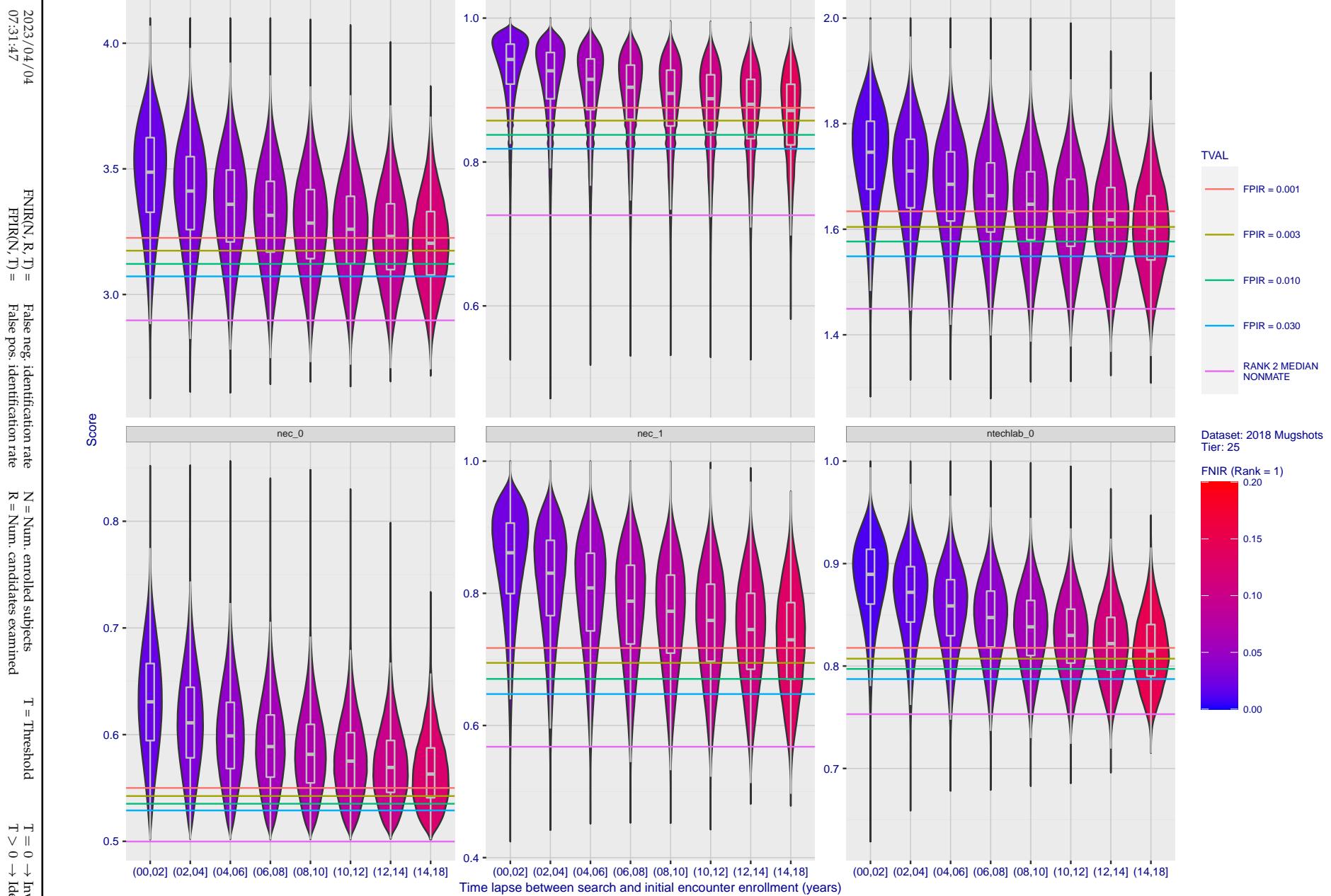


Figure 130: [FRVT-2018 Mugshot Ageing Dataset] Native mate scores vs. time-elapsed. The oldest image of each individual is enrolled. Thereafter, all more recent images are searched. Mated score distributions are computed over all searches noted in row 17 of Table 1 binned by number of years between search and initial enrollment.

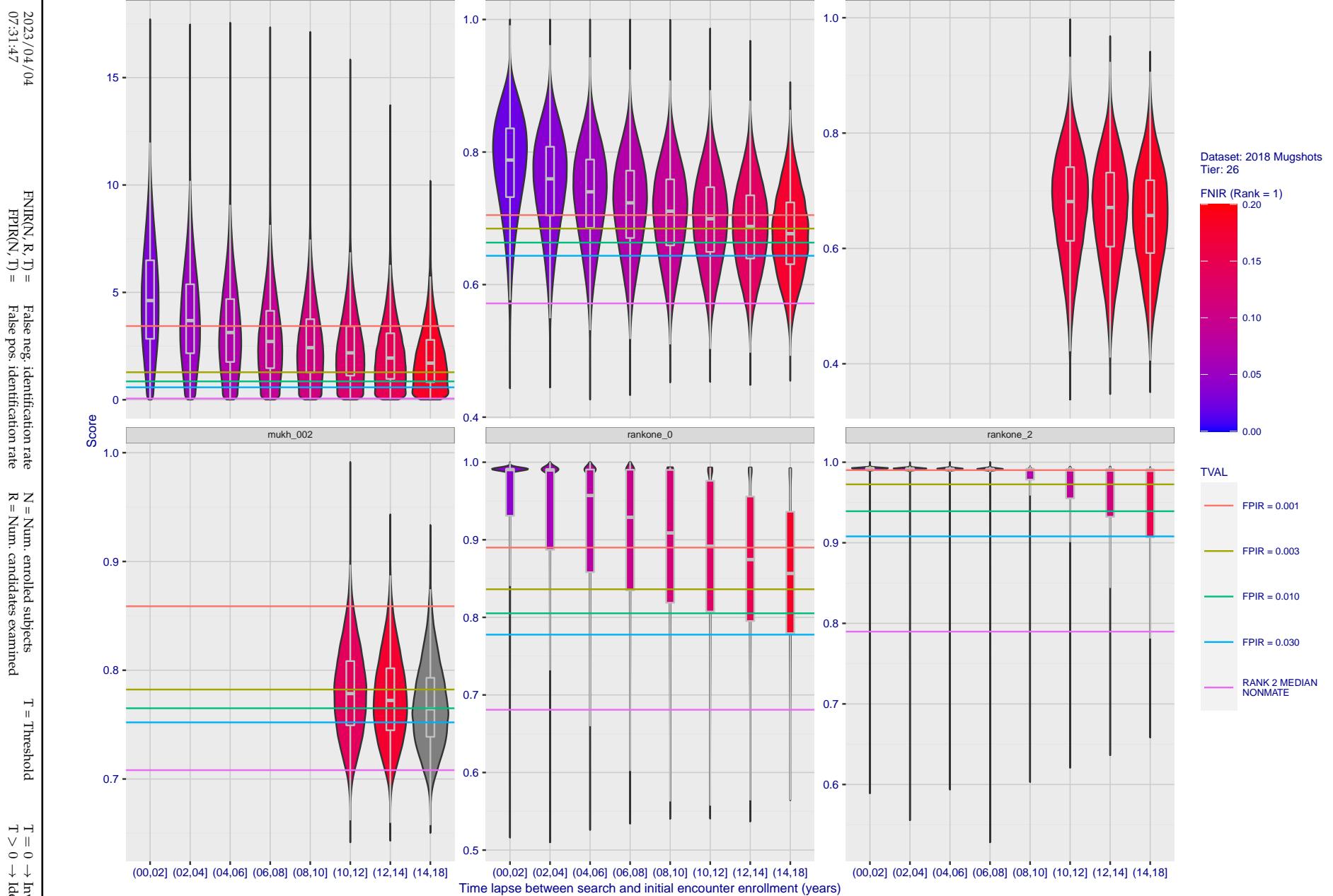


Figure 131: [FRVT-2018 Mugshot Ageing Dataset] Native mate scores vs. time-elapsed. The oldest image of each individual is enrolled. Thereafter, all more recent images are searched. Mated score distributions are computed over all searches noted in row 17 of Table 1 binned by number of years between search and initial enrollment.

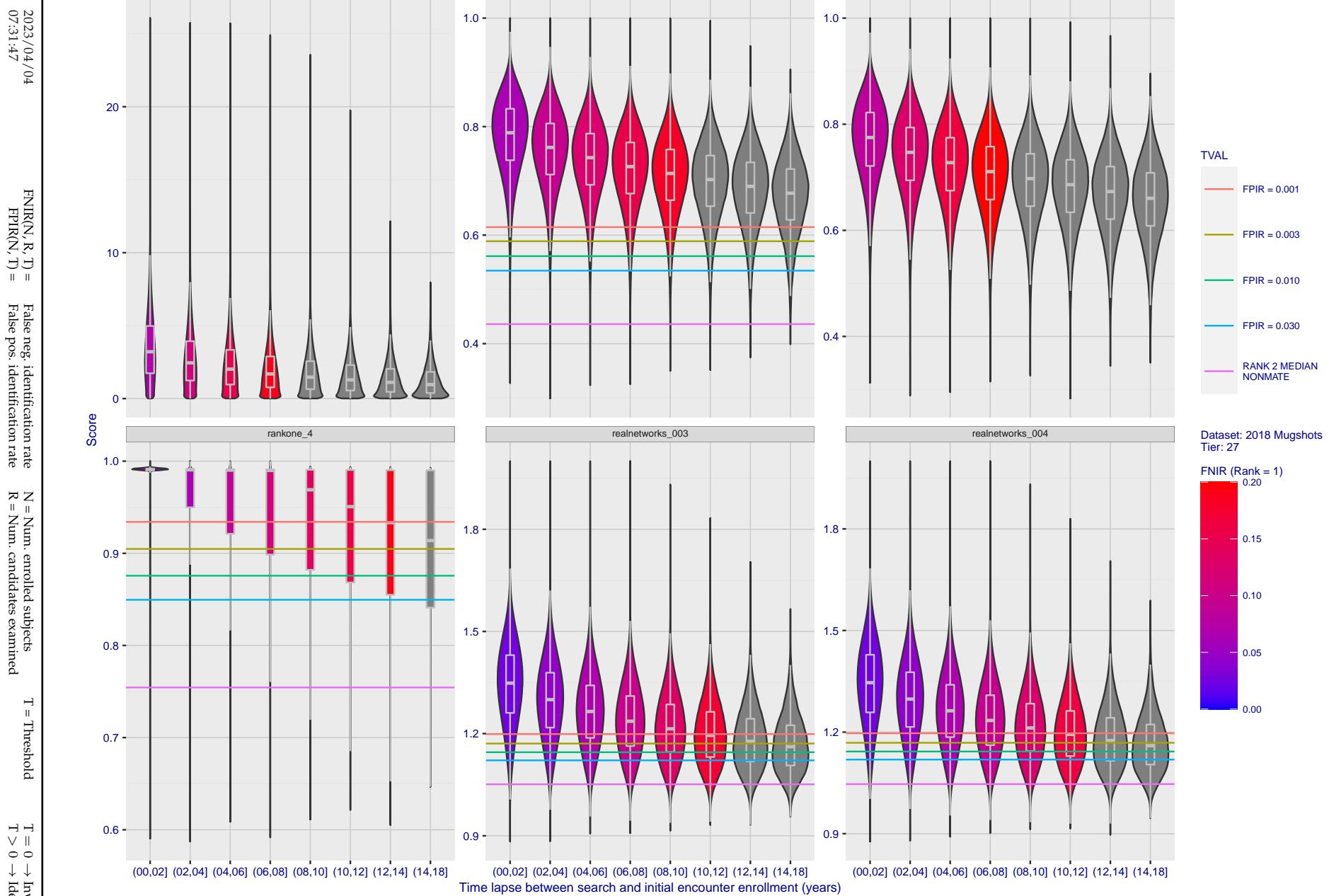


Figure 132: [FRVT-2018 Mugshot Ageing Dataset] Native mate scores vs. time-elapsed. The oldest image of each individual is enrolled. Thereafter, all more recent images are searched. Mated score distributions are computed over all searches noted in row 17 of Table 1 binned by number of years between search and initial enrollment.

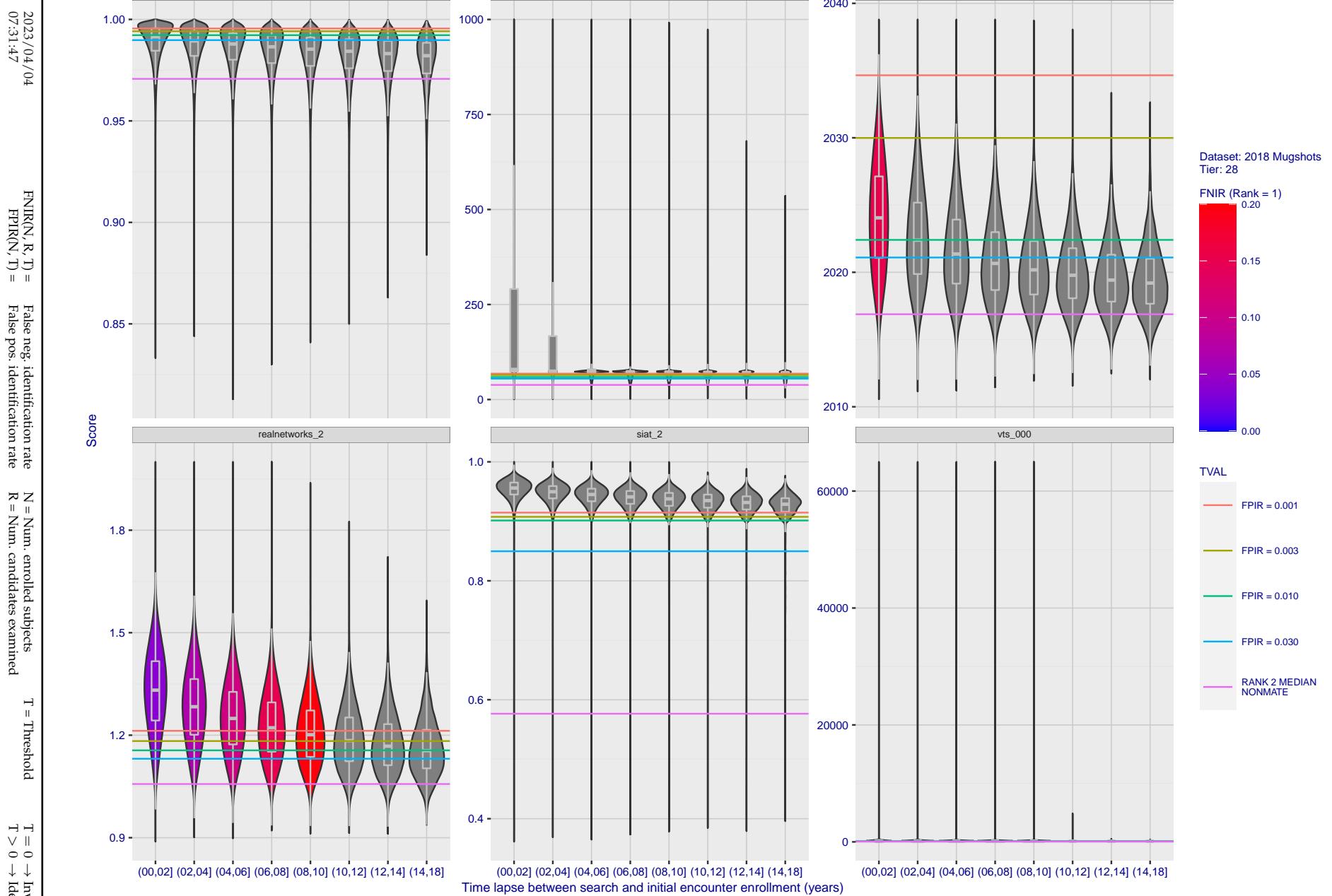


Figure 133: [FRVT-2018 Mugshot Ageing Dataset] Native mate scores vs. time-elapsed. The oldest image of each individual is enrolled. Thereafter, all more recent images are searched. Mated score distributions are computed over all searches noted in row 17 of Table 1 binned by number of years between search and initial enrollment.

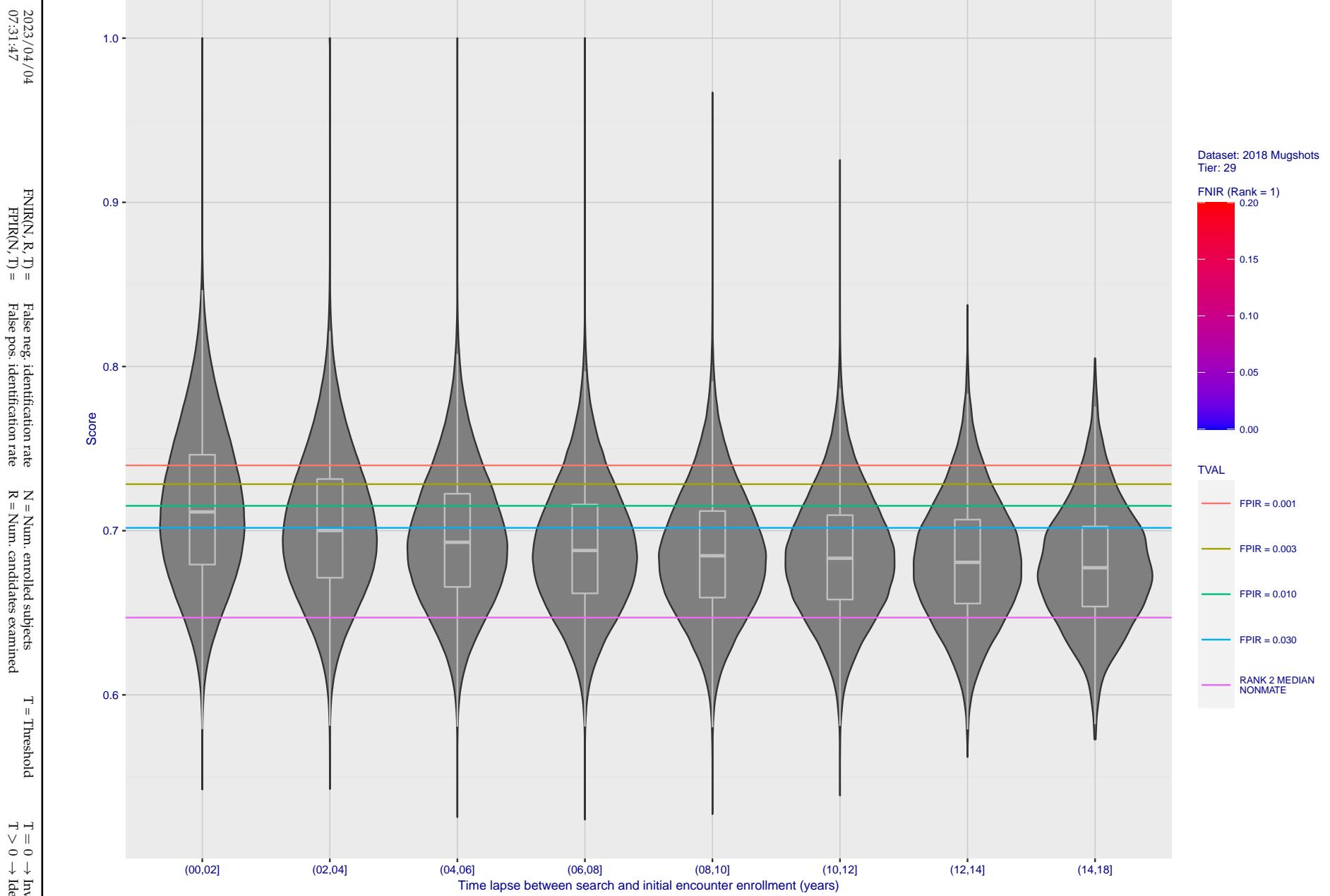


Figure 134: [FRVT-2018 Mugshot Ageing Dataset] Native mate scores vs. time-elapsed. The oldest image of each individual is enrolled. Thereafter, all more recent images are searched. Mated score distributions are computed over all searches noted in row 17 of Table 1 binned by number of years between search and initial enrollment.

Appendix C Effect of enrolling multiple images

2023/04/04
07:31:47FNIR(N, R, T) = False neg. identification rate
FPIR(N, T) = False pos. identification rateN = Num. enrolled subjects
R = Num. candidates examined

T = Threshold

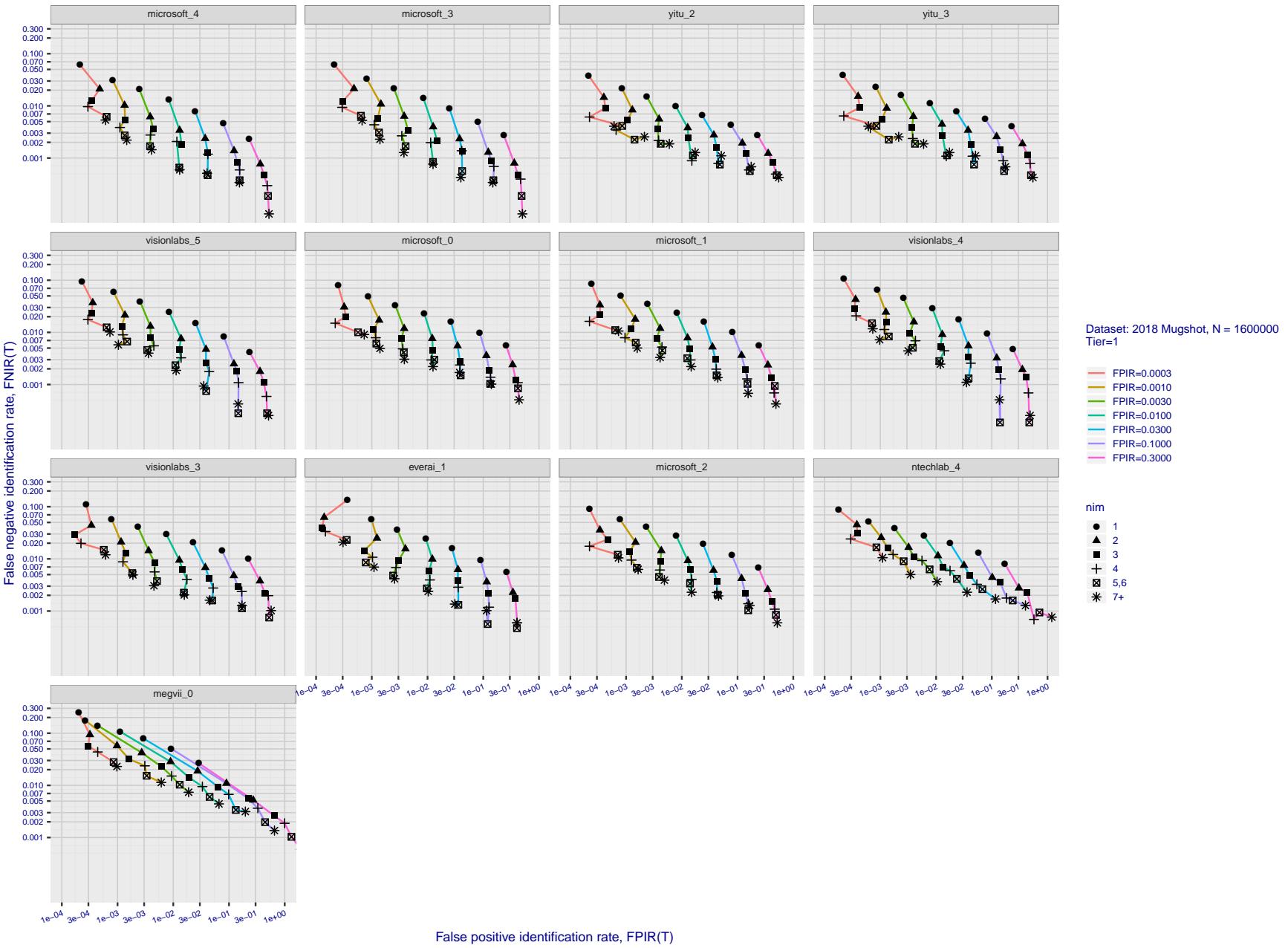
T = 0 → Investigation
T > 0 → Identification

Figure 135: [FRVT-2018 Mugshot Dataset] Effect of enrolling multiple images for each identity. The plot shows an identification miss rates vs. false positive rates, at seven operating thresholds. The enrolled population size is fixed. The images are enrolled with lifetime-consolidation - see section 2.3.

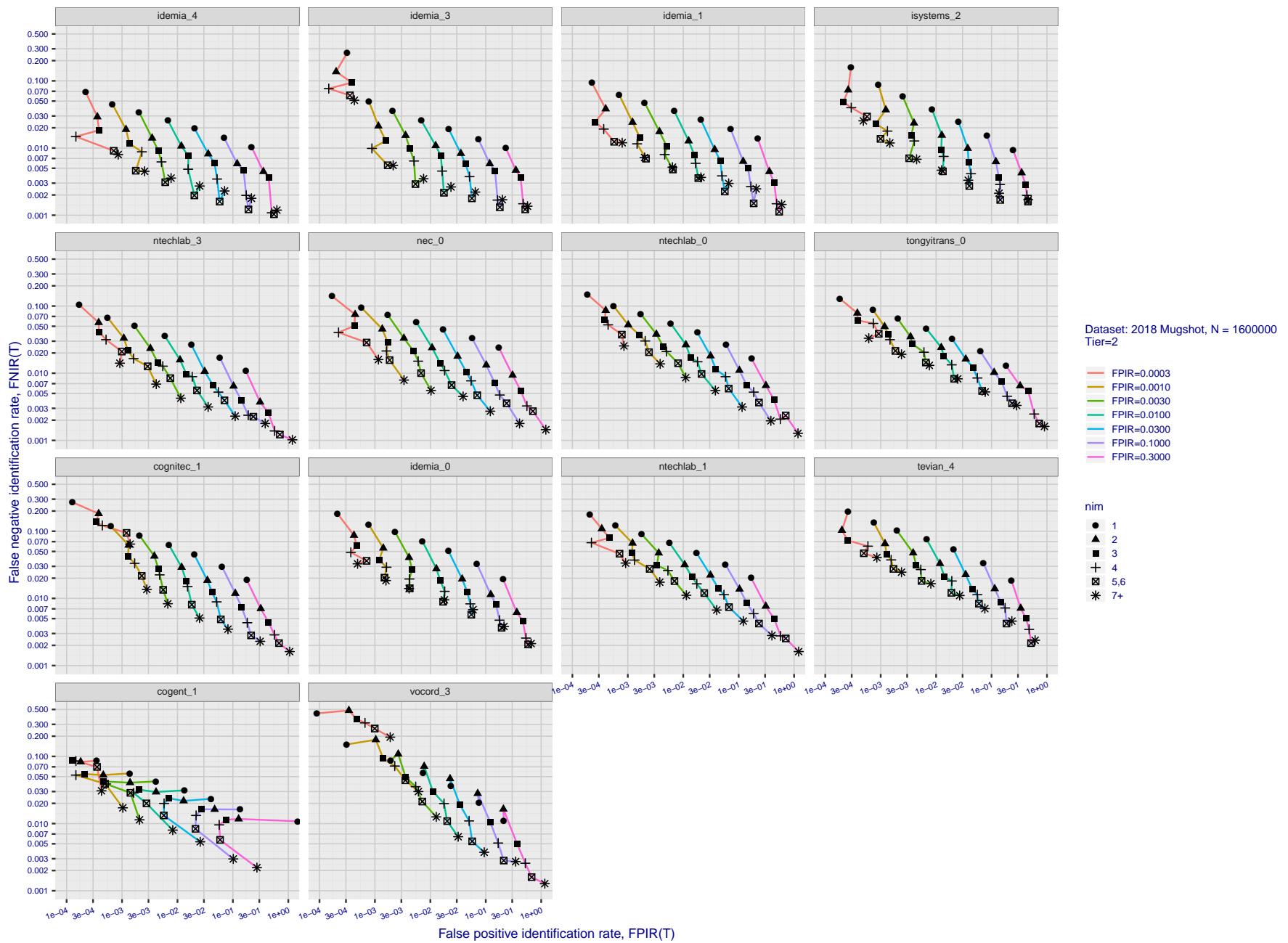


Figure 136: [FRVT-2018 Mugshot Dataset] Effect of enrolling multiple images for each identity. The plot shows an identification miss rates vs. false positive rates, at seven operating thresholds. The enrolled population size is fixed. The images are enrolled with lifetime-consolidation - see section 2.3.

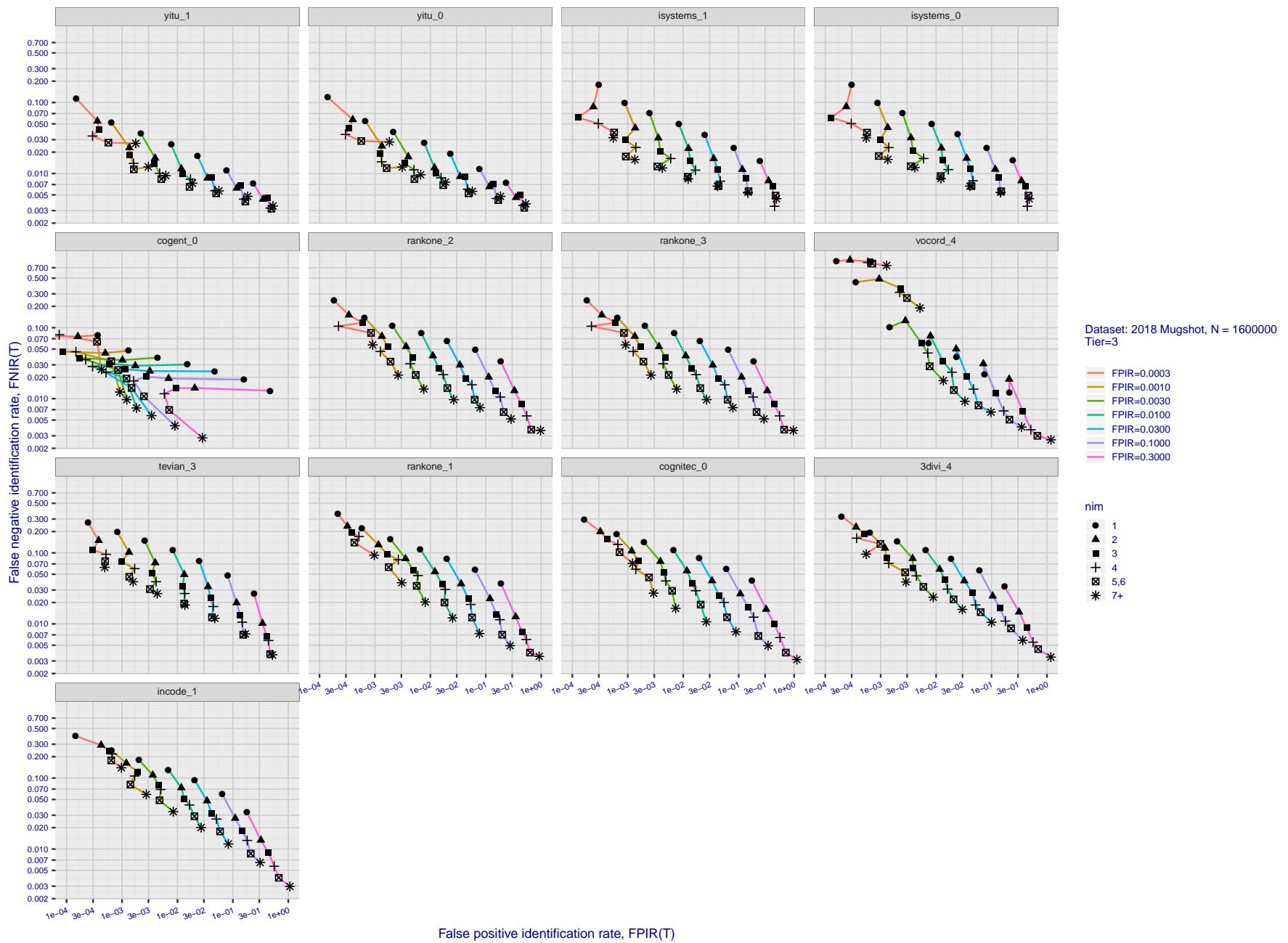


Figure 137: [FRVT-2018 Mugshot Dataset] Effect of enrolling multiple images for each identity. The plot shows an identification miss rates vs. false positive rates, at seven operating thresholds. The enrolled population size is fixed. The images are enrolled with lifetime-consolidation - see section 2.3.

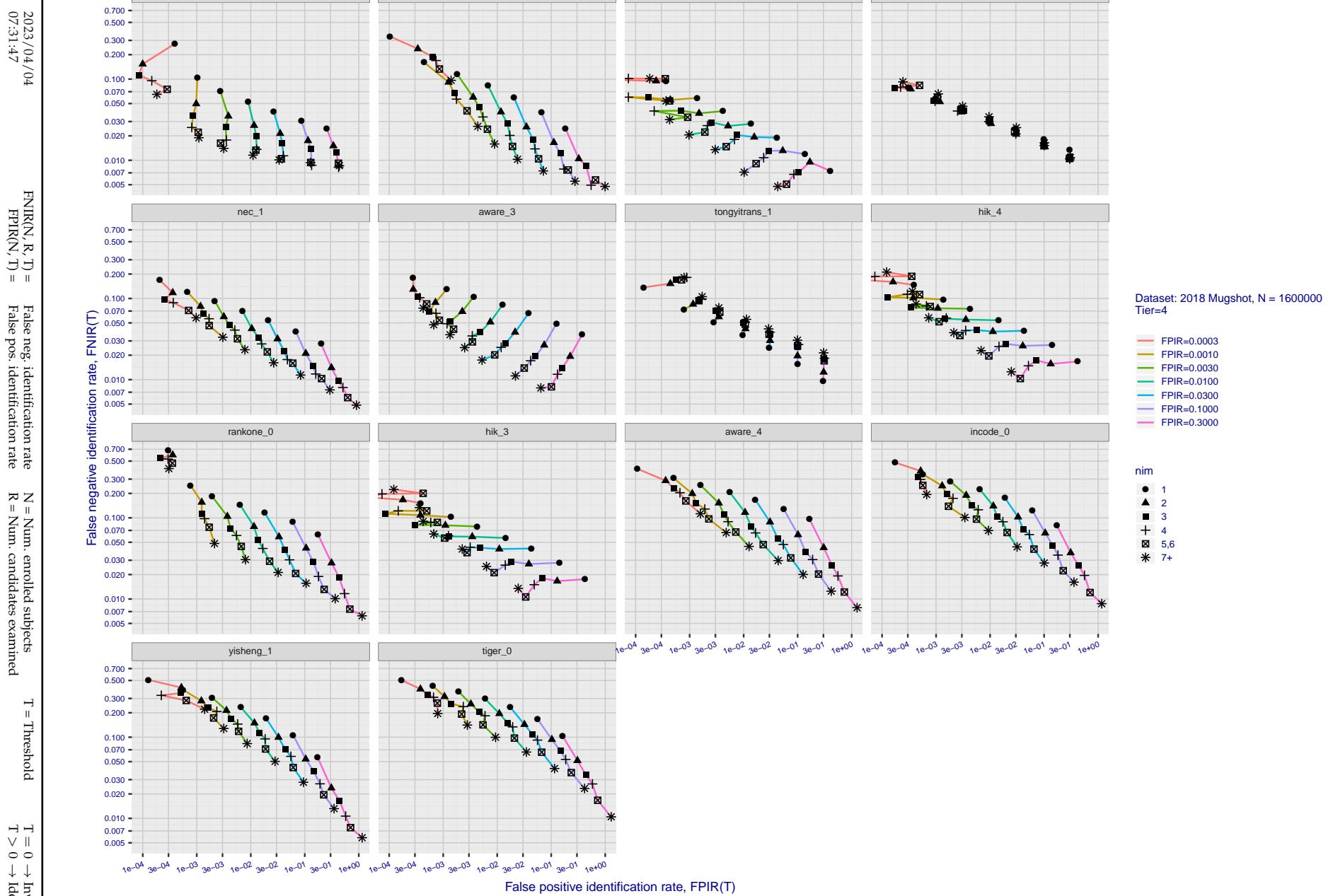


Figure 138: [FRVT-2018 Mugshot Dataset] Effect of enrolling multiple images for each identity. The plot shows an identification miss rates vs. false positive rates, at seven operating thresholds. The enrolled population size is fixed. The images are enrolled with lifetime-consolidation - see section 2.3.

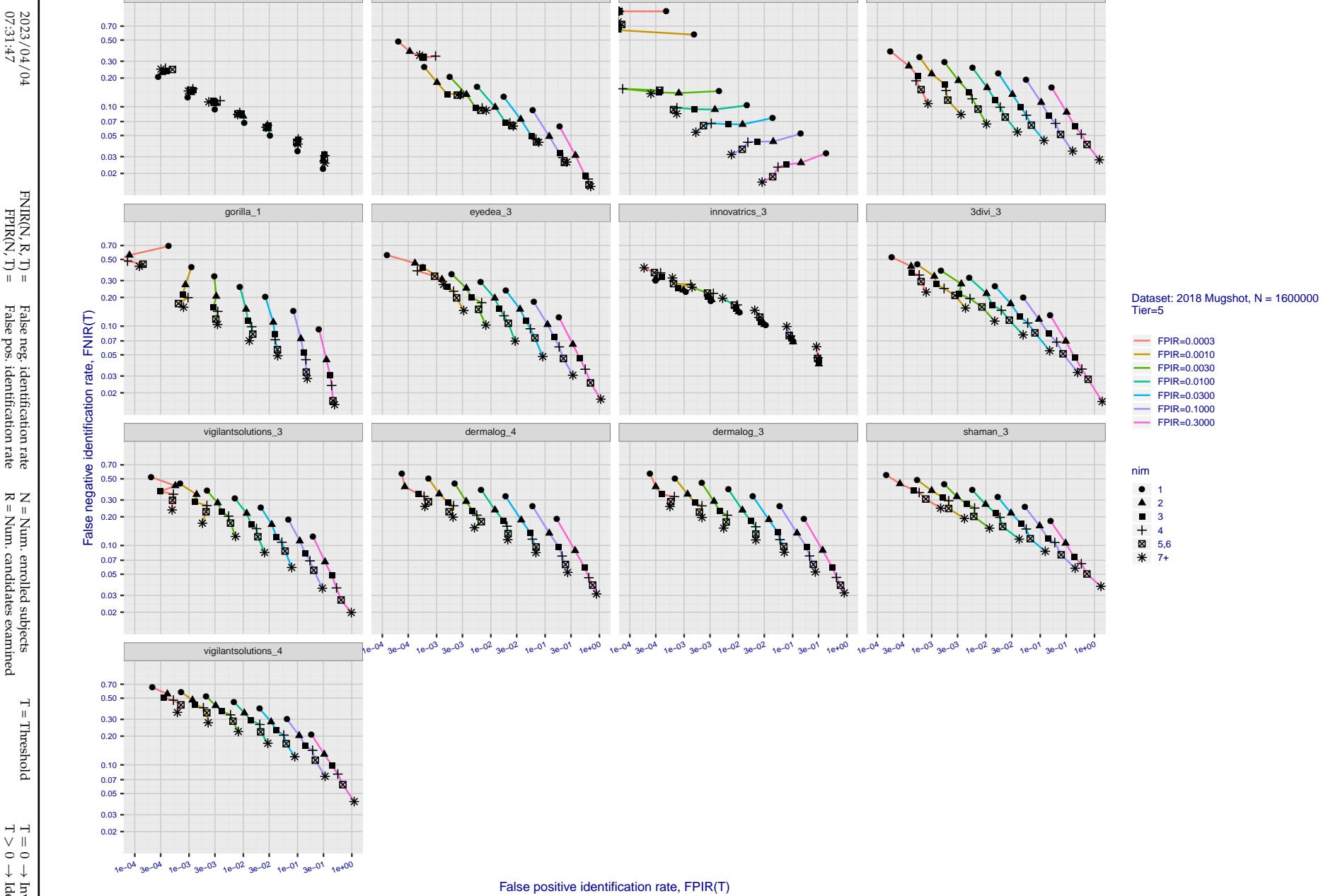


Figure 139: [FRVT-2018 Mugshot Dataset] Effect of enrolling multiple images for each identity. The plot shows an identification miss rates vs. false positive rates, at seven operating thresholds. The enrolled population size is fixed. The images are enrolled with lifetime-consolidation - see section 2.3.

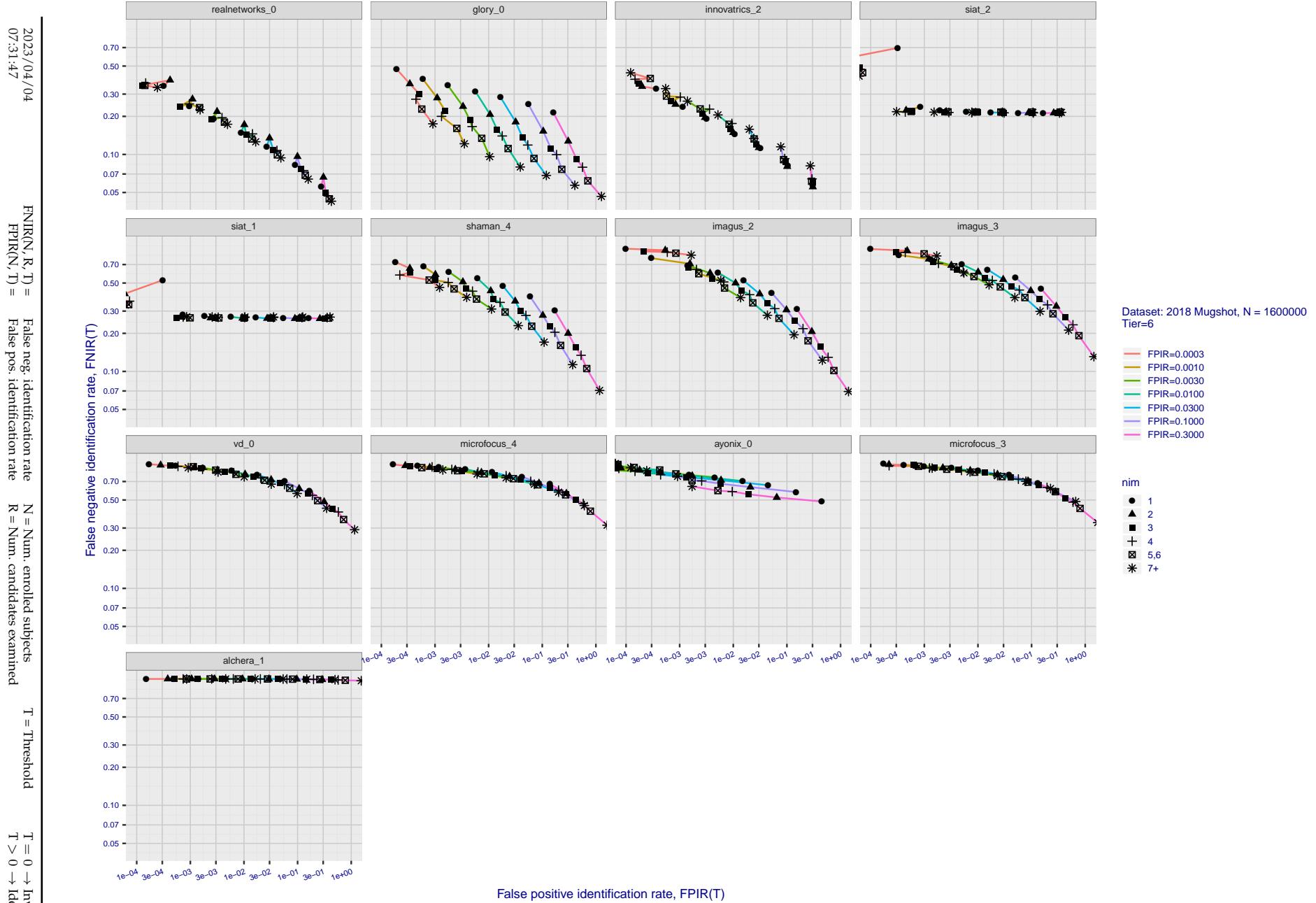


Figure 140: [FRVT-2018 Mugshot Dataset] Effect of enrolling multiple images for each identity. The plot shows an identification miss rates vs. false positive rates, at seven operating thresholds. The enrolled population size is fixed. The images are enrolled with lifetime-consolidation - see section 2.3.

Appendix D Accuracy with poor quality webcam images

2023/04/04
07:31:47

FNIR(N, R, T) = False neg. identification rate
FPTR(N, T) = False pos. identification rate

N = Num. enrolled subjects
R = Num. candidates examined

T = Threshold
T = 0 → Investigation
T > 0 → Identification

2023/04/04
07:31:47

 $\text{FNIR}(N, R, T) =$ False neg. identification rate
 $\text{FPFR}(N, T) =$ False pos. identification rate
 $N =$ Num. enrolled subjects
 $R =$ Num. candidates examined
 $T =$ Threshold
 $T = 0 \rightarrow$ Investigation
 $T > 0 \rightarrow$ Identification

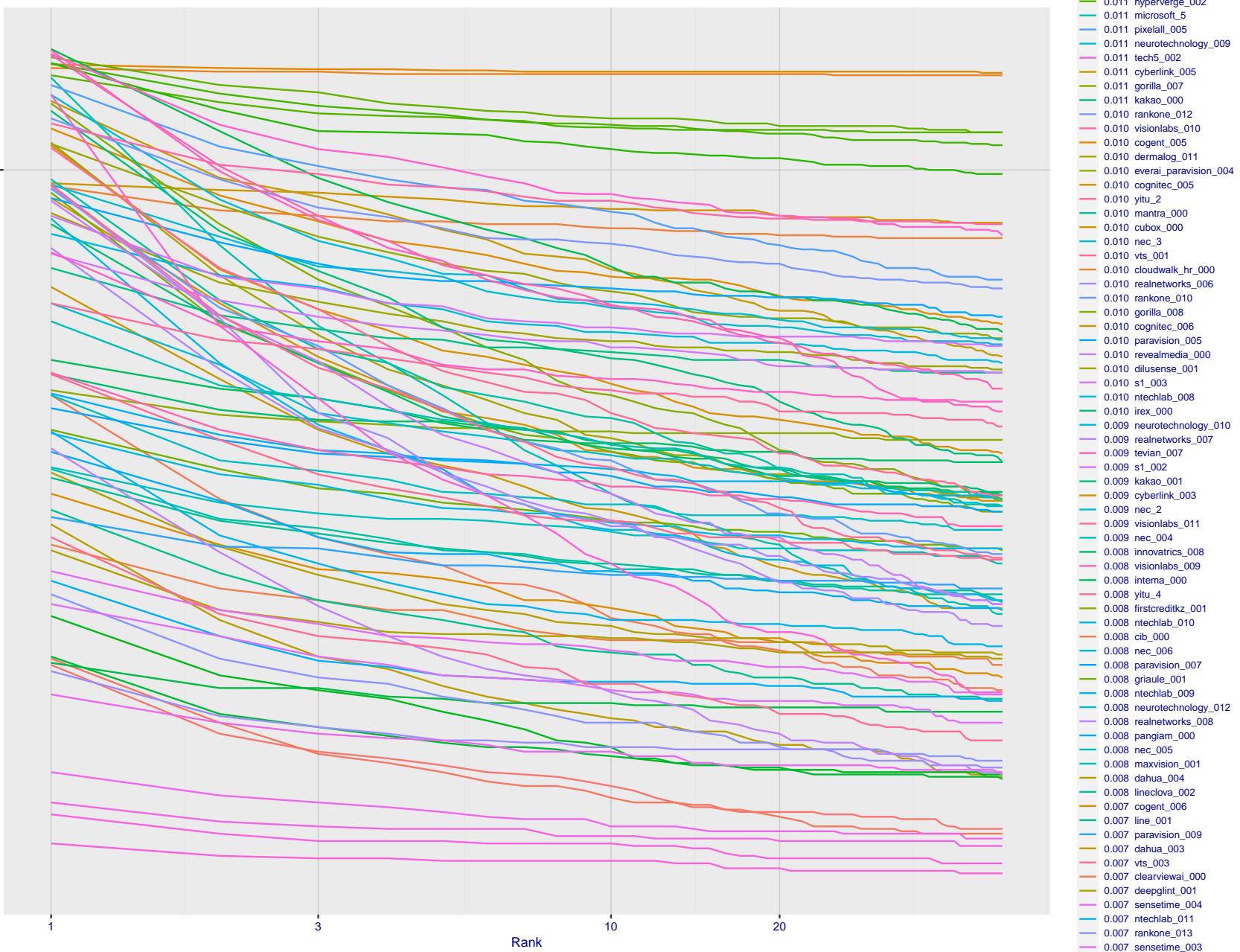


Figure 141: [Webcam Dataset] Identification miss rates vs. rank. The results apply to cross-domain recognition in which webcams are searched against enrolled mugshots. The FNIR values are higher than those for mugshot-mugshot identification due to low image resolution, lighting and less constrained subject pose in webcam images - see Figure 6.

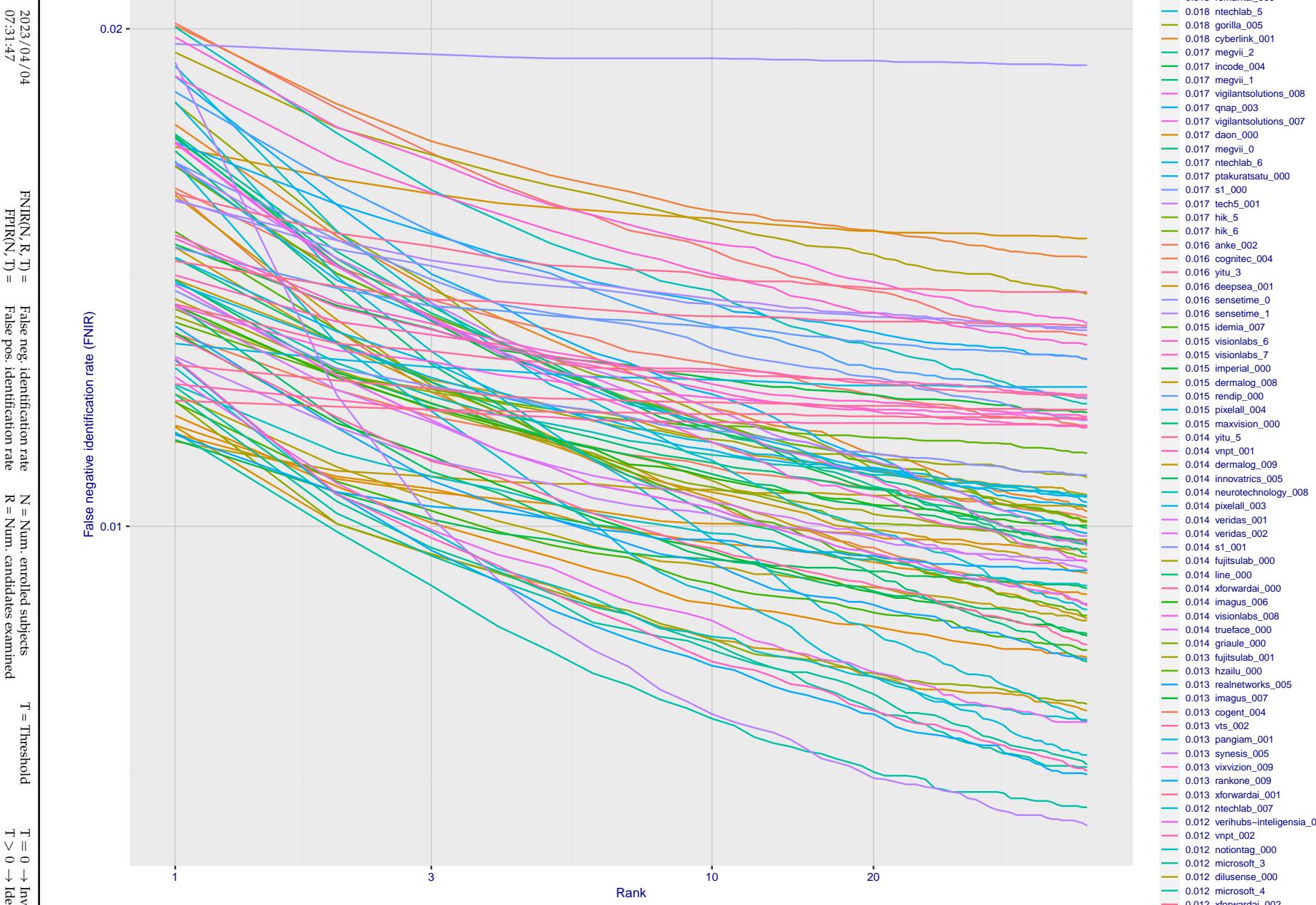


Figure 142: [Webcam Dataset] Identification miss rates vs. rank. The results apply to cross-domain recognition in which webcams are searched against enrolled mugshots. The FNIR values are higher than those for mugshot-mugshot identification due to low image resolution, lighting and less constrained subject pose in webcam images - see Figure 6.

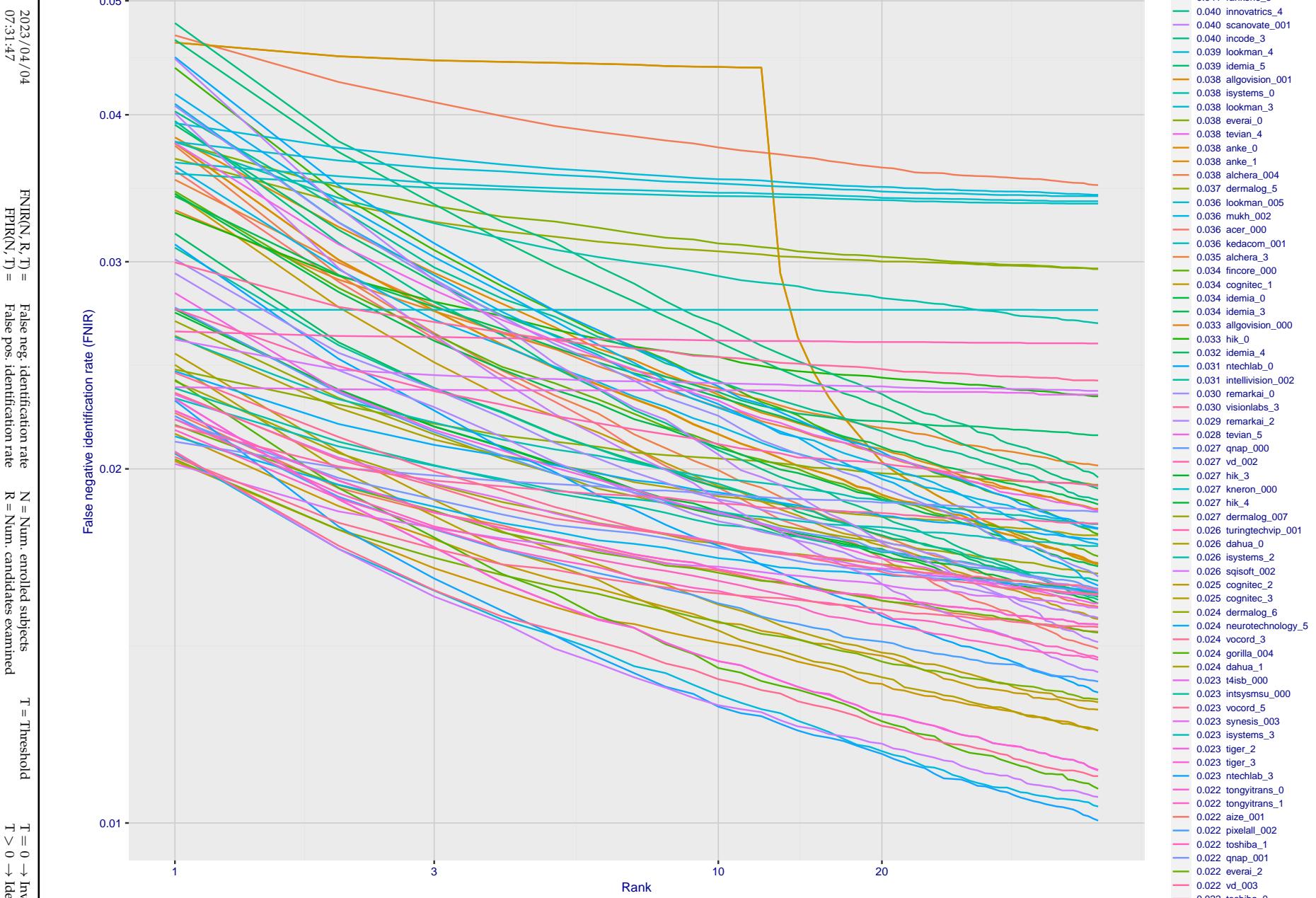


Figure 143: [Webcam Dataset] Identification miss rates vs. rank. The results apply to cross-domain recognition in which webcams are searched against enrolled mugshots. The FNIR values are higher than those for mugshot-mugshot identification due to low image resolution, lighting and less constrained subject pose in webcam images - see Figure 6.

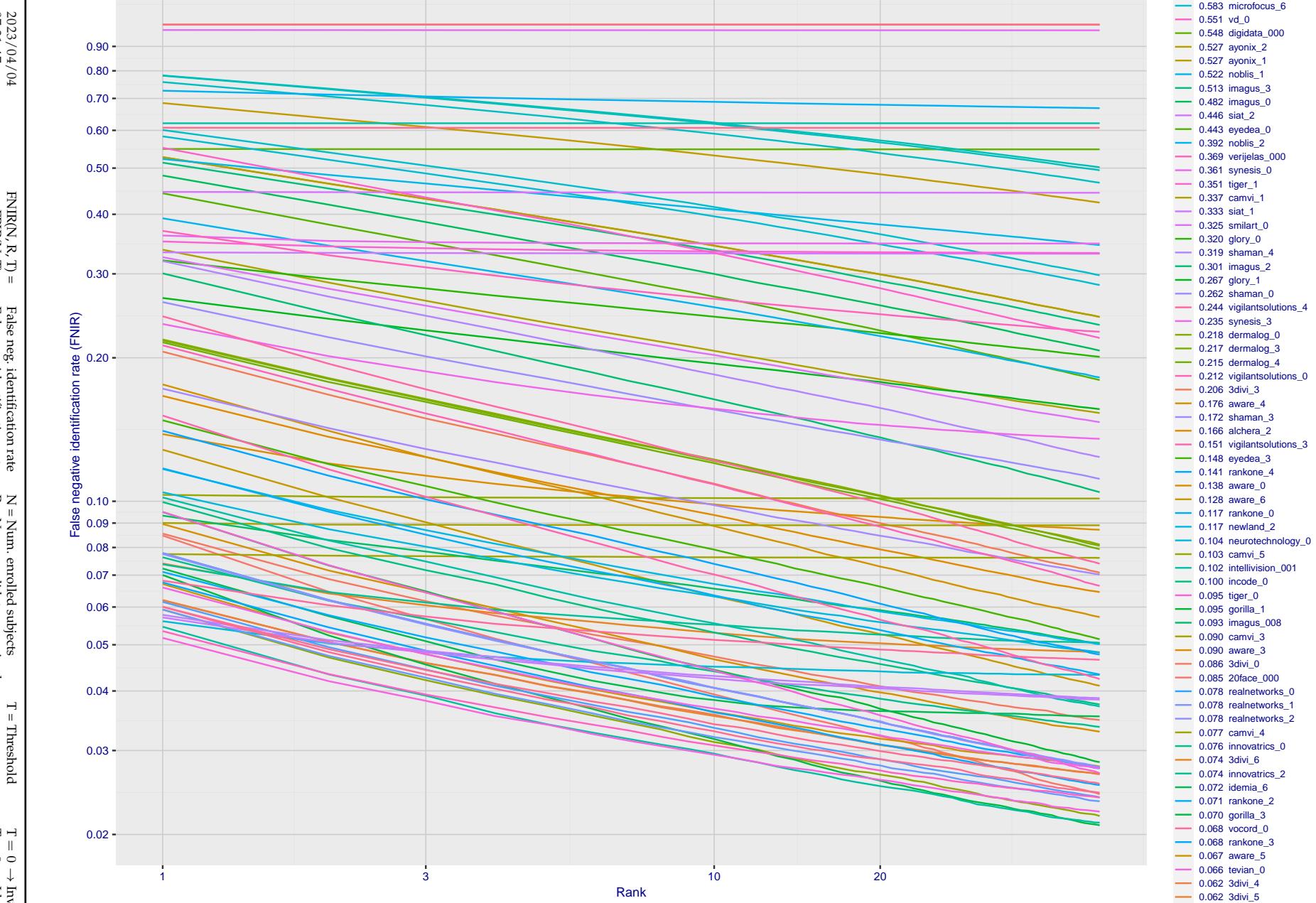


Figure 144: [Webcam Dataset] Identification miss rates vs. rank. The results apply to cross-domain recognition in which webcams are searched against enrolled mugshots. The FNIR values are higher than those for mugshot-mugshot identification due to low image resolution, lighting and less constrained subject pose in webcam images - see Figure 6.

2023/04/04
07:31:47

FNIR(N, R, T) = False neg. identification rate
FPTR(N, T) = False pos. identification rate

N = Num. enrolled subjects
R = Num. candidates examined

T = Threshold
T > 0 → Identification

T = 0 → Investigation

2023/04/04
07:31:47FNIR(N, R, T) = False neg. identification rate
FPIR(N, T) = False pos. identification rateN = Num. enrolled subjects
R = Num. candidates examinedT = Threshold
T = 0 → Investigation

T > 0 → Identification

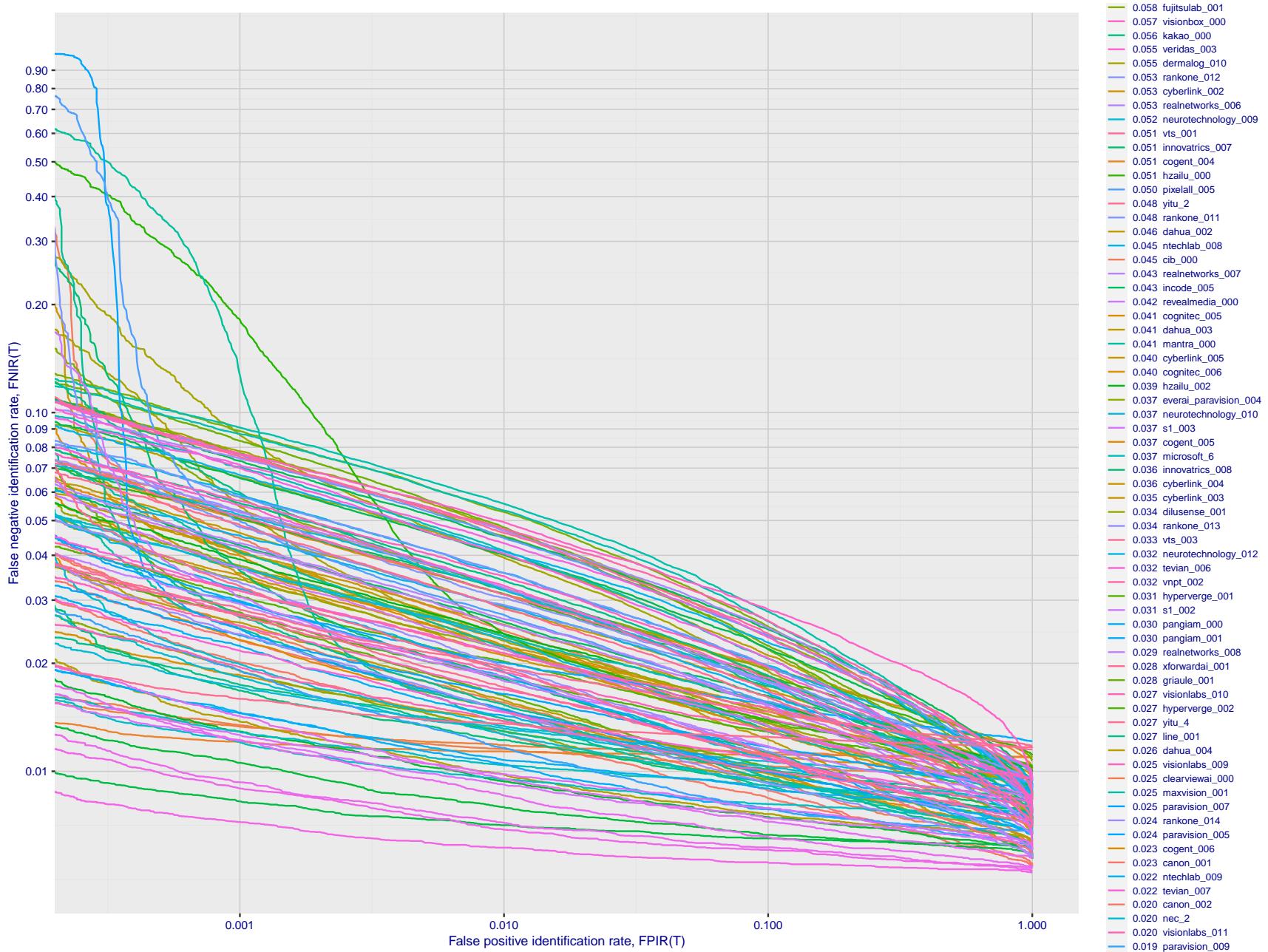


Figure 145: [Webcam Dataset] Identification miss rates vs. false positive rates. The results apply to cross-domain recognition in which webcams are searched against enrolled mugshots. The FNIR values are higher than those for mugshot-mugshot identification due to low image resolution, lighting and less constrained subject pose in webcam images - see Figure 6.

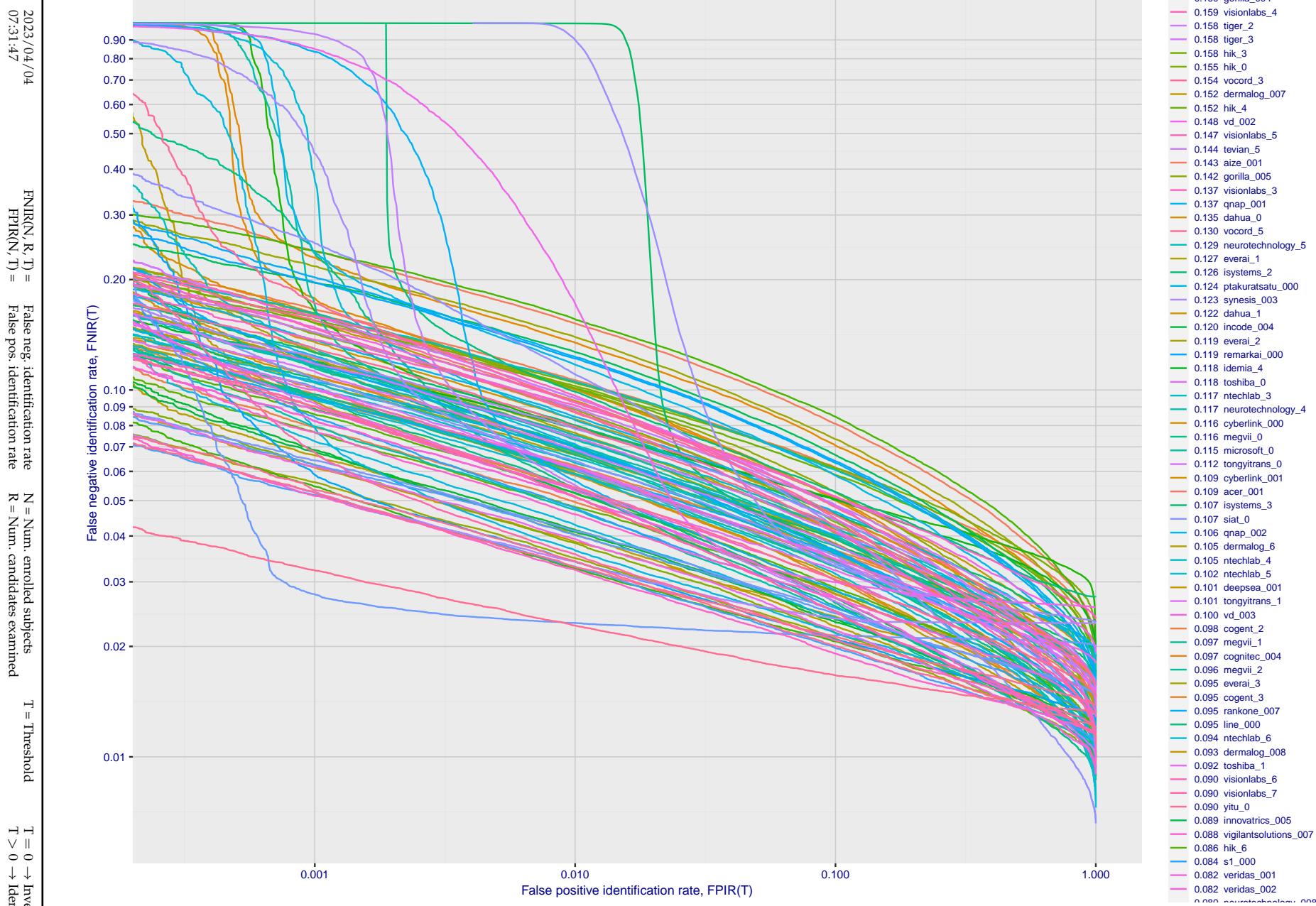


Figure 146: [Webcam Dataset] Identification miss rates vs. false positive rates. The results apply to cross-domain recognition in which webcams are searched against enrolled mugshots. The FNIR values are higher than those for mugshot-mugshot identification due to low image resolution, lighting and less constrained subject pose in webcam images - see Figure 6.

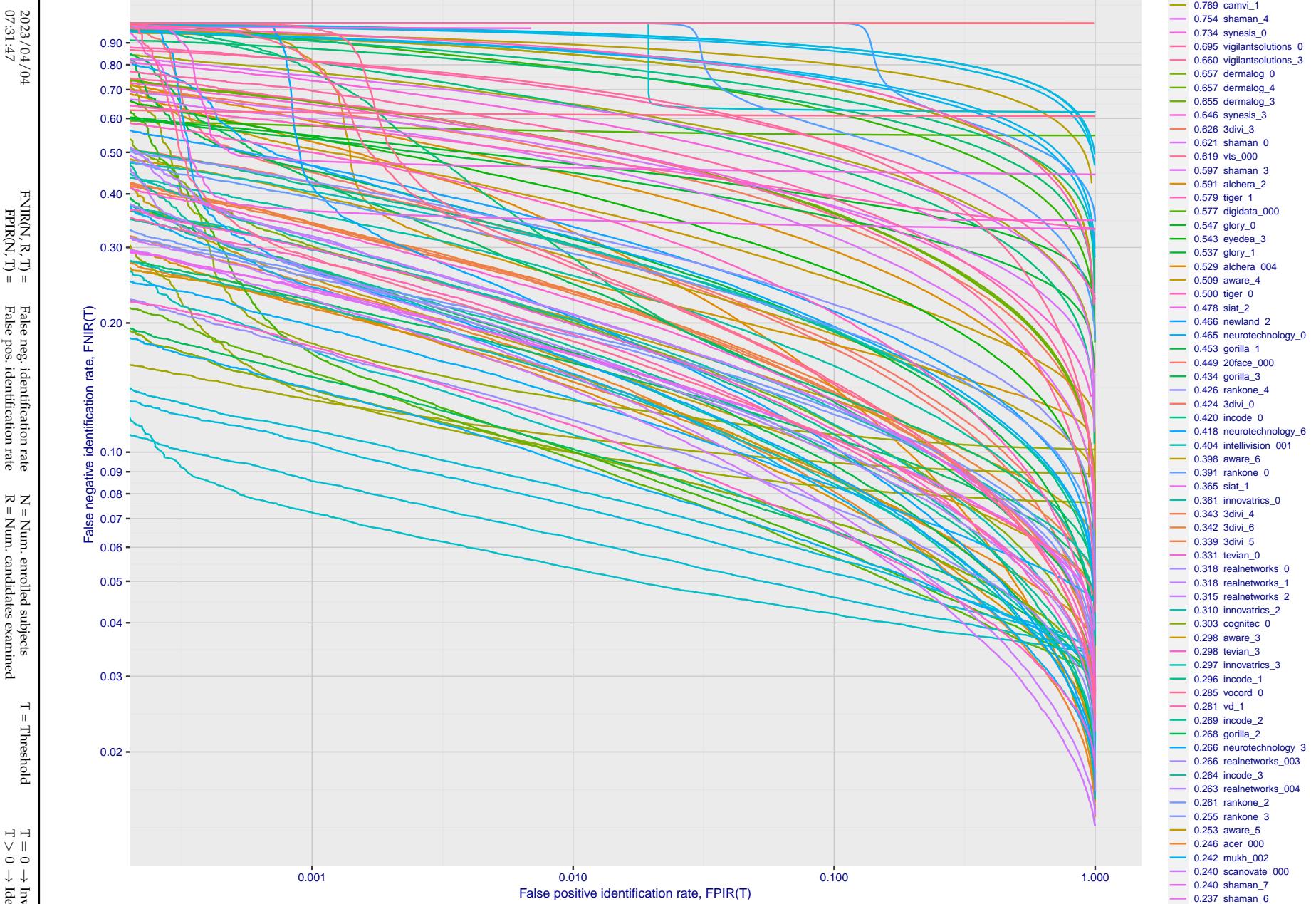


Figure 147: [Webcam Dataset] Identification miss rates vs. false positive rates. The results apply to cross-domain recognition in which webcams are searched against enrolled mugshots. The FNIR values are higher than those for mugshot-mugshot identification due to low image resolution, lighting and less constrained subject pose in webcam images - see Figure 6.

2023 / 04 / 04

FNIR(N, R, T) = False neg. identification rate
FPIR(R, T) = False pos. identification rateN = Num. enrolled subjects
R = Num. candidates examinedT = Threshold
T = 0 → Investigation
T > 0 → Identification

Appendix E Accuracy for profile-view to frontal recognition

Figures 148 - 150 gives accuracy results for searching 100 000 mated and 100 000 non-mated profile-view images against the same FRVT 2018 frontal enrollment dataset, $N = 1\,600\,000$, used in the main mugshot trials. This experiment corresponds to row-13 of Table 1. An example of profile-view image is given in Figure 7.

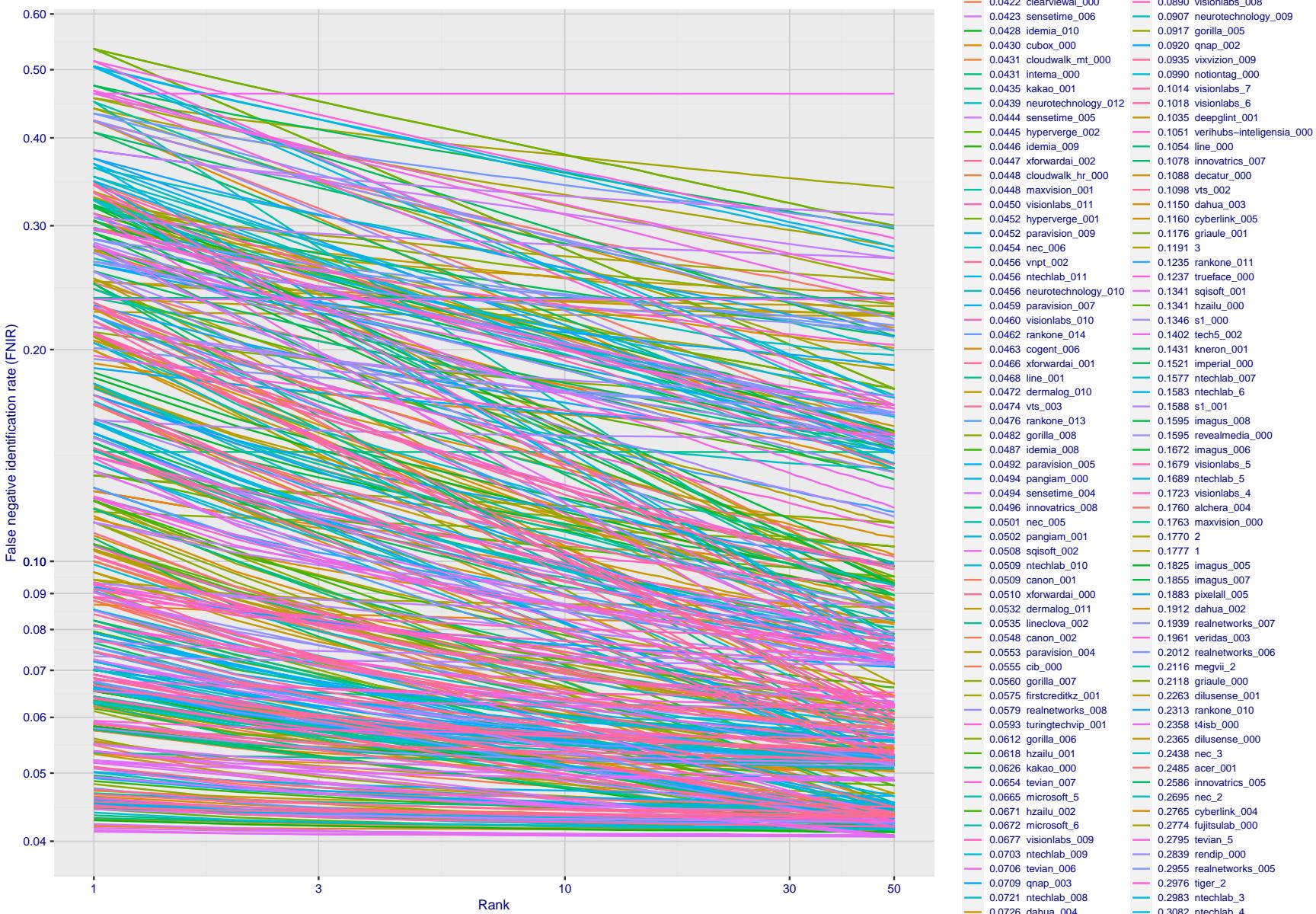


Figure 148: [Mugshot and profile-view dataset] Rank-based accuracy. For some of the more accurate Phase 3 algorithms the figure plots error tradeoff characteristics for frontal and profile-view searches into an enrolled set of $N = 1\,600\,000$ frontal images. Note that some algorithms fail on profile-view images with $\text{FNIR} \rightarrow 1$ - this evaluation did not ask developers to provide profile-view capability. Some algorithms, on the other hand, give FNIR approaching that for frontal-view searches using c. 2010 algorithms. The best result is that 91% of profile-view searches yield the correct mate at rank 1, and better than 94% in the top-50 candidates.

2023/04/04
07:31:47

 $\text{FNIR}(N, R, T) =$
False neg. identification rate
 $\text{FPIR}(N, T) =$
False pos. identification rate

 $N = \text{Num. enrolled subjects}$
 $R = \text{Num. candidates examined}$
 $T = \text{Threshold}$
 $T = 0 \rightarrow \text{Investigation}$
 $T > 0 \rightarrow \text{Identification}$

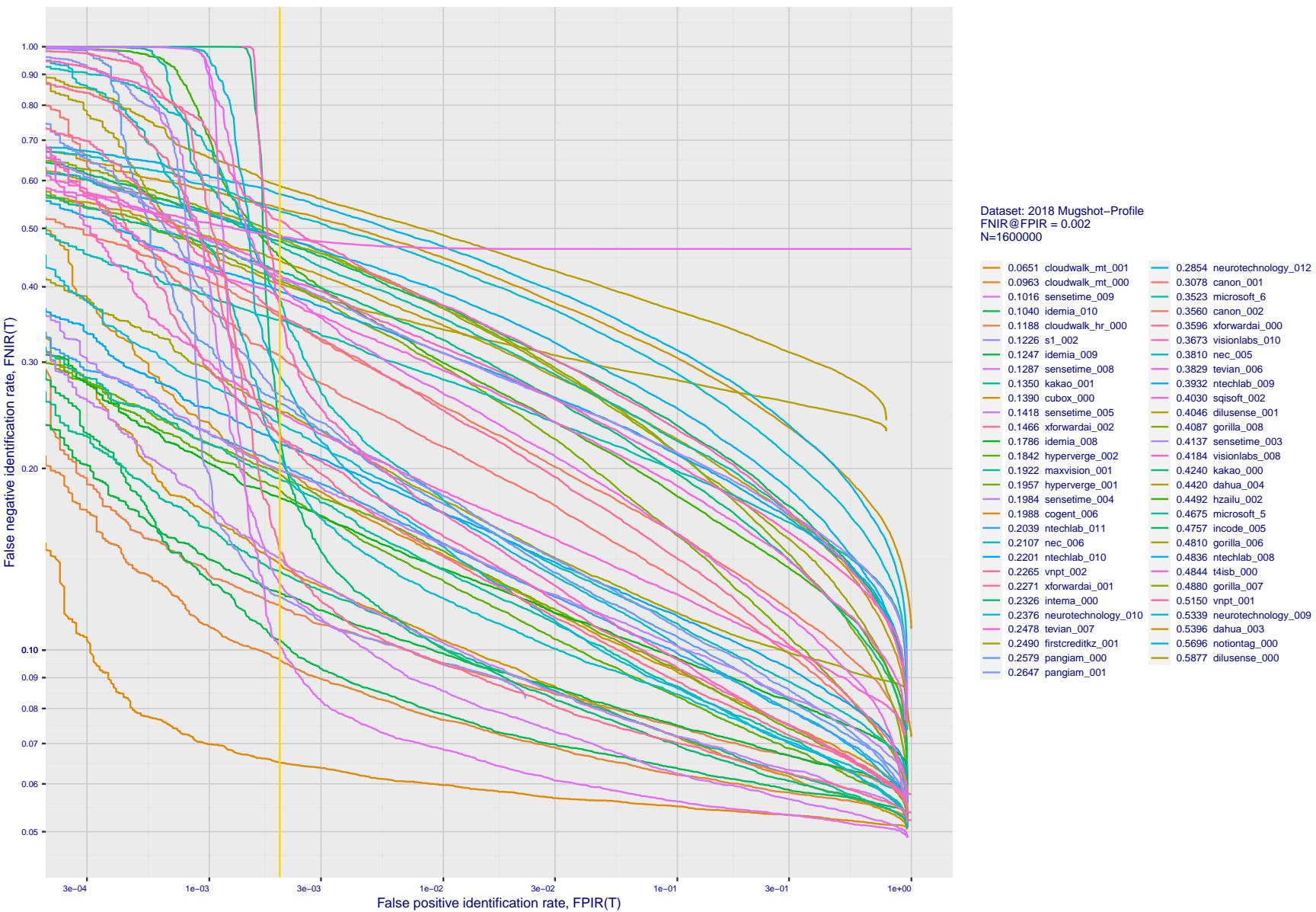


Figure 149: [Mugshot and profile-view dataset] Threshold-based accuracy. For some of the more accurate Phase 3 algorithms the figure plots error tradeoff characteristics for frontal and profile-view searches into an enrolled set of $N = 1600000$ frontal images. Note that some algorithms fail on profile-view images with $\text{FNIR} \rightarrow 1$ - this evaluation did not ask developers to provide profile-view capability. Some algorithms, on the other hand, give FNIR approaching that for frontal-view searches using c. 2010 algorithms.

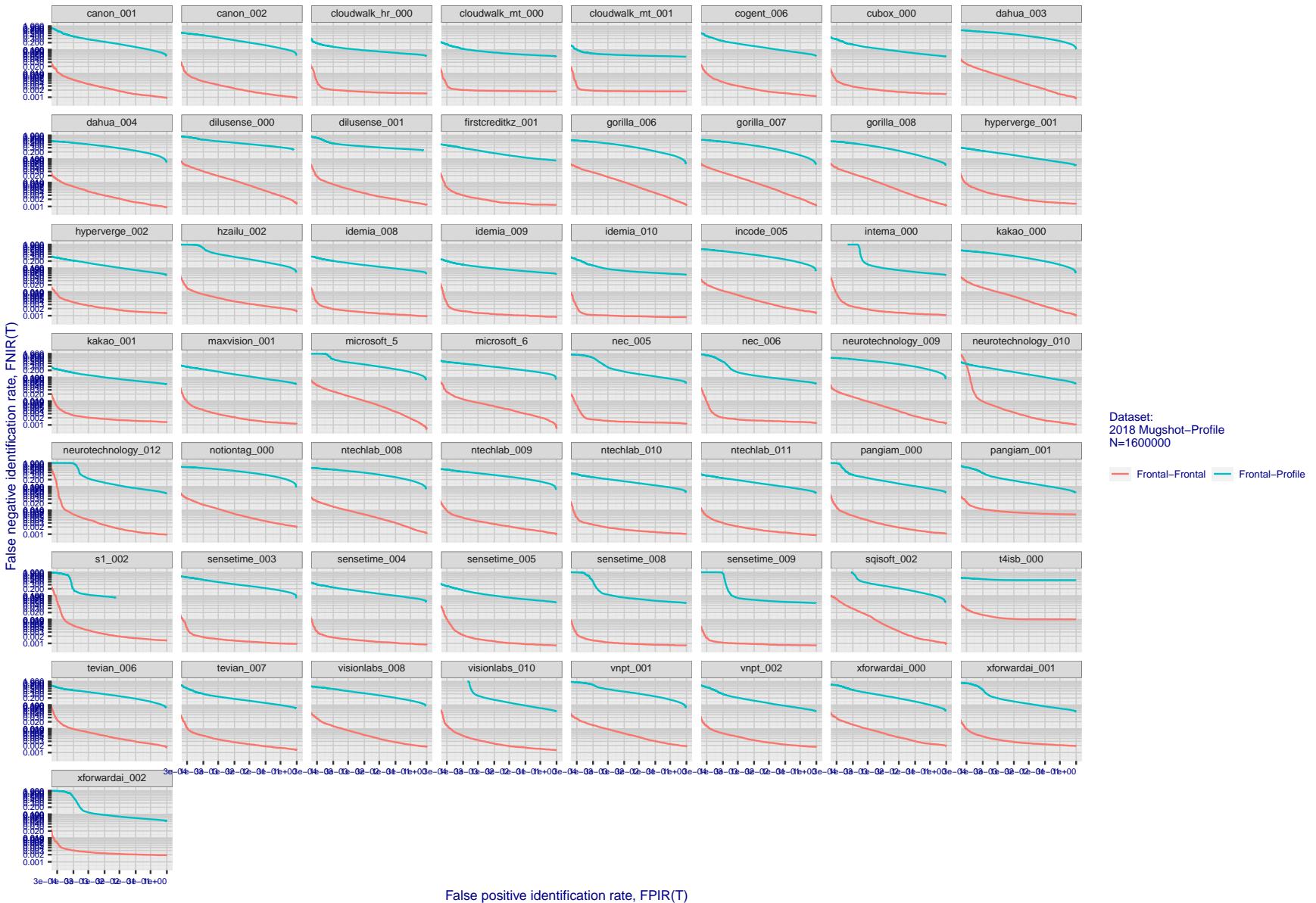


Figure 150: [Mugshot and profile-view dataset] Speed-accuracy tradeoff. For some of the more accurate Phase 3 algorithms the figure plots error tradeoff characteristics for frontal and profile-view searches into an enrolled set of $N = 1\,600\,000$ frontal images. Some algorithms fail on profile-view images with $\text{FNIR} \rightarrow 1$ - this evaluation did not ask developers to provide profile-view capability. Some algorithms, on the other hand, give FNIR approaching that for frontal-view searches using c. 2010 algorithms. Blue lines connect points of equal threshold from which it is evident that some algorithms would give markedly higher false positive outcomes if profile-view images were searched in a system configured for frontal searches. This would be a vulnerability in an access control system.

Appendix F Search duration

As in and prior tests, this section documents search speeds spanning three orders of magnitude. In applications where search volumes are high enough, this will have implications for hardware requirements especially for large N or when search duration is appreciably larger than the time it takes to prepare a template from the search image(s). Further, given very large (and growing) operational databases, the scalability of algorithms is important. It has been reported previously [8] that search duration can scale sublinearly with enrolled population size N. Further there has been considerable recent research on indexing, exact [13] and approximate nearest neighbor search [1,13] and fast-search [14,16].

Figure 151 charts the search duration measurements presented earlier in Tables 2 - 4.

- ▷ Most algorithms scale linearly. For those in that category, there is a wide range in speed with search durations ranging from 82 milliseconds for a 12 million gallery (for NEC-3) to more than 40 seconds (for Yitu-3, Toshiba-2) and even higher for less accurate algorithms.
- ▷ Some developers (Camvi, Dermalog, EverAI, Innovatrics, and Visionlabs) provide algorithms whose template search durations grow approximately logarithmically i.e. $T(N) \sim \log N$ with the constant a varying between implementations. In the figure this model is fit using the point $T(1) = 0$, and $T(640\,000)$. This very sublinear behaviour affords extremely fast search times in very large galleries. One caveat for the sublinear algorithms is that their fast-search data structures can require considerable computation time - on the order of hours - for N in the millions, and this scales mildly super-linearly, i.e. $O(N^b)$, $b > 1$. There are exceptions: the Camvi algorithms take minutes; and Innovatrics' scale sublinearly.

2023/04/04
07:31:47

FNIR(N, R, T) = False neg. identification rate
FPTR(N, T) = False pos. identification rate

N = Num. enrolled subjects
R = Num. candidates examined

T = Threshold
T > 0 → Identification

T = 0 → Investigation

2023/04/04
07:31:47FNIR(N, R, T) = False neg. identification rate
FPFR(N, T) = False pos. identification rateN = Num. enrolled subjects
R = Num. candidates examinedT = Threshold
T = 0 → Investigation

T > 0 → Identification

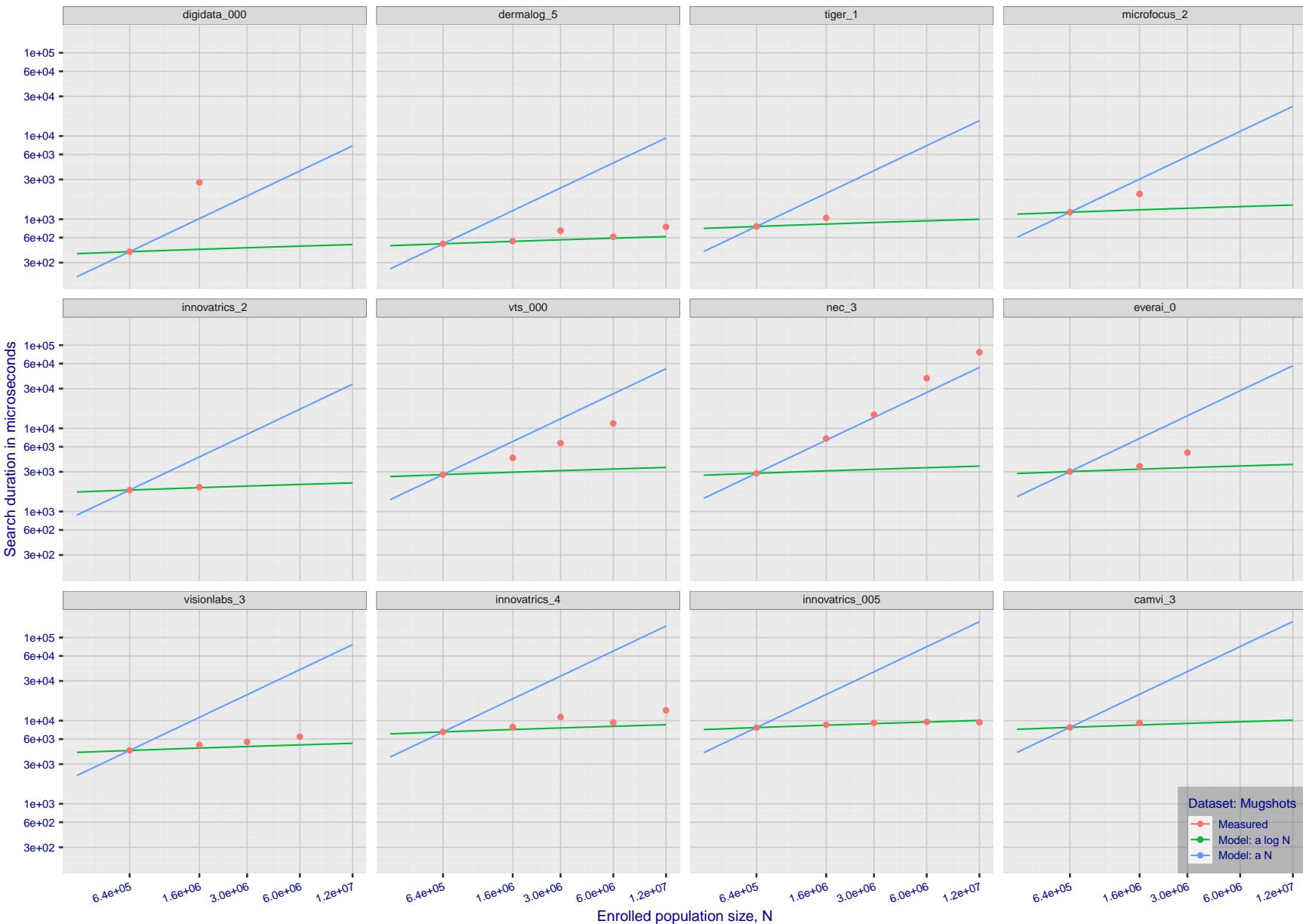


Figure 151: [Mugshot Dataset] Search duration vs. enrolled population size. In red are the actual point durations measured on a single c. 2016 core. The blue shows linear growth from $N = 640\,000$. The green line shows logarithmic growth from that point to $N = 1\,600\,000$. Note the sublinear growth from algorithms from Camvi, Dermalog, EverAI, Innovatrics, and Visionlabs. The tiger_1 algorithm is also sublinear, but inaccurate and inoperable at $N \geq 3000000$. This capability sometimes comes at the additional expense of converting a linear gallery data structure into whatever fast-search data structure is used. Note that search times are sometimes dominated by the template generation times shown in Table 29.

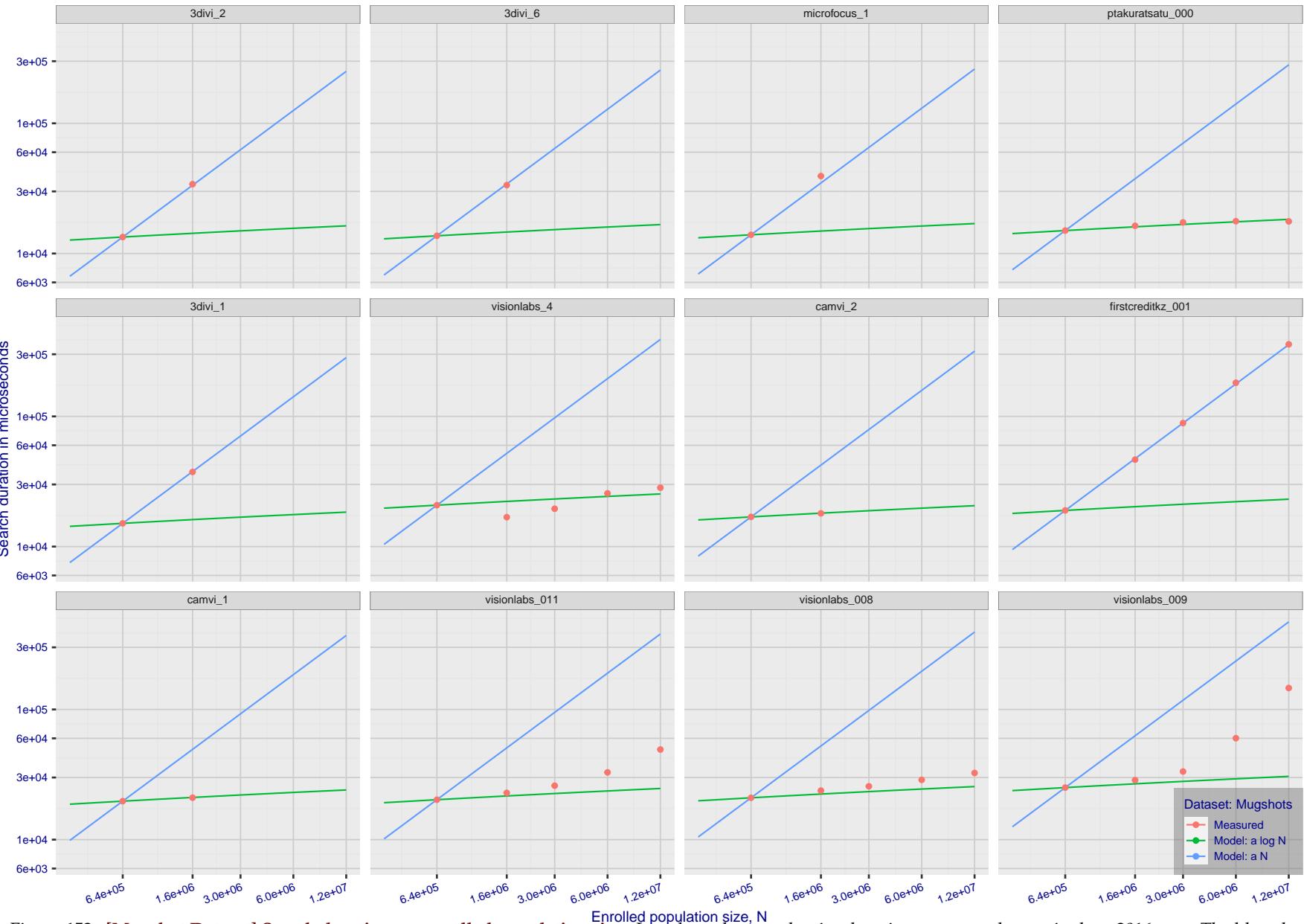
2023/04/04
07:31:47FNIR(N, R, T) = False neg. identification rate
FPIR(N, T) = False pos. identification rate
N = Num. enrolled subjects
R = Num. candidates examined
T = Threshold
T = 0 → Investigation
T > 0 → Identification

Figure 152: [Mugshot Dataset] Search duration vs. enrolled population size. In red are the actual point durations measured on a single c. 2016 core. The blue shows linear growth from $N = 640\,000$. The green line shows logarithmic growth from that point to $N = 1\,600\,000$. Note the sublinear growth from algorithms from Camvi, Dermalog, EverAI, Innovatrics, and Visionlabs. The tiger_1 algorithm is also sublinear, but inaccurate and inoperable at $N \geq 3000000$. This capability sometimes comes at the additional expense of converting a linear gallery data structure into whatever fast-search data structure is used. Note that search times are sometimes dominated by the template generation times shown in Table 29.

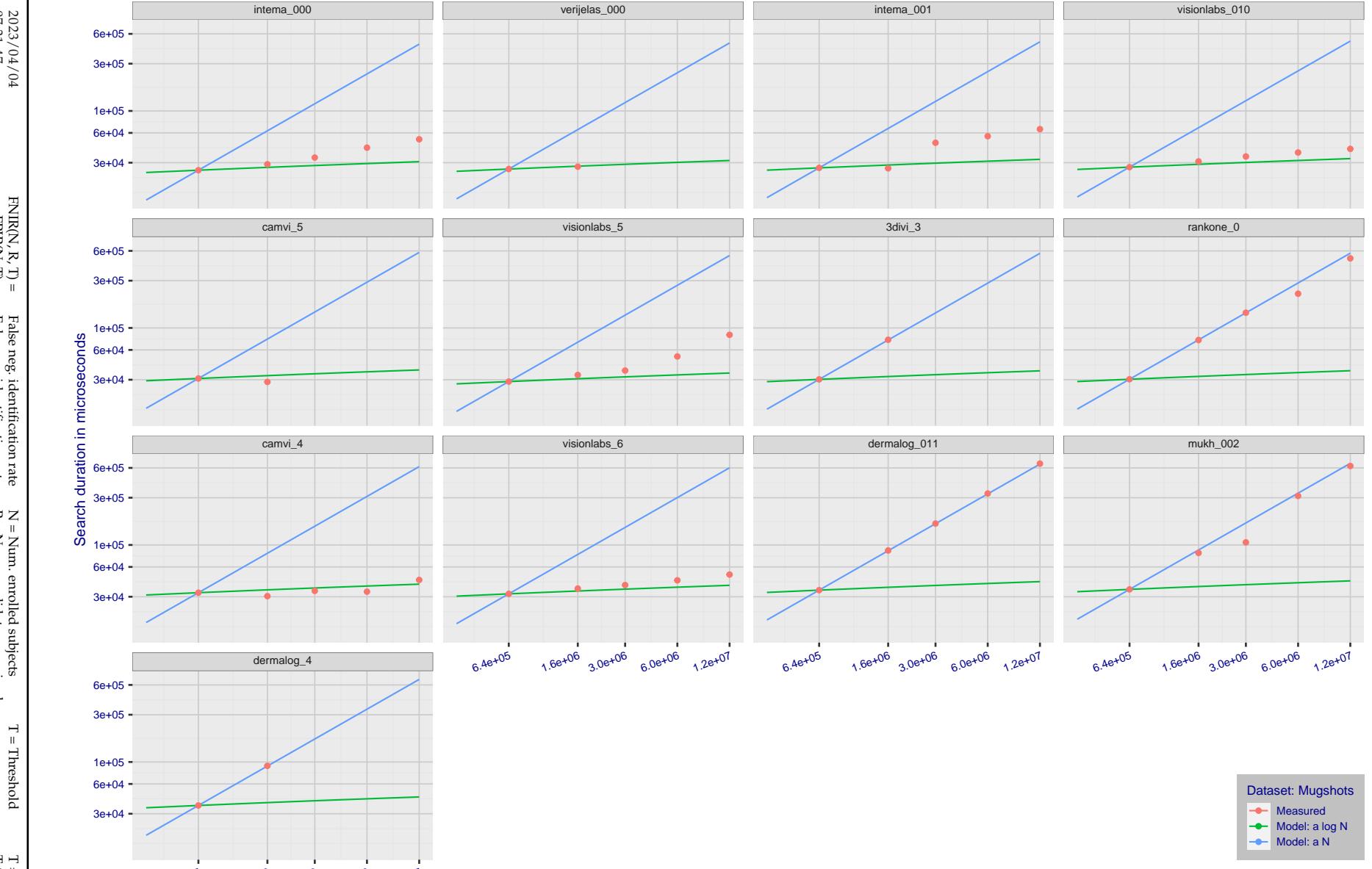


Figure 153: [Mugshot Dataset] Search duration vs. enrolled population size. In red are the actual point durations measured on a single c. 2016 core. The blue shows linear growth from $N = 640\,000$. The green line shows logarithmic growth from that point to $N = 1\,600\,000$. Note the sublinear growth from algorithms from Camvi, Dermalog, EverAI, Innovatrics, and Visionlabs. The tiger_1 algorithm is also sublinear, but inaccurate and inoperable at $N \geq 3000000$. This capability sometimes comes at the additional expense of converting a linear gallery data structure into whatever fast-search data structure is used. Note that search times are sometimes dominated by the template generation times shown in Table 29.

2023/04/04
07:31:47FNIR(N, R, T) = False neg. identification rate
FPIR(N, T) = False pos. identification rateN = Num. enrolled subjects
R = Num. candidates examined

T = Threshold

T = 0 → Investigation
 $T > 0 \rightarrow$ Identification

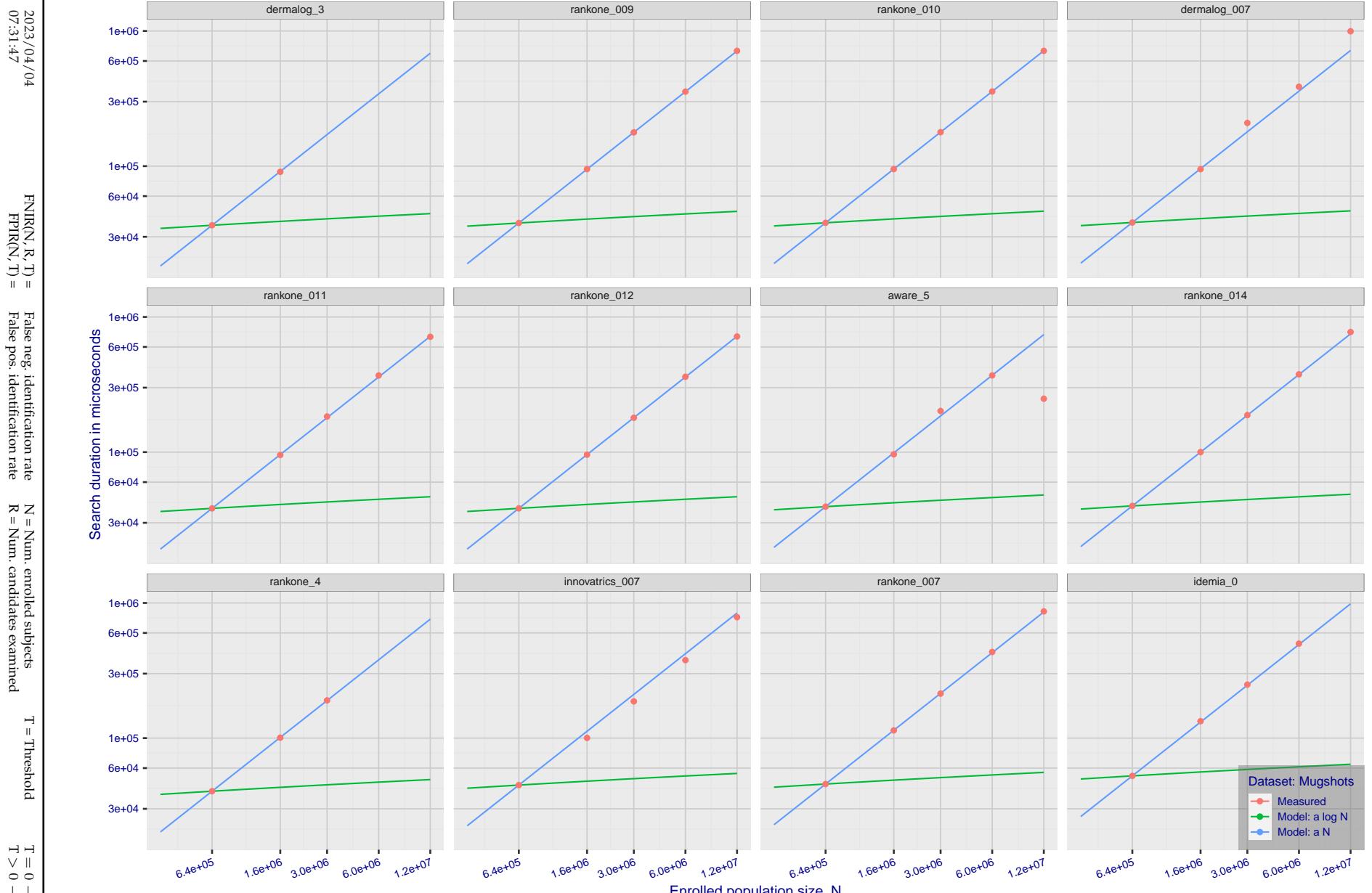


Figure 154: [Mugshot Dataset] Search duration vs. enrolled population size. In red are the actual point durations measured on a single c. 2016 core. The blue shows linear growth from $N = 640\,000$. The green line shows logarithmic growth from that point to $N = 1\,600\,000$. Note the sublinear growth from algorithms from Camvi, Dermalog, EverAI, Innovatrics, and Visionlabs. The tiger_1 algorithm is also sublinear, but inaccurate and inoperable at $N \geq 3000000$. This capability sometimes comes at the additional expense of converting a linear gallery data structure into whatever fast-search data structure is used. Note that search times are sometimes dominated by the template generation times shown in Table 29.

2023/04/04
07:31:47FNIR(N, R, T) = False neg. identification rate
FPIR(N, T) = False pos. identification rateN = Num. enrolled subjects
R = Num. candidates examined

T = Threshold

T = 0 → Investigation
 $T > 0 \rightarrow$ Identification

2023/04/04
07:31:47FNIR(N, R, T) = False neg. identification rate
FPIR(N, T) = False pos. identification rateN = Num. enrolled subjects
R = Num. candidates examined

T = Threshold

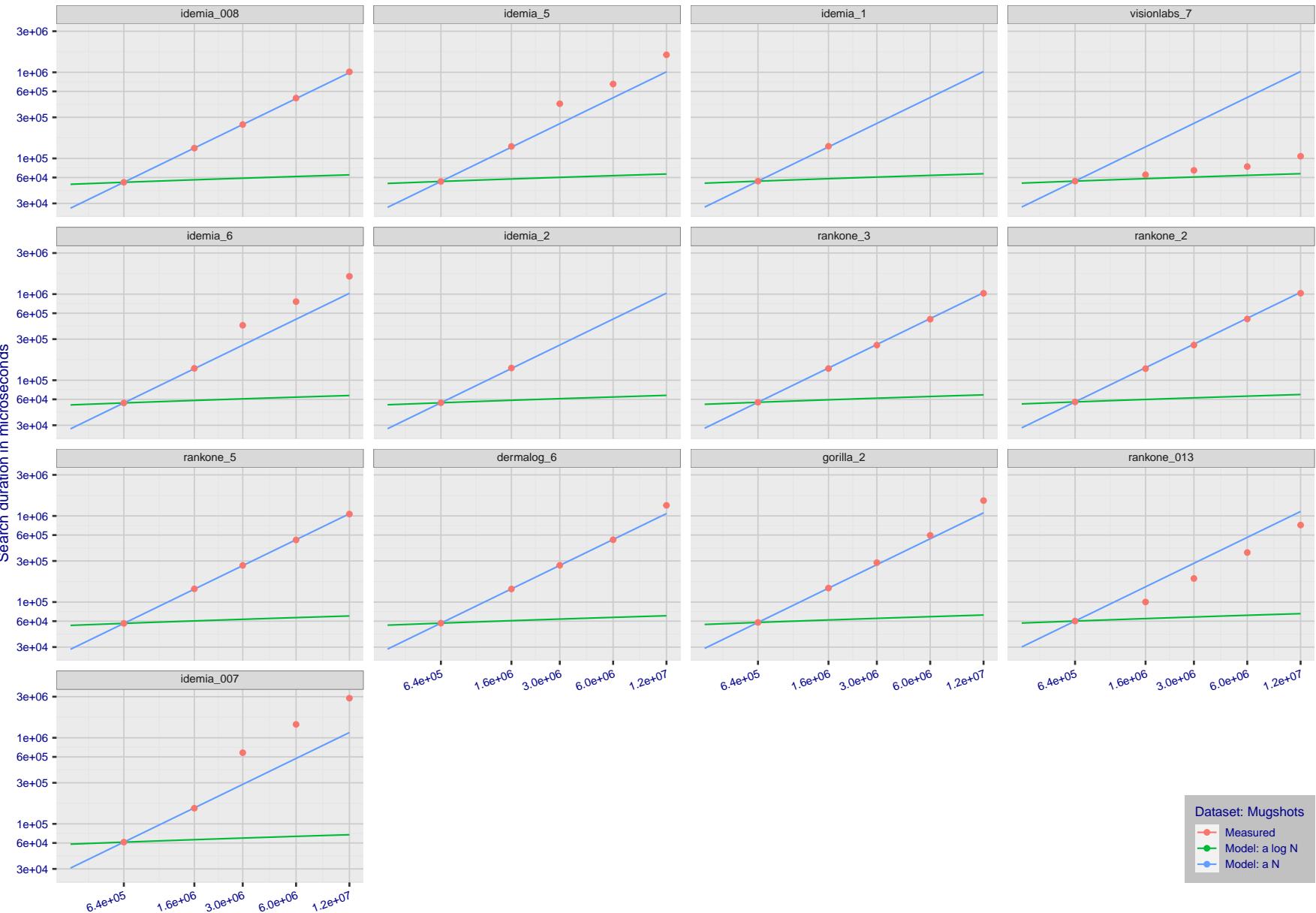
T = 0 → Investigation
 $T > 0 \rightarrow$ Identification

Figure 155: [Mugshot Dataset] Search duration vs. enrolled population size. In red are the actual point durations measured on a single c. 2016 core. The blue shows linear growth from $N = 640\,000$. The green line shows logarithmic growth from that point to $N = 1\,600\,000$. Note the sublinear growth from algorithms from Camvi, Dermalog, EverAI, Innovatrics, and Visionlabs. The tiger_1 algorithm is also sublinear, but inaccurate and inoperable at $N \geq 3000000$. This capability sometimes comes at the additional expense of converting a linear gallery data structure into whatever fast-search data structure is used. Note that search times are sometimes dominated by the template generation times shown in Table 29.

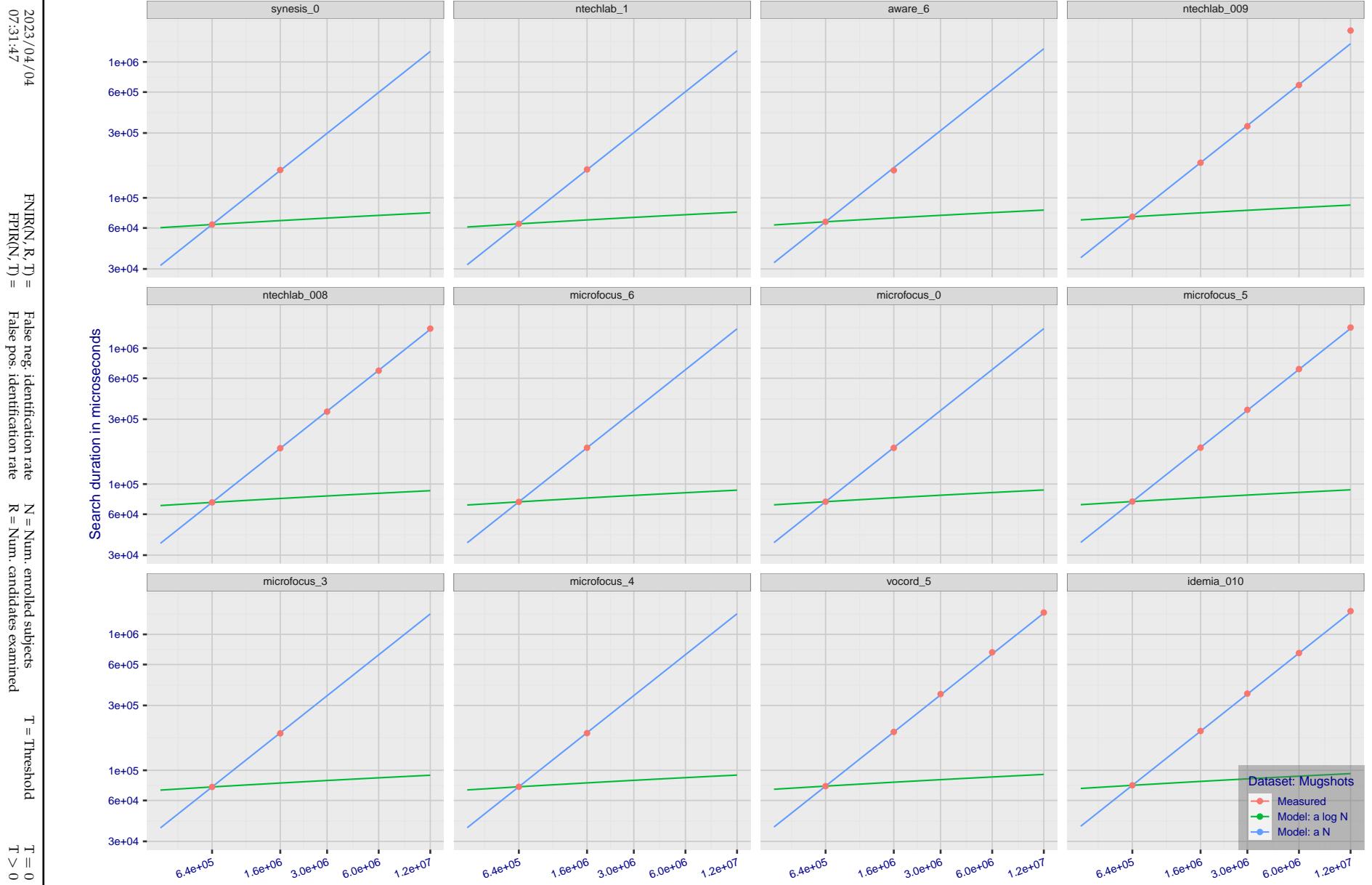


Figure 156: [Mugshot Dataset] Search duration vs. enrolled population size. In red are the actual point durations measured on a single c. 2016 core. The blue shows linear growth from $N = 640\,000$. The green line shows logarithmic growth from that point to $N = 1\,600\,000$. Note the sublinear growth from algorithms from Camvi, Dermalog, EverAI, Innovatrics, and Visionlabs. The tiger_1 algorithm is also sublinear, but inaccurate and inoperable at $N \geq 3000000$. This capability sometimes comes at the additional expense of converting a linear gallery data structure into whatever fast-search data structure is used. Note that search times are sometimes dominated by the template generation times shown in Table 29.

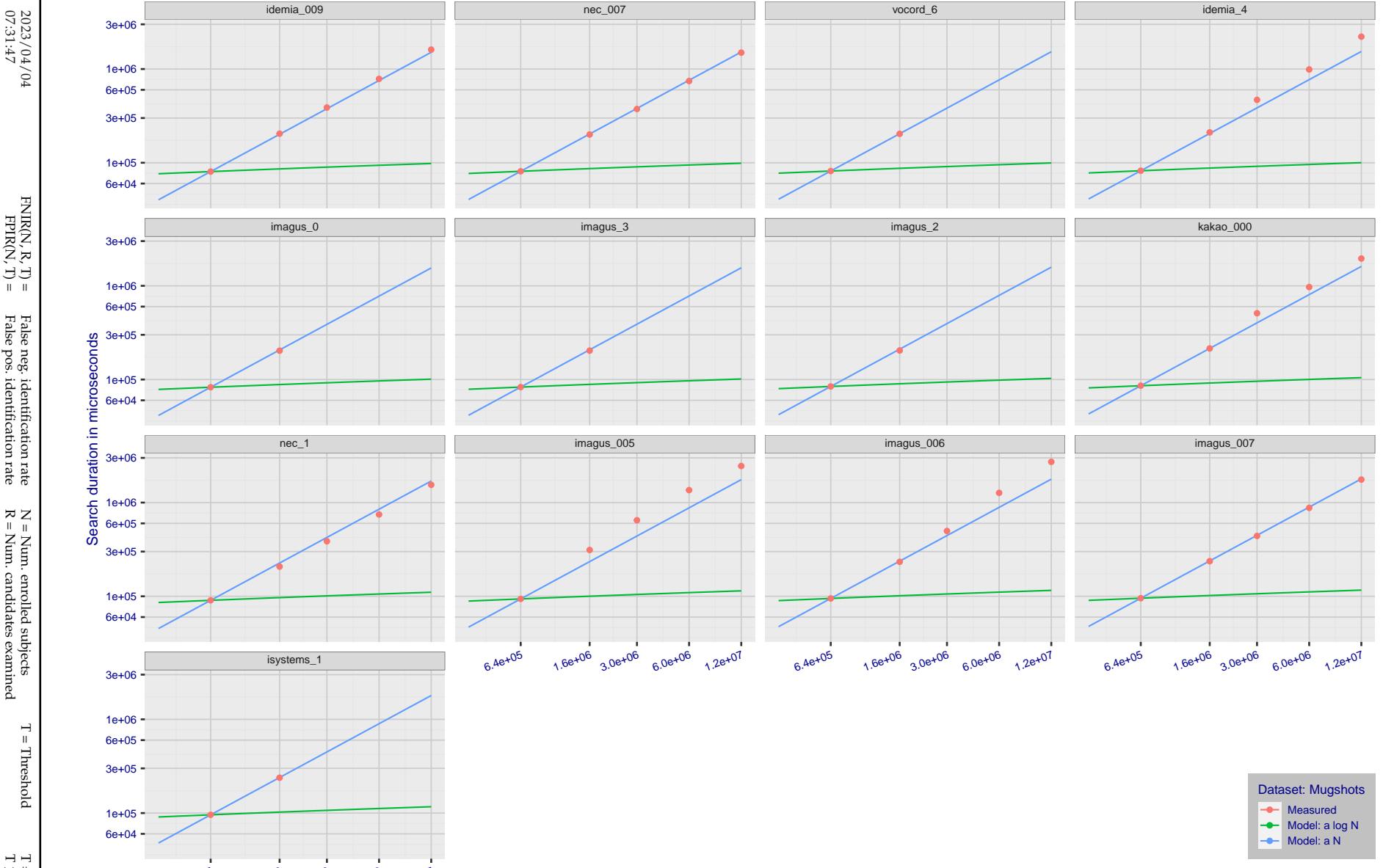


Figure 157: [Mugshot Dataset] Search duration vs. enrolled population size. In red are the actual point durations measured on a single c. 2016 core. The blue shows linear growth from $N = 640\,000$. The green line shows logarithmic growth from that point to $N = 1\,600\,000$. Note the sublinear growth from algorithms from Camvi, Dermalog, EverAI, Innovatrics, and Visionlabs. The tiger_1 algorithm is also sublinear, but inaccurate and inoperable at $N \geq 3000000$. This capability sometimes comes at the additional expense of converting a linear gallery data structure into whatever fast-search data structure is used. Note that search times are sometimes dominated by the template generation times shown in Table 29.

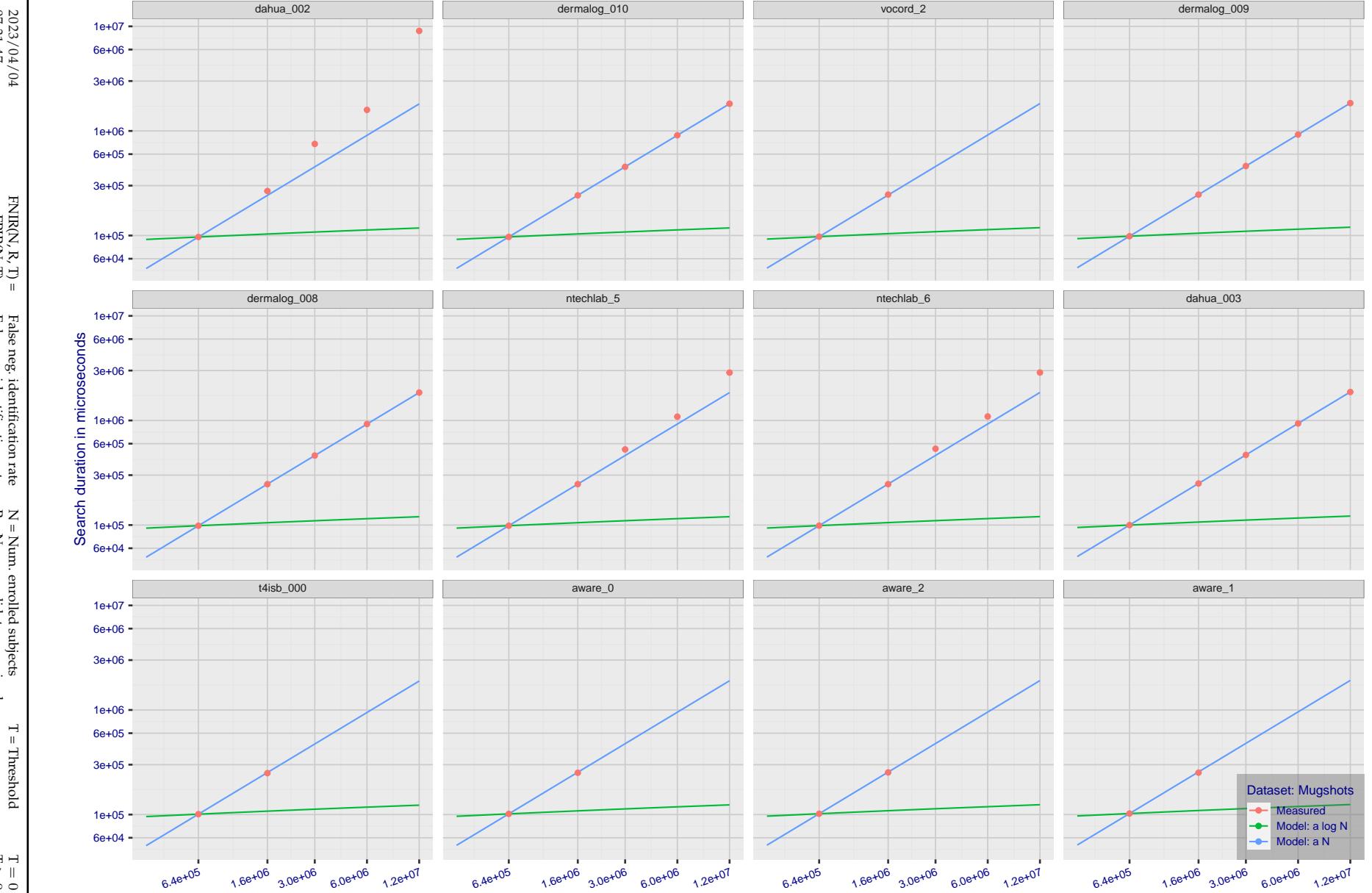


Figure 158: [Mugshot Dataset] Search duration vs. enrolled population size. In red are the actual point durations measured on a single c. 2016 core. The blue shows linear growth from $N = 640\,000$. The green line shows logarithmic growth from that point to $N = 1\,600\,000$. Note the sublinear growth from algorithms from Camvi, Dermalog, EverAI, Innovatrics, and Visionlabs. The tiger_1 algorithm is also sublinear, but inaccurate and inoperable at $N \geq 3000000$. This capability sometimes comes at the additional expense of converting a linear gallery data structure into whatever fast-search data structure is used. Note that search times are sometimes dominated by the template generation times shown in Table 29.

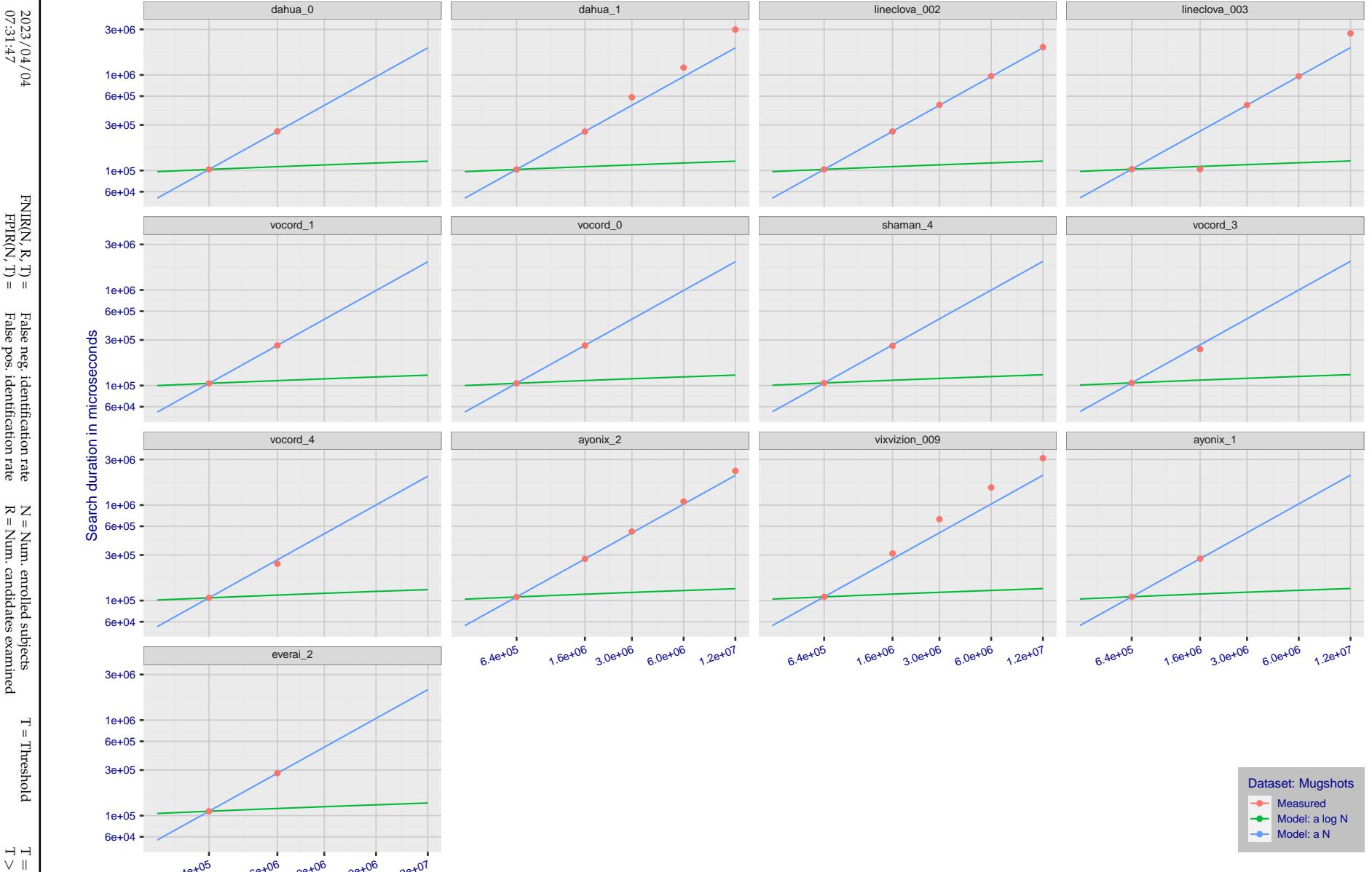


Figure 159: [Mugshot Dataset] Search duration vs. enrolled population size. In red are the actual point durations measured on a single c. 2016 core. The blue shows linear growth from $N = 640\,000$. The green line shows logarithmic growth from that point to $N = 1\,600\,000$. Note the sublinear growth from algorithms from Camvi, Dermalog, Innovatrics, and Visionlabs. The tiger_1 algorithm is also sublinear, but inaccurate and inoperable at $N \geq 3000000$. This capability sometimes comes at the additional expense of converting a linear gallery data structure into whatever fast-search data structure is used. Note that search times are sometimes dominated by the template generation times shown in Table 29.

2023/04/04
07:31:47FNIR(N, R, T) = False neg. identification rate
FPIR(N, T) = False pos. identification rateN = Num. enrolled subjects
R = Num. candidates examined

T = Threshold

T = 0 → Investigation
 $T > 0 \rightarrow$ Identification

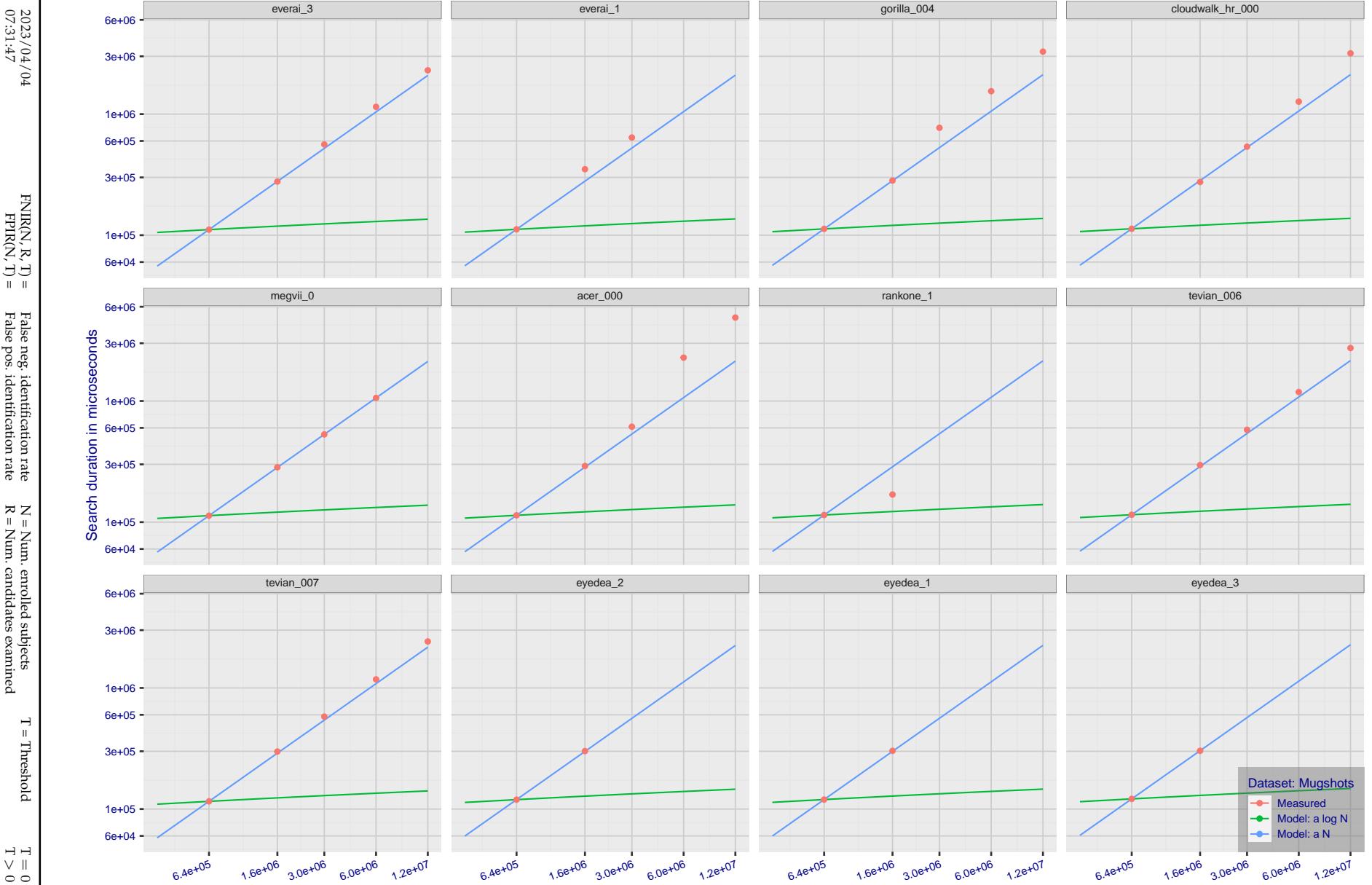


Figure 160: [Mugshot Dataset] Search duration vs. enrolled population size. In red are the actual point durations measured on a single c. 2016 core. The blue shows linear growth from $N = 640\,000$. The green line shows logarithmic growth from that point to $N = 1\,600\,000$. Note the sublinear growth from algorithms from Camvi, Dermalog, EverAI, Innovatrics, and Visionlabs. The tiger_1 algorithm is also sublinear, but inaccurate and inoperable at $N \geq 3000000$. This capability sometimes comes at the additional expense of converting a linear gallery data structure into whatever fast-search data structure is used. Note that search times are sometimes dominated by the template generation times shown in Table 29.

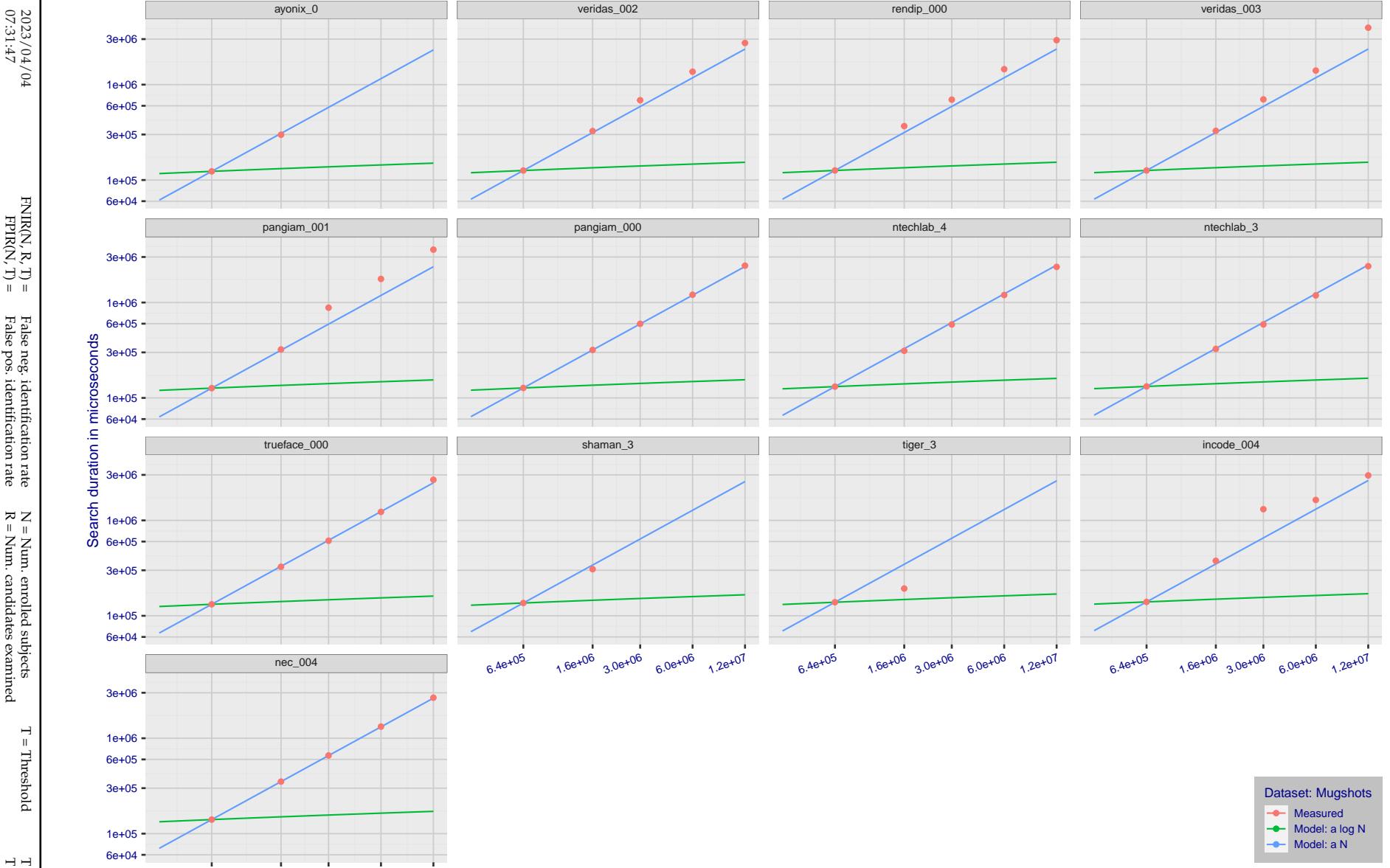


Figure 161: [Mugshot Dataset] Search duration vs. enrolled population size. In red are the actual point durations measured on a single c. 2016 core. The blue shows linear growth from $N = 640\,000$. The green line shows logarithmic growth from that point to $N = 1\,600\,000$. Note the sublinear growth from algorithms from Camvi, Dermalog, EverAI, Innovatrics, and Visionlabs. The tiger_1 algorithm is also sublinear, but inaccurate and inoperable at $N \geq 3000000$. This capability sometimes comes at the additional expense of converting a linear gallery data structure into whatever fast-search data structure is used. Note that search times are sometimes dominated by the template generation times shown in Table 29.

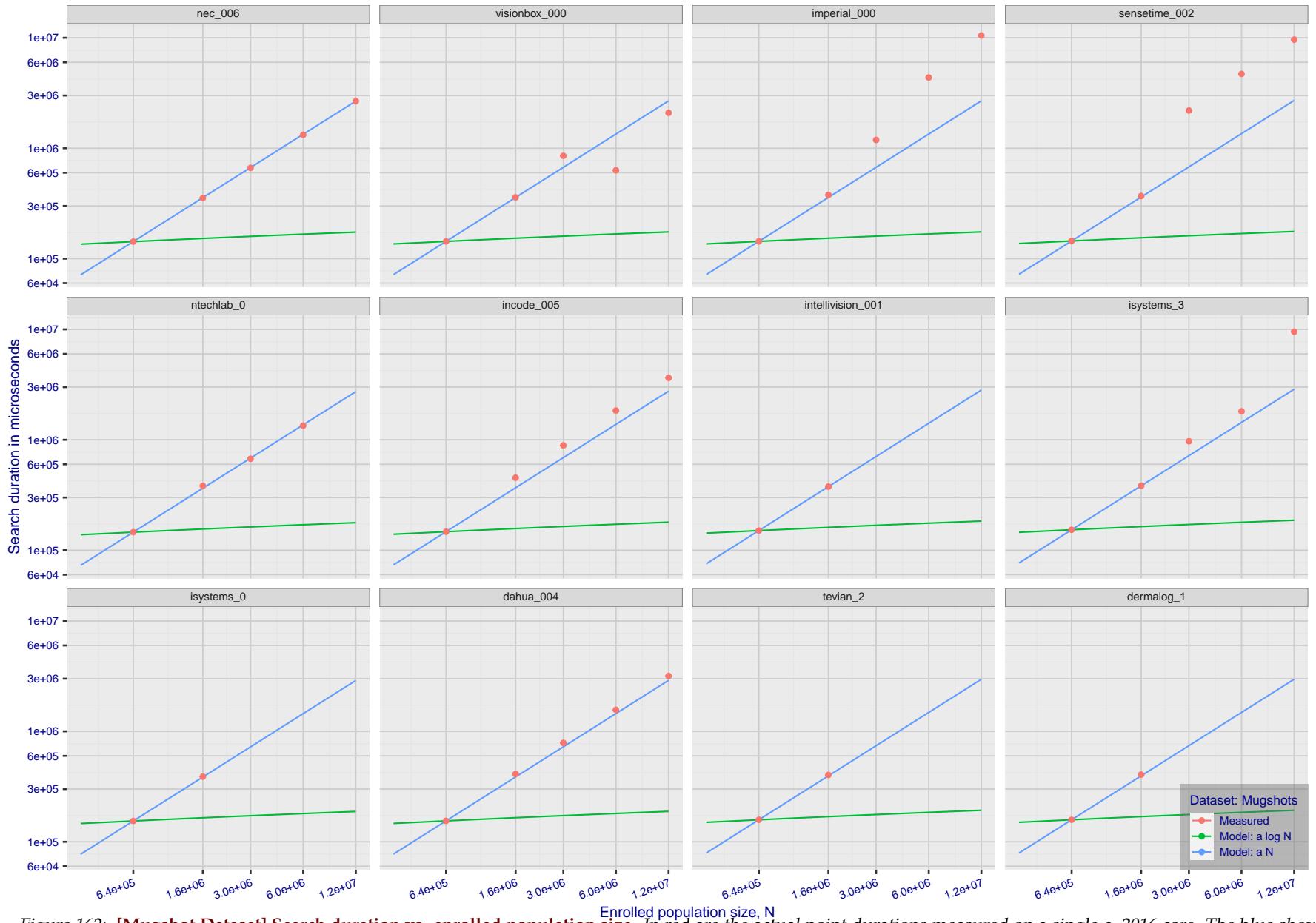


Figure 162: [Mugshot Dataset] Search duration vs. enrolled population size. In red are the actual point durations measured on a single c. 2016 core. The blue shows linear growth from $N = 640\,000$. The green line shows logarithmic growth from that point to $N = 1\,600\,000$. Note the sublinear growth from algorithms from Camvi, Dermalog, EverAI, Innovatrics, and Visionlabs. The tiger_1 algorithm is also sublinear, but inaccurate and inoperable at $N \geq 3000000$. This capability sometimes comes at the additional expense of converting a linear gallery data structure into whatever fast-search data structure is used. Note that search times are sometimes dominated by the template generation times shown in Table 29.

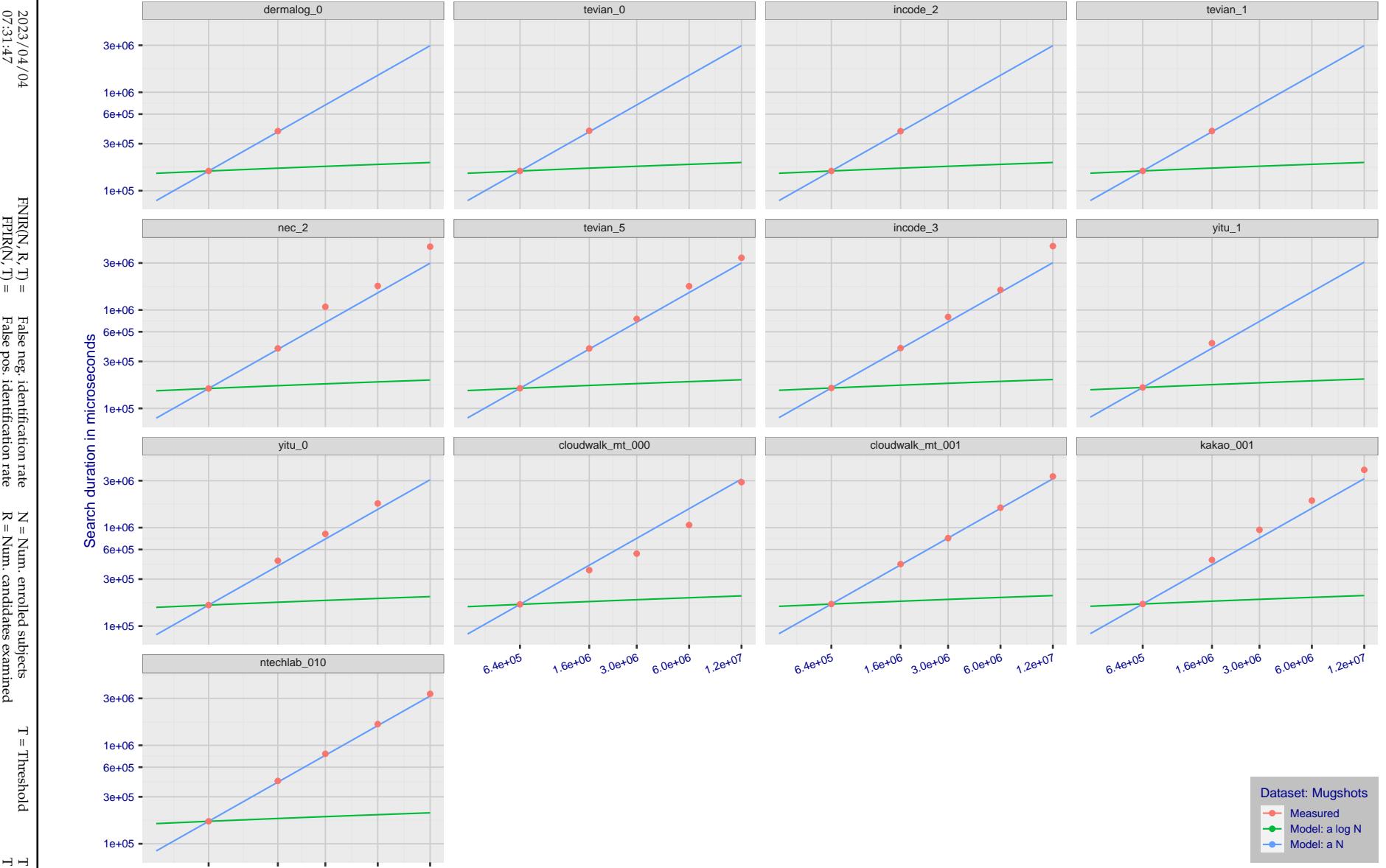


Figure 163: [Mugshot Dataset] Search duration vs. enrolled population size. In red are the actual point durations measured on a single c. 2016 core. The blue shows linear growth from $N = 640\,000$. The green line shows logarithmic growth from that point to $N = 1\,600\,000$. Note the sublinear growth from algorithms from Camvi, Dermalog, EverAI, Innovatrics, and Visionlabs. The tiger_1 algorithm is also sublinear, but inaccurate and inoperable at $N \geq 3000000$. This capability sometimes comes at the additional expense of converting a linear gallery data structure into whatever fast-search data structure is used. Note that search times are sometimes dominated by the template generation times shown in Table 29.

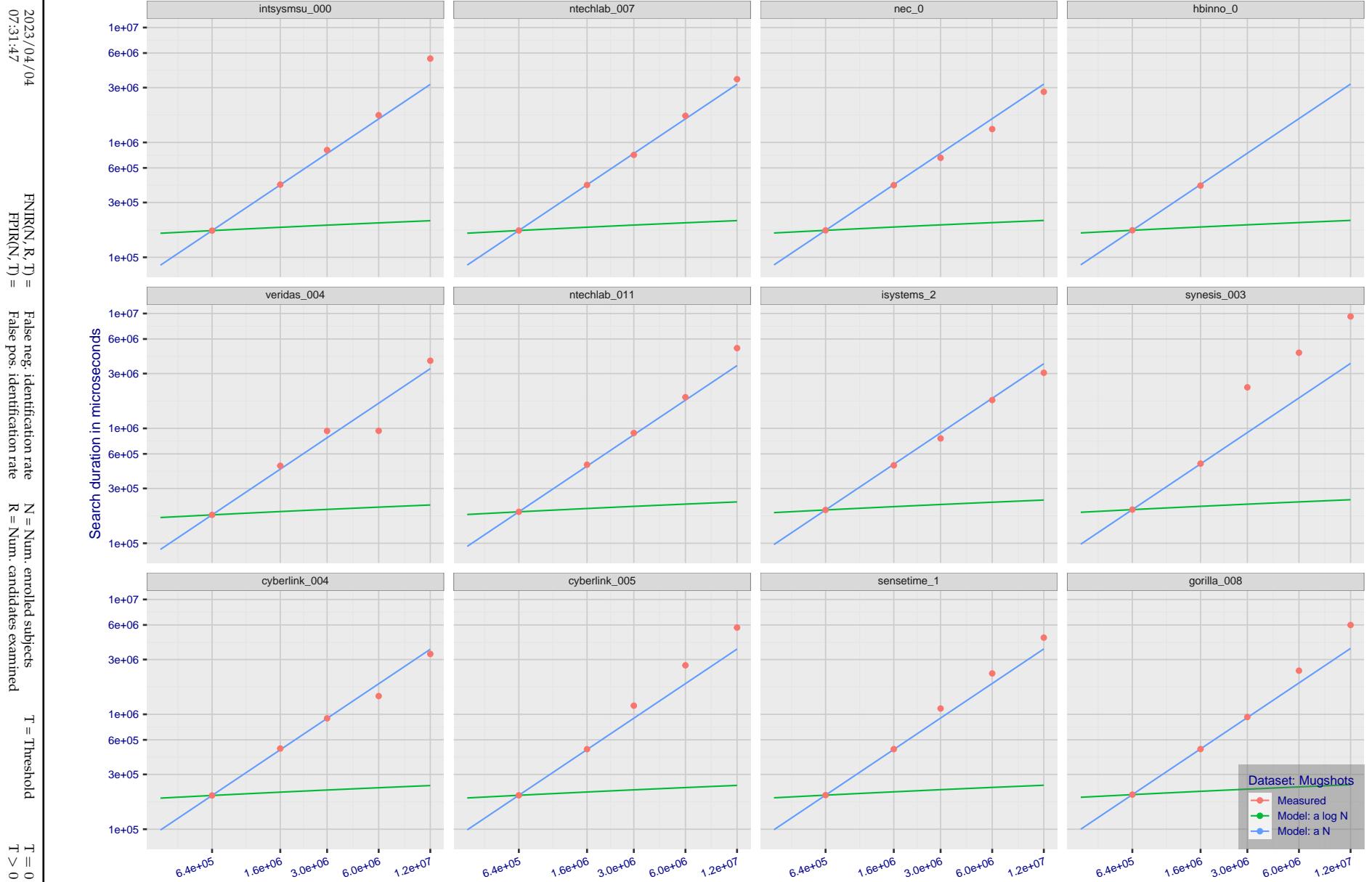


Figure 164: [Mugshot Dataset] Search duration vs. enrolled population size. In red are the actual point durations measured on a single c. 2016 core. The blue shows linear growth from $N = 640\,000$. The green line shows logarithmic growth from that point to $N = 1\,600\,000$. Note the sublinear growth from algorithms from Camvi, Dermalog, EverAI, Innovatrics, and Visionlabs. The tiger_1 algorithm is also sublinear, but inaccurate and inoperable at $N \geq 3000000$. This capability sometimes comes at the additional expense of converting a linear gallery data structure into whatever fast-search data structure is used. Note that search times are sometimes dominated by the template generation times shown in Table 29.

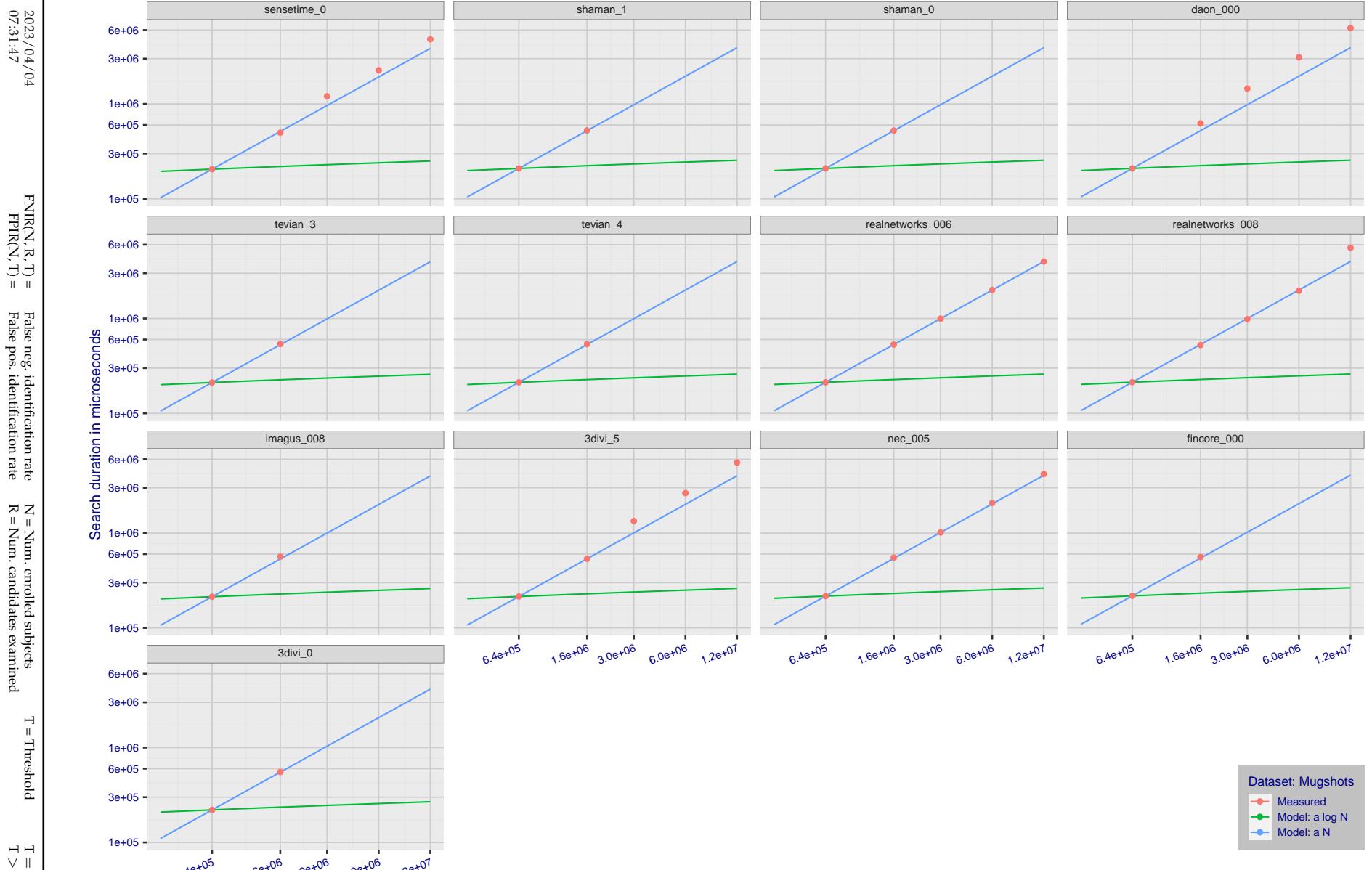


Figure 165: [Mugshot Dataset] Search duration vs. enrolled population size. In red are the actual point durations measured on a single c. 2016 core. The blue shows linear growth from $N = 640\,000$. The green line shows logarithmic growth from that point to $N = 1\,600\,000$. Note the sublinear growth from algorithms from Camvi, Dermalog, EverAI, Innovatrics, and Visionlabs. The tiger_1 algorithm is also sublinear, but inaccurate and inoperable at $N \geq 3000000$. This capability sometimes comes at the additional expense of converting a linear gallery data structure into whatever fast-search data structure is used. Note that search times are sometimes dominated by the template generation times shown in Table 29.

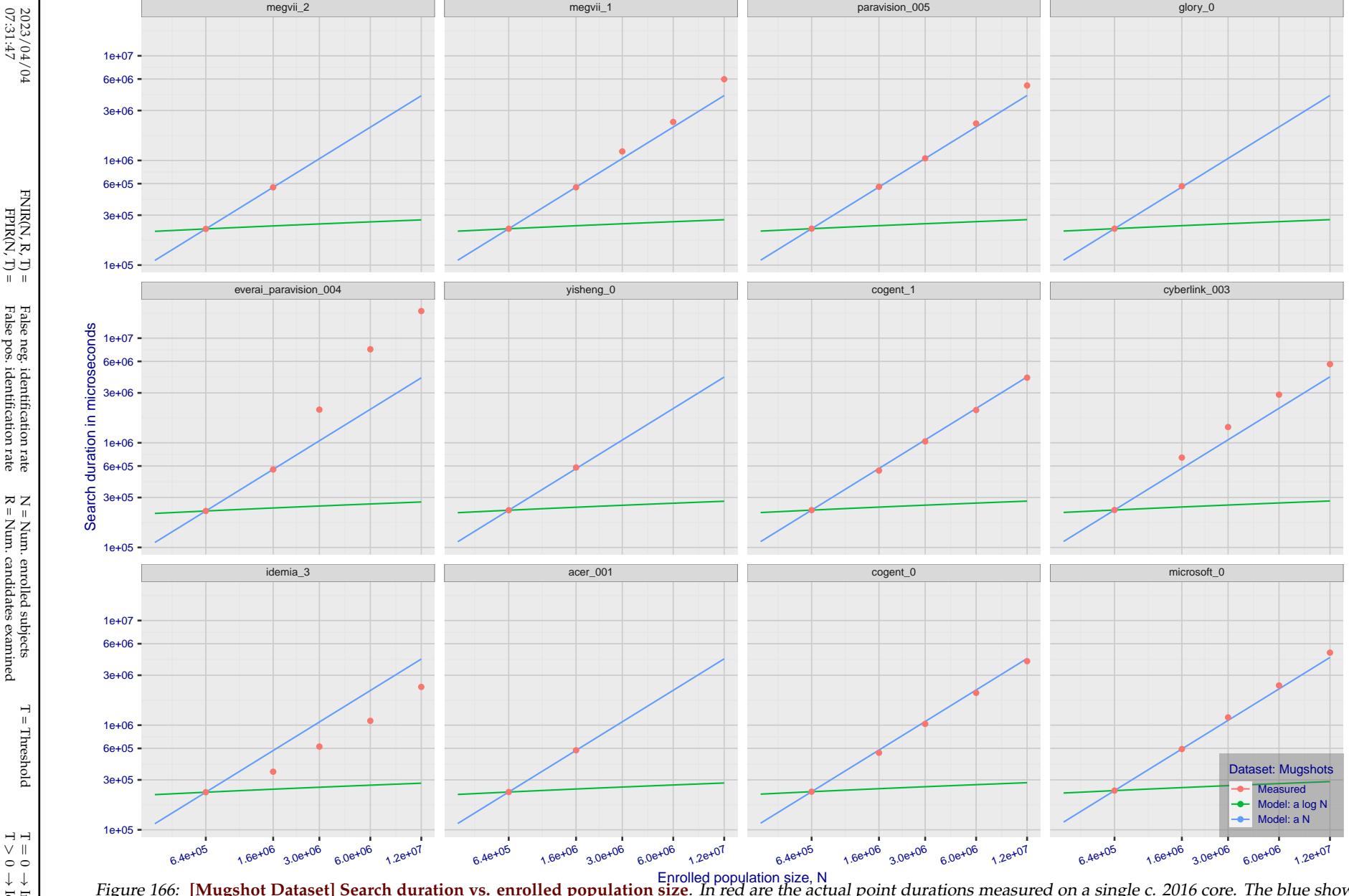


Figure 166: [Mugshot Dataset] Search duration vs. enrolled population size. In red are the actual point durations measured on a single c. 2016 core. The blue shows linear growth from $N = 640\,000$. The green line shows logarithmic growth from that point to $N = 1\,600\,000$. Note the sublinear growth from algorithms from Camvi, Dermalog, EverAI, Innovatrics, and Visionlabs. The tiger_1 algorithm is also sublinear, but inaccurate and inoperable at $N \geq 3000000$. This capability sometimes comes at the additional expense of converting a linear gallery data structure into whatever fast-search data structure is used. Note that search times are sometimes dominated by the template generation times shown in Table 29.

2023/04/04

FNIR(N, R, T) = False neg. identification rate
FPIR(N, T) = False pos. identification rateN = Num. enrolled subjects
R = Num. candidates examinedT = Threshold
T = 0 → Investigation

T > 0 → Identification

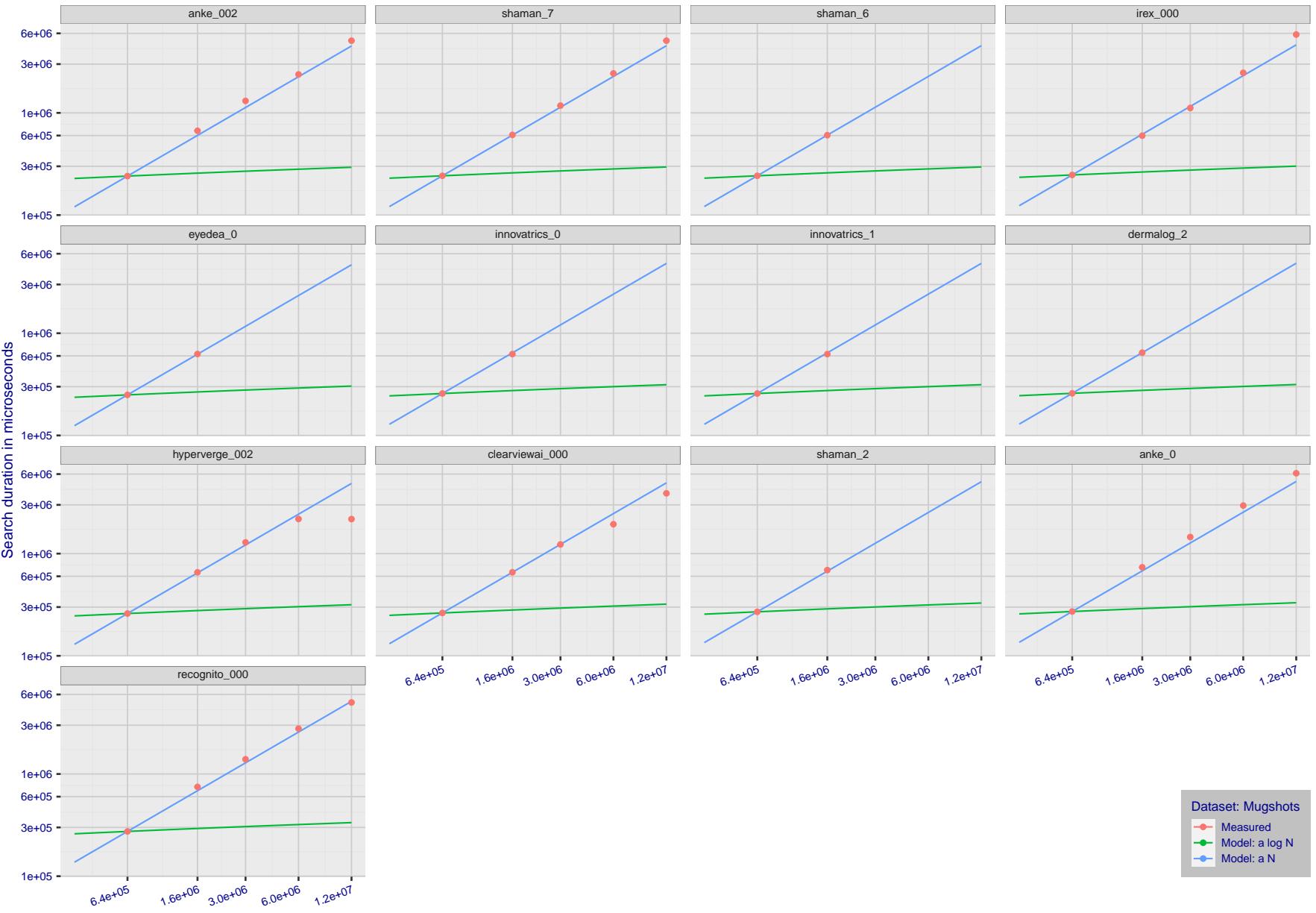


Figure 167: [Mugshot Dataset] Search duration vs. enrolled population size. In red are the actual point durations measured on a single c. 2016 core. The blue shows linear growth from $N = 640\,000$. The green line shows logarithmic growth from that point to $N = 1\,600\,000$. Note the sublinear growth from algorithms from Camvi, Dermalog, EverAI, Innovatrics, and Visionlabs. The tiger_1 algorithm is also sublinear, but inaccurate and inoperable at $N \geq 3000000$. This capability sometimes comes at the additional expense of converting a linear gallery data structure into whatever fast-search data structure is used. Note that search times are sometimes dominated by the template generation times shown in Table 29.

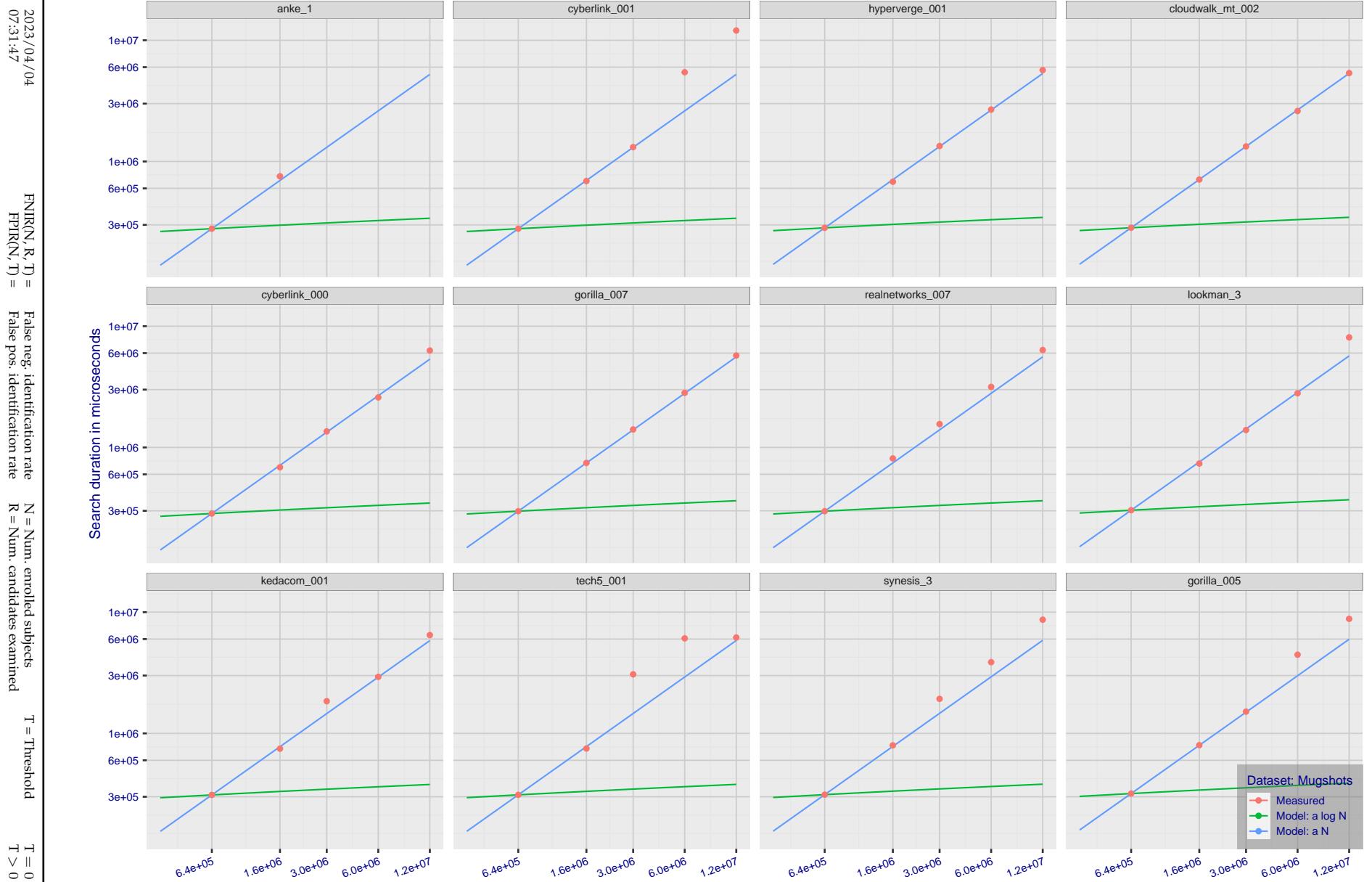


Figure 168: [Mugshot Dataset] Search duration vs. enrolled population size. In red are the actual point durations measured on a single c. 2016 core. The blue shows linear growth from $N = 640\,000$. The green line shows logarithmic growth from that point to $N = 1\,600\,000$. Note the sublinear growth from algorithms from Camvi, Dermalog, EverAI, Innovatrics, and Visionlabs. The tiger_1 algorithm is also sublinear, but inaccurate and inoperable at $N \geq 3000000$. This capability sometimes comes at the additional expense of converting a linear gallery data structure into whatever fast-search data structure is used. Note that search times are sometimes dominated by the template generation times shown in Table 29.

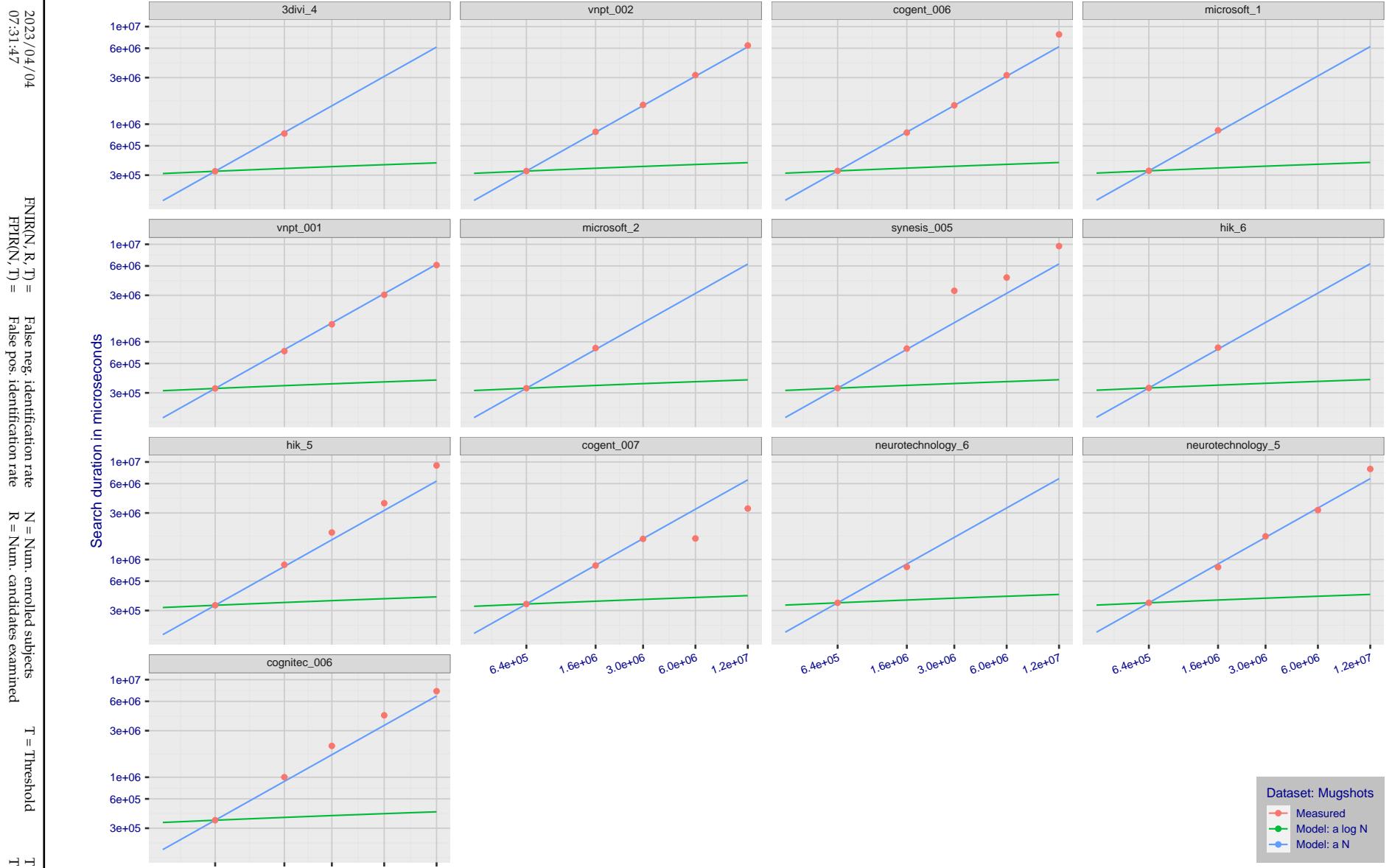


Figure 169: [Mugshot Dataset] Search duration vs. enrolled population size. In red are the actual point durations measured on a single c. 2016 core. The blue shows linear growth from $N = 640\,000$. The green line shows logarithmic growth from that point to $N = 1\,600\,000$. Note the sublinear growth from algorithms from Camvi, Dermalog, EverAI, Innovatrics, and Visionlabs. The tiger_1 algorithm is also sublinear, but inaccurate and inoperable at $N \geq 3000000$. This capability sometimes comes at the additional expense of converting a linear gallery data structure into whatever fast-search data structure is used. Note that search times are sometimes dominated by the template generation times shown in Table 29.

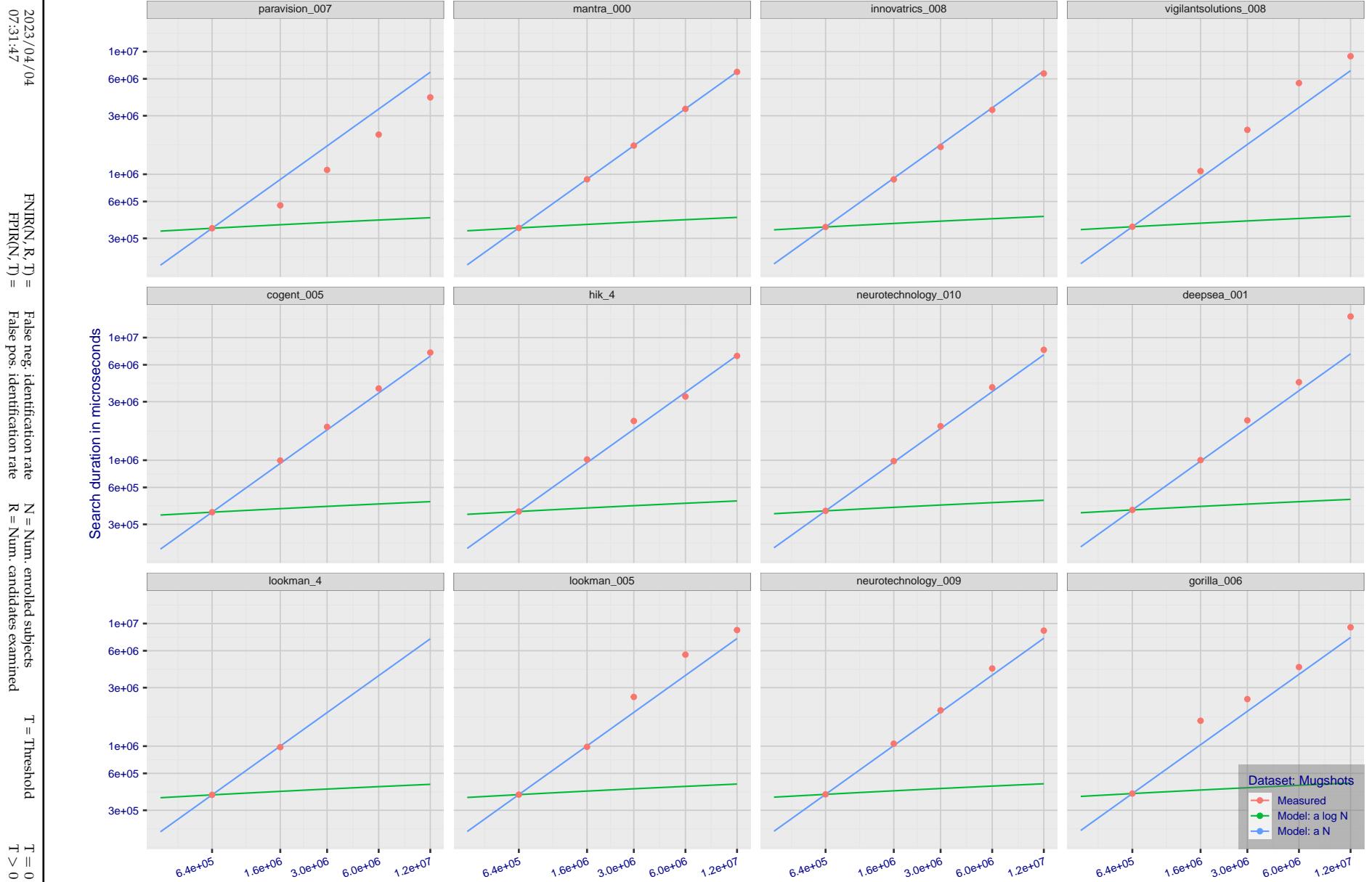


Figure 170: [Mugshot Dataset] Search duration vs. enrolled population size. In red are the actual point durations measured on a single c. 2016 core. The blue shows linear growth from $N = 640\,000$. The green line shows logarithmic growth from that point to $N = 1\,600\,000$. Note the sublinear growth from algorithms from Camvi, Dermalog, EverAI, Innovatrics, and Visionlabs. The tiger_1 algorithm is also sublinear, but inaccurate and inoperable at $N \geq 3000000$. This capability sometimes comes at the additional expense of converting a linear gallery data structure into whatever fast-search data structure is used. Note that search times are sometimes dominated by the template generation times shown in Table 29.

2023 / 04 / 04

FNIR(N, R, T) = False neg. identification rate
FPTR(N, T) = False pos. identification rateN = Num. enrolled subjects
R = Num. candidates examined

T = Threshold

T = 0 → Investigation
 $T > 0 \rightarrow$ Identification

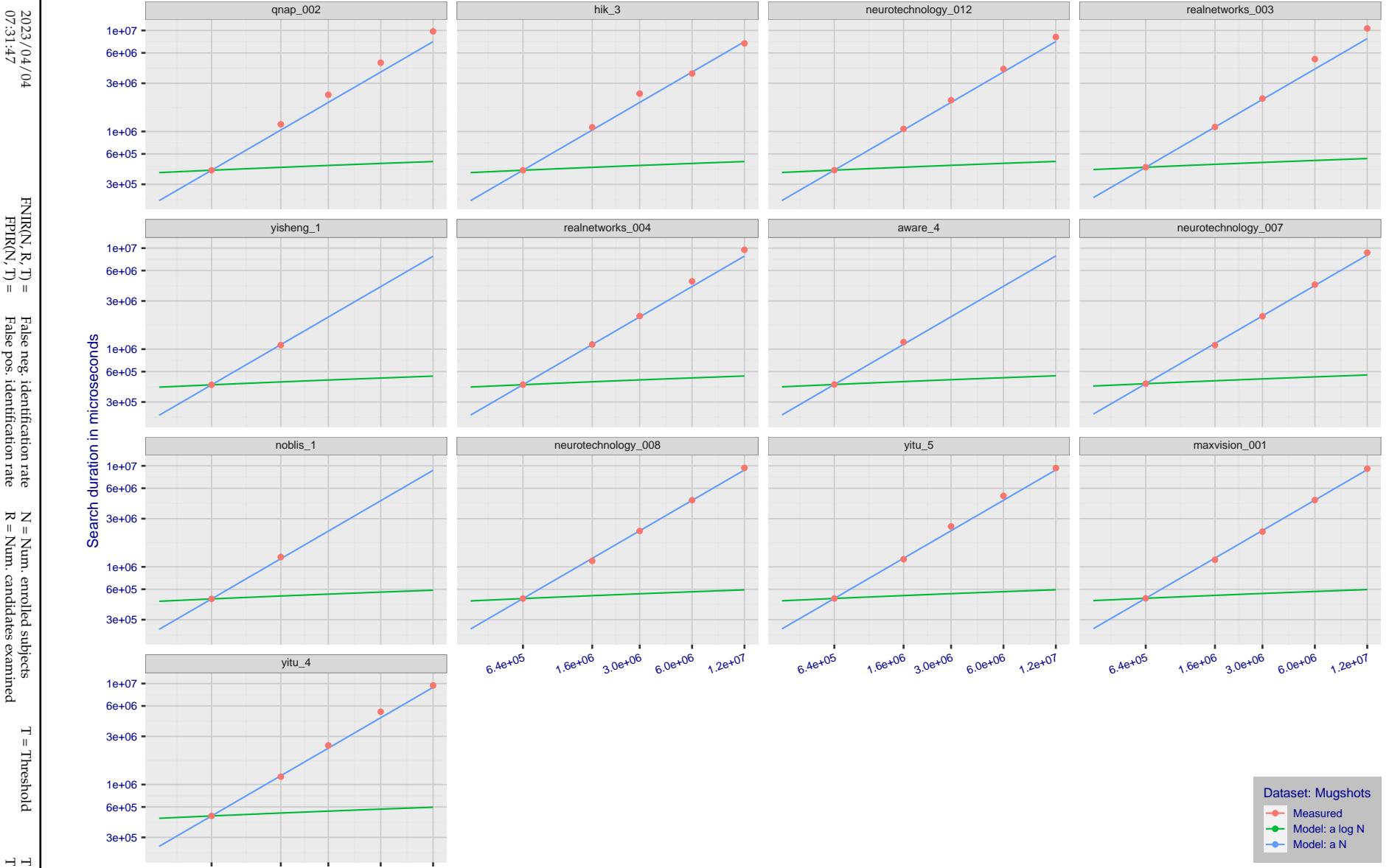


Figure 171: [Mugshot Dataset] Search duration vs. enrolled population size. In red are the actual point durations measured on a single c. 2016 core. The blue shows linear growth from $N = 640\,000$. The green line shows logarithmic growth from that point to $N = 1\,600\,000$. Note the sublinear growth from algorithms from Camvi, Dermalog, EverAI, Innovatrics, and Visionlabs. The tiger_1 algorithm is also sublinear, but inaccurate and inoperable at $N \geq 3000000$. This capability sometimes comes at the additional expense of converting a linear gallery data structure into whatever fast-search data structure is used. Note that search times are sometimes dominated by the template generation times shown in Table 29.

2023 / 04 / 04

FNIR(N, R, T) =

False neg. identification rate
FPIR(N, T) =
False pos. identification rateN = Num. enrolled subjects
R = Num. candidates examined

T = Threshold

T = 0 → Investigation
 $T > 0 \rightarrow$ Identification

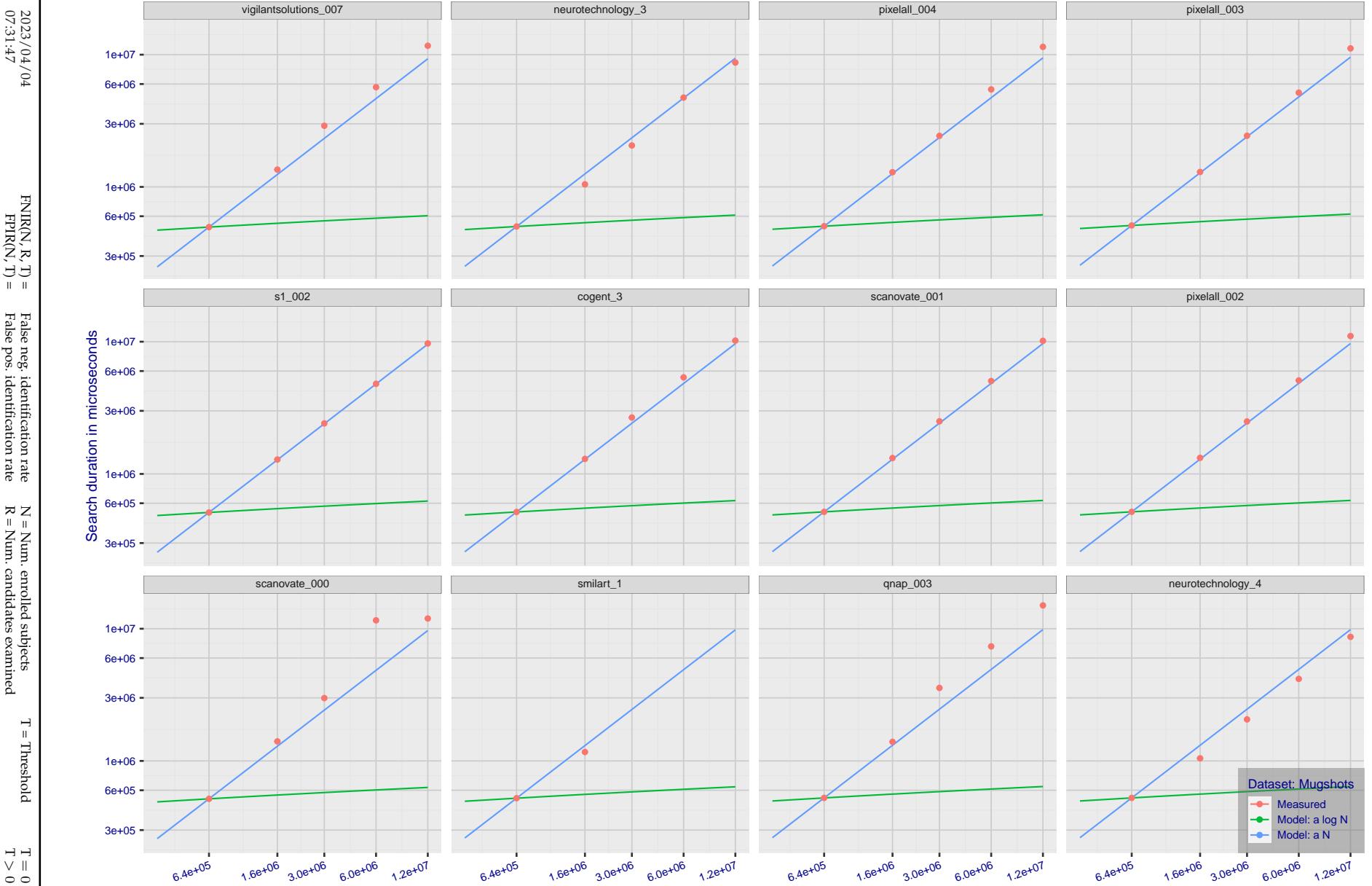


Figure 172: [Mugshot Dataset] Search duration vs. enrolled population size. In red are the actual point durations measured on a single c. 2016 core. The blue shows linear growth from $N = 640\,000$. The green line shows logarithmic growth from that point to $N = 1\,600\,000$. Note the sublinear growth from algorithms from Camvi, Dermalog, EverAI, Innovatrics, and Visionlabs. The tiger_1 algorithm is also sublinear, but inaccurate and inoperable at $N \geq 3000000$. This capability sometimes comes at the additional expense of converting a linear gallery data structure into whatever fast-search data structure is used. Note that search times are sometimes dominated by the template generation times shown in Table 29.

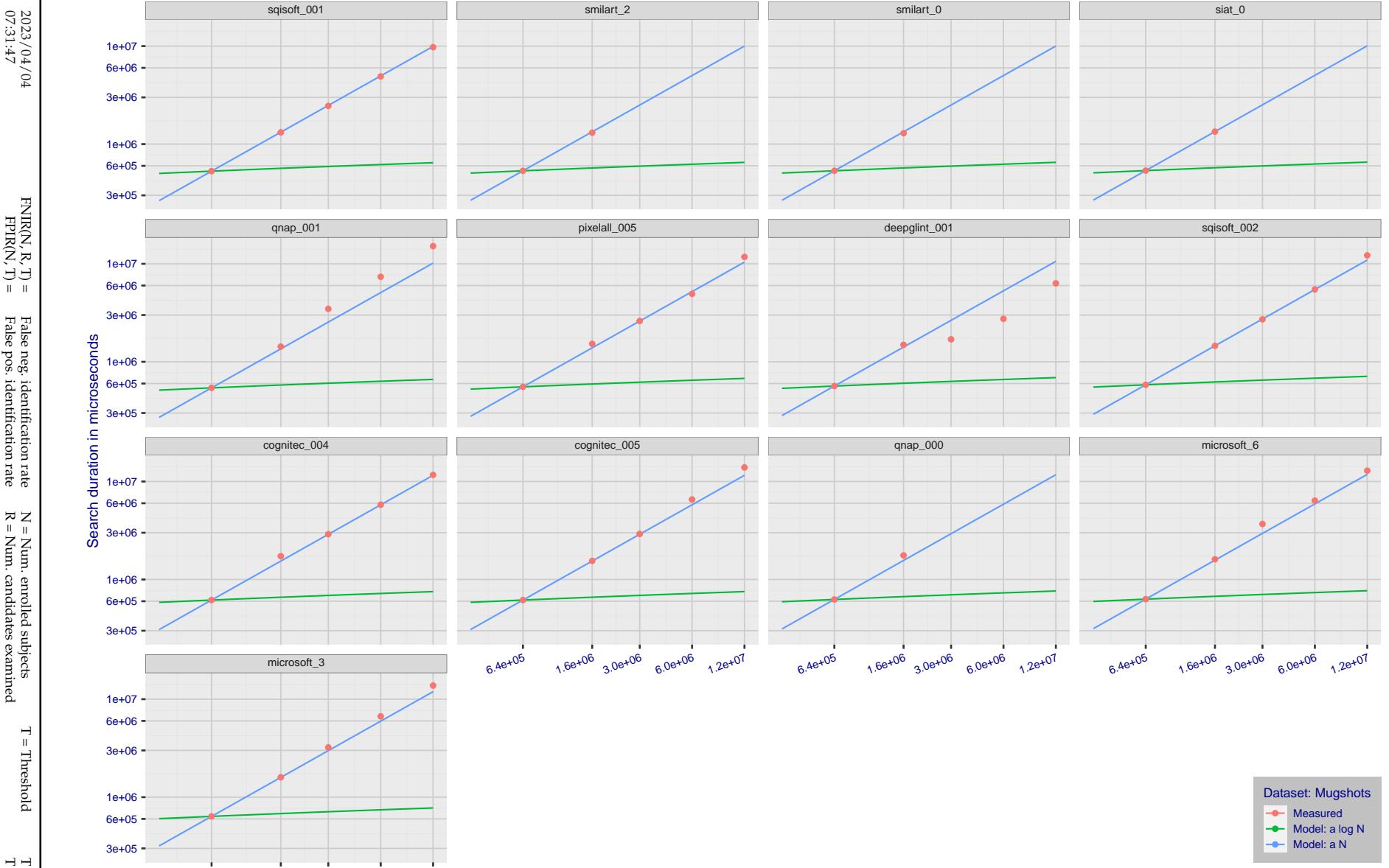


Figure 173: [Mugshot Dataset] Search duration vs. enrolled population size. In red are the actual point durations measured on a single c. 2016 core. The blue shows linear growth from $N = 640\,000$. The green line shows logarithmic growth from that point to $N = 1\,600\,000$. Note the sublinear growth from algorithms from Camvi, Dermalog, EverAI, Innovatrics, and Visionlabs. The tiger_1 algorithm is also sublinear, but inaccurate and inoperable at $N \geq 3000000$. This capability sometimes comes at the additional expense of converting a linear gallery data structure into whatever fast-search data structure is used. Note that search times are sometimes dominated by the template generation times shown in Table 29.

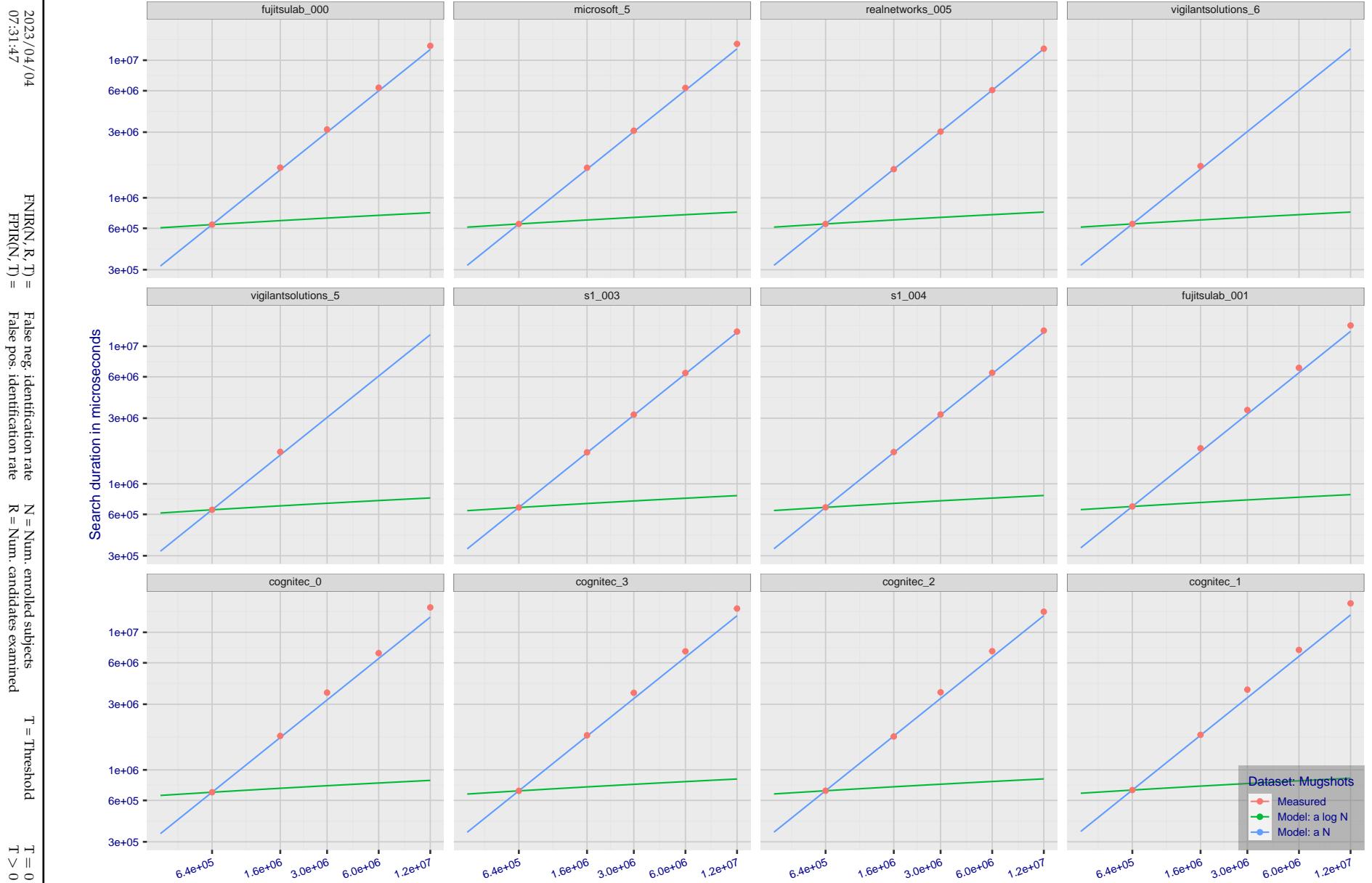


Figure 174: [Mugshot Dataset] Search duration vs. enrolled population size. In red are the actual point durations measured on a single c. 2016 core. The blue shows linear growth from $N = 640\,000$. The green line shows logarithmic growth from that point to $N = 1\,600\,000$. Note the sublinear growth from algorithms from Camvi, Dermalog, EverAI, Innovatrics, and Visionlabs. The tiger_1 algorithm is also sublinear, but inaccurate and inoperable at $N \geq 3000000$. This capability sometimes comes at the additional expense of converting a linear gallery data structure into whatever fast-search data structure is used. Note that search times are sometimes dominated by the template generation times shown in Table 29.

2023/04/04

FNIR(N, R, T) = False neg. identification rate
FPIR(N, T) = False pos. identification rateN = Num. enrolled subjects
R = Num. candidates examinedT = Threshold
T = 0 → Investigation

T > 0 → Identification

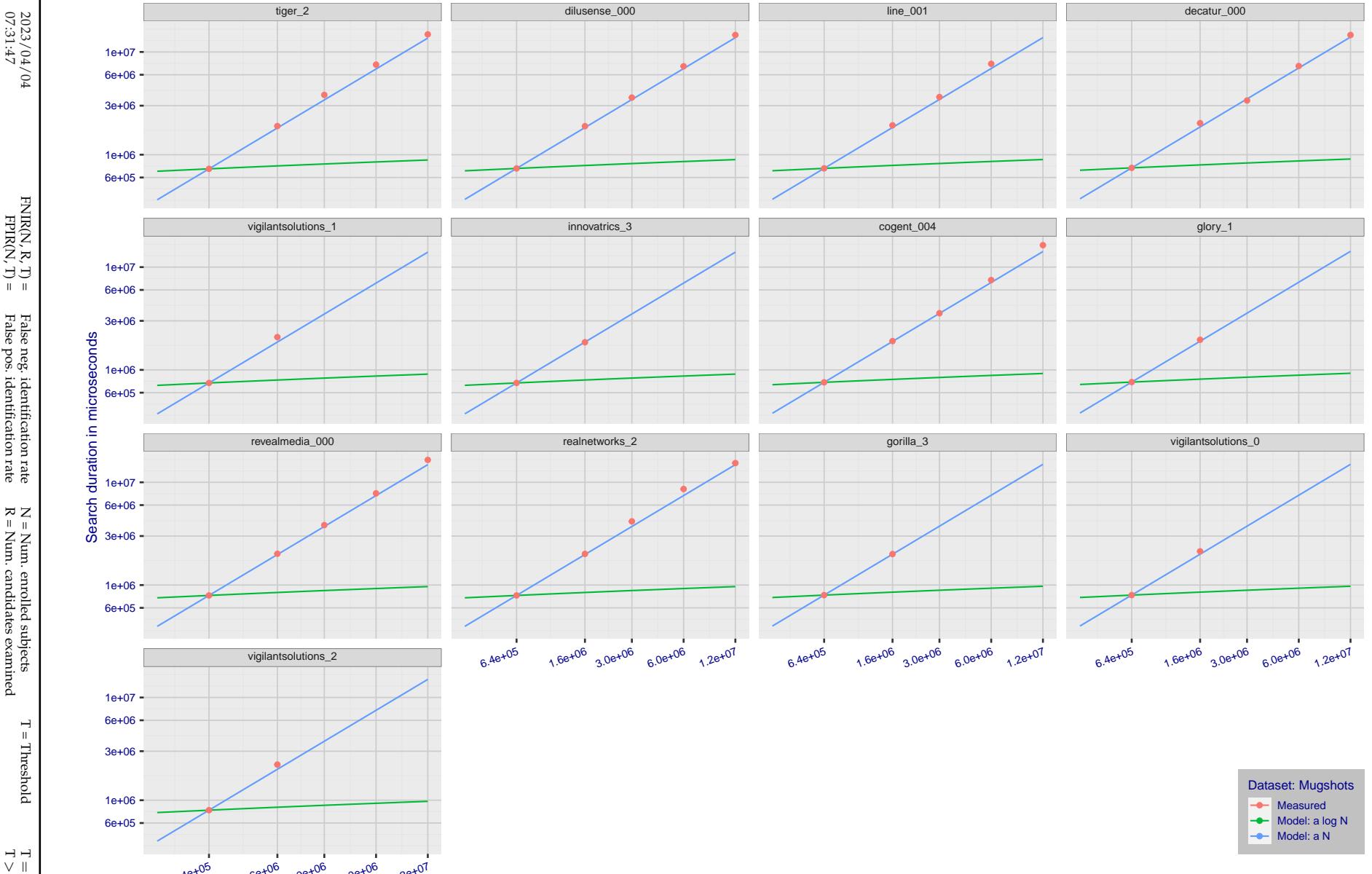


Figure 175: [Mugshot Dataset] Search duration vs. enrolled population size. In red are the actual point durations measured on a single c. 2016 core. The blue shows linear growth from $N = 640\,000$. The green line shows logarithmic growth from that point to $N = 1\,600\,000$. Note the sublinear growth from algorithms from Camvi, Dermalog, EverAI, Innovatrics, and Visionlabs. The tiger_1 algorithm is also sublinear, but inaccurate and inoperable at $N \geq 3000000$. This capability sometimes comes at the additional expense of converting a linear gallery data structure into whatever fast-search data structure is used. Note that search times are sometimes dominated by the template generation times shown in Table 29.

2023/04/04

FNIR(N, R, T) = False neg. identification rate
FPIR(N, T) = False pos. identification rateN = Num. enrolled subjects
R = Num. candidates examined

T = Threshold

T = 0 → Investigation
 $T > 0 \rightarrow$ Identification

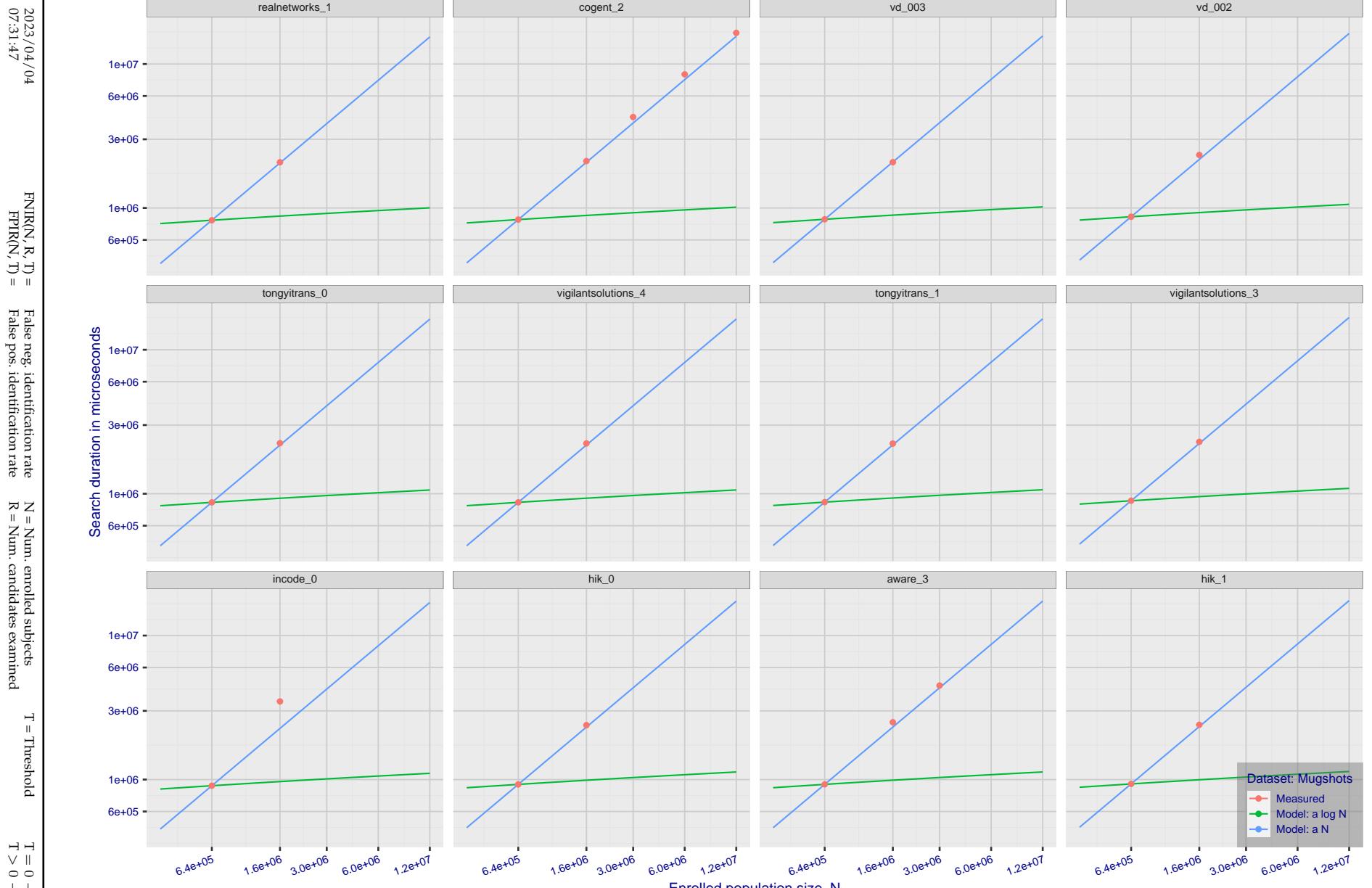


Figure 176: [Mugshot Dataset] Search duration vs. enrolled population size. In red are the actual point durations measured on a single c. 2016 core. The blue shows linear growth from $N = 640\,000$. The green line shows logarithmic growth from that point to $N = 1\,600\,000$. Note the sublinear growth from algorithms from Camvi, Dermalog, EverAI, Innovatrics, and Visionlabs. The tiger_1 algorithm is also sublinear, but inaccurate and inoperable at $N \geq 3000000$. This capability sometimes comes at the additional expense of converting a linear gallery data structure into whatever fast-search data structure is used. Note that search times are sometimes dominated by the template generation times shown in Table 29.

2023/04/04

FNIR(N, R, T) =

False neg. identification rate

N = Num. enrolled subjects

R = Num. candidates examined

T = Threshold

T = 0 → Investigation

 $T > 0 \rightarrow$ Identification

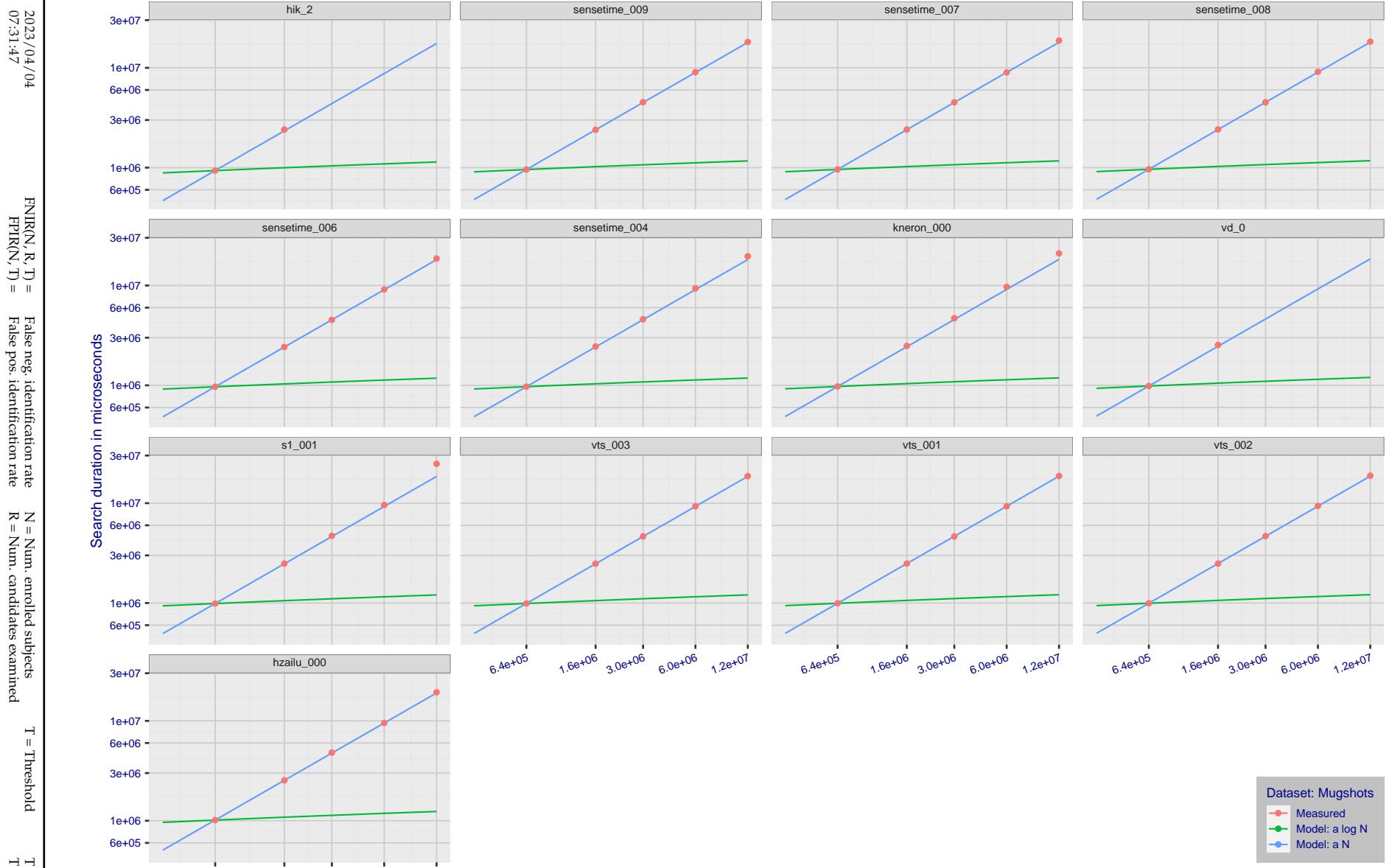


Figure 177: [Mugshot Dataset] Search duration vs. enrolled population size. In red are the actual point durations measured on a single c. 2016 core. The blue shows linear growth from $N = 640\,000$. The green line shows logarithmic growth from that point to $N = 1\,600\,000$. Note the sublinear growth from algorithms from Camvi, Dermalog, EverAI, Innovatrics, and Visionlabs. The tiger_1 algorithm is also sublinear, but inaccurate and inoperable at $N \geq 3000000$. This capability sometimes comes at the additional expense of converting a linear gallery data structure into whatever fast-search data structure is used. Note that search times are sometimes dominated by the template generation times shown in Table 29.

2023/04/04
07:31:47FNIR(N, R, T) = False neg. identification rate
FPTR(N, T) = False pos. identification rateN = Num. enrolled subjects
R = Num. candidates examined

T = Threshold

T = 0 → Investigation
 $T > 0 \rightarrow$ Identification

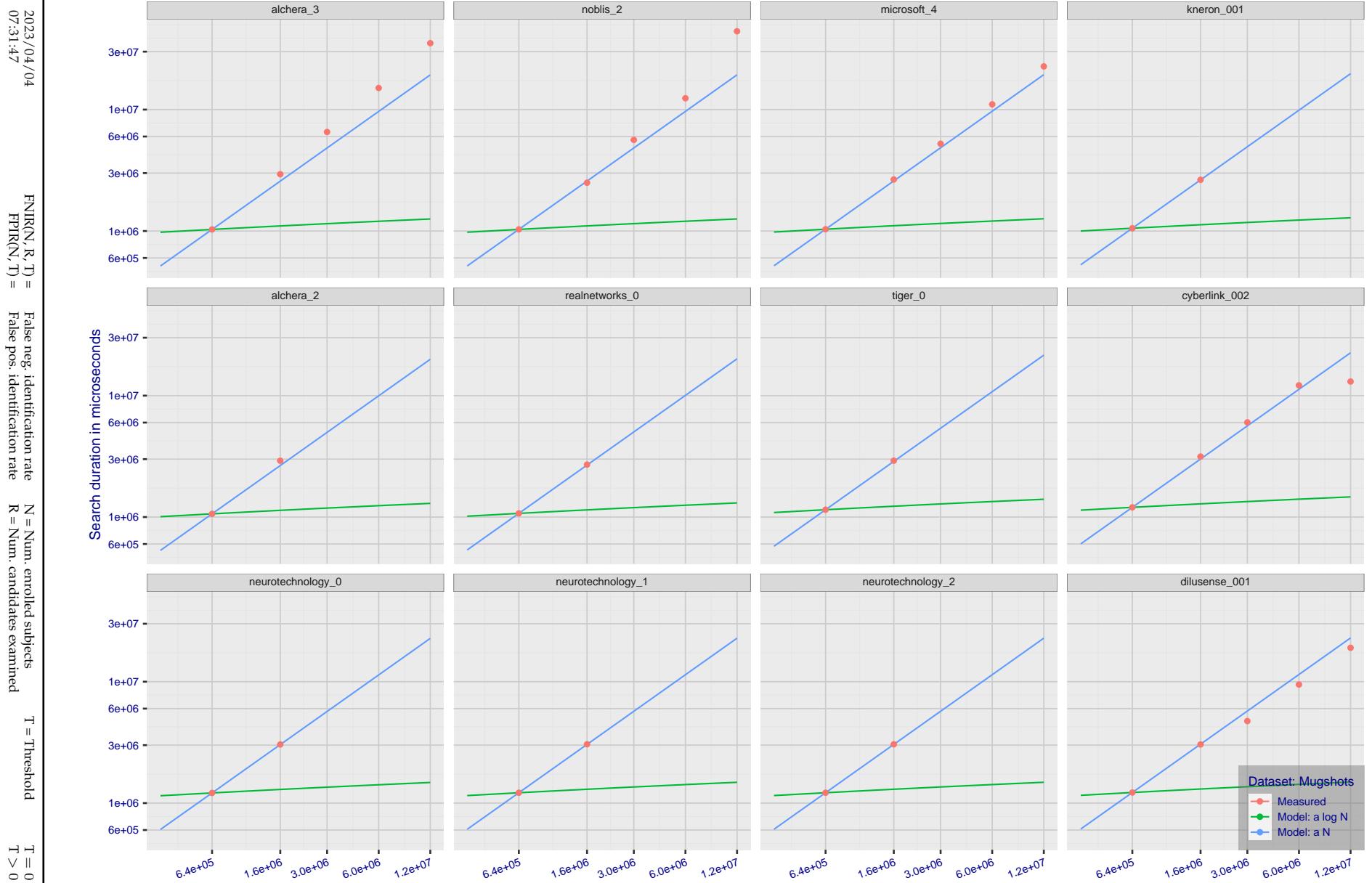


Figure 178: [Mugshot Dataset] Search duration vs. enrolled population size. In red are the actual point durations measured on a single c. 2016 core. The blue shows linear growth from $N = 640\,000$. The green line shows logarithmic growth from that point to $N = 1\,600\,000$. Note the sublinear growth from algorithms from Camvi, Dermalog, EverAI, Innovatrics, and Visionlabs. The tiger_1 algorithm is also sublinear, but inaccurate and inoperable at $N \geq 3000000$. This capability sometimes comes at the additional expense of converting a linear gallery data structure into whatever fast-search data structure is used. Note that search times are sometimes dominated by the template generation times shown in Table 29.

2023 / 04 / 04

FNIR(N, R, T) = False neg. identification rate
FPIR(N, T) = False pos. identification rateN = Num. enrolled subjects
R = Num. candidates examined

T = Threshold

T = 0 → Investigation
 $T > 0 \rightarrow$ Identification

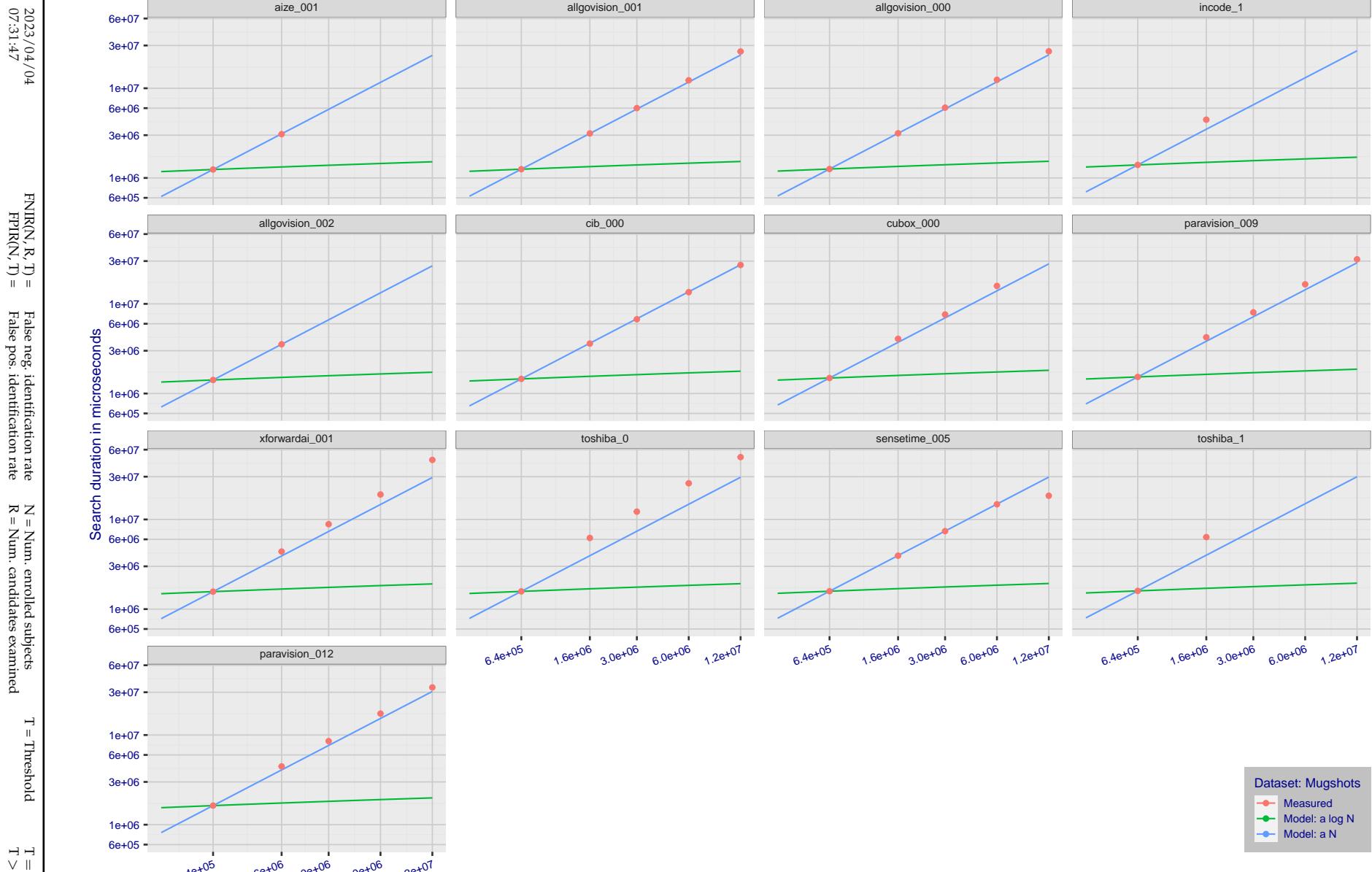


Figure 179: [Mugshot Dataset] Search duration vs. enrolled population size. In red are the actual point durations measured on a single c. 2016 core. The blue shows linear growth from $N = 640\,000$. The green line shows logarithmic growth from that point to $N = 1\,600\,000$. Note the sublinear growth from algorithms from Camvi, Dermalog, EverAI, Innovatrics, and Visionlabs. The tiger_1 algorithm is also sublinear, but inaccurate and inoperable at $N \geq 3000000$. This capability sometimes comes at the additional expense of converting a linear gallery data structure into whatever fast-search data structure is used. Note that search times are sometimes dominated by the template generation times shown in Table 29.

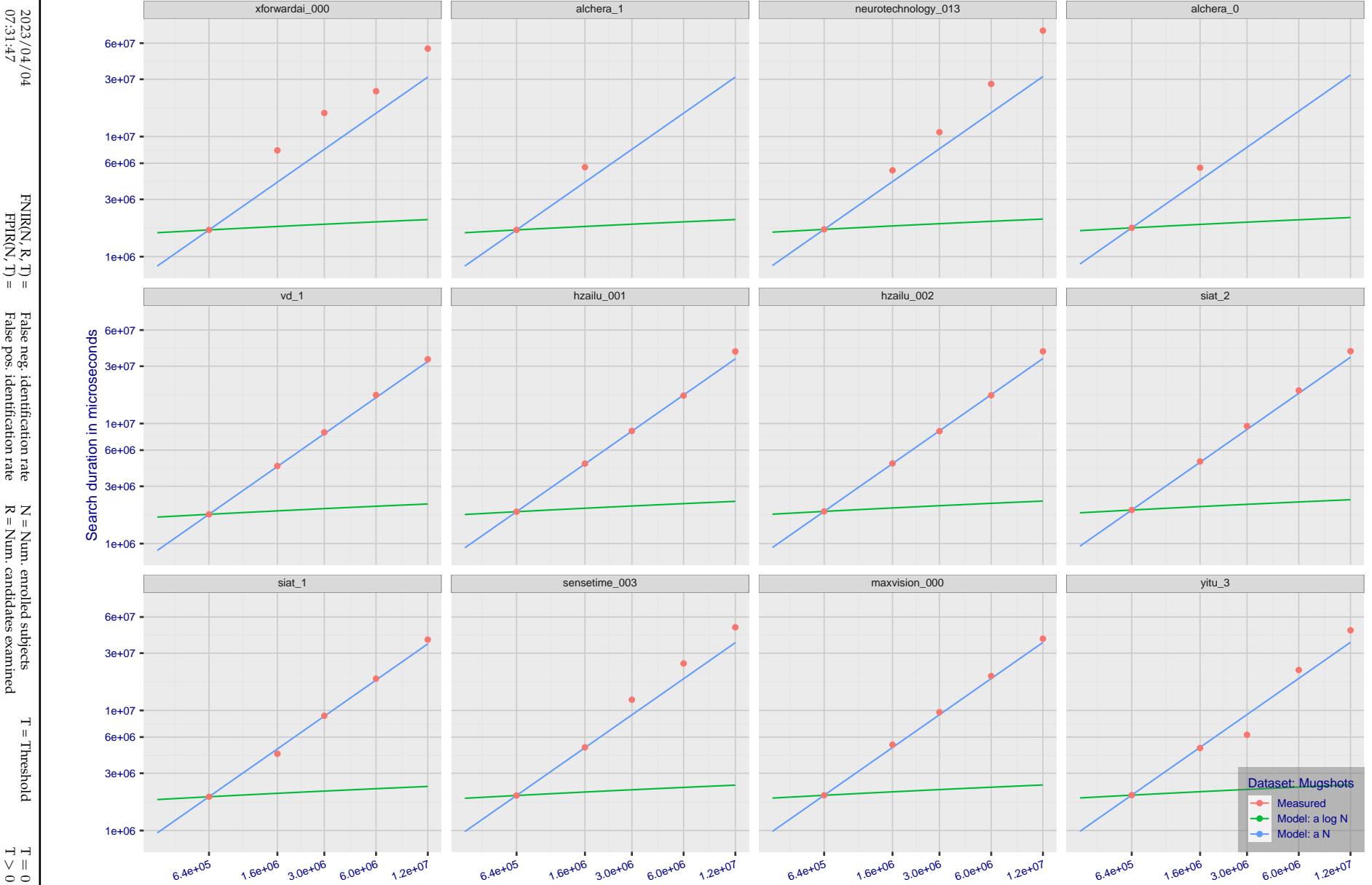


Figure 180: [Mugshot Dataset] Search duration vs. enrolled population size. In red are the actual point durations measured on a single c. 2016 core. The blue shows linear growth from $N = 640\,000$. The green line shows logarithmic growth from that point to $N = 1\,600\,000$. Note the sublinear growth from algorithms from Camvi, Dermalog, EverAI, Innovatrics, and Visionlabs. The tiger_1 algorithm is also sublinear, but inaccurate and inoperable at $N \geq 3000000$. This capability sometimes comes at the additional expense of converting a linear gallery data structure into whatever fast-search data structure is used. Note that search times are sometimes dominated by the template generation times shown in Table 29.

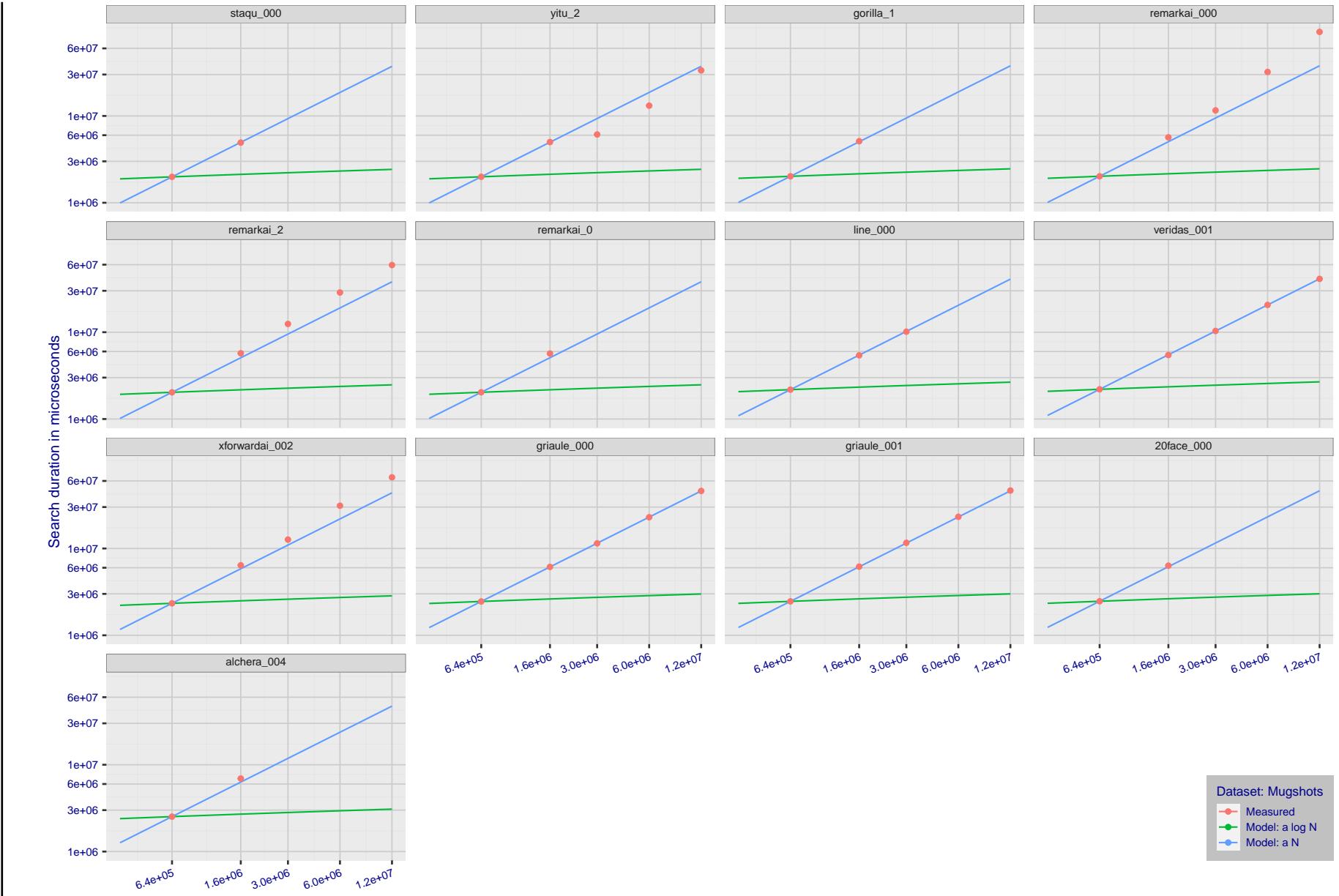


Figure 181: [Mugshot Dataset] Search duration vs. enrolled population size. In red are the actual point durations measured on a single c. 2016 core. The blue shows linear growth from $N = 640\,000$. The green line shows logarithmic growth from that point to $N = 1\,600\,000$. Note the sublinear growth from algorithms from Camvi, Dermalog, EverAI, Innovatrics, and Visionlabs. The tiger_1 algorithm is also sublinear, but inaccurate and inoperable at $N \geq 3000000$. This capability sometimes comes at the additional expense of converting a linear gallery data structure into whatever fast-search data structure is used. Note that search times are sometimes dominated by the template generation times shown in Table 29.

2023/04/04 07:31:47

FNIR(N, R, T) = False neg. identification rate
FPIR(N, T) = False pos. identification rateN = Num. enrolled subjects
R = Num. candidates examined

T = Threshold

T = 0 → Investigation
 $T > 0 \rightarrow$ Identification

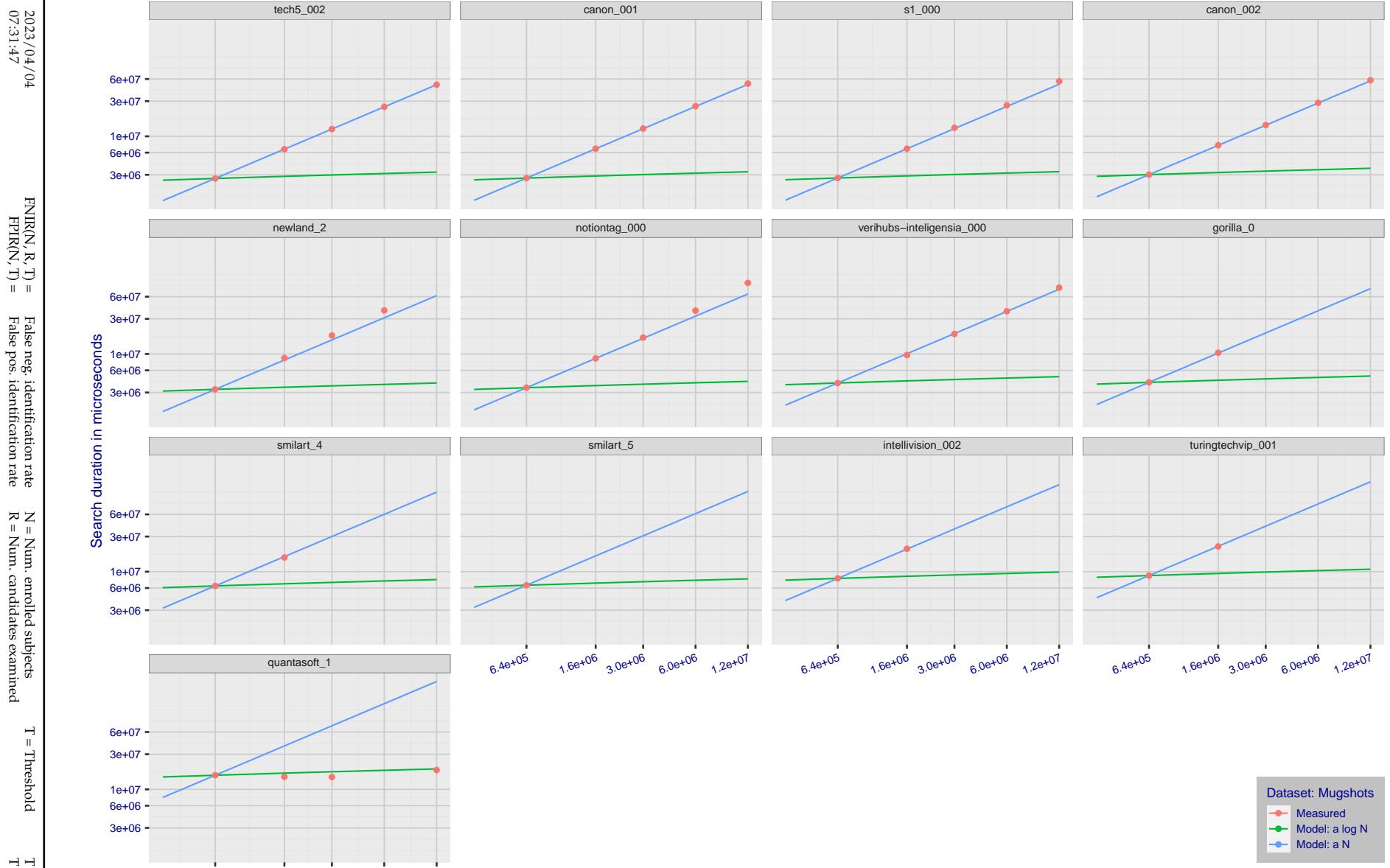


Figure 182: [Mugshot Dataset] Search duration vs. enrolled population size. In red are the actual point durations measured on a single c. 2016 core. The blue shows linear growth from $N = 640\,000$. The green line shows logarithmic growth from that point to $N = 1\,600\,000$. Note the sublinear growth from algorithms from Camvi, Dermalog, EverAI, Innovatrics, and Visionlabs. The tiger_1 algorithm is also sublinear, but inaccurate and inoperable at $N \geq 3000000$. This capability sometimes comes at the additional expense of converting a linear gallery data structure into whatever fast-search data structure is used. Note that search times are sometimes dominated by the template generation times shown in Table 29.

2023/04/04

FNIR(N, R, T) = False neg. identification rate
FPIR(N, T) = False pos. identification rateN = Num. enrolled subjects
R = Num. candidates examined

T = Threshold

T = 0 → Investigation
 $T > 0 \rightarrow$ Identification

Appendix G Gallery Insertion Timing

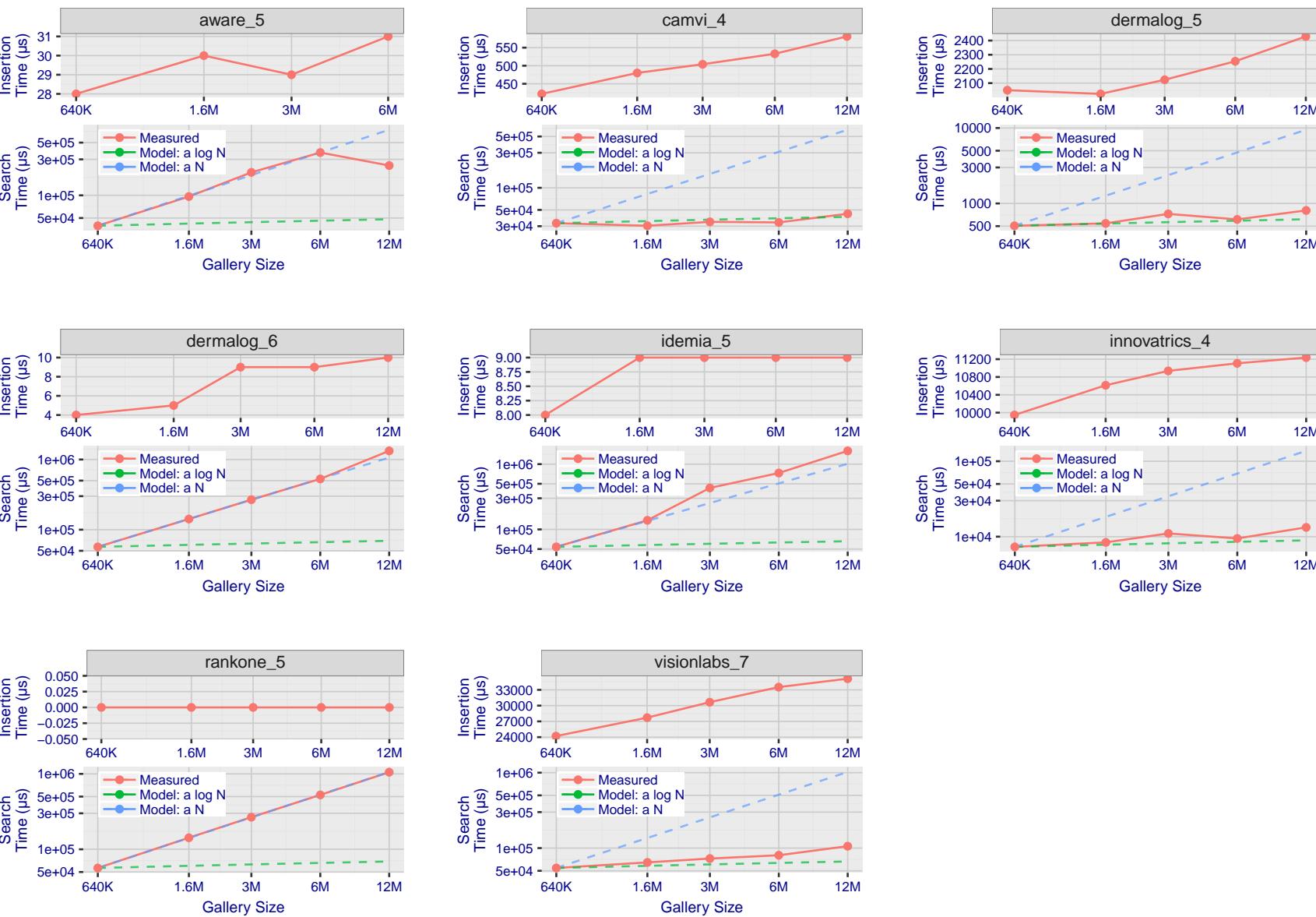
2023/04/04
07:31:47FNIR(N, R, T) = False neg. identification rate
FPIR(N, T) = False pos. identification rateN = Num. enrolled subjects
R = Num. candidates examinedT = Threshold
T = 0 → Investigation
T > 0 → Identification

Figure 183: [Mugshot Dataset] Gallery insertion duration vs. enrolled population size. This chart plots the time it takes to insert a single template into a finalized gallery, illustrated over increasing gallery sizes. For reference, search times on finalized galleries of corresponding sizes are plotted right underneath. Gallery insertion time plots were generated on algorithms that 1) successfully implemented gallery insertion with no errors and 2) that were run on galleries with N up to 12 000 000. Generally, only the more accurate algorithms were run on galleries with N up to 12 000 000.

2023/04/04

FNIR(N, R, T) = False neg. identification rate

FPFR(N, T) = False pos. identification rate

N = Num. enrolled subjects

T = Threshold

T = 0 → Investigation

T > 0 → Identification

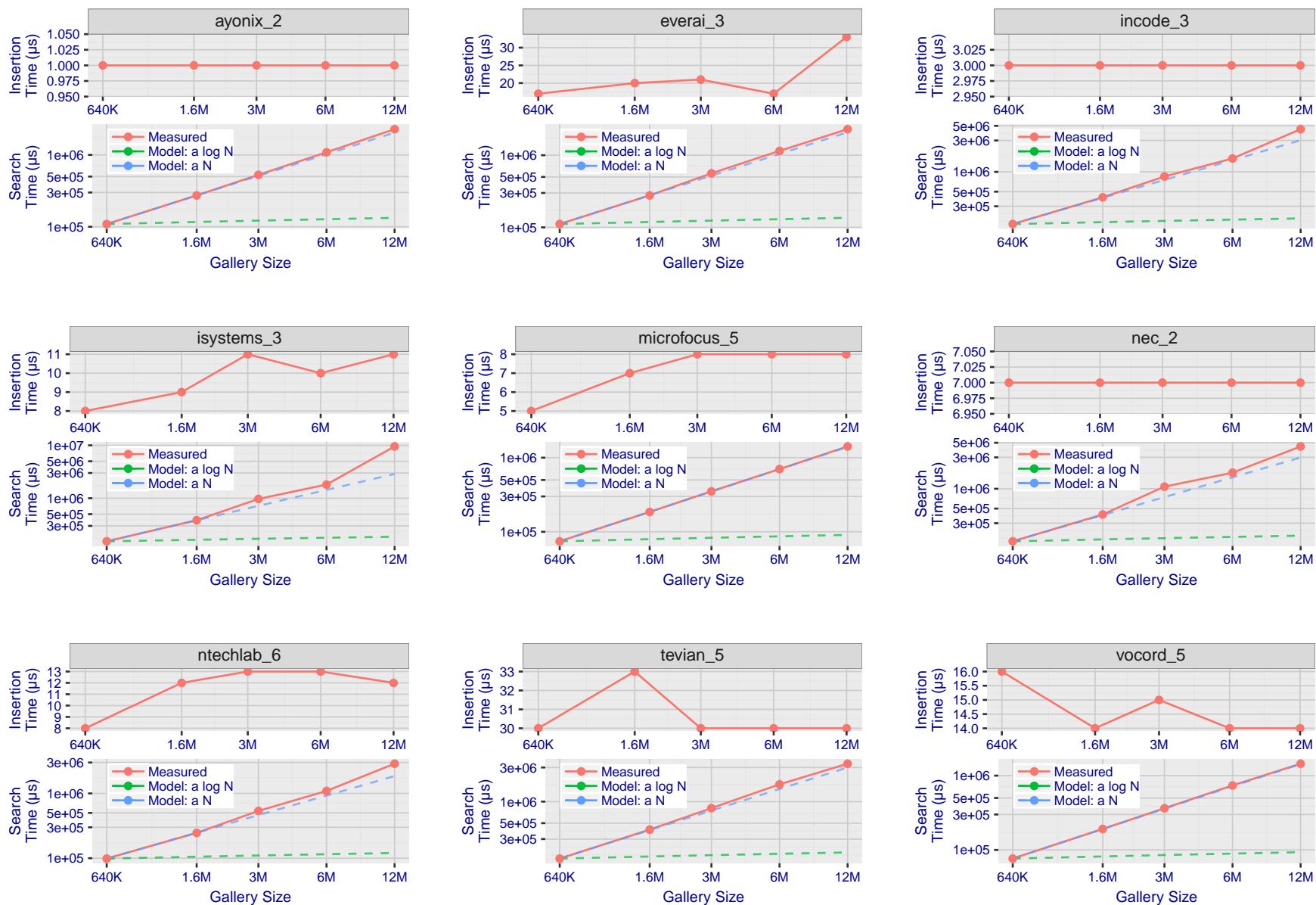


Figure 184: [Mugshot Dataset] Gallery insertion duration vs. enrolled population size. This chart plots the time it takes to insert a single template into a finalized gallery, illustrated over increasing gallery sizes. For reference, search times on finalized galleries of corresponding sizes are plotted right underneath. Gallery insertion time plots were generated on algorithms that 1) successfully implemented gallery insertion with no errors and 2) that were run on galleries with N up to 12 000 000. Generally, only the more accurate algorithms were run on galleries with N up to 12 000 000.

2023/04/04

FNIR(N, R, T) = False neg. identification rate

FPTR(N, T) = False pos. identification rate

N = Num. enrolled subjects

R = Num. candidates examined

T = Threshold

T = 0 → Investigation

T > 0 → Identification

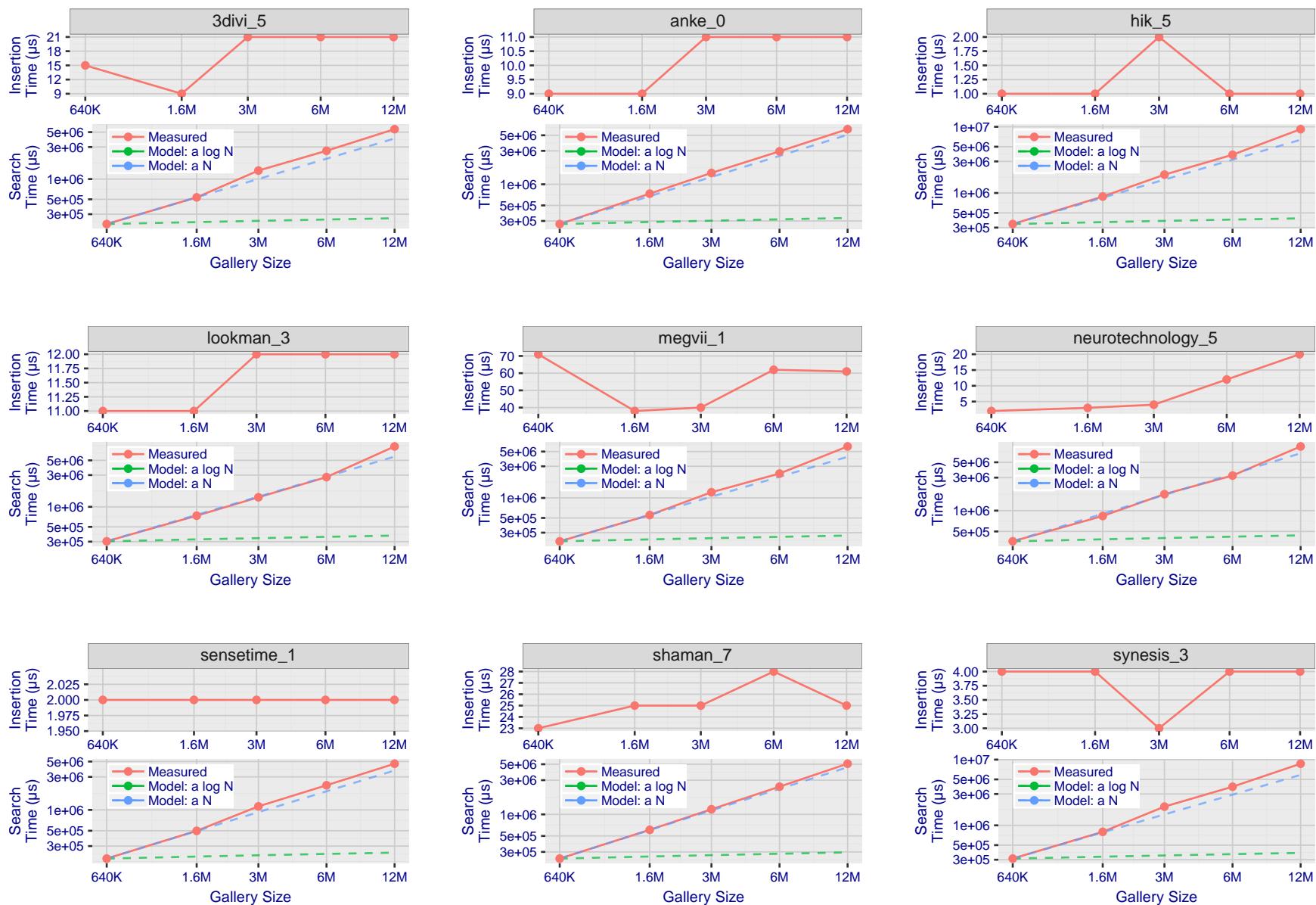


Figure 185: [Mugshot Dataset] Gallery insertion duration vs. enrolled population size. This chart plots the time it takes to insert a single template into a finalized gallery, illustrated over increasing gallery sizes. For reference, search times on finalized galleries of corresponding sizes are plotted right underneath. Gallery insertion time plots were generated on algorithms that 1) successfully implemented gallery insertion with no errors and 2) that were run on galleries with N up to 12 000 000. Generally, only the more accurate algorithms were run on galleries with N up to 12 000 000.

2023/04/04

FNIR(N, R, T) = False neg. identification rate

FPTR(N, T) = False pos. identification rate

N = Num. enrolled subjects

R = Num. candidates examined

T = Threshold

T = 0 → Investigation

T > 0 → Identification

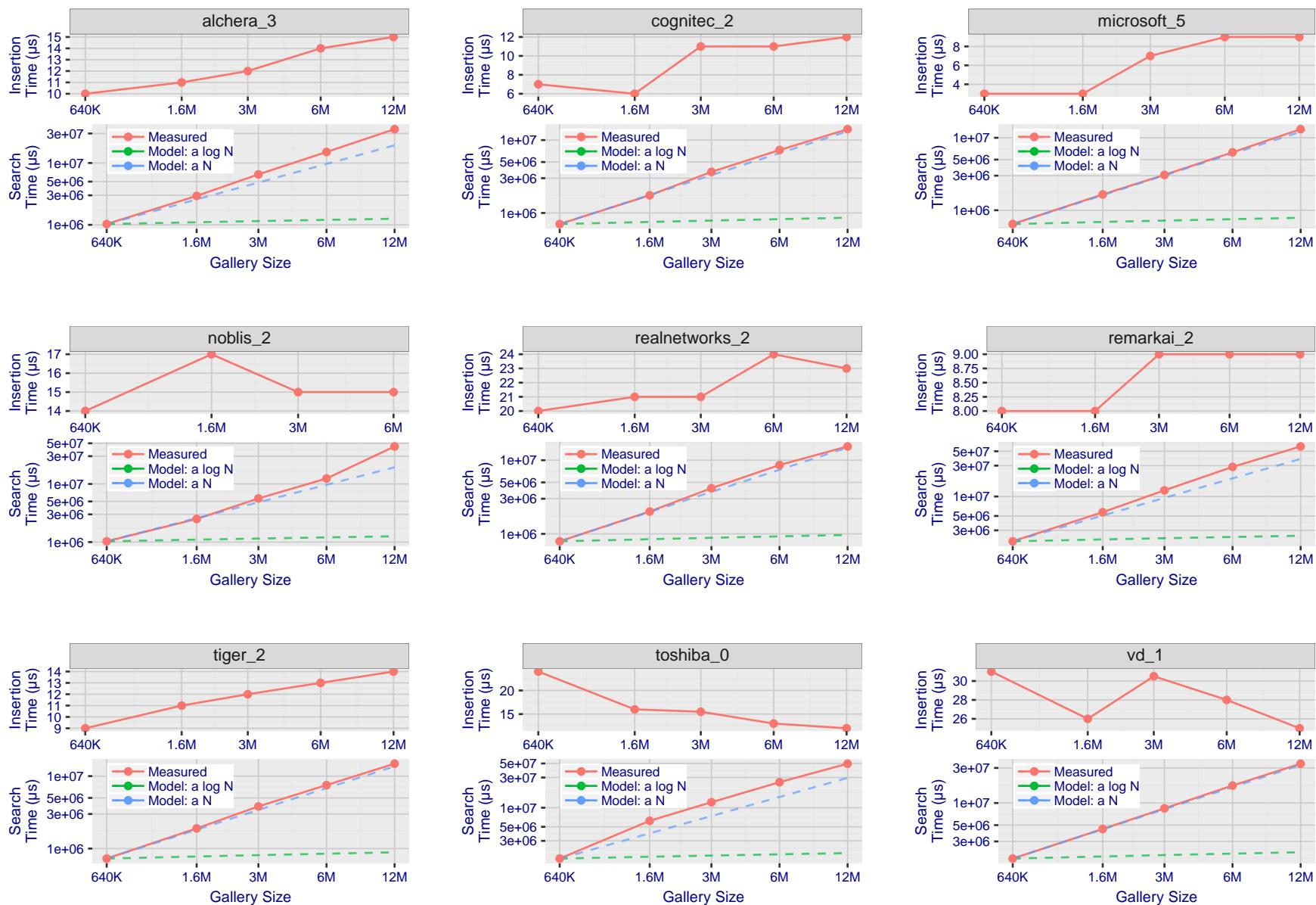


Figure 186: [Mugshot Dataset] Gallery insertion duration vs. enrolled population size. This chart plots the time it takes to insert a single template into a finalized gallery, illustrated over increasing gallery sizes. For reference, search times on finalized galleries of corresponding sizes are plotted right underneath. Gallery insertion time plots were generated on algorithms that 1) successfully implemented gallery insertion with no errors and 2) that were run on galleries with N up to 12 000 000. Generally, only the more accurate algorithms were run on galleries with N up to 12 000 000.

References

- [1] Artem Babenko and Victor Lempitsky. Efficient indexing of billion-scale datasets of deep descriptors. In *The IEEE Conference on Computer Vision and Pattern Recognition (CVPR)*, June 2016.
- [2] L. Best-Rowden and A. K. Jain. Longitudinal study of automatic face recognition. *IEEE Transactions on Pattern Analysis and Machine Intelligence*, 40(1):148–162, Jan 2018.
- [3] Blumstein, Cohen, Roth, and Visher, editors. *Random parameter stochastic models of criminal careers*. National Academy of Sciences Press, 1986.
- [4] Thomas P. Bonczar and Lauren E. Glaze. Probation and parole in the united statesm 2007, statistical tables. Technical report, Bureau of Justice Statistics, December 2008.
- [5] White D., Kemp R. I., Jenkins R., Matheson M, and Burton A. M. Passport officers' errors in face matching. *PLoS ONE*, 9(8), 2014. e103510. doi:10.1371/journal.pone.0103510.
- [6] P. Grother, G. W. Quinn, and P. J. Phillips. Evaluation of 2d still-image face recognition algorithms. NIST Interagency Report 7709, National Institute of Standards and Technology, 8 2010. <http://face.nist.gov/mbe> as MBE2010 FRVT2010.
- [7] P. J. Grother, R. J. Micheals, and P. J. Phillips. Performance metrics for the frvt 2002 evaluation. In *Proceedings of Audio and Video Based Person Authentication Conference (AVBPA)*, June 2003.
- [8] Patrick Grother and Mei Ngan. Interagency report 8009, performance of face identification algorithms. *Face Recognition Vendor Test (FRVT)*, May 2014.
- [9] Patrick Grother, George Quinn, and Mei Ngan. Face in video evaluation (five) face recognition of non-cooperative subjects. Interagency Report 8173, National Institute of Standards and Technology, March 2017. <https://doi.org/10.6028/NIST.IR.8173>.
- [10] Patrick Grother, George W. Quinn, and Mei Ngan. Face recognition vendor test - still face image and video concept, evaluation plan and api. Technical report, National Institute of Standards and Technology, 7 2013. http://biometrics.nist.gov/cs.links/face/frvt/frvt2012/NIST_FRVT2012.api_Aug15.pdf.
- [11] K. He, X. Zhang, S. Ren, and J. Sun. Deep residual learning for image recognition. In *2016 IEEE Conference on Computer Vision and Pattern Recognition (CVPR)*, pages 770–778, June 2016.
- [12] Gary B. Huang, Manu Ramesh, Tamara Berg, and Erik Learned-Miller. Labeled faces in the wild: A database for studying face recognition in unconstrained environments. Technical Report 07-49, University of Massachusetts, Amherst, October 2007.
- [13] Masato Ishii, Hitoshi Imaoka, and Atsushi Sato. Fast k-nearest neighbor search for face identification using bounds of residual score. In *2017 12th IEEE International Conference on Automatic Face & Gesture Recognition (FG 2017)*, pages 194–199, Los Alamitos, CA, USA, May 2017. IEEE Computer Society.
- [14] Jeff Johnson, Matthijs Douze, and Hervé Jégou. Billion-scale similarity search with gpus. *CoRR*, abs/1702.08734, 2017.

- [15] Ira Kemelmacher-Shlizerman, Steven M. Seitz, Daniel Miller, and Evan Brossard. The megaface benchmark: 1 million faces for recognition at scale. *CoRR*, abs/1512.00596, 2015.
- [16] Yury A. Malkov and D. A. Yashunin. Efficient and robust approximate nearest neighbor search using hierarchical navigable small world graphs. *CoRR*, abs/1603.09320, 2016.
- [17] Joyce A. Martin, Brady E. Hamilton, Michelle J.K. Osterman, Anne K. Driscoll, , and Patrick Drake. National vital statistics reports. Technical Report 8, Centers for Disease Control and Prevention, National Center for Health Statistics, National Vital Statistics System, Division of Vital Statistics, November 2018.
- [18] O. M. Parkhi, A. Vedaldi, and A. Zisserman. Deep face recognition. In *British Machine Vision Conference*, 2015.
- [19] P. Jonathon Phillips, Amy N. Yates, Ying Hu, Carina A. Hahn, Eilidh Noyes, Kelsey Jackson, Jacqueline G. Cava-zos, Géraldine Jeckeln, Rajeev Ranjan, Swami Sankaranarayanan, Jun-Cheng Chen, Carlos D. Castillo, Rama Chellappa, David White, and Alice J. O'Toole. Face recognition accuracy of forensic examiners, superrecognitioners, and face recognition algorithms. *Proceedings of the National Academy of Sciences*, 115(24):6171–6176, 2018.
- [20] Florian Schroff, Dmitry Kalenichenko, and James Philbin. Facenet: A unified embedding for face recognition and clustering. *CoRR*, abs/1503.03832, 2015.
- [21] Jeroen Smits and Christiaan Monden. Twinning across the developing world. *PLOS ONE*, 6(9):1–5, 09 2011.
- [22] Yaniv Taigman, Ming Yang, Marc'Aurelio Ranzato, and Lior Wolf. Deepface: Closing the gap to human-level performance in face verification. In *Proceedings of the 2014 IEEE Conference on Computer Vision and Pattern Recognition, CVPR '14*, pages 1701–1708, Washington, DC, USA, 2014. IEEE Computer Society.
- [23] A. Towler, R. I. Kemp, and D White. *Unfamiliar face matching systems in applied settings*. Nova Science, 2017.
- [24] Working Group 3. Ed. M. Werner. *ISO/IEC 19794-5 Information Technology - Biometric Data Interchange Formats - Part 5: Face image data*. JTC1 :: SC37, 2 edition, 2011. <http://webstore.ansi.org>.
- [25] David White, James D. Dunn, Alexandra C. Schmid, and Richard I. Kemp. Error rates in users of automatic face recognition software. *PLoS ONE*, 10:1–14, October 2015.
- [26] Bradford Wing and R. Michael McCabe. Special publication 500-271: American national standard for information systems data format for the interchange of fingerprint, facial, and other biometric information part 1. Technical report, NIST, September 2015. ANSI/NIST ITL 1-2015.
- [27] Andreas Wolf. Portrait quality - (reference facial images for mrtd). Technical report, ICAO, April 2018.
- [28] D. Yadav, N. Kohli, P. Pandey, R. Singh, M. Vatsa, and A. Noore. Effect of illicit drug abuse on face recognition. In *2016 IEEE Winter Conference on Applications of Computer Vision (WACV)*, pages 1–7, Los Alamitos, CA, USA, mar 2016. IEEE Computer Society.